The Effect of Metal Ions on Splice Site Formation of Group II Intron Ribozymes

DISSERTATION

zur

Erlangung der naturwissenschaftlichen Doktorwürde

(Dr. sc. nat.)

vorgelegt der

Mathematisch-naturwissenschaftlichen Fakultät

der

Universität Zürich

von

Daniela Kruschel

aus

Deutschland

Promotionskomitee

Prof. Dr. Roland K. O. Sigel (Vorsitz, Leitung der Dissertation)

Prof. Dr. Roger Alberto

Zürich 2008

My very special thanks go to my Ph.D. advisor

Prof. Dr. Roland K. O. Sigel

for giving me the opportunity to come to Switzerland to work in his group on this fascinating and challenging project. Thank you very much for supporting me over the past 4 years, for your manifold ideas, suggestions and your endless enthusiasm

and to

Prof. Dr. Roger Alberto

for kindly acting as referee

Content

List of Abbreviations

COSY correlation spectroscopy

D1, D2, D3, D4, D5, and D6, domains 1, 2, 3, 4, 5, and 6 of the group II intron *Sc*.ai5γ

d3'-EBS1 hairpin including d3'-stem and EBS1 of the group II intron *Sc*.ai5γ

d3'-EBS1* hairpin including d3'-stem and EBS1 of the group II intron *Sc*.ai5γ, including two mutations

d3'-EBS1·IBS1, hairpin including d3'-stem and EBS1 together with IBS1 of the group II intron *Sc*.ai5γ

d3'-EBS1*·IBS1*, hairpin including d3'-stem and EBS1 together with IBS1 of the group II intron *Sc*.ai5γ, including two mutations

d3'-TL hairpin including d3'-stem with a GAAA tetraloop

D56 domains 5 and 6

D6-27 shortened domain 6 construct that branches actively *in vitro*

DLS Dynamic light scattering

DOSY Diffusion ordered spectroscopy

DP 5'-terminal diphosphate group of an in vitro transcribed RNA

EBS1·IBS1 wildtype interaction between EBS1 and IBS1

EBS1*·IBS1*, modified interaction between EBS1 and IBS1

EBS exon binding site

EDTA ethylenediamine-N,N,N',N'-tetraacetic acid disodium salt

HDV Hepatitis delta virus

HSQC heteronuclear single quantum coherence

IBS intron binding site

MOPS [3-(N-morpholino)propane-sulfonic acid]

mRNA messenger ribonucleic acid

NMR nuclear magnetic resonance

NOE nuclear overhauser effect

NOESY nuclear overhauser effect spectroscopy

nt nucleotide

NTP nucleoside 5'-triphosphate

PAGE polyacrylamide gel electrophoresis

PNK polynucleotide kinase

ppm	parts per million
RDC	residual dipolar coupling
r.m.s.d.	root-mean-square deviation
RNP	ribonucleoprotein
rRNA	ribosomal ribonucleic acid
Sc.ai5γ	yeast mitochondrial group II selfsplicing intron in the gene of cytochrome c oxidase subunit 1 (*Sc*.cox1/5 intron)
snRNA	small nuclear ribonucleic acid
SRP	signal recognition particle
sw	sweep width
TOCSY	total correlation spectroscopy
TP	5'-terminal triphosphate group of an *in vitro* transcribed RNA
TR	tetraloop receptor
Tris	2-amino-2-(hydroxymethyl) propane-1,3-diol
tRNA	transfer ribonucleic acid
VS	Varkud satellite
wt	wildtype

1 Introduction

1.1 RNA - diversity of structure and function

1.1.1 The central dogma of molecular biology and the RNA World

In 1970, Francis Crick proposed the central dogma of molecular biology, which anticipated ribonucleic acid (RNA) as an intermediate between the genetic information stored in deoxyribonucleic acid (DNA) and the cellular activities, which are carried out by proteins after translation (Figure 1).[1] This simplified scheme represents several important cellular processes. The genetic information, which is stored in the sequence of the DNA building blocks, is copied accurately into the building blocks of RNA by transcription. Subsequently, RNA is translated by the ribosomal machinery inside the cell into proteins. These nucleic acids are responsible for a large variety of biochemical processes *in vivo*. The function of the transfer of information from DNA to proteins is carried out by messenger RNAs (mRNAs). In addition, other cellular processes exist, which are not depicted in this scheme. Besides mRNAs, DNA is transcribed into other RNA molecules like (i) transfer RNA (tRNA), which transports aminoacids to the site of proteins synthesis; (ii) ribosomal RNA (rRNA), which catalyzes and regulates protein synthesis; and (iii) small nuclear RNAs (snRNA), which are involved in intron splicing in the nucleus.[2] Additional classes of RNA are riboswitches, which play an important role in gene regulation, and the signal recognition particle (SRP), which is responsible for the protein transport over membranes.[3-5]

Before the discovery of this large variety of functions of RNA and its catalytic activity many scientists have struggled with the question of the origin of life. They faced the proverbial chicken-and-egg paradoxon, which states the question whether DNA or proteins came first. In 1967/68 Woese,[6] Crick[7] and Orgel[8] independently proposed that neither the egg nor the chicken came first, but the intermediate, i.e. the RNA. This suggestion became

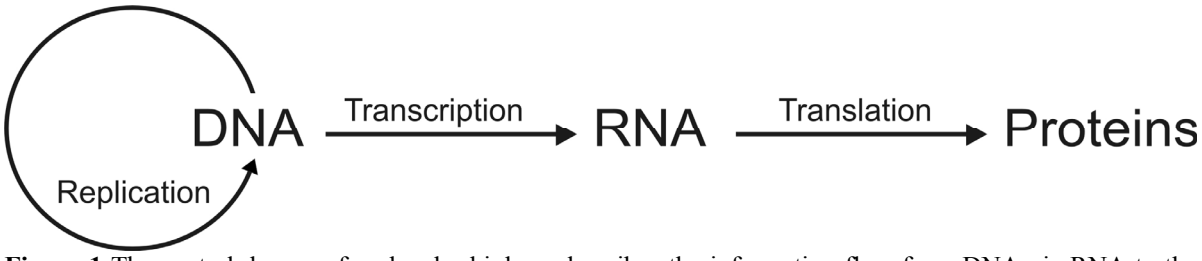

Figure 1 The central dogma of molecular biology describes the information flow from DNA via RNA to the proteins that perform catalytic functions. The genetic information, which resides in the DNA, is passed through cellular generations by replication, and transferred to RNA via transcription. Through translation the information is then transferred into proteins. This scheme is a simplified representation of the central dogma, for the complete representation see reference (1).

more and more prominent after the discovery of Cech and Altman that RNA can catalyze reactions in much the same way as proteins.[9,10] In 1982 Thomas Cech and his coworkers found that the *Tetrahymena* rRNA intron accomplishes autocatalytic activity by undergoing splicing without the help of enzymes, small nuclear RNAs and folding of the pre-rRNA into a RNP.[9] One year later, in 1983, Sidney Altman and his coworkers corroborated the hypothesis of the existence of true RNA enzymes, which were subsequently called "ribozymes". They showed that the RNA moieties of ribonuclease P can cleave its tRNA precursors in the absence of its protein moieties.[10] For their discovery of RNA-based catalysis, Altman and Cech were awarded the Nobel Prize in Chemistry in 1989. With this discovery the "RNA World" emerged, a term which was first coined by Walter Gilbert in 1986 and is today widely used.[11]

1.1.2 Basic structural features of RNA

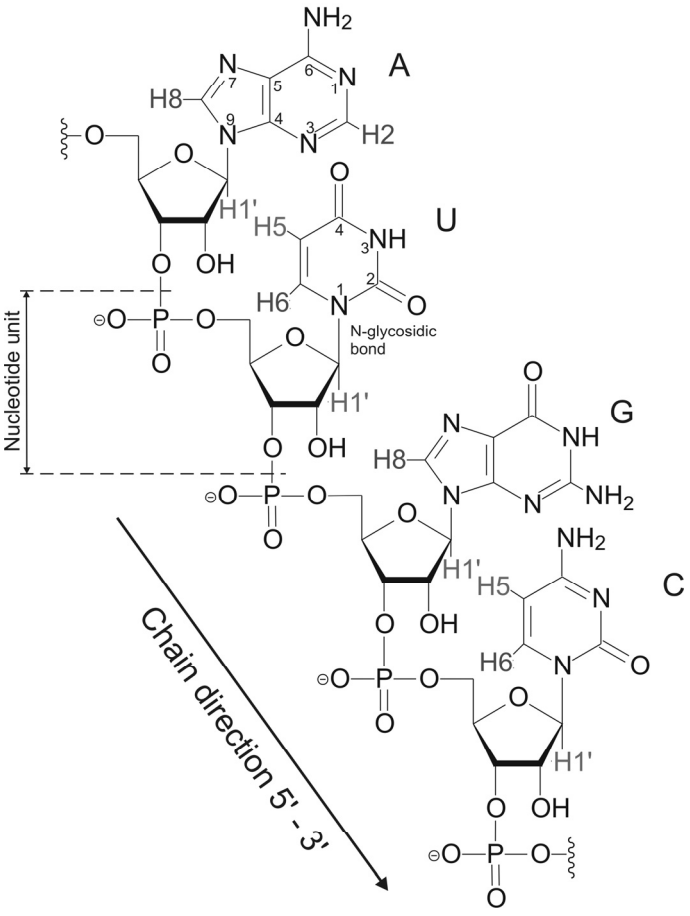

Figure 2 Section of a RNA strand showing an adenosine (A), an uridine (U), a guanosine (G) and a cytidine (C) linked by 3', 5'-phosphodiester bonds. The chain direction from 5'- to 3'-end is indicated by an arrow. The numbering scheme of the protons is shown.

In respect of the structural focus of this thesis, this chapter will discuss the basic structural features of RNA.

The basic repeating motif in RNA is the nucleotide (Figure 2). It is composed of a 5'-phosphorylated β-D-ribose that is substituted at position C1' by one of four bases via a N-glycosidic bond.[12] There are two purine bases, adenine (A) and guanine (G) and two pyrimidine bases, cytosine (C) and uracil (U). In addition to these four common nucleobases, a variety of other naturally occurring nucleobase analogues can be found, and also the sugar moieties can be posttranscriptionally modified. The most frequently occuring modifications are pseudouridylation, 2'-O-methylation and base methylation.[13,14]

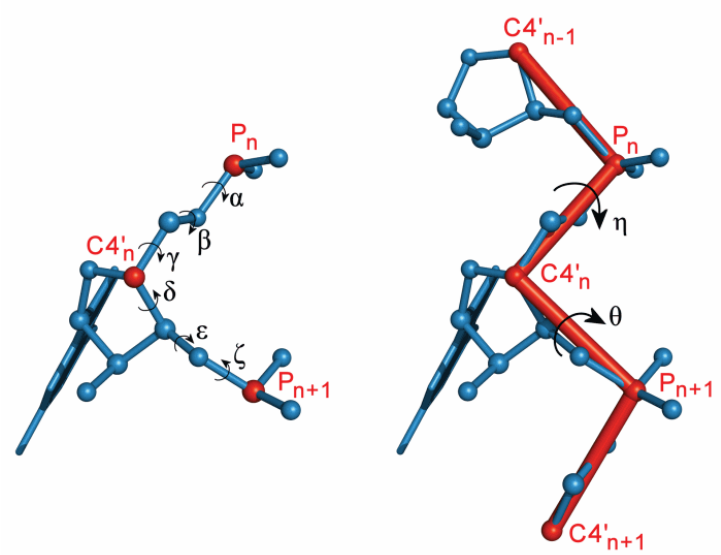

Figure 3 A nucleotide showing the standard backbone torsional angles (χ is not shown) (left) together with the depiction of the pseudotorsions η and θ (right) as used in the program AMIGOS. The red lines indicate the pseudo-bonds that connect successive P and C4' atoms. P and C4' atoms are shown in red and are labeled for reference. Figure was adapted from reference (16).

It is not only important to know the identity of the nucleobases, but also the backbone and sugar pucker conformation to fully describe the structure of RNA. Six standard torsion angles (α, β, γ, δ, ε, and ζ) describe the backbone conformation of every nucleotide linkage. To reduce the six standard backbone angles of RNA to a more simple description the pseudotorsions η ($C4'_{n-1}$, P_n, $C4'_n$, P_{n+1}) and θ (P_n, $C4'_n$, P_{n+1}, $C4'_{n+1}$) were introduced (Figure 3).[15,16] The program AMIGOS makes use of these pseudotorsions, allowing to perform a so-called "wormsearch", which compares the pseudotorsional angles of a given structural motif with those from previously reported RNA structures.[16] AMIGOS was used in this study to find similar structural motifs as discussed in Section 2.2.9.

The seventh torsion angle χ defines the orientation about the glycosidic bond, which can either adopt a *syn* or an *anti* conformation (Figure 4A and B). The latter one is mainly found in nucleic acids since it allows to maximize hydrogen bonding and base stacking in the secondary structure of nucleic acids and minimizes the electrostatic repulsion of the phosphate groups. The *syn* conformation appears less frequently, e.g. at guanosines in the $(dC\text{-}dG)_3$ DNA, which forms left-handed Z-DNA.[17] The *syn* and *anti* conformation can be distinguished with the help of nuclear magnetic resonance (NMR) spectroscopy: Nuclear Overhauser Effects (NOEs), which are dependent on the distance between protons, can be measured between the sugar H1' protons and the purine H8 or pyrimidine H6 base protons, respectively. The internuclear distance in a *syn* conformation is about 2.2 Å and is as such smaller than in an *anti* conformation which shows a distance of about 3.7 Å.[18,19] Therefore, a very strong crosspeak is expected for a *syn* conformation, whereas for an *anti* conformation only a weak or intermediate NOE will occur.

Another important feature of nucleic acid structures is the sugar pucker conformation. The most common sugar pucker conformations in nucleic acids are the C3'-endo (or North) conformation, which is mainly found in A-form RNA, and the C2'-endo (or South)

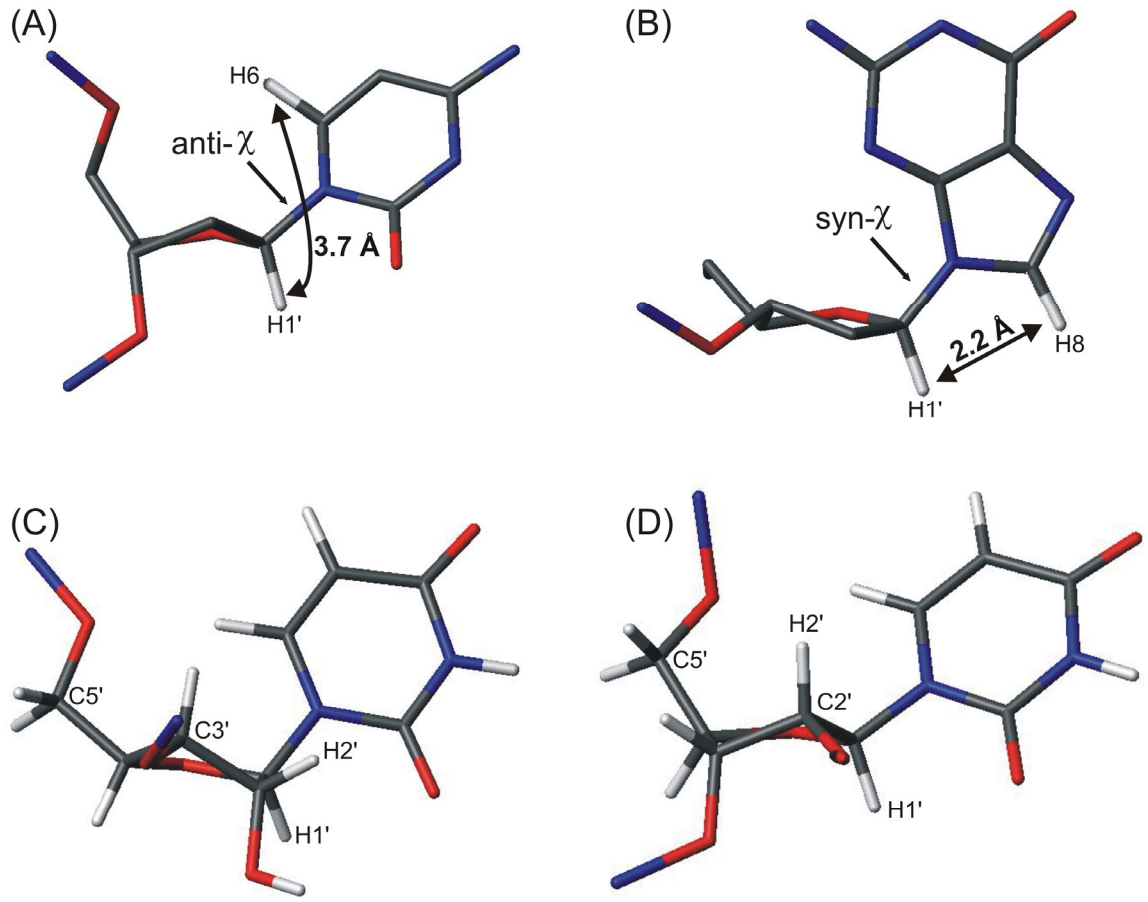

Figure 4 Typical glycosidic and sugar pucker conformations in RNA and DNA. (A) The *anti* glycosidic bond conformation is commonly found in A-form RNA and B-form DNA. The ≈3.7 Å distance between H6 and H1' results in moderate to weak NOE crosspeak. (B) The *syn* glycosidic bond conformation is not typically found in DNA and RNA structures. The small distance of ≈2.2 Å between H8 and H1' results in a very strong NOE crosspeak. (C) A C3'-endo sugar pucker conformation is usually found in A-form RNA. (D) A C2'-endo sugar pucker conformation is usually found in B-form DNA. Carbon atoms are coloured in grey, oxygens in red, hydrogens in white, and nitrogens in blue. In (A) and (B) all hydrogens except H1', H8 and H6 are omitted for clarity.

conformation, which is found in B-form DNA. The atom termed endo describes the atom, which points towards the same side as C5' in respect to the plane of the ribose (Figure 4C and D). To differentiate between a C3'-endo and a C2'-endo conformation, NMR can be the method of choice. For example, 2D [^{1}H,^{1}H]-TOCSY experiments give information about the sugar pucker conformation. In a C3'-endo sugar pucker, the angle between H1' and H2' is about 90° and thus coupling cannot be observed in NMR through-bond correlation experiments. The angle between H1' and H2' in a C2'-endo conformation is about 180° and therefore, a coupling is observable.[19] From these examples it is already obvious that NMR is a powerful tool to characterize RNA structures. Therefore, in this thesis NMR was used to elucidate structural properties of several RNA molecules. Further strategies to solve a solution structure by NMR will be discussed in Section 1.2.

1.1.3 The diversity of structural elements in RNA

The discovery that RNA molecules are not only working copies of the genome, but can also catalyze a variety of reactions, changed the view of RNA function and increased the interest in the structure of RNA. In this section, structural moieties of previously characterized RNAs will be discussed.

Most functional RNAs fold into a compact, stable and unique conformation.[20-22] These folded RNA molecules are stabilized by a variety of interactions, e.g. stacking of and hydrogen bonding between bases. The most common base-pairs are thereby Watson-Crick base-pairs (Figure 5A and B). Further base-base interactions are found regularly, including the GU wobble (Figure 5C) as well as bifurcated, triple and quadruplets interactions. A set of the observed base-base interactions in RNA structures is tabulated in the NCIR database: http://prion.bchs.uh.edu/bp_type/.[23] Base triples, especially the UAU base triple (Figure 5D), will be discussed in more detail in Section 2.2.9.

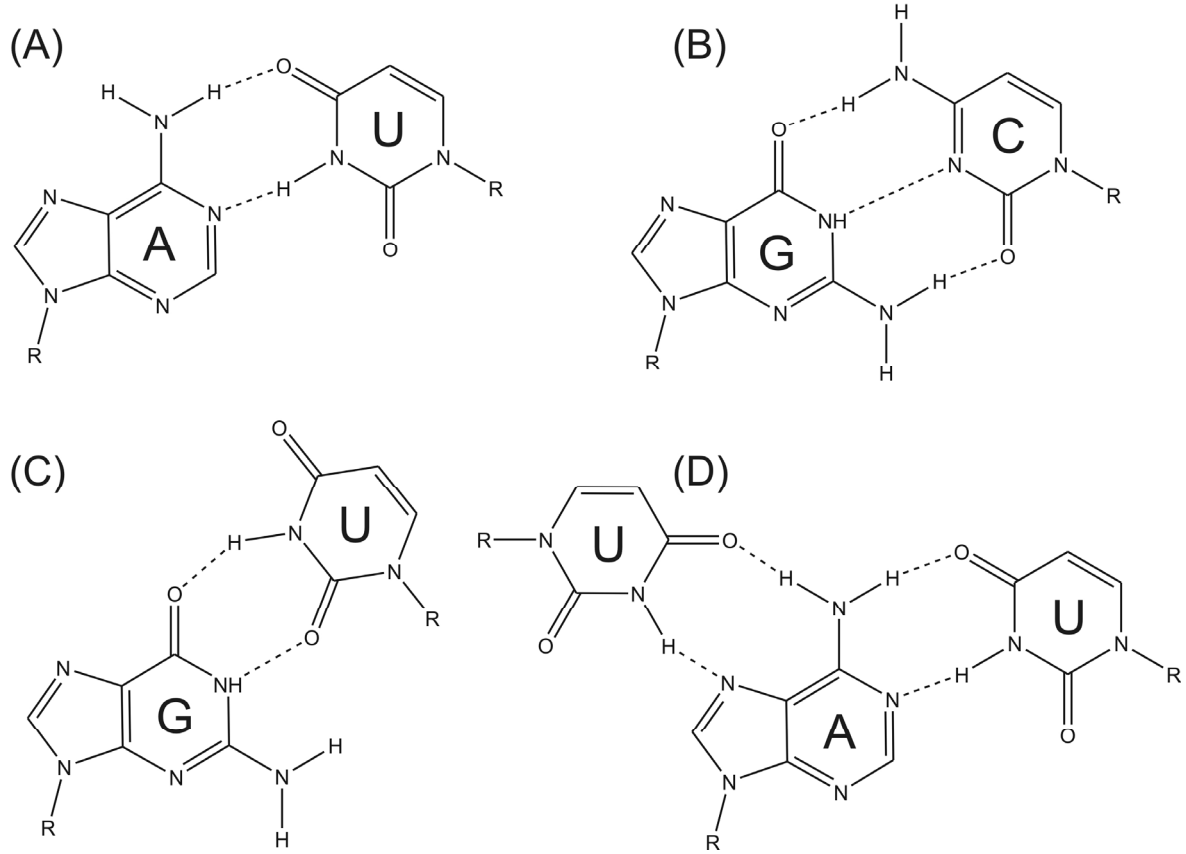

Figure 5 In the classical Watson-Crick base-pairs adenine pairs with uracil (A) and guanine with cytosine (B). Non Watson-Crick base-pairs like the G-U wobble pair (C) and triple base-pairs like the here depicted U-A-U (D) also occur sometimes in RNA.

Secondary as well as tertiary elements are found in a three-dimensional structure of RNA. The secondary structure of RNAs includes duplexes, single-stranded regions, hairpins, internal loops or bulges, and junctions.[24] Figure 6 gives an overview of different types of secondary and tertiary structural elements. Programs are available for the prediction of RNA secondary structure, which are mainly based on energy minimization using nearest neighbour energy parameters.[26] The mfold server (http://frontend.bioinfo.rpi.edu/applications/mfold/cgi-bin/rna-form1.cgi) was used in this study to predict the secondary structure of a hairpin (see Section 2.2.5). The most often encountered secondary structures in this thesis are hairpins and duplexes. Therefore, these two moieties will be discussed in more detail.

RNA duplexes are comprised of two single strands that interact via hydrogen bonds forming a right-handed double helix in the so-called A-form. In comparison to RNA, DNA is mainly found in the B-form, but also examples of DNA in A-form exist like in poly(dG)·poly(dC).[27] Both helices are right-handed and stabilized by stacking interactions between neighbouring bases. In 1979, Alexander Rich and coworkers found a left-handed polynucleotide helix, which is known as the Z-form.[17] Table 1 summarizes the parameters for the A-form RNA, and the B-, as well as the Z-form DNA. A-form RNA differs in several ways from B-form DNA. The different ribose conformations were already mentioned in

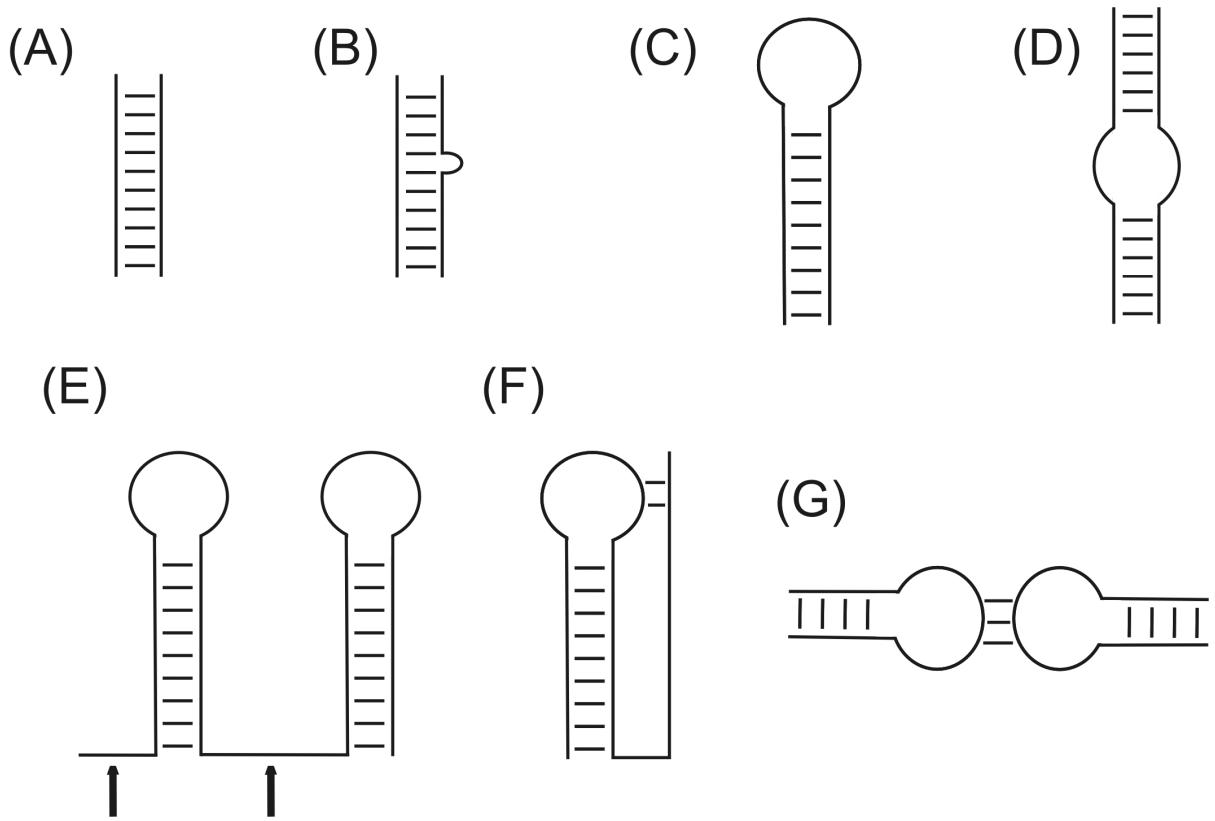

Figure 6 Secondary and tertiary structural elements in RNA. (A) Duplex, (B) bulge, (C) hairpin with stem and loop, (D) internal loop, (E) single stranded regions (depicted with arrows), (F) pseudoknot, and (G) kissing hairpins. The magnitude of bulges and loops can vary. Junctions are not shown. Figure is adapted from references (24) and (25).

Table 1 Parameters for the A-form RNA, B-form DNA and Z-form DNA of polynucleotide helices.[12]

	A-form RNA	B-form DNA	Z-form DNA
Direction of helix rotation	Right	Right	Left
Number of residues/turn	11	10	12
Pitch	30 Å	33.8 Å	31 Å
Turn angle/nucleotide residue	32.7°	36°	38.6
Axial rise/nucleotide residue	2.9 Å	3.38 Å	3.7 Å
Diameter	26 Å	20 Å	18 Å

Section 1.1.2. The base-pairs in A-form helices are tilted with respect to the helix axis of about 17°.[12] In contrast to the wide major groove of a B-form helix, an A-form helix has a deep and narrow major groove that is ideal suited for metal ions to bind and a broad and shallow minor groove (Figure 7). The reason why RNAs exist in the A-form is due to the fact that the B-form helix formation is sterically unfavoured by the additional 2'-OH group if the riboses are in C2'-endo conformation.[28]

Next to duplexes, the most common secondary structural elements in RNA are hairpins. The loop size typically ranges from three to six nucleotides. In this thesis, a hairpin which comprises a loop of 11 nucleotides will be described. It has been shown that hairpins with four or five nucleotides in the loop are the most stable ones, independent of the loop composition.[32] In this thermodynamic study, loop sequences $(U)_n$, $(C)_n$, or $(A)_n$ were used with loop magnitudes between three and nine nucleotides. A further thermodynamic study of

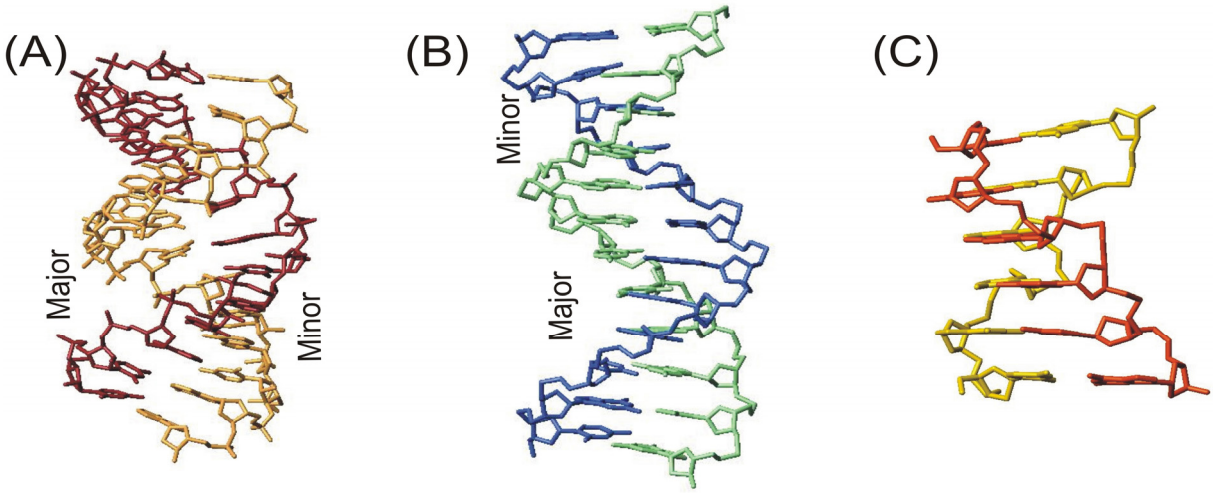

Figure 7 Different forms of nucleic acids. (A) A-form RNA, (B) B-form DNA, (C) Z-form DNA. The deep and narrow major groove in A-form and the wide major groove of B-form as well as the minor grooves are shown. Figures were prepared with MOLMOL[29] based on the PDB files 1RNA[30], 1BNA[31] and 2DCG[17], respectively.

tetraloop-hairpins showed that the UUCG tetraloop closed by a CG base-pair is the most stable of the studied tetraloops.[33] Besides UUCG tetraloops, also GAAA tetraloops are found to form stable hairpins in DNA as well as RNA.[34-36] NMR studies revealed that nucleotides in hairpin loops are stabilized by interactions between loop bases and between bases in the loop and the sugar-phosphate backbone.[37] A hairpin with a GAAA tetraloop was studied in this thesis and will be discussed in Section 2.3.

Besides secondary structural elements a variety of tertiary structural elements are known, e.g. pseudoknots, kissing loops, loop-receptor interactions, and coaxial stacking. Moreover, these and other distinct three-dimensional motifs play an important role in the modulation of specific functions of RNAs.[39] First insights into the architecture of RNAs was gained in 1974 by Robertus *et al*. by solving the crystal structure of Phenylalanine-tRNA from yeast (Figure 8A).[38] The structure of this 25 kD RNA molecule revealed the geometry of a few non-Watson-Crick base interactions that still adopt an A-form like helical structure, and also base triples were found in this structure.[40] In addition, coaxial stacking of RNA helices was observed for the first time. For two decades, this structure and regular helices of double stranded RNA were the only examples of three-dimensional folds. Due to technical improvements in the synthesis of RNA and developments in structure determination methods, many three-dimensional structures of RNAs could be solved thereafter. In 1996, Cate *et al.* solved the crystal structure of the P4-P6 domain of a self-splicing group I intron (Figure

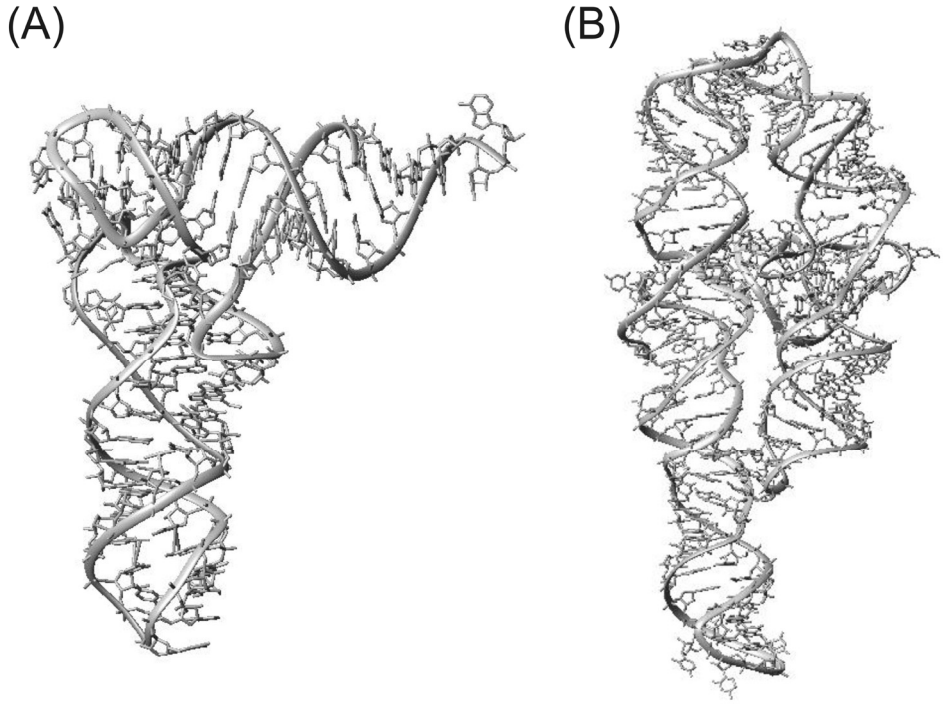

Figure 8 (A) Crystal structure of the 76-nt phenylalanine tRNA from yeast at 2.0 Å resolution[38] and (B) crystal structure of the 160-nt P4-P6 domain of a self-splicing group I intron at 2.8 Å resolution.[21] Figures were prepared with MOLMOL[29] based on the PDB files 1EVV and 1GID.

8B).[21] The structure of this *Tetrahymena thermophila* intron was solved at 2.8 Å resolution and revealed the A-minor motif which is one of the most abundant long-range interactions in RNA.[41] The term derives from the interaction of single-stranded adenosines with the minor grooves of double helices, making hydrogen bonds and van-der-Waals contacts. In this structure, the GAAA tetraloop-receptor motif was found, which comprises the interaction between a tetraloop and a tetraloop receptor. This motif also provides an example of a GACG quadruplet in which four bases are in a plane connected via hydrogen bonds. Davis *et al.* used NMR to solve the solution structure of a 30kDa GAAA tetraloop-receptor complex (Figure 9A) and confirmed the suggested hydrogen bond pattern of this motif.[42]

In the years 1999 and 2000 the first high-resolution X-ray structure of the ribosomal subunits were solved, thereby not only extending the size of the molecule that can be structurally studied, but also gaining information on additional RNA tertiary structural motifs.[43-47] The ribosome comprises 20 out of the 25 possible kinds of noncanonical base-pairs involving two or more hygrogen bonds.[12] In addition, single stranded regions were found to be highly structured, being involved in hydrogen bonds and stacking interactions with other elements of the RNA. In the ribosome, short helices are connected by bulges or internal loops of different lengths, thereby revealing recurring motif structures, e.g. the S-turn motif (Figure 10A) and the kink turn, which connects two adjacent helices by an obtuse 120° angle.[48] The compact and stable structure of the ribosome is stabilized by long-range base-pairs as well as by the A-minor motif. Mg^{2+}-bridges and RNA-protein crosslinks also contribute to the stability.[49] The crystal structures of the ribosomal subunits show that the rRNA serves as a molecular scaffold and is also involved in ribosomal function by forming the main features of the ribosome's functional sites. Thus, it was proposed that the ribosome is also a ribozyme.[49,50] Ribozymes will be discussed in further detail in Section 1.3.

Besides the already mentioned S-turn and kink turn motifs also U- and C-turns belong to the structural family of turns (Figure 10B and C). U-turns, which were first identified in the anticodon loop and T-loop in tRNA, follow a UNR (N is any nucleotide, R is a purine) consensus and are stabilized by specific hydrogen bonding and base-phosphate stacking interactions along the bend.[39,51] However, the stabilization of turns only involves a few functional groups, thus many sites are free to form further tertiary interactions. The C-turn shares some structural similarities with the U-turn and has been described in a ribosomal frameshifting pseudoknot.[52] U- and C-turns are classified by the nucleotide preceding the turning phosphates. The expression S-turns derives from the S-shaped kink in the RNA strand, which is induced by a sugar moiety with a C2'-endo pucker, thereby causing a locally

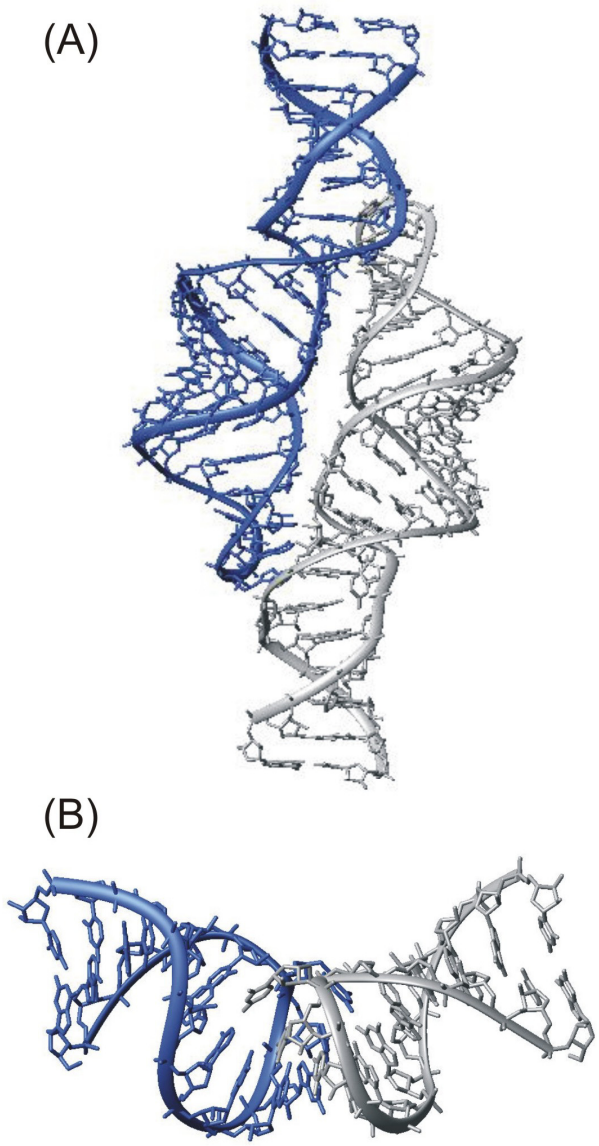

Figure 9 (A) Solution structure of the GAAA tetraloop-receptor complex. The lowest energy structure with one half of the homodimer in blue and the other in grey is shown.[42] (B) Solution structure of the kissing hairpin complex of the HIV TAR hairpin loop (blue) and its counterpart (grey).[53] Figures were prepared with MOLMOL[29] based on the PDB files 2ADT and 1KIS, respectively.

reversed backbone. The overall linear conformation is maintained in S-turns, whereas U- and C-turns globally reverse the strand direction of RNAs. Figure 10 exemplifies several of the mentioned recurring motifs in RNA structures.

Two further three-dimensional distinct motifs are pseudoknots and kissing loops (Figure 6F and G). Pseudoknots involve base-pairing between unpaired nucleotides within a stem-loop and nucleotides that flank the stem-loop. The stem-loop can either be a hairpin-loop, a bulge or an internal loop. The first pseudoknot was identified at the 3'-end of a plant RNA.[54] Through the pseudoknot formation, these molecules fold into a tertiary structure functionally similar to tRNA. Using the example of the coronavirus IBV, it has been shown that the formation of pseudoknots enhances frameshifting during translation.[55] Owing to its diverse structures, pseudoknots are known to play further roles in biological processes, including the formation of the catalytic core of the Neurospora VS ribozyme,[56] the hepatitis delta virus ribozyme,[57] group I intron ribozymes,[58] and telomerase.[59] The best characterized pseudoknot topology is the H-type, in which the bases in the loop of a hairpin form hydrogen bonds with bases outside of the stem.

Loop-loop interactions between RNA hairpins, also known as kissing loops, are important in antisense regulation.[60] Kissing loops are often found to offer sites for metal ion and protein binding. The solution structure of the RNA kissing hairpin complex from the HIV TAR hairpin loop and its counterpart revealed that the loop-loop helix of the kissing complex

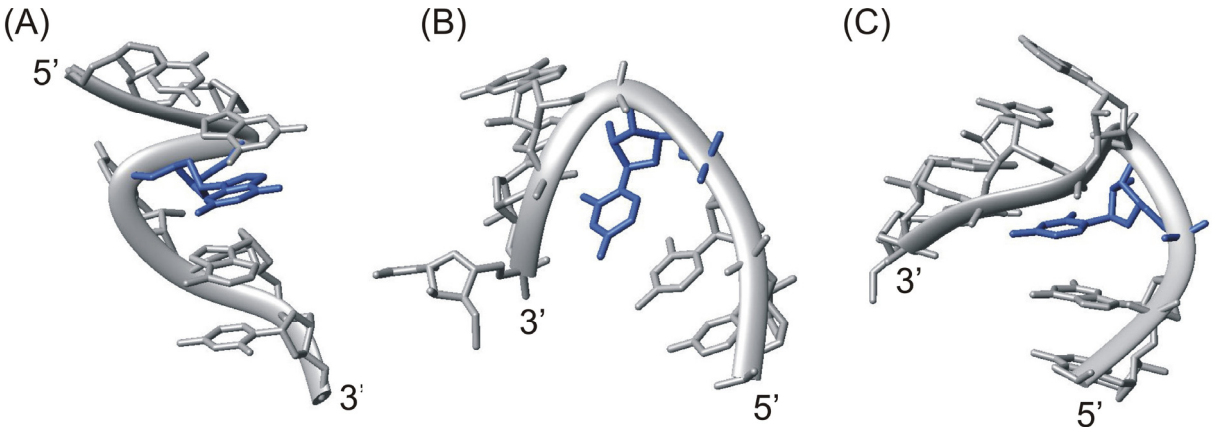

Figure 10 (A) In S-turns a locally reversed backbone is caused by a sugar moiety with a C2'-endo pucker (blue), which leads to a S-shaped kink in the RNA strand as exemplified here by the RRE RNA (PDB entry 1ETF).[61] (B) In U-turns, a sharp bend is introduced at a phosphate, which follows an uridine base (blue). The active site of the hammerhead ribozyme comprises this motif. (PDB entry 1HMH).[62] (C) In C-turns, the sharp bend follows a cytosine base (blue). A C-turn is found in a ribosomal frameshifting pseudoknot (PDB entry 437D).[52] Figures were prepared with MOLMOL.[29]

is distorted compared to usual A-form RNA (Figure 9B). It adopts an alternating helical twist pattern, which may be important for protein recognition of the kissing hairpin complex.[53]

It is already obvious from these examples that RNA can adopt a large variety of different folds. To assess the question, what factors guide RNAs into their folds, the next chapter will deal with some requirements of RNA folding.

1.1.4 The role of metal ions in RNA folding and catalysis and methods of metal ion detection

Metal ions are crucial for proper folding and function of RNA molecules. RNA is a highly negatively charged polyanion and thus higher order structures cannot form without charge compensation.[63,64] A simplified pathway for folding of large RNAs consists of a first transition from a random coil to secondary structure followed by a second step of compaction to the tertiary structure, in which specialized long-range interactions orient all the structural elements in space (Figure 11).[65] Monovalent ions play an important role in charge-screening, thereby allowing the secondary structure to form. The most common of these monovalent ions is K^+.[66,67] Divalent metal ions stabilize the tertiary structure, but also potassium appears to

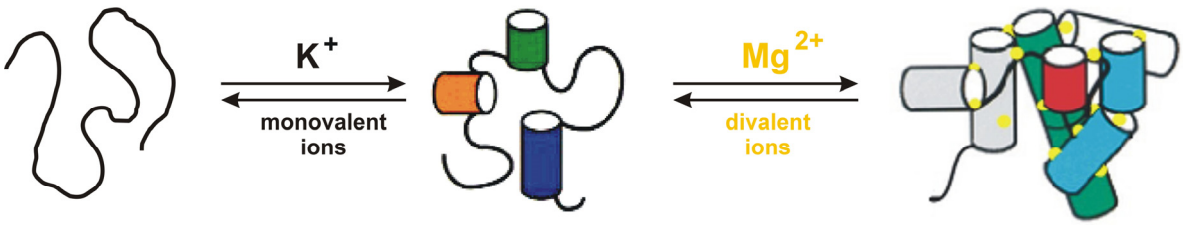

Figure 11 Simplified folding pathway of RNA. The secondary structure is formed in the presence of monovalent ions only. Divalent metal ions bind to specific sites and induce the active tertiary structure.

have a special additional role in binding to high affinity sites.[66] The most abundant divalent metal ion thereby is Mg^{2+}. Due to its small size and high charge density, Mg^{2+} is an adequate ion for stabilizing tertiary structural elements.[65,68-71] Although K^+ and Mg^{2+} play a main role in RNA metabolism, they can be replaced by other metal ions. K^+ can be substituted in some cases by Na^+, Li^+ and NH_4^+ and Mg^{2+} can be substituted by Ca^{2+}, Mn^{2+}, Zn^{2+}, Pb^{2+} and Cd^{2+}, although these substitutes are rarely the natural cofactors.[72,73] It has been shown that some ribozymes and DNAzymes are catalytically active in the absence of Mg^{2+} (see also Section 1.3.1).[74-77] These findings led to the assumption that in these cases divalent metal ions are not directly involved in catalysis but rather compensate only the negative charge of the phosphodiester backbone or stabilize structural components.

In general, three types of metal ion binding to RNA are known:

(i) *Diffuse binding*: this binding mode has the main purpose to compensate the negative charges of the RNA backbone.[78-80]

(ii) *Site-bound outer-sphere binding*: Metal ions coordinate to RNA bases and phosphate groups via bridging H_2O molecules (Figure 12A).[21,81,82] Because of the inert nature of the NH_3 groups, $[Co(NH_3)_6]^{3+}$ is typically used to mimic this binding mode in experiments.[81-83]

(iii) *Site-bound inner-sphere binding* (Figure 12B): Such inner-sphere bound metal ions are often directly involved in RNA structure formation and function,[68,79] where they may effect the pK_a values of nucleobases.[84,85] Metal ion specificity switch experiments can be used to investigate direct inner-sphere contacts and to give information about the role of the divalent metal ion in catalysis.[67,86,87]

Binding of the type (ii) or (iii) can occur at phosphoryl oxygens, purine N7 heteroatoms, purine and pyrimidine keto oxygens, as well as at ribose 2'-OH groups. In a typical A-form helix, metal ions usually bind in the deep, narrow major groove because of its pronounced negative electrostatic potential.[80] In addition, Mg^{2+} binding motifs are known to bind to RNA in the major groove of tandem GU wobble pairs,[21] or at internal loop structures like the loop E motif, where cations are bound as binuclear cluster.[88] The so-called A-platform is another known metal ion binding motif. It has been biochemically and crystallographically shown that the A-platform binds a partly dehydrated K^+ ion.[67]

Although metal ions are crucial for the correct function and catalysis of RNA molecules, investigations have been hindered because Mg^{2+} and K^+ are spectroscopically "silent". Studies on divalent ions are further complicated because these metal ions serve multiple roles in the same molecule, as well as the fact that Mg^{2+} binding sites are often weak, leading to a requirement of high concentrations of Mg^{2+} in the studies. Therefore, alternative methods

were applied in the past few years to investigate the role of metal ions in RNAs.[89-91] First of all, crystallographic studies have provided information on the diversity of metal ion binding motifs in RNA. Also the so-called "metal ion rescue experiment" is one of the most common methods for the detection of metal ion binding sites.[86,92-96] Lanthanide(III)-mediated (Tb^{3+} and Eu^{3+}) cleavage experiments have been used to identify metal ion binding sites in large ribozymes.[91,97,98] The use of spectroscopic (Mn^{2+}),[99,100] hydrolytic (Pb^{2+}, Mn^{2+}, Zn^{2+}),[101-106] or redoxactive (Fe^{2+})[107,108] mimics of Mg^{2+} are other methods to study interactions between metal ions and RNA. In addition, NMR spectroscopy has established itself as a new method to determine RNA structures and the detection of metal ion binding sites by using NMR-active isotopes (^{23}Na, ^{113}Cd),[109,110] mimicking ions (NH_4^+, $[Co(NH_3)_6]^{3+}$),[83,111] or paramagnetic ions (Mn^{2+}).[81,112-114] But even Mg^{2+} binding to RNA can be directly observed.[34,115] Upon addition of Mg^{2+} to a RNA sample, specific protons experience a chemical shift change. This change is induced by direct Mg^{2+} binding at a neighbouring atom or by a structural change in the local geometry, which is caused by Mg^{2+} binding in close proximity of this site.

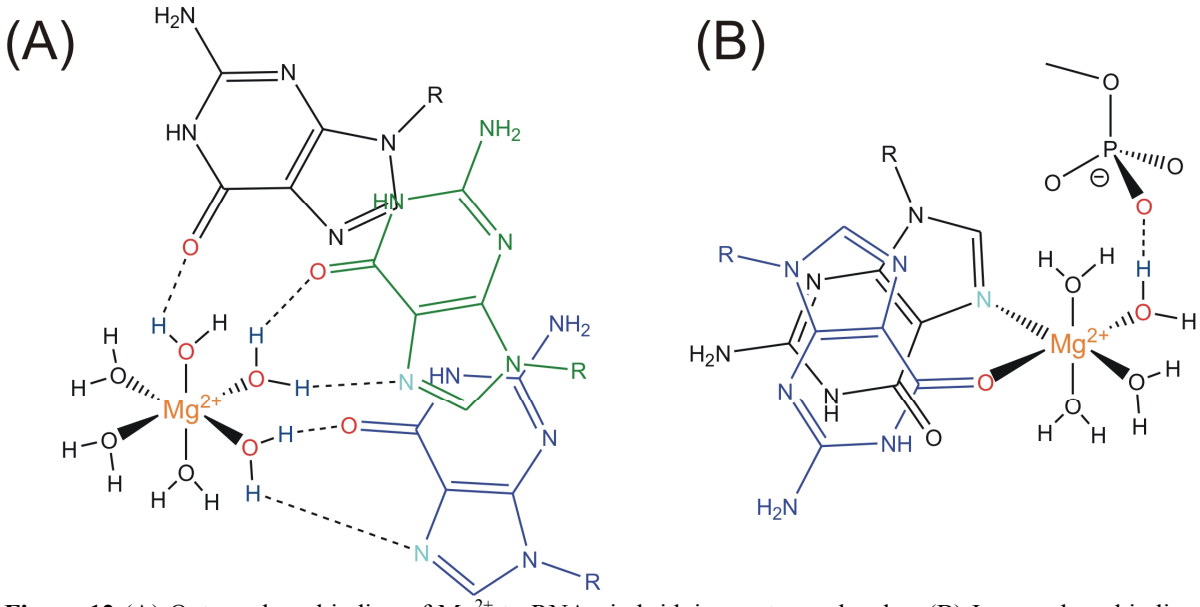

Figure 12 (A) Outer-sphere binding of Mg^{2+} to RNA via bridging water molecules. (B) Inner-sphere binding mode. Mg^{2+} coordinates directly to the base N7, to carbonyl oxygen and to a nonbridging phosphate oxygen via a water molecule. Mg^{2+} is coloured in orange, the atoms involved in coordination are highlighted in red, cyan, and dark blue.

1.2 Determination of RNA structures by NMR

A method to determine RNA structures at high resolution is single crystal X-ray diffraction. This method reveals three-dimensional structures even of large biomolecules. Unfortunately, obtaining single crystals suitable for X-ray analysis is often a difficult task. Another disadvantage is that a crystal structure represents a "frozen snapshot" of the structure and thus does not answer the question, if the molecule adopts the same structure in solution. This problem is solved by NMR spectroscopy.[19] In this section, the basics of NMR to determine a high resolution structure of RNA molecules will be briefly discussed.

Three types of informations can be gained from NMR: (i) distances between protons by the nuclear Overhauser effects (NOE), (ii) scalar couplings and (iii) chemical shifts. The NOE is the main effect used to elucidate a three-dimensional structure. The NOE phenomenon describes the transfer of magnetization due to magnetic dipole-dipole coupling between nuclei. NOEs can only be observed when two protons are close in space (up to 5-6 Å), independent of the nature of the proton, i.e. if it is an exchangeable or a non-exchangeable proton. 2D and 3D NOE spectroscopy (NOESY) experiments measure the transferred magnetization as a function of time, which is called the mixing time.[116] By measuring the NOE intensity, approximate distances of protons can be derived. The NOE intensity is dependent on the interatomic distance by r^{-6}.[19] The most valuable distance information is obtained by 2D [^{1}H,^{1}H]-NOESY spectra in D_2O. These spectra include the so-called "sequential walk" region, in which one can sequentially assign the NOEs: Not only intraresidual nucleobase-protons (H6/H8) and sugar H1' protons are close in space, but also interresidual H6/H8 and the upstream H1' (Figure 13) (see also Results and Discussion). By walking through the sequence, it is possible to assign the spectra to subsequentially extract the distance information. After the integration of NOEs, they are classified into three different ranges as strong,

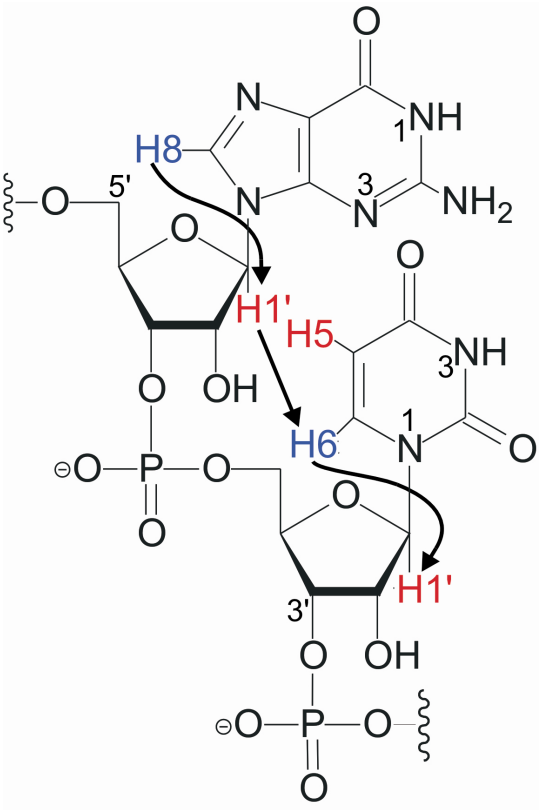

Figure 13 The "sequential walk". Through-space connectivities of nucleobase and sugar protons are indicated by black arrows. The protons, which are of great importance for structure determination by NMR, are highlighted in blue (H8/H6) and red (H1'/H5). The imino protons H1 of G and H3 of U are indicated by numbers.

medium and weak (for details see Materials and Methods) and will then be included in the structure calculation.

In addition to the sequential walk region, NOESY spectra include information about base-stacking and also about sugar-sugar interactions. Therefore, these spectra are the major source for structural restraints containing the non-exchangeable protons. In general, about 21 intranucleotide distances can be found in a nucleotide. In addition to that, up to 11 internucleotide distances can be measured. Of course, the number of distances found highly depends on the sequence and structure of the RNA. Differentiation between pyrimidines and purines can easily be achieved by through-bond correlation experiments (such as TOCSY), which give strong resonances for H5-H6 of the pyrimidines. Recording of [^{1}H,^{13}C]-HSQCs of ^{13}C-labeled samples give information about the nature of the pyrimidine, i.e. if it is a cytosine or an uracil, because C5 in C and U resonates in different spectral regions. C5 of C resonates between 95 and 100 ppm, whereas signals of uracil's C5 appear between 100 and 105 ppm. In addition, ^{13}C-labeled samples help to identify the H2 of adenine as C2 resonates in a separated spectral region between 150 and 157 ppm.

Base-pairing information can be obtained from NOEs between imino resonances assigned to specific nucleotides. Since imino protons resonate between 10 and 15 ppm, they are well separated from other proton resonances. Guanines and uracils have one imino proton each (Figure 13). Only imino-protons, which are included in a base-pair are observable in NMR spectra due to the decreased exchange rate of free imino-protons with the bulk solvent.[117] If the imino-proton is not included in a base-pair the exchange with the solvent is in the range of milliseconds or even faster. Base-pairs at the end of helical stems often have broadened imino proton resonances because they can exchange rapidly with the water.[116] Imino protons of Watson-Crick base-pairs are found between 12 and 15 ppm, whereas non-canonical base-pairs, such as the G-U wobble pair, are shifted upfield to about 10 ppm. In addition, G-U wobbles can be easily distinguished from Watson-Crick base-pairs because of the strong NOE contact between the guanine and uracil imino protons. Additionally, base-pairs can be assigned and confirmed by J_{NN} HNN-COSY experiments.[118] These experiments give direct evidence for Watson-Crick base-pairs. G-U wobble pairs cannot be detected by these experiments since no hydrogen bond from an imino-NH to another N across the helix exists in such a conformation.

The determination of the conformation of the sugar pucker and the glycosidic bond was already described in Section 1.1.2.

The calculation of RNA structures depends on the collection of distance and dihedral restraints. Different programs make use of a molecular dynamics simulated annealing protocol.[119,120] Starting from an extended strand, the program CNS uses the simulated annealing protocol to obtain a first structure. During a molecular dynamics simulation, the positions of the atoms are slightly shifted in order to minimize their overall energy. Contributions to this energy can derive from bonding, torsional movement, repulsion, van-der-Waals attraction, and electrostatics.[116] In a first step of simulated annealing, the RNA is heated to high temperatures to obtain a single unstructured strand. At this high temperature, experimental restraints are gradually applied as quadratic, square-well energy functions. An output including energies and violation is obtained after the protocol is completed. The energy is dependent on the number of violations of distance and dihedral restraints, thus giving a positive energy if a restraint is not satisfied and a zero energy contribution at satisfaction. An energy minimization step is performed in the final structure. XPLOR uses the simulated annealing protocol as well, but an input structure from CNS or another program is required. In this study, CNS and XPLOR are the programs of choice for the final structure calculation.

After the final structure is obtained, it is of great importance to judge the quality of the NMR structure. One criteria for this evaluation is the number of restraints used in the calculation. This reflects how well the structure is defined. In addition, statistics of final restraint violations as well as the superposition of the final structures give information about the quality of a structure. The obtained root mean square deviation (r.m.s.d.) for all heavy atoms of an ensemble of 20 structures lies usually between 1 – 3 Å.[34,115] Compared to protein structures these r.m.s.d. values are quite large. However, RNA structures are not as compact as protein structures and thus are much more flexible justifying the higher r.m.s.d. values.

The here described methods for RNA structure determination are supposed to give a brief overview over the basics of NMR. In Section 2 these and further applications like the implementation of residual dipolar couplings (RDCs) and X-filtered experiments will be discussed. For further details and other methods please refer to references (19,121-123).

1.3 Ribozymes - autocatalytic RNAs

Many folded RNA molecules are "ribozymes", i.e. catalytically active enzymes that are completely composed of RNA. Natural ribozymes either catalyze the cleavage and/or joining of RNA and DNA molecules through reaction at phosphate centers,[65,124] or catalyze peptidyl transfer during protein synthesis.[50] But ribozymes can also be designed to perform particular catalytic functions.[125,126] The number of structurally different naturally occurring types of ribozymes has grown from seven, which were identified until 2003[127], to 10, which are known today.[128] According to their differences in size, ribozymes are divided into two classes, i.e. the small and the large ribozymes. But ribozmyes can also be classified due to their main function: cleaving ribozymes and splicing ribozymes. In general, the small ribozymes are cleaving, whereas the large ribozymes are splicing ribozymes with the exception of RNase P, which belongs to the group of large and cleaving ribozymes.[127,128]

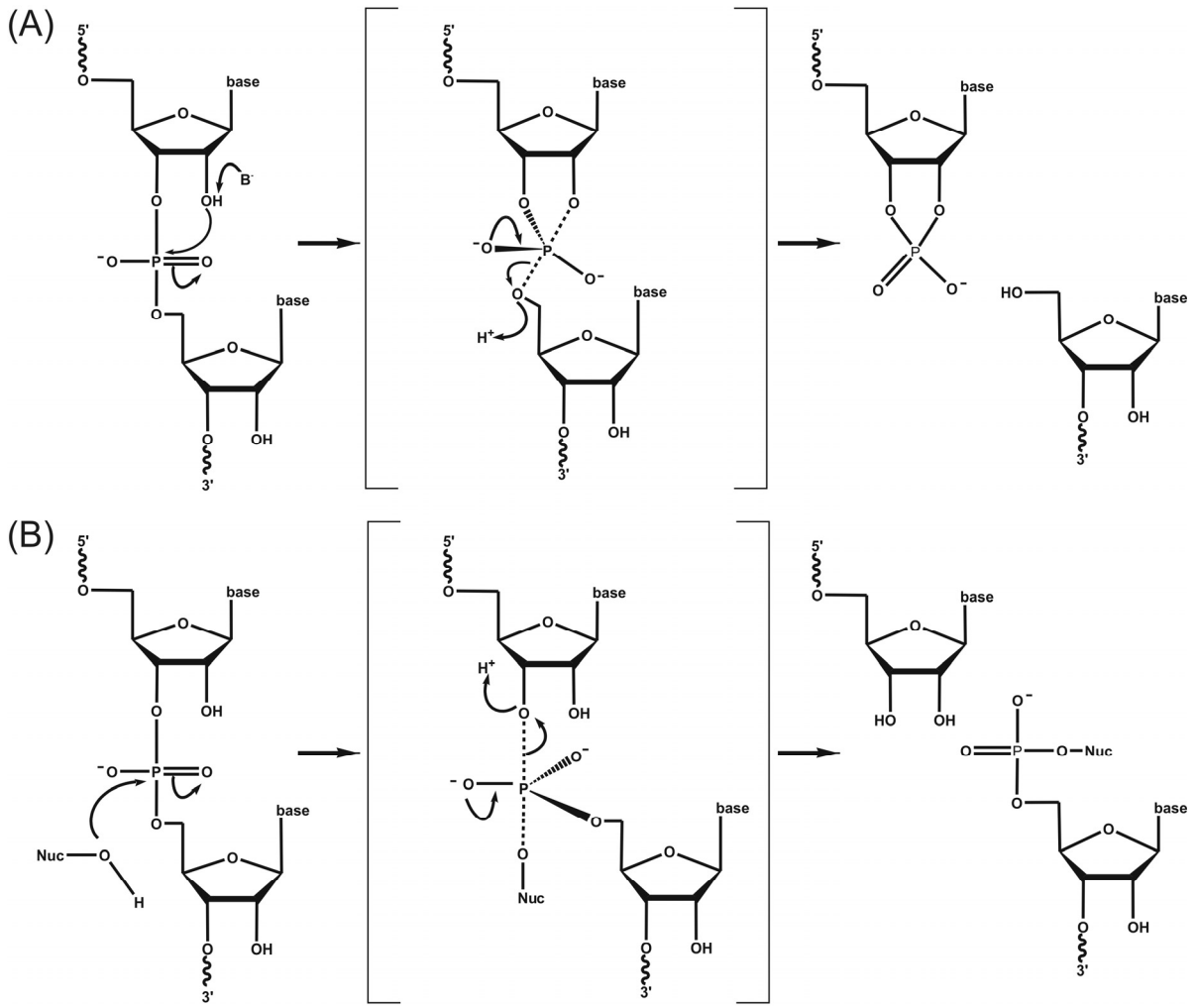

Figure 14 Cleavage mechanism of small and large ribozymes. (A) The small ribozymes use an internal 2'-OH group to carry out the nucleophilic attack on the adjacent scissile phosphate. The reaction proceeds via a penta-coordinated transition state to give products with a 2',3'-cyclic phosphate and with a 5'-OH terminus. (B) Large ribozymes make use of an external 2'-OH in the first splicing step to give products with a 5'-phosphate and a 3'-OH terminus. Both reactions proceed via a S_N2 mechanism.

The small ribozymes perform a transesterification reaction by an in-line S_N2 mechanism (Figure 14A). The phosphate is attacked by the internal 2'-OH group of the ribose next to the phosphodiester bond leading to an inversion of configuration around the phosphor atom. The reaction yields products with a 2',3'-cyclic phosphate and a 5'-hydroxyl terminus. A two-metal ion mechanism has been proposed for the class of small ribozymes.[129] The theory is based on a metal ion binding region in the ribozyme that contains binding sites for two metal ions, which are 4 Å apart. In the transition state, one metal coordinates to the leaving group oxygen, whereas the other coordinates to the nucleophile, thus stabilizing the trigonal bipyramidal intermediate.

In contrast to the small ribozymes, the large ribozymes use an external 2'-OH group as a nucleophile in the first step of splicing generating products with a 5'-phosphate and a 3'-hydroxyl. The catalysis of the large ribozymes proceeds also in an in-line S_N2 type manner. Metal ions play an important role in structure and function of ribozymes and will be discussed in the subsequent sections directly on the example of the specific ribozymes.

1.3.1 Small ribozymes

1.3.1.1 An overview

The hammerhead ribozyme,[130] hairpin ribozyme,[131] human *Hepatitis delta virus* (HDV)[132] and the *Neurospora* Varkud satellite (VS) ribozyme[133] belong to the class of small ribozymes due to the relatively small size of less than 200 nucleotides.[127,134,135] They are mainly found in satellite RNAs of plant origin. Each of them folds into a well-defined tertiary structure and undergoes self-cleavage in the presence of divalent metal ions. Three of the small ribozymes, i.e. the hammerhead, hairpin and VS ribozyme, were identified not to require divalent metal ions for efficient self-cleavage if very high monovalent ions are present.[74] For the hammerhead ribozyme, cleavage in 4 M LiCl is ~30-fold slower than under standard conditions of 10 mM $MgCl_2$. It is obvious that very high concentrations of monovalent cations have to be present in order to obtain sufficient self-cleavage. The same holds true for the hairpin and the VS ribozyme. Both ribozymes show significant catalytic activity in the absence of divalent metal ions.[74-76] It is suggested that under appropriate conditions of high ionic strength, at which the ribozymes fold correctly, there is no strict requirement for any metal ions for a successful cleavage reaction. Rather, the presence of a positive charge at high density seems to be crucial to neutralize phosphate repulsion and faciliate folding into an active conformation.

Recently, a couple of new small ribozymes have been discovered. In 2004, the *glmS* ribozyme has been identified.[124] It occurs in certain Gram-positive bacteria, where it resides within mRNAs encoding glutamine-fructose-6-phosphate amidotransferase. The *glmS* ribozyme functions as a riboswitch, i.e. undergoes structural changes upon binding a metabolite, and as a ribozyme, i.e. cleaves the mRNA encoding the protein that controls the metabolism of the same metabolite. Like other ribozymes, the *glmS* ribozyme folds into a complex structure to be able to undergo catalytic reactions.[136] It has been shown that divalent metal ions do not participate directly in the catalysis of the *glmS* ribozyme.[137]

Two other new ribozymes were found within eukaryotic pre-mRNAs: (i) the CPEB3 ribozyme, which is structurally and biochemically related to the HDV ribozyme[138] and (ii) the co-transcriptional cleavage CoTC ribozyme that was found in the 3'-flanking region of primate β-globin genes and promotes transcription termination.[139]

Although all small ribozymes catalyze the same chemical reaction (see Figure 14A), they are very diverse in structure and mechanism. Some structural and metal ion binding properties of the hammerhead ribozyme, hairpin ribozyme, HDV ribozyme, and VS ribozyme will be discussed in the next sections.

1.3.1.2 The hammerhead ribozyme

The hammerhead ribozyme was first discovered in viroids and satellite RNAs of plant viruses.[130,140] Hammerhead ribozymes have been found to recognize their substrate immediately upstream of the cleavage site (↓) following the "NUX↓" rule: N must be paired, U is conserved and X can be any nucleotide but G (Figure 15).[141] The hammerhead ribozyme can be truncated to a minimal, but still catalytically active motif that consists of three helical stems flanking a core of 15 mostly invariant residues.[141-143] Most of the biochemical and structural studies have employed such a minimal construct.[144-147]

The first hammerhead structure solved was a RNA-DNA ribozyme inhibitor complex at 2.6 Å resolution.[62] A second structure was solved, in which the cleavage-site nucleophile was replaced with an inert 2'-O-methyl ether linkage in an all-RNA construct.[148] Both structures were based on the minimal construct. In 2006, the full-length hammerhead ribozyme from *Schistosoma mansoni* was solved at 2.2 Å resolution.[149] It contains a hairpin loop at the end of stem II and a bulged loop in the extended stem I in addition to the minimal core sequence (Figure 15). The crystal structure of the full-length ribozyme (Figure 15) allowed Martick *et al.* to explain some contradicting hypotheses, which resulted from biochemical and structural analyses. At the scissile phosphate, an inversion of configuration

was observed. This proved an in-line attack mechanism, in which the 2' oxygen of C-17, which is the nucleotide at the cleavage site, is the nucleophile.[150,151] However, C-17 was not in a position for an in-line attack in the minimal crystal structures of the hammerhead.[62,148] The full-length hammerhead ribozyme structure now showed that the attacking nucleophile is in a position for an in-line attack, thus demonstrating that the additional nucleotides (see above) lead to structural rearrangements of the catalytic core.[149] In addition, another puzzle was solved by the full-length crystal structure of the hammerhead ribozyme: A9 and the scissile phosphate appear to create a binding site for a metal ion,[152] but in the initial crystal structures these phosphates are 20 Å apart, i.e. too far apart to bind one metal ion. In the full-length ribozyme these nonbridging oxygens have a distance of about 4 Å, thus providing a metal ion binding platform without further rearrangements.[149,153]

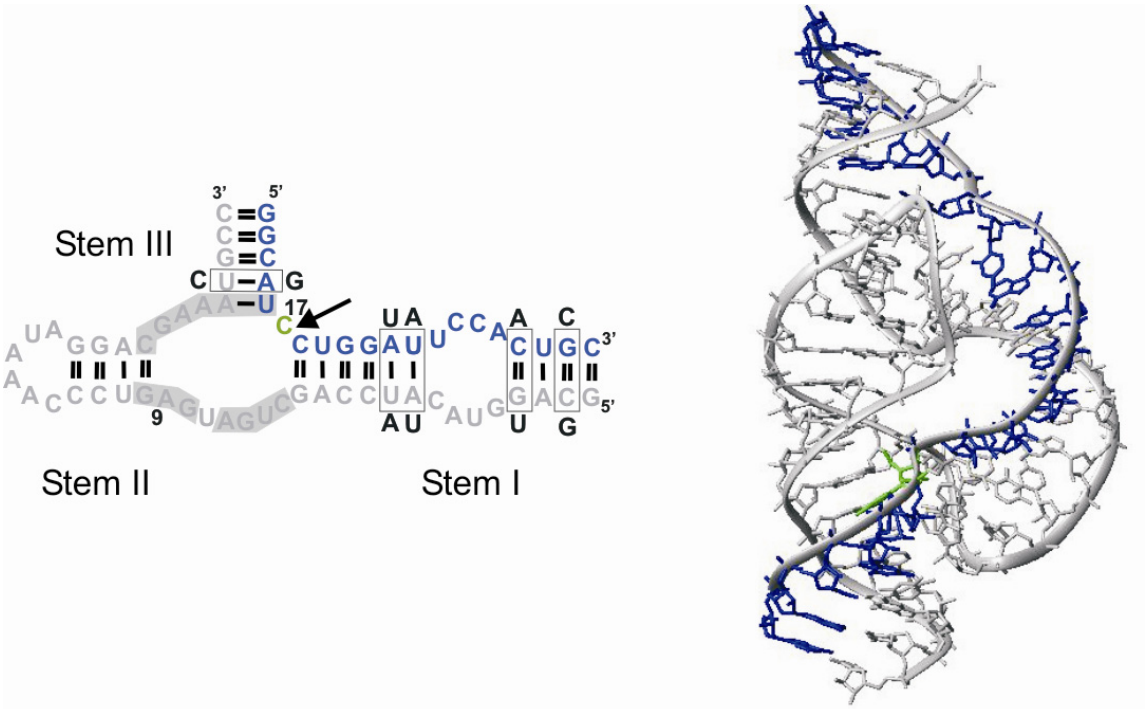

Figure 15 Secondary structure together with the crystal structure of the extended hammerhead ribozyme (PDB entry 2GOZ).[149] The upper substrate strand is coloured in blue, the lower enzyme strand in grey and the active cytosine in green. A9, which is involved in metal ion coordination together with the scissile phosphate, is indicated as well as C17. The conserved nucleotides are shown in a grey background. To aid crystallization, some nucleotides were changed from the wildtype-sequence (boxes), the base substitutions are indicated adjacent to the boxes. The arrow indicates the scissile bond. The figure was prepared with MOLMOL.[29]

1.3.1.3 The hairpin ribozyme

The hairpin ribozyme comprises a functional length of 50 nucleotides and is therefore the second smallest catalytic RNA molecule.[134] It was found on the negative-polarity strand of the tobacco ringspot satellite virus RNA, the same RNA genome that harbors a hammerhead ribozyme in the positive strand.[157,158] The hairpin ribozyme constists of two internal loops (loop A and B), which comprise the catalytically essential nucleotides. Loop A contains thereby the bound RNA substrate, whereas loop B is essential for catalysis.[155] In its natural form, these loop regions are connected by a four-way junction. In the hairpin ribozyme, the cleavage site is surrounded by a set of conserved nucleotides, i.e. N↓GUC (↓ denotes the cleavage site).[159,160] The solution structures of the individual loops have been solved.[154,155] It has been shown that the two domains are catalytivally active when they are not covalently bound.[161] A model of the individual domains was build based on the solution structures and is shown in Figure 16B.[155] In the solution structure of loop B, a wide range of stacked non-Watson-Crick base-pairs were found leading to an irregular helix. This leads to an exposure of functional groups in the minor groove. These functional groups would be non-accessible in a normal helix.[155]

The docking of the two domains is mediated by the binding of metal ions, but the ionic requirements are in a nonspecific fashion. Therefore, it is assumed that metal ions play a role in folding of the ribozyme and are probably only required for structural arrangements. It is proposed that functional groups of the RNA participate directly in catalysis.[134,135] NMR studies have shown that cations prefer to bind to the B domain.[162] Tb(III) hydrolysis and

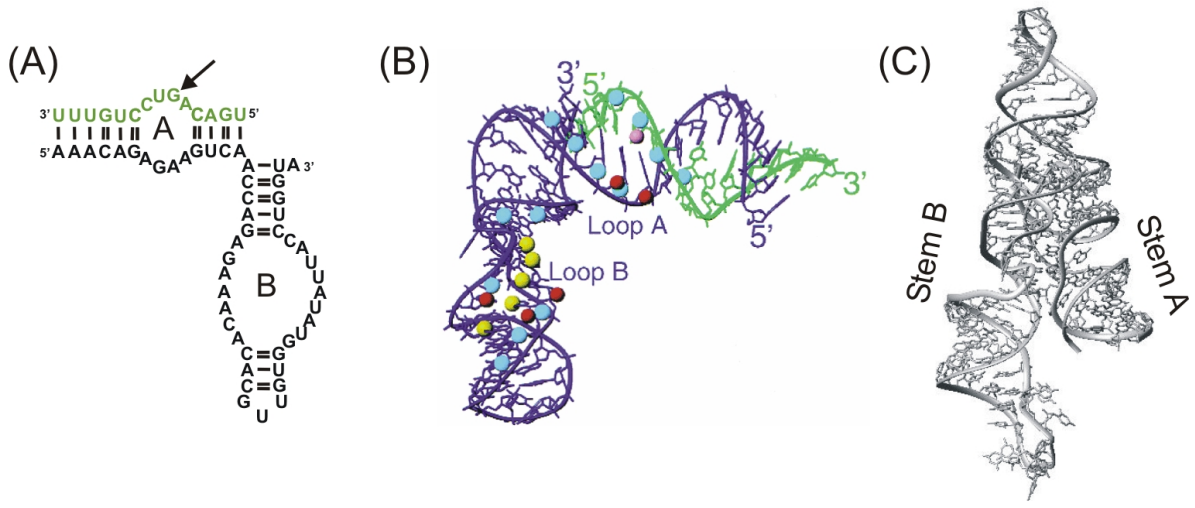

Figure 16 The hairpin ribozyme. (A) Secondary structure of the hairpin ribozyme with its substrate (green). The arrow indicates the scissile bond. (B) Model of the hairpin ribozyme based on the solution structures of the individual domains.[154,155] Figure is taken from reference (155). The cleavage site 2'-OH is indicated with a pink sphere. Atoms implicated in domain docking are shown as red, yellow and cyan spheres. (C) Crystal structure as solved by Rupert *et al.* in 2001 (PDB entry 1M5K).[156] Figure was prepared with MOLMOL.[29]

luminescence studies corroborate the presence of metal ion binding sites in loop B, but were found to be at slightly different locations than in the NMR structure.[163]

In 2001, Rupert *et al.* solved the first crystal structure of a full hairpin ribozyme at 2.4 Å resolution (Figure 16C).[156] The central portions of stem A and B dock via interactions between their minor grooves to form the active site of the ribozyme. No metal ion was found in the active site. In stem B, non-canonical base-pairs were identified that stack in an irregular helix as was already depicted in the NMR structure of loop B. The narrow major groove of stem B is stabilized by several divalent metal ions.

1.3.1.4 The Hepatitis delta virus ribozyme

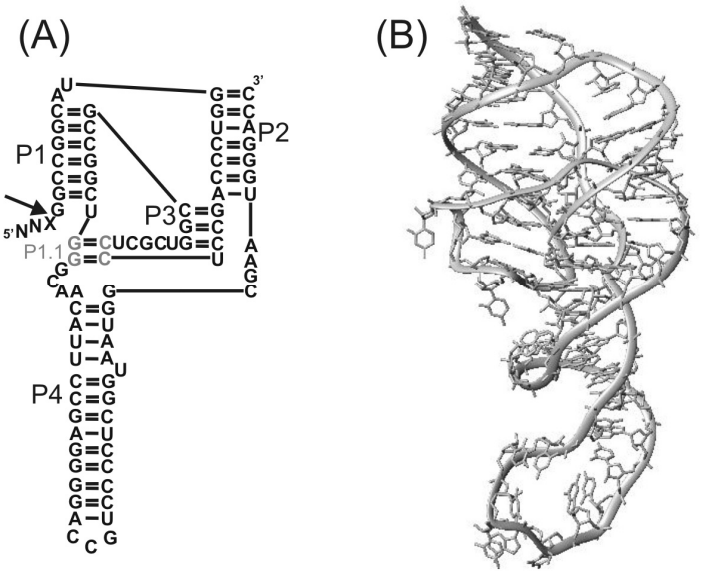

Figure 17 The HDV ribozyme. (A) Secondary pseudoknot structure of a genomic HDV ribozyme.[164] The arrow indicates the scissile bond and X is the nucleotide preceding the cleavage site, which can be any base. The fifth base-paired region P1.1 as identified by the crystal structure is shown in grey. (B) Crystal structure of the 72-nucleotide, self-cleaved form of the genomic HDV ribozyme (PDB entry 1CX0).[165] Figure was prepared with MOLMOL.[29]

The human *Hepatitis delta virus* (HDV) is a RNA satellite virus of hepatitis B.[134,165] It was discovered in both the genomic and antigenomic viral RNA strand. The minimal active HDV ribozyme comprises about 85 nucleotides, which adopts a secondary structure with four paired regions P1 to P4 (Figure 17A).[166,167] Remarkable, this atypical pseudoknotted ribozyme achieves sufficient cleavage also when only a single nucleotide 5' of the cleavage site is present. Thereby, the identity of this nucleotide (in Figure 17 denoted as X) plays a minor role. A G-U wobble plays an important role for cleavage site specification.[168] As for the hairpin ribozyme, the HDV ribozyme shows a nonspecific requirement for divalent metal ions. It has been shown that cleavage occurs even at low concentrations of Ca^{2+}, Mg^{2+}, Mn^{2+} or Sr^{2+}.[169]

The crystal structure of a 72-nucleotide, self-cleaved form of the genomic HDV ribozyme has been solved at a resolution of 2.3 Å (Figure 17B).[165] The crystal structure reveals a fifth base-paired region (P1.1) in addition to the four biochemically identified ones. Two coaxial stacks were found, one between P1, P1.1 and P4, the other one between P2 and P3. In the

crystal structure of the HDV ribozyme no tightly bound metal ion is found, suggesting that the stabilization is only generated by base-pairing, stacking, non-canonical base-backbone and backbone-backbone interactions. The HDV ribozyme folds into a complex three-dimensional structure that buries the active site deep within a catalytic cleft.[165] Although no atomic-resolution structure exists for the antigenomic version of the HDV ribozyme, it has been suggested that its fold is similar to the one of the genomic HDV ribozyme.[170,171]

1.3.1.5 The *Neurospora* VS ribozyme

The *Neurospora* varkud satellite (VS) ribozyme was found in the mitochondria of the Varkud-1c natural isolate of *Neurospora*.[134,174] The VS ribozyme is the largest of the small ribozymes and comprises a complex secondary structure (Figure 18A). Little is known about its three-dimensional structure so far. The solution structure of a analogous substrate hairpin was solved in 2000 (Figure 18B).[174] The structure of the cleavage site domain revealed two tandem G·A base-pairs and a protonated A^{+}·C wobble pair. It has been shown on the example of the VS ribozyme that not all RNAs undergo a hierarchical folding pathway, i.e. secondary structure formation precedes tertiary structure. Anderson *et al.* found that Mg^{2+}-dependent tertiary formation disrupts a stable RNA secondary structure element during catalysis.[175]

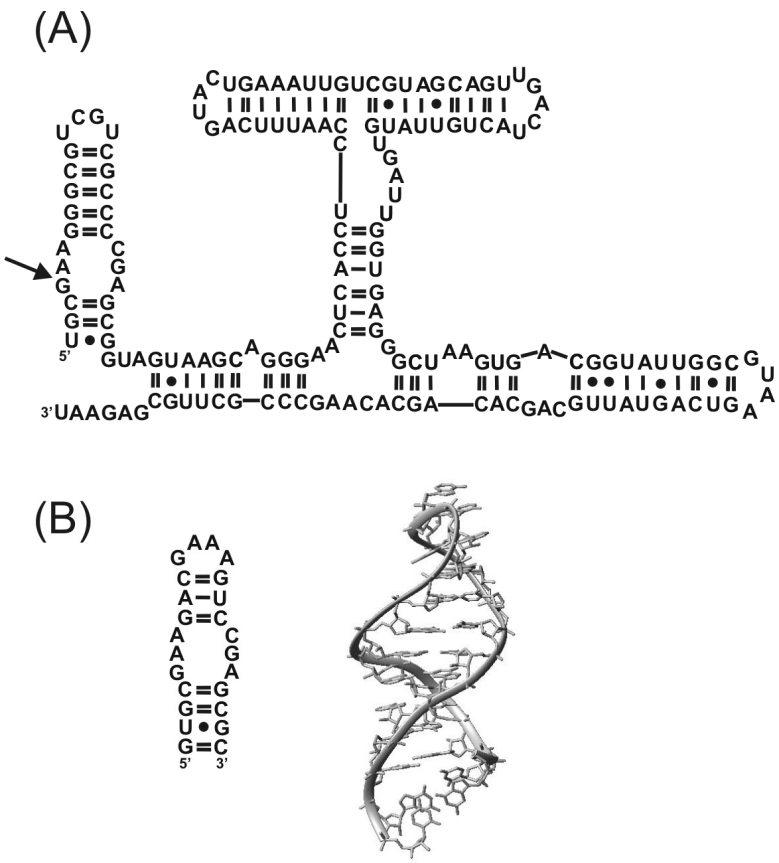

Figure 18 The *Neurospora* VS ribozyme. (A) Secondary structure of the VS ribozyme.[172,173] The arrow indicates the scissile bond. (B) Secondary structure of VSm1, the VS substrate analog used in the NMR study together with the solution structure (PDB entry 1E4P).[174] Figure was prepared with MOLMOL.[29]

1.3.2 Large ribozymes

1.3.2.1 RNase P and Group I introns

As already mentioned in Section 1.1.3, there is strong evidence that the ribosome is also a ribozyme.[49,50] In addition, the spliceosome, composed of five different snRNA molecules and numerous proteins is also assumed to be a ribozyme. This large ribonucleoprotein complex occurs in higher eukaryotes and performs splicing of newly transcribed RNAs.[176,177]

In addition to the ribosome and the spliceosome, ribonuclease P (RNase P) with a length of 140 to 500 nucleotides and group I introns with a length of 200 to 1500 nucleotides belong to the group of the large ribozymes.

RNase P, found in prokaryotes as well as eukaryotes, is a site-specific endoribonuclease that processes precursor RNA substrates, i.e. the 5'-end of tRNAs or 5S rRNA.[180,181] In fact, RNAse P is a RNA-protein complex, but the activity solely stems from the RNA component. Phylogenetic covariation analysis revealed information about the secondary as well as tertiary structure.[182] Despite differences in sequence, length and secondary structure, RNase P RNAs contain five conserved regions that constitute the structural core.[183] In 2005, the crystal structure of a bacterial ribonuclease P RNA was solved at 3.3 Å resolution (Figure 19A).[178] The 417 nucleotide long RNA forms six coaxially stacked helical subdomains that are stabilized by long-range tertiary contacts. Since RNase P is a metalloenzyme, special interest lies in the detection of metal ion binding sites.

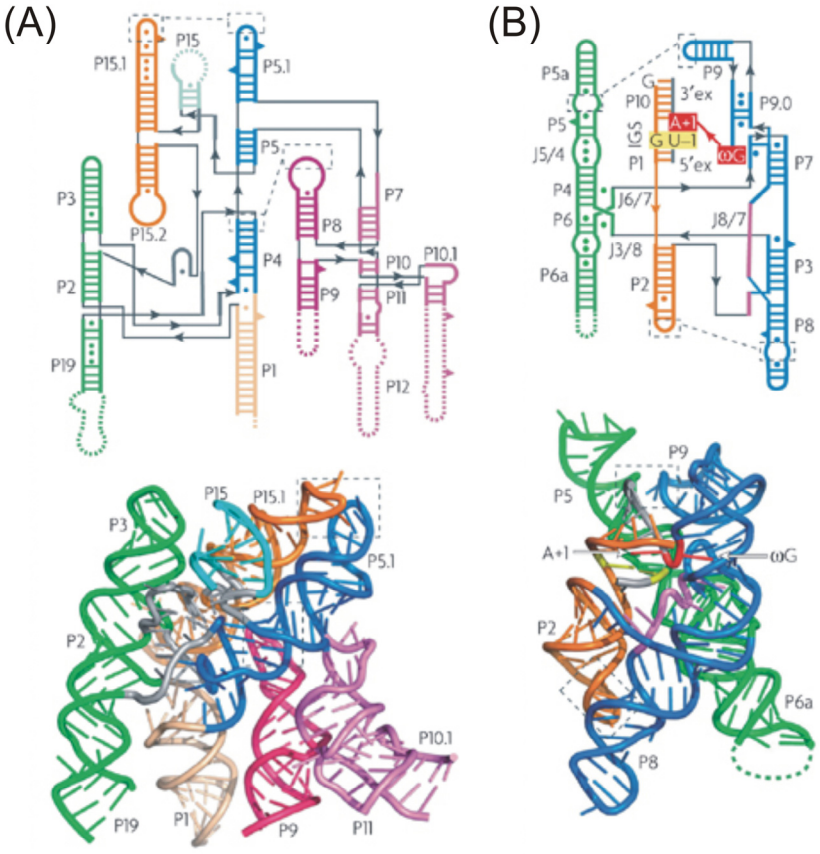

Figure 19 Two examples of large ribozymes: RNase P and group I introns. (A) Secondary structure of RNase P together with the crystal structure as solved by Kazantsev *et al.*[178] (B) Secondary structure of a group I intron together with the crystal structure in the state that precedes the second step of splicing as solved by Stahley *et al.*[179] Subdomains are coloured for clarity. Figure is taken from reference (128).

Metal ions play a threefold role in RNase P: (i) they are involved in the correct folding of the ribozyme,[184] (ii) they participate in substrate binding[185] and (iii) they are directly involved in hydrolysis of the substrate phosphodiester bond.[184,186,187] In the crystal structure, the majority of metal ions was found in major grooves of double stranded helices that are often distorted from typical A-form helices due to helical junctions and non-canonical base-pairs. In addition, metal ion binding sites were identified in the highly conserved helix P4, which makes up part of the active site.[178]

Group I introns are mainly found in protists, bacteria and bacteriophages,[188] but are also detected in the mitochondria of some animals.[128] They are classified based on their secondary structure, which consists of an arrangement of ten base-paired elements (P1-P10) capped by loops and connected by junctions (Figure 19B).[189] Another important feature of group I introns is their splicing mechanism. Group I introns perform splicing through a two-step transesterification mechanism using an exogenous guanosine as a nucleophile to cleave the 5'-splice site. This site is located within the base-paired region P1, which comprises the last few nucleotides of the 5'-exon base-paired to an internal guide sequence (IGS) within the intron.[189,190] A conserved G-U wobble pair in this region contributes to the recognition of the 5'-splice site.[191] Helix P10 is formed after the first step of splicing and includes base-pairs between the intron and the 3'-exon.

Different groups were interested in solving the crystal structure of group I introns to gain an understanding of the cleavage and ligation mechanisms. As already mentioned in Section 1.1.3, the crystal structure of the P4-P6 domain gave first insights into the architecture at the atomic level of group I introns (Figure 8B).[21] It took about eight years until three groups solved the crystal structures of three different group I introns within 6 months independently of each other. The first intron stems from the purple bacterium *Azoarcus* sp. BH72,[58,192] the second from the ciliate *Tetrahymena thermophila*[193] and the third from *Staphylococcus aureus bacteriophage* Twort.[194] The constructs were designed to represent different states along the splicing pathway (reviewed in [191]). The three crystal structures reveal a defined set of structural domains assembling into a conserved core, which organizes the catalytic site.

As in other ribozymes metal ions are also involved in folding and function of group I intron ribozymes. A two-metal ion mechanism was proposed for the splicing reaction based on computational studies[195], comparisons with protein enzyme active sites[196], biochemical and modelling studies.[105,129,197] However, a three-metal ion mechanism was proposed for the *Tetrahymena* group I intron.[198] These inconsistent findings let scientists to perform further investigations on the metal ion properties on the atomic level. In 2005, a second crystal

structure of *Azoarcus* sp. BH72 was solved.[179] This structure contains the complete intron, both exons, the scissile phosphate, and all functional groups, which are predicted to be involved in metal ion coordination. This structure revealed that the functional groups in the active site are fully satisfied with two metal ions.[179] The two Mg^{2+} ions were found to be 3.9 Å apart from each other and are directly coordinated to the hydroxyl and phosphate oxygen groups of the catalytically relevant ligands. Strobel and co-workers were not yet satisfied with these results and further continued to crystallize group I introns in different stages. Just as recently as this year, they solved the crystal structure of the intron together with spliced exons and two additional structures that examine the role of metal ions in the active site during the second step of splicing.[199] Two Mg^{2+} ions were observed in all three structures. The scissile phosphate is directly coordinated to metal ions before exon ligation, yet after exon ligation, the direct metal ion coordination is lost. Based on these crystal structures and additional biochemical data, they propose a revised model for substrate binding and docking, which gives further insights into the splicing mechanism of group I intron ribozymes.

1.4 Group II introns

Like group I introns, group II introns belong to the family of large phosphoryl transfer ribozymes.[65] These introns are large molecular machines consisting of 600 – 2500 nucleotides and are therefore second in size only to ribosomal RNA. Group II introns are found primarily in organellar genes of plants, fungi, and yeast, but also in many bacteria.[200-203] Recently, a group II intron was found in an animal mitochondrial genome.[204] The class of group II intron was first identified in 1982.[205] Group II introns have been divided into two main families IIA and IIB based on conserved features of their RNA secondary structures. Each class is further divided into two subdivisions A1, A2, B1 and B2, thereby A2 introns are found very rarely.[200,206] More recently, the third main class IIC has been recognized. These introns are typically located downstream of transcriptional terminator motifs or other inverted repeats in bacterial genomes.[206,207] In general, group IIC introns are smaller in size (420-480 nucleotides) compared to the well-studied group IIA and IIB introns. The EBS1-IBS1 interaction of group IIC introns consists of 3-4 base-pairs and therefore is smaller than the one of group IIA and IIB introns, which comprises 6-7 base-pairs. Further differences arise from the facts that IIC introns lack an EBS2 motif and that they self-splice *in vitro* through a hydrolytic pathway,[208] forming a linear intron instead of a lariat.[207,209]

Group II introns have been found to act as mobile genetic elements, i.e. they are able to reversibly insert themselves into RNA as well as DNA (see also Section 1.4).[210,211] To keep

track of the increasing number of mobile group II introns, the group of Steven Zimmerly initiated a database for information about group II introns, in particular from bacterial origin. The database can be accessed via http://www.fp.ucalgary.ca/group2introns/.[212]

Among the best studied *in vitro* active group II introns regarding folding, catalytic activity and tertiary structure is *Sc*.ai5γ (Figure 20). *Sc*.ai5γ is located in the cytochrome oxidase 1 gene of mitochondria in *Saccharomyces cerevisiae*.[127,213] Further details about this particular group II introns, which also plays a major role in this thesis will be dicussed in the next section.

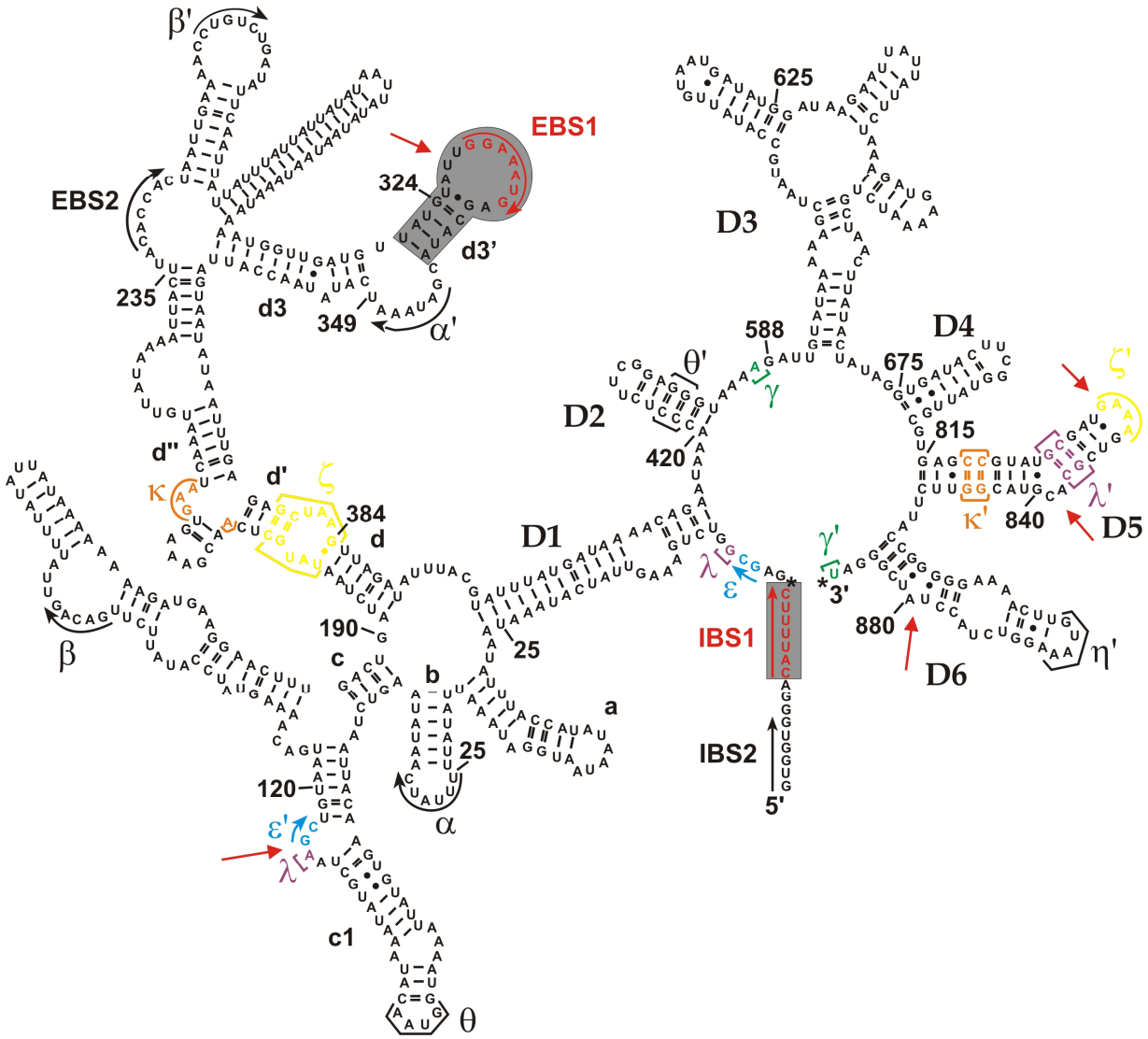

Figure 20 Secondary structure map of the group II intron *Sc*.ai5γ from yeast mitochondrial *cox1* gene with exonic IBS1 and IBS2. The 5'- and 3'-splice sites are marked with an asterisk. Shaded regions of D1d3' and IBS1 are the primary focus of this thesis. Nucleotides involved in tertiary contacts (coloured, Greek letters) and metal ion binding sites (red arrows) within these regions, as determined by Tb^{3+} induced cleavage,[97] are marked.

1.4.1 Group II introns and their individual domains

Biochemical and mutational analysis together with modelling studies have shown that group II introns consist of a conserved set of six domains that contain well-defined secondary structural elements (Figure 20).[70,127,203,214-217] One interesting property of group II introns is that their domains are independent folding units, i.e. individually separated domains will reassemble to the active three-dimensional structure when they are added together in *trans*.[218-221] Each domain is designated to a specific function: Domain 1 (D1) as the largest of the six domains is further divided into four subdomains a, b, c, and d.[127] D1 is an independent folding domain and serves as a molecular scaffold for docking of the other domains.[213,218,222] Folding of D1 is rate-limiting for the folding of the entire ribozyme, and it requires similar amounts of Mg^{2+} for folding as the full-length ribozyme.[223] In addition, this domain recognizes the 5'-exon through base-pairing interactions of two different regions within the subdomain d (exon-binding sites 1 and 2, EBS1 and EBS2) with their cognate partners, which are located in the last 10-15 nucleotides at the 3'-end of the 5'-exon. The EBS-IBS motif is not conserved in sequence but always co-varies.[200,224,225] EBS1 and EBS2 are located in the center of D1 (Figure 20) and are separated by several stem-loop structures. Mutational studies of EBS1/IBS1 in a ribozyme derived from the *Sc*.ai5γ intron revealed that the ribozyme shows high fidelity and high interaction specificity for cleavage site selection.[226] It has been shown that EBS1 forms the most stable duplex with a given substrate. After formation of the duplex the ribozyme recognizes the structural transition between single and double-stranded regions, thus explaining the fact that there is no need for phylogenetic conservation of the EBS1-IBS1 interaction. In addition, it has been shown that the identity of the divalent metal ion affects the cleavage site selection, suggesting that Mg^{2+} plays an important role in forming the proper cleavage site and creates a structural marker for recognition of the cleavage site.[226] Tb^{3+} cleavage experiments detected a strong metal ion binding site just 5' of EBS1.[97] While there is no absolute requirement for conserved nucleotides within the EBS1/IBS1 and EBS2/IBS2 recognition helices, two conserved intronic nucleotides contribute to the 5'-splice site selection, made up by the ε-ε' interaction (Figure 20), which is an essential component of the active site of the intron.[227] D1, as well as domain 5 (D5), are the only domains of group II introns that are essential for catalysis.[228,229] Domain 2 (D2) is not phylogenetically conserved in sequence and deletion of this domain shows little effect on the efficiency of *cis* splicing.[230] However, D2 contains structural elements that form tertiary interactions to D1 and D6 in some introns.[229,231]

Domain 3 (D3) is a catalytic effector that increases the rate of catalysis.[232,233] A linker region between D2 and D3, called J2/3, is highly conserved and plays an important role in splicing.[215,234] Domain 4 (D4) has no effect on splicing but it often contains an open reading frame (ORF) from which a multifunctional protein involved in splicing and mobility is translated.[201,235]

Domain 5 (D5) is the most phylogenetically conserved region of the intron and represents the most critical acive-site component. D5 binds to the central region of D1 through the ζ-ζ'[236] and the κ-κ'[219] tertiary interaction. D5 also binds the 5'-splice site through two tertiary interactions, λ-λ' and ε-ε'.[70,219,227,237,238] D5 comprises a hairpin structure with two helical regions that are separated by a two-nucleotide bulge. The hairpin is closed by a GNRA tetraloop (Figure 21B). The so-called catalytic triad is the most conserved sequence within D5. The triad usually comprises a AGC sequence, but often also CGC is found.[239] The G-U wobble pair at the base of D5 seems to be necessary for the splicing activity of the intron.[239] Mutational studies of the two-nucleotide bulge in D5 revealed that these nucleotides are also crucial for catalysis, although the nature of the nucleotides seems to play a minor role.[240] The solution structure of D5 of *Sc*.ai5γ was the first individual domain of a group II intron ribozyme, which was solved by NMR (Figure 21).[34] The bulge region in solution considerably differs from the previously proposed ones[200,238,241] as well as from the crystal structure of a construct comprising D5 as well as D6 (Figure 21A).[242] G840 adopts a *syn* conformation and is flipped down into the major groove of helix one. Hence, G840 comes to lay close to the catalytic AGC triad suggesting a potential role in catalysis. The hydrophobic surface of the adjacent A-U base-pair is exposed to the solvent due to a kink in the backbone near G840. The kink causes the bases of the bulge to be stacked on top of each other. In the D56 crystal structure, the bulge nucleotide A838 is not stacked as depicted in the solution structure but points out into the solvent (Figure 21A and B). NMR metal titration experiments with Mg^{2+} revealed a strong metal ion binding site in the minor groove of the D5 bulge. Further chemical shift changes are observed at C843 and in the tetraloop, yet these shifts upon Mg^{2+} binding are smaller than what is found in the bulge. An additional metal ion binding site was found at the minor groove site of the catalytic triad by paramagnetic line broadening studies with Mn^{2+}. This metal ion binding site at the AGC triad was already proposed by functional group mutagenesis experiments.[243]

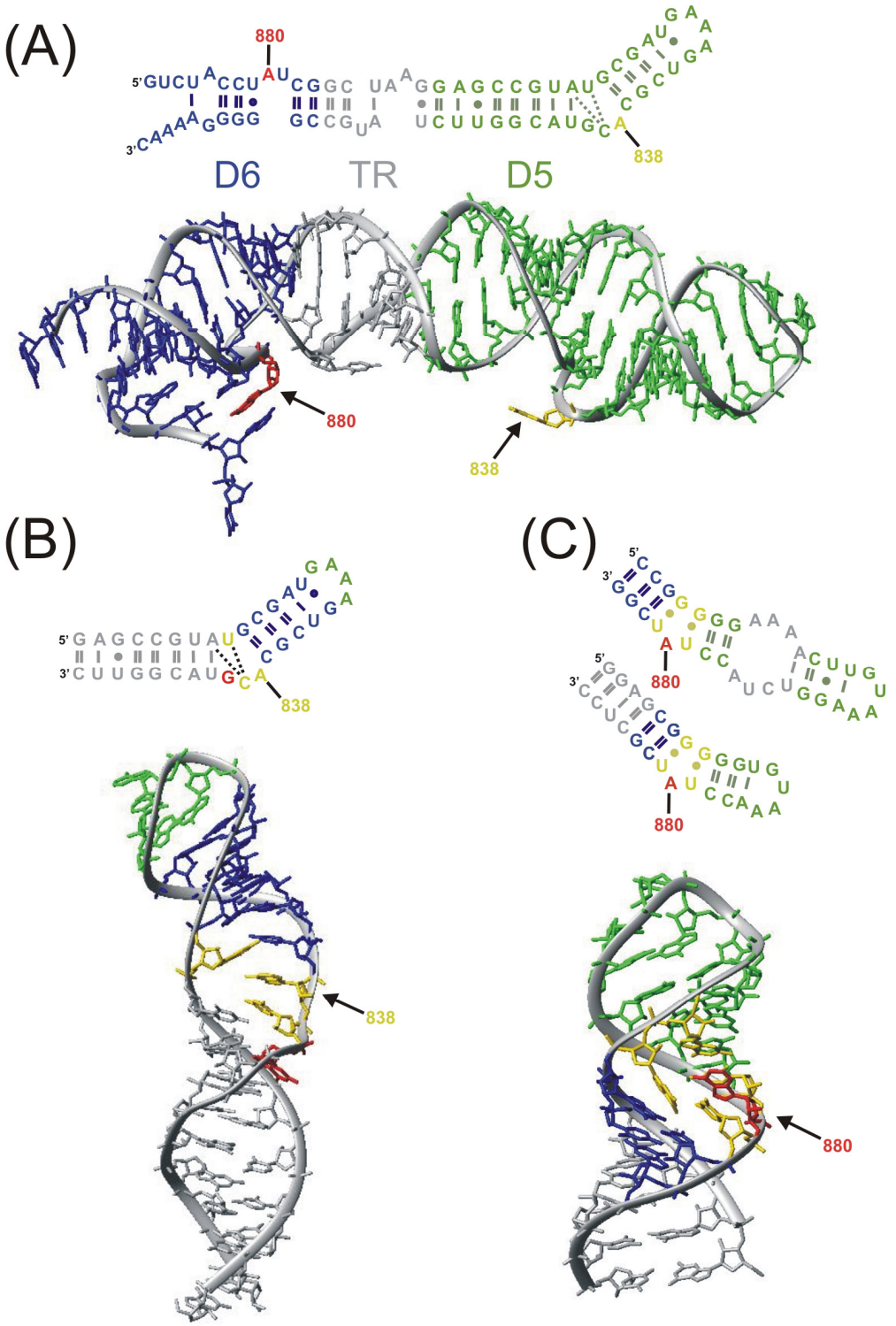

Figure 21 Comparison of D5 and D6 in the crystal and solution structure. (A) Secondary structure of D56-TR of *Sc*.ai5γ together with the crystal structure (PDB entry 1KXK).[242] Domains 5 (green) and 6 (blue) are separated by the tetraloop receptor (TR) (grey). A838 (yellow) is located in the bulge of D5 and A880 (red) is the branch-adenosine of D6. The numbering is according to their positions in the intact intron. The construct for crystallization lacks the terminal loop of D6. (B) Secondary structure of D5 of *Sc*.ai5γ together with the solution structure (PDB entry 1R2P).[34] The tetraloop is coloured in green, the bulge nucleotides (including A838) in yellow. G840, which adopts a syn conformation and therefore is flipped down on top of the catalytic triad, is coloured in red. Helix 1 is coloured in grey and helix 2 in blue. (C) Secondary structure of the wildtype D6 (top) and D6-27 (middle), a minimal D6 construct that lacks the internal loop as used for structure analysis by NMR. The solution structure of D6-27 is shown at the bottom (PDB entry 2AHT).[115] Additional nucleotides, which were added to improve transcription yield, are coloured in grey, and helix 1 is shown in blue. Upper helix including the tetraloop is highlighted in green, and the two G-U wobble pairs which flank the branch-adenosine (red) are in yellow. Figures were prepared with MOLMOL.[29]

Domain 6 (D6) includes the branch point – the 2'-OH of a highly conserved adenosine. Together with neighbouring functionalities, D6 positions this bulged adenosine relative to the active-site components in D1 and D5.[244,245] To investigate the importance of the identity of the branch-point, mutational studies of the adenosine were performed showing that with cytosine the transesterification reaction does not take place and guanosine and uracil allow the reaction to take place but to a very low extent.[246,247] The solution structure of D6 of the group II intron *Sc*.ai5γ was solved recently (Figure 21C).[115] NMR experiments of the wildtype D6 turned out to be very difficult due to the flexibility of the internal loop, which complicated the assignment of the spectra. Thus, a shortened construct (D6-27) (Figure 21C, middle) was used, which shows a slightly reduced activity compared to the wildtype D6. [115] Similar to D5, the solution structure of D6 is different from the crystal structure of the D56-TR construct. In the crystal structure, a two-nucleotide bulge with a shifted base-pairing pattern (Figure 21A) was found. The solution structure of the truncated D6-27 construct revealed the branch-adenosine to be a single nucleotide bulge, which resides within the helix and is partially stacked between the flanking G-U wobble pairs. These wobble pairs are suggested to be important for efficient branching due to their structural flexibility.[115,127] To locate metal ion binding sites in D6 NMR titration studies were performed by monitoring chemical shift changes upon addition of metal ions. The largest shifts appear at the branch adenosine and the two flanking G-U wobble pairs. Using paramagnetic line broadening studies with Mn^{2+}, it has been shown that a metal ion does not directly bind to the adenosine, but rather coordinates to the neighbouring G-U wobble pairs. A further binding site was proposed at the tandem GC base-pair in helix 1. Two metal ions are located at the tetraloop,[115] being in accordance with earlier fluorescence studies.[248]

These structures provide detailed insights into structural and metal ion requirements of isolated domains of a group II intron ribozyme. Yet information on the structure in the context of the full-length ribozyme is still missing. Attempts to crystallize the structure of a full-length ribozyme were fruitless for a long time and were only successful this year.[249] The crystal structure of a full-length class IIC intron will be discussed in the next section.

1.4.2 The crystal structure of a class IIC intron

Although biochemical studies, modelling efforts and NMR studies of the individual domains revealed many information about secondary and tertiary interactions of group II intron ribozymes,[34,70,115,127,203,214-216] molecular details about the active site as well as the

exact orientation of the domains towards each other remained unknown. This year, this situation changed because the first structure of an intact, self-spliced group II intron was published.[249]

Crystallization was successful with a class IIC intron from *Oceanobacillus iheyensis*. Main differences between class IIB and class IIC introns are discussed in Section 1.4. The crystal structure at 3.1 Å resolution revealed a network of unusual RNA tertiary interactions. This intron self-spliced during *in vitro* transcription, proving that it is active already at low magnesium concentrations and at high temperature. The construct contains all six domains (Figure 22), thus the crystal structure gives information about the organization of a full-length

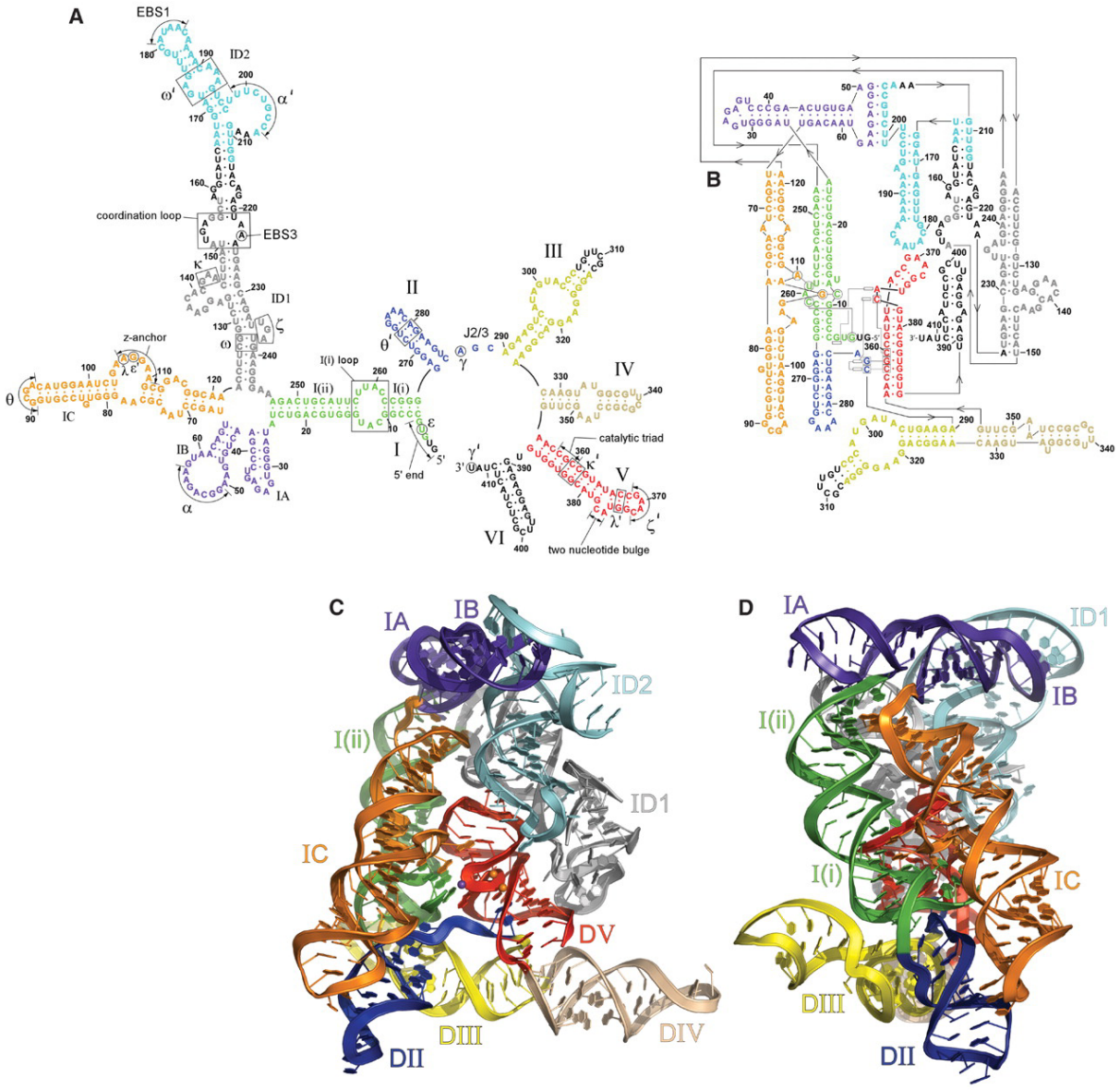

Figure 22 Overall secondary and tertiary structure of the crystallized intron. (A) Secondary structure of the intron from *Oceanobacillus iheyensis*. Roman numerals indicate domains and greek letters tertiary interactions. Disordered bases are shown in black. The domains are highlighted in different colours for clarity. (B) This secondary structure shows the coaxial stacking and domain arrangement like it was found in the crystal structure. (C) Ribbon presentation of the overall structure. (D) 90° orientation of the image in (C). Figure is taken from reference (249).

intron. The crystal structure revealed that the active site components are located around the catalytic center D5 (Figure 22C).

Analysis of the tertiary interactions shows that some corroborate the predicted ones, e.g. θ-θ' [231]. In contrast, the tertiary interactions α-α' and ζ-ζ' show an unexpected structural form. The long-range interaction of α-α' forms a kissing loop structure in the crystal structure. α becomes correctly positioned by coaxial stacking of stems IA ands IB. The tetraloop-receptor interaction of ζ-ζ exhibits an unusual conformation and consists only of base stacking between the AAC of the tetraloop and a single, bulged guanosine within the receptor (Figure 22). The tetraloop of the θ-θ'-interaction of stem IC docks into a receptor in DII, thereby bringing the conserved ε' sequence within the core of the intron. Since there are analogous tertiary interactions in class IIB and IIC introns, conclusions can be drawn from one to the other. However, due to the shortened lengths of group IIC introns some parts are missing, such as μ-μ'[250] and the EBS2-IBS2 interaction.[207] Therefore, no structural links can be made concerning these interactions.

As already suggested by previous folding studies, D1 is an independent folding scaffold for organization of the other domains.[213,218,222] D5 as the catalytic core of the intron is bound to D1 by several tertiary interactions, the most important of which is ζ-ζ'. An unusal conformation was found for this tetraloop-receptor in the crystal structure, consisting of base stacking between the AAC of the tetraloop in D5 and a bulged guanosine in the receptor. The κ-κ' connection between D1 and D5 was also confirmed. The J2/3 linker between D2 and D3 was suggested to be located near the catalytic triad in the folded ribozyme.[217,251] The crystal structure corroborates this suggestion and even shows that the nucleotides of J2/3 form a triple helix with the stem of D5. The structure of D5 in the full ribozyme substantially differs from the above described structures in isolation. The upper and lower stem of D5 are at an angle of ~ 45° oriented to each other in the crystal structure and are not coaxially stacked as depicted in the isolated structures. The bulge region of D5 in the full-length ribozyme is distorted because of interactions with other parts of the intron, thus showing that folding of D5 to a catalytically relevant form is essentially dependent on the presence of the full-length intron.

To investigate metal ion binding sites in the full-length ribozyme Yb^{3+} soaks were performed, which is a mimic for the coordination state of Mg^{2+}. Only four Yb^{3+} binding sites in the intron were found, of which two are located near the catalytic triad and one is at the bulge of D5. The fourth site is located outside the core of the intron. These findings are in

good agreement with the proposed metal ion binding sites in the solution structure of isolated D5.[34]

The crystal structure lacks electron density for D6, thus only assumptions can be made that D6 lies next to D5 as it was already suggested by biochemical methods.[252]

The part of the intron, which comprises EBS1 and also the 5'-end of the intron, are located near the bulge of D5. The 5'-splice site is located in the active site. The 3'-splice site is also located near the D5 bulge. Thus, both splice sites are positioned in the catalytic core in close proximity to the metal ions in D5. Based on these observations it has been suggested that the crystal structure is a catalytically relevant structure.[249]

1.4.3 Self-splicing of group II introns

Most RNAs undergo several steps of post-transcriptional modifications before they are able to carry out their assigned functions. One of the major modifications occur during the splicing process. In this process, the non-coding introns (*in*tervening sequences) are removed from the coding exons (*ex*pressed regions). Group II introns have the ability to catalyze their own excision out of the pre-mRNA. This is achieved as follows: First, the splice site is recognized by base-pair formation of two different sequences within the intron (EBS1 and EBS2) to their cognate partners consisting of the last nucleotides at the 3'-end of the 5'-exon (IBS1 and IBS2) (see also Section 1.4).[200] After the exon is recognized, two sequential transesterification steps follow. In the first splicing step, the 2'-OH group of a bulged adenosine within D6 nucleophilically attacks the scissile phosphate at the 5'-splice site and the 5'-exon is released in a typical S_N2 reaction while the intron forms a lariat (Figure 23A).[254] The 5'-exon is still bound via the EBS1-IBS1 and EBS2-IBS2 interactions and thus its free 3'-OH is in a correct position to attack the 3'-splice

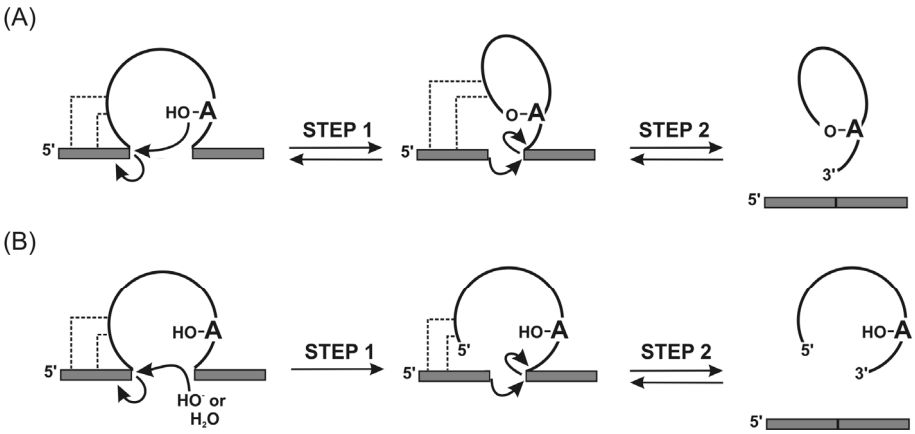

Figure 23 Pathways of group II intron splicing. (A) Branch-point splicing with the adenosine 2'-OH acting as a nucleophile in the first step of splicing. (B) Hydrolytic splicing, OH^- or H_2O act as a nucleophile in the first splicing step. The intron is shown in black, exons are shown as grey boxes. Binding interactions between intron and exon nucleotides (EBS1/IBS1 and EBS2/IBS2) are indicated by dotted lines. Figure adapted from reference (253).

site in the second splicing step. The 5'- and 3'-exons are ligated and the intron is released in the form of a lariat.[255] Both splicing steps are reversible reactions. The first step is rate-limiting, whereas the second step is extremly fast.[210,253,256] It has been shown *in vitro* and *in vivo* that water or hydroxide can also act as a nucleophile in the first splicing step[208,253,257-259] (Figure 23B) and that this reaction occurs in parallel to the branching reaction with the internal adenosine.[253] The products of the hydrolytic pathway are ligated exons and a linear intron but in contrast to the branch-point splicing the first step is irreversible.[260]

The splicing pathways of group II introns is very similar to the one of the spliceosome, with the difference that the catalytic components responsible for splicing of group II introns exclusively reside within the intron itself.[257,261,262] In the spliceosomal pathway numerous snRNAs and proteins assemble and the RNP-complex subsequently performs splicing. The second splicing step is no longer reversible compared to the one in group II introns. But the fundamental similarities in the reaction pathways fueled speculations that an evolutionary link exists between these two molecular machineries.[263-265]

Group II introns are best known for their ability to perform self-splicing, but they are also capable of performing other reactions like RNA and DNA hydrolysis and intron mobility among others.[203] The latter will be discussed in the next section.

1.4.4 Group II introns as mobile genetic elements

Additional interest in group II intron ribozymes stems from their activity as infectious genetic elements that are capable of migrating into new hosts or new positions within a host genome.[210-212,266-271] The insertion occurs via reversed splicing, which is catalyzed by the intron itself. The RNA is then converted into DNA by reverse transcription.[272] An intron-encoded protein (IEP) stabilizes the active RNA structure and provides reverse transcriptase (RT) activity.[203,272] Unlike in other systems capable of genetic transportation, the processing reactivity of group II introns depends on the ribozymes themselves. Intensive studies of group II intron mobility have shown that group II introns can be designed for the insertion at any desired location, either knocking out or transforming a gene.[267,270,273] Thus, new protein sequences can be introduced into an organism by the use of intron mobility. Recent work has shown that group II intron ribozymes are exceptionally accurate in targeting specific sequences in contrast to all other ribozymes[274-276] and that such specificity is controlled by folding of the group II intron ribozyme.[277] The exon binding sites (EBS) of the intron, which are bound to the exon, are of particular interest: The base-pairing interactions between EBS1

and IBS1 as well as EBS2 and IBS2 are not only required for RNA splicing, but since the transesterification reactions are reversible, the same base-pairings are essential for reverse splicing into RNA or DNA target sites during intron mobility.[266,278]

The biomedical application of group II introns will therefore depend on the ability to understand and manipulate their three-dimensional architecture, one important aspect of which is a detailed knowledge on the role of metal ions.

1.4.5 Metal ions and group II introns

Metal ions are inextricably involved in the splicing mechanism of group II intron ribozymes, i.e. group II introns are metalloenzymes. The requirements for group II introns to be catalytically efficient lies in the range of 0.2-2.0 M for monovalent cations (KCl, NH_4Cl or $(NH_4)_2SO_4$) and additionally, about 100 mM Mg^{2+}.[213,253,258,261] In addition to the Mg^{2+} requirement for catalysis, it has been shown that Mg^{2+} is also needed for folding [70,97,216] and substrate binding.[218] Mn^{2+} has been found to be the only divalent metal ion that can partly substitute for Mg^{2+} in catalysis.[256] The hydrolytic pathway dominates the splicing reaction at low salt concentrations, thus high salt concentrations are required in order to branch via an intramolecular pathway (see Section 1.4).[253]

Table 2 Metal ion requirements for group II introns in different organisms. The listed concentrations of monovalent (K^+, NH_4^+) and divalent (Mg^{2+}) are needed for a successful splicing event *in vitro*.

Organism	Group II intron	Subgroup	Location[a]	$[K^+/NH_4^+]$[M]	$[Mg^{2+}]$[mM]	Ref
Saccharomyces cerevisiae	aI1	IIA	cox1	1	100	[279]
Saccharomyces cerevisiae	aI2	IIA	cox1	2	100	[280]
Saccharomyces cerevisiae	*Sc*.ai5γ	IIB	cox1	0.5	50-100	[90,258]
Saccharomyces cerevisiae	*Sc*.bI1	IIB	cob	1.25	10	[106]
Pylaiella littoralis	*Pl*.lsu/1	IIB	lsu rRNA	1	100	[281]
Pylaiella littoralis	*Pl*.lsu/2	IIB	lsu rRNA	1	0.1-5	[281]
Azotobacter vinelandii	*Av*.hsp60	IIB	hsp60	0.5	100	[282]

[a]cox1, cytochrome oxidase 1; cob, apocytochrome B; lsu rRNA, large subunit of ribosomal RNA; hsp60, heat shock protein 60kD.

The concentration of monovalent cations *in vivo* is usually between 2 and 150 mM (depending on the organism and kind of cell).[70] The large three-dimensional structures of group II introns are additionally stabilized by protein cofactors, protamines and polyamines. Such group II introns can form stable structures under physiological conditions.[283-285]

In vitro, the metal ion requirements for monovalent as well as divalent metal ions differ substantially for individual group II introns (Table 2). It is interesting to note that *Pl*.lsu/2 still carries out accurate splicing at very low magnesium concentrations of about 0.1 mM, whereas *Pl*.lsu/1 from the same organism needs about 1000-fold more magnesium.[281] So far it is not quite understood why these molecules have so different metal ion requirements, although they are conserved in secondary structure. The extensively studied model ribozyme D135 from *Sc*.ai5γ folds properly at 100 mM Mg^{2+} by an apparent two-state mechanism, but at physiological concentrations of about 2-3 mM Mg^{2+} it compacts very slowly.[284,286] In contrast, the intron *Sc*.bI1, which also stems from *Saccharomyces cerevisiae* and belongs to the group IIB, splices at only 10 mM Mg^{2+}.

The twofold role of Mg^{2+} in catalysis as well as folding of the ribozyme makes it very difficult to differentiate between them. In 1999, it was suggested that only one Mg^{2+} is involved in the catalytic reactions of group II intron ribozymes.[287] This metal ion stabilizes the 3'-oxoanion leaving group by binding to the 3'-oxygen of the scissile phosphodiester bond in both splicing steps. Such a coordination was also observed in the spliceosome, thus showing another parallel between group II introns and the spliceosome.[287,288] However, in the recently solved crystal structure of a group IIC intron two metal ions were found in close proximity to the catalytic center suggesting a two-metal ion mechanism.[249]

As already mentioned in Section 1.1.4, lanthanide(III) cleavage experiments can be used to locate metal ion binding sites in large RNA molecules. This has been performed for the group II intron *Sc*.ai5γ with Tb^{3+} as the mediating lanthanide.[97] Similar to Mg^{2+}, lanthanides are redox inactive and prefer to coordinate to hard ligands such as phophate oxygens. Strong metal ion binding sites occur in the catalytically important domains 1, 3, 5 and 6. In particular major metal ion binding sites are observed in regions where ribozyme reaction chemistry occurs. This includes the Jd"/d"' motif, the λ and ε' nucleotides, the branch site and the nucleotides just 5' of EBS1. Further metal ion binding sites are located in regions of the catalytic apparatus, e.g. the bulge in D5 and the J2/3 linker, supporting the concept that D5 provides a metal ion binding platform within the active site.[129] Metal ion binding sites have also been observed close to regions, which are involved in tertiary interactions such as the α-

α' and β-β' helices. The three-way junction in D1c, nonconserved regions of D3 and linkers surrounding D4 provide further binding sites.

The Tb^{3+} clevage studies have revealed many important metal ion binding sites, but it is likely that additional strong binding sites are still undetected. Ions such as Tb^{3+}, and Mg^{2+} mediate RNA hydrolysis through the formation of metal hydroxides, which cleave RNA by activating the 2'-OH in the minor groove. But this cleavage is unfavourable in helical regions. Therefore, strong metal ion binding sites that are located within helices may be undetected by Tb^{3+} cleavage.[97] Other methods are needed to detect these metal ion binding sites, e.g. the ones mentioned in Section 1.1.4. Metal ion binding studies on the individual domains 5 and 6 of the group II intron *Sc*.ai5γ were conducted using NMR as discussed in Section 1.4. One part of this thesis focuses on the detection of metal ion binding sites by NMR (see Results and Discussion).

1.5 Aims of the project

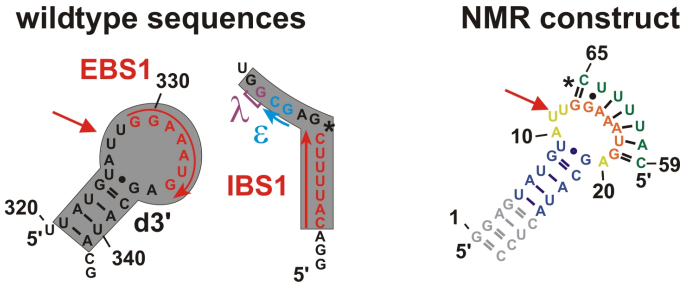

Figure 24 Comparison of wildtype sequence (left) and the NMR construct d3'-EBS1·IBS1 (right) of the EBS1-IBS1 interaction together with the D1d3'-stem in *Sc*.ai5γ, which is the focus of this thesis. The red arrow indicates a metal ion binding site. In the NMR construct additional nucleotides (G1-G4, C26-C29) are coloured in grey, the upper helical part (U5-U9, G21-A25) in blue, the unpaired nucleotides (A10-U12, A20) in yellow, EBS1 (G13-G19) in orange and IBS1 (C59-C65) in green.

As already mentioned in Section 1.4, before splicing of group II introns can be successfully carried out, the exon has to be recognized site specifically by the intron. The correct recognition of the splice site is therefore crucial for correct functioning of the RNA, e.g. the error free translation of mRNAs into proteins or the correct function of the mature RNA molecule. This recogniton process is still poorly understood: Watson-Crick base pairing between intronic and exonic nucleotides, i.e. the EBS1-IBS1 interaction, as well as the structural integrity mediated by at least one metal ion, seems to be crucial in group II intron splicing. Thus, the EBS1-IBS1 interaction is together with D5 and D6 part of the catalytic core.

As there is still little structural information available about the recognition site of group II introns, the first aim of this thesis is the structure determination of the hairpin including the d3'-stem and EBS1 in the absence and presence of the substrate, i.e. IBS1, by NMR. An initial attempt to solve the structure of d3'-EBS1 (Figure 25A) and d3'-EBS1·IBS1 (Figure 24) failed due to crowded regions in the NMR spectra. Despite of putting a lot of effort into stabilizing these RNAs, no conditions to record well-resolved NMR spectra could be found. Thus, another approach was aspired through stabilization of the base pairing interaction by changing two AU base pairs by two GC base pairs (Figure 25B and C). It was found that this change has no effect on the catalytic rate of splicing.[289] Thus, the solution structures with the more

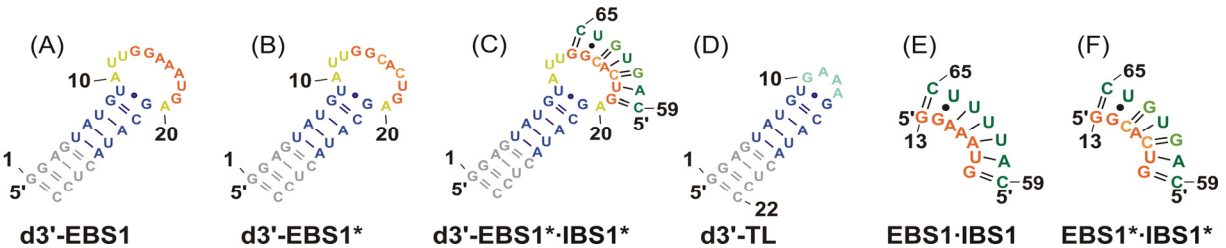

Figure 25 Summary of the constructs used in this project. (A) The wildtype construct d3'-EBS1 from *Sc*.ai5γ in the absence of IBS1. (B) The modified construct d3'-EBS1*. (C) The whole modified construct d3'-EBS1*·IBS1*. (D) The short construct d3'-TL with a GAAA tetraloop. (E) The wildtype EBS1·IBS1 interaction. (F) The modified EBS1*·IBS1* interaction. Residues that were added to improve transcription yield and to stabilize the helical stem are coloured in grey and the wildtype residues in the d3'-helix in blue. The unpaired nucleotides (A10-U12, A20) are yellow, EBS1 and EBS1*, respectively, in orange. IBS1 and IBS1*, respectively, are coloured in green. The altered GC basepairs are highlighted.

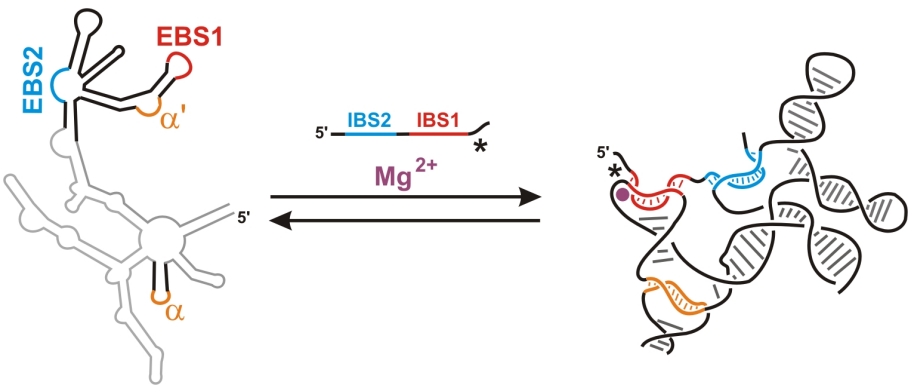

Figure 26 Formation of the 5'-splice site. A Mg^{2+} (●) is located right next to the EBS1-IBS1 interaction to possibly stabilize both a strong kink in the backbone and the transition state of catalysis.

stable EBS1*·IBS1* interaction was aimed to be solved, i.e. (i) the sole hairpin d3'-EBS1* (Figure 25B), (ii) the hairpin in the presence of the substrate, d3'-EBS1*·IBS1* (Figure 25C) and (iii) the EBS1*·IBS1* interaction only (Figure 25F). In addition, the helical stem leading to the splice site d3'-TL (Figure 25D) was of great importance, because it supported the spectral assignment of d3'-EBS1* and d3'-EBS1*·IBS1*.

The structures of d3'-EBS1* and d3'-EBS1*·IBS1* serve then as a profound basis to define the role of M^{n+} at this crucial part at the interface between 5'-exon and intron, which leads to the second aim of this thesis. It has been shown that most major metal ion binding sites in the *Sc*.ai5γ group II intron ribozyme are located around the catalytic core.[97] The EBS1-IBS1 interaction is the crucial region for recognition of the 5'-splice site through double helix formation, which induces heavy stress on the backbone just 5' of the EBS1 site (Figure 26). Two helices are arranged perpendicular to each other, linked by just two or three nucleotides. This leads to a close positioning of several negatively charged phosphate oxygen just 5' of EBS1. The Mg^{2+} ion could easily neutralize such repulsive interactions and thus stabilize the structure. This consideration is underlined by three previous results: a) Mg^{2+} is essential for substrate (i.e. exon) binding[218], b) one of the most intense Tb^{3+} cleavage sites is located just 5' of EBS1 and thus also next to the 5'-splice site[97] and c) in the crystal structure of a class IIC intron from *Oceanobacillus iheyensis* two metal ions are located close to the catalytic center of D5 being also accessible for EBS1.[249] Consequently, studying the role of this metal ion on the structures of d3'-EBS1* and d3'-EBS1*·IBS1* in detail was a second important aim of this project. Special focus was given on the determination of the affinity constants of divalent metal ions, such as Mg^{2+} and Cd^{2+}, to d3'-EBS1* and d3'-EBS1*·IBS1*.

In addition to NMR spectroscopy, circular dichroism (CD) is a good tool to monitor structural changes in nucleic acids. Thus, CD was additionally used to elucidate the metal ion requirements for the binding of IBS1* to EBS1* and to reveal further knowledge about the structural changes induced upon IBS1* and/or M^{n+} binding, respectively.

Such a study has – to the best of our knowledge – never been done before, yet it will shed light on the importance of metal ions on the formation of local RNA structures. This two-way approach ensures that (i) the process of splice site formation, (ii) the stability of the splice site structure, as well as (iii) the structure of the splice site in context of the whole D1d3' domain can be examined at atomic resolution.

To summarize the aims of this project, a combination of techniques from the fields of Coordination Chemistry, Bioinorganic Chemistry, Biochemistry, and Structural Biology was used to characterize the role of metal ions on the structure and formation of the splice-site recognition sequence within group II intron ribozymes. The results of this study provide an important basis for research related to either structure, folding, and/or catalysis of RNAs, to the mechanism of the spliceosome, as well as the biomedical application of group II introns (see also Section 1.4).

2 Results and Discussion

2.1 The wildtype d3'-EBS1 and d3'-EBS1·IBS1

2.1.1 Construct design and spectral features

The exon binding site 1 of the group II intron *Sc*.ai5γ is located within the loop of a hairpin structure in the subdomain d of D1 (Figure 20). This hairpin comprises nucleotides 321 to 341, of which 11 are encompassed by the loop. The d3'-stem consists of three consecutive alternating AU base pairs followed by a GC base pair and a GU wobble pair. The intron binding site 1 is located at the 3'-end of the 5'-exon and includes seven nucleotides (Figure 20).[69,70,200]

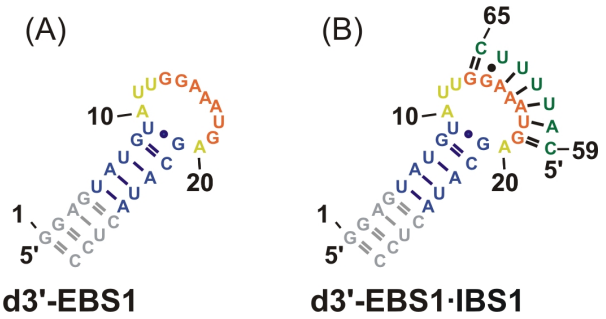

Figure 27 Secondary structures of d3'-EBS1 (A) and d3'-EBS1·IBS1 (B). Additional nucleotides (G1-G4, C26-C29) are coloured in grey and the upper helical part (U5-U9, G21-A25) in blue. The unpaired nucleotides (A10-U12, A20) are yellow, EBS1 (G13-G19) is orange and IBS1 (C59-C65) is coloured in green.

To design a construct suitable for NMR measurements some points have to be taken into consideration in order to obtain good yields by the *in vitro* transcription and to stabilize the helical region. It is known that aside from the RNA sequence itself the yield is mainly dominated by the first two or three nucleotides at the 5'-end of the RNA, i.e. the transcription initiation.[290-292] Pyrimidines are notoriously poor for transcription initiation, and guanosines are much better than adenosines.[290] The first two nucleotides at the 5'-end of the wildtype d3'-helix of *Sc*.ai5γ, being an uridine and an adenosine, imply a very poor transcription start (Figure 24). Therefore a GGAG sequence was added at the 5'-end of the helix and its complement at the 3'-end, thus leading to a stabilization of the helix and to an improvement of the transcription efficiency of the T7 RNA polymerase. It is expected that elongating the helix by four base pairs does not alter the structure of the EBS1 site,[200] but instead that the stabilization of the helix increases the quality of the NMR spectra. Very short constructs (<11 nucleotides) are very difficult to transcribe,[290] thus the seven nucleotide long IBS1 sequence was obtained commercially (for details see Materials and Methods).

First NMR spectra of d3'-EBS1 showed severe overlap in the central region of the sequential walk, probably due to the flexibility of the loop, hindering the complete and unambigious sequential assignment (Figure 28). The assignment of the helical part of the hairpin was only possible with the help of the spectrum of a shortened construct, namely d3'-

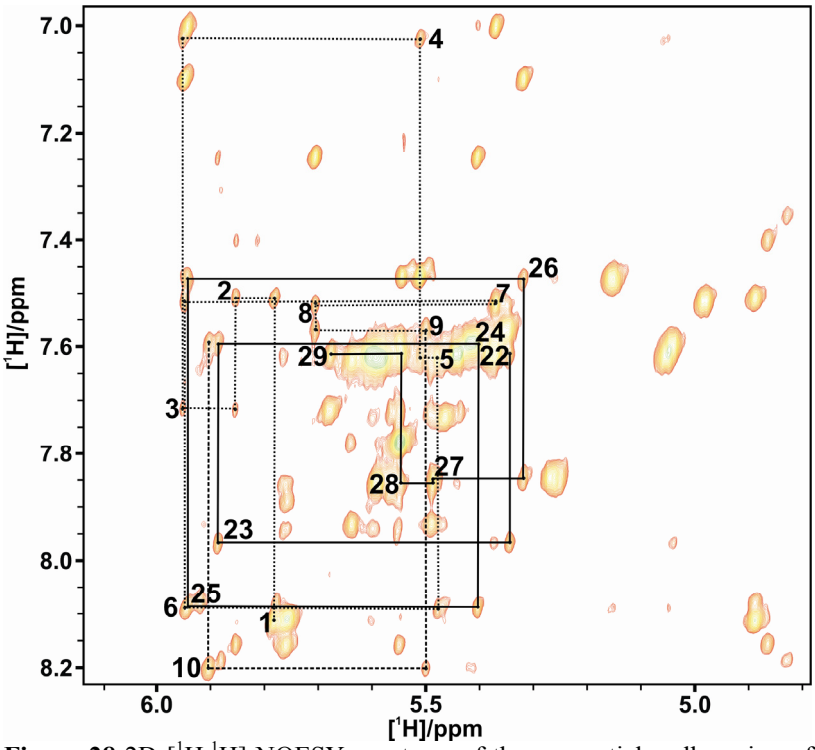

Figure 28 2D [^{1}H,^{1}H]-NOESY spectrum of the sequential walk region of d3'-EBS1 (99.99% D_2O, pD = 6.45, 10 mM KCl, 10 µM EDTA) recorded at 700 MHz and 303 K. The sequencial walk of the helical region is indicated by dotted (5'-end) and solid (3'-end) lines.

TL, where the 11-nucleotide long loop is replaced by a classical GAAA tetraloop (see Section 2.3.1).

In order to stabilize the 11 nt-loop of d3'-EBS1, different attempts were performed. The first one was to record spectra at different temperatures as it is assumed that the loop is less agile at lower temperature. However, lower temperatures lead to line broadening and thus making it even more difficult to assign the spectrum. In a second attempt, DMSO was added to the NMR samples in order to increase the viscosity of the solution and therefore decreasing the flexibility of the loop, but also this did not lead to a better resolution of the spectrum. With the consideration that metal ions might stabilize the loop, Mg^{2+} was added to d3'-EBS1, but also this try only led to line broadening. As the described efforts did not result in an improvement of the spectra quality of d3'-EBS1, IBS1 was added to the hairpin in order to stabilize the loop by the formation of a second helix. This experiment only resulted in an even more crowded sequential walk region (Figure 29). It was assumed and later confirmed by UV melting studies (see Section 2.2.3) that IBS1 is not completely bound to EBS1 under the used conditions. As it is known that a metal ion binding

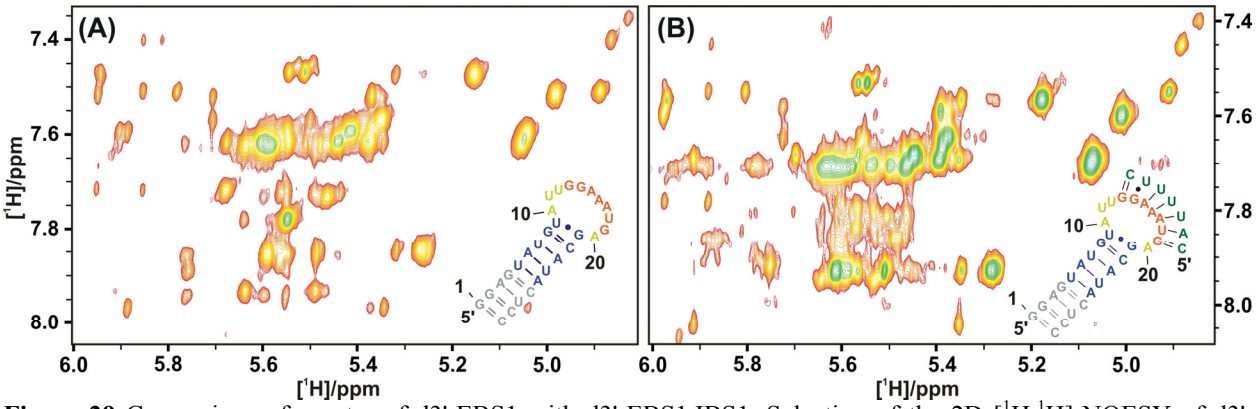

Figure 29 Comparison of spectra of d3'-EBS1 with d3'-EBS1·IBS1. Selection of the 2D [^{1}H,^{1}H]-NOESY of d3'-EBS1 (A) and d3'-EBS1·IBS1 (B) are shown. It is obvious that the resolution of the spectrum gets worse when IBS1 is added.

site exists 5' to EBS1,[97] metal ion titration studies of d3'-EBS1·IBS1 were performed in order to help stabilize the EBS1-IBS1 interaction. The addition of Cd^{2+} caused shifting of several peaks but also led to line broadening and was therefore not successful. Hence, to improve the quality of the spectra and to be able to completely assign them new approaches had to be considered, which will be discussed in the next section.

2.2 The altered d3'-EBS1* and d3'-EBS1*·IBS1*

2.2.1 Construct design of d3'-EBS1* and d3'-EBS1*·IBS1*

Recent discoveries have shown that EBS1·IBS1 lacks phylogenetic conservation[200,224,226,277,293] and a model was suggested, in which the cleavage site is not determined through recognition of specific nucleotides. Instead, it appears that the ribozyme recognizes the helical part of the EBS1·IBS1 interaction and cleaves at the junction between single and double stranded nucleotides. It is proposed that the specification of the cleavage site is defined by the most stable EBS1-IBS1 interaction.[226] Therefore, in order to stabilize the interaction between EBS1 and IBS1 and thus receive well resolved NMR spectra, two AU base pairs were changed to GCs (Figure 30). An additional construct (d3'-EBS1*·IBS1*-GC) was tested in which the GU wobble pair in the EBS1-IBS1 interaction was additionally changed to a GC (Figure 30C). However, as this latter construct is not as active as d3'-EBS1*·IBS1* (see Section 2.2.2), it was discarded and the main focus for the structure determination was set on d3'-EBS1*·IBS1*. Activity, thermal stability and spectral features of the altered d3'-EBS1* and d3'-EBS1*·IBS1* constructs will be discussed in the next sections.

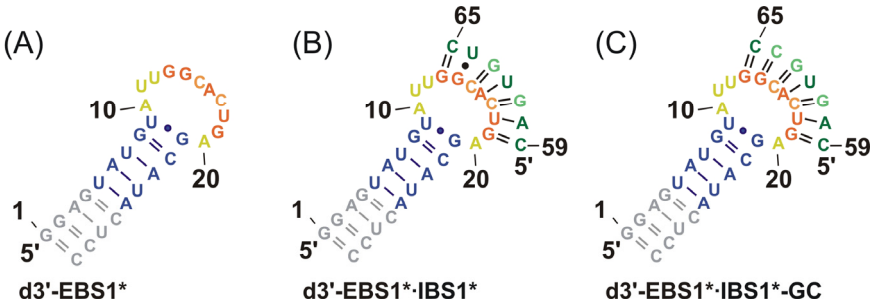

Figure 30 Secondary structures of the altered d3'-EBS1* (A), d3'-EBS1*·IBS1* (B) and d3'-EBS1*·IBS1*-GC (C) constructs. Additional nucleotides (G1-G4, C26-C29) are coloured in grey and the upper helical part (U5-U9, G21-A25) in blue. The unpaired nucleotides (A10-U12, A20) are yellow, EBS1 (G13-G19) is orange and IBS1 (C59-C65) is coloured in green. Modified nucleotides are highlighted.

2.2.2 d3'-EBS1*·IBS1* is active *in vitro*

If mutations are introduced into a biologically significant site one has to verify that this mutation does not have any effects on the activity of the system. Thus, to check if the modified interactions as they appear in d3'-EBS1*·IBS1* and d3'-EBS1*·IBS1*-GC do not hamper splicing *in vitro*, trans-splicing assays under single turnover conditions were performed as already described by Su *et al*.[286] In this activity assay, the 17/7 approach was carried out, i.e. a 24 nucleotide long so-called 17/7 substrate, which consists of the 17 nucleotides spanning IBS1 and IBS2 as well as the first 7 nucleotides of the intron, was used. 17/7* thereby includes the mutation corresponding to the EBS1* sequence and 17/7-GC the

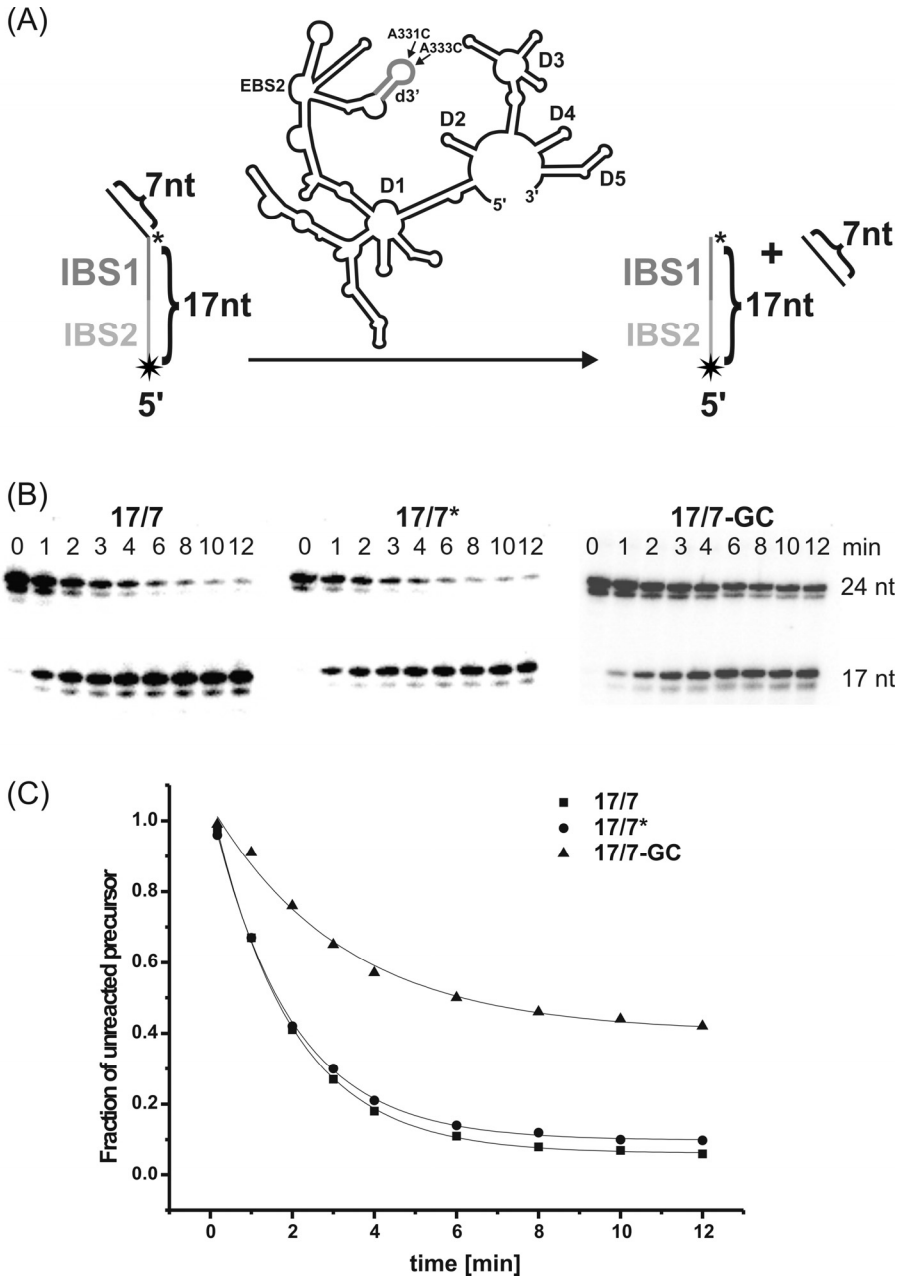

Figure 31 Activity assay. (A) Schematic representation of the cleavage reaction. The 17/7-substrate is ^{32}P-labeled at the 5'-end (star). IBS1 and IBS2 of the 5'-exon are indicated as grey lines. The cleavage site is indicated by an asterisk. The location of the A331C and A333C mutations in the ribozyme D135 are shown. (B) Time course of the trans-splicing assay showing the reduction of the precursor band (24 nts) and the appearance of the product band (17 nts) for the wildtype 17/7 (left), altered 17/7* (middle) and 17/7-GC (right) sequences. (C) Cleavage rates for both 17/7 and 17/7* are $k_{obs} = 0.52 \pm 0.01$ min^{-1}, whereas 17/7-GC cleaves only with a reaction rate of 0.3 ± 0.01 min^{-1}.

mutation corresponding to the EBS1*-GC sequence (Table 3). Accordingly, the mutations A331C and A333C were introduced into D135 giving D135GC (Figure 31A) to allow for proper base pairing with 17/7* and 17/7-GC. The wildtype substrate 17/7, the altered substrates 17/7* and 17/7-GC (see Table 3) were radioactively labeled with [γ-^{32}P]-ATP at the 5'-end to be able to observe their cleavage and with that the dissapearence of the uncleaved 24 nucleotide long band and the appearance of the 17 nucleotide long cleaved band (Figure 31B). Both, D135 and D135GC cleave 17/7 and 17/7*, respectively, to about 90% within 12 minutes with equal reaction rates k_{obs} = 0.52 ± 0.01 min^{-1} (Figure 31B and C; Table 3). The reaction with 17/7-GC containig no GU wobble shows a reaction rate of only 0.3 ± 0.01 min^{-1} and a conversion of 60% (Table 3), thus this construct was not taken into account in NMR investigations.

The observed activity of the altered 17/7* is in excellent agreement with a recent study that showed that the EBS1·IBS1 interaction lacks phylogenetic conservation[224,226,277,293] and a model, in which the cleavage site is not determined through recognition of specific nucleotides at the cleavage site. Instead, it appears that the ribozyme recognizes the helical part of the EBS1·IBS1 interaction and cleaves at the junction between single- and double-stranded nucleotides. It is proposed that the specification of the cleavage site is defined by the most stable EBS1·IBS1 interaction, i.e. correct base pairing,[226] thus confirming our findings of the same reaction rates of the wildtype and the modified EBS1*·IBS1* interaction. However, the obtained results with the 17/7-GC substrate, which lacks a G-U wobble in the corresponding EBS1-IBS1 interaction, suggests that the G-U wobble pair is absolutely necessary for splicing. Thus, the altered d3'-EBS1* and d3'-EBS1*·IBS1* constructs, which include a G-U wobble in the EBS1-IBS1 interaction, were the main focus in the structure determination and metal ion titration experiments (Section 2.2.5, 2.2.7, 2.2.8, 2.2.9 and 2.5).

Table 3 Kinetic parameters for cleavage of 5'-^{32}P-labeled 17/7, 17/7* and 17/7-GC.

substrate	sequence	ribozyme		k_{obs} [min^{-1}]	% cleavage
		D135	D135GC		
17/7	5'-CGUGGUGGGACAUUUUCGAGCGGU-3'	+	-	0.52 ± 0.01	90
17/7*	5'-CGUGGUGGGACA***G***U***G***UCGAGCGGU-3'	-	+	0.52 ± 0.01	90
17/7-GC	5'-CGUGGUGGGACA***G***U***GC***CGAGCGGU-3'	-	+	0.30 ± 0.01	60

2.2.3 Thermal stability of the wildtype and the modified EBS1·IBS1 interactions

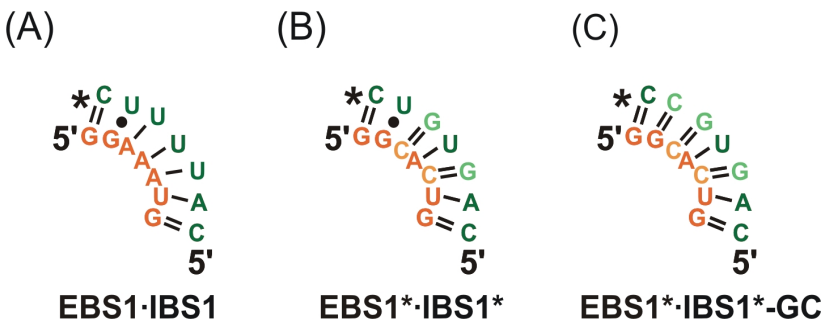

Figure 32 Secondary structures of the wt-EBS1·IBS1 (A), EBS1*·IBS1* (B) and EBS1*·IBS1*-GC (C) constructs as used in the UV melting studies. Altered nucleotides are highlighted.

In order to confirm the low stability of the wildtype EBS1·IBS1 interaction as found by NMR, UV melting studies were performed. Melting temperatures T_m give an estimate of the thermal stability of oligonucleotides and of the homogeneity of the sample. At the melting temperature T_m 50% of the oligonucleotide is melted, i.e. is single stranded. To investigate the stability of the wildtype as well as the altered EBS1-IBS1 interactions, three constructs were designed, which include only the EBS1·IBS1 interaction without the stem (Figure 32A-C). The melting temperatures are summarized in Table 4. The UV melting studies of the EBS1·IBS1 interaction (Figure 32A) reveal a melting point T_m of 15.5 °C (100 mM KCl). Higher concentrations of KCl do not lead to a considerable increase of T_m (Table 4), thus indicating a poor stability of the EBS1·IBS1 complex in the absence of the covalent exon-intron linkage and/or EBS2·IBS2. These results confirm the observations made by NMR (see Section 2.1). NMR studies are normally carried out between 20 °C and 30 °C, thus the wildtype EBS1·IBS1 interaction with its low stability is not suitable for NMR studies as at usual measurement temperatures IBS1 is not completely bound to EBS1.

The altered EBS1*·IBS1* and EBS1*·IBS1*-GC interactions result in significantly higher melting temperatures. Indeed, an increase in T_m by a factor of more than two to 34.3 °C (100 mM KCl, Table 4) was achieved for EBS1*·IBS1*. Even when reducing the KCl

Table 4 Melting temperatures T_m [°C] of EBS1·IBS1, EBS1*·IBS1*, EBS1*·IBS1*-GC and d3'-EBS1*·IBS1* (see also Figure 32 and 30B) at different KCl concentrations [mM].

[KCl]/mM	T_m (EBS1·IBS1)	T_m (EBS1*·IBS1*)	T_m (EBS1*·IBS1*-GC)	T_m (d3'-EBS1*·IBS1*)
10	nd	27.5 ± 0.3	nd	27.9 ± 0.5 / 51.0 ± 0.2
100	15.5 ± 1.0	34.3 ± 0.2	49.9 ± 0.1	40.6 ± 0.2 / 63.5 ± 0.2
150	17.0 ± 1.1	nd	nd	nd
200	17.5 ± 2.0	nd	nd	nd

nd, not determined

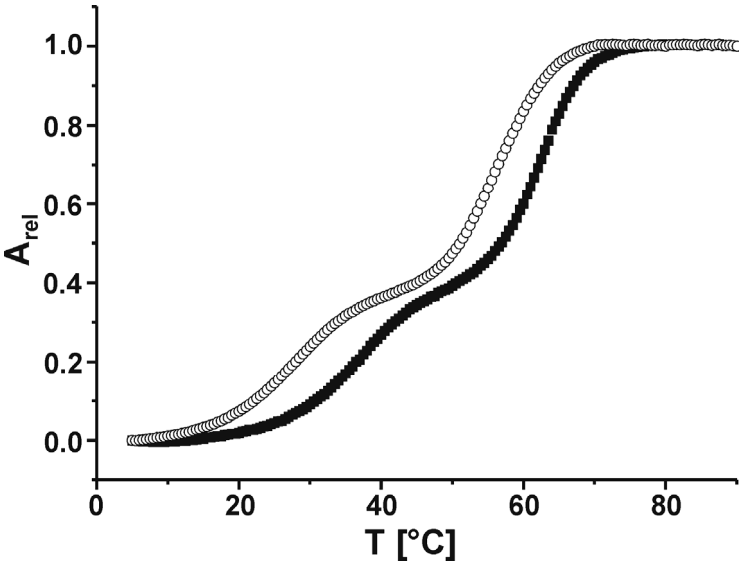

Figure 33 UV-melting curves for d3'-EBS1*·IBS1* in the presence of 10 mM KCl (○) and 100 mM KCl (■). The curves were acquired by measuring the absorbance at 260 nm. The first transition corresponds to the melting of the EBS1*·IBS1* interaction and the second to the one of the d3'-stem (see also Table 4).

concentration to 10 mM, T_m is with 27.5 °C still higher than the one of the wildtype interaction. Such a stabilizing effect by KCl is no surprise as the higher ionic strength reduces the charge repulsion of the two negatively charged RNA strands. A further small increase in stability of the EBS1*·IBS1* interaction is achieved by including the d3'-stem, i.e. having the corresponding full-length d3'-EBS1*·IBS1* interaction as found in the full D135GC ribozyme: Melting temperatures of 28 °C (10 mM KCl) and 40 °C (100 mM KCl) are reached. The melting curve of this RNA dimer shows a second transition at higher temperature, which originates from the dissociation of the hairpin stem (Figure 33, Table 4). Taken together, the modified d3'-EBS1*·IBS1* construct shows a very good thermal stability even in the absence of divalent metal ions and was therefore used in all further experiments.

The construct EBS1*·IBS1*-GC (Figure 32C) has with 49.9 °C (100 mM KCl) an even higher melting temperature than EBS1*·IBS1*. But as already mentioned in Section 2.2.2 the change from wobble to Watson-Crick base pairing results in very poor activity *in vitro*.

In order to determine the thermodynamic parameters for the EBS1*·IBS1* and EBS1*·IBS1*-GC interaction the melting curves were converted into plots showing the percentage of folded fraction (α) versus temperature as it has been previously described for other RNAs[294] and fit with a two-state transition model using linear sloping of the upper and lower baselines (Figure 34A).[295,296] Because of the low thermal stability of the wildtype EBS1·IBS1 interaction, the linear region of the RNA duplex could not be reached. This lower baseline is needed for the calculation of ΔH^0-values. Hence, a van't Hoff analysis was only performed for the EBS1*·IBS1* interaction in the presence of 10 mM and 100 mM KCl and for EBS1*·IBS1*-GC (100 mM KCl). A van't Hoff plot (ln*K vs* 1/T) was drawn by using the equilibrium constant *K* as determined for each temperature using equation 1 for bimolecular transitions (Figure 34B):[294]

$$K = \frac{\alpha}{c_{ss}\left(1-\alpha\right)^2} \qquad \text{equation 1}$$

where c_{ss} is the concentration of each single strand. This expression is used for non-self-complementary associations. *K* values are most precise in the α-range between 0.2 and 0.8,[296,297] and hence only the values within this region were used (Figure 34A). For a concentration-independent monomolecular transition as in the case of the d3'-stem *K* is determined with equation 2.[295,298]

$$K = \frac{\alpha}{1-\alpha} \qquad \text{equation 2}$$

ΔH^0 is assumed to be independent of temperature for a two-state transition.[296] Therefore, the van't Hoff plot is linear with $-\Delta H^0/R$ as the slope and $\Delta S^0/R$ as the axis intercept. All standard errors for ΔH^0 and ΔS^0 are in the range of 5-8%. As the errors of ΔH^0 and ΔS^0 compensate, the analysis of optical melting curves provides a precise way of determining ΔG_{37} yielding standard errors of ±2-5%.[297] The thermodynamic data for the EBS1*·IBS1* and EBS1*·IBS1*-GC interaction are summarized in Table 5. ΔH^0 for the melting of EBS1*·IBS1* decreases from –313.8 ± 15.7 kJmol^{-1} to –334.3 ± 16.7 kJmol^{-1} when raising the KCl concentration from 10 mM to 100 mM. At the same time, ΔG_{37} only slightly decreases (–20.3 ± 1.4 kJmol^{-1} *vs* –28.8 ± 2.0 kJmol^{-1}) illustrating that the thermodynamic stability of EBS1*·IBS1* is only little stabilized by increasing the

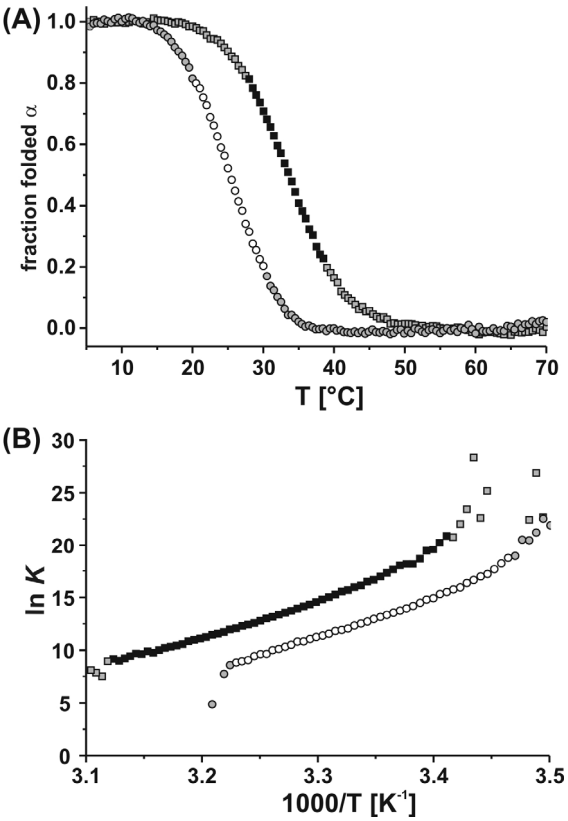

Figure 34 (A) UV-melting curves for EBS1*·IBS1* in the presence of 10 mM KCl (○) and 100 mM KCl (■). The curves were acquired by measuring the absorbance at 260 nm. (B) Van't Hoff plot (ln *K vs* 1/T) for EBS1*·IBS1* at 10 mM KCl (○) and 100 mM KCl (■). For the final calculation of the thermodynamic parameters, only the data points between 20 and 80% folded were used, i.e. the points shown in grey were omitted.

Table 5 Thermodynamic parameters for the folding of EBS1*·IBS1* at 10 and 100 mM KCl and of EBS1*·IBS1*-GC at 100 mM KCl as determined by UV melting experiments. The errors given correspond to one standard deviation.

Construct ([KCl]/mM)	ΔH^0/kJ·mol^{-1}	ΔG_{37}/kJ·mol^{-1}	ΔS^0/J·mol^{-1} K^{-1}
EBS1*·IBS1* (10)	–313.8 ± 15.7	–20.3 ± 1.4	–946.2 ± 66.2
EBS1*·IBS1* (100)	–334.3 ± 16.7	–28.8 ± 2.0	–985.2 ± 69.0
EBS1*·IBS1*-GC (100)	–314.3 ± 15.7	–43.3 ± 3.0	–874.0 ± 61.2

Table 6 Thermodynamic parameters for the folding of d3'-EBS1*·IBS1* at 10 mM and 100 mM KCl as determined by UV melting experiments. The errors given correspond to one standard deviation.

	[KCl]/mM	ΔH^0/kJ·mol^{-1}	ΔG_{37}/kJ·mol^{-1}	ΔS^0/J·mol^{-1} K^{-1}
d3'-stem	10	–346.3 ± 17.3	–19.8 ± 1.4	–1053.0 ± 73.7
EBS1*·IBS1* interaction	10	–317.1 ± 15.9	–17.7 ± 1.2	–965.0 ± 67.6
d3'-stem	100	–447.2 ± 22.4	–41.3 ± 2.9	–1308.7 ± 91.6
EBS1*·IBS1* interaction	100	–336.3 ± 16.7	–35.3 ± 2.5	–965.1 ± 67.6

concentration of monovalent cations. However, illustrated by the construct EBS1*·IBS1*-GC with a ΔG_{37} of –43.3 ± 3.0 kJmol^{-1}, the exchange of a G-U wobble pair by a G-C base pair leads to a more stable interaction. The compiled thermodynamic parameters in Table 6 illustrate that the d3'-stem has no influence on the EBS1*·IBS1* interaction: The ΔH^0 and ΔS^0 values are the same within the error limits and also ΔG_{37} is not significantly different for the melting of isolated EBS1*·IBS1* and the same sequence embedded within d3'-EBS1*·IBS1*.

Taken together, the thermodynamic parameters show that the stability of double helices can be increased rather by replacing A-U and G-U pairs, respectively, with G-C base pairs than by increasing the ionic strength.

2.2.4 Hairpin *versus* duplex: Which one exists in solution?

2.2.4.1 General considerations

Because of its partly palindromic sequence, d3'-EBS1* tends to form besides a hairpin structure in addition a homo-dimer, i.e. a duplex. The exclusion of a duplex is of importance for NMR structural studies on RNA oligonucleotides. The symmetry of a duplex leads to a spectrum, which can be similar to the one of a hairpin. Therefore, a series of experiments was performed to proof the existence of a hairpin in solution and thus excluding dimerization.

It has been shown that the stability of hairpins is dependent on the size of the loop and on the number of base pairs in the stem.[110,299,300] Small loops tend to form more stable hairpins and Kirchner *et al.* demonstrated that a 7-nucleotide loop predominently forms dimers.[110,299] The influence of the stem length on the stability was analyzed showing that increasing the number of base pairs in the stem stabilizes the hairpin.[300] The here studied 29-mer includes a 11 nucleotide long loop and thus the stability of the hairpin is decreased compared to shorter loops. Four base pairs were added to the wildtype stem to increase the stability. It was important to demonstrate that even with this large loop size indeed a hairpin structure exists in solution.

In the case of short oligonucleotides, high salt and high strand concentrations favour the duplex formation, whereas at low salt and low strand concentrations the equilibrium is driven to the hairpin.[301,302] Low salt concentrations favour formation of the species that possesses the lower charge density, which is the hairpin structure. It has been shown that hairpins are kinetically stabilized by rapid cooling after thermal denaturation.[110,303] Thus, the 29 long oligonucleotide was treated as follows: The oligonucleotide was dissolved in 100 mL double distilled water, denatured at 85 °C and rapidly cooled on ice to have a low RNA and a low salt concentratrion. Afterwards it was concentrated at 14 °C to get an appropriate volume for NMR measurements (for details see Materials and Methods). At this point it was important to proof if this procedure led to the hairpin formation:

There is a great variety of experiments, which investigate the problem of distinction between hairpin and duplex: (i) monitoring the hyperchromic UV shift of melting at different oligonucleotide concentrations,[302,304] (ii) measurement of X-filter-NOESY-HSQC experiments with G-U wobble pairs as probe,[305,306] determination of the hydrodynamic radii of the oligonucleotides by measurement of the diffusion coefficient by (iii) NMR (DOSY),[301,307] and (iv) dynamic light scattering (DLS).[307] These four experiments were carried out and will be discussed below.

2.2.4.2 Concentration dependent UV melting studies

Concentration dependent UV melting studies were carried out at 1.0, 1.7, 3.5, 5.8, 13.3, 19.0, 36.5 and 70.1 μM RNA strand concentration. UV melting curves at each concentration show a single transition (Figure 35) revealing a homogenous structure melting. The melting temperature does not change within the error limits as a function of oligomer concentration (Table 7). The concentration independent T_m of ~ 49.5 °C thus corresponds to a monomolecular process, such as melting of a hairpin. A distinct dependence of the melting temperature on concentration would provide evidence that a bimolecular complex such as a dimer exists in solution.[308] This concentration independency of the melting point gives a first proof of the existence of the d3'-EBS1* hairpin in solution.

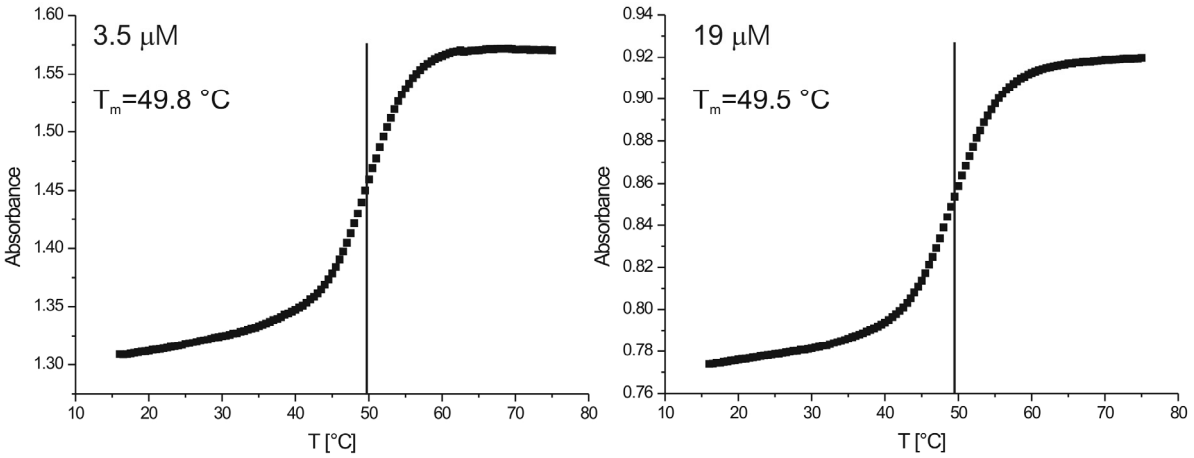

Figure 35 Two examples of UV melting curves of d3'-EBS1* at 3.5 μM (left) and 19 μM oligomer concentration (right). Both melting curves show a single transition at ~49.5 °C. The concentration independence gives evidence for a hairpin structure.

Table 7 Melting temperatures T_m [°C] of d3'-EBS1* at different oligomer concentrations [μM].[a]

[RNA]/μM	1.0	1.7	3.5	5.8	13.3	19.0	36.5	70.1
T_m	50.1 ± 0.5	49.9 ± 0.3	49.8 ± 0.2	49.8 ± 0.2	49.5± 0.2	49.5 ± 0.2	49.0± 0.2	48.7 ± 0.2

[a]Measurements were performed with 10 mM KCl at pH 6.8. Errors given correspond to one standard deviation.

2.2.4.3 X-filter-NOESY-HSQC experiments

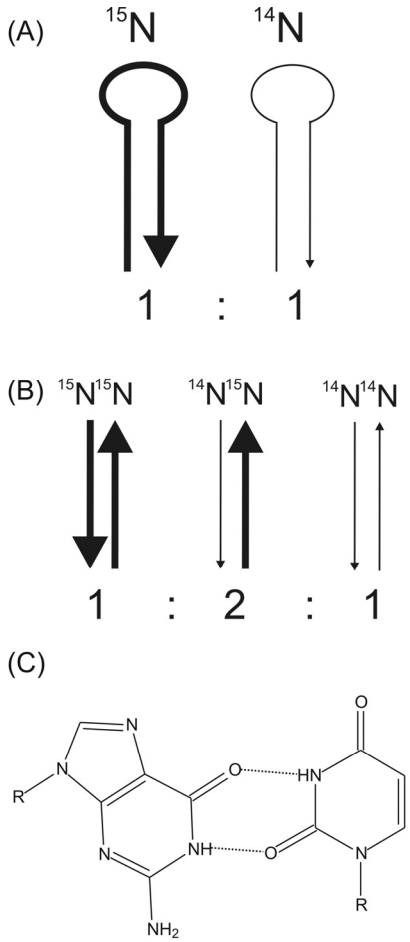

Figure 36 Schematic representation of (A) hairpin and (B) duplex formation. The relative ratios of labeled versus unlabeled RNA is given below, the bold arrow represents ^{15}N labeled RNA, whereas the narrow arrow represents the unlabeled RNA. (C) The imino protons of a G-U wobble pair are close in space (< 3 Å) and serve as a probe for distinguishing between hairpin and duplex.

Double half isotope filtered-NOESY-HSQC experiments with a 1:1 mixture of ^{15}N,^{13}C-labeled and unlabeled molecules can be used to distinguish RNA hairpins from RNA duplexes.[305] With the help of this experiment, it is possible to distinguish between inter- and intramolecular NOEs, because cross peaks are only observed when one proton is bound to ^{15}N and the other one is bound to ^{14}N. For a 1:1 mixture of ^{15}N,^{13}C-labeled and unlabeled RNA, hairpin formation can occur either of unlabeled or of labeled RNA (Figure 36A). Since all NOEs in a hairpin are intramolecular, no NOEs will be observed in the double half filtered experiment. When duplex formation in a 1:1 mixture of labeled and unlabeled RNA is assumed, three different strand combinations can exist, ^{15}N:^{15}N and ^{14}N:^{14}N homodimers and ^{15}N:^{14}N heterodimer in a 1:1:2 ratio (Figure 36B). The double half filtered experiment shows resonances only for NOEs between labeled and unlabeled molecules, therefore in the ^{15}N:^{14}N heterodimer NOEs can be observed. G-U wobble pairs serve as a distinctive marker for the identification of intermolecular NOEs, because GU wobble pairs give a very strong cross peak for the G and U imino protons (Figure 36C). Figure 37A shows the double half isotope filtered-NOESY-HSQC of a 1:1 mixture of ^{15}N,^{13}C-labeled and unlabeled d3'-EBS1*. No NOE for the U9-G21 wobble is observed in this spectrum proofing that only intramolecular interactions occur and with that demonstrating unambiguously that a hairpin is present. In order to test whether this experiment is working, a double half isotope filtered-NOESY-HSQC of d3'-EBS1*·IBS1* with only the d3'-EBS1* part ^{15}N,^{13}C-labeled and IBS1* at natural abundance was recorded. Indeed, there is clearly an intermolecular NOE between G14H1 of the ^{15}N,^{13}C-labeled d3'-EBS1* and U64H3 of the unlabeled IBS1* observed

(Figure 37B). Thus, it is shown that this experiment indeed can be a proof for the existence of a hairpin or a duplex in solution.

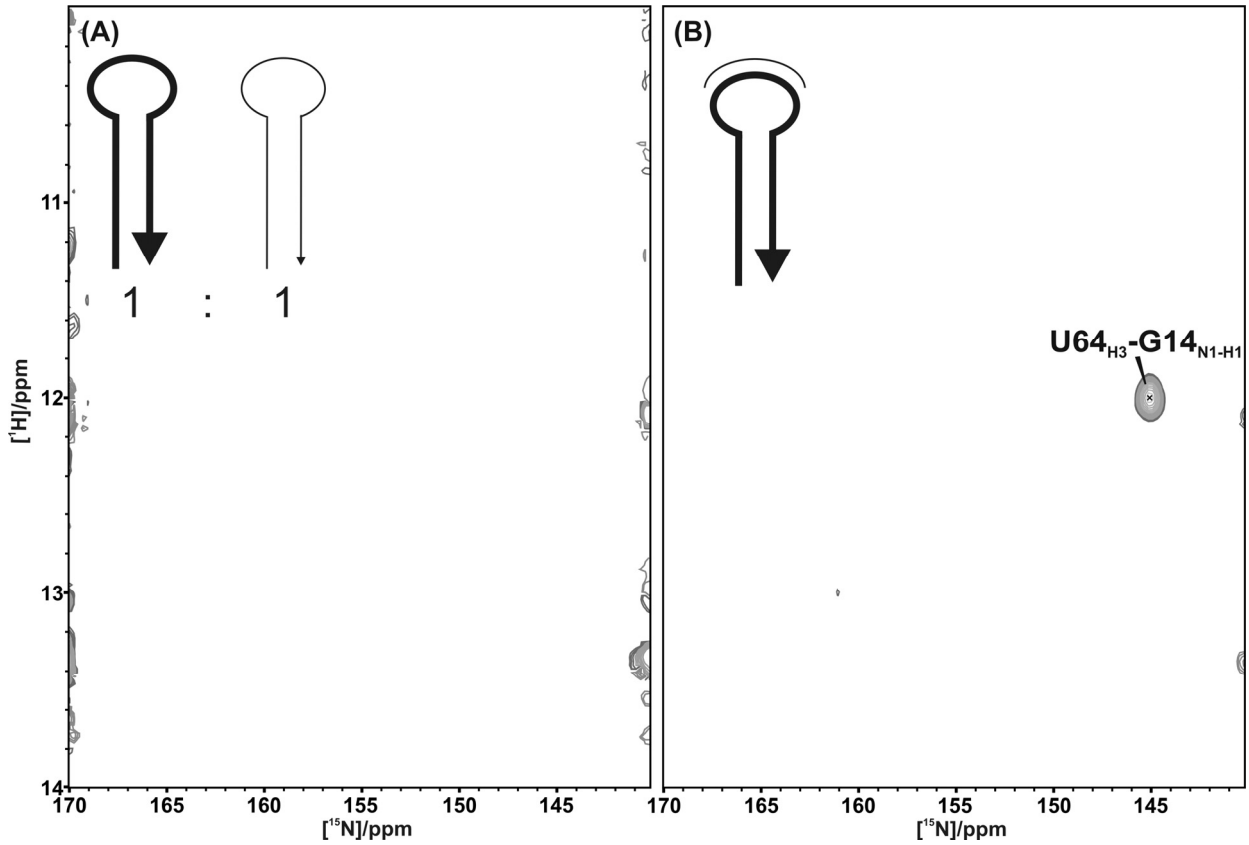

Figure 37 Double half isotope filtered-NOESY-^{15}N-HSQC of a 1:1 mixture of ^{15}N,^{13}C-labeled and unlabeled d3'-EBS1* (A) and of d3'-EBS1*·IBS1* (B) with the d3'-EBS1* part ^{15}N,^{13}C-labeled only. Shown is a projection onto the HSQC-plane. A NOE is only observed for the G-U wobble pair, which is formed by the interaction of IBS1* with EBS1* (U64H3-G14H1). With the absence of a NOE of U9H3-G21H1 it is proven that d3'-EBS1* forms a stable hairpin.

2.2.4.4 Diffusion ordered spectroscopy and dynamic light scattering

The determination of the hydrodynamic radii by diffusion ordered spectroscopy (DOSY) and dynamic light scattering (DLS) give an estimate of the size of the molecules and thus further methods to discriminate between hairpin and duplex. DOSY and DLS experiments were carried out under identical conditions for d3'-EBS1*, d3'- EBS1*·IBS1*, d3'-TL, and EBS1*·IBS1*, respectively. The latter three constructs are listed here for reasons of completeness and comparison.

Particles can either be modelled by the spherical or the symmetrical cylinder model dependent on the ratio of its length L and its diameter d ($q = L/d$). With a ratio of length to diameter $q < 2$ the spherical model can be used according to equation 3:

$$r_H = \frac{L}{2} \qquad \text{equation 3}$$

The symmetrical cylinder model is applied when $2 < q < 30$ with equation 4[301,307,309]:

$$r_H = \frac{L}{2\left(\ln q + 0.312 + 0.565q^{-1} - 0.1q^{-2}\right)} \qquad \text{equation 4}$$

The length of the particles was measured from the PDB file of the lowest energy structure of the corresponding construct. A typical A-form RNA has a diameter of 2.4 nm. The length of RNA molecules often exceed the RNA helix diameter of 2.4 nm and can therefore not considered spherical.

In Table 8 the apparent hydrodynamic radii for hairpin and duplex formation are given, calculated with respect to *q* using the spherical model or the symmetrical cylinder model, respectively, together with the experimental data obtained by DOSY and DLS measurements. As *q* for d3'-EBS1* in the case of a hairpin is with a value of 2.08 close to 2 the apparent hydrodynamic radius was calculated with both models. Judging from the obtained hydrodynamic radii from the measurements, the spherical model for a hairpin is in good agreement with the value obtained by DOSY and the symmetrical cylinder model fits better to the value obtained from DLS measurments. However, the theoretical hydrodynamic radius for a duplex calculated with the symmetrical cylinder model is also in good agreement with the experimental DOSY-values of d3'-EBS1*. Since in the case of d3'-EBS1* the DOSY-values fit within the error limits to a hairpin as well as to a duplex (when different models are used), a distinction between hairpin and duplex in this case cannot be made. However, the values obtained for d3'-EBS1*·IBS1* clearly show that the experimental DOSY values fit to the hydrodynamic radius of a hairpin. Since the only difference between d3'-EBS1*·IBS1* and d3'-EBS1* is the additional 7-mer IBS1*, it is expected that the d3'-EBS1* part behaves correspondingly in both constructs. Therefore, it can be concluded that d3'-EBS1* prefers to

Table 8 Hydrodynamic radii r_H of EBS1*·IBS1*, d3'-TL, d3'-EBS1* and d3'-EBS1*·IBS1* as determined by DLS ($r_{H,DLS}$) and DOSY ($r_{H,DOSY}$) experiments. Shown are also the length L as measured from the PDB file of the lowest energy solution structure, the ratio q = L/d (with d = 2.4 nm being the diameter of A-RNA), and the theoretical hydrodynamic radius r_H of a hairpin. The latter was calculated according to a spherical model for q < 2 or to a symmetrical cylinder model for q > 2.

[nm]	Hairpin			Duplex			$r_{H,DOSY}$	$r_{H,DLS}$[c]
	L	q	r_H	L	q	r_H		
EBS1*·IBS1*	–	–	–	2.60	1.08	1.30[a]	1.78 ± 0.08 (25°C) 1.92 ± 0.20 (20°C)	1.67 ± 0.03 (25°C) 1.71 ± 0.03 (20°C)
d3'-TL	3.80	1.58	1.90[a]	7.60	3.17	2.33[b]	2.34 ± 0.12 (25°C) 2.32 ± 0.10 (20°C)	1.49 ± 0.01 (25°C) 1.49 ± 0.01 (20°C)
d3'-EBS1*	5.00	2.08	2.50[a] 1.93[b]	10.0	4.17	2.67[b]	2.42 ± 0.20 (25°C) 2.67 ± 0.15 (20°C)	1.59 ± 0.01 (25°C) 1.61 ± 0.02 (20°C)
d3'-EBS1*·IBS1*	6.20	2.58	2.49[b]	12.4	5.17	3.01[b]	2.52 ± 0.18 (25°C) 2.69 ± 0.20 (20°C)	2.06 ± 0.01 (25°C) 1.96 ± 0.02 (20°C)

[a] r_H values were calculated according the spherical cylinder model. [b] r_H values were calculated according the symmetrical cylinder model. [c] All values are average values of at least five measurements. Errors given correspond to one standard deviation.

form a hairpin. This assumption is corroborated by the DLS measurements, which give values closer to the theoretical hydrodynamic radius of a hairpin (Table 8). These results show that distinction between hairpin and duplex highly depends on the size of the molecule and the chosen model. In addition, the values obtained by DOSY measurements show that indeed the size of EBS1*·IBS1* < d3'-TL < d3'-EBS1* < d3'-EBS1*·IBS1* (Table 8). For the DLS mesurements this trend is only observed for the hairpin structures d3'-TL, d3'-EBS1*, and d3'-EBS1*·IBS1*.

Taken together, the results of the concentration dependent UV melting studies, the X-filter-NOESY-HSQC experiments, the DOSY and DLS measurements proof that indeed d3'-EBS1* forms a stable hairpin in solution under the above mentioned conditions.

2.2.5 Spectral features of d3'-EBS1* and comparison with wt-d3'-EBS1

It is assumed that the change of the two nucleotides in d3'-EBS1* does not have any influence on the flexibility of the loop in the absence of IBS1*. This assumption is confirmed by comparison of the imino region of 2D [^{1}H,^{1}H]-NOESY spectra acquired in 90% H_2O/10% D_2O (Figure 38). Both imino regions show the same pattern for the helical part of the hairpin showing eight Watson-Crick base pairs and only one strong crosspeak originating from a G-U wobble pair. This implicates that the loop region does not form any further base pairs as it was proposed by theoretical folding, which was performed with the mfold server (http://frontend.bioinfo.rpi.edu/applications/mfold/cgi-bin/rna-form1.cgi).[26,310] Figure 39 shows the possibilities and the corresponding energies for the different conformations of wt-d3'-EBS1 and the modified d3'-EBS1*. The mfold server suggests three possibilities how the bases in the loop can be arranged. Besides the existence of a big loop consisting of 11 nucleotides, two or even three additional basepairs can be formed, both including a bulged adenosine at position 10. G-U wobble pairs show the strongest crosspeak in the imino region

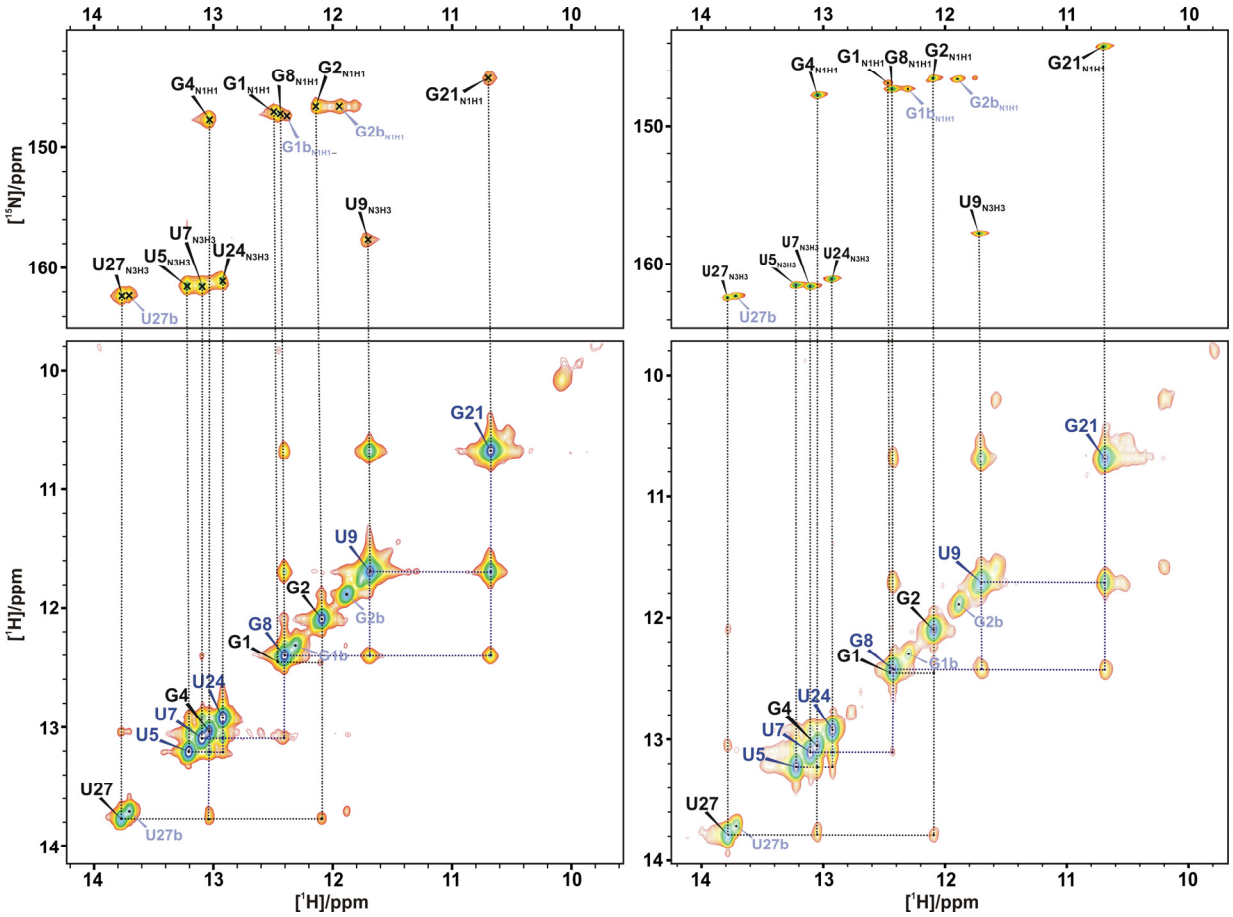

Figure 38 Assignment of imino resonances in d3'-EBS1 (left) and d3'-EBS1* (right). The imino section of the 2D [^{1}H,^{1}H]-NOESY spectra acquired in 90% H_2O/10% D_2O at 278 K is shown in the lower panel and the corresponding section of the 2D [^{1}H,^{15}N]-HSQC at 278 K in the upper panel. The letter "b" indicates the resonances of the n+1 derivative, which gives additional resonances for G1, G2 and U27 in the imino spectra.

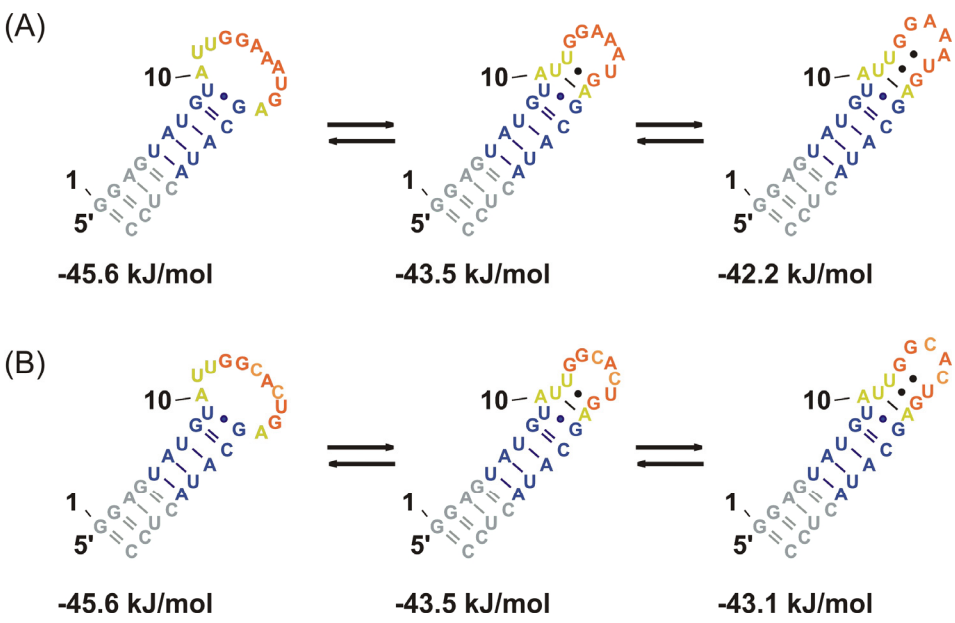

Figure 39 Secondary structures of the possible conformations of the wildtype d3'-EBS1 (A) and the altered d3'-EBS1* (B) as predicted by mfold.[26,310] The given ΔG_{37} values were calculated for the folding at 37 °C in 1 M NaCl being the standard conditions used in mfold.

of 2D [^{1}H,^{1}H]-NOESY spectra, therefore the existence of either one, two or three G-U wobbles can be easily distinguished. As clearly only one strong crosspeak is observed, indeed a 11 nucleotide long unpaired loop prior to IBS1* binding is present in solution. The absence of crosspeaks for the imino protons of the loop indicates that these protons are in fast exchange with the solvent, i.e. no hydrogen bonds are formed. Only one additional small crosspeak in d3'-EBS1* was observed at 10.2 ppm. It was not possible to assign this peak to a specific proton, but it is assumed that it belongs to the loop region. Thus, indicating that in the altered d3'-EBS1* construct the residues in the loop have the possibility to be closer in space due to the smaller sterical hindrance of cytosine than adenosine. A 2D J_{NN} HNN-COSY[118] confirms the Watson-Crick base pairs (Appendix 4). GU wobble pairs cannot be seen in this experiment because a hydrogen bond from an imino-NH to another N across the helix does not exist in such a conformation. The lack of observable imino resonances for the loop makes the structure determination extremely challenging, since NOE distance restraints have to be solely derived from non-exchangeable protons. Furthermore no additional hydrogen bond restraints can be included for the loop residues in the structure calculation.

A striking observation was made in the imino region: two resonances each were found for G1, G2 and U27 (Figure 38). These peaks were assigned to a RNA, which has a n+1 nucleotide, i.e. 30 nt, due to transcription. It is known that T7 RNA polymerase tends to add random nucleotides to the 3'-terminus of "run-off" transcripts.[290] By running the complete transcription solution on a 15% PAGE gel, it was not possible to separate the n+1 band from the 29 nucleotide long RNA due to the very good transcription yields of the d3'-EBS1* construct. In order to enhance the separation, only small amounts of the transcription solution

were applied to a 15% PAGE. To yield sufficient RNA for a NMR sample this procedure was performed several times. With this method the two bands were relatively good separated. 2D [^{1}H,^{1}H]-NOESY spectra in 90% H_2O/10% D_2O of the separated samples were acquired in order to confirm and assign the doubled resonances of G1, G2 and U27. The spectra with the corresponding assignment is shown in Appendix 1. Comparison of 2D [^{1}H,^{1}H]-NOESY spectra acquired in D_2O of the separated and the non-separated RNA species show that the chemical shifts are not influenced, thus indicatig that the structure of the RNA is not affected when n+1 is present. In addition, no resonance for a 30th nucleotide was observed as well as no second resonances for the beginning or the ending.

The modified d3'-EBS1* construct shows, like the wt-d3'-EBS1, severe overlap in the sequential walk region (Figure 41C). With common NTPs it was not possible to perform the complete and unambiguous sequential assignment. The sequential assignment could only be done for the helical part as it does not differ from the one of wt-d3'-EBS1 and d3'-TL (see Section 2.1 and 2.3.1). Therefore, transcription of d3'-EBS1* was performed with selectively deuterated NTPs, which were just newly commercially available. These deuterated NTPs (Figure 40) are labeled at the position 5 of the bases U and C and at position 3', 4', 5' and 5'' of the sugar moieties. With the deuterated RNA greatly simplified 2D [^{1}H,^{1}H]-NOESY spectra were achieved (Figure 41). The spectral overlap for the crowded ribose region is significantly reduced allowing the complete assignment of the spectrum of d3'-EBS1* (see Appendix 2 for chemical shifts). In the H1'-H2' region (Figure 41B) 29 strong crosspeaks were observed, which could be assigned to each single residue. The sequential walk was assigned from the bases to the H1' (Figure 41D) as well as to H2' (Figure 41F).

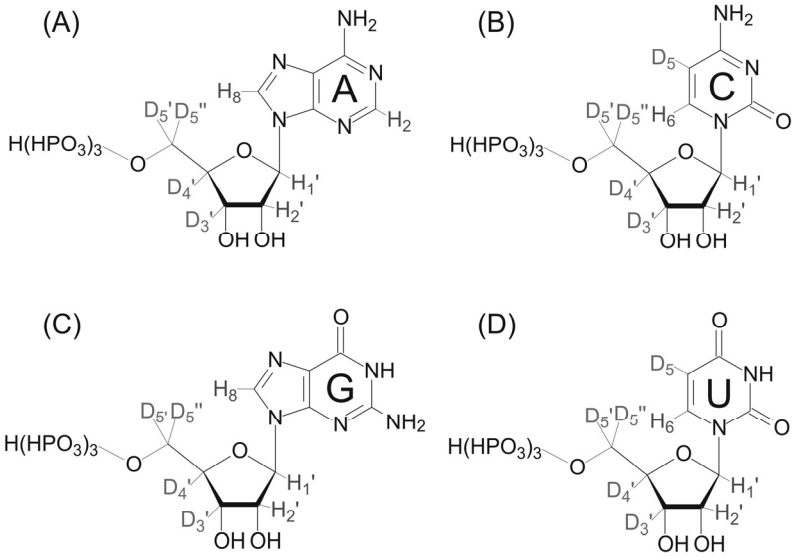

Figure 40 Selectively deuterated ribonucleotides. (A) Adenosine triphosphate, (B) Cytidine triphosphate, (C) Guanosine triphosphate, and (D) Uridine triphosphate are shown. The use of these NTPs significantly reduces the spectral overlap for the crowded ribose region. The D5-labeled nucleotides were supplied as an equimolar mixture of the ammonium salts of ATP, CTP, GTP, and UTP and were used in the transcription using T7 RNA polymerase.

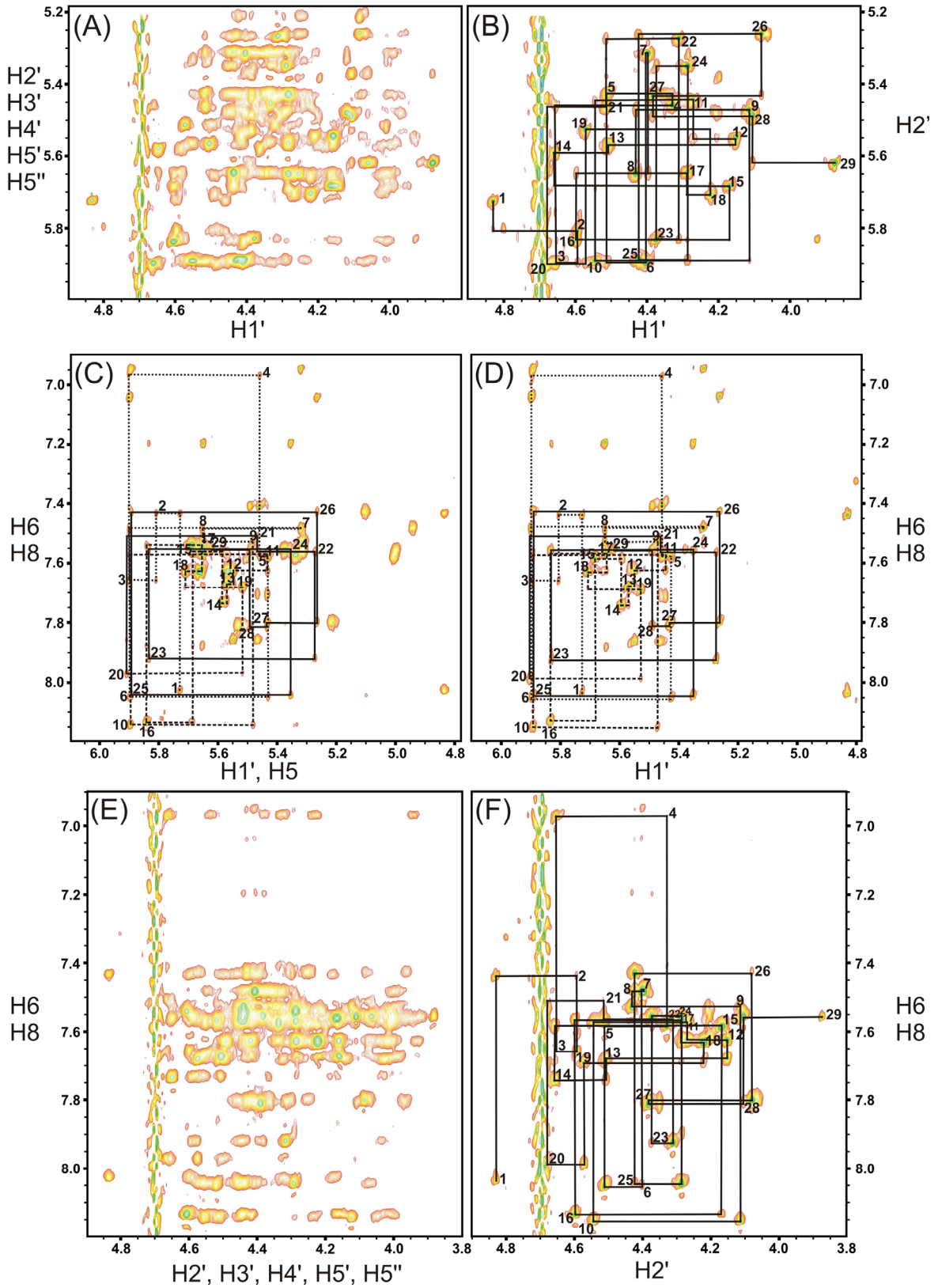

Figure 41 2D [^{1}H,^{1}H]-NOESY spectra of d3'-EBS1*. Spectra on the left are from unlabeled RNA (A, C, E) and spectra on the right are from deuterated RNA (B, D, F). The top two panels (A, B) show NOEs between the H1' proton and all other ribose protons. The middle two panels (C, D) show NOEs between the base protons and H1' protons. The bottom two panels (E, F) show NOEs between the base and other ribose protons. The sequential assignment of inter- and intranucleotide NOEs is shown for the deuterated d3'-EBS1* as well as for the sequential walk region between H1' and H6/H8 of the non-deuterated d3'-EBS1* (C).

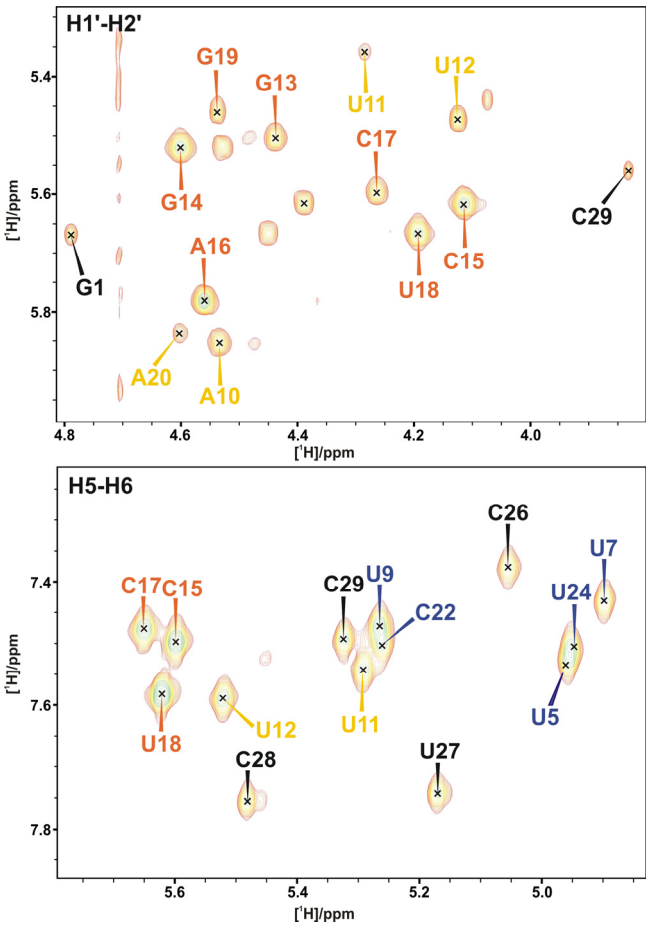

Figure 42 Two sections of the 2D [^{1}H,^{1}H]-TOCSY of d3'-EBS1*. The upper panel shows the H1'-H2' crosspeaks that indicate a 2'-endo sugar conformation. In d3'-EBS1* such a sugar pucker is found at the helix end (black), and in the loop (yellow and orange). The H5-H6 crosspeaks of d3'-EBS1* are shown in the lower panel. These crosspeaks help to assign the pyrimidines in the 2D [^{1}H,^{1}H]-NOESY. The colouring scheme corresponds to Figure 30.

At this point it has to be noted that for the loop region the internucleotide crosspeaks were very weak indicating that the loop does not adopt a rigid structure as it was already shown by the imino region of 2D [^{1}H,^{1}H]-NOESY spectra acquired in 90% H_2O/10% D_2O. This is also confirmed by the chemical shift pattern of the adenosine H2 protons. The H2s of A10, A16, and A20 that belong to the loop resonate between 7.69 and 7.82 ppm (Appendix 35). This shift is more downfield than H2 located in an AU base pair but still more upfield than the adenosine H2 protons of GAAA tetraloops which are flipped out[34,115] (see Appendix 35 for comparison of chemical shifts). Such a chemical shift pattern indicates that A10, A16 and A20 are neither fully buried within the helix nor flipped out.

With the help of the spectra of the deuterated sample, the spectra of the non-deuterated sample could be assigned and even most of the other sugar protons (H3', H4', H5', and H5''; Appendix 2). Most of the C1', C2, C5, C6, and C8 carbon resonances could be assigned by 2D [^{1}H,^{13}C]-HSQCs (Appendix 3). These experiments also helped to assign and confirm the corresponding protons.

With the help of 2D [^{1}H,^{1}H]-TOCSY spectra the sugar conformation can be elucidated. A strong H1'-H2' crosspeak indicates a 2'-endo conformation (also known as south conformation), which is usually present in B-DNA. The absence of a H1'-H2' crosspeak reveals a 3'-endo conformation (also known as north conformation), which is in general present in A-form RNA and A-form DNA. The 2D [^{1}H,^{1}H]-TOCSY experiment of d3'-EBS1* (Figure 42) confirmed a 3'-endo sugar pucker conformation for most of the helical part. The sugar puckers of G1, and C29 as well as A10 to A20 of the loop showed H1'-H2' crosspeaks in the 2D [^{1}H,^{1}H]-TOCSY and were left unconstrained in the structure calculation. 2D

[^{1}H,^{1}H]-TOCSY experiments comprise a second important region, in which H5-H6 resonates. This region not only helps to assign the H5-H6 resonances in 2D [^{1}H,^{1}H]-NOESY spectra, but also give a quick and easy way to confirm the number of pyrimidines in the RNA.

2.2.6 Residual dipolar couplings of d3'-EBS1* and d3'-EBS1*·IBS1*

This section deals with the theory, measurement and implementation of residual dipolar couplings (RDCs) into a structure calculation. Solving a solution structure primarily relies on measuring a large number of cross-relaxation effects (NOEs) between protons, which are close in space (<5-6 Å), yielding approximate distance information.(123) These restraints are mainly derived from NOEs between sequential nucleotides or neighbouring base pairs giving only information about the local geometry, but making the definition of global structure difficult. Solution structures, which base only on NOEs can therefore result in ill-defined relative orientation of distant regions towards each other (like two helices in RNAs). Protein structures, in which only NOEs and torsion angle restraints were included are often more well defined than solution structures of nucleic acids of the same size. The main reason is the lower proton density for nucleic acids (0.35 protons/atom) compared to proteins (0.52 protons/atom).(311) It has been shown that standard NMR methods define very well local conformational parameters like sugar pucker and glycosidic torsion angle, but long-range parameters like helical twist, helical rise, and backbone torsion angles are less well defined.(312) The definition of the global conformation becomes increasingly difficult as molecular size increases. In addition, in larger protonated molecules NOEs become difficult to measure due to prohibitive transverse relaxation effects.(313) Therefore it was necessary to develop new approaches for the structure determination of larger biomolecules such as the introduction of RDCs.

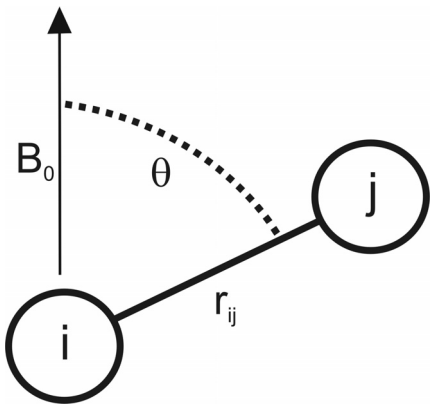

Figure 43 Schematic representation of the orientation of two spins i and j in an external magnetic field B_0. r_{ij} represents the distance between the spins and θ the angle between r_{ij} and B_0. Residual dipolar couplings only depent on the orientation of the internuclear vector $\vec{ij}$ in solution because i and j are covalently bound and therefore r_{ij} is constant.

The dipolar contribution derives from the magnetic dipole-dipole interaction between two spins i and j.(314) This dipolar interaction is dependent on the angle θ between the internuclear vector and the external magnetic field B_0 and on the distance r between the two nuclei as described in equation 5. The latter does not have to be taken into account as residual dipolar

couplings are usually measured between two nuclei at a fixed distance, such as ^{1}H-^{15}N or ^{1}H-^{13}C bonds (Figure 43).[315,316]

$$D_{ij} = -\frac{\gamma_i \gamma_j}{8\pi^3}\left\langle \frac{3\cos^2\theta - 1}{2r_{ij}^3} \right\rangle \qquad \text{equation 5}$$

where γ_i and γ_j are the gyromagnetic ratios of the two nuclei i and j. In solution, dipolar couplings average to zero due to the fast molecular tumbling and thus cannot be measured by standard NMR methods. RDCs can only be observed in anisotropic solutions. Therefore, alignment media have to be introduced to partially orient the macromolecules and thus to measure RDCs. In the presence of such an alignment medium the contribution of RDCs can be directly observed by NMR and provide additional distance and angle information. The alignment medium used in this study was filamentous bacteriophage Pf1. Pf1 phages consist of single-stranded, circular DNA, which is surrounded by α-helical coat proteins.[317] They measure about 60 Å in diameter and 20000 Å in length and align in magnetic fields orienting with its long axis parallel to the magnetic field.[318] These rod-like phages align even at low field strengthes (300 MHz) and the degree of alignment can be adjusted by simply changing the phage concentration.[315,319,320] 1D ^{2}H spectra of 90% H_2O/10% D_2O at different phage concentrations were recorded to find the right phage concentration for an appropriate final splitting. The 1D ^{2}H spectra of 90% H_2O/10% D_2O containing 17 mg/ml and 25.6 mg/ml Pf1 phage, respectively, are shown in Figure 44. The splitting of the HOD signal arises from the large deuterium quadrupole moment that is not isotropically averaged for water bound to the aligned phages. The observed line splitting is with 9.7 Hz at 17 mg/ml phage smaller than at 25.6 mg/ml phage, which shows a line splitting of 24.2 Hz. The order of sufficient line splitting for measuring RDCs is around 20 Hz. Due to the desired degree of line splitting a phage concentration of 25.6 mg/ml phage was used in this study.

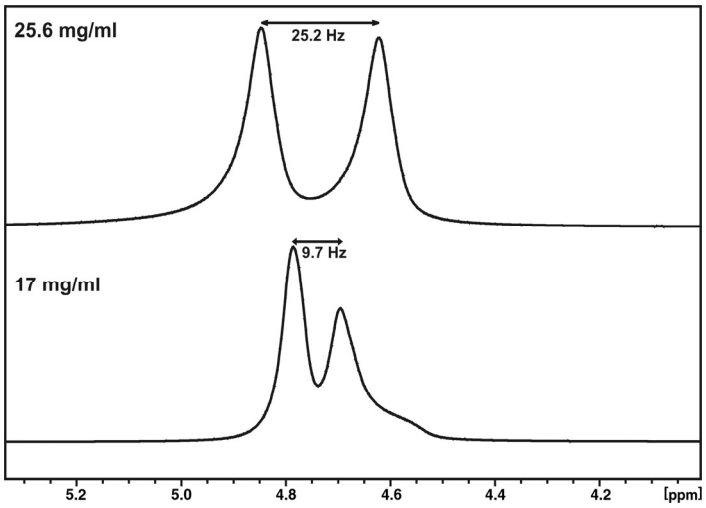

Figure 44 1D ^{2}H spectra of 90% H_2O/10% D_2O containing 17 mg/ml (lower panel) and 25.6mg/ml (upper panel) Pf1 phage. These spactra were collected at 700 MHz at 298 K with 4 scans. The vertical scales of the individual spectra were adjusted in order to get the same heights for both spectra.

Pf1 phages are stable over a wide range of temperature (5-45 °C), pH and buffer conditions[315,319,320] and thus have benefits compared to other alignment media, e.g. liquid crystalline bicelles.[321] Phages have a

negatively charged surface at physiological pH and therefore do not bind to the negatively charged RNA. Alignment results from collisions that occur between the RNA and the surface of the aligned phage particles.[320] It has been shown that the relaxation times for individual imino nitrogens are identical in the absence and presence of Pf1 phage, thus demonstrating that the phage does not have a measurable effect on the rotational correlation time and therefore high resolution spectra can be obtained.[319]

The observed residual dipolar coupling between two nuclei can also be described by:[321]

$$D_{ij} = S\frac{\mu_0}{4\pi}\gamma_i\gamma_j h\left[D_A\left(3\cos^2\theta - 1\right) + \frac{3}{2}R\sin^2\theta\cos 2\phi\right]4\pi^2 r_{ij}^3 \qquad \text{equation 6}$$

D_A and R are the axially symmetric and rhombic components of the molecular alignment tensor of the macromolecule, respectively. S is the generalized order parameter for internal motions of the $\vec{ij}$ vector, θ and ϕ are the spherical coordinates describing the orientation of the vector $\vec{ij}$ in the principal axis system of the alignment tensor. μ_0 is the magnetic permeability of vacuum and h the Planck constant. The only dependence of D_{ij} is the orientation of the internuclear vector in respect to the magnetic field (see above).

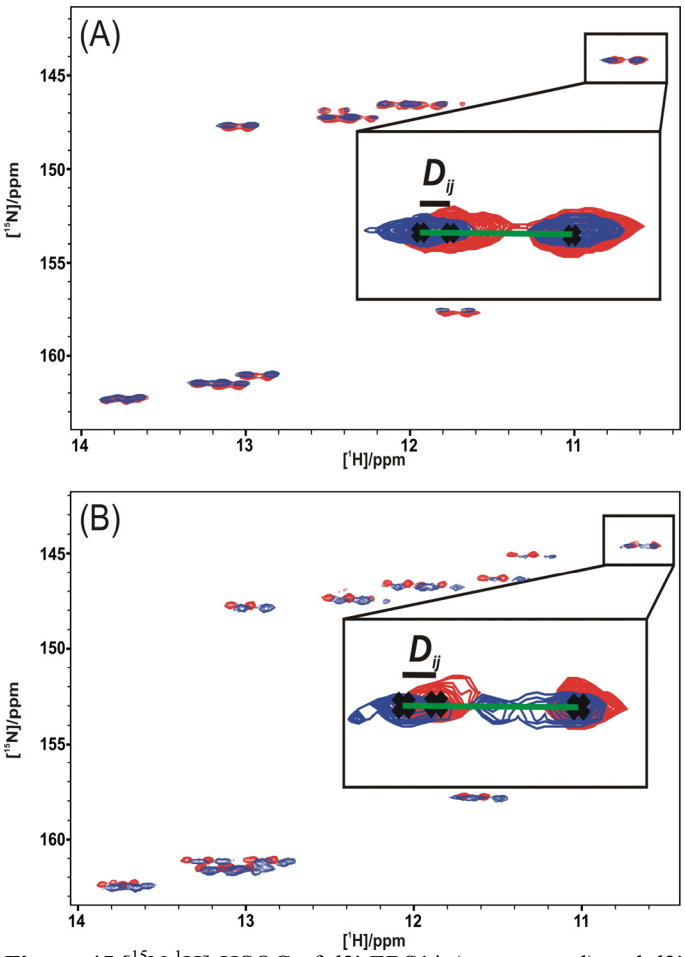

Figure 45 [^{15}N,^{1}H]-HSQC of d3'-EBS1* (upper panel) and d3'-EBS1*·IBS1* (lower panel) with (blue) and without (red) Pf1 phage with the decoupling turned off in the f2 dimension. An example of extracting RDCs is shown: the green line shows the combined spin-spin and residual dipolar couplings ($^{1}J_{ij}$+D_{ij}), and the black line only the RDC contribution D_{ij}.

Various 2D [^{1}H,^{13}C]-HSQC and 2D [^{1}H,^{15}N]-HSQC spectra were recorded to extract RDCs for the structure calculation. In these HSQCs, a 180° pulse in the middle of the evolution period of the second nucleus is omitted to provide $^{1}J_{ij}$ and $^{1}J_{ij}$+D_{ij} coupled spectra. An example of extracting RDCs is shown in Figure 45. At first, HSQCs of d3'-EBS1* as well as for d3'-EBS1*·IBS1* were recorded in isotropic solution, i.e. without phages, with the decoupling in one dimension turned off. From these spectra the spin-spin couplings ($^{1}J_{ij}$) were extracted. Accordingly, HSQCs

of the two constructs were recorded in anisotropic solution, i.e. with phages and the combined spin-spin and residual dipolar couplings ($^1J_{ij}+D_{ij}$) were extracted. The dipolar contribution can now be calculated by:

$$(^1J_{ij}+D_{ij}) - (^1J_{ij}) = (D_{ij}) \qquad \text{equation 7}$$

In general, RDCs can be obtained with this method, but a disadvantage of the frequency-based method is the probability of highly overlapped spectra. Especially for large RNA molecules the extraction of ^1H-^{13}C residual dipolar couplings is difficult. For ^1H-^{15}N residual dipolar couplings the frequency based method can be easily used as these spectra are usually well resolved (Figure 45). An alternative method for the determination of RDCs are *J*-modulated HSQC experiments. In these experiments the observed signal is passed through a period, in which the intensity is modulated by a known function of the spin-spin coupling. An array of 2D spectra with incremented t1 delays is recorded, from which the coupling constants ($^1J_{ij}$) and ($^1J_{ij}+D_{ij}$) can be measured.[322]

The axial and rhombic components D_A and R of the alignment tensor are constant for the whole molecule and were obtained by a manual gridsearch, i.e. calculating a series of structure ensembles for different estimates of D_a and R. The final values for D_a and R, which were used in the final structure calculation, were taken from the gridsearch, which provided the lowest energies. Starting values for D_a and R were obtained by the program PALES (prediction of alignment from structure).[323,324] This software is used for the analysis of residual dipolar couplings and contains the PALES simulation, which predicts the magnitude and orientation of a sterically induced alignment tensor from a pdb input structure. Experimentally determined RDC values were compared to the ones calculated by PALES (Figure 46). Values, which differed in a high degree, were not included in the structure calculation. In total, 28 RDCs were obtained for d3'-EBS1*, of which 18 are ^1H-^{13}C- and 10 ^1H-^{15}N- based (Appendix 7), and for the full construct d3'-EBS1*·IBS1* 37 RDCs were included into the final structure calculation, 26 ^1H-^{13}C and 11 ^1H-^{15}N residual dipolar couplings (Appendix 18). For the final structure calculation of d3'-EBS1* see Section 2.2.7 and for d3'-EBS1*·IBS1* Section 2.2.9.

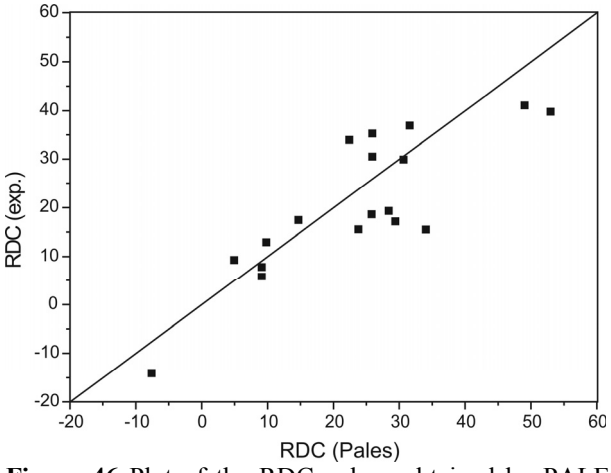

Figure 46 Plot of the RDC values obtained by PALES versus the experimental ones. Shown is one example of d3'-EBS1* for one input structure. 25 pdb input structures were tested in total.

2.2.7 The solution structure of d3'-EBS1*

The structure determination of d3'-EBS1* was performed by including 514 conformationally restrictive NOE distance restraints collected from 2D [^{1}H,^{1}H]-NOESY spectra in 100% D_2O as well as in 90% H_2O/10% D_2O and 28 RDC constraints (Table 9, appendices 6 and 7, for calculation details see Materials and Methods). d3'-EBS1* adopts a stable hairpin structure closed by the 11 nucleotide long loop including EBS1*, which is in the absence of IBS1* rather flexible. The relatively low number of NOEs per residue of 17.72

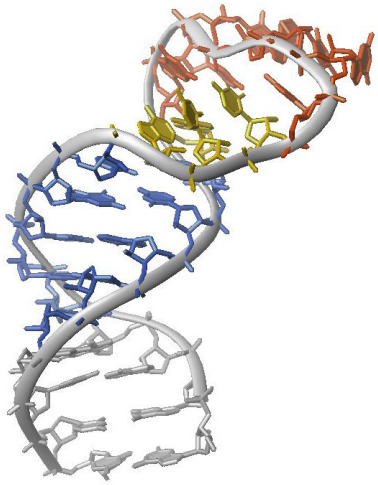

Figure 47 Lowest energy structure of d3'-EBS1* out of 200 calculated.

Table 9 NMR restraints and structural statistics for the d3'-EBS1* structure.[a]

	With RDCs	Without RDCs
NOE-derived distance restraints	514	514
Intranucleotide	178	178
Internucleotide ($\|i - j\| = 1$)	252	252
Long-range ($\|i - n\| \geq 2$)	84	84
Repulsive	0	0
NOE restraints per residue		
Total	17.72	17.72
Helix (1-9, 21-29)	20.17	20.17
Loop (10-20)	13.72	13.72
Dihedral restraints	180	180
Hydrogen bond restraints	45	45
Dipolar coupling restraints	28	0
r.m.s.d. (for all heavy atoms to the best structure (Å))		
Overall	2.06 ± 0.86	2.50 ± 0.65
Helix (1-9, 21-29)	0.41 ± 0.10	0.81 ± 0.35
Loop (10-20)	2.59 ± 1.23	2.73 ± 1.03
NOE violations > 0.2 Å	0	0
Dihedral violations > 5°	0	0

[a]All statistics are given for the 20 lowest energy structures out of 200 calculated structures.

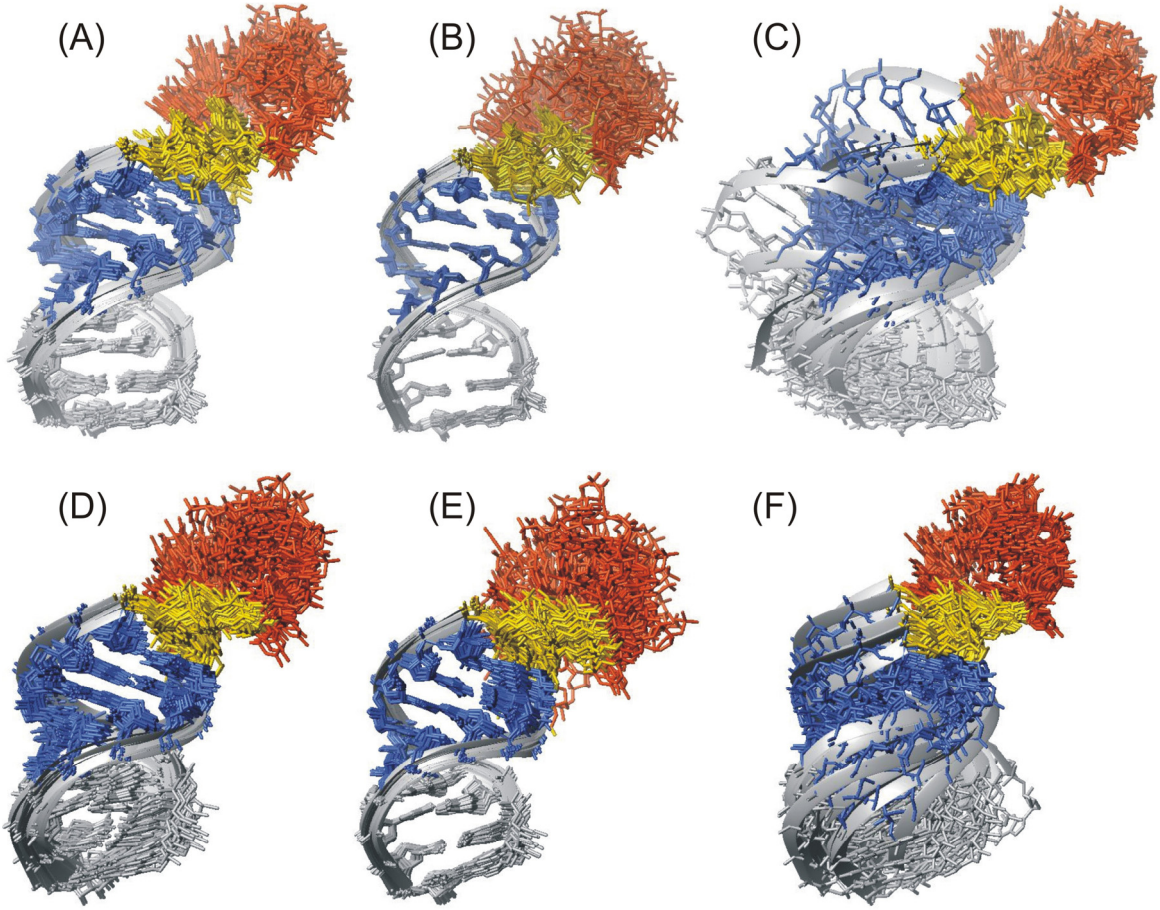

Figure 48 Solution structure of d3'-EBS1* as determined by NMR. The upper panel shows the 20 lowest energy structures of d3'-EBS1* with residual dipolar couplings, the lower panel the ones without residual dipolar couplings. (A and D) Overall superposition of all heavy atoms in d3'-EBS1*. (B and E) Superposition of all heavy atoms in the stem (nucleotides 1-9, and 21-29) of d3'-EBS1* of the 20 lowest energy structures. (C and F) Superposition of all heavy atoms in the loop (nucleotides 10-20) of d3'-EBS1* of the 20 lowest energy structures.

derives from the unstructured loop region, for which only 13.72 NOEs per residue were observed in comparison to the helix where 20.16 were found. As already shown by the base pairing situation (see Section 2.2.5), the loop does not adopt a rigid structure, thus being rather flexible and free to bind IBS1*. The overall r.m.s. deviation of all heavy atoms from the 20 lowest energy structures with the inclusion of RDCs is with 2.06 ± 0.86 Å rather low compared to the r.m.s. deviation for the 20 lowest energy structures without RDCs with 2.50 ± 0.65 Å (Table 9, Figure 48). However, independent superposition of the helical region (nucleotides 1-9 and 21-29) results in much lower r.m.s. deviations in both cases, whereas the independent superposition of the loop (nucleotides 10-20) gives much higher r.m.s. deviations (Table 9, Figure 48B, C, E, and F, and Figure 48).

The loop is the least well defined part of d3'-EBS1*. The reasons for the relatively poor definition of the loop are twofold. First, as already mentioned, distance constraints for the amino and imino protons could not be obtained due to the fast exchange rate of these protons with the solvent (see Section 2.2.5). Second, the majority of the assigned NOEs to the loop

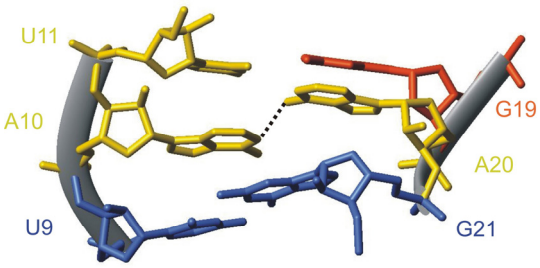

Figure 49 Section of d3'-EBS1* of the lowest energy structure showing the first and the last nucleotide of the loop A10 and A20 pointing into the inside of the loop, a possible hydrogen bond is visualized.

are either intranucleotide or between sequential nucleotides, and therefore are not useful in defining tertiary structural features.

However, apart from the overall unpaired situation in the loop, some special structural features can be discovered in the loop within the 20 lowest energy structures. The stem leading to the loop is closed by the U9-G21 wobble pair. The bases of A10 and A20, being the first and the last nucleotide of the loop, are pointing towards each other on the inside of the loop (Figure 49), but they are not completely buried as it has been already shown by the chemical shift pattern of H2 resonances described in Section 2.2.5. A10 remains partly stacked onto U9 defined by five NOE cross peaks associated with non-exchangeable protons as well as A20 onto G21, which is defined by seven NOEs. In the 20 lowest energy structures these stacking interactions are pronounced differently illustrating the loop flexibility. The arrangement of A10 and A20 is also confirmed by the observation of crosspeaks between A10H2 and A20H2 as well as A10H2 and G21H1' in the 2D [^{1}H,^{1}H]-NOESY spectrum in 100% D_2O (see Appendix 6). All other nucleotides in the loop show no specific arrangements. The bases belonging to EBS1* are in majority protruded being therefore solvent exposed. This also explains the absence of observable imino proton resonances for the loop region, because they are in fast exchange with the solvent and thus not detectable on the NMR timescale. These structural observations have immediate biological implications. The major function of the EBS1* is to recognize the substrate, thus building tertiary contacts. Therefore the loop is in a favoured position to bind IBS1* when it comprises a certain flexibility to expose the bases to the outside.

The only known structure of a full group II intron ribozyme and thus also of the hairpin including the exon binding site 1 was just published recently.[(249)] The crystal structure of an intact, self-spliced group II intron from *Oceanobacillus iheyensis* was solved at 3.1 Å resolution (see also Introduction Section 1.3.2.). The exon binding site in this system comprises only four nucleotides (AUAA) and is located in a loop of eight nucleotides (Figure 50). The stem of the hairpin consists only of four base pairs starting with a GC base pair and followed by three AU base pairs. The last four nucleotides in the loop, of which two belong to EBS1, show partial stacking interactions. In contrast to this the first four nucleotides are completely unstructured, of which U182 is missing due to lacking electron density. A

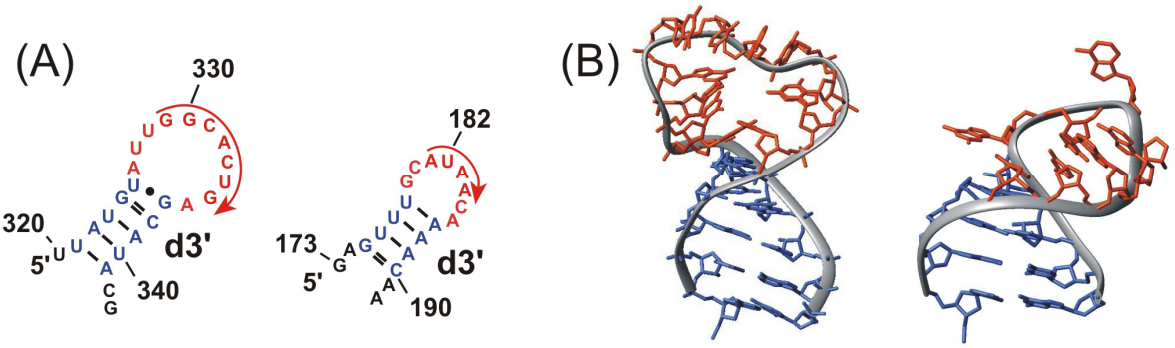

Figure 50 Comparison of (A) the secondary structures of d3'-EBS1* (left) together with the section of the hairpin including EBS1 of the group II intron from *Oceanobacillus iheyensis*[249] (right) and (B) of the solution structure of d3'-EBS1* (left) with the crystal structure of the corresponding section (right). The nucleotides in the loop are coloured in red and the d3'-stem nucleotides in blue. EBS1 is indicated by a red arrow. Numbering of the nucleotides corresponds to the one in the full ribozymes.

comparison of the crystal structure with d3'-EBS1* is shown in Figure 50. Both structures show a stable stem but for the loop only some partial stacking interactions. Unfortunately no conclusion about the relevance of the partial stacking can be drawn from this structures as they differ from each other not only in the stacking situation of the loop but also in their size.

2.2.8 Spectral features of d3'-EBS1*·IBS1*

In order to solve the solution structure of the full d3'-EBS1*·IBS1* construct (Figure 51), IBS1* (numbered 59-65) was added in a 1:1 ratio to d3'-EBS1*. First NMR measurements resulted in very well resolved spectra. Even without the help of partially deuterated samples the sequential walk could be completely assigned. Figure 52A shows the sequential walk region and its assignment of d3'-EBS1*·IBS1*. It can be easily seen that even with the addition of seven nucleotides the resolution of the spectra is much better than in the absence of IBS1*. This is due to the formation of a second helix and this includes the stabilization of the loop leading to a well structured part, which is confirmed by the very good dispersion of the resonances throughout the spectrum. With 2D [^{1}H,^{1}H]-NOESY spectra that were acquired at different temperatures and mixing times (see Materials and Methods) all H1', H2, H5, H6, and H8 protons could be assigned (Appendix 13). The H2' sugar protons were assigned by using a deuterated sample. The H3' resonances were then assigned with the help of 2D [^{1}H,^{1}H]-NOESY spectra with 60 ms and 120 ms mixing time. Subsequently, the assignment of most other sugar protons became possible (H4', H5', and H5''; Appendix 13).

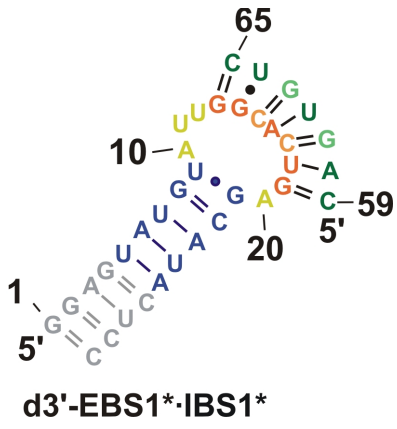

Figure 51 Secondary structure of d3'-EBS1*·IBS1*. The colouring scheme corresponds to Figure 30.

To confirm the sequential walk of IBS1*, a phase sensitive ge-2D w_1,w_2 $^{13}C,^{15}N$-filtered/edited-NOESY experiment using a watergate H_2O suppression was recorded.(325-328) In this spectrum only protons that are bound to ^{14}N or ^{12}C are detected, but they have to interact through H-bonds with a $^{15}N,^{13}C$ labeled substrate. The X-filter is based on the evolution of $J_{(XH)}$ for ^{1}H-^{13}C systems whereas ^{1}H-^{12}C remains unaltered during a spin echo period. Thus, at the end of this period, ^{1}H-^{12}C is on the y-axis whereas ^{1}H-^{13}C is on the x-axis. A 90° proton pulse applied from the x or y axis rotates only one of these two magnetizations to the z-axis, whereas the other component remains in the transverse plane. This experiment is widely used to study protein-ligand complexes where the protein is $^{15}N,^{13}C$ labeled and the ligand is at natural abundance.(325-328) In our case, the hairpin d3'-EBS1* is $^{15}N,^{13}C$ labeled and IBS1* is at natural abundance, thus only NOEs of IBS1* are detected. Figure 52B shows the double filtered-NOESY spectrum and Figure 52C the corresponding TOCSY spectrum. The sequential walk of IBS1* is identical with the one in the NOESY of the completely unlabeled d3'-EBS1*·IBS1*, thus confirming the assignment. The TOCSY spectrum shows the four H5-H6 crosspeaks of the pyrimidines of IBS1*.

In Appendix 42 the double X half-filtered-NOESY-HSQC with ^{15}N as third dimension of

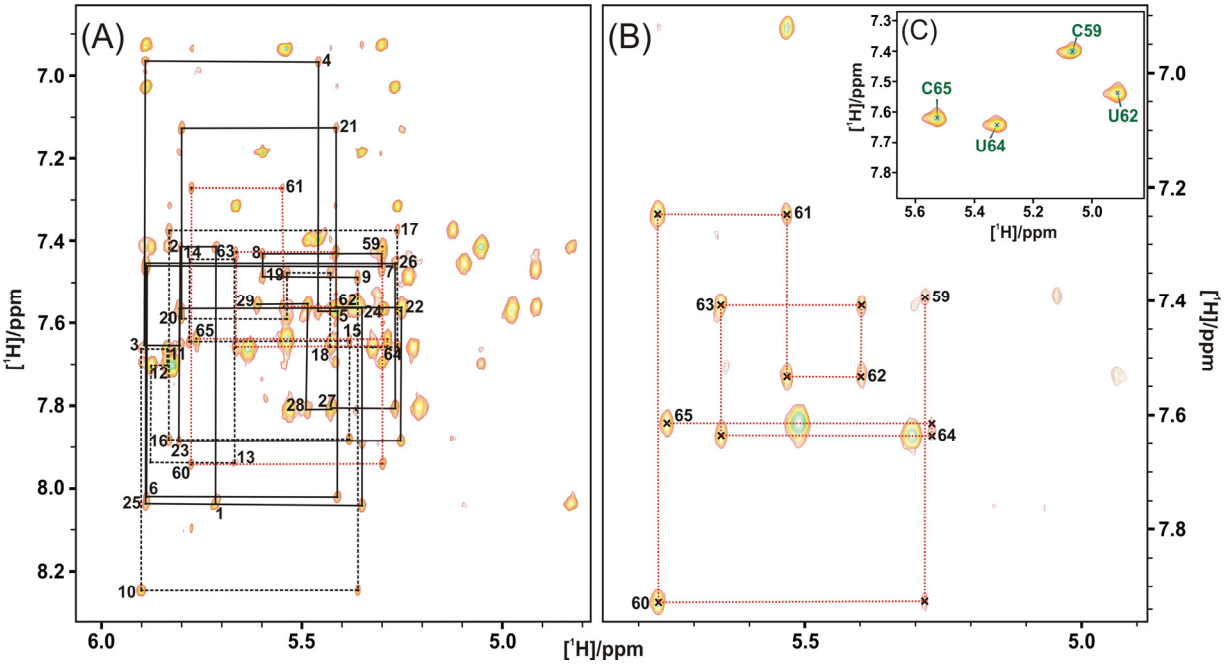

Figure 52 (A) 2D [$^{1}H,^{1}H$]-NOESY spectrum of the sequential walk region of d3'-EBS1*·IBS1* (100% D_2O, pD = 6.83, 110 mM KCl, 10 µM EDTA) recorded at 700 MHz and 298 K. The solid line shows the sequential walk through the helical region, black broken lines the one of the loop including EBS1*, and red dotted lines the one of IBS1. (B) ge-2D w_1,w_2 $^{13}C,^{15}N$-filtered-NOESY spectrum of d3'-EBS1*·IBS1* (90% H_2O/10% D_2O, pH = 6.45, 50 mM KCl, 10 µM EDTA) to detect the unlabeled IBS1* protons that are bound to labeled d3'-EBS1*. The sequential walk through IBS1* confirms the one in the 2D [$^{1}H,^{1}H$]-NOSEY spectrum of the unlabeled RNA. (C) Double filtered TOCSY spectrum of d3'-EBS1*·IBS1* (90% H_2O/10% D_2O, pH = 6.45, 50 mM KCl, 10 µM EDTA) showing the four H5-H6 resonances of the pyrimidines of IBS1*.

d3'-EBS1*·IBS1* is shown. Only resonances from the ^{15}N,^{13}C-labeled d3'-EBS1* to unlabeled IBS1* are visible. Resonances to H_2O from labeled d3'-EBS1* are also observed.

The chemical shift pattern of the adenosine H2 protons of A10, A16 and A20 in the absence of IBS1* resonates more downfield as the usual ones observed for AU base pairs (see Section 2.2.5, Appendix 35). Upon addition of IBS1* the chemical shift of A10H2 is hardly affected showing that A10 is still neither fully buried within the helix nor flipped out. In comparison the chemical shifts of A16H2 as well as A20H2 experience an upfield shift (Appendix 35). A16H2 shifts about 0.5 ppm upfield being now in the area where H2 resonances appear in AU base pairs. Since A16 basepairs with U62 this additionally shows that IBS1* binds to EBS1*. The resonance of the H2 of A20 shifts only about 0.2 ppm to smaller ppm values. A20 is not involved in a base pair but this intermediate shift shows that it is stuck in between two neighbouring base pairs.

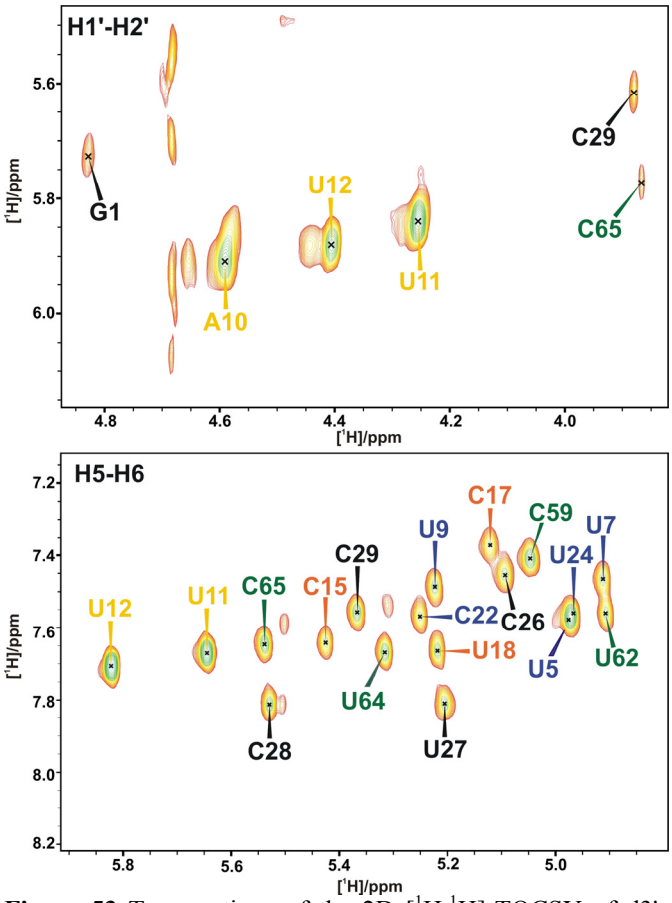

Figure 53 Two sections of the 2D [^{1}H,^{1}H]-TOCSY of d3'-EBS1*·IBS1*. The upper panel shows the H1'-H2' crosspeaks that indicate a 2'-endo sugar conformation. In d3'-EBS1*·IBS1* such a sugar pucker is found at the helix end (black), and in the unpaired nucleotides A10, U11 and U12 (yellow). The H5-H6 crosspeaks of d3'-EBS1* are shown in the lower panel. These crosspeaks help to assign the pyrimidines in the 2D [^{1}H,^{1}H]-NOESY.

Table 10 Unusual NOEs observed in the 2D [^{1}H,^{1}H]-NOESY from C59 to A10, U11, U12 and A20 (see also Appendix 17).

NOE from:	to:
A10H1'	C59H5, C59H6
A10H2'	C59H5
A10H2	C59H1', C59H2', C59H5, and C59H6
U11H1'	C59H1', C59H5, and C59H6
U11H5	C59H5
U11H6	C59H5 and C59H6
U12H1'	C59H1', C59H5, C59H6 and C59H5
U12H5	C59H5
U12H6	C59H5
A20H2	C59H1'

Very weak correlations for U12H6-G13H1', G13H8-H1', G13H8-G14H1' as well as for G14H8-H1' already indicate an unusual conformation in this region. NOEs were found from the unpaired nucleotides in the loop A10, U11, U12, and A20 to C59 of IBS1* and are listed

in Table 10. All these NOEs show that C59 is embedded within the loop pointing into the direction of the three unpaired nucleotides A10, U11, and U12 (see also Section 2.2.9 and Figure 58).

The sugar pucker of the individual residues was investigated by a 2D [^{1}H,^{1}H]-TOCSY experiment acquired at 298 K (Figure 53). Very strong H1'-H2' correlations were found for A10, U11, and U12. These nucleotides are besides A20 the only ones, which are not incorporated in a base pair. A H1'-H2' crosspeak is not found for A20, suggesting that this nucleotide is indeed stuck in between the flanking nucleotides and therefore connecting EBS1* to the stem in an A-form like manner (see Section 2.2.9). G1, C29 and C65 at the helical ends show a weak, but still visible H1'-H2' correlation. For C59 located at the 5'-end of IBS1* no H1'-H2' crosspeak is found, what one might have expected. As already mentioned C59 is pointing towards the middle of the loop thus being trapped. Figure 53 shows another region in the TOCSY spectrum that comprises H5-H6 correlations. 18 H5-H6 resonances of d3'-EBS1*·IBS1* were clearly observed, which confirm the assignments in 2D [^{1}H,^{1}H]-NOESY spectra.

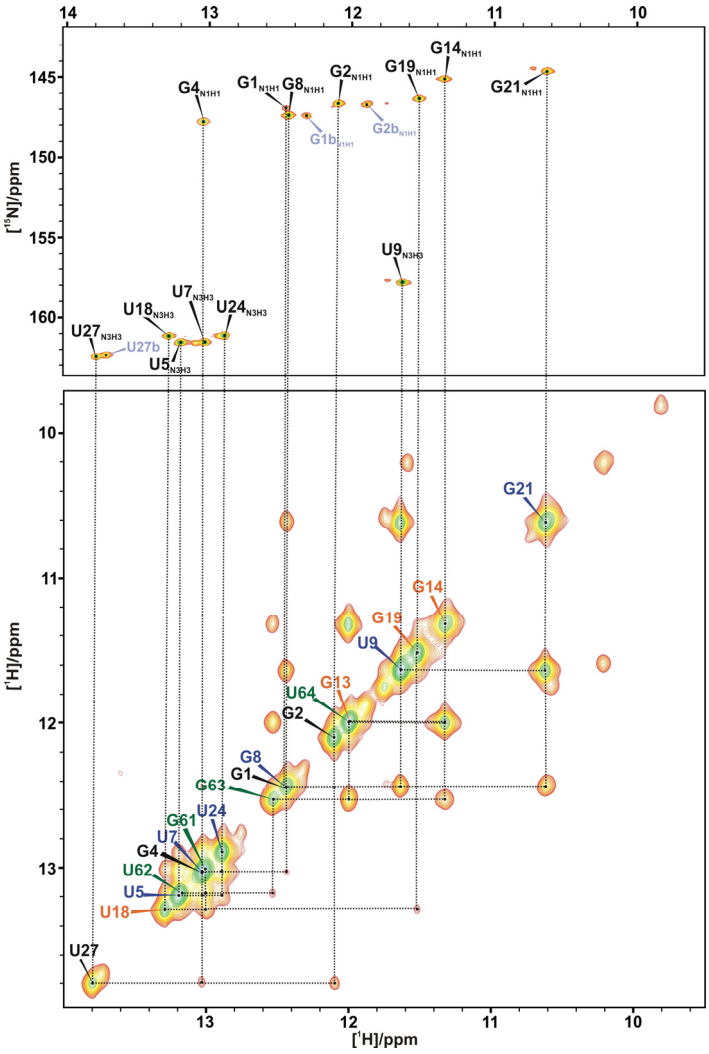

Figure 54 Assignment of imino resonances in d3'-EBS1*·IBS1*. The imino section of the 2D [^{1}H,^{1}H]-NOESY spectra acquired in 90% H_2O/10% D_2O at 278 K is shown in the lower panel. In the upper panel the corresponding section of the 2D [^{1}H,^{15}N]-HSQC at 278 K is shown.

Exchangeable protons were assigned by 2D [^{1}H,^{1}H]-NOESY spectra in 90% H_2O/10% D_2O at 278 K and 293 K with a mixing time of 150 ms and watergate H_2O suppression (Figure 54). The assignment was supported by a 2D [^{1}H,^{15}N]-HSQC, which only shows the NH-resonances of the ^{15}N,^{13}C-labeled part, i.e. the d3'-EBS1* hairpin. The imino region reveals two strong crosspeaks originating from G21-U9 and G14-U64. In addition to the eight Watson-Crick base pairs of the stem, which were already observed in d3'-EBS1*, six additional Watson-Crick base pairs were found in d3'-EBS1*·IBS1*. This shows that IBS1* is

completely bound to EBS1*. To confirm the base pairing pattern, a 2D J_{NN} HNN-COSY[118] was recorded with the d3'-EBS1* hairpin $^{15}N,^{13}C$-labeled and IBS1* at natural abundance (Appendix 15). This spectrum revealed for the stem the same base pairs like in d3'-EBS1*. G14N1-H1, U18N3-H3 and G19N1-H1 resonances were observed showing that these nucleotides are not solvent exposed anymore like it was the case in the absence of IBS1*. A missing correlation for G13 in the 2D J_{NN} HNN-COSY as well as in the 2D [$^{1}H,^{15}N$]-HSQC experiment suggests that this imino proton is partly solvent exposed. This suggestion is confirmed by the solution structure, which shows that G13 is pointing outwards (see Section 2.2.9). In addition, the missing crosspeak can derive from a fraying end of the EBS1*·IBS1* duplex as is well known for other RNA as well as DNA structures.[329-336]

2.2.9 The solution structure of d3'-EBS1*·IBS1*

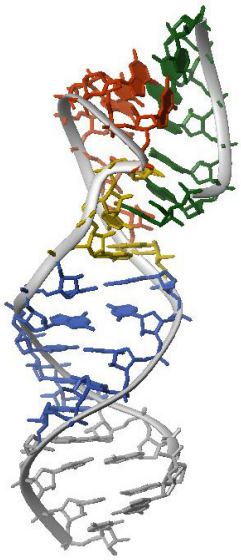

Figure 55 Lowest energy structure of d3'-EBS1*·IBS1* out of 200 calculated.

The structure calculation of the full construct d3'-EBS1*·IBS1* is based on 751 conformationally restrictive NOE distance restraints that were collected with 2D [^{1}H,^{1}H]-NOESY spectra in 100% D_2O and in 90% H_2O/10% D_2O as well as on 37 residual dipolar coupling constraints (Table 11, appendices 17 and 18, for calculation details see Materials and Methods). Like in the absence of IBS1* the hairpin adopts a stable stem. Upon addition of IBS1* the loop is stabilized due to the formation of a second helical region. The same overall conformation of d3'-EBS1*·IBS1* was obtained with and without RDC restraints. However, the RDC restraints helped to define the angle between the two helical axes. A comparison of the superpositions of the 20 lowest energy structures with and without RDCs is shown in Figure 56. It is obvious that the introduction of residual dipolar couplings straightens the overall structure.

Table 11 NMR restraints and structural statistics for the d3'-EBS1*·IBS1* structure.[a]

	With RDCs	Without RDCs
NOE-derived distance restraints	751	751
Intranucleotide	259	259
Internucleotide ($\|i - j\| = 1$)	347	347
Long-range ($\|i - n\| \geq 2$)	145	145
Repulsive	0	0
NOE restraints per residue	20.86	20.86
Dihedral restraints	288	288
Hydrogen bond restraints	82	82
Dipolar coupling restraints	37	0
r.m.s.d. (for all heavy atoms to the best structure (Å))		
Overall	0.69 ± 0.17	1.32 ± 0.65
Helix (1-9, 21-29)	0.45 ± 0.11	0.77 ± 0.32
EBS1*·IBS1* (13-19, 59-65)	0.27 ± 0.10	0.21 ± 0.06
NOE violations > 0.2 Å	0	0
Dihedral violations > 5°	0	0

[a]All statistics are given for the 20 lowest energy structures out of 200 calculated structures.

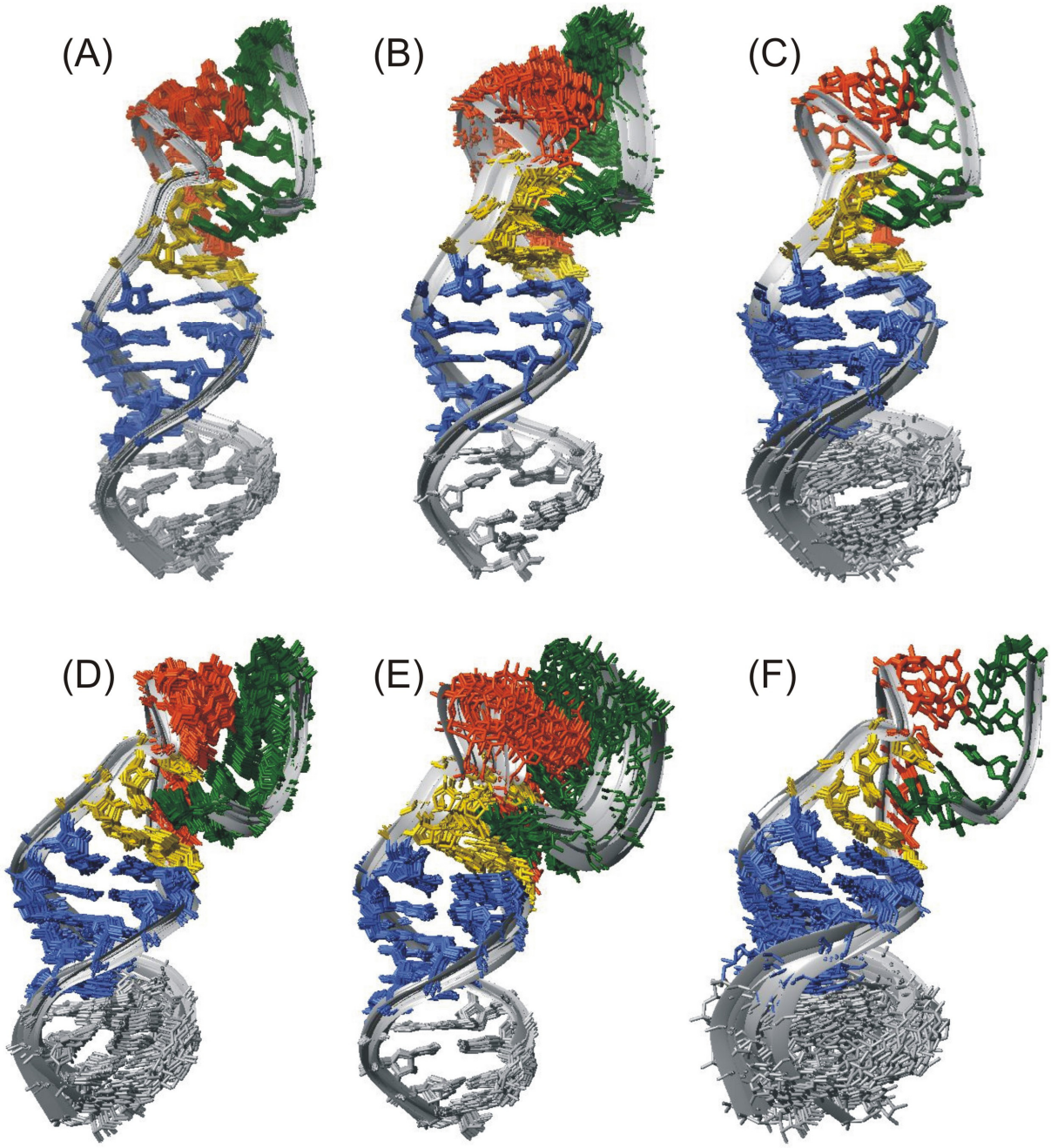

Figure 56 Solution structure of d3'-EBS1*·IBS1* as determined by NMR. The upper panel shows the 20 lowest energy structures of d3'-EBS1*·IBS1* with residual dipolar couplings, the lower panel the ones without residual dipolar couplings. (A and D) Overall superposition of all heavy atoms in d3'-EBS1*·IBS1*. (B and E) Superposition of all heavy atoms in the stem (nucleotides 1-9 and 21-29) of d3'-EBS1*·IBS1* of the 20 lowest energy structures. (C and F) Superposition of all heavy atoms in EBS1*·IBS1* (nucleotides 13-19 and 59-65) of d3'-EBS1*·IBS1* of the 20 lowest energy structures.

The overall r.m.s.d. of all heavy atoms of the 20 lowest energy structures with RDCs (0.69 ± 0.17 Å) is very low compared to the 20 lowest energy structures without RDCs (1.32 ± 0.65 Å; Figure 56, Table 11). However, independent superpositions of the stem (nucleotides 1-9 and 21-29) and the EBS1*·IBS1* interaction (nucleotides 13-19 and 59-65) result in lower r.m.s. deviations for the structures in the absence and presence of residual dipolar couplings

(Table 11). Thus, the higher total r.m.s deviation is due to the unpaired nucleotides A10, U11 and U12 as well as A20, which encompass the least defined part of the structure.

The activity assays described in Section 2.2.2 have shown that the G14-U64 wobble pair is crucial for successful splicing. However, in the solution structure this G-U wobble pair exhibits no anomalous configurations, i.e. it is an usual G-U wobble pair. Thus, from the structural point of view no information can be obtained about the importance of this wobble pair for splicing.

Taking a closer look at the three unpaired nucleotides A10, U11, and U12 it is obvious that U12 is the least defined nucleotide of the structure in the sense that it adopts two positions: In the six lowest energy structures the base of U12 is pointing towards EBS1*, whereas in the other 14 lowest energy structures the base of U12 shows stacking interactions with U11 lying in a parallel fashion to it (Figure 57A). The base of U12 is possibly involved in a putative UAU base triple in a *cis* Hoogsteen-Watson-Crick fashion (Figure 57B). A60 and U18 thereby capture the normal Watson-Crick base pairing, and U12 with A60 adopts a Hoogsteen base pair with the sugars in *cis* position towards each other. Additional hydrogen bond restraints for this triple base pair were included in the structure calculation to force and check if it might have an influence on the structure (Appendix 38). No additional NOE or dihedral violations were observed, thus suggesting that it is indeed possible that a triple base pair exists in this structure. The best 20 structures of this ensemble show an increase in the overall r.m.s.d. to 0.91 ± 0.36 Å (Appendix 39), which lies with its value in between the ensembles of d3'-EBS1*·IBS1* with and without residual dipolar couplings (Table 11). Individual superpostion of the helix and the EBS1*·IBS1* interaction also led to an increase in r.m.s.d. to 0.6 ± 0.2 Å for the helix and 0.31 ± 0.1 Å for EBS1*·IBS1*. The latter one

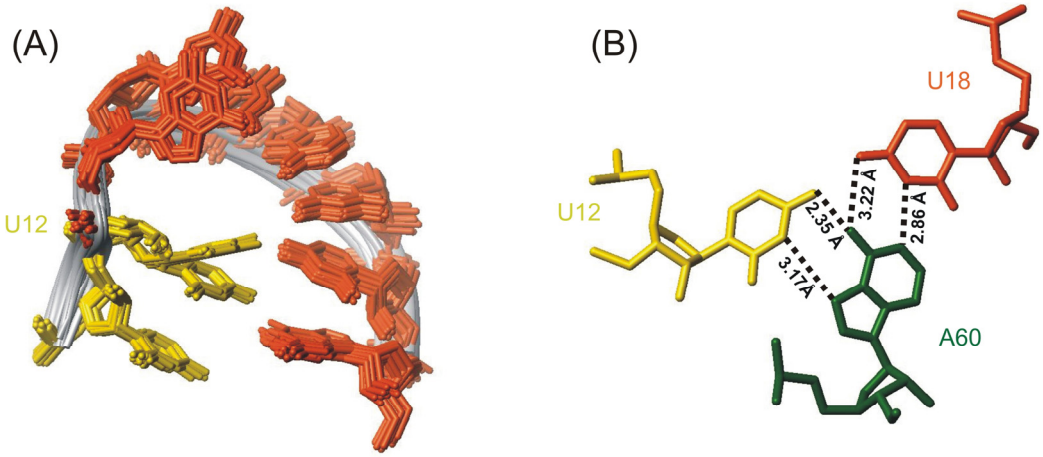

Figure 57 (A) Superposition of nucleotides U11 to G19 of the 20 lowest energy structures of d3'-EBS1*·IBS1* showing that U12 flips out in some of the structures being therefore the least defined nucleotide. (B) A putative major groove triple base pair is shown between U12, A60 and U18 in a *cis* Hoogsteen-Watson-Crick fashion that was forced by additional hydrogen bond restraints but does not influence the overall structure.

shows only a slight increase in r.m.s.d., which seems surprising as the forced triple base pair is located closer to EBS1*·IBS1* than to the helix. The overall conformation of the helix and the EBS1*·IBS1* interaction does not change with the forced triple base pair, it only leads to a less defined overall structure.

Non-canonical base pairs including triple base pairs have been observed in several crystal and NMR structures of RNA molecules.[12,23,344] Such non-standard interactions are now widely accepted to stabilize secondary as well as tertiary structural elements in RNAs.[39] Due to the increasing number of these structural players and their potential involvement in structure stabilization the NCIR database (http://prion.bchs.uh.edu/bp_type/) was created.[23] This database includes the known occurences of non-Watson-Crick base-base interactions, of which today 1860 entries are listed. 12 of the listed entries are UAU Hoogsteen-Watson-Crick

Table 12 Known UAU Hoogsteen-Watson-Crick base triples and its sugar and glycosidic conformation.

Structure	Residue number	Method	Sugar conformation	Glycosidic comformation	Special features	Lit.
Large ribosomal subunit	5' U U(2116) U 3' 5' U A(2118) C 3' 5' G U(2276) U 3'	X-ray	C3'-endo	*anti*	-	(46)
Large ribosomal subunit	5' U U(2277) U 3' 5' A A(2470) G 3' 5' C U(2115) U 3'	X-ray	C3'-endo	*anti*	-	(46)
Large ribosomal subunit	5' U U(2116) U 3' 5' U A(2118) C 3' 5' G U(2276) U 3'	X-ray	C3'-endo	*anti*	-	(46)
HIV-2 TAR-argininamide complex	5' A U(23) U 3' 5' G A(27) G 3' 5' C U(38) C 3'	NMR	U23 is C2'-endo	-	Forms a part of argininamide binding site	(337,338)
Dienococcus Radiodurans 23S RNA	5' U U(2223) U 3' 5' A A(2414) G 3' 5' C U(2057) U 3'	X-ray	C3'-endo	*anti*	–	(339)
RNA triplex	5' G U(12) C 3' 5' G A(7) U 3' 5' C U(30) * 3'	NMR	C3'-endo	–	–	(340)
HIV-1 TAR RNA-Tat peptide complex	5' A U(23) C 3' 5' G A(27) G 3' 5' C U(38) C 3'	NMR	–	–	The base triplet forms upon binding the Tat peptide	(341)
Human Telomerase RNA psuedoknot	5' U U(10) U 3' 5' A A(40) G 3' 5' C U(21) U 3'	NMR	C3'-endo	*anti*	–	(59)
Human Telomerase RNA psuedoknot	5' U U(9) U 3' 5' A A(39) A 3' 5' U U(22) U 3'	NMR	C3'-endo	*anti*	–	(59)
Human Telomerase RNA psuedoknot	5' U U(8) U 3' 5' A A(38) A 3' 5' U U(23) C 3'	NMR	C3'-endo	*anti*	–	(59)
HIV-1 rev-RNA complex	5' C U(23) G 3' 5' G A(26) G 3' 5' C U(9) C 3'	NMR	U23 is C2'-endo	–	Forms a part of ariginine binding site	(342)
Tat-peptide:TAR RNA complex	5' G U(10) G 3' 5' U A(13) G 3' 5' C U(24) C 3'	NMR	U10 is C2'-endo	–	I79 of the peptide interacts with the major groove edge of the triplet	(343)

base pairs as it was found in the here reported structure of d3'-EBS1*·IBS1*. All of the so far known UAU base triples and also the here reported one are major groove triples. The known UAU Hoogsteen-Watson-Crick base triples are listed together with its sugar and glycosidic conformation in Table 12. Of the 12 reported UAU triple base pairs the majority forms a C3'-endo conformation and the glycosidic bond is in an *anti* position. These base triples have stabilizing effects on the structures and/or are involved in interactions with other ligands. In d3'-EBS1*·IBS1* U12, which is part of the Hoogsteen base pair, adopts an intermediate conformation between C3' and C2'-endo, whereas all three glycosidic bonds adopt *anti* conformation. The putative UAU triplet might support the binding of IBS1* upon EBS1* by including the unpaired nucleotide U12 and thus stabilizing the structure. This suggests that the unpaired region in the loop, especially U12, is needed for support of the recognition of the substrate.

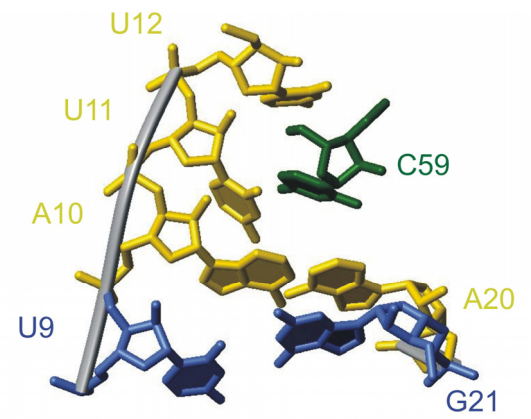

Figure 58 Section of the lowest energy structure of d3'-EBS1*·IBS1* showing C59 of IBS1* embedded between the unpaired nucleotides A10, U11, U12, and A20.

As already discussed in Section 2.2.8 the first nucleotide of IBS1* C59 is embedded within the unpaired nucleotides (Figure 58). Although C59 is surrounded by intronic nucleotides, there is still enough space for the 5'-positioned nucleotides of the full-length exon. The 3'-end of IBS1* sticks out of the structure giving room for the following nucleotides of the exon. Thus, this structure of the recognition site shows that binding of EBS1* to IBS1* is not hindered by sterical obstacles.

To put the 5'-splice site into context of the full ribozyme, the EBS1-sites of d3'-EBS1*·IBS1* with the one in the crystal structure of the group II intron from *Oceanobacillus iheyensis*[249] were superimposed. Figure 59 shows the overlay based on the stacked nucleotides together with domain 5 of the crystal structure. This superposition shows that the 5'-splice site resides right in the catalytic center of the ribozyme close to the bulged nucleotides and the catalytic triad of D5, which are known to play a major role in catalysis.[34] Even in the presence of D5 no sterical hindrances are present, which could prevent binding of IBS1 to EBS1.

The unpaired nucleotide A20 is stacked between G19 and G21, thus a helical pattern is observed from G13 to the last nucleotide C29 (Figure 56). This is also confirmed by the software AMIGOS (Algorithmic Method of Identifying and Grouping Overall Structure; for a detailed description see below), which reveals for A20 a position of η=183.4° and θ=221.3°

(Figure 61). This numbers are in the range of a normal helical region, which is centered at η=170° and θ=225° (Figure 61).[15] In comparison to d3'-EBS1* the stacking interactions of A20 are much more pronounced showing that the addition of IBS1* not only stabilizes EBS1* but also the loop in total. For the loop nucleotides A10 to A20 in d3'-EBS1* the 20 lowest energy structures were plotted with AMIGOS. No defined spot for the single nucleotides was found, thus giving additional evidence for the unstructured loop (Appendix 37).

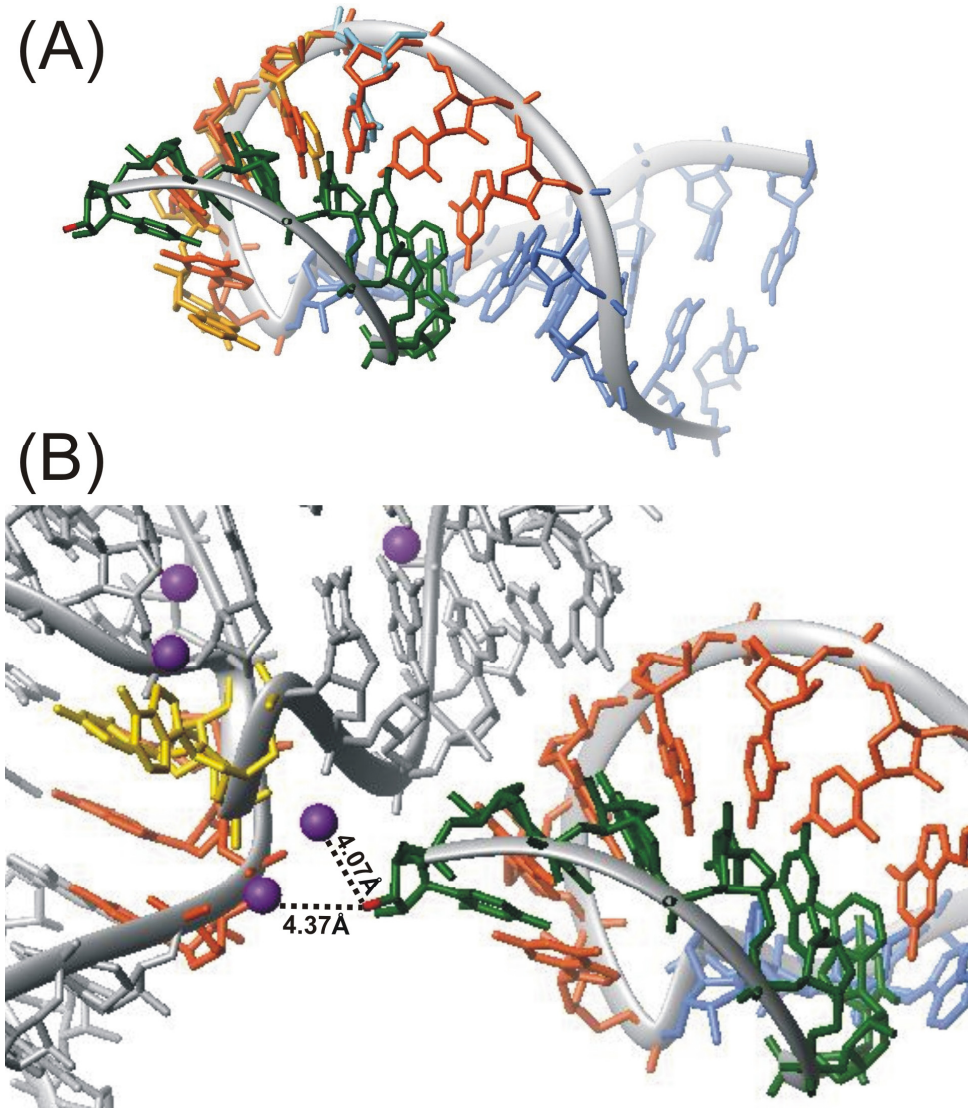

Figure 59 (A) Overlay of the EBS1-site of the crystal structure of the group II intron from *Oceanobacillus iheyensis*[249] with the solution structure of d3'-EBS1*·IBS1*. The fit is based on the sugar and N9 atoms of the stacked nucleotides in EBS1 (residue number 182-185). The splice site (3'-OH of C65) is coloured in red. EBS1 of the group IIC intron is shown in light orange and the preceding nucleotide in light blue. In d3'-EBS1*·IBS1* the stem nucleotides and the unpaired nucleotides A10,U11, U12 and A20 are dark blue, EBS1* dark orange and IBS1* dark green. (B) d3'-EBS1*·IBS1* together with D5 from the crystal structure. EBS1 of the group IIC intron is not shown for clarity. D5 is shown in grey, the catalytic CGC triad in orange and the bulge nucleotides in gold. The Mg^{2+} ions as found in the crystal structure are depicted as violet balls. Two magnesium ions are in very close proximity (4.07 and 4.37 Å) to the splice site indicated by dotted lines.

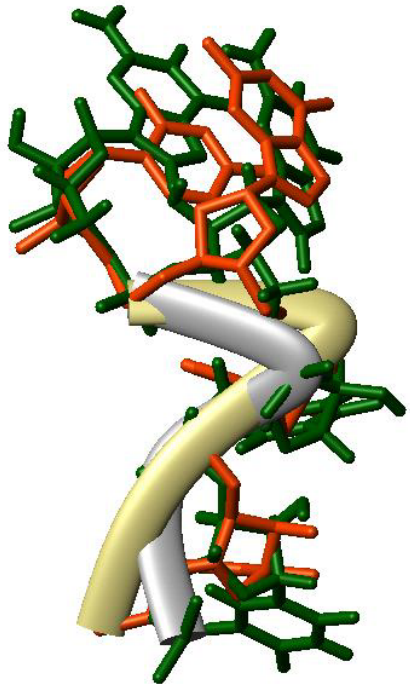

Figure 60 Overlay of nucleotides 11-14 of d3'-EBS1*·IBS1* with nucleotides 59-62 of 2B66 to visualize the kinks. The superposition is based on the backbone. Nucleotides of d3'-EBS1*·IBS1* are coloured in dark green and the ribbon in grey. The nucleotides of 2B66 are highlighted in orange red and the ribbon in khaki.

An unusual kink between nucleotides U12 and G13 5' of EBS1* is observed (Figure 60). In order to judge if such a motif is already known, a detailed wormsearch with the program AMIGOS[15,16] of the protein data bank (RCSB PDB) was performed. AMIGOS is a software, which reduces the seven standard torsion angles and the sugar pucker, which are necessary to characterize the conformation of a RNA nucleotide completely to two pseudotorsions η and θ. These pseudotorsions can be used to describe RNA conformations in a similar way like ϕ and ψ are used to describe backbone configurations in proteins in a so called Ramachandran plot.[345] The AMIGOS program provides a way to analyze new RNA structures for regions that contain unusual conformation. A structure analysis by AMIGOS provides a complete set of conventional and pseudotorsion angles. From these angles deviations the standard A-form RNA as well as other structures can be easily detected. All current available pdb-files of RNA structures (also RNA/proteins or RNA/DNA structures) were downloaded from the protein data bank (http://www.rcsb.org) giving 1465 structures to perform the wormsearch. Dependend on the size, batches of the pdb-file were made because AMIGOS has problems reading all 1465 pdb-files at once. Every single batch was loaded into AMIGOS as well as the lowest energy structure of d3'-EBS1*·IBS1*. A wormsearch with nucleotides A10 to G14 and U11 to G14, respectively, of d3'-EBS1*·IBS1* was performed. Subsequently, the individual matches were overlaid with d3'-EBS1*·IBS1* in MOLMOL and visually the best matches were extracted. In Appendix 37 these matches and the corresponding absolute values as given by AMIGOs are summarized. The PDB entry 2B66 revealed the best fit with nucleotides 11 to 14 of d3'-EBS1*·IBS1*. This entry is the crystal structure of the 50S ribosomal subunit with release factor RF1, tRNAs and mRNA bound to the ribosome.[346] The overlay of nucleotides 59-62 of 2B66 with nucleotdies 11-14 of d3'-EBS1*·IBS1* is shown in Figure 60. The other found matches show also a kink in the backbone, but in these cases the kink is not as pronounced as in d3'-EBS1*·IBS1*. Figure 61 shows the η-θ plot of d3'-EBS1*·IBS1* together with the position of the four nucleotides of 2B66, which revealed the best fit with the wormsearch of the nucleotdies U11, U12, G13 and G14 in d3'-EBS1*·IBS1*.

In addition the position of the four nucleotides of the gene 32 messenger RNA pseudoknot from bacteriophage T2[347] (PDB entry 2TPK) are shown, which give a match with the nucleotides 10-14 of d3'-EBS1*·IBS1*. The absolute values between the positions of the corresponding nucleotides give the dimension for the deviation of the pseudotorsions.

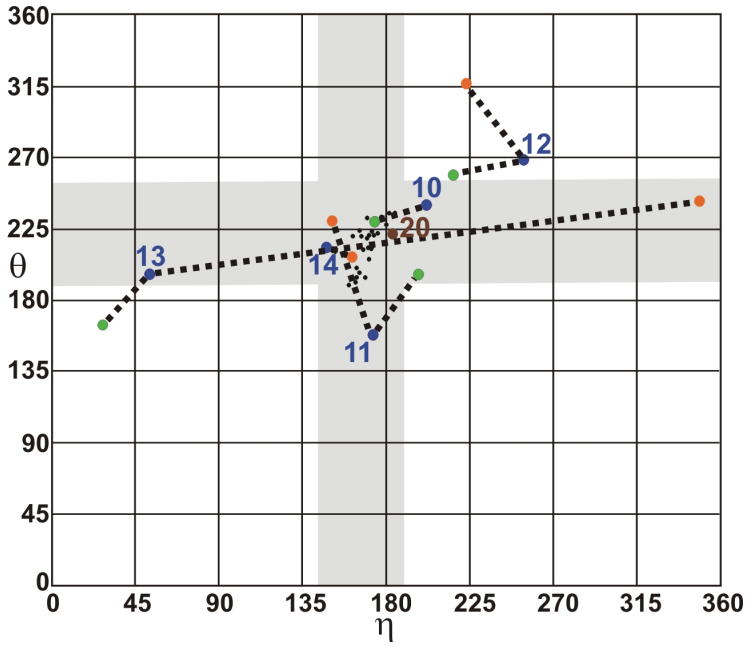

Figure 61 η-θ plot of d3'-EBS1*·IBS1*. The positions of the nucleotides 59-62 of 2B66 and 6-9 of 2TPK are shown. The positions of the nucleotides A10, U11, U12, G13 and G14 of d3'-EBS1*·IBS1* are indicated by blue dots. The corresponding positions of the nucleotides in 2B66 are shown in orange and the ones of 2TPK in green. The absolute values, which represents the deviation between the corresponding positions in the η-θ plot, are indicated by dotted lines (absolute values for 2B66: U11: 76.8, U12: 57.03, G13: 76.77, G14: 14.93, and for 2TPK2: A10: 29.7, U11: 46.1, U12: 38.5, and G13: 40.9). Grey bars represent areas of the plot where either η or θ is in the same range as nucleotides in the helical region. A20 (brown) is located at around η=170° and θ=225°, which is the center of the helical region.

The kink motif in 2B66, 2TPK and d3'-EBS1*·IBS1* share some features: In the three structures, the last two nucleotides, which correspond to G13 and G14 in d3'-EBS1*·IBS1* are paired, whereas the second nucleotide corresponding to U12 in d3'-EBS1*·IBS1* is unpaired. This indicates that the unpaired nucleotides are required to overcome sterical hindrances. In 2B66 and 2TPK this requirement is already fulfilled by one single nucleotide, whereas in d3'-EBS1*·IBS1* three unpaired nucleotides are present.

2.2.10 d3'-EBS1* *versus* d3'-EBS1*·IBS1*: A chemical shift comparison

As already discussed in Section 2.2.8, the spectra of d3'-EBS1*·IBS1* are very well resolved due to the formation of a second helix upon IBS1* binding and thus stabilization of the loop. This is not only confirmed by the solution structures of d3'-EBS1* (Figure 48) and d3'-EBS1*·IBS1* (Figure 56), but also by the good dispersion of crosspeaks throughout the sequential walk of d3'-EBS1*·IBS1* (Figure 52). To investigate the differences of the two constructs in more detail, the chemical shift changes upon IBS1* binding were mapped for the hairpin nucleotides (G1 – C29) (Figure 62). The chemical shift values of d3'-EBS1*(*I* = 10 mM KCl, 10 µM EDTA, pD = 6.96, 298 K) were subtracted from the values of d3'-EBS1*·IBS1* (*I* = 110 mM KCl, 10 µM EDTA, pD = 6.83, 298 K) to yield the chemical shift map shown in Figure 62. It sticks out that the helical stem in d3'-EBS1* and d3'-EBS1*·IBS1* is the least influenced part. Besides U9H1' and G21H8, which show with 0.12 and 0.379 ppm, respectively, a relative large upfield shift, all resonances shift less than 0.1 ppm. This observation is not surprising since IBS1* binds to the loop region thereby inducing a structural rigidity leaving the stem unaffected. The wobble pair U9-G21 is the last base pair in the helical stem and thus in close proximity to the loop. Therefore, it is possible that the electronic environment around U9-G21 is influenced, thereby inducing a change in chemical shift. It has to be noted that the differences in ionic strength by 100 mM

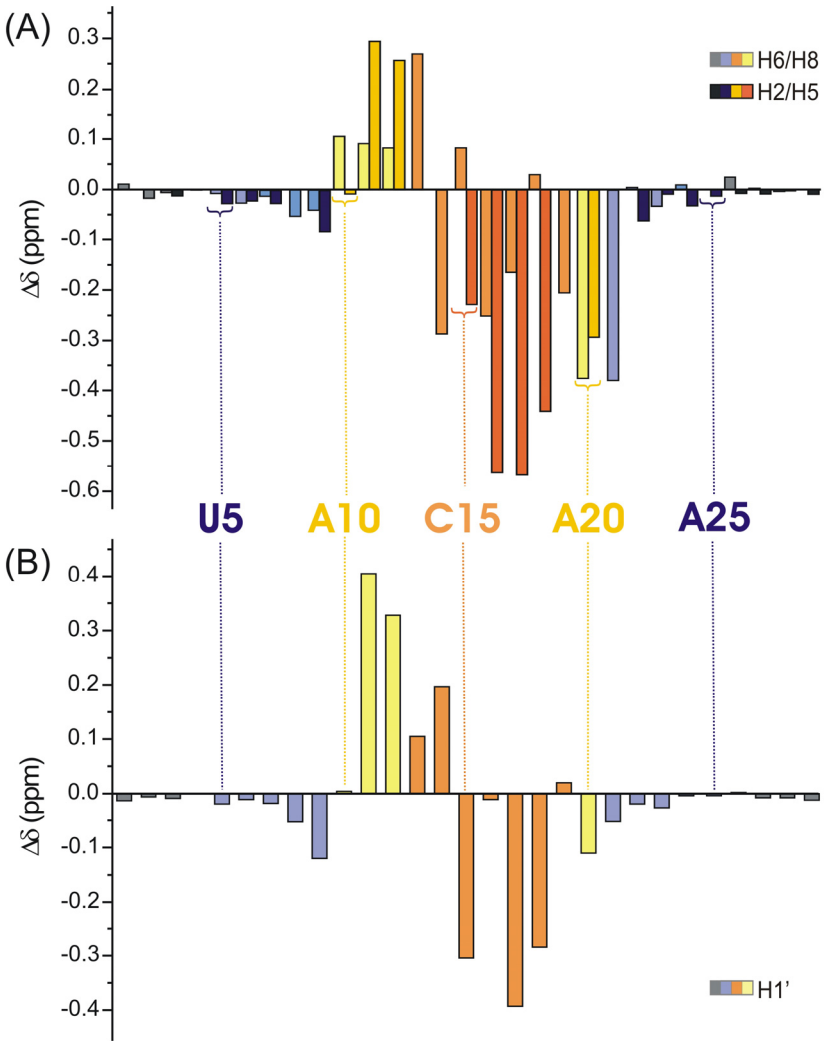

Figure 62 Chemical shift changes upon IBS1* binding. Chemical shift changes are given for (A) all aromatic protons and (B) for H1'. Colouring of the boxes corresponds to that of the secondary structures in Figure 30A and B.

KCl as well as the slight different pD might also have an influence on the chemical shift of the proton resonances. However, the effect induced by IBS1* is certainly much larger and thus the influence of the ionic strengthes and the pD can be neglected.

The protons of the loop are the most affected ones. A chemical shift of up to 0.567 (C17H5) is observed. It is interesting to note that the majority of the protons of the nucleotides G14 to A20 experience an upfield shift, whereas A10 to G13 shift downfield or are hardly influenced. In general, an upfield shift suggests that stacking interaction of the bases is increased. Upon IBS1* binding and the subsequent formation of a second helix, it is obvious that the nucleobases of EBS1* stack onto each other. Although A20 is not involved in a base pair, its proton resonances shift upfield, suggesting that also A20 stacks in a larger extent between G19 and G21. This is also confirmed by the solution structure, which shows elongation of the helix before G21, i.e. a helical pattern is observed from G13 up to C29.

The downfield shifts of U11 to G13 suggest that the stacking interactions are decreased, thus upon IBS1* addition it is no longer possible that base pairing in the loop including EBS1* occurs as suggested by mfold (Figure 39). Although the 2D [^{1}H,^{1}H]-NOESY spectra in 90% H_2O/10% D_2O (Figure 38) imply that a 11 nt long loop exists in solution, it cannot be excluded that the loop does not partially form additional base pairs. Although G13 is involved in a base pair, the downfield chemical shift can easiliy be explained by the solution structure of d3'-EBS1*·IBS1*: G13 stacks upon G14, but the unusual kink 5' of G13 leads to a nearly perpendicular position to U12 (Figure 57A). Thus, no stacking interactions between U12 and G13 exist explaining the absence of an upfield shift.

Interestingly, the unpaired nucleotide A10 is hardly influenced by IBS1*. Only A10H8 shifts downfield by 0.105 ppm. This suggests that A10 stays in its position, only experiencing a slight change upon IBS1* binding.

In summary, as expected, upon addition of IBS1* the loop nucleotides are the most affected part of the hairpin. The stacking interactions of G14 to A20 are thereby increased, whereas U11 and U12 experience partly unstacking. These observations corroborate the suggestion that U11 and U12 need to be unpaired to provide a certain flexibility to bind IBS1*.

2.3 The individual components of the splice site: d3'-TL and EBS1*·IBS1*

2.3.1 Spectral features of d3'-TL

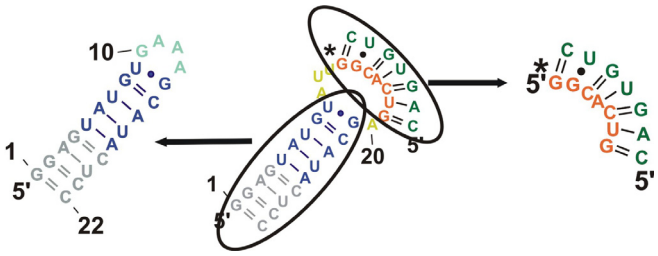

Figure 63 Schematic representation of the individual components of d3'-EBS1*·IBS1* as investigated by NMR. The hairpin d3'-TL including a GAAA tetraloop (left) represents the stem and the duplex the EBS1*·IBS1* interaction (right).

Two further constructs were designed to investigate the single components of the splice site recognition complex individually and to support the assignment of the full constructs, i.e. d3'-TL and EBS1*·IBS1* (Figure 63). In this section, the spectral features of d3'-TL, which comprises the stem helix of d3'-EBS1* and instead of a 11 nucleotide long loop only a GAAA tetraloop, will be discussed. The replacement of the loop by the GAAA sequence led to a tremendous improvement of the NMR spectra (Figure 64). With 2D [^{1}H,^{1}H]-NOESY spectra at different mixing times, the assignment of all H1', H5, H6, H2, and H8 protons in the sequential walk region as well as most sugar protons (H2', H3', H4', H5', and H5") was possible (Appendix 24).

The sequential walk of the GAAA tetraloop runs in a similar resonance pattern as already reported previously for tetraloops.[34] The H1' just 3' of the GAAA tetraloop (here G14H1') is far upfield shifted to 4.05 ppm. This is due to stacking interactions with

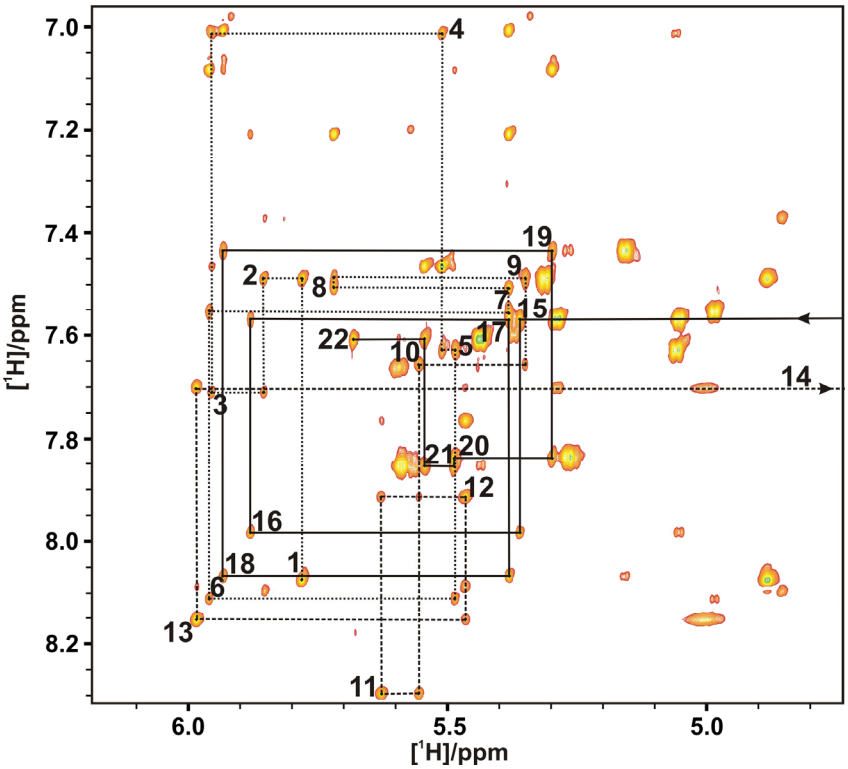

Figure 64 (A) 2D [^{1}H,^{1}H]-NOESY spectrum of the sequential walk region of d3'-TL (100% D_2O, pD = 6.61, 10 mM KCl, 10 µM EDTA) recorded at 700 MHz and 303 K. The dotted line shows the sequential walk through the 5'-helical region, dashed lines the one of the tetraloop, and solid lines the one through the 3'-helical region.

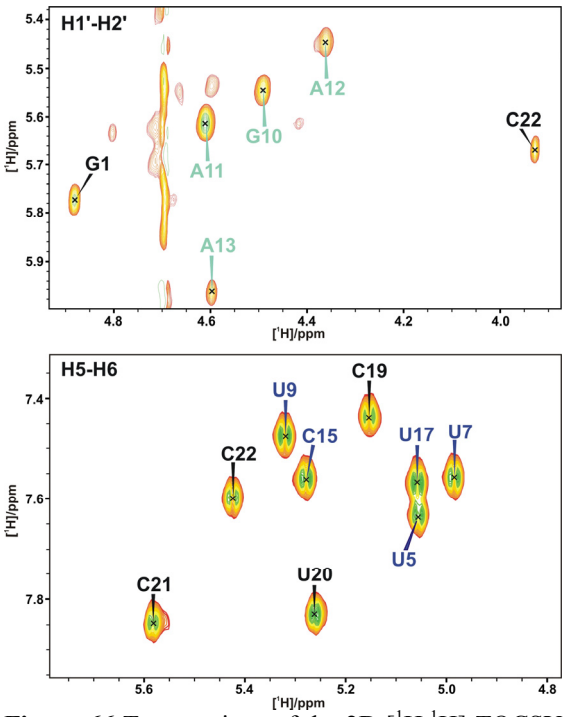

Figure 66 Two sections of the 2D [^{1}H,^{1}H]-TOCSY of d3'-TL. The upper panel shows the H1'-H2' crosspeaks that indicate a 2'-endo sugar conformation. In d3'-TL such a sugar pucker is found at the helix end (black), and in the tetraloop (green). The H5-H6 crosspeaks of d3'-EBS1* are shown in the lower panel. These crosspeaks helped to assign the pyrimidines in the 2D [^{1}H,^{1}H]-NOESY.

showed H1'-H2' crosspeaks but only A11 was constrained to south due to its strong H1'-H2' resonance.

NMR spectra acquired in 90% H_2O/10% D_2O reveal eight Watson-Crick base pair and one G-U wobble pair, thus corresponding to the imino region of d3'-EBS1, d3'-EBS1* and d3'-EBS1*·IBS1* (Figure 65). An imino resonance for G10 in the GAAA tetraloop is observed at around 11.4 ppm (Figure 65). A J_{NN} HNN-COSY[118] confirmed this base pairing scheme (Appendix 26).

As it is expected for a sequence that has the same order of nucleotides, the sequential walk in the helical region of d3'-the most 3' A in the tetraloop. The H2 of this last A (A13H2) is downfield shifted to 8.1 ppm and shows NOEs to A12H1' and A13H1'. The H8 of the first A in the tetraloop (A11H8) is far downfield shifted to 8.3 ppm.

Most of the C1', C2, C5, C8 and C6 resonances were assigned by 2D [^{1}H,^{13}C]-HSQCs (Appendix 25). Figure 66 shows two sections of the 2D [^{1}H,^{1}H]-TOCSY spectrum. A 3'-endo sugar pucker conformation is confirmed for the helical regions except the helix end. Due to the intermediate intensities of the H1'-H2' crosspeaks of G1 and C22 their sugar puckers were left unconstrained in the structure calculation. G10, A11, A12, and A13 also

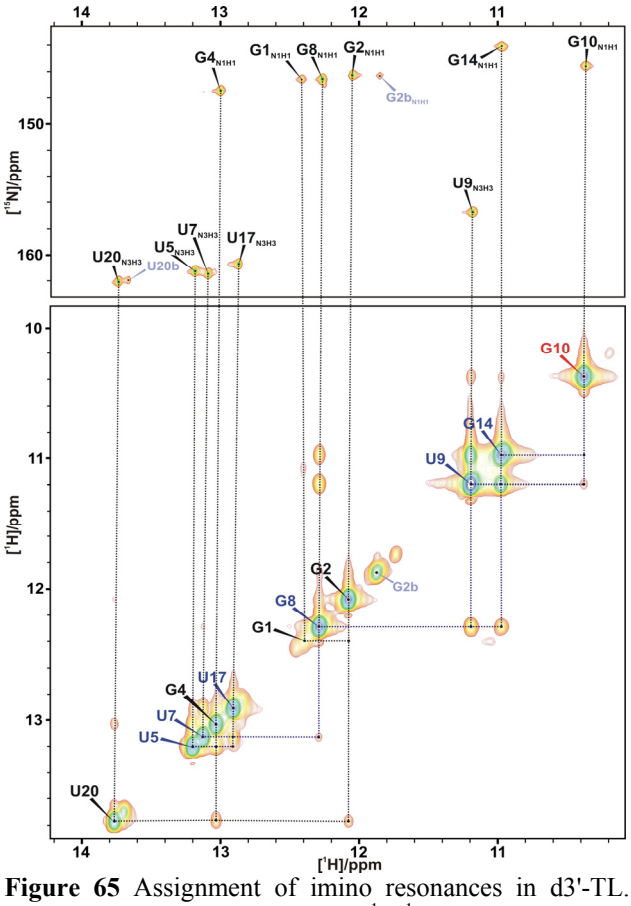

Figure 65 Assignment of imino resonances in d3'-TL. The imino section of the 2D [^{1}H,^{1}H]-NOESY spectra acquired in 90% H_2O/10% D_2O at 278 K is shown in the lower panel. In the upper panel the corresponding section of the 2D [^{1}H,^{15}N]-HSQC at 278 K is shown.

TL shows the same pattern like in the corresponding regions of d3'-EBS1, d3'-EBS1* and d3'-EBS1*·IBS1* (see Section 2.1.1, 2.2.5, and 2.2.8). The well resolved spectra of d3'-TL supported the assignment of the less well defined spectra of d3'-EBS1, d3'-EBS1* and d3'-EBS1*·IBS1* in the helical region of the d3'-stem. For comparison the chemical shifts of the helix in the four structures are summarized in Appendix 41. It is obvious that the shifts of the different RNAs deviate in a higher degree for nucleotides closer to the loop. For the nucleotides G1-U5 and A25-C29 the chemical shifts for the sugar as well as for the base protons are nearly identical for all four structures. This shows that the loop does not have any influence on the helix end, but only influences the nucleotides nearby. The protons of the helices of d3'-EBS1 and d3'-EBS1* besides A10, which already belongs to the loop, resonate at nearly the same frequency suggesting that the change in the loop does not have any effect on the helix. But with a GAAA tetraloop or in the presence of IBS1* the chemical shifts of the nucleotides nearby the loop deviate in a higher degree. Thus indicating that the size of the loop does have an effect on the neighbouring nucleotides in the helix rather than the sequence itself. It has to be considered that the spectrum of the full construct d3'-EBS1*·IBS1* was recorded in the presence of 110 mM KCl, whereas the spectra of the other three constructs were measured in the presence of only 10 mM KCl. This difference in ionic strength can also influence the chemical shifts. Only the chemical shift of G1H1' in d3'-EBS1*·IBS1* differs from the other three structures, whereas the other nucleotides of the 5'-strand of the helix are in good agreement with the chemical shifts of the other constructs. Therefore, it is assumed that the higher amount of KCl influences only the first nucleotide and that the chemical shift difference of the nucleotides close to the loop originate from the addition of IBS1*.

2.3.2 The structure of d3'-TL

The structure of d3'-TL was solved by including 471 conformationally restrictive NOE distance restraints that have been collected with 2D [^{1}H,^{1}H]-NOESY spectra in 100% D_2O as well as in 90% H_2O/10% D_2O (Table 13, Appendix 28, for calculation details see Materials and Methods). The RNA adopts a stable hairpin structure, which is closed by a classical GAAA tetraloop. This tetraloop does not differ from other published GNRA tetraloop structures.[34,82,242,348] The overall r.m.s.d. of all heavy atoms from the final 20 lowest energy conformers is 0.57 ±

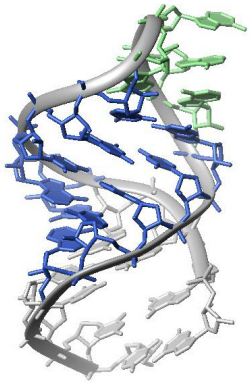

Figure 67 Lowest energy structures of d3'-TL out of 200 calculated.

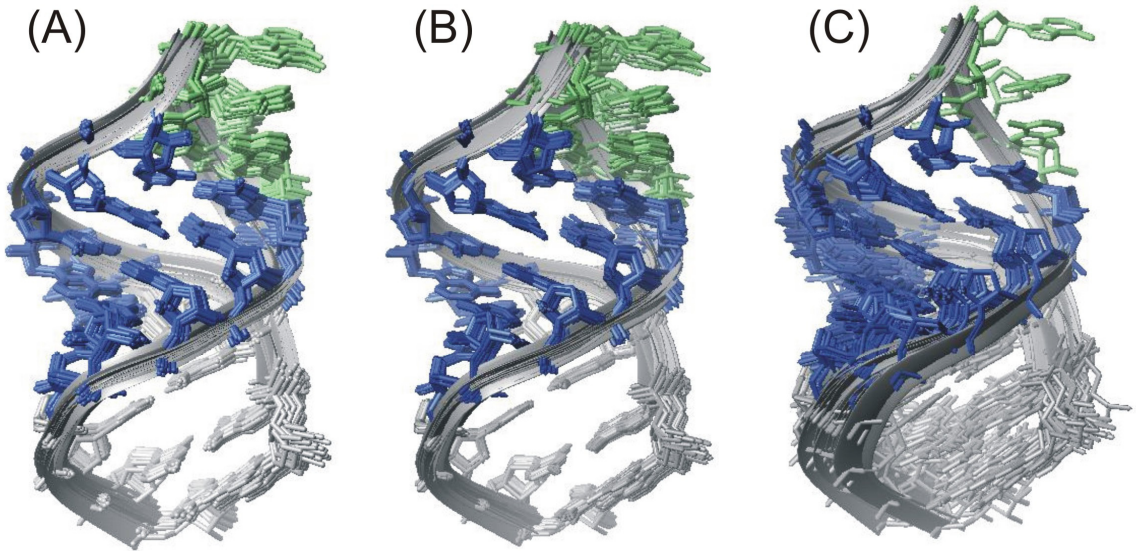

Figure 68 Solution structure of d3'-TL as determined by NMR. (A) Overall superposition of all heavy atoms in d3'-TL of the 20 lowest energy structures. (B) Superposition of all heavy atoms in the stem (nucleotides 1-9 and 14-22) of d3'-TL of the 20 lowest energy structures. (C) Superposition of all heavy atoms in the tetraloop (nucleotides 10-13) of d3'-TL of the 20 lowest energy structures.

0.19 Å (Table 13, Figure 68A). The individual superposition of the helical region and the tetraloop result in even lower r.m.s.d. values of only 0.46 ± 0.19 Å for the helix and 0.11 ± 0.05 Å for the tetraloop (Table 13, Figure 68B and C).

Table 13 NMR restraints and structural statistics for the d3'-TL structure.[a]

NOE-derived distance restraints	471
Intranucleotide	157
Internucleotide ($\|i - j\| = 1$)	228
Long-range ($\|i - n\| \geq 2$)	86
Repulsive	0
NOE restraints per residue	21.41
Dihedral restraints	162
Hydrogen bond restraints	49
r.m.s.d. (for all heavy atoms to the best structure (Å))	
Overall	0.57 ± 0.19
Helix (1-9, 14-22)	0.46 ± 0.16
Loop (10-13)	0.11 ± 0.05
NOE violations > 0.2 Å	0
Dihedral violations > 5°	0

[a]All statistics are given for the 20 lowest energy structures out of 200 calculated structures.

2.3.3 Spectral features of EBS1*·IBS1*

The EBS1*·IBS1* interaction consists of a seven base pair long duplex (Figure 63). With 2D [^{1}H,^{1}H]-NOESY spectra acquired at different temperatures and mixing times, the assignment of all H1', H5, H6, H2 and H8 protons in the well resolved sequential walk region was possible. The sugar protons H2', H3', H4', H5', and H5'' were mostly assigned (Appendix 30).

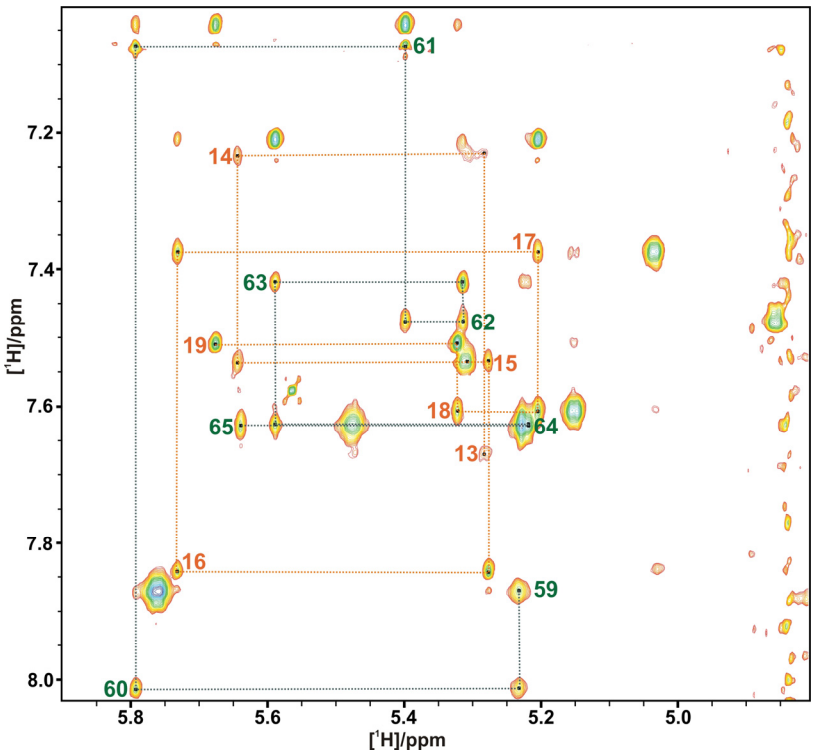

Figure 69 (A) 2D [^{1}H,^{1}H]-NOESY spectrum of the sequential walk region of EBS1*·IBS1* (100% D_2O, pD = 6.7, 100 mM KCl, 10 µM EDTA) recorded at 700 MHz at 288 K. The orange line shows the sequential walk through EBS1* and the green line the one through IBS1*.

Except for the H6 of C59, which is shifted downfield, the sequential walk pattern of IBS1* is very similar to the one of IBS1* in the full d3'-EBS1*·IBS1* construct (compare Figure 52 with 69, and Appendix 13 with 30). The sequential walk of EBS1* follows in both constructs the same way. This shows that the independent structure of EBS1*·IBS1* does not differ from the EBS1*·IBS1* interaction in the full construct d3'-EBS1*·IBS1*. Only C59 of IBS1* exhibits a different chemical shift due to the missing close neighbourhood to the unpaired nucleotides A10, U11, and U12.

Since short oligonucleotides are very difficult to transcribe, the two seven nucleotide long sequences were obtained commercially (see Materials and Methods). On this account no ^{15}N,^{13}C-labeled constructs could be obtained. Thus, [^{1}H,^{13}C]-HSQCs were recorded over 24 hours at natural abundance. Assignment of most of the C1', C2, C5, C8 and C6 resonances was possible (Appendix 31). No [^{1}H,^{15}N]-HSQCs as well as no J_{NN} HNN-COSY could be obtained due to the low natural abundance of ^{15}N nuclei of 0.364% compared to ^{13}C with a 3-fold higher natural abundance of 1.07%.[349]

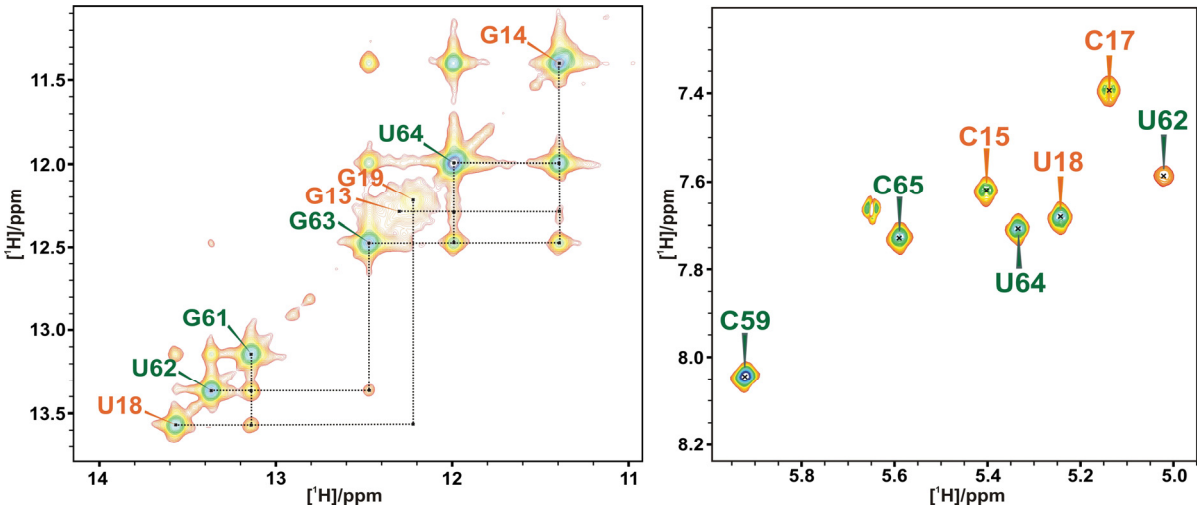

Figure 70 Assignment of imino and H5-H6 resonances in EBS1*·IBS1*. The imino section of the 2D [^{1}H,^{1}H]-NOESY spectra acquired in 90% H_2O/10% D_2O at 278 K is shown (left) together with the H5-H6 section of a 2D [^{1}H,^{1}H]-TOCSY (right).

The exchangeable imino protons are in a very well resolved region between 11 and 14 ppm (Figure 70). The assignment of these protons was possible by recording 2D [^{1}H,^{1}H]-NOESY spectra in 90% H_2O/10% D_2O. G13 at the 5'-end and G19 at the 3'-end of EBS1* show relative weak resonances indicating a certain flexibility at the helix end.

2.3.4 The structure of EBS1*·IBS1*

The structure calculation for EBS1*·IBS1* is based on 281 conformationally restrictive NOE distance restraints collected from 2D [^{1}H,^{1}H]-NOESY spectra in 100% D_2O as well as in 90% H_2O/10% D_2O (Table 14, Appendix 33, for calculation details see Materials and Methods). EBS1*·IBS1* adopts a stable double helical conformation (Figure 71). The overall r.m.s.d. of all heavy atoms from the 20 lowest energy structures is 0.22 ± 0.08 Å (Table 14, Figure 71).

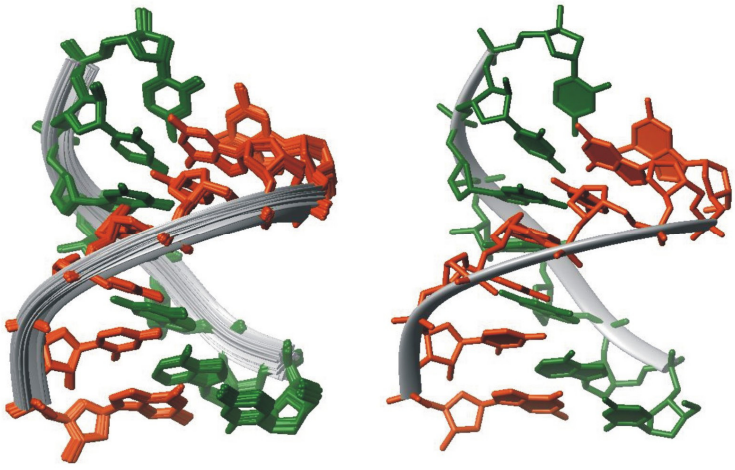

Figure 71 Solution structure of EBS1*·IBS1*: Superposition of all heavy atoms in EBS1*·IBS1* of the 20 lowest energy structures (left) together with the view of the lowest energy structure of EBS1*·IBS1* (right).

Table 14 NMR restraints and structural statistics for the EBS1*·IBS1* structure.[a]

NOE-derived distance restraints	281
Intranucleotide	105
Internucleotide ($\|i - j\| = 1$)	126
Long-range ($\|i - n\| \geq 2$)	50
Repulsive	0
NOE restraints per residue	20.07
Dihedral restraints	118
Hydrogen bond restraints	37
r.m.s.d. (for all heavy atoms to the best structure (Å))	
Overall	0.22 ± 0.08
NOE violations > 0.2 Å	0
Dihedral violations > 5°	0

[a]All statistics are given for the 20 lowest energy structures out of 200 calculated structures

2.4 Structural comparison of d3'-EBS1*, d3'-EBS1*·IBS1*, d3'-TL and EBS1*·IBS1*

The four structures discussed above comprise the full or individual parts of the splice site recognition complex. Thus, they share sequencial and structural features. In this section, we will compare and discuss the structures with each other.

d3'-EBS1*, d3'-EBS1*·IBS1* and d3'-TL include the helical stem that leads to EBS1. The structures of d3'-EBS1* and d3'-EBS1*·IBS1* were calculated including RDCs, whereas d3'-TL and EBS1*·IBS1* were calculated without the inclusion of RDCs. Even d3'-TL did not contain RDC values the superspositions of the helix of the 20 lowest energy structures of each

Table 15 Statistical comparison of d3'-EBS1*, d3'-EBS1*·IBS1*, d3'-TL, and EBS1*·IBS1*

construct	r.m.s.d. (helical stem, Å)[a]	NOE/residue (helical stem)	r.m.s.d. (EBS1*·IBS1*, Å)[a]	NOE/residue (EBS1*·IBS1*)
d3'-EBS1*	0.41 ± 0.10	20.17	-	-
d3'-EBS1*·IBS1*	0.45 ± 0.11	21.39	0.27 ± 0.10	19.07
d3'-TL	0.46 ± 0.16	22.22	-	-
EBS1*·IBS1*	-	-	0.22 ± 0.08	20.07

[a]For d3'-EBS1' and d3'- EBS1*·IBS1* values are given for the structures with RDCs.

structure give within the error limits the same r.m.s. deviation (Table 15, column 2). Comparing the d3'-stem in d3'-TL with the one in d3'-EBS1* and d3'-EBS1*·IBS1* without RDCs the r.m.s. deviation of d3'-TL is rather low (0.46 ± 0.16 Å for d3'-TL *vs* 0.81 ± 0.35 Å for d3'-EBS1* *vs* 0.77 ± 0.32 Å for d3'-EBS1*·IBS1*). The reason for that is twofold. First, in the calculation of d3'-TL more distance restraints were included (Table 15, column 3) due to the better resolution of the spectra of d3'-TL, and thus leading to a better definition of the overall structure. Second, the relative orientation between the loop and/or EBS1*·IBS1*, respectively, to the helical stem and the global conformation in general can only be determined by additional distance constraints like RDCs that give long-range informations (see Section 2.2.6).

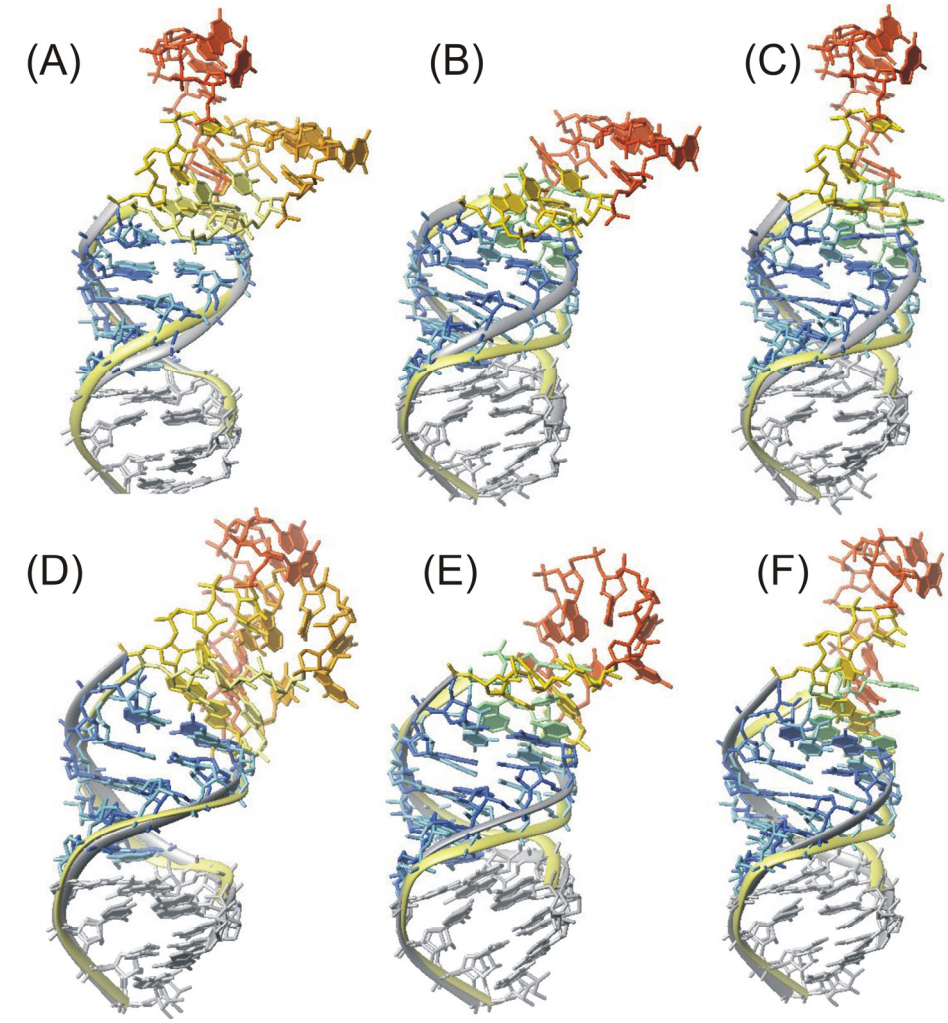

Figure 72 Overlay of the lowest energy structures of d3'-EBS1*, d3'-EBS1*·IBS1*, and d3'-TL. (A) Overlay of d3'-EBS1* (light colours, yellow ribbon) and d3'-EBS1*·IBS1* (dark colours, grey ribbon), both structures with RDCs, (B) overlay of d3'-EBS1* (dark colours, grey ribbon) with RDCs and d3'-TL (light colours, yellow ribbon), (C) overlay of d3'-EBS1*·IBS1* (dark colours, grey ribbon) with RDCs and d3'-TL (light colours, yellow ribbon), (D) Overlay of d3'-EBS1* (light colours, yellow ribbon) and d3'-EBS1*·IBS1* (dark colours, grey ribbon), both structures without RDCs, (E) overlay of d3'-EBS1* (dark colours, grey ribbon) without RDCs and d3'-TL (light colours, yellow ribbon), and (F) overlay of d3'-EBS1*·IBS1* (dark colours, grey ribbon) without RDCs and d3'-TL (light colours, yellow ribbon).

Table 16 R.m.s.d. values of the different superpositions of the 20 lowest energy structures of d3'-EBS1* (1), d3'-EBS1*·IBS1* (2), d3'-TL (3), and EBS1*·IBS1* (4).

construct	1:2:3[a]	1:2 [a]	1:3 [a]	2:3 [a]	1:4[b]
r.m.s.d. (Å) (with RDCs)[c]	1.74 ± 1.10	0.87 ± 0.45	1.64 ± 1.19	1.75 ± 1.27	0.92 ± 0.70
r.m.s.d. (Å) (without RDCs)	1.62 ± 0.81	1.31 ± 0.64	1.22 ± 0.65	1.63 ± 1.06	-

[a]r.m.s.d. values are given for the superposion of the helical stem (1-9, 21-29 (14-22 for d3'-TL)). [b]r.m.s.d. values are given for the superposion of EBS1*·IBS1* (13-19, 59-65). [c]RDCs are included in d3'-EBS1*, and d3'-EBS1*·IBS1*.

The 20 best structures each of d3'-EBS1*, d3'-EBS1*·IBS1* and d3'-TL were overlaid. The superposition of the helical stem (nucleotides 1-9, 21-29 or 14-22 for d3'-TL, respectively) of the 60 lowest energy structures results in a r.m.s.d. value for all heavy atoms of 1.74 ± 1.10 Å including RDCs in d3'-EBS1* and d3'- EBS1*·IBS1*. Without RDCs the 60 structures could be fitted to a r.m.s.d. for all heavy atoms to 1.62 ± 0.81 Å showing a better fit because d3'-TL does not include RDCs. These results suggest that RDCs would help to define the global conformation even in short hairpins like d3'-TL. Also the individual superposition of the 20 lowest energy structures of two constructs each support this result. The superposition of d3'-EBS1* and d3'-EBS1*·IBS1* result in a r.m.s.d. for all heavy atoms of 0.87 ± 0.45 Å (Table 16, column 3) with the inclusion of RDCs, showing a very good fit for the helical stem. Without RDCs included in the structure calculations, the r.m.s.d. gives a higher value for the superposition of this 40 structures for all heavy atoms of 1.31 ± 0.64 Å (Figure 72, column 3). The superposition of d3'-TL with d3'-EBS1* or d3'-EBS1*·IBS1* with RDCs, respectively, gives higher r.m.s.d. values than the superposition of d3'-TL with d3'-EBS1* and d3'-EBS1*·IBS1* without RDCs (Figure 72, column 4 and 5). Thus, RDCs not only help to define the relative orientation of two helices towards each other but also help to define the global conformation of helices with a length of nine base pairs.

The superposition of the EBS1*·IBS1* interaction of the 20 lowest energy structures in d3'-EBS1*·IBS1* and EBS1*·IBS1* leads to a r.m.s.d. of 0.92 ± 0.70 Å (Table 16, column 6). Figure 73 shows the overlay of the lowest

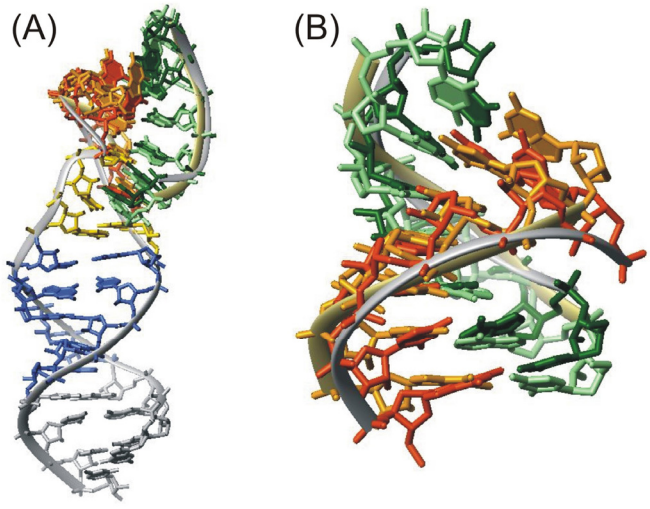

Figure 73 Overlay of d3'-EBS1*·IBS1* (dark colours, grey ribbon; with RDCs) with EBS1*·IBS1* (light colours, yellow ribbon) (A) together with the section of the EBS1*·IBS1* interaction only (B).

energy structures of d3'-EBS1*·IBS1* with EBS1*·IBS1*. In the full construct d3'-EBS1*·IBS1* the EBS1*·IBS1* interaction is bent to a small degree. This bending occurs due to the integration of EBS1*·IBS1* in the loop and because of sterical reasons EBS1*·IBS1* is forced to abandon the straightness that it adopts when only two seven nucleotide long strands are present (Figure 73).

In general the r.m.s.d. values show that no large change in the overall conformation of the helix or the EBS1*·IBS1* interaction, respectively, occurs by changing the lengths of the loop or by the presence of a second helix, respectively.

2.5 Metal ion location in d3'-EBS1* and d3'-EBS1*·IBS1*

2.5.1 Detection of metal ion binding sites in d3'-EBS1* and d3'-EBS1*·IBS1* by Mg^{2+} titration studies

The EBS1-IBS1 interaction is the crucial region for recognition of the 5'-splice site through double helix formation. Already the solution structure described in Section 2.2.9 shows that heavy stress is induced on the backbone just 5' of the EBS1* site. Two helices are arranged nearly perpendicular to each other linked by just three nucleotides, inducing an unusual kink at this site. This leads to a close positioning of several negatively charged phosphate oxygens just 5' of EBS1*. Such repulsive interaction can be neutralized and unusual conformations stabilized by Mg^{2+} ions. This view is supported by the following results: (i) Hydrolytic cleavage experiments have shown that one of the most prominent binding sites is located just 5' of EBS1 and thus being part of the catalytic core.[97] (ii) In addition, the recently solved crystal structure of the group IIC intron from *Oceanobacillus iheyensis* revealed that two metal ions, which are located in close

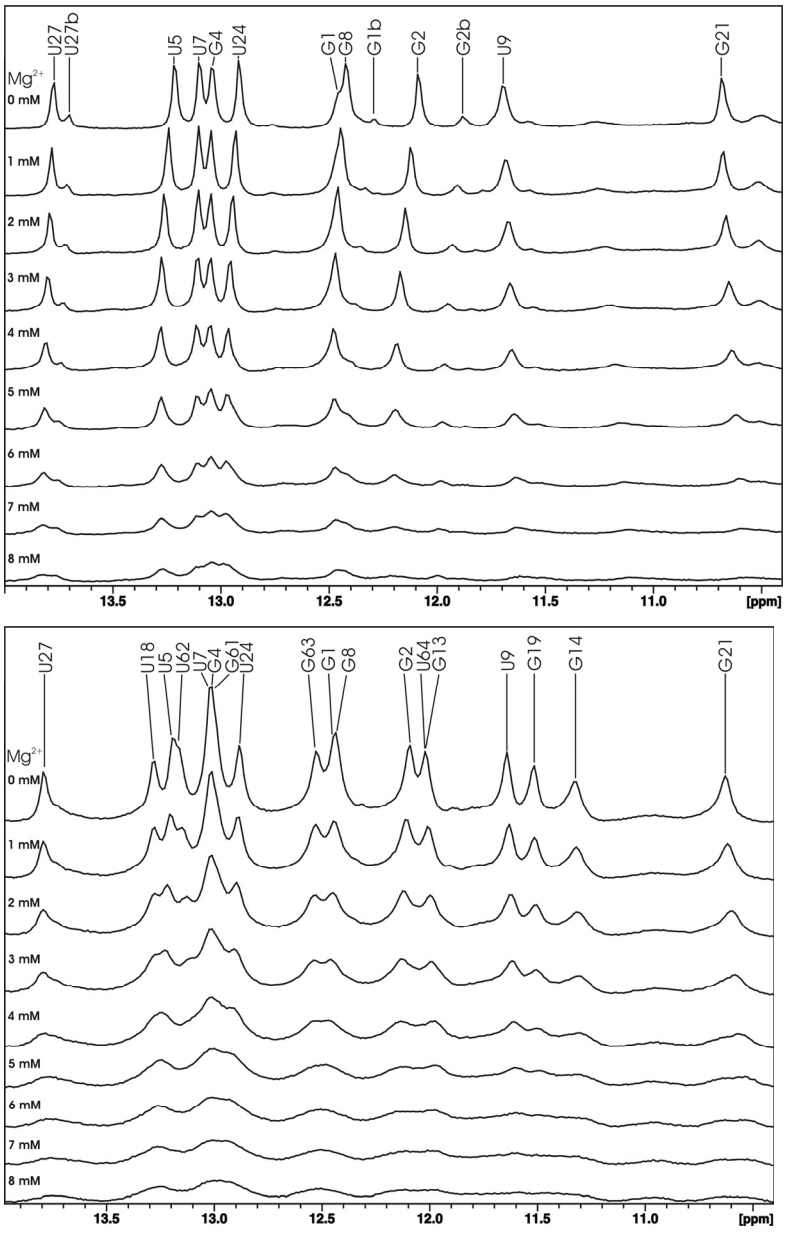

Figure 74 A series of 1D [^{1}H]-NMR spectra of d3'-EBS1* (upper panel; pH = 6.52, 10 mM KCl, 10 µM EDTA) and d3'-EBS1*·IBS1* (lower panel; pH = 6.58, 110 mM KCl, 10 µM EDTA) in 90% H_2O/10% D_2O upon stepwise addition of Mg^{2+}. Spectra were recorded at 700 MHz and 278 K. The letter "b" indicates the resonances of the n+1 derivative, which gives additional resonances for G1, G2 and U27 in the imino spectra (see also text and Section 2.2.5).

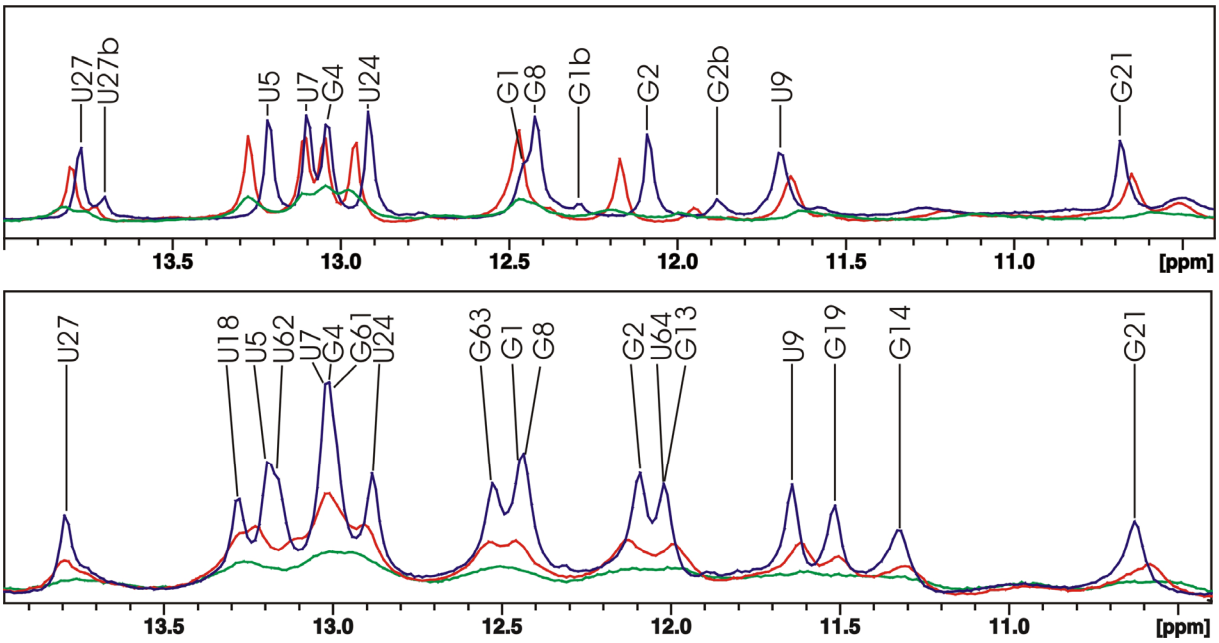

Figure 75 Overlay of 1D [^{1}H]-NMR spectra of the imino resonaces in d3'-EBS1* (upper panel) and d3'-EBS1*·IBS1* (lower panel) without (blue), with 3 mM Mg^{2+} (red) and with 7 mM Mg^{2+} (green). It is obvious that all resonances become severely broadened. The letter "b" indicates the resonances of the n+1 derivative, which gives additional resonances for G1, G2 and U27 in the imino spectra (see also text and Section 2.2.5).

proximity to the catalytic center of D5, are accessible for EBS1.[249] (iii) It has been shown that Mg^{2+} is essential for substrate binding.[218]

To obtain a more detailed view on the atomic level on metal ion binding to EBS1* in the absence and presence of IBS1*, NMR titration studies were conducted to determine the effect of Mg^{2+} on the splice site recognition complex. Since chemical shift changes of imino protons can give informations about the effect of metal ions on local structure[34], a series of 1D [^{1}H]-NMR spectra of d3'-EBS1* and d3'-EBS1*·IBS1* were recorded, each in 90% H_2O/10% D_2O (see Materials and Methods). The stack plots of d3'-EBS1* and d3'-EBS1*·IBS1* upon stepwise addition of Mg^{2+} are shown in Figure 74. It is obvious that in both cases all imino proton resonances become severely broadened and even disappear upon addition of Mg^{2+} (Figure 75). Unfortunately, changes in the chemical shift of imino protons are often difficult to interpret:[34] (i) imino protons are located far away from metal ion coordination sites, (ii) chemical shifts are dependent on the local structure as well as the exchange rate with the solvent, and (iii) since adenine and cytosine do not contain imino protons, A and C moieties cannot be observed. Especially for d3'-EBS1* the imino protons of the loop cannot be observed due to the fast exchange rate with the bulk solvent. In the case of d3'-EBS1*·IBS1* the unpaired nucleotides U11 and U12 are not observable for the same reason. Thus, only information about the paired regions can be obtained.

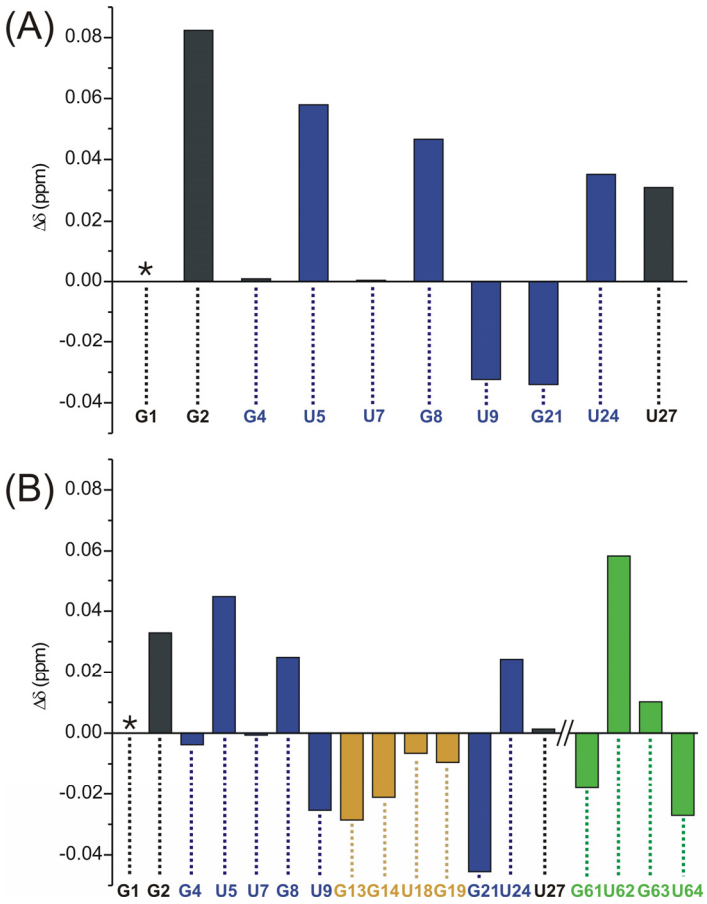

Figure 76 Chemical shift changes of the observed imino resonances upon Mg^{2+} binding. (A) shows the difference in chemical shift between 0 and 3 mM Mg^{2+} for d3'-EBS1* and (B) the one for d3'-EBS1*·IBS1*. Colouring of the boxes corresponds to that of the secondary structures in Figure 30A and B. Resonances of G1 could not be followed upon addition of Mg^{2+} and are marked with an asterisk.

Chemical shifts were extracted for 0 mM and 3 mM Mg^{2+} for d3'-EBS1* and d3'-EBS1*·IBS1* because at this Mg^{2+} concentration it was still possible to assign the resonances for both constructs despite line broadening. The chemical shift changes are shown in Figure 76.

In both cases, the resonance for G1H1 lies underneath G8H1 and thus, no chemical shift change could be obtained for resonance G1H1. However, for the other helical imino-protons it was possible to obtain chemical shifts. In the case of d3'-EBS1* as well as d3'-EBS1*·IBS1* G2 is strongly affected. This is due to the close proximity to G1, which usually still has a triphosphate attached from *in vitro* transcription and triphosphates are known to be good metal ion binding sites. G2 experiences the largest chemical shift change with 0.082 ppm in d3'-EBS1*, whereas in d3'-EBS1*·IBS1*, i.e. in the presence of IBS1*, G2 is not the most affected imino proton. In d3'-EBS1*·IBS1* the largest chemical shift change upon Mg^{2+} addition is observed at U62H3 with 0.058 ppm, followed by G21H1 and U5H3 with –0.0455 ppm and 0.0448 ppm, respectively. Other protons in IBS1* and EBS1* experience chemical shift changes, but to a smaller degree, thereby G13H1, G14H1 and U64H3 are the most affected ones with -0.0286, -0.0212, and 0.0271 ppm, respectively. The almost same change in chemical shift indicates a similar change in the electronic environment around these protons. Additionally, comparing the chemical shift changes of both constructs in the stem of the hairpin, they behave in a similar way. G2H1, U5H3, G8H1, and U24H3 experience a downfield shift, U9H3 and G21H1 an upfield shift, whereas G4H1 and U7H3 are hardly affected in both cases.

From these imino-proton titrations we can postulate for d3'-EBS1* that Mg^{2+} has an influence at the helix end (G1), in the helical stem, mainly around U5, and at the upper part of the helix including mainly the G21-U9 wobble pair just below the loop. Since imino protons in the loop cannot be observed, it is not evident yet, if the latter one is influenced by direct metal ion binding or if metal ion coordination to the loop also influences the environment around the G-U wobble pair.

It is assumed that Mg^{2+} has a similar effect on the helix of the stem in d3'-EBS1*·IBS1*. In addition, two further affected sites are observed in the EBS1*-IBS1* interaction, one at G13/G14, the second one located close to U62, experiencing the largest chemical shift upon Mg^{2+} binding. As in the case of d3'-EBS1* it cannot be excluded that the non-detectable imino protons of U11 and U12 in d3'-EBS1*·IBS1* also experience changes upon Mg^{2+} binding and if this binding has an indirect influence on the surrounding.

To overcome the above mentioned problems and to investigate protons in closer proximity to potential metal ion binding sites, 2D [^{1}H,^{1}H]-NOESY spectra in D_2O were recorded. That way, the effect of proton exchange with the solvent was excluded and thus detection of chemical shift changes was additionally possible in the loop region. The effect of Mg^{2+} to the RNA was monitored at sugar as well as at nucleobase residues (Appendix 9 and 20). The observed H8, H6, H2, and H5 protons are positioned close to potential metal ion coordination sites, such as the phosphate oxygens, N7 of purines, the carbonyl oxygens of purines and pyrimidines, or the 2'-OH at the sugars. Addition of Mg^{2+} to a solution of d3'-EBS1* and d3'-EBS1*·IBS1*, respectively, leads to increasing changes in the chemical shifts ($\Delta\delta$) of specific resonances in both constructs. $\Delta\delta$ values were extracted for aromatic as well as H1' protons (Figure 77). Chemical shifts can be affected either by direct metal ion coordination or by structural changes, which are induced by coordination of the metal ion in close proximity, i.e. reduced or increased stacking interactions. Another observed effect during these titration studies is substantial line broadening of some peaks. This effect is well known and can be traced back to binding kinetics of the metal ion at its binding site being in the intermediate exchange regime on the NMR timescale.[42,350] Line broadening experiments can therefore be used to detect specific Mg^{2+}-binding sites, since their effect should be visible only on protons in close proximity to the bound Mg^{2+}.[351] Thorough evaluation of the chemical shift changes $\Delta\delta$ and the line broadening upon Mg^{2+} binding led to the identification of numerous specific metal ion binding sites in both constructs:

Analysis of chemical shift changes for aromatic as well as H1' protons indicates that in d3'-EBS1*, A10, U11, A20 and G21 are stronger affected by Mg^{2+} than other regions (Figure 77A and B). In fact, the largest overall chemical shift with > 0.1 ppm was found for A10H2. H2 together with H1' protons are located in the minor groove region of RNAs, which offers potential binding sites for hard ions like Mg^{2+}, but metal ion binding to the major groove cannot be excluded since resonances at this site are also affected, i.e. H8 of A10, H5 and H6 of U11 and H8 of A20 (Figure 77A). These observations led to the identification of a first strong metal ion binding site in d3'-EBS1* (denoted as "loop 1" in Figure 78A). Line broadening, which is observed upon Mg^{2+} binding, corroborates these findings. In d3'-EBS1* resonances including U11 to G13 and around A20 are broadened or even disappear with increasing Mg^{2+} concentration. In addition, crosspeaks including protons of G21 also experience line broadening, thus indicating that Mg^{2+} is in close proximity to this site. It is interesting to note that the intraresidue crosspeak A10H1'-H8 does not broaden upon addition of Mg^{2+}, although it shows a very large chemical shift change (Figure 79). This observation indicates that the metal ion just 5' of EBS1* does not directly coordinate to A10, but rather to

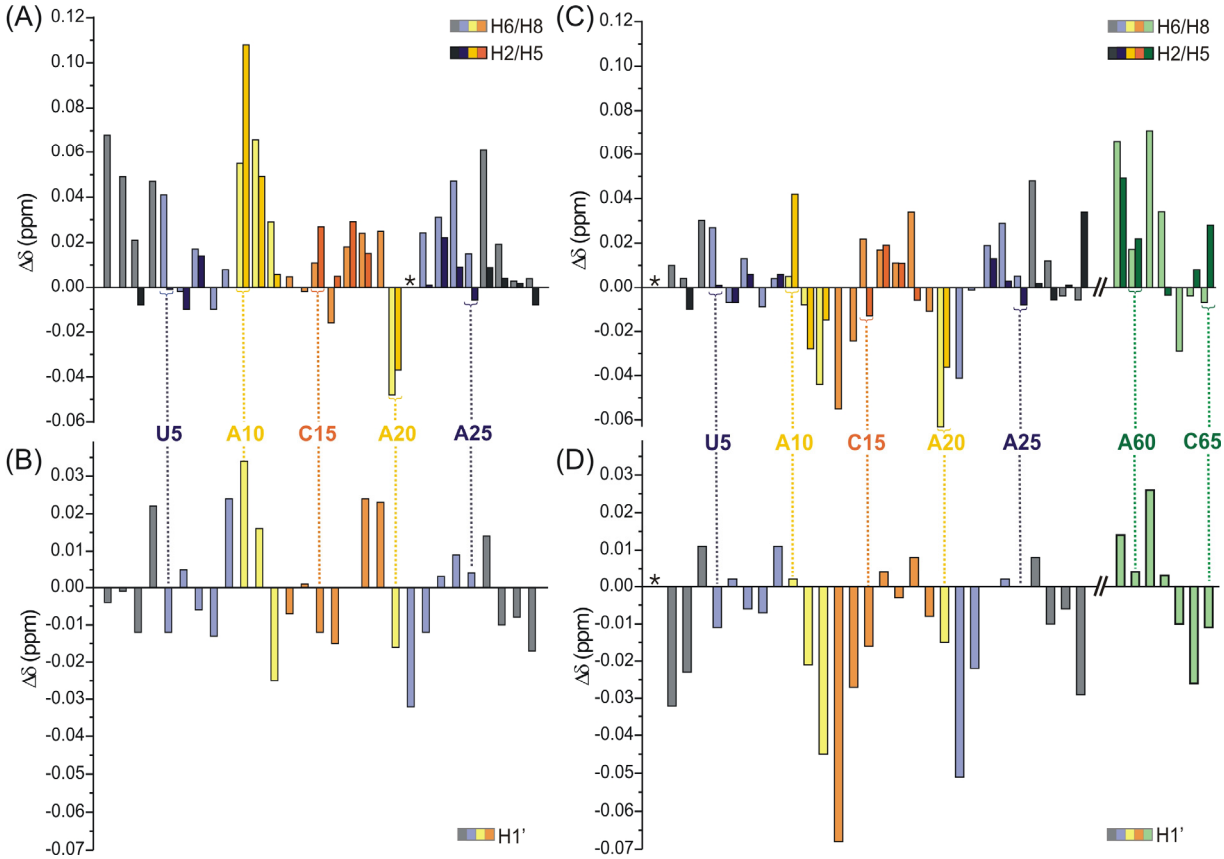

Figure 77 Chemical shift changes upon Mg^{2+} binding. Chemical shift changes are given for all aromatic protons in (A) d3'-EBS1* and (C) d3'-EBS1*·IBS1*. Chemical shift changes are given for H1' in (B) d3'-EBS1* and (D) d3'-EBS1*·IBS1*. Resonances that disappear upon addition of Mg^{2+} are marked with an asterisk. Colouring of the boxes corresponds to that of the secondary structures in Figure 30A and B.

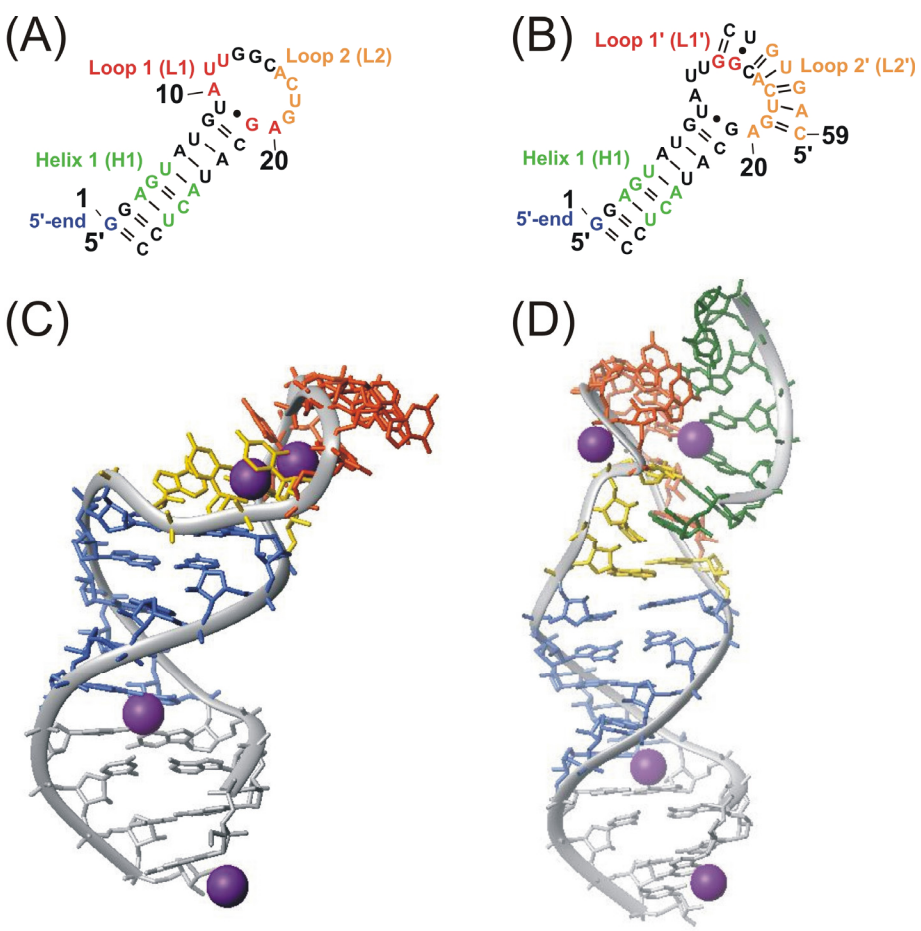

Figure 78 Potential metal ion binding sites. (A) Secondary structure of d3'-EBS1* with the four detected metal ion binding sites coloured in blue (5'-end), green (helix 1), red (loop 1) and orange (loop 2). (B) Secondary structure of d3'-EBS1*·IBS1*. The four determined binding sites are coloured in blue (5'-end), green (helix 1), red (loop 1) and orange (loop 2). (C) The lowest energy structure of d3'-EBS1* with four bound metal ions. (D) The lowest energy structure of d3'-EBS1*·IBS1* with four metal ions at its binding sites as observed by Mg^{2+} titration experiments (see text). The colour code of (C) and (D) corresponds to the one in Figure 30A and B.

U11, U12 and A20, inducing thereby a change in the local geometry, which indirectly influences A10.

One of the strongest line broadening effects were observed at the 5'-end, including G1 and G2 of d3'-EBS1*, leading to a second metal ion binding site (denoted as "5'-end" in Figure 78A). In addition, the H1' of C29, being at the 3'-end of the helix, experiences a moderate change in chemical shift. These observations correlate well with the assumption of 5'-terminal phosphate groups being the strongest binding sites due to their multiple negative charge. It is well possible that Mg^{2+} also coordinates to N7 and O6 of G1, thereby forming a macrochelate, as it has been shown to occur in $Mg(GDP)^{-}$ and $Mg(GTP)^{2-}$.[352-355]

A third potential metal ion binding site is located in the helical stem of d3'-EBS1*, i.e. "helix 1" (Figure 78A). Although the interresidual crosspeak between A3H1' and G4H8 shows hardly any line broadening effect, the intraresidual G4 crosspeak broadens significantly at around 5 mM Mg^{2+}. In addition, G4H8, G4H1', and C26H6 experience strong chemical shift changes corroborating a possible Mg^{2+} binding directly to this site. The neighbouring base pairs A3-U27 and U5-A25 were included in the binding site of helix 1 due to their similar affinity constants, which are discussed in Section 2.5.5.

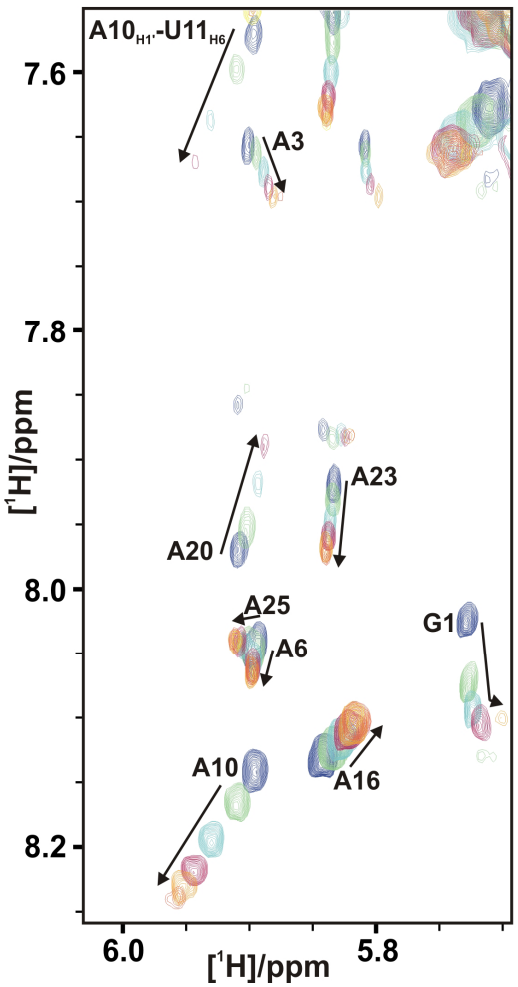

Figure 79 Section of the 2D [^{1}H,^{1}H]-NOESY of d3'-EBS1* showing an overlay of the titration from 0 (blue) to 5 mM Mg^{2+} (tomato). Significant broadening is observed at the 5'-end (G1), the interresidual A10H1'-U11H6 and the intraresidual A20 crosspeak. The intraresidual A10 crosspeak is not affected. Arrows indicate the direction of the shift change.

Another region in d3'-EBS1* is strongly affected by line broadening, namely C17 to G19, indicating a fourth metal ion binding site "loop 2" in d3'-EBS1* (Figure 78A). In addition, a set of protons, showing a large influence upon Mg^{2+} addition, is found in this region, indicating a further binding site for metal ions. However, as already discussed in the previous sections, the loop is rather flexible. Thus, the two metal ions found in this region might not be fixed, but rather "rolling" between different locations in the loop. Furthermore, chemical shifts might be affected due to structural changes in close proximity to the protons. However, the line broadening and chemical shift change data together with the magnitude of the loop (11 nucleotides in total) suggest that indeed two metals are located in the loop of d3'-EBS1*.

The chemical shift change as well as line broadening analysis of d3'-EBS1*·IBS1* revealed also four metal ion binding sites: upon addition of IBS1* not only A10, U11, A20 and G21 are strongly affected by Mg^{2+}, but additionally U12, G13 and G14 show a very strong chemical shift change and also the nucleotides in IBS1* (C59 to C65) are strongly influenced (Figure 77C and D). The resonance of G13H1' experiences the largest chemical shift change with 0.7 ppm in d3'-EBS1*·IBS1*. As already mentioned, H1' as well H2 protons are located in the minor groove, which are potential Mg^{2+} binding sites, but like in the case of d3'-EBS1*, metal ion binding to the major groove cannot be excluded since resonances at this site are also affected, especially G13H8 with a change of –0.055 ppm (Figure 77C). It appears that upon addition of IBS1* the metal ion binding site just 5' of EBS1* experiences a shift. In d3'-EBS1*·IBS1* line broadening upon Mg^{2+} addition is not observed for resonances of A10, but resonances including U12 to G14 are strongly affected. The intraresidual crosspeak A10H1'-H8 does not only show no line broadening, but also hardly experiences any chemical shift change upon Mg^{2+} addition (Figure 77C and D and

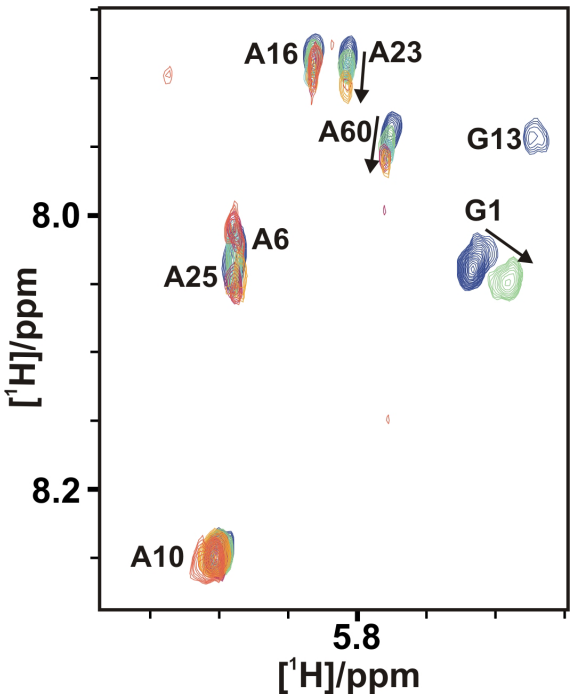

Figure 80 Section of the 2D [^{1}H,^{1}H]-NOESY of d3'-EBS1*·IBS1* showing an overlay of the titration from 0 (blue) to 5 mM Mg^{2+} (tomato). Significant broadening is observed at the 5'-end (G1), and the intraresidual G13 crosspeak. The intraresidual A10 crosspeak is not affected by line broadening and does not shift upon Mg^{2+} addition. Arrows indicate the direction of the shift change.

Figure 80). Together with the chemical shift changes upon addition of Mg^{2+}, the Mg^{2+} line broadening studies suggest that the metal ion binding site just 5' of EBS1* shifts downstream from U11/U12 in d3'-EBS1* to G13/G14 in d3'-EBS1*·IBS1*.

For d3'-EBS1*·IBS1* the 5'-end of the helical stem is strongly affected as well: The resonances of G1 disappear very soon in the titration, thus indicating a strong metal ion binding site. Although no information about the chemical shift changes of the G1 protons can be obtained, the large chemical shift of the proton resonances at the 3'-end of the helix at C29, which is in close proximity to G1, corroborates the metal ion binding site at the 5'-end. Thus, it can be concluded that d3'-EBS1* and d3'-EBS1*·IBS1* share the metal ion binding site at the 5'-end (Figure 78). This is not surprising since d3'-EBS1* and d3'-EBS1*·IBS1* share the same hairpin-sequence. This leads to a further binding site, which the two constructs have in common, namely "helix 1" (Figure 78A and B). In d3'-EBS1*·IBS1*, the crosspeak of A3H1'-G4H8 shows no line broadening effect, whereas G4H1'-H8 broadens at around 4 mM Mg^{2+}. In addition, in d3'-EBS1*·IBS1*, the interresidual crosspeak between G4H1' and U5H6, as well as the intraresidual U5 crosspeak show broadening upon Mg^{2+} addition. Moderate chemical shift changes are observed for protons of G4 and U5. These observations show that indeed a metal ion binding site in "helix 1" in d3'-EBS1*·IBS1* exists as it is the case for d3'-EBS1*.

In d3'-EBS1*·IBS1* a fourth metal ion binding site is found in the EBS1*-IBS1* interaction. This assumption is based on line broadening and chemical shift data: upon Mg^{2+} addition, line broadening is observed at nucleotides C17 to G19 as well as on the opposite strand at A60 and G61 and at the intraresidual G63 crosspeak. Strong chemical shift changes are observed in IBS1* at C59, G61, U62H6, G63H8 and U64H1'. Protons of C17 and G19 experience only a slight chemical shift, although its resonances broaden severely upon Mg^{2+}

addition. However, these observations suggest a metal ion to bind to this site being the fourth metal ion in this construct.

Interesting to note is that U11H5, H6 and H1', U12H5 and H6, as well as G13H8 experience chemical shift changes in opposite direction when comparing d3'-EBS1* with d3'-EBS1*·IBS1*. U11H5, H6 and H1', U12H5 and H6 experience a downfield shift in d3'-EBS1*, whereas the corresponding protons in d3'-EBS1*·IBS1* shift upfield. In general, it can be assumed that a downfield shift indicates metal ion coordination to a nucleobase, thereby decreasing stacking interactions. Thus, the stacking within the unpaired nucleotides U11 and U12 in d3'-EBS1* gets even decreased upon metal ion binding. This might be an indication that Mg^{2+} helps to destroy even the smallest structural parts in the loop leading to a larger flexibility of the loop. This flexibility allows IBS1* to bind easier. This observation is supported by CD-titration studies, which are discussed in Section 2.6. By contrast, an upfield shift is an indication for an increase in stacking. Thus it can be assumed that in d3'-EBS1*·IBS1* the nucleobases of the unpaired nucleotides U11 and U12 are stabilized by increasing stacking interactions. This is consistent with the solution structure of d3'-EBS1*·IBS1*, which shows that U11 and U12 are embedded within the loop (Figure 55 and 56), U12 thereby being partly flexible. Upon metal ion binding this flexibility is decreased. This indicates that the structural changes are dependent on the absence and presence of the substrate and thus also on the site at which Mg^{2+} is bound. In other words, if IBS1* is present, a different structural change in the local geometry around the unpaired nucleotides U11 and U12 occurs. Taken all aforementioned observations together, the proposed metal ion binding site just 5' of EBS1[(97)] is corroborated, thereby providing a more detailed view of this metal ion binding site in the absence and presence of the substrate.

To summarize, the data from the Mg^{2+} titration experiments reveal for d3'-EBS1* and d3'-EBS1*·IBS1* four metal ion binding sites (Figure 78). Both constructs share two metal ion binding sites: one at the 5'-end of the helix, and the second one in the helical stem around G4 (helix 1). In d3'-EBS1* a third binding site is located at U11/U12/A20/G21, which is shifted to G13/G14 in d3'-EBS1*·IBS1* (loop 1). A fourth binding site (loop 2) in d3'-EBS1* is located in the middle of the loop comprising C17 to G19. However, it is well possible that the two metal ions in the loop of d3'-EBS1* are not fixed at a specific position, but presumably they are flexible like the loop itself. Upon addition of IBS1* this site is also coordinated by the fourth metal ion, which is bound to the loop region. Thus, in d3'-EBS1*·IBS1* not only the 3'-half of the loop is included in the fourth metal ion binding site, but also the 5'-end of IBS1*.

2.5.2 Line broadening studies with Mn^{2+}

Line broadening cannot only be observed upon binding of the diamagnetic Mg^{2+} ion, but also paramagnetic ions like Mn^{2+} are applied to detect potential metal ion binding sites. The unpaired electron spin of the paramagnetic ion strongly interacts with the nearby nuclear spin in a distance-dependent manner and leads to significant broadening of the line width of the protons in close vicinity.(81) Thus, Mn^{2+} can be used as a qualitative probe for direct metal ion coordination to RNA as already shown by different examples in the literature.(112,162,356)

With this approach the assigned metal ion binding sites were further validated by observing line broadening of exchangeable as well as non-exchangeable protons. 1D [^{1}H]-NMR spectra for d3'-EBS1* and d3'-EBS1*·IBS1* recorded in 90% H_2O/10% D_2O and with increasing amounts of Mn^{2+} are shown in Figure 81. For both constructs it is obvious that G2H1 broadens out fast. For G1 no information can be obtained since the resonance for G1H1 lies beneath G8. In the spectra of d3'-EBS1*, small amounts of a n+1 derivative, i.e. a 30th nucleotide, are present, and hence two resonances each for G1H1, G2H1 and U27H3 are observed (indicated by "b"; for further details about n+1 see Section 2.2.5). These resonances experience a large line broadening effect indicating that indeed a metal ion binds to the 5'-end

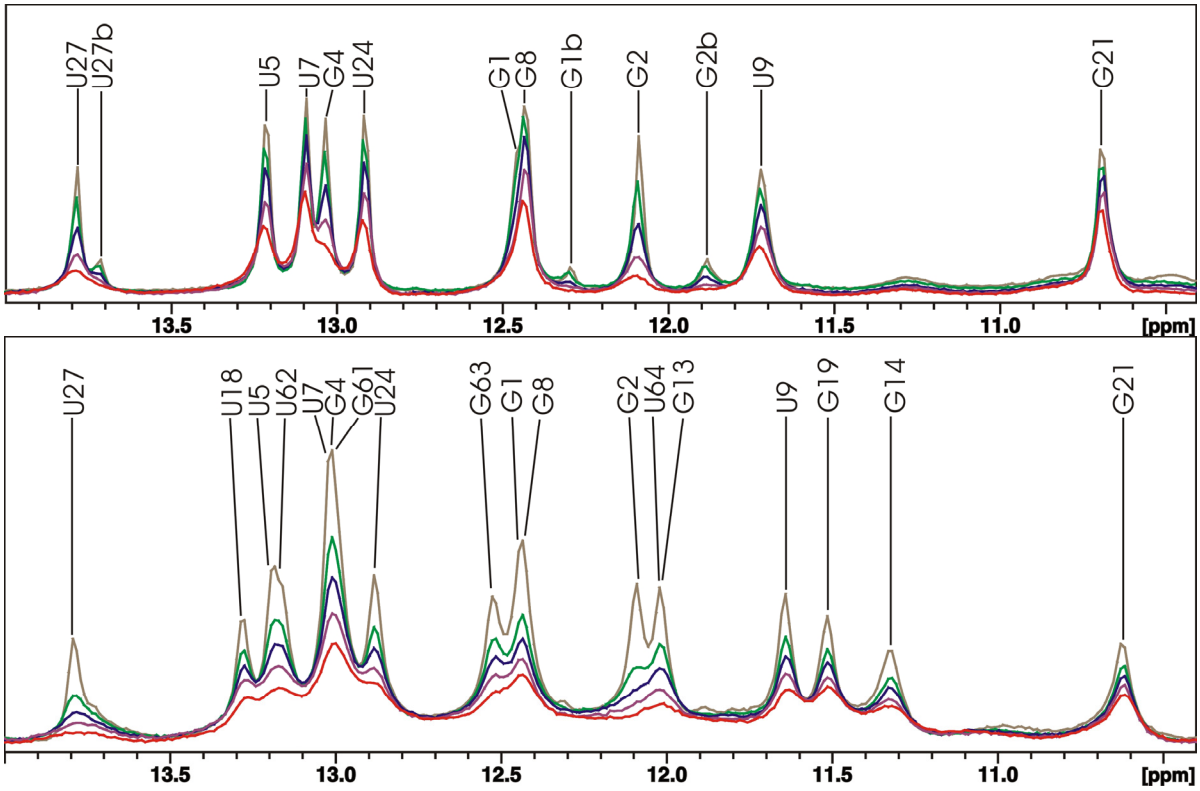

Figure 81 Line broadening of the imino protons in d3'-EBS1* (upper panel; pH = 6.79, 10 mM KCl, 278 K) and d3'-EBS1*·IBS1* (lower panel; pH = 6.89, 110 mM KCl, 278 K) upon addition of the paramagnetic ion Mn^{2+}. 1D [^{1}H]-NMR spectra recorded in 90% H_2O/10% D_2O are shown at 0 (grey), 120 (green), 150 (blue), 180 (purple) and 210 (red) µM Mn^{2+}. The letter "b" indicates the resonances of the n+1 derivative, which gives additional resonances for G1, G2 and U27 in the imino spectra (see also text and Section 2.2.5).

of the hairpin. This observation in the 30 nt long RNA can easily be transferred to the 29 nt RNA, as the only difference in these two RNAs is the non-specific 30th nucleotide. In the sample of d3'-EBS1*·IBS1*, which was used in this study, it was possible to separate the n+1 (30 nt) band from n (29 nt) almost completely. Thus, no G1b, G2b and U27b resonances are assigned in these spectra.

In d3'-EBS1*, another imino proton that broadens significantly upon addition of Mn^{2+} is G4H1. This observation corroborates the finding of a metal ion binding site in the helix around G4. In d3'-EBS1*·IBS1* the imino resonance of G4 falls together with the ones of U7 and G61, thus no precise information can be obtained about the line broadening of these three imino protons in d3'-EBS1*·IBS1*. However, line broadening is observed at the peak, which includes the resonances of G4, U7 and G61. Thus, and together with the assumption that the metal ion binding sites in the helical stem are independent of the absence or presence of IBS1*, it is suggested that Mn^{2+} binds in close proximity to G4 in d3'-EBS1*·IBS1* as well.

All other imino resonances in d3'-EBS1* become broadened evenly upon addition of Mn^{2+}. Again, no information about the loop can be obtained as already discussed in Section 2.2.5 and 2.5.1. In summary, the line broadening of imino resonances at the 5'-end and at around G4 in d3'-EBS1* reflects the results obtained by the Mg^{2+} titration studies.

For d3'-EBS1*·IBS1* further observations can be made due to the second helix formed upon IBS1* binding: The resonance of G13H1 is of specific interest since a metal ion binding site is suggested at this site. However, G13H1 falls together with U64H3, and thus, no conclusion can be drawn regarding the broadening of G13H1. Nevertheless, G14H1 broadens severely upon Mn^{2+} addition, supporting the proposed metal ion binding site at G13/G14. In addition, G63 experiences a significant line broadening effect, supporting a second metal ion binding site at the EBS1*-IBS1* interaction. All other resonances broaden out evenly or no conclusion can be drawn due to the overlay of several peaks, which is the case for U5, G8, G61, U62 and U64.

To conclude, the observations of paramagnetic line broadening of imino resonances corroborate metal ion binding sites at the terminal phosphate group and around G4 in both constructs. In addition, in d3'-EBS1*·IBS1* the two metal ion binding sites at the EBS1*-IBS1* interaction are confirmed. To obtain a more detailed picture of the metal ion binding sites and to be able to get information about the loop region and residues, which are generally not involved in base pairing, we recorded 2D [^{1}H,^{1}H]-NOESY spectra in D_2O at different Mn^{2+} concentrations. Since numerous crosspeaks lie beneath H5-H6 resonances, partially

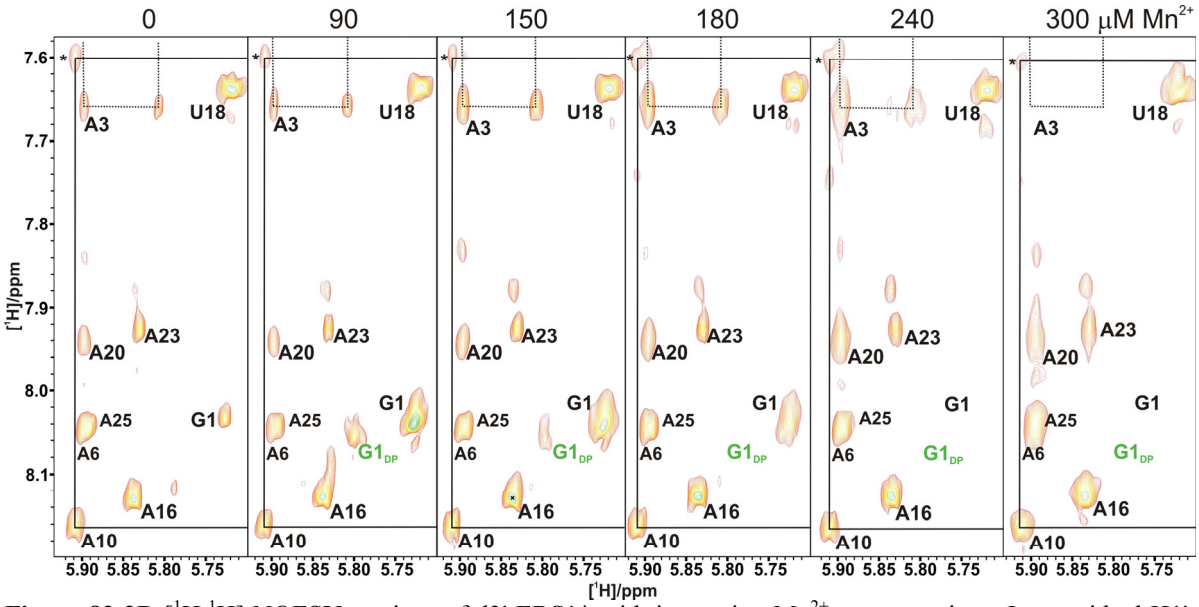

Figure 82 2D [^{1}H,^{1}H]-NOESY sections of d3'-EBS1* with increasing Mn^{2+} concentrations. Intraresidual H1'-H8 crosspeaks are assigned with the corresponding nucleotide, e.g. G1. At 90 µM Mn^{2+} a second starting point appears that is indicated with $G1_{DP}$ (green). This resonance is assumed to be G1 of a derivative bearing a diphosphate group at the 5'-terminus. All peaks of protons close to the 5'-end disappear with subsequent addition of Mn^{2+}. The sequential walk around A3 (dotted lines) and around A10 (solid lines) is indicated in every panel. The interresidual A10H1'-U11H6 (*) broadens upon addition of Mn^{2+}, whereas the intraresidual A10 crosspeak is hardly affected. Mn^{2+} concentrations are indicated at the top.

deuterated samples of d3'-EBS1* and d3'-EBS1*·IBS1* were used in the Mn^{2+} titration experiments (for details see Materials and Methods).

An interesting observation was made at the 5'-terminus in d3'-EBS1* as well as in d3'-EBS1*·IBS1*. Upon addition of Mn^{2+} a second starting point appears (denoted as "$G1_{DP}$" in Figure 82 and 83), this additional peak was not observed in the Mg^{2+} titration studies, suggesting that Mn^{2+} has a different effect on the 5'-end. This additional peak could also be traced back to the beginning of the n+1 RNA (30 nucleotides in length). Since special care was taken to remove the n+1 compound, it is more likely that the additional starting point derives from a different phosphate moiety, i.e. a diphosphate instead of the triphosphate, usually obtained by *in vitro* transcription. A mixture between di- and triphosphate at the 5'-end was previously observed in D6-27, a shortened form of domain 6 of the group II intron *Sc*.ai5γ.[115] Mn^{2+} binds with different affinities to di- and triphosphate moieties, thereby inducing different chemical shifts at G1. In the absence of Mn^{2+} it is well possible that the crosspeaks for the di- and triphosphate resonate at the same frequency.

The additional resonance G1b disappears again at 180 µM Mn^{2+}, whereas G1 is broadened beyond detection at 240 µM Mn^{2+} in d3'-EBS1* and d3'-EBS1*·IBS1* (Figure 82 and 83). The broadening of G1 together with other resonances at the beginning of the helix, i.e. G2 and A3, confirm the strong metal ion binding site at the 5'-terminus. In addition, in d3'-EBS1* and d3'-EBS1*·IBS1* the intraresidual G4 crosspeak disappears and G4H1'-U5H6 becomes

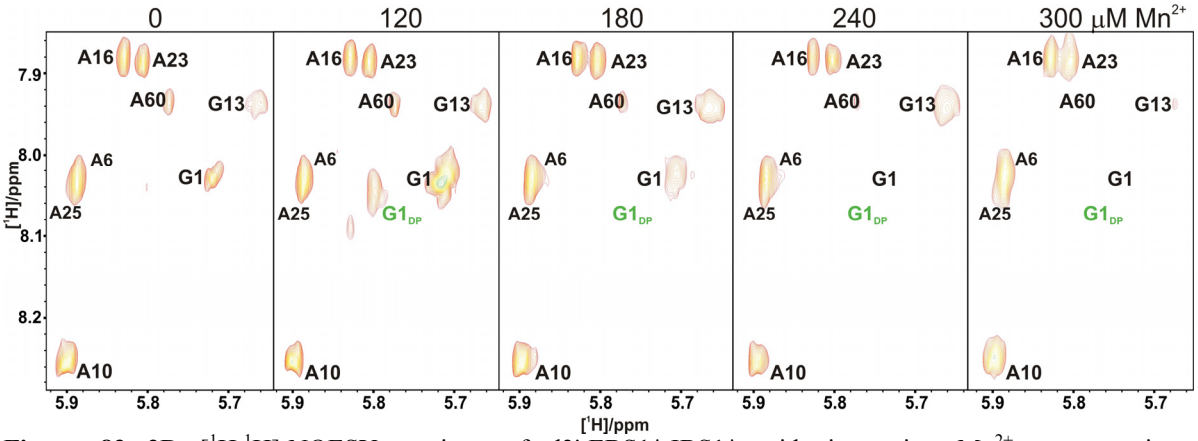

Figure 83 2D [^{1}H,^{1}H]-NOESY sections of d3'-EBS1*·IBS1* with increasing Mn^{2+} concentrations. Intraresidual H1'-H8 crosspeaks are assigned with the corresponding nucleotide, e.g. G1. At 120 µM Mn^{2+} a second starting point appears indicated with $G1_{DP}$ (green). This resonance is assumed to be G1 of a derivative bearing a diphosphate group at the 5'-terminus. All peaks at the 5'-end and in addition G13 and A60 disappear with subsequent addition of Mn^{2+}. The intraresidual A10 crosspeak is hardly affected. Mn^{2+} concentrations are indicated at the top.

severely broadened with increasing Mn^{2+} concentration. This observation additionally supports the metal ion binding site in the helix around G4 in both constructs. Line broadening is also observed for the 3'-end of d3'-EBS1* and d3'-EBS1*·IBS1*, this includes the intraresidual crosspeaks of U27, C28 and C29 as well as the interresidual peaks.

Like in the case of Mg^{2+}, the line width of the intraresidual A10 crosspeak is hardly affected in d3'-EBS1*, whereas the interesidual A10H1'-U11H6 disappears with increasing Mn^{2+} concentration (Figure 82). The intraresidual as well as the interresidual crosspeak between U11, U12, G13 and G14 broaden upon Mn^{2+} binding in d3'-EBS1*. Only for U12H1'-G13H8 no information is available due to its position in a crowded region. However, the line broadening effects at this site support the metal ion binding site "loop 1" (Figure 78A), showing also that A10 is not involved in Mg^{2+} binding.

In d3'-EBS1* paramagnetic line broadening is additionally observed at the end of the loop at G19H1'-H8, while the G19H1'-A20H8 crosspeak even disappears at higher concentrations of Mn^{2+}. In addition, the intraresidual G21H1'-H8 crosspeak broadens out. Resonances between C15 and C17 are hardly affected, neither is the intraresidual U18H1'-H6. Although the measurements were performed with deuterated samples, overlap cannot be avoided. Thus, it was not possible to extract information for C17H1'-U18H6 and U18H1'-G19H8. Nevertheless, the extensive line broadening in the loop further promotes the assumption that two metal ions exist in the loop.

The following picture was obtained for the EBS1*-IBS1* region and the unpaired nucleotides in the loop of d3'-EBS1*·IBS1*: The intraresidual A10 crosspeak (Figure 83) as well as the interresidual A10H1'-U11H6 are hardly affected. Line broadening is observed from U11H1'-H6 up to G14H1'-C15H6, thereby the crosspeaks including G13 (Figure 83) and

G14 even disappear at higher Mn^{2+} concentrations, indicating a strong binding of divalent metals to this site. These findings corroborate the downstream shift of the metal ion binding site at the beginning of EBS1*. At the 3'-half of the loop U17H1'-U18H6, U18H1'-G19H8, G19H1'-H8, G19H1'-A20H8 and A20H1'-H8 experience signal broadening upon Mn^{2+} addition. For IBS1* the crosspeaks A60H1'-H8 (Figure 83), A60H1'-G61H8 and G61H1'-H8 disappear at around 240 μM Mn^{2+}, whereas broadening is observed for G61H1'-U62H6, U62H1'-G63H8 and G63H1'-H8. The extensive line broadening in the region of EBS1*-IBS1* interaction shows that indeed a second metal ion binds to this site.

To summarize, the Mg^{2+} and Mn^{2+} line broadening data confirm the four metal ion binding sites in d3'-EBS1* and d3'-EBS1*·IBS1* (Figure 78), which were defined mainly by the chemical shift titration data (Figure 77). The phosphate groups at the 5'-end are the strongest metal ion binding sites in d3'-EBS1* and d3'-EBS1*·IBS1*. In both constructs a metal ion binding to the region around G4 is observed. Guanine moieties in general offer with the carbonyl oxygen and the N7 position a good coordination site. In addition, U5 might contribute to the coordination of a metal ion with its carbonyl oxygens, most probably in an outer-sphere mode. The metal ion binding site "loop 1" at EBS1*, which was seen in Tb^{3+} cleavage experiments,[97] was confirmed by these titration experiments. In addition to that, a more detailed view was obtained: In the absence of IBS1* the metal ion binding site is located around U11/U12. When IBS1* comes into play, a second helix is formed, which induces an unusual kink 5' of EBS1* (see Section 2.2.9). This structural change protrudes the phosphate oxygens of G13 and G14 and therefore these sites are coordinated more easily by metal ions. Additionally, metal ions such as Mg^{2+} must stabilize the unusual conformation. In both structures a second metal ion is found in the loop, presumably at the 3'-end of EBS1*, including also the 5'-end of IBS1* in d3'-EBS1*·IBS1* ("loop 2" in Figure 78). It has been shown that Mg^{2+} is needed in group II intron for catalysis,[213,253,258,261] as well as folding[70,97,216] and substrate binding.[218] Since it is known that two metal ions can bind in close proximity to each other,[357] it is possible that there are two Mg^{2+} binding to the loop region in d3'-EBS1*, waiting for the substrate to "arrive" and then locate themselves in a defined position. It is still not quite clear if the metal ions found in the loop region are the ones, which also participate in catalysis. That the metal ions stabilize the structure and the unusal kink motif and additionally help to bind the substrate was shown by circular dichroism experiments, which are discussed in Section 2.6. In the crystal structure of the group IIC intron from *Oceanobacillus iheyensis* seven Mg^{2+} ions were found to be centered around D5, thus being in the heart of the catalytic site.[249] In the superposition as shown in Figure 59 two

of the seven Mg^{2+} ions, which are found in the crystal structure, are located in close proximity (4.07 Å and 4.37 Å, repectively, from the oxygen of the 3'-OH) to the 5'-splice site, thus in addition supporting the crucial role of divalent metal ions in splice site recognition and catalysis. This observation corroborates the localization of a metal ion binding site just 5' of EBS1 as it was found in this study. Since no further metal ion was found at EBS1 in the crystal structure, it is possible that at least one of the two metal ions found in the crystal structure corresponds to the one at the 5'-end of EBS1 in the solution structure. In the solution structure of D5 metal ion binding sites were found to be located at the catalytic triad as well as at the bulge nucleotides.[34] It is therefore well possible that in the active form of the group II intron D5 and the EBS1 site share a common metal ion.

2.5.3 The electrostatic surface potential of d3'-EBS1* and d3'-EBS1*·IBS1*

Since nucleic acids contain negatively charged residues, which are uniformly distributed throughout the molcule, it is difficult to estimate, how distinct regions of electrostatic potentials are and how they contribute to the binding of metal ions. To accurately determine interactions between metal ions and RNA the electrostatic surface potential of a known three-dimensional RNA structure can be calculated.[80] In this approach, the solution of the complete nonlinear Poisson-Boltzmann equation (NLPB) is required due to the high charge density of nucleic acids, rather than the linearized equation (LPB), which is generally used for proteins.[80] To calculate the electrostatic surface potential of d3'-EBS1* and d3'-EBS1*·IBS1* the program QNIFFT[80] was used. Visualization as shown in Figure 84 was performed with PYMOL (W. L. DeLano, 2002, http://www.pymol.org).

The visualized electrostatic surface potential in d3'-EBS1* shows a highly negative charge dispersion in the major groove around A20 and A10 (Figure 84A), thus supporting the hypothesis that the unstructured loop region offers potential binding sites for metal ions. In the case of d3'-EBS1*·IBS1* a negatively charged "hole" is found in the major groove of the EBS1*-IBS1* double helix (Figure 84B). In addition, a high negative charge is observed at the backbone of G13 (Figure 84C). These results are in good agreement with the Mg^{2+} titration studies, which suggest a potential metal ion binding site on the 5'-end of EBS1* as well as at the other side of the EBS1*-IBS1* interaction (Figure 78).

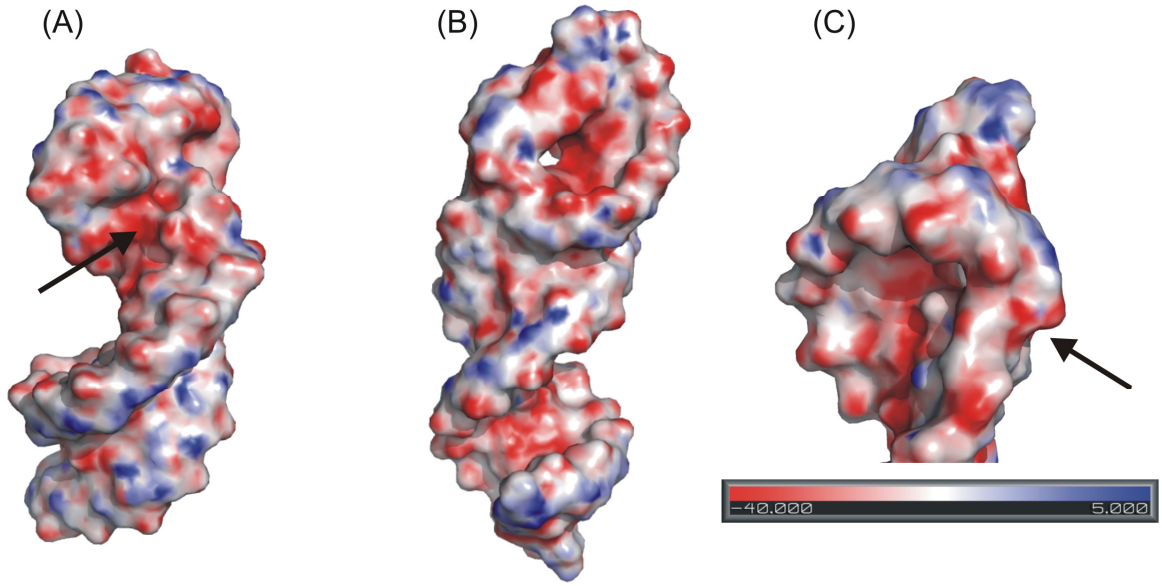

Figure 84 Electrostatic surface potential map of d3'-EBS1* and d3'-EBS1*·IBS1* as calculated with QNIFFT.[80] (A) Calculated surface potential of d3'-EBS1* showing the highly negative charge in the major groove at A20 and A10 (arrow). (B) Calculated surface potential of d3'-EBS1*·IBS1*. It can be seen that the major groove of the EBS1*-IBS1* interaction comprises a negatively charged "hole". (C) Section of d3'-EBS1*·IBS1* showing high negative charges at the backbone of G13 (arrow). Red indicates negative (–40 kTe^{-1}), white neutral (–5 kTe^{-1}), and blue positive (5 kTe^{-1}) charges.

2.5.4 Outer-sphere coordination of $[Co(NH_3)_6]^{3+}$ to d3'-EBS1* and d3'-EBS1*·IBS1*

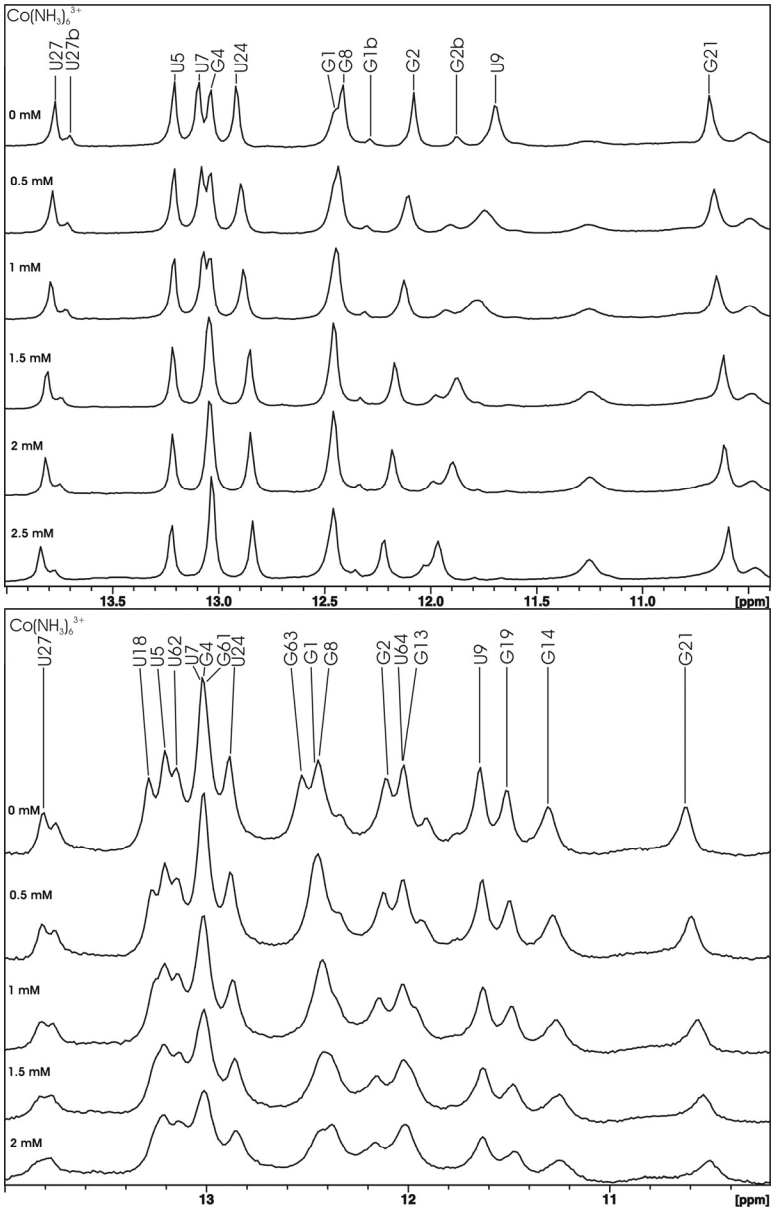

Figure 85 A series of 1D [^{1}H]-NMR spectra of d3'-EBS1* (upper panel; pH = 6.52, 10 mM KCl, 10 µM EDTA) and d3'-EBS1*·IBS1* (lower panel; pH = 6.61, 110 mM KCl, 10 µM EDTA) in 90% H_2O/10% D_2O upon stepwise addition of $[Co(NH_3)_6]^{3+}$. Spectra were recorded at 700 MHz at 278 K. The letter "b" indicates the resonances of the n+1 derivative, which gives additional resonances for G1, G2 and U27 in the imino spectra (see also text and Section 2.2.5).

Besides inner-sphere coordination of metal ions to RNA, also outer-sphere binding can occur (see Section 1.1.4). To investigate outer-sphere coordination to d3'-EBS1* and d3'-EBS1*·IBS1*, $[Co(NH_3)_6]^{3+}$ was used as a mimic for the spectroscopically silent $[Mg(H_2O)_6]^{2+}$.[81-83,162,356] The hexammine cobalt (III) ion is similar in shape, size and binding surface to a magnesium ion, thus providing a good tool to determine interactions of this important biological ion.[83] Because the NH_3 groups of hexammine cobalt (III), in contrast to $[Mg(H_2O)_6]^{2+}$, are kinetically inert, NMR can be used as a tool to monitor intermolecular NOEs between the metal ion complex and the imino protons of RNAs.[81-83,162] The 18 ammine protons of the hexammine cobalt (III) resonate at a single frequency at about 3.6 ppm. In this region no protons of the RNA are found, therefore NOEs between the $[Co(NH_3)_6]^{3+}$ protons and the imino H1 and H3 protons of guanine and uracil, respectively, are easily detectable and outer-sphere binding can easily be observed. Hexammine cobalt (III) not only gives NOEs to specific regions in the RNA, but additionally induces chemical shifts giving further information about the binding conditions.

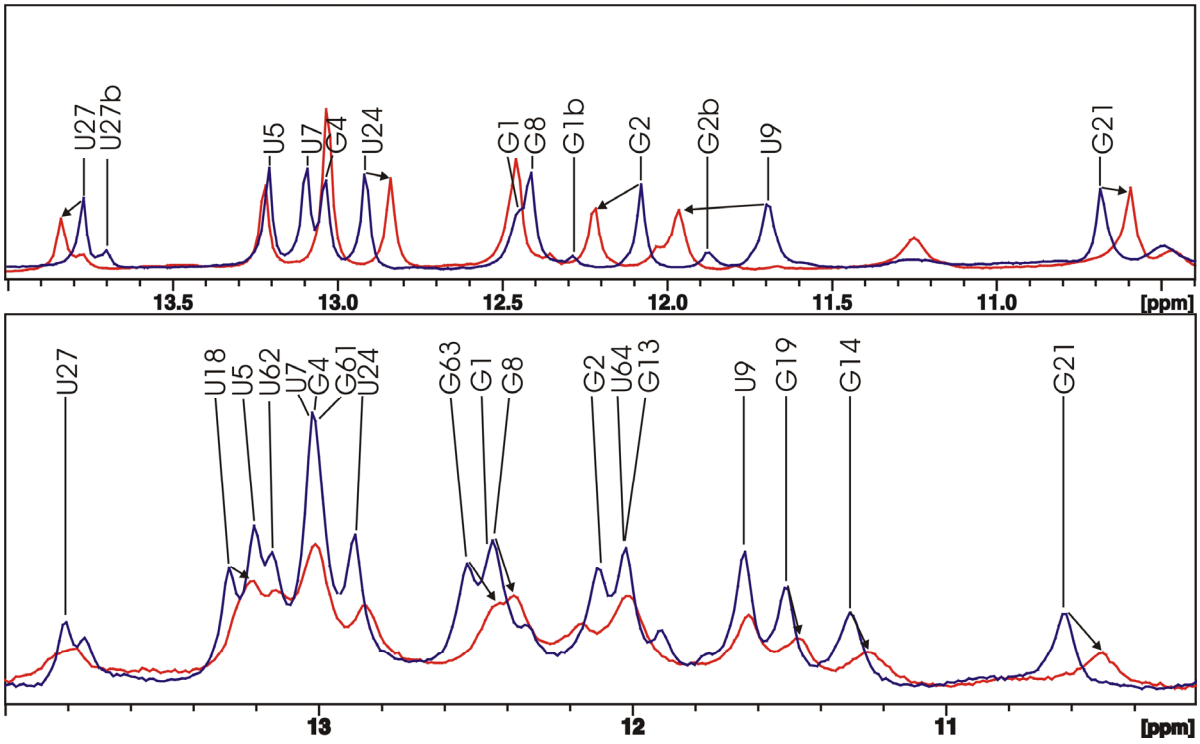

Figure 86 Overlay of the 1D [^{1}H]-NMR spectra of d3'-EBS1* (upper panel) and d3'-EBS1*·IBS1* (lower panel) upon addition of 0 (blue) and 2.5 mM (red) $[Co(NH_3)_6]Cl_3$ for d3'-EBS1* and 2 mM (red) $[Co(NH_3)_6]Cl_3$ for d3'-EBS1*·IBS1*. The chemical shifts, which experienced quite large changes, are indicated by arrows. The letter "b" indicates the resonances of the n+1 derivative, which gives additional resonances for G1, G2 and U27 in the imino spectra (see also text and Section 2.2.5).

To apply this method to d3'-EBS1* and d3'-EBS1*·IBS1*, a series of 1D [^{1}H]-NMR spectra in 90% H_2O/10% D_2O at 278 K were recorded first for both constructs, in which $[Co(NH_3)_6]Cl_3$ was added stepwise (Figure 85 and 86). Using the 1D [^{1}H]-NMR titration experiments, chemical shift changes were observed and additionally line broadening was used as an estimate of a sufficient $[Co(NH_3)_6]Cl_3$ concentration. Comparison of the 1D [^{1}H]-NMR spectra of d3'-EBS1* with the one of d3'-EBS1*·IBS1* shows that in the latter case line broadening is happening already at around 2 mM $[Co(NH_3)_6]Cl_3$, whereas in d3'-EBS1* the lines are still sharp at 2.5 mM $[Co(NH_3)_6]Cl_3$. For d3'-EBS1* the largest chemical shift change is clearly occuring for U9H3, followed by G2H1 (Figure 86A and 87A). In addition G21H1 and U24H3 experience an intermediate change in chemical shift. As already discussed in Section 2.2.1 and 2.5.1, NOEs of imino protons in the loop cannot be observed due to the fast exchange with the solvent. Thus, with these experiments, outer-sphere binding can only be observed to the helical stem. The major chemical shift change at U9 indicates that this site is affected by a $[Co(NH_3)_6]^{3+}$ ion. This chemical shift change can either derive from a direct coordination to U9, or from a structural change in the local environment. Since no metal ion binding site was found at U9 by Mg^{2+} titration experiments (Section 2.5.1), but at "loop 1" comprising A10 – U12, an indirect influence on U9H3 is well possible. Although imino

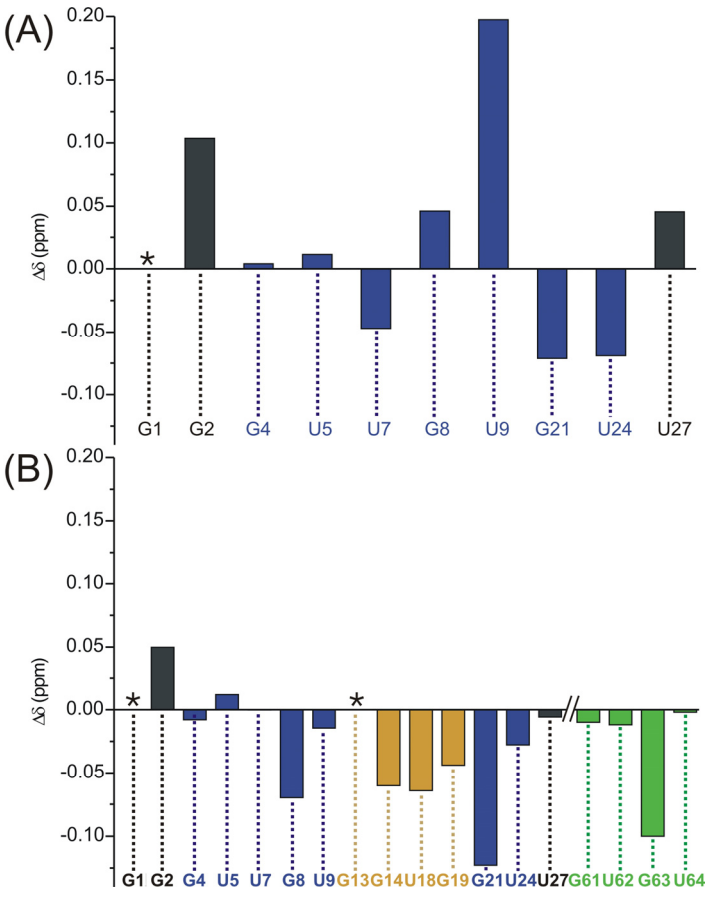

Figure 87 Chemical shift changes of the observed imino resonances upon $[Co(NH_3)_6]^{3+}$ binding. (A) shows the difference in chemical shift in d3'-EBS1* in the absence and presence of 2.5 mM $[Co(NH_3)_6]^{3+}$ and (B) the one in the absence and presence of 2 mM $[Co(NH_3)_6]^{3+}$ for d3'-EBS1*·IBS1*. Colouring of the boxes corresponds to that of the secondary structures in Figure 30A and B. Resonances, which could not be assigned due to overlap, are marked with an asterisk.

protons in the loop of d3'-EBS1* cannot be observed, it cannot be excluded that the binding site "loop 1" accommodates a $[Co(NH_3)_6]^{3+}$ ion.

In d3'-EBS1*·IBS1* an interesting observation is made compared to d3'-EBS1*: The chemical shift of U9H3 is hardly affected by $[Co(NH_3)_6]^{3+}$. This indicates that the local environment around U9 hardly changes. Thus, the $[Co(NH_3)_6]^{3+}$ ion, which is assumed to be located at the binding site "loop 1" in d3'-EBS1*, is not located at the same position in d3'-EBS1*·IBS1*. Although the chemical shift change of G13H1 could not be extracted, one can assume that the $[Co(NH_3)_6]^{3+}$ ion is now located at G13/G14 since G14 experiences a relative large chemical shift. G21H1 experiences the largest chemical shift upon $[Co(NH_3)_6]^{3+}$ addition in d3'-EBS1*·IBS1* (Figure 86B and 87B). In addition, U18H3 and G19H1, which are part of EBS1*, shift upfield (Figure 87B). G63H1 of IBS1* has the most affected chemical shift in the EBS1*-IBS1* interaction and is the only affected imino proton in IBS1* (Figure 87B). These observations suggest that $[Co(NH_3)_6]^{3+}$ coordinates in the EBS1*-IBS1* interaction, thereby inducing structural changes in the local environment, which results in chemical shift changes. So far, one can only speculate about the exact position of the $[Co(NH_3)_6]^{3+}$ in the EBS1*-IBS1* helix, as chemical shift changes cannot be directly transferred to a coordination of $[Co(NH_3)_6]^{3+}$ to the proton, which experiences the chemical shift change.

To get a more detailed picture of the outer-sphere coordination mode to both constructs, 2D [^{1}H,^{1}H]-NOESY experiments were acquired to find NOEs between the imino protons and the ammine protons of $[Co(NH_3)_6]^{3+}$. Figure 88 shows the 2D [^{1}H,^{1}H]-NOESY spectra of d3'-EBS1* and d3'-EBS1*·IBS1*. The $[Co(NH_3)_6]^{3+}$-proton line is located at 3.6 ppm showing

several NOEs to the imino protons in both constructs. The strongest NOEs between an imino proton of d3'-EBS1* and $[Co(NH_3)_6]^{3+}$ appears for U9, suggesting indeed an outer-sphere coordination of $[Co(NH_3)_6]^{3+}$ to this site. Another relative strong NOE to $[Co(NH_3)_6]^{3+}$ was found for G8, as well as intermediate NOEs to U7 and G21. Although no binding site was determined at the upper helical end with Mg^{2+}, these observations indicate that an outer-sphere coordination of $[Co(NH_3)_6]^{3+}$ occurs at the upper helix. Additionally, the NOE between G21H1 and the protons of $[Co(NH_3)_6]^{3+}$, together with the moderate chemical shift change of G21H1 indicate that at the 3'-end of the loop a coordination of $[Co(NH_3)_6]^{3+}$ is possible. This is in good agreement with the binding site postulated in Section 2.5.1. Only a very weak NOE is found to U24H3, thus $[Co(NH_3)_6]^{3+}$ either very weakly coordinates to this site or this weak crosspeak stems from unspecific binding of excess of $[Co(NH_3)_6]^{3+}$. The first assumption is more probable since a metal ion binding site was postulated to occur in close proximity to U24, i.e. "helix 1". Thus, it cannot be excluded that U24 is partially involved in an outer-sphere coordination to $[Co(NH_3)_6]^{3+}$.

In d3'-EBS1*·IBS1* the picture changes: A NOE between U9H3 and the protons of $[Co(NH_3)_6]^{3+}$ is found, but this NOE is much weaker than the one observed in d3'-EBS1*. This observation is consistent with the chemical shift change of U9H3. Unfortunately, NOEs of imino protons often resonate at similar frequencies in the spectrum of d3'-EBS1*·IBS1*, thus some NOEs cannot be clearly identified, e.g. U7H3 resonates together with G61H1 and G4H1. In addition, the chemical shifts of these three imino protons are hardly affected. Thus, it is well possible that two or even three of these protons give NOEs to $[Co(NH_3)_6]^{3+}$. However, very strong NOEs, which can easily be identified, are observed for G14H1, U62H3, G63H1 and U64H3. A crosspeak to G13H1 can be assumed to lie beneath the one of U64H3. Furthermore, the strong NOE to G14 clearly shows that an outer-sphere coordination to this site is present. For IBS1* $[Co(NH_3)_6]^{3+}$ most probably coordinates directly to G63 as could be deduced from its large chemical shift change, thereby coordinating also to the previous and following nucleotide. Surprisingly, no NOE was found for G21H1 to the protons of $[Co(NH_3)_6]^{3+}$, indicating that the large chemical shift change stems from structural changes, which are induced by $[Co(NH_3)_6]^{3+}$ coordination to sites nearby and not directly to G21.

In conclusion, $[Co(NH_3)_6]^{3+}$ coordinates in d3'-EBS1* to U9-G21 at the end of the stem, thereby presumably including G8. It is well possible that a further $[Co(NH_3)_6]^{3+}$ complex around U7 and U24 is formed since both imino protons show an intermediate chemical shift change upon $[Co(NH_3)_6]^{3+}$ addition as well as an interresidual NOE to the protons of $[Co(NH_3)_6]^{3+}$.

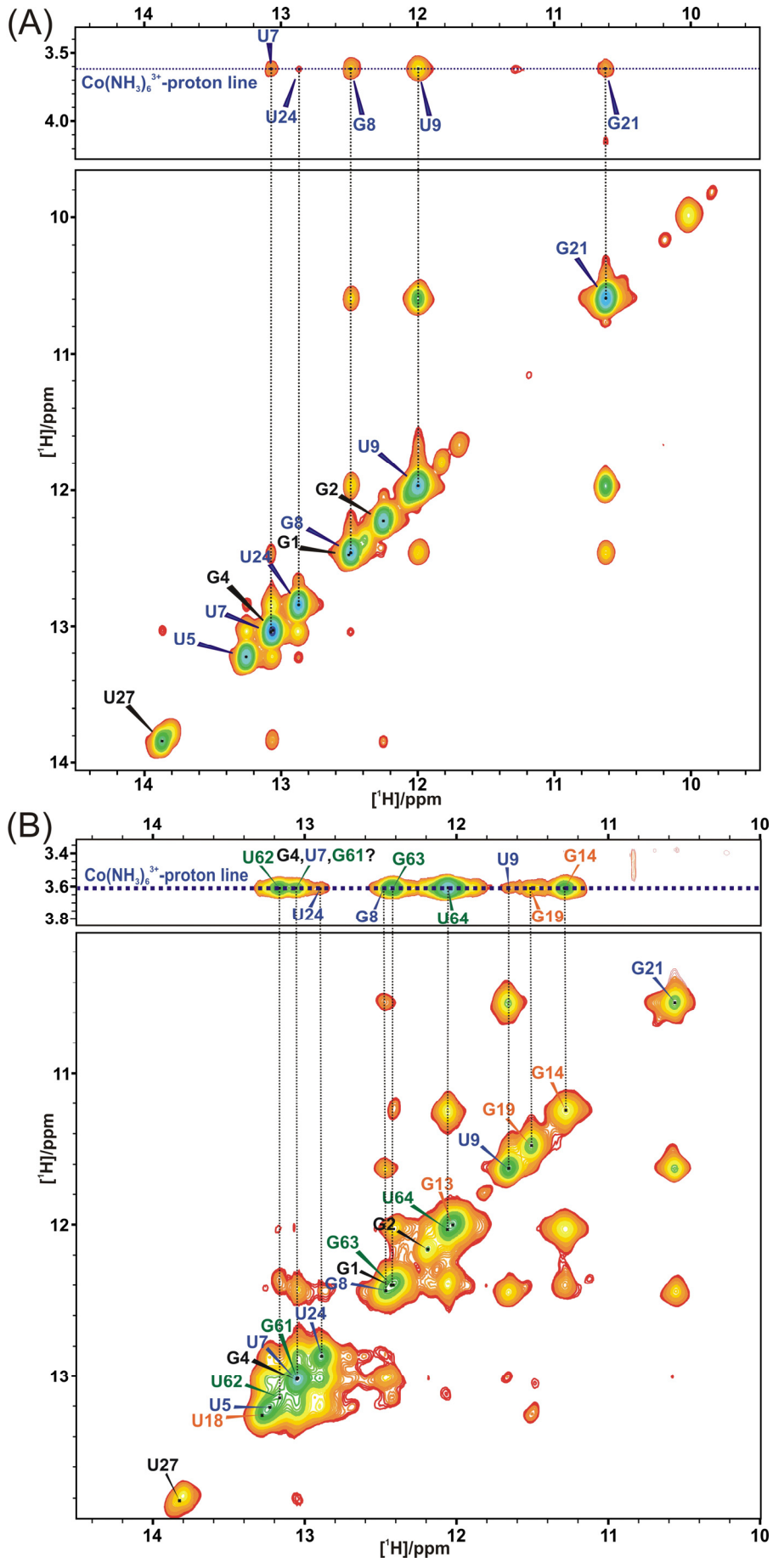

Figure 88 Sections of the 2D [^{1}H,^{1}H]-NOESY spectra of (A) d3'-EBS1* (pH = 6.52, 10 mM KCl, 10 µM EDTA) and (B) d3'-EBS1*·IBS1* (pH = 6.61, 110 mM KCl, 10 µM EDTA) with $[Co(NH_3)_6]^{3+}$ acquired in 90% H_2O/10% D_2O at 278 K. The spectra of d3'-EBS1* was recorded in the presence of 2.5 mM $[Co(NH_3)_6]^{3+}$, whereas to d3'-EBS1*·IBS1* 1.5 mM $[Co(NH_3)_6]^{3+}$ were added. The resonance of the $[Co(NH_3)_6]^{3+}$-protons is shown as a blue dotted line. Imino protons are labeled in the same colour as in Figure 30.

In d3'-EBS1*·IBS1* a $[Co(NH_3)_6]^{3+}$ molecule binds to the EBS1*·IBS1* double helix. The outer-sphere binding site is located at G14 and G63, thereby including U62 and U64 and presumably also G13. In the helix a weak $[Co(NH_3)_6]^{3+}$ binding site is assumed at G8/G9, which is corroborated by the relative large chemical shift change of G8H1. In addition, G21H1 experiences a large chemical shift change, but no NOE to the protons of $[Co(NH_3)_6]^{3+}$ is observed, thus suggesting a conformational change around G21H1, but no direct coordination to $[Co(NH_3)_6]^{3+}$.

2.5.5 Calculation of affinity constants of M^{n+} to RNAs

2.5.5.1 Iterative calculation with ISTARv2.2

Chemical shift studies and line broadening analysis are two approaches to determine metal ion binding sites qualitatively. To assess the metal ion binding sites quantitatively, affinity constants of M^{n+} to the RNA are calculated from the NMR chemical shift change data. Traditionally, affinities of metal ions towards RNA are estimated by plotting the chemical shift changes of the observed proton *versus* the M^{n+} concentration. By fitting these plots assuming a 1:1 binding behaviour (equation 8) the affinity constants are calculated for each individual proton (see also Materials and Methods):

$$\Delta\delta_{obs} = \Delta\delta_{RNA_i} + \left(\Delta\delta_{RNA \bullet M} - \Delta\delta_{RNA}\right) \frac{\left[M^{n+}\right]_{tot} + \left[RNA_i\right]_{tot} + \frac{1}{K_{Ai}} - \sqrt{\left(\left[M^{n+}\right]_{tot} + \left[RNA_i\right]_{tot} + \frac{1}{K_{Ai}}\right)^2 - 4\left[M^{n+}\right]_{tot}\left[RNA_i\right]_{tot}}}{2\left[RNA_i\right]_{tot}} \qquad \text{equation 8}$$

However, a single metal ion affects not necessarily only a single proton, but rather several protons close to its coordination site. Multiple coordination sites can be present in nucleic acids, and thus also multiple metal ions can bind simultaneously. Depending on the affinity of the metal ion, coordination sites can fill up in parallel. As a consequence, a metal ion, which is bound to one site, cannot be available at the same time to bind another site. Thus, the effective $[M^{n+}]$ concentration at each binding site is lower than the total concentration of $[M^{n+}]$ that was added.(351) To calculate intrinsic M^{n+} affinities of a single site, the binding of M^{n+} to all the other sites has to be taken into account. Therefore an iterative correction procedure was used, which was recently developed in our lab.(351)

ISTARv2.2 is a MatLab script that performs an iterative procedure to calculate affinity constants from NMR chemical shift data. The here described procedures are fully automized in ISTAR, simplifying the calculation of intrinsic affinity constants and thereby reducing the time needed for the calculations. ISTAR calculates the $[M^{n+}]$ concentration, which is actually available at each specific coordination site, by subtracting the amount of $[M^{n+}]$ that is bound at the same time to all other binding sites within the same molecule. With this information at hand, ISTAR iteratively calculates the intrinsic affinity constants for each binding site from the NMR chemical shift data.

In other words, ISTARv2.2 is run in two phases: The first phase is the traditional estimation of the affinity constants of each proton towards a designated metal ion according to equation 8. A single iteration is run, resulting in a nonlinear least square fit for each titration point. The quality of the data is thereby not taken into account. Therefore, the fits have to be

evaluated manually and poor fits are discarded. This first round of calculation, in which the M^{n+} concentration still corresponds to the total amount of M^{n+} added at each titration point, yields log $K_{A,est}$ values for each proton. From these first estimates log $K_{A,est}$ and the line broadening data, the individual binding sites are defined. Subsequently, the second phase can be performed resulting in an average affinity constant (log $K_{A,av}$) for each individual binding site. Thereby, each binding site contains one or more ensembles of protons, which were evaluated in the first phase. In the second phase, the available $[M^{n+}]$ concentration for each site is taken into account through an iterative procedure. The first average affinity constants log $K_{A,av1}$ are used to determine the amount of Mg^{2+} bound to each site at every point of the titration by using the following equation:

$$\left[M^{n+}\right]_{bound,i} = \frac{\left(K_{A_i}\left[M^{n+}\right]_{tot} + K_{A_i}\left[RNA_i\right]_{tot} + 1\right) - \sqrt{\left(-\left(K_{A_i}\left[M^{n+}\right]_{tot} + K_{A_i}\left[RNA_i\right]_{tot} + 1\right)\right)^2 - 4K_{A_i}{}^2\left[M^{n+}\right]_{tot}\left[RNA_i\right]_{tot}}}{2K_{A_i}}$$

equation 9

According to:

$$\left[M^{n+}\right]_{avail,i} = \left[M^{n+}\right]_{tot} - \sum\left[M^{n+}\right]_{bound,tot} + \left[M^{n+}\right]_{bound,i}$$ equation 10

the amount of M^{n+}, which is available for binding to a specific site "*i*", is given by the M^{n+} coordinated to this site plus the free concentration of M^{n+}. These corrected M^{n+} concentrations for each individual site are then used in the next iteration round. Again, the corrected data are fitted to a 1:1 binding behaviour resulting in an improved second estimate of the affinity constant log $K_{A,est2}$. To obtain the affinity constants log $K_{A,av2}$ for the individual binding sites, the log $K_{A,est2}$ values are again averaged for each binding site. The corrected affinity constants of the second round serve as a basis to calculate again the amount of M^{n+} at each binding site "*i*" according to equation 9. Subsequently, the concentration of available metal ions for each binding site is again determined. A next round of iteration uses these corrected concentrations to yield new individual log $K_{A,est3}$ as well as new averaged log $K_{A,av3}$ values and so on (see also Materials and Methods). As many iteration rounds are performed until a final averaged log K_A value is achieved, i.e. the log K_A values do not change anymore within their error limits.

The final affinity constants log $K_{A,fin}$ are obtained by plotting the average log $K_{A,av}$ values of each round *versus* the number of the iteration round. The data is then fitted by an asymptotic function (Figure 91, see also Materials and Methods). ISTAR automatically checks for convergence, and thus the iteration procedure is stopped when the change in the

calculated stability constant is below the error limit. But if one wishes to perform a certain number of iterations, this can be manually specified.

2.5.5.2 Iterative calculation with ISTARv2.3

Due to severe line broadening of some resonances in NMR spectra, one might not be able to reliably fit the chemical shift change data to a 1:1 binding isotherm, e.g. in the case of the 5'-end of d3'-EBS1*·IBS1* as discussed in Section 2.5.5.6. In these special cases one has to use known log K_A values of similar binding sites as an estimation to calculate the average affinity constants for the other binding sites. If a relativly high log K_A value is set fixed at the beginning of the iteration, some values for the available M^{n+} concentration may turn negative. In the standard calculation procedure of ISTARv2.2, each binding site can bind as much M^{n+} from the solution as is available, taking into account its affinity constant. At low $[M^{n+}]$ concentrations, this can lead to negative values for the available $[M^{n+}]$ at other binding sites due to the fact that the fixed high affinity site drags almost all available Mg^{2+} just from the beginning of the iteration. Because these results make no physical sense, the $[M^{n+}]$ concentrations bound to each site have to be put into relation to each other. Thus, the equilibrium concentrations of free and bound $[M^{n+}]$ have to be considered. The law of mass action for the formation of the $[RNA{\cdot}M^{n+}]$ complex is given by the following equilibrium:

$$\left[\mathrm{RNA}\right]_{\mathrm{i,free}} + \left[\mathrm{M}^{n+}\right]_{\mathrm{free}} \rightleftharpoons \left[\mathrm{RNA{\bullet}M}^{n+}\right]_{\mathrm{i}}$$

and the equilibrium constant:

$$K_{\mathrm{A,i}} = \frac{\left[\mathrm{RNA{\bullet}M}^{n+}\right]_{\mathrm{i}}}{\left[\mathrm{M}^{n+}\right]_{\mathrm{free}}\left[\mathrm{RNA}\right]_{\mathrm{i,free}}} \qquad \text{equation 11}$$

with $[RNA{\cdot}M^{n+}]_i$, $[M^{n+}]_{free}$ and $[RNA]_{i,free}$ being the concentrations of the metal ion bound to the RNA, the unbound metal ion and the free RNA, respectively, in the equilibrium.

To treat the different binding sites separately with respect to the RNA concentration, it has to be assumed that only two species of RNA with respect to the single binding sites exist in solution, (i) those with a metal ion bound to this special site and (ii) those, which have no metal ion coordinated at this site. With this approximation, $[RNA]_{i,free}$ can be defined as:

$$\left[\mathrm{RNA}\right]_{\mathrm{i,free}} = \left[\mathrm{RNA}\right]_{\mathrm{i,total}} - \left[\mathrm{RNA{\bullet}M}^{n+}\right]_{\mathrm{i}} \qquad \text{equation 12}$$

with $[RNA]_{i,total}$ being the total RNA concentration.

Insertion of equation 12 into 11 gives:

$$K_{A,i} = \frac{\left[RNA \bullet M^{n+}\right]_i}{\left[M^{n+}\right]_{i,free}\left(\left[RNA\right]_{i,total} - \left[RNA \bullet M^{n+}\right]_i\right)} \qquad \text{equation 13}$$

and rearrangement of equation 13 yields:

$$\left[RNA \bullet M^{n+}\right]_i = \frac{K_{A,i}\left[M^{n+}\right]_{i,free}\left[RNA\right]_{i,total}}{\left(K_{A,i}\left[M^{n+}\right]_{i,free}\right)+1} \qquad \text{equation 14}$$

$[M^{2+}]_{i,free}$ is unknown and has therefore to be estimated by minimization of the factor *f*:

$$f\left(\left[M^{n+}\right]_{i,free}\right) = \sum_{1}^{n}\left[RNA \bullet M^{n+}\right]_i + \left[M^{n+}\right]_{i,free} - \left[M^{n+}\right]_{i,total} =$$

$$\sum_{1}^{n}\frac{K_{A,i}\left[M^{n+}\right]_{i,free}\left[RNA\right]_{i,total}}{\left(K_{A,i}\left[M^{n+}\right]_{i,free}\right)+1} + \left[M^{n+}\right]_{i,free} - \left[M^{n+}\right]_{i,total} \qquad \text{equation 15}$$

In this study this minimization step was performed with the *fsolve* command in Matlab. Implementation of these considerations yields the adapted version ISTARv2.3. ISTARv2.2 and ISTARv2.3 were used for the calculation of the intrinsic affinity constants of Mg^{2+} and Cd^{2+} to d3'-EBS1* and d3'-EBS1*·IBS1*, respectively, and will be discussed in the next sections.

2.5.5.3 Calculation of affinity constants of Mg^{2+} to d3'-EBS1* using ISTARv2.2

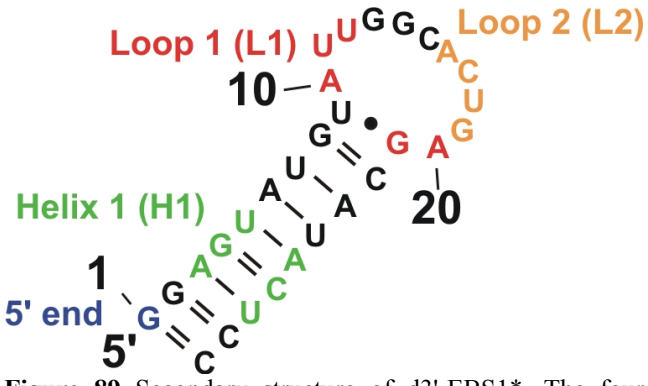

Figure 89 Secondary structure of d3'-EBS1*. The four detected metal ion binding sites are coloured in blue (5'-end), green (helix 1), red (loop 1) and orange (loop 2).

Using ISTARv2.2 the intrinsic affinity constants of Mg^{2+} towards d3'-EBS1* were calculated. The chemical shift data of 79 protons were collected from the titration of d3'-EBS1* with Mg^{2+} for the first phase of ISTAR. 39 of these protons could be fitted to a 1:1 binding isotherm (equation 8). The remaining 40 protons either hardly experienced a chemical shift upon Mg^{2+} addition or could not be found in all spectra recorded due to line broadening or severe overlap. This approach resulted in a first estimation of individual affinities (log $K_{A,est}$) between 1.39 ± 0.29 and 3.3 ± 0.13 at a pD of 6.96 (Appendix 10A). Thorough examination of these values together with the chemical shift and line broadening data revealed four metal ion binding sites in d3'-EBS1* (Figure 89, Appendix 10). The individual log $K_{A,est}$ for each

Table 17 Affinity values log K_A for Mg^{2+} binding to d3'-EBS1* in D_2O. Listed are the averaged log K_A values (1σ) at the four high affinity binding sites, obtained from the change in chemical shifts of all aromatic and H1' protons after various rounds of iterative corrections for the Mg^{2+} concentration that is available at a certain site. The log K_A values are shown for the calculation with ISTARv2.2 (non-shaded lines) and the modified version of ISTARv2.3 (see text), which takes the equilibrium concentrations of the free and bound M^{2+} species in solution into account (shaded lines).

Calculation method[a]	Binding site	log $K_{A,av1}$ [mM^{-1}]	log $K_{A,av2}$ [mM^{-1}]	log $K_{A,av3}$ [mM^{-1}]	log $K_{A,av4}$ [mM^{-1}]	log $K_{A,av5}$ [mM^{-1}]	log $K_{A,fin}$ [b] [mM^{-1}]	$\Delta_{fin-av1}$ [c] [mM^{-1}]
ISTARv2.2	5'-end	3.30 ± 0.13	3.48 ± 0.14	3.64 ± 0.15	3.70 ± 0.17	3.73 ± 0.17	3.76 ± 0.05	0.46 ± 0.13
ISTARv2.3	5'-end	3.30 ± 0.13	3.41 ± 0.13	3.46 ± 0.14	3.47 ± 0.14	3.48 ± 0.14	3.48 ± 0.01	0.18 ± 0.13
ISTAR v2.2	Helix 1 (H1)	2.38 ± 0.04	2.63 ± 0.03	2.72 ± 0.02	2.75 ± 0.03	2.76 ± 0.03	2.77 ± 0.01	0.39 ± 0.04
ISTARv2.3	Helix 1 (H1)	2.38 ± 0.04	2.59 ± 0.03	2.64 ± 0.03	2.65 ± 0.03	2.65 ± 0.03	2.65 ± 0.01	0.27 ± 0.04
ISTARv2.2	Loop 1(L1)	2.13 ± 0.05	2.40 ± 0.03	2.46 ± 0.02	2.48 ± 0.02	2.49 ± 0.02	2.50 ± 0.01	0.37± 0.05
ISTARv2.3	Loop 1(L1)	2.13 ± 0.05	2.39 ± 0.03	2.43 ± 0.03	2.44 ± 0.03	2.45 ± 0.03	2.45 ± 0.01	0.32 ± 0.05
ISTARv2.2	Loop 2 (L2)	2.11 ± 0.06	2.42 ± 0.05	2.48 ± 0.05	2.50 ± 0.05	2.51 ± 0.05	2.52 ± 0.01	0.41 ± 0.06
ISTARv2.3	Loop 2 (L2)	2.11 ± 0.06	2.40 ± 0.05	2.44 ± 0.05	2.45 ± 0.05	2.45 ± 0.05	2.45 ± 0.01	0.34 ± 0.06

The chemical shift changes were obtained from 2D [^{1}H,^{1}H]-NOESY spectra of a 0.5 mM d3'-EBS1* RNA at pD 6.96 in 10 mM KCl at 25 °C. All error limits correspond to one standard deviation (1σ). [a]In the modified ISTARv2.3 version an additional variable *v* is defined, taking the equilibrium between the bound and unbound state of the metal ion into account (see text). [b]The maximal log $K_{A,fin}$ values correspond to the limiting value of an asymptotic fit, which was obtained by plotting log K_a values after each iteration round *versus* the number of the iteration rounds. The errors from the fits were multiplied by three to obtain reasonable error limits. [c]Difference in log K_A between log $K_{A,av1}$ and the maximal log $K_{A,fin}$ of the asymptotic fit.

proton evaluated show similar values for the specific binding site: The first binding site is located at the 5'-end of d3'-EBS1*, a second one encompasses the A3-U27, G4-C26, and U5-A25 base pairs in the helical stem (H1). The third and fourth binding sites are located in the loop. One is found 5' of EBS1* at A10 to U12, including A20 and G21 in this binding site. The second binding site in the loop includes A16 to G19. As already discussed in Section 2.5.1, these two metal ions in the loop might not be fixed at a specific position, but rather cover the entire loop region, waiting for the substrate to bind and thereby stabilizing the interaction and the unusual conformation as discussed in Section 2.2.9.

Having determined these four binding sites, the second phase of ISTAR can be performed yielding log $K_{A,av}$ values (Table 17). The highest affinity was found for the 5'-end with a log $K_{A,av1,5'\text{-end}} = 3.3 \pm 0.13$ after the first iteration round. This relatively high affinity is due to the terminal phosphate groups, which carry the highest negative charge density within transcribed RNA. It is assumed that the value for the 5'-end stands for a mean value of Mg^{2+} binding to a di- and triphosphate moiety located at the 5'-end of the RNA. This assumption is based on two results: (i) upon addition of Mn^{2+} as well as Cd^{2+} a second crosspeak for G1H1'-H8 is observed in the 2D [^{1}H,^{1}H]-NOESY spectra (see Sections 2.5.2 and 2.5.6). This additional resonance illustrates that Mn^{2+} as well as Cd^{2+} form different complexes with di- and triphosphates, leading to different chemical shifts. Mg^{2+} binds not as strongly as Mn^{2+} and Cd^{2+}, and thus no additional resonance in the spectra of the Mg^{2+} titration is observed. Rather

the 5'-ends with either a di- or a triphophate group shift comparably. (ii) Investigations of the metal ion binding properties of a shortened construct of domain 6 of *Sc*.ai5γ suggest that in this transcribed D6-27 construct a diphosphate as well as a triphosphate at the 5'-end is present.[115,351] D6-27 shares the 5'-GGAG sequence with d3'-EBS1*. As both constructs are products of *in vitro* transcription, it is assumed that their 5'-ends have similar properties. However, in the spectra of D6-27 two beginnings are observed even without addition of any metal ions. Thus, the sequence of the full-length RNA has an influence on the spectra. This is supported by 2D [^{1}H,^{1}H]-NOESY spectra of d3'-TL, which has the same sequence in the helical stem as d3'-EBS1*, but instead of the big loop d3'-TL contains a GAAA tetraloop. In the spectra of d3'-TL the sequential walk up to G2 gives two resonances for each crosspeak (Figure 90). However, the observation of a second beginning might not only depend on the sequence, but also on the transcription conditions. Since d3'-TL and d3'-EBS1* were transcribed using different $MgCl_2$ concentrations (30 mM for d3'-EBS1* and 50 mM for d3'-TL), it is likely that the hydrolysis of the triphosphate to a diphosphate at the 5'-end happened during transcription to a greater extent in d3'-TL due to the higher Mg^{2+} concentrations.

The affinity constant at the helical region (H1), involving the nucleotides A3, G4, U5, A25, C26 and U27, was determined to be log $K_{A,av1,H1}$ = 2.38 ± 0.04 mM^{-1} after the first iteration. Although the neighbouring nucleotides A6, U7, G8, U9, C22, A23 and U24 exhibit similar results for the individual log $K_{A,est}$ than H1, these sites were neither considered as an independent binding site nor included in H1 (Appendix 10). This exclusion is based on two considerations: (i) Mn^{2+} as well as Mg^{2+} line broadening data show no effect on the resonances in the helical region above H1 (see Section 2.5.1 and 2.5.2), and (ii) the size of the resulting binding site would be around 18 Å, being too large to be covered by only one metal ion.

The loop encompasses two binding sites: The first one involves the nucleotides A10, U11, U12, A20 and G21, giving an affinity constant of log $K_{A,av1,L1}$ = 2.13 ± 0.05 mM^{-1}. The second one is located at A16, C17, U18 and G19, resulting in a log $K_{A,av1,L2}$ of 2.11 ± 0.06 mM^{-1}. The fact that L1 and L2 experience nearly the same affinity towards Mg^{2+} could be an indication that one single metal ion rolls over this area. However, this assumption can be excluded due to the extent of the loop: The evaluated protons span over a distance

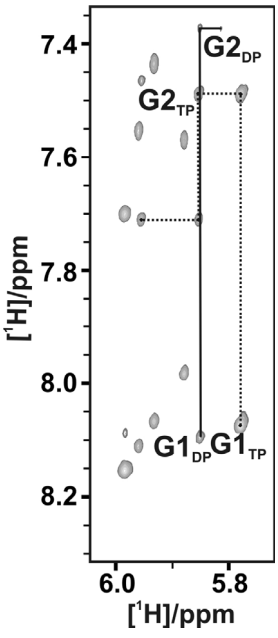

Figure 90 Section of a 2D [^{1}H,^{1}H]-NOESY of d3'-TL recorded at 700 MHz and 303 K. The first nucleotides in the sequential walk are shown. For G1 and G2 two crosspeaks can be distinguished, one for the construct with a triphosphate and one with a diphosphate at the 5'-terminus.

of approximately 17 Å, which is too large for a single metal ion to cover the complete range of the loop. It is well possible that two metal ions are delocalized and thereby an average value is obtained. Thus, a two metal ion coordination to the loop is anticipated and it is feasible that these binding sites are filled up simultaneously.

As mentioned in Section 2.5.5.1 during the first round of calculation of the averaged affinity constants for specific binding sites, the simultaneous occupation of all binding sites by Mg^{2+} is not taken into account. Thus, the total Mg^{2+} concentration present in the sample at each step of the titration was used, resulting in the log $K_{A,av1}$ values (see Table 17, column 3). However, the four binding sites in d3'-EBS1* compete for the free Mg^{2+} ions present in solution. Depending on their individual affinities, some binding sites become loaded with Mg^{2+} before other sites do. As a consequence, the amount of Mg^{2+} available for each site is smaller than the total concentration by the amount bound to the other three sites (Table 18). As already mentioned, the 5'-end of *in vitro* transcribed RNA contains at least partly a triphosphate. Because the 5'-terminus has a significantly higher affinity to Mg^{2+} than the internal binding sites (Table 17) at low Mg^{2+} concentration, a large amount of the metal ions added to the solution binds to the 5'-end, before they occupy other sites. This is reflected by the values given in Table 18, i.e. the 5'-end is at a total Mg^{2+} concentration of 1 mM already occupied by Mg^{2+} to approximately 58%, whereas the other three binding sites are loaded less than 18% each. However, after saturation of all binding sites, approximately 50% of the total Mg^{2+} concentration remains freely available in solution. This exemplifies the inaccuracy, which is obtained when the total amount of Mg^{2+} is used in the calculation.

Table 18 Percentages of Mg^{2+} freely available in solution and bound to each of the binding sites identified in d3'-EBS1* after the first (1st rd) and the fifth iteration round (5th rd). The first number of each entry represents the percentage of the total Mg^{2+} concentration bound to one specific binding site, and the number in parentheses represents the corresponding loading factor of this site in %.[a] The bottom row shows the amount (in percentages) of Mg^{2+} still free in solution as calculated with respect to the total concentration of Mg^{2+}.

$[Mg^{2+}]_{tot}$		1mM	2 mM	3 mM	4 mM	5 mM	6 mM	7 mM
5'-end	1st rd	29.3 (58.6)	19.1 (76.4)	14.0 (83.8)	11.0 (78.7)	9.0 (90.1)	7.6 (91.7)	6.6 (92.9)
	5th rd	38.3 (76.7)	22.3 (89.2)	15.5 (93.1)	11.9 (95.0)	9.6 (96.0)	8.1 (96.7)	6.9 (97.2)
H1	1st rd	8.9 (17.8)	7.6 (30.5)	6.7 (39.9)	5.9 (47.2)	5.3 (52.9)	4.8 (57.5)	4.4 (61.4)
	5th rd	16.4 (32.7)	12.6 (50.4)	10.2 (61.1)	8.5 (68.0)	7.3 (72.9)	6.4 (76.6)	5.7 (79.3)
L1	1st rd	5.6 (11.2)	5.1 (20.3)	4.6 (27.8)	4.2 (34.0)	3.9 (39.2)	3.6 (43.7)	3.4 (47.6)
	5th rd	10.9 (21.8)	9.1 (36.2)	7.7 (46.4)	6.7 (53.8)	5.9 (59.5)	5.3 (63.9)	4.8 (67.5)
L2	1st rd	5.4 (10.8)	4.9 (19.6)	4.5 (26.9)	4.1 (33.0)	3.8 (38.2)	3.6 (38.2)	3.3 (46.5)
	5th rd	11.2 (22.5)	9.3 (37.2)	7.9 (47.5)	6.9 (54.9)	6.1 (60.6)	5.4 (64.5)	4.9 (68.5)
$[Mg^{2+}]_{free}$	1st rd	50.8	63.7	70.2	74.8	78.0	80.4	82.3
	5th rd	23.2	46.7	58.7	66.0	71.1	74.8	77.7

[a]The total RNA concentration is 0.5 mM.

Correction of this inaccuracy leads to an increase for all affinity constants from the first to the second iteration round between 0.18 and 0.31 log units (Table 17). Such an increase for all binding sites is expected, as less Mg^{2+} is available at each data point. From the first to the fifth round an increase for the four binding sites in d3'-EBS1* in the average log K_A values by 0.36 to 0.43 log units is observed (Table 17). The 5'-end, which is reflected by G1H8, experiences thereby the largest change in log K_A from 3.3 ± 0.13 mM^{-1} to 3.73 ± 0.17 mM^{-1}.

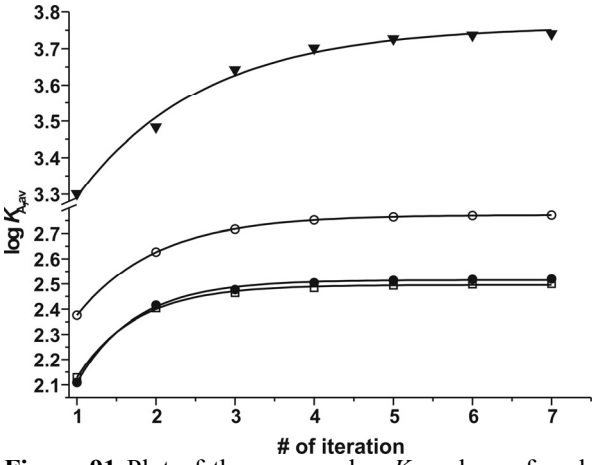

Figure 91 Plot of the average log K_A values of each binding site of d3'-EBS1* towards Mg^{2+} after every round *versus* the number of iterations and fitted by an asymptotic function. The plots for the binding sites at the 5'-end (▼), the helical region (H1, ○), loop 1 (L1, □) and loop 2 (L2, ●) are shown.

The final log $K_{A,fin}$ values, which are obtained by an asymptotic function (see Section 2.5.5.1 and Materials and Methods, Figure 91), for the binding sites in d3'-EBS1* are given in column 8 of Table 17. As already discussed, the 5'-end has the highest affinity to Mg^{2+} with a log $K_{A,fin}$ value of 3.76 ± 0.05 mM^{-1}. The other three binding sites show similar affinities towards Mg^{2+}, the binding site in helix H1 has with 2.77 ± 0.01 mM^{-1} a slightly higher affinity than the two in the loop. However, the similar affinity constants support the parallel occupation of the binding sites.

In the light of the full length ribozyme three of the four binding sites in d3'-EBS1* have to be considered, as the 5'-end of d3'-EBS1* is in the complete ribozyme covalently linked to domain 1 of the intron. Thus, out of the 29 negative charges of the phosphate diester bridges in d3'-EBS1*, six are compensated by the three Mg^{2+} ions. This corresponds to about 20%, which is much higher than the 10% usually expected,[64] and as it is found in the crystal structure of the large ribosomal subunit with 10.6%[358] and the HIV dimerization initiation site with 13%.[359] However, as d3'-EBS1* accomodates the crucial exon binding site 1, which forms tertiary interactions to the exon, the need for metal ions to compensate the repulsive negative charges is obvious. Thus, a high number of equally bound metal ions would support binding of IBS1. It has already been shown that divalent metal ions are necessary for binding of the substrate.[218] In addition to the support of substrate binding, the divalent metal ions located in the loop might also play a crucial role in catalysis. It is known that the excision of the intron is mediated by Mg^{2+} ions and that Mg^{2+} is needed for folding of the intron into the catalytically active form.[213,253,258,261] Hence, the metal ions in the structure of d3'-EBS1*

might play a twofold role. However, in the light of the individual part of the ribozyme, the metal ions seem to play a major role in compensating the negative charge of the backbone, thus allowing IBS1* to bind and subsequently stabilizing tertiary interactions and unusual conformations as observed in the solution structure of d3'-EBS1*·IBS1* (see Section 2.2.9).

2.5.5.4 Calculation of affinity constants of Mg^{2+} to d3'-EBS1* using ISTARv2.3

To compare the results obtained by ISTARv2.2 with the ones of ISTARv2.3, the affinity constants for d3'-EBS1* were recalculated using ISTARv2.3. All steps were performed as described above. The individual affinity constants log $K_{A,est}$ of every evaluated proton obtained after the fifth round of calculation are summarized in Appendix 10C. The average log $K_{A,av}$ together with the final log $K_{A,fin}$ values are listed in Table 17 (shaded lines). The data obtained with ISTARv2.3 give smaller values for the affinity constants than ISTARv2.2, and hence lead to smaller overall changes $\Delta_{fin-av1}$ between 0.18 ± 0.13 and 0.34 ± 0.06, compared to 0.39 ± 0.04 and 0.46 ± 0.13 for ISTARv2.2. It is interesting to note that the largest change in $\Delta_{fin-av1}$ is observed for the 5'-end when calculating with ISTARv2.2, whereas in the new calculation with ISTARv2.3 the 5'-end experiences the smallest change of all binding sites. The 5'-end therefore shows the largest difference in log $K_{A,fin}$ between the two procedures (0.28 ± 0.05 log units). The values for all other binding sites differ only slightly (0.05 to 0.12 log units). Thus, for sites with similar and moderate affinity constants, both procedures are in good agreement with each other. However, the 5'-end of d3'-EBS1*, being the highest affinity binding site, coordinates most of the available Mg^{2+} at low metal ion concentrations. By plotting the chemical shift change *versus* the [Mg^{2+}] concentration, a very steep curve for the 5'-end binding site is obtained in the case of ISTARv2.2. This curve is difficult to fit reliably by a 1:1 binding behaviour. When taking the equilibrium between bound and unbound metal ion into account, i.e. using ISTARv2.3 the plots show a less steep slope due to less bound Mg^{2+}. This also explains the lower log K_A values, which are obtained by the new procedure. Thus, we believe that including the equilibrium concentrations of free and bound metal ions in solution yields more reliable values, as soon as one site exhibits an augmented affinity towards the investigated metal ion.

2.5.5.5 Evaluation of the rearrangement of the metal ion binding sites in d3'-EBS1*

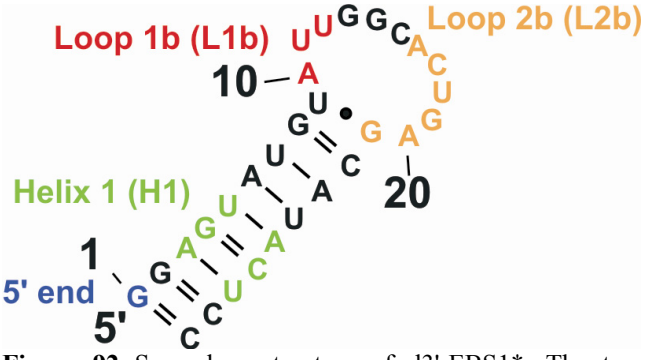

Figure 92 Secondary structure of d3'-EBS1*. The two metal ion binding sites in the loop were rearranged and the calculation repeated. The binding sites are coloured in blue (5'-end), green (helix 1), red (loop 1b) and orange (loop 2b).

Up to this stage, two metal ions were defined to bind at specific regions in the loop. However, it is not clear yet, if the metal ions stick to these sites. Since the loop shows a certain flexibility, the metal ions, which are bound to the loop, might be also influenced by the dynamic behaviour of the loop. Thus, the calculation of the metal ion binding sites in the loop was repeated with newly defined binding sites (Figure 92). The first binding site in the loop L1b now includes the nucleotides A10, U11 and U12. At these nucleotides a binding site was previously determined by Tb^{3+} cleavage assays.[97] The second binding site in the loop L2b is located at the end of the loop, involving A16 to G21.

The affinity constants were calculated with and without the incorporation of the equilibrium concentrations of free and bound metal ions, i.e. with ISTARv2.2 and ISTARv2.3, respectively. The results for all four binding sites in d3'-EBS1* with the newly defined binding sites in the loop are listed in Table 19. After the first round of calculation, in which the total amount of [Mg^{2+}] is considered for every binding site, the log $K_{A,av1}$ values for the 5'-end and the helix 1 are the same as in the previous calculation (Table 17 and 19). This is of course not surprising as these binding sites are defined equally in both calculations. However, the final log $K_{A,fin}$ values are slightly increased, i.e. with the newly defined binding sites, the stability of the Mg^{2+} complex of the 5'-end is increased by 0.08 ± 0.05 log units with the classical ISTARv2.2 version and by 0.02 ± 0.01 log units with ISTARv2.3, which includes the equilibrium concentrations. The final log $K_{A,fin}$ value of helix 1 experiences an increase of 0.03 ± 0.01 log units with ISTARv2.2 and with ISTARv2.3 it is the same within the error limits.

Comparing the log $K_{A,av1}$ values of the binding sites loop 1b and loop 2b after the first iteration round, it is already obvious that the binding site loop 1b with a log $K_{A,av1}$ of 2.31 ± 0.05 mM^{-1} has now a higher affinity to Mg^{2+} than loop 2b with 2.02 ± 0.05 mM^{-1}. The log $K_{A,fin}$ of loop 1b gives a value of 2.71 ± 0.01 mM^{-1} with ISTARv2.2 and 2.63 ± 0.03 mM^{-1} with ISTARv2.3, whereas loop 2b has a log $K_{A,fin}$ value of 2.47 ± 0.02 mM^{-1} if calcultated

Table 19 Affinity values log K_A for Mg^{2+} binding to d3'-EBS1* in D_2O with newly defined binding sites in the loop (see Figure 92). Listed are the averaged log K_A values (1σ) at the four high affinity binding sites, obtained from the change in chemical shifts of all aromatic and H1' protons after various rounds of iterative corrections for the Mg^{2+} concentration that is available at a certain site. The log K_A values are shown for the calculation with ISTARv2.2 (non-shaded lines) and the modified version of ISTARv2.3 (see text), which takes the equilibrium concentrations of the free and bound M^{2+} species in solution into account (shaded lines).

Calculation method[a]	Binding site	log $K_{A,av1}$ [mM^{-1}]	log $K_{A,av2}$ [mM^{-1}]	log $K_{A,av3}$ [mM^{-1}]	log $K_{A,av4}$ [mM^{-1}]	log $K_{A,av5}$ [mM^{-1}]	log $K_{A,fin}$ [b] [mM^{-1}]	$\Delta_{fin-av1}$ [c] [mM^{-1}]
ISTARv2.2	5'-end	3.30 ± 0.13	3.50 ± 0.14	3.68 ± 0.16	3.75 ± 0.18	3.79 ± 0.19	3.84 ± 0.06	0.54 ± 0.13
ISTARv2.3	5'-end	3.30 ± 0.13	3.41 ± 0.13	3.48 ± 0.14	3.49 ± 0.14	3.49 ± 0.14	3.50 ± 0.01	0.20 ± 0.13
ISTARv2.2	Helix 1 (H1)	2.38 ± 0.04	2.64 ± 0.02	2.74 ± 0.03	2.78 ± 0.03	2.79 ± 0.03	2.80 ± 0.01	0.42 ± 0.04
ISTARv2.3	Helix 1 (H1)	2.38 ± 0.04	2.60 ± 0.03	2.65 ± 0.03	2.66 ± 0.03	2.66 ± 0.03	2.66 ± 0.01	0.28 ± 0.04
ISTARv2.2	Loop 1(L1b)	2.31 ± 0.05	2.60 ± 0.03	2.66 ± 0.02	2.69 ± 0.02	2.71 ± 0.02	2.71 ± 0.01	0.40 ± 0.05
ISTARv2.3	Loop 1(L1b)	2.31 ± 0.05	2.56 ± 0.03	2.61 ± 0.03	2.62 ± 0.03	2.63 ± 0.03	2.63 ± 0.03	0.32 ± 0.05
ISTARv2.2	Loop 2 (L2b)	2.02 ± 0.05	2.34 ± 0.03	2.41 ± 0.02	2.45 ± 0.02	2.47± 0.02	2.47 ± 0.02	0.45 ± 0.05
ISTARv2.3	Loop 2 (L2b)	2.02 ± 0.05	2.32 ± 0.04	2.37 ± 0.03	2.38 ± 0.03	2.38 ± 0.03	2.38 ± 0.02	0.36 ± 0.05

The chemical shift changes were obtained from 2D [^{1}H,^{1}H]-NOESY spectra of a 0.5 mM d3'-EBS1* RNA at pD 6.96 in 10 mM KCl at 25 °C. All error limits correspond to one standard deviation (1σ). [a]In the modified ISTAR version an additional variable *v* is defined, taking the equilibrium between the bound and unbound state of the metal ion into account (see text). [b]The maximal log $K_{A,fin}$ values correspond to the limiting value of an asymptotic fit, which was obtained by plotting log K_a values after each iteration round *versus* the number of the iteration rounds. The errors from the fits were multiplied by three to obtain reasonable error limits. [c]Difference in log K_A between log $K_{A,av1}$ and the maximal log $K_{A,fin}$ of the asymptotic fit.

without the equilibrium concentrations of bound and unbound M^{2+}, and 2.38 ± 0.02 mM^{-1} including the equilibrium, respectively. These results can be traced back to the individual log $K_{A,est}$ values of the single protons in the loop region (see Appendix 10A). Since the individual log $K_{A,est}$ values contribute to the final affinity constants for each binding site, these values are highly dependent on the individual log $K_{A,est}$ values. A20H2, A20H8 and G19H8 have log $K_{A,est}$ values below 2, thus the final log $K_{A,fin}$ values for the single binding sites depend on the incorporation of these protons into the site. However, besides these three relatively low log $K_{A,est}$ values, all other values of the individual protons in the loop are roughly in the same range. Thus, it can be generally accepted that the two metal ions bind with the same affinity to the loop and that these metal ions are somehow spread over the loop to cover a large range. Having a look at the solution structure of d3'-EBS1*, the first suggestion of the binding sites in the loop as shown in Figure 89 is the more likely one. This assumption is based on the arrangement of the nucleotides in the loop. A10, U11, U12, A20 and G21 are located such that one Mg^{2+} ion can cover this range, whereas the nucleotides at the 3'-end of the loop, A16 to G21, span a relatively large range which cannot be covered by only one metal ion. Thus, it is assumed that the binding sites shown in Figure 89 are the more reliable ones.

2.5.5.6 Calculation of affinity constants of Mg^{2+} to d3'-EBS1*·IBS1* using ISTARv2.3

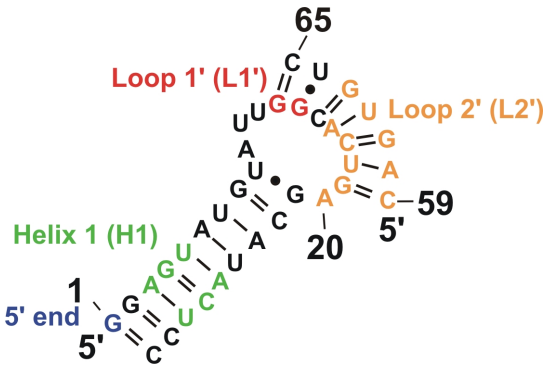

Figure 93 Secondary structure of d3'-EBS1*·IBS1*. The four determined binding sites are coloured in blue (5'-end), green (helix 1), red (loop 1') and orange (loop 2').

To evaluate the influence of IBS1* on the Mg^{2+} affinities towards the determined binding sites, the affinity constants for each Mg^{2+} binding site in d3'-EBS1*·IBS1* were calculated. Four metal ions specifically binding to d3'-EBS1*·IBS1* were detected by chemical shift and line broadening studies (Section 2.5.1 and 2.5.2). In order to localize all Mg^{2+} binding sites better, the chemical shifts of all base and sugar protons were plotted *versus* the titrated Mg^{2+} concentration, and the millimolar affinity constants calculated by fitting these plots by a 1:1 binding mode analogous to d3'-EBS1* (see Section 2.5.5.1 and Materials and Methods). Out of 98 evaluated protons, 51 could be fitted to a 1:1 binding isotherm (equation 8). The remaining 47 protons experience hardly any chemical shift, or could not be evaluated in all spectra due to severe overlap or line broadening. The fits reveal first estimates for the individual log $K_{A,est}$ values between 1.24 ± 0.10 mM^{-1} and 3.13 ± 0.32 mM^{-1} at a pD of 6.83 (Appendix 21A). These values together with the chemical shift and the Mg^{2+} as well as Mn^{2+} line broadening data were thoroughly evaluated and revealed four metal ion binding sites within d3'-EBS1*·IBS1* (Figure 93, Appendix 21). The evaluated protons were grouped according to similar affinities towards Mg^{2+}, suggesting that one metal binds with the same affinity to the specific site. Two metal ion binding sites in d3'-EBS1*·IBS1* are at the same locations as in d3'-EBS1*, the one at the 5'-end of the hairpin and the other one in the helix (H1) including the base pairs A3-U27, G4-C26, and U5-A25. The third and the fourth binding site are also located in the loop, but at slightly different locations. The binding site, which is in d3'-EBS1* just 5' of EBS1* including A10 to U12 (L1), is shifted downstream to G13 and G14 (L1'). As already discussed in Section 2.5.1 and 2.5.2, it is well possible that G13 and G14 provide a metal ion binding platform due to the structural change, which is induced upon IBS1* binding. On one hand the metal ion might stabilize the unusual conformation just 5' of EBS1* (Section 2.2.9 and Figure 55), on the other hand it binds preferentially to this site because the phosphate oxygens protrude and are therefore more accessible to metal ion binding. The second binding site in the loop (L2') seems to cover a relative large area, including the nucleotides A16 to A20 and C59 to G63 (see also Figure 93 and Appendix 21). However, this binding site was assigned on the basis of

similar log $K_{A,est}$ values, suggesting a single Mg^{2+} to bind to this region. A20H2 as well as C17H6 were not included in the evaluation of this binding site due to their relativly low log $K_{A,est}$ values. Although G21H1' and U64H1' enlarge the range, which the metal ion has to cover, they were included in this binding site due to a similar log $K_{A,est}$ value. It is assumed that the averaged affinity constant for the binding site is not affected by the inclusion of these two protons. In order to cover a distance of 20 Å, the single Mg^{2+} ion has to roll over the whole binding site L2'. Two further considerations underline the assumption of only two metal ion binding sites in the loop: (i) in the absence of IBS1* only two metal ions are found in the loop, which are considered to "wait" for IBS1* to bind in order to compensate the negative charges and to stabilize the new arrangement. As discussed in Section 2.5.5.3, these specifically bound metal ions neutralize double the amount of negative charge from the phosphate diester bridges as usually expected. The binding of IBS1* delivers 7 additional nucleotides and thus out of the 36 negative charges of the phosphate diester bridges six are compensated by totally three Mg^{2+} ions, corresponding to about 16.5%. This amount is now closer to the expected 10%.[64] (ii) In the crystal structure of an intact, self-spliced group II intron from *Oceanobacillus iheyensis* only two metal ions were found to reside on the surface of D5, and are therefore accessible to EBS1.[249] This corroborates the suggestion of only two metal ions close to the EBS1*·IBS1* interaction.

The resonances of the 5'-end of d3'-EBS1*·IBS1* disappear very early in the titration. Thus, the data for G1 and G2 could not be fitted to a 1:1 binding mode. However, this fast broadening indicates a high affinity of Mg^{2+} to the 5'-end of d3'-EBS1*·IBS1*, as it was already observed in d3'-EBS1*.

To calculate the averaged affinity constants log $K_{A,av}$ for all binding sites in d3'-EBS1*·IBS1* despite the missing information of the 5'-end, the following approach was used: Since both constructs share the sequence in the helical stem of the hairpin, it is assumed that this part exhibits a similar metal ion binding behaviour in both constructs. Thus, d3'-EBS1* and d3'-EBS1*·IBS1* should have approximately the same affinity towards Mg^{2+} at the 5'-end. However, it has to be considered that the titrations were performed under different conditions, i.e. d3'-EBS1* was measured in the presence of 10 mM KCl at a pD of 6.96, whereas the ionic strenght in the sample of d3'-EBS1*·IBS1* was 110 mM KCl at a pD of 6.83. As it cannot be excluded that the binding sites are partly occupied by K^+ ions that influence the affinity towards Mg^{2+}, the log $K_{A,fin}$ values of d3'-EBS1* cannot directly be transferred to d3'-EBS1*·IBS1*. Thus, a second value is needed to determine an estimate for the 5'-end of d3'-EBS1*·IBS1*. The log $K_{A,fin}$ values that have recently been calculated for

D6-27[351] were used as a second starting point for the calculation. It can be assumed that the log $K_{A,fin}$ values of D6-27 (2.57 ± 0.01 mM^{-1} for the 5'-DP and 3.35 ± 0.01 mM^{-1} for 5'-TP) are more appropriate than other literature values for Mg^{2+} coordination to GTP and GDP residues,[353] because the sequence at the helix end is identical for D6-27 and d3'-EBS1* (Figure 21C). The log $K_{A,fin}$ values of D6-27 were determined at an ionic strength of 100 mM (KCl) at a pD of 6.7.[351]

However, before calculating the estimate for log $K_{A,fin}$ of d3'-EBS1*·IBS1*, the following considerations have to be taken into account:

(i) Due to the implementation of the fixed value for the 5'-end in the calculation for log $K_{A,fin}$ of d3'-EBS1*·IBS1*, ISTARv2.3 was used (see section 2.5.5.2). The following log $K_{A,fin}$ values for the 5'-terminus were used in the calculation: 3.48 ± 0.01 mM^{-1} for d3'-EBS1* at 10 mM KCl and 2.57 ± 0.01 mM^{-1} for the the 5'-diphosphate end and 3.35 ± 0.01 mM^{-1} for the 5'-triphosphate end of D6-27 at 100 mM KCl.[322,351]

(ii) This leads to the second consideration: For D6-27, two values for the 5'-end were determined, i.e. for a 5'-terminus with either a di- or a triphosphate residue. In d3'-EBS1* it is assumed that these two ends exist as well in solution, but as their crosspeaks resonate at the same frequency, their log K_A values could not be determined individually (for details see Sections 2.5.1 and 2.5.5.3). Thus, to use the log K_A value of D6-27, an average value of the di- and triphosphate has to be determined. The two sets of NOE peaks for the 5'-terminal G1 in D6-27 were found in a 1:2 ratio, the one with lower intensity belonging to the triphosphate (TP) residue and the other to the diphosphate (DP) moiety.[322,351] Before averaging the values for the 5'-TP and DP end of D6-27, a third consideration has to be taken into account:

(iii) The above mentioned values 2.57 ± 0.01 mM^{-1} for the 5'-DP and 3.35 ± 0.01 mM^{-1} for 5'-TP of D6-27 are *apparent* constants, i.e. these values are only valid at pD 6.7, at which the experiments were carried out. At this pD a competition between the proton (actually a D^+ ion) and Mg^{2+} occurs at the terminal phosphate residue. It has to be noted that such a competition does not exist for internal phosphate binding sites, because their pK_a values are not in the physiological pH range.

The proton competition at the terminal diphosphate or triphosphate residue can be determined by considering the corresponding pK_a values of the monoprotonated phosphate groups. Since the acidity constants are not known for D6-27 nor for d3'-EBS1*, one has to assume that they are very similar to those of nucleoside 5'-triphosphates ($pK^{H}_{H(NTP)}$ = 6.50 ± 0.05)[360,361] and nucleoside 5'-diphosphates ($pK^{H}_{H(NDP)}$ = 6.40 ± 0.05).[352,362] The reason for the similarity of these two values is that the nucleoside is rather far apart from the site of deprotonation, i.e. the

monoprotonated terminal phosphate group. The values for $H(GTP)^{3-}$ ($pK^{H}_{H(GTP)}$ = 6.50 ± 0.02)[355] and $H(GDP)^{2-}$ ($pK^{H}_{H(GDP)}$ = 6.38 ± 0.01)[363] fit well into this picture and were used for the evaluation.

In addition, it has to be considered that the measurements were performed in D_2O and not in H_2O. To account for D_2O as solvent, the following equation was used:[364]

$$pK_{a/D_2O} = 1.015 \cdot pK_{a/H_2O} + 0.45 \qquad \text{equation 16}$$

to give $pK^{D}_{D(GTP)}$ = 7.05 and $pK^{D}_{D(GDP)}$ = 6.93. These two values were then used to estimate the competition between D^+ and the metal ion by using equation 17

$$\log K_{A,DP/TP} = \log K^{app}_{A,fin,DP/TP} + \log\left(1+\frac{[D^+]}{K_{a,\,D_2O}}\right) \qquad \text{equation 17}$$

with $\log K_{A,DP/TP}$ being the actual local stability constant, $\log K^{app}_{A,fin,DP/TP}$ the apparent stability constant at a given pD, and $[D^+] = 10^{-pD}$. Using equation 17 the actual $\log K_A$ is calculated, resulting in a value independent of the pD, i.e. no competition with D^+ occurs.

By inserting the apparent affinity constants $\log K^{app}_{A,fin,DP}$ = 2.57 ± 0.01 mM^{-1} and $\log K^{app}_{A,fin,TP}$ = 3.35 ± 0.01 mM^{-1} of D6-27 into equation 17, the actual local stability constants of $\log K_{A,DP}$ = 3.00 ± 0.01 mM^{-1} for a 5'-diphosphate and $\log K_{A,TP}$ = 3.86 ± 0.01 mM^{-1} for a 5'-triphosphate helix end were calculated. These two values were then adjusted to pD = 6.96, which is the pD value used for measurements of d3'-EBS1* to yield the apparent $\log K^{app}_{A,fin,DP}$ and $\log K^{app}_{A,fin,TP}$ values at this specific pD. equation 17 yields apparent affinity constants of $\log K^{app}_{A,fin,DP}$ = 2.71 ± 0.01 mM^{-1} and $\log K^{app}_{A,fin,TP}$ = 3.51 ± 0.01 mM^{-1}.

As for d3'-EBS1* only one value is available for the 5'-end, which is assumed to be an averaged value for a 5'-terminus with a di- and triphosphate residue (see also above), the apparent stability constants of DP and TP for D6-27 have to be averaged. Calculating a weighted average of these values assuming a TP:DP ratio of 1:2, resulted in a $\log K^{app}_{A,fin}$ = 3.15 ± 0.01 mM^{-1} for a mixture of di- and triphosphate at the 5'-end at an ionic strength of 100 mM KCl.

The $\log K^{app}_{A,fin}$ = 3.48 ± 0.01 mM^{-1} of d3'-EBS1* at 10 mM KCl together with the $\log K^{app}_{A,fin}$ = 3.15 ± 0.01 mM^{-1} of D6-27 at 100 mM KCl were used to obtain an estimate for the 5'-end of d3'-EBS1*·IBS1* at 110 mM KCl. Extrapolation of the values at 10 and 100 mM KCl resulted in a $\log K^{app}_{A,fin}$ = 3.11 ± 0.01 mM^{-1} at 110 mM KCl (Figure 94). This slightly lower

value seems reasonable since at 110 mM KCl the 5'-end is easier occupied by K^+ than at 10 or 100 mM KCl, resulting in a lower affinity of Mg^{2+} to this site.

The calculated affinity constant $\log K_{A,fin}^{app}$ = 3.11 ± 0.01 mM^{-1} for 110 mM KCl is an apparent stability constant, i.e. in this case it is valid for a pD of 6.96. The measurements of d3'-EBS1*·IBS1* were performed at a pD of 6.83. Thus, the value of 3.11 ± 0.01 mM^{-1} has to be adjusted for pD = 6.83 to be used in the calculation of the averaged affinity constants for all binding sites. equation 18 accounts for the differences in pD:

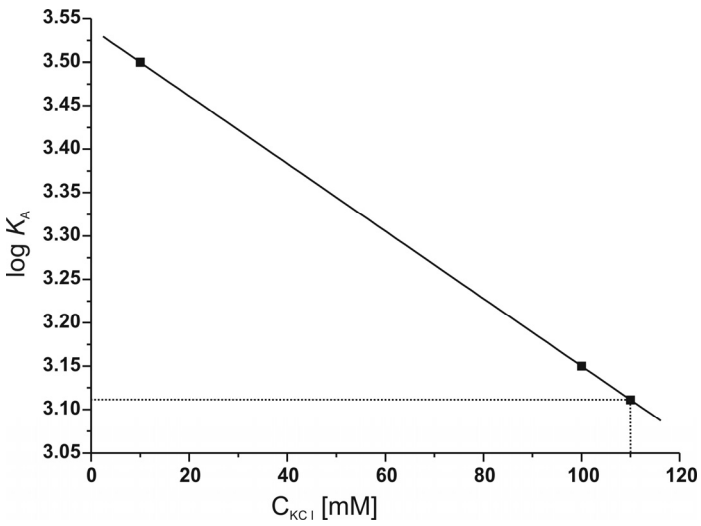

Figure 94 Extrapolation (solid line) of the $\log K_{A,fin}^{app}$ values at 10 and 100 mM KCl resulting in the $\log K_{A,fin}^{app}$ value for 110 mM KCl (dotted lines).

$$\log K_{A,2} = \log K_{A,1} + \log\left(1+\frac{[D^+]_1}{K_{a,D_2O}}\right) - \log\left(1+\frac{[D^+]_2}{K_{a,D_2O}}\right) \qquad \text{equation 18}$$

with $\log K_{A,2}$ being the unknown affinity constant, $\log K_{A,1}$ = 3.11 ± 0.01 mM^{-1}, $[D^+]_1 = 10^{-pD}$ with the pD of 6.96, at which $\log K_{A,1}$ was determined, and $[D^+]_2 = 10^{-pD}$ with the pD of 6.83, at which the measurements of d3'-EBS1*·IBS1* were carried out.

Having now approximated an affinity constant for the 5'-end of d3'-EBS1*·IBS1*, log $K_{A,av}$ values for the other three binding sites could be determined. For this purpose ISTARv2.3 was used, which considers the equilibrium concentrations of free and bound [Mg^{2+}] (see Section 2.5.5.2). The iteration was then performed analogously to the case with d3'-EBS1*, resulting in the affinity constants listed in Table 20a. The plot of the average log $K_{A,av}$ values of each binding site after every iteration round versus the iteration number together with the asymptotic fit is shown in Figure 95.

The first binding site in the loop, L1', including G13 and G14, shows thereby with log $K_{A,fin}$ = 3.06 ± 0.01 mM^{-1} a slightly higher affinity to Mg^{2+} than the 5'-end with 3.03 ± 0.1 mM^{-1}. This result may seem surprising, since usually the 5'-end with its multiple negative charge is assumed to be the site with the highest affinity towards Mg^{2+}. However, having a closer look at the structure of d3'-EBS1*·IBS1*, it can be seen that the phosphate oxygens of G13 and G14 protrude to the outside (Figure 55 and 84C), thus the negative charges of the backbone at this site are exposed and easily accessible for metal ions to bind. In addition, the

unusual kink needs to be stabilized by metal ions, thus a high affinity towards divalent metal ions at this site is expected. The observation of a strong metal ion binding site located at the 5'-end of EBS1* is in good agreement with Tb^{3+} cleavage experiments, which revealed a high affinity metal ion binding site at the 5'-end of EBS1.[97]

The binding site in the helix (H1) and the second one in the loop (L2') show similar affinities towards Mg^{2+} (Table 20a), suggesting a parallel occupation of these two binding sites. Both have in common that they are located in helical regions, thus suggesting that the metal ions at these sites are crucial for stabilizing structural elements. However, it cannot be excluded that the second metal ion in the loop is additionally participating in catalysis.

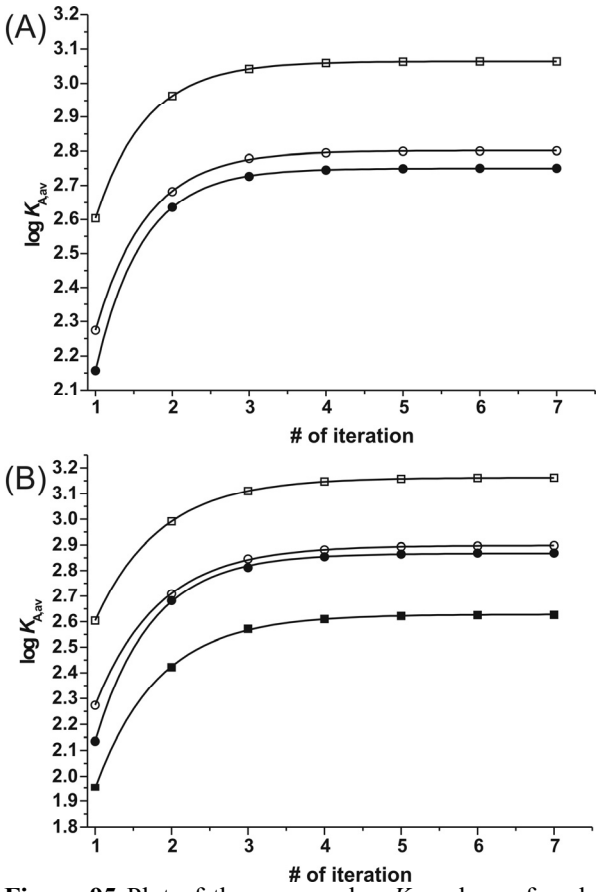

Figure 95 Plot of the average log K_A values of each binding site of d3'-EBS1*·IBS1* towards Mg^{2+} after every round *versus* the number of iterations and fitted by an asymptotic function. The plots for the binding sites at the helical region (H1, ○), loop 1' (L1', □), loop 2' (L2', ●) and loop 3' (L3', ■) are shown. (A) shows the plots for the consideration of 4 binding sites and (B) the ones for 5 binding sites.

The affinity constants of the binding sites in the loop of d3'-EBS1*·IBS1* are higher than the ones in d3'-EBS1* (Table 17 and Table 20a), showing that a tighter binding of

Table 20 Affinity values log K_A for Mg^{2+} binding to d3'-EBS1*·IBS1* in D_2O. Listed are the averaged log K_A values (1σ) of four (a) and five (b) high affinity binding sites, obtained from the change in chemical shifts of all aromatic and H1' protons after various rounds of iterative corrections for the Mg^{2+} concentration that is available at a certain site. The log K_A values were calculated with ISTARv2.3, which takes the equilibrium concentrations of the free and bound M^{2+} species in solution into account. A fixed value for the 5'-end was given as input due to early disappearance of resonances at the 5'-end in the 2D [^{1}H,^{1}H]-NOESY (see text).

(a)

Binding site	log $K_{A,av1}$ [mM^{-1}]	log $K_{A,av2}$ [mM^{-1}]	log $K_{A,av3}$ [mM^{-1}]	log $K_{A,av4}$ [mM^{-1}]	log $K_{A,av5}$ [mM^{-1}]	log $K_{A,fin}$ [a] [mM^{-1}]	$\Delta_{fin-av1}$ [b] [mM^{-1}]
5'-end	-	-	-	-	-	3.03 ± 0.10	-
Helix 1 (H1)	2.27 ± 0.05	2.68 ± 0.06	2.78 ± 0.06	2.80 ± 0.06	2.80 ± 0.06	2.80 ± 0.01	0.53 ± 0.05
Loop 1' (L1')	2.60 ± 0.13	2.96 ± 0.12	3.04 ± 0.13	3.06 ± 0.13	3.06 ± 0.13	3.06 ± 0.01	0.46 ± 0.13
Loop 2' (L2')	2.16 ± 0.04	2.64 ± 0.03	2.73 ± 0.03	2.75 ± 0.03	2.75 ± 0.03	2.75 ± 0.01	0.59 ± 0.04

(b)

Binding site	log $K_{A,av1}$ [mM^{-1}]	log $K_{A,av2}$ [mM^{-1}]	log $K_{A,av3}$ [mM^{-1}]	log $K_{A,av4}$ [mM^{-1}]	log $K_{A,av5}$ [mM^{-1}]	log $K_{A,fin}$ [a] [mM^{-1}]	$\Delta_{fin-av1}$ [b] [mM^{-1}]
5'-end	-	-	-	-	-	3.03 ± 0.05	-
Helix 1 (H1)	2.27 ± 0.05	2.71 ± 0.06	2.85 ± 0.06	2.88 ± 0.06	2.89 ± 0.06	2.90 ± 0.01	0.63 ± 0.05
Loop 1'b (L1'b)	2.60 ± 0.13	2.99 ± 0.12	3.11 ± 0.13	3.15 ± 0.14	3.16 ± 0.14	3.16 ± 0.01	0.56 ± 0.13
Loop 2'b (L2'b)	2.14 ± 0.06	2.68 ± 0.04	2.81 ± 0.04	2.85 ± 0.04	2.86 ± 0.04	2.87 ± 0.01	0.73 ± 0.06
Loop 3' (L3')	1.95 ± 0.06	2.42 ± 0.04	2.57 ± 0.04	2.61 ± 0.04	2.62 ± 0.04	2.63 ± 0.01	0.68 ±0.06

The chemical shift changes were obtained from 2D [^{1}H,^{1}H]-NOESY spectra of a 0.9 mM d3'-EBS1*·IBS1* RNA at pD 6.83 in 110 mM KCl at 25 °C. All error limits correspond to one standard deviation (1σ). [a]The maximal log $K_{A,fin}$ values correspond to the limiting value of an asymptotic fit, which was obtained by plotting log K_a values after each iteration round *versus* the number of the iteration rounds. The errors from the fits were multiplied by three to obtain reasonable error limits. [b]Difference in log K_A between log $K_{A,av1}$ and the maximal log $K_{A,fin}$ of the asymptotic fit.

divalent metal ions is required when the substrate is bound. This observation confirms the assumption that divalent metal ions are required to bind EBS1* and to stabilize the interaction between IBS1* and its substrate.

2.5.5.7 Four *versus* five metal ion binding to d3'-EBS1*·IBS1*

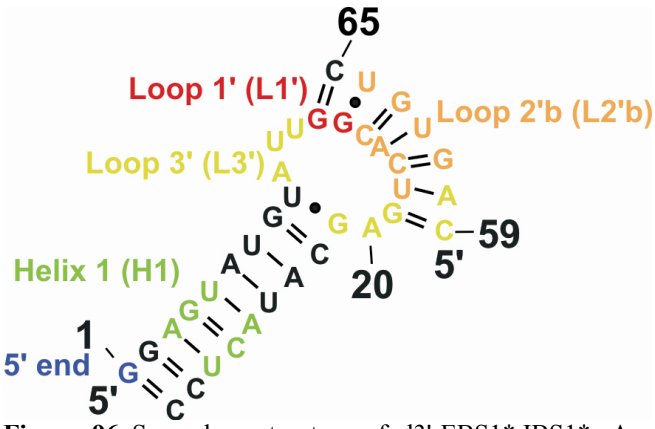

Figure 96 Secondary structure of d3'-EBS1*·IBS1*. An additional binding site was defined in the loop and the calculation repeated. The binding sites are coloured in blue (5'-end), green (helix 1), red (loop 1'), orange (loop 2'b), and yellow (loop 3').

In the previous section a four metal ion binding model to d3'-EBS1*·IBS1* has been discussed. To evaluate the possibility of five binding sites in d3'-EBS1*·IBS1*, the iteration procedure was used to calculate the averaged log $K_{A,fin}$ values with five defined binding sites, i.e. three of them in the loop (Figure 96). With five metal ions bound to d3'-EBS1*·IBS1* it is assumed that the downstream shift of the metal ion binding site at EBS1* upon binding of IBS1* does not occur, but an additional metal ion comes into play, binding to the EBS1* site at G13/G14 (Figure 96). The definition of the three binding sites in the loop of d3'-EBS1*·IBS1* may seem inexpertly when looking only at the secondary structure. Having a closer look at the solution structure of d3'-EBS1*·IBS1* (Figure 55) it can easily be seen that C59 and A60 are positioned in between U11, U12, and G19. Thus, including C59 and A60 into the second binding site L2'b in the loop is well possible. In contrast to the definition of four binding sites, U11 and U12 as well as C15 were also considered in the definition of the binding sites. The second binding site in the loop encompasses the nucleotides C15, A16, C17, U18, G61, U62, G63 and U64, thus the protons of G19, A20, G21, C59, and A60 are not included in this binding site as it was the case with four defined sites. In return, the third newly defined binding site in the loop L3' involves these protons, i.e. it includes the nucleotides A10, U11, U12, G19, A20, G21, C59 and A60.

Compared to the calculation assuming four binding sites the log $K_{A,fin}$ values of H1, L1', and L2'b increase by about 0.1 log units when five binding sites are considered (Table 20). This trend is not surprising, since an additional binding site was included in the calculation, which reduces the available Mg^{2+} concentration and leads to an increase of the values for the affinity constants. However, the tendency of the averaged affinity constants for the individual binding sites H1', L1' and L2' is independent of the number of binding sites, i.e. the binding site L1' is still the one with the highest affinity towards Mg^{2+}, followed by H1 and L2'. The additional site L3', which was included for these calculations, shows with log $K_{A,fin}$ = 2.63 ± 0.01 mM^{-1} the lowest value of all binding sites. This observation is due to the individual affinity constants of the protons of U11 and U12, which contribute with relatively small log

$K_{A,est}$ values to the averaged value of the binding site (see Appendix 21A). These small log $K_{A,est}$ values led to the suggestion that U11 and U12 are not affected by M^{2+} when IBS1* is bound and thus, they were first not included into the calculation leading to the assumption of only four binding sites in d3'-EBS1*·IBS1*.

Comparison of the asymptotic fits for the individual sites in the case of four and five binding sites (Figure 95) shows that with four binding sites the fit is slightly better than the one with five binding sites. This observation, together with the low value of log $K_{A,est}$ for U11 and U12, suggests that indeed only two metal ions bind to the loop region. Although a chemical shift change is induced at U11 and U12 (Figure 77), it is still assumed that these two nucleotides are not included in a metal ion binding site. It should be noticed that chemical shift changes are not only observed when a metal ion binds directly to the investigated proton, but are also induced by structural changes in the local environment. Thus, it is well possible that the observed chemical shift changes of U11 and U12 are induced by structural changes at G13 and G14, which constitute a strong metal ion binding platform.

To conclude, the described iteration procedure is more sensitive to the number of defined binding sites than to its exact location. Thus, the number of binding sites has to be carefully defined before the iteration process begins. The individual log K_A values of each investigated proton, the chemical shifts upon Mg^{2+} addition and Mg^{2+} as well as Mn^{2+} line broadening studies give valuable information about the number of individual binding sites. Having thoroughly evaluated these data (Sections 2.5.1, 2.5.2, 2.5.5.3 and 2.5.5.6) four metal ion binding sites each were found in d3'-EBS1* as well as in d3'-EBS1*·IBS1*. In d3'-EBS1* two metal ions are located in the loop with the same affinity towards Mg^{2+}, which are assumed not to be fixed at a certain position, but rather "waiting impatiently" for IBS1* to arrive. Upon IBS1* addition one of these two metal ions is then fixed at the 5'-end of EBS1* (at G13/G14), stabilizing thereby the unusual conformation at this site. The second metal ion in the loop of d3'-EBS1*·IBS1* is stabilizing the EBS1*·IBS1* interaction in general, covering a relative large range. Thus, it is assumed that this metal ion rolls over the whole region.

2.5.6 Cd^{2+} binding to d3'-EBS1* and d3'-EBS1*·IBS1*

Since Mg^{2+} has a ligand exchange rate on the submillisecond range and thus close to the NMR timescale, the resonances become broadened relatively fast. In the case of d3'-ESB1* severe line broadening is observed already at 7 mM Mg^{2+} and in some cases even earlier (see Appendix 9). The signals for the d3'-EBS1*·IBS1* construct become broad at around 7-8 mM Mg^{2+} (see Appendix 20). To overcome this problem, alternative metal ions can be used to replace Mg^{2+}. For example, Cd^{2+} has been widely used in biochemical studies to mimic Mg^{2+},[75,100,365-367] especially in thio-rescue experiments.[94,368,369] With a ligand exchange rate of the hexaqua complex of $4.0 \cdot 10^8$ s^{-1}, compared to $5.3 \cdot 10^5$ s^{-1} for Mg^{2+}, Cd^{2+} exchanges significantly faster with the solvent.[370,371] It is obvious that the line broadening based on the intermediate exchange phenomena is avoided, when metal ions with a faster solvent exchange kinetic are used. Thus, the chemical shifts upon addition of Cd^{2+} were analyzed, and additionally the affinities of Cd^{2+} towards d3'-EBS1* and d3'-EBS1*·IBS1* were determined in the same way as for Mg^{2+} (see Sections 2.5.1 and 2.5.5). The calculation of the affinity constants will be discussed in the next section. In this chapter, the effect of Cd^{2+} will be examined qualitatively.

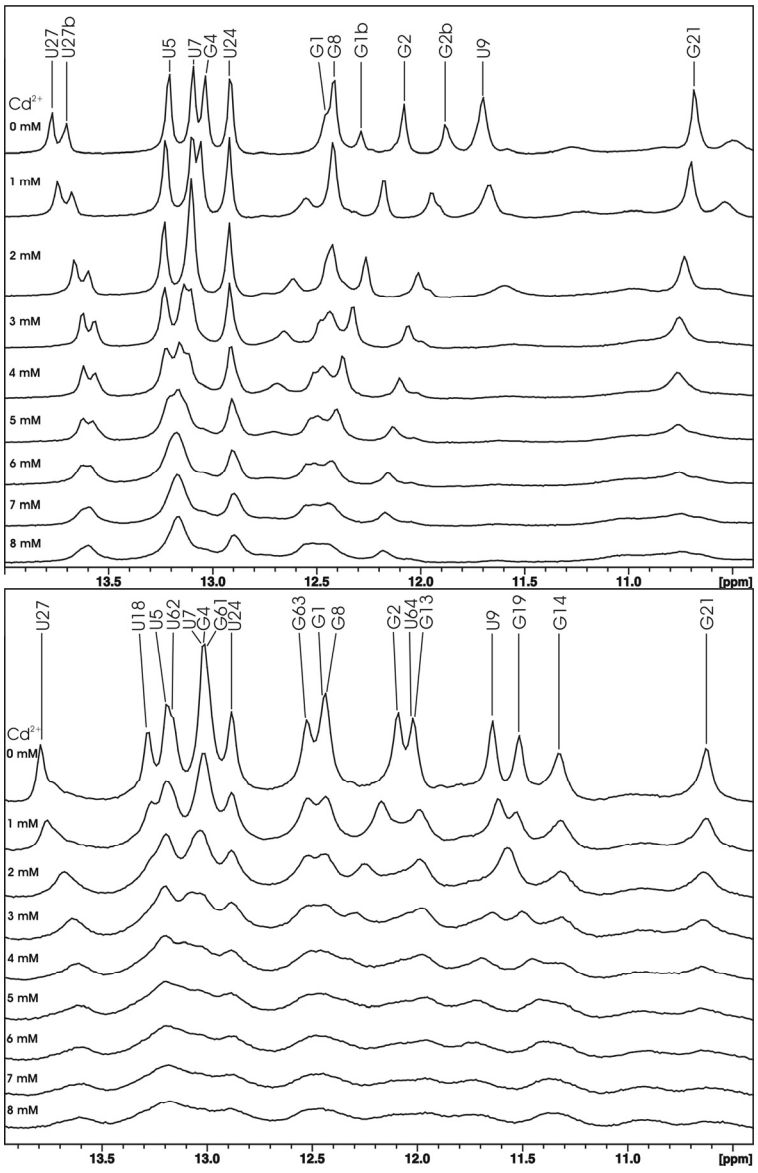

Figure 97 A series of 1D [^{1}H]-NMR spectra of d3'-EBS1* (upper panel; pH = 6.72, 10 mM KCl, 10 µM EDTA) and d3'-EBS1*·IBS1* (lower panel; pH = 6.71, 110 mM KCl, 10 µM EDTA) in 90% H_2O/10% D_2O upon stepwise addition of Cd^{2+}. Spectra were recorded at 700 MHz and 278 K. The letter "b" indicates the resonances of the n+1 derivative, which gives additional resonances for G1, G2 and U27 in the imino spectra (see also text and Section 2.2.5).

The chemical shift changes

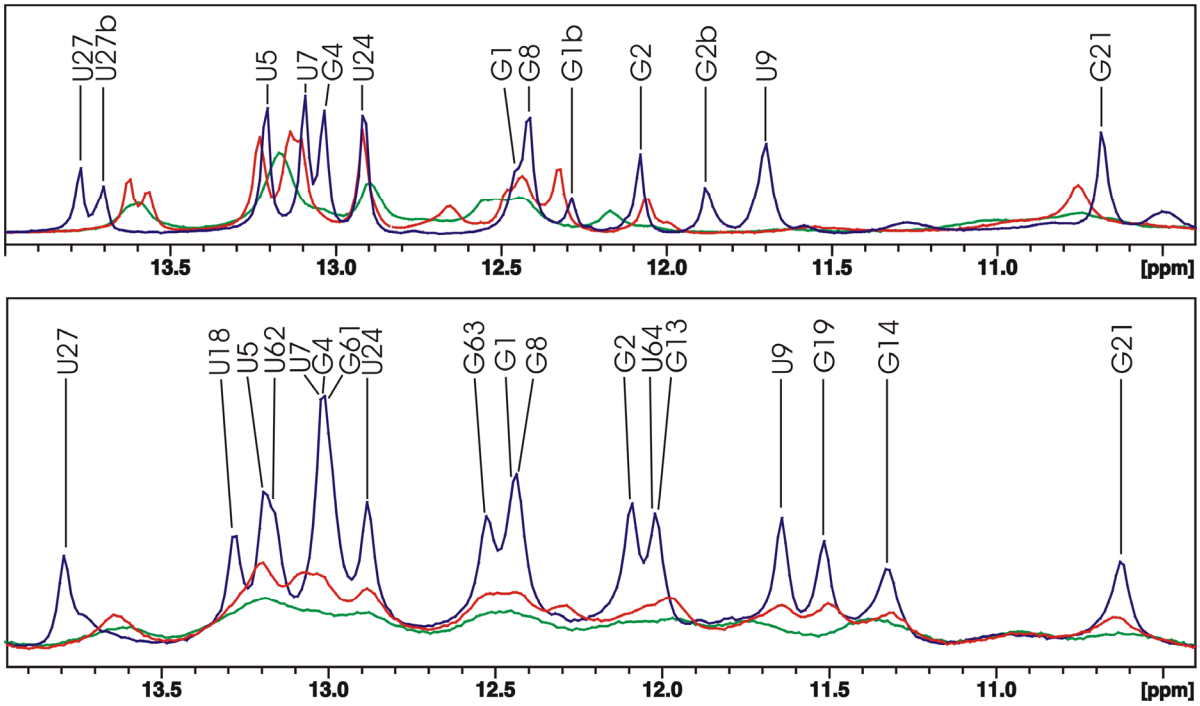

Figure 98 Overlay of 1D[^{1}H] NMR spectra of the imino resonances in d3'-EBS1* (upper panel) and d3'-EBS1*·IBS1* (lower panel) without (blue), with 3 mM (red) and with 7 mM Cd^{2+} (green), respectively. It is obvious that all resonances become severely broadened. The letter "b" indicates the resonances of the n+1 derivative, which gives additional resonances for G1, G2 and U27 in the imino spectra (see also text and Section 2.2.5).

of exchangeable as well as non-exchangeable protons upon Cd^{2+} binding were recorded. For the imino protons, a series of 1D [^{1}H]-NMR spectra of d3'-EBS1* and d3'-EBS1*·IBS1* were measured (see Materials and Methods). The stack plots of d3'-EBS1* and d3'-EBS1*·IBS1* upon stepwise addition of Cd^{2+} are shown in Figure 97. As in the Mg^{2+} titration (Figure 75, Section 2.5.1), the resonances become severely broadened and even disappear upon Cd^{2+} addition (Figure 97 and 98). Since imino protons of unpaired nucleotides cannot be observed due to the fast exchange with the solvent, chemical shift changes were extracted for the helical regions in both constructs only. A plot of the chemical shift change pattern for all observable imino proton resonances at a Cd^{2+} concentration of 2 mM is shown in Figure 99.

As expected, the largest influence of Cd^{2+} is observed at the helix end including G1H1, G2H1 and U27H3 due to the terminal triphosphate moiety, which offers a very strong binding site for Cd^{2+}. In d3'-EBS1*·IBS1* the resonance for G1H1 could not be extracted due to its position in a crowded region (Figure 97 and 98). Thus, it was not possible to locate the resonance of G1H1 in d3'-EBS1*·IBS1* upon Cd^{2+} binding. Nevertheless, since d3'-EBS1* and d3'-EBS1*·IBS1* share the sequence in the helix and the chemical shift changes of G2H1 and U27H3 are similar in both constructs, it is expected that Cd^{2+} binds in the same fashion to the 5'-ends of d3'-EBS1* and d3'-EBS1*·IBS1*. Additionally, U9H3 experiences in both constructs a large chemical shift change of about –0.15 ppm. In d3'-EBS1* all other imino

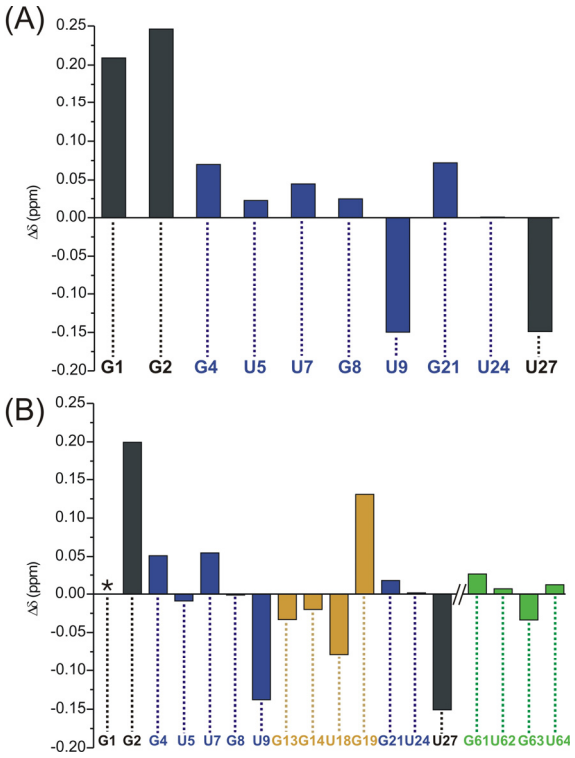

Figure 99 Chemical shift changes of the observed imino resonances in the helical parts of d3'-EBS1* and d3'-EBS1*·IBS1* upon Cd^{2+} binding. (A) shows the difference in chemical shift between 0 and 2 mM Cd^{2+} for d3'-EBS1* and (B) the one for d3'-EBS1*·IBS1*. Colouring of the boxes corresponds to that of the secondary structures in Figure 30A and B. Resonances of G1 in d3'-EBS1*·IBS1* could not be followed upon addition of Cd^{2+} and are marked with an asterisk.

to U9. It is well possible that this metal ion is located at the metal ion binding site "loop 1" (see Figure 78A) found for Mg^{2+} at A10 to U12 in d3'-EBS1*, since chemical shift changes can also be induced by structural changes in the local geometry. Compared to the Mg^{2+} titrations (Figure 100), one striking difference is observed: Upon addition of Cd^{2+} only moderate chemical shift changes are observed at the binding site "helix 1" (G4H1 and U5H3 in Figure 100A). Upon addition of Mg^{2+} a relatively large chemical shift change is observed at U5H3, but hardly at G4H1 (Figure 100A). This indicates that resonances experience moderate or even no chemical shifts. The loop region in d3'-EBS1*·IBS1* is mostly affected by Cd^{2+} at U18H3 and G19H1. Thus, a Cd^{2+} ion is presumably located in this region within the loop.

To conclude, from these titration experiments it is already obvious that the Cd^{2+} binds strongly to the 5'-end of the helical stem in both constructs. This is consistent with the existence of 5'-terminal phosphate groups, being the strongest metal ion binding sites due to their high negative charge. In addition, in d3'-EBS1* a Cd^{2+} ion binds presumably in close proximity

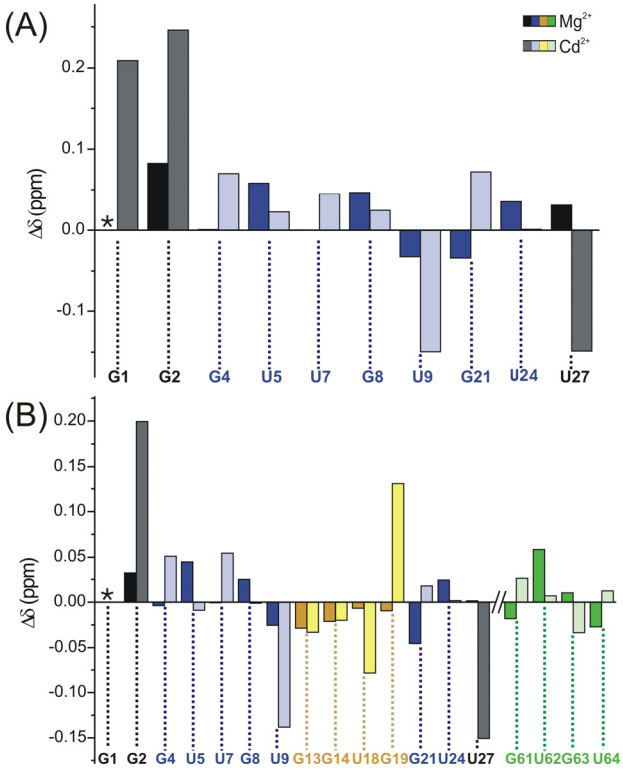

Figure 100 Comparison of the chemical shift changes of the observed imino resonances in the helical parts of d3'-EBS1* and d3'-EBS1*·IBS1* upon Mg^{2+} (dark colours) and Cd^{2+} (light colours) binding. Chemical shift changes are given for imino protons in (A) d3'-EBS1* and (B) d3'-EBS1*·IBS1*. Colouring of the boxes corresponds to that of the secondary structures in Figure 30A and B. Resonances of G1, which could not be followed upon addition of M^{2+} are marked with an asterisk.

Mg^{2+} and Cd^{2+} bind in different ways to "helix 1". At the U9-G21 wobble pair, Cd^{2+} induces larger chemical shift changes than Mg^{2+}, thus supporting different binding modes of Cd^{2+} and Mg^{2+}. In addition, Cd^{2+} has a higher affinity to the terminal phosphate groups than Mg^{2+}, which is corroborated by the large chemical shift change of G1H1, G2H1 and U27H3 upon Cd^{2+} addition.

The chemical shift changes of the imino protons in the helical stem of d3'-EBS1* are very similar to the ones in d3'-EBS1*·IBS1* (Figure 99), thus it can be concluded that Cd^{2+} binds to the helical stem in the same way in the absence or presence of IBS1*. Since a second helix is formed upon addition of IBS1*, the exchange rate of the imino protons in the loop is reduced and thus, imino protons of the EBS1*-IBS1* helix in d3'-EBS1*·IBS1* can also be observed. From the Cd^{2+} titration experiments it appears that a Cd^{2+} binds additionally in the region of U18 and G19, even though the imino proton resonances of IBS1* are hardly affected by Cd^{2+}. Upon addition of Mg^{2+} U62H3 in IBS1* experiences a relative large chemical shift change. All other imino protons of IBS1* are affected to about the same degree upon Mg^{2+} or Cd^{2+}, respectively. Thus, Cd^{2+} additionally influences the 3'-end of EBS1*, whereas Mg^{2+} has a stronger effect on IBS1*. The differences in chemical shifts upon addition of Mg^{2+} or Cd^{2+}, respectively, indicate that the binding mode of one type of metal ion cannot be directly transferred to another one.

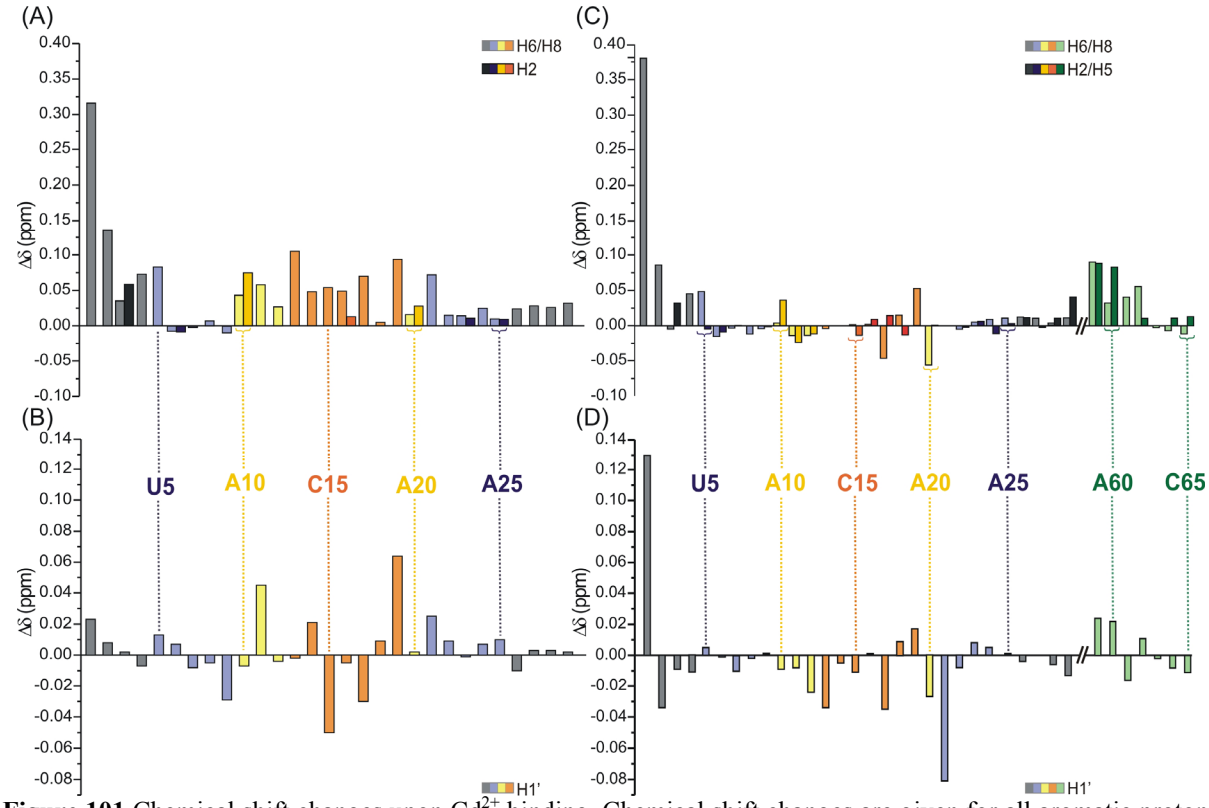

Figure 101 Chemical shift changes upon Cd^{2+} binding. Chemical shift changes are given for all aromatic protons in (A) d3'-EBS1* and (C) d3'-EBS1*·IBS1*, and for H1' in (B) d3'-EBS1* and (D) d3'-EBS1*·IBS1*. For G1 the chemical shift change for the construct bearing a diphosphate moiety is shown. Colouring of the boxes corresponds to that of the secondary structures in Figure 30A and B.

To monitor the non-exchangeable protons, 2D [^{1}H,^{1}H]-NOESY spectra of d3'-EBS1* and d3'-EBS1*·IBS1* in D_2O were recorded upon stepwise addition of Cd^{2+}. Although it was expected that line broadening does not occur as fast as with Mg^{2+}, the lines become very broad at around 7-8 mM Cd^{2+} (Appendix 11) for d3'-EBS1* and at 7 mM for d3'-EBS1*·IBS1* (Appendix 22). It might be possible that even with Cd^{2+} the fast kinetic regime cannot be reached in these constructs. Nevertheless, the chemical shift changes were monitored for all aromatic protons except of H5 of pyrimidine bases (see below) as well as for H1' of the sugar moieties. A selectively deuterated d3'-EBS1* sample (see Materials and Methods) was used in the Cd^{2+} titration, thus no chemical shift change could be observed for H5. However, due to the missing H5-H6 crosspeaks, overlap is reduced and thus the chemical shift changes of the other resonances could be easier followed. A plot of the chemical shift changes for all observed protons at 2 mM Cd^{2+} is shown in Figure 101.

As mentioned earlier, a special situation is observed for the 5'-end of the helix: Without any divalent metal ion present, only one starting point is observed in the 2D [^{1}H,^{1}H]-NOESY

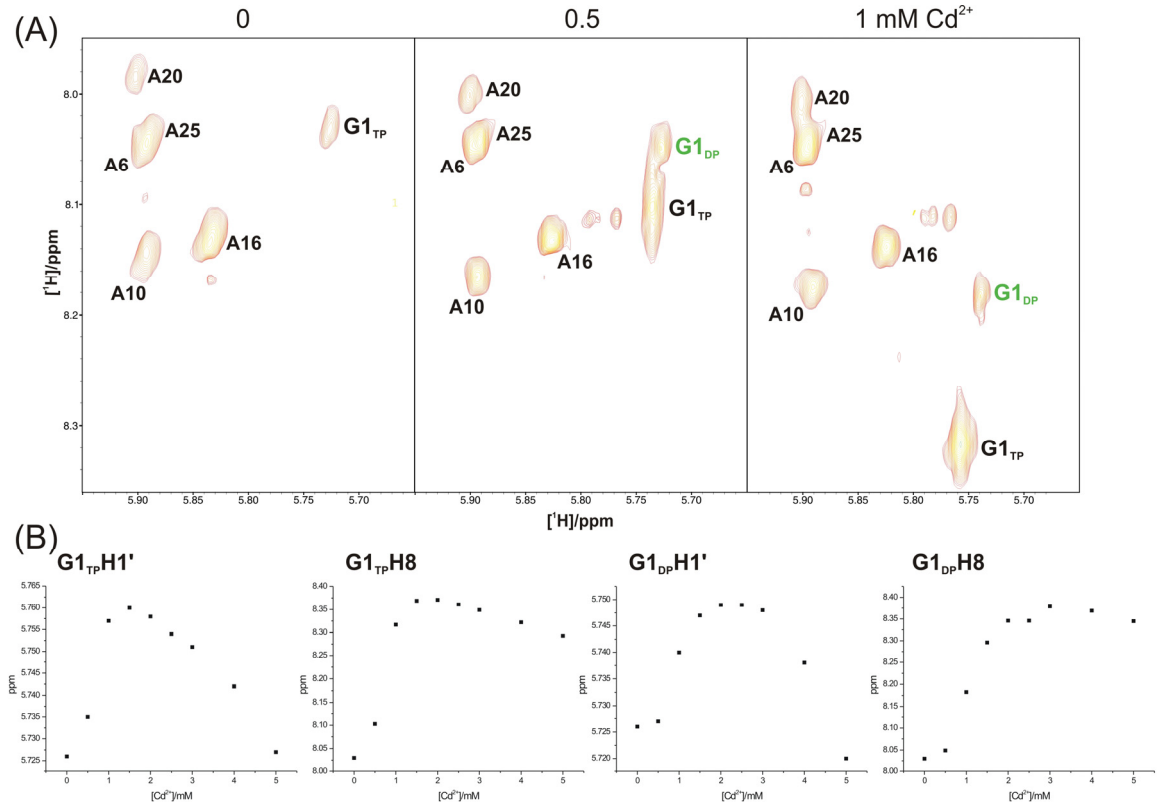

Figure 102 Illustration of the chemical shift behaviour at the 5'-end in d3'-EBS1*. (A) 2D [^{1}H,^{1}H]-NOESY sections of d3'-EBS1* in the presence of different Cd^{2+} concentrations. Intraresidual H1'-H8 crosspeaks are assigned with the corresponding nucleotide, e.g. G1. At 0.5 mM Cd^{2+} a second starting point appears indicated with $G1_{DP}$ (green). This resonance is assumed to be G1 of a derivative, bearing a diphosphate group at the 5'-terminus. The large chemical shift change of $G1_{TP}$ and $G1_{DP}$ is obvious. (B) Plots of the chemical shift change of $G1_{TP}$H1', $G1_{TP}$H8, $G1_{DP}$H1' and $G1_{DP}$H8 upon addition of Cd^{2+}, demonstrating the anomalous direction of chemical shifts.

spectra of d3'-EBS1* and d3'-EBS1*·IBS1*. When 0.5 mM Cd^{2+} are added, a second starting point appears like in the case with Mn^{2+} (see Section 2.5.2, Figure 102). This second starting point is assumed to be a derivative, bearing a diphosphate group at the 5'-terminus instead of a triphosphate. As illustrated in Figure 102B, the H1' and H8 protons of G1, bearing a tri- and diphosphate moiety, experience a large downfield chemical shift up to a concentration of 1.5 mM Cd^{2+} and shift upfield again when more Cd^{2+} is added. This behaviour is more pronounced for the H1' protons. In the case of $G1_{TP}$H1' and $G1_{DP}$H1' at 5 mM Cd^{2+} the resonance goes even back to the starting point, i.e. to the value in the absence of Cd^{2+} (Figure 102B). This chemical shift pattern adumbrate that not only one Cd^{2+} is binding to the phosphate derivatives at the 5'-end of the helix. It is assumed, and will later on taken into account in the calculation of the affinity constants (see Section 2.5.7 and 2.5.8), that two metal ions are bound to the triphosphate and one to the diphosphate moiety. Such a two-metal ion coordination behaviour has been found already in 1974 for a nucleoside 5'-triphosphate,[372,373] and further experiments have proven this fact, mainly for M_2(ATP) complexes.[374-381]

In the case of d3'-EBS1*·IBS1* a second starting point upon addition of Cd^{2+} is also observed, but the resonances of G1 disappear upon further addition of Cd^{2+}. Thus, the chemical shifts of the G1 protons can only be followed in the downfield direction. Nevertheless, since the hairpin sequence in d3'-EBS1*·IBS1* is identical with the one in d3'-EBS1*, it is assumed that Cd^{2+} binds in the same fashion to the 5'-end in d3'-EBS1*·IBS1* and d3'-EBS1*.

Next to the strongest metal ion binding site at the 5'-end of the hairpin stem, the most affected regions in d3'-ESB1* are in the 5'-strand at G4 and U5, as well as in the loop region (A10 to G21). At G4 and U5 mainly the aromatic protons seem to be affected by Cd^{2+}. In the loop region all H8/H6 protons experience in general a very similar chemical shift, except of U18H6 and A20H8, which are hardly affected (Figure 101). Regarding the H1' protons, those of U11, C15, C17, and G19 show the strongest chemical shift changes in the loop upon Cd^{2+} addition.

In general, chemical shift changes are difficult to interpret, since they can stem from different origins, e.g. direct metal ion binding to a site or structural changes in the close environment. However, the chemical shift changes of nearly all resonances in the loop region of d3'-EBS1* upon Cd^{2+} addition indicate that at least one metal ion is bound to this site. It can be well possible that, due to the magnitude of the loop and the overall chemical shift

changes, a second Cd^{2+} ion is located in the loop as it was observed in the Mg^{2+} titration experiments (Section 2.5.1).

Next to the 5'-end of the hairpin, Cd^{2+} also influences G4 and U5 in d3'-EBS1*·IBS1*. As in d3'-EBS1*, the aromatic protons show a larger chemical shift change upon Cd^{2+} addition than the H1' protons, which is expected due to the similarity of the two constructs. G21H1' in d3'-EBS1*·IBS1* shows with -0.081 ppm a large chemical shift change. In addition to that, the protons of A20, C59 and A60 are also affected significantly by Cd^{2+} (Figure 101). These chemical shift changes indicate that a Cd^{2+} binds in close proximity to this site. Other moderate chemical shift changes are spread between A10 and C19, indicating that a possible second Cd^{2+} binds to the loop region.

As already mentioned, it is difficult to state exactly, where a chemical shift change originate from. Thus, other experiments are required to directly locate a metal ion binding site, such as the above mentioned Mn^{2+} and Mg^{2+} line broadening studies (Section 2.5.1 and 2.5.2). Nevertheless, it cannot be excluded that Cd^{2+} has a different binding behaviour than Mg^{2+}. To draw conclusions about Cd^{2+} being capable of mimicking Mg^{2+}, the two chemical shift maps of d3'-EBS1* and d3'-EBS1*·IBS1* were compared (Figure 103). In general, it can be stated that a similar chemical shift pattern indicates an analogous binding mode.

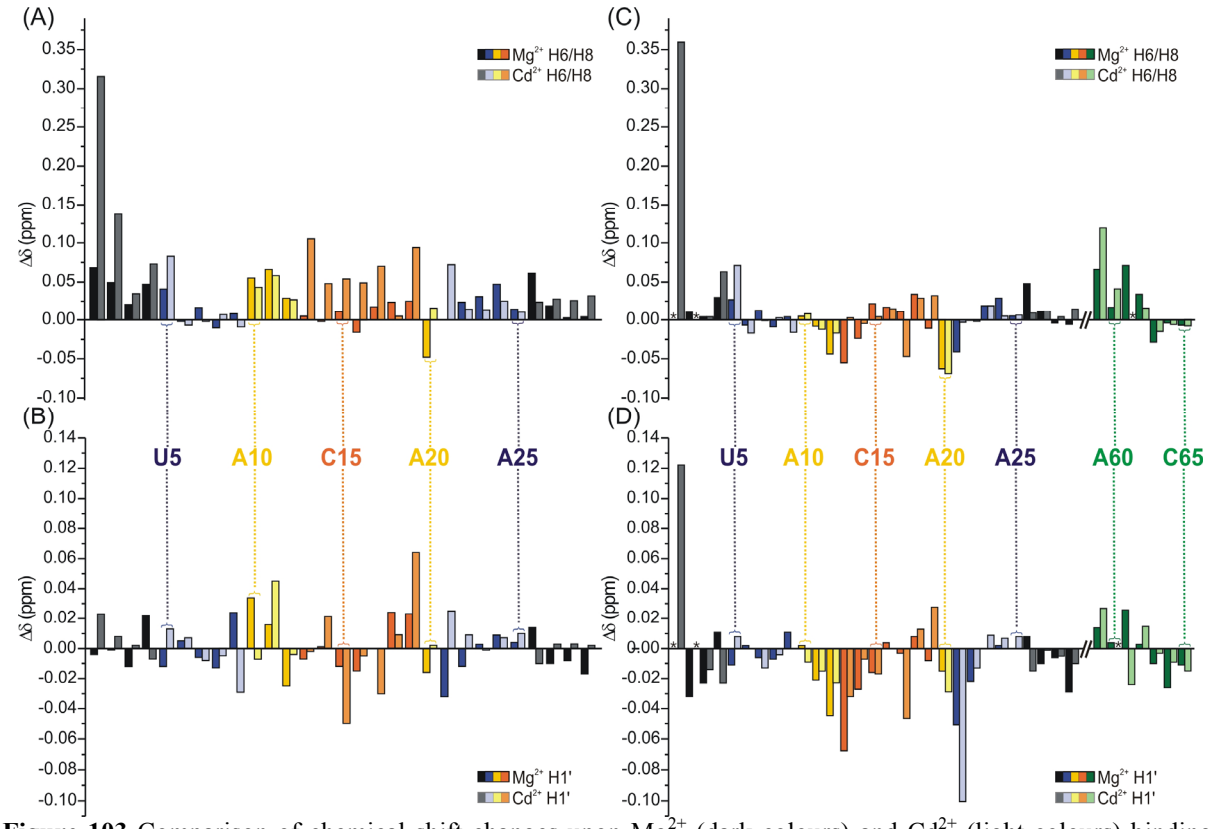

Figure 103 Comparison of chemical shift changes upon Mg^{2+} (dark colours) and Cd^{2+} (light colours) binding. Chemical shift changes are given for H6/H8 protons in (A) d3'-EBS1* and (C) d3'-EBS1*·IBS1* and (B) d3'-EBS1* and (D) d3'-EBS1*·IBS1*. Resonances that disappear upon addition of M^{2+} are marked with an asterisk. Colouring of the boxes corresponds to that of the secondary structures in Figure 30 A and B.

In the aromatic region, the chemical shift changes in d3'-EBS1* induced by Cd^{2+} and Mg^{2+} follow a similar pattern in the helical region of the stem from G1 to U5 and C22 to C29 (Figure 103A). The chemical shifts of A6H8, U7H6, G8H8 and U9H6 are hardly affected by the addition of either Mg^{2+} or Cd^{2+}. Especially at the 5'- and 3'-end of the helix (G1 to U5 and U27 to C29), Cd^{2+} induces a larger chemical shift than Mg^{2+}, corroborating the very strong binding of Cd^{2+} to the 5'-end. The chemical shifts of H1' at the 5'-end between G1 and U5 and at the 3'-end between C26 and C29 show shifts in opposite directions upon addition of Mg^{2+} and Cd^{2+}, respectively. However, these chemical shift changes are relative small, and thus this observation can be neglected.

In addition, U9H1' and G21H1' show about the same chemical shift change when titrated with Mg^{2+} or Cd^{2+}, respectively, but they shift in opposite directions, i.e. one downfield, the other one upfield. This indicates that the two metal ions have a different influence on the environment around the U9-G21 wobble pair. However, the base protons of A10, U11 and U12 show not only a similar chemical shift change upon addition of Mg^{2+} or Cd^{2+}, respectively, but both shift downfield. Thus, it can be assumed that the two metal ions have a similar influence at the bases of the binding site "loop 1" (Figure 78A). In the region of the binding site "loop 2" (Figure 78A), Cd^{2+} has a much stronger effect on the chemical shift than Mg^{2+}. In addition, upon addition of Cd^{2+}, relative large chemical shift changes are observed at G13H8, G14H1', G14H8, C15H1' and C15H6, whereas upon Mg^{2+} addition these chemical shifts are hardly affected. This may reflect that Cd^{2+} induces more structural changes in the loop region than Mg^{2+} does and certainly binds in a different mode.

To summarize the observations regarding d3'-EBS1* upon addition of either Mg^{2+} or Cd^{2+}, it can generally be concluded that these two metal ions bind at similar sites in d3'-EBS1*, but the difference in chemical shift as well as the different direction of the shifts in some cases imply a different binding mode for the two metal ions. Cd^{2+} seems to bind stronger to the binding sites than Mg^{2+}, inducing larger structural changes, especially at the nucleotides of EBS1*. This conclusion is based on the overall larger chemical shifts upon Cd^{2+} binding and is in agreement with the general tendency of Cd^{2+} to form more stable complexes than Mg^{2+}.[64]

In d3'-EBS1*·IBS1* a large chemical shift change is observed at the 5'-end of the hairpin stem upon addition of Cd^{2+}. The effect of Mg^{2+} at the 5'-end is not as pronounced, which shows again that Cd^{2+} binds stronger to the 5'-terminus of the hairpin than Mg^{2+}. At the binding site "helix 1", as it was determined by Mg^{2+} titration studies (Section 2.5.1, Figure 78B), Mg^{2+} and Cd^{2+} have a similar influence on A3H8, G4H8, U5H6, A25H8, C26H6 and

U27H6. The resonances of the H1' protons of the binding site "helix 1" either experience only a minor chemical shift or shifts in opposite directions. As the H1' protons are located in the minor groove, it appears as if Cd^{2+} and Mg^{2+} have different binding modes at this site.

At the binding site "loop 1" of d3'-ESB1*·IBS1*, which comprises G13 and G14 (Figure 78B), Cd^{2+} has hardly any influence on the aromatic protons. In addition, the change of 0.032 ppm of G13H1' upon Cd^{2+} addition is only about half of what is observed with Mg^{2+} and the change of 0.007 ppm of G14H1' is roughly a quarter compared to the one of Mg^{2+}. One is tempted to assume that Cd^{2+} does not bind to "loop 1" at all due to these findings. Nevertheless, based on the calculated affinity constants (see Section 2.5.8) Cd^{2+} is still assumed to bind to the binding site "loop 1", which will be discussed in the preceding sections. However, Cd^{2+} certainly binds in a different way to this site than Mg^{2+}.

A very striking similarity of the influence of Mg^{2+} and Cd^{2+} is observed in IBS1*. Except of G61H1', all proton resonances have a similar chemical shift pattern, albeit the extend of the shift change is different in some cases. Thus, it can be assumed that Mg^{2+} and Cd^{2+} induce the same structural change in IBS1*, but in a slightly different extent. By contrast, EBS1* shows a similar chemical shift pattern upon Mg^{2+} or Cd^{2+} binding, respectively, only at C15H6, A16H8, U18H6, G13H1', G14H1', C15H1', and U18H1' and also at the unpaired nucleotide A20. All other proton resonances of EBS1* shift in opposite directions, showing that Cd^{2+} induces partly different structural changes at this site. Thus, the metal ion binding site "loop 2" as determined by Mg^{2+} titration studies (Section 2.5.1, Figure 78B) appears to bind the two metal ions investigated differently.

Based on the chemical shift pattern of d3'-EBS1*·IBS1* upon addition of either Mg^{2+} or Cd^{2+}, it can generally be assumed that these two metal ions bind to similar sites in d3'-EBS1*·IBS1*. However, a stronger binding of Cd^{2+} is indicated by the higher extent in chemical shift change than in the case of Mg^{2+} and a different binding mode is assumed by the shift changes of some resonances in opposite directions.

Since d3'-EBS1* and d3'-ESB1*·IBS1* share the hairpin-sequence, it is expected that the binding behaviour of Mg^{2+} and Cd^{2+} towards the stem is similar. Besides some exceptions, this is indeed the case from G1 to U9 and A23 to C29. G21, which is still part of the helical stem, shows a different picture in d3'-EBS1* and d3'-ESB1*·IBS1*: Whereas in d3'-EBS1* G21H1' experiences chemical shift changes in opposite direction upon Mg^{2+} or Cd^{2+} addition, in d3'-ESB1*·IBS1* the chemical shift changes lead to the same direction. This indicates that the presence of IBS1* indeed influences the binding modes of Cd^{2+} and Mg^{2+}. The same is true for A20H8 and A20H1': In both structures this nucleotide is unpaired, but in d3'-

ESB1*·IBS1* it is stacked upon G19 and G21, thereby elongating the helix (see Section 2.2.9). Thus, the upfield shift of A20H8 and A20H1' upon addition of Cd^{2+} or Mg^{2+}, respectively, shows that both metal ions increase the stacking interactions of this nucleotides in d3'-ESB1*·IBS1*. In contrast, Cd^{2+} reduces the stacking interactions of A20 in d3'-EBS1*, which is obvious from the downfield shift of A20H8 and A20H1' upon Cd^{2+} addition.

In summary, this study shows that Cd^{2+} cannot universally replace Mg^{2+} at all sites, but may be a mimic for Mg^{2+} at certain specific sites. This view is supported by a recent study of the HIV dimerization site, which shows that Cd^{2+} selectively replaces Mg^{2+} if inner-sphere coordination to a phosphate oxygen as well as a guanine N7 can take place.[359] Although Cd^{2+} has a much higher affinity towards nucleic acids than Mg^{2+}, it has been shown that Cd^{2+} does not replace Mg^{2+} at all positions. This indicates that the coordination sites, their geometry and accessibility are of great importance.

2.5.7 Calculation of affinity constants of Cd^{2+} to d3'-EBS1*

To assess the metal ion binding properties of Cd^{2+} not only qualitatively, but also in a quantitative way, the intrinsic affinity constants of Cd^{2+} to d3'-EBS1* and d3'-EBS1*·IBS1* were determined by the same calculation procedure as for Mg^{2+} (Section 2.5.5). Comparison of the affinities of Mg^{2+} with Cd^{2+} will help to gain more knowledge about the coordination behaviour of different divalent metal ions towards RNA.

To calculate the intrinsic affinity constants, ISTARv2.3 was employed, which takes the equilibrium concentrations of bound and unbound metal ions into account (see Section 2.5.5). As already discussed in Section 2.5.5, the different phosphate moieties at the 5'-terminus of d3'-EBS1* display a special case when discussing Cd^{2+} binding to this sequence. It is assumed that two metal ions are binding to $G1_{TP}$ and one metal ion to $G1_{DP}$. Since a 1:1 fit was not possible to perform for G1, literature values for the affinity of Cd^{2+} towards the mononucleotides GTP ($\log K_A = 5.82 \pm 0.05$),[355] and $\log K_A = 2.52 \pm 0.15$ for the first and second binding, respectively, and GDP ($\log K_A = 4.86 \pm 0.03$)[382] were used for the calculation (see Materials and Methods). By integration of the two starting points G1H1'-H8 in Sparky (see Materials and Methods) a triphosphate:diphosphate ratio of 70:30 was determined and was taken into account in the calculations. The Cd^{2+} titration for d3'-EBS1* was performed with a selectively deuterated sample (see 2.2.5 and Materials and Methods), thus no resonances for the H5 protons of pyrimidine nucleobases could be evaluated. This results in a decreased number of evaluated protons compared to the ones in the Mg^{2+} titration

Table 21 Affinity values log K_A for Mg^{2+} and Cd^{2+} (grey backgrounds) binding to d3'-EBS1* in D_2O. Listed are the averaged log K_A values (1σ) at the four high affinity binding sites, obtained from the change in chemical shifts of all aromatic and H1' protons after various rounds of iterative corrections for the metal ion concentration that is available at a certain site. The log K_A values are shown for the calculation with ISTARv2.3, which takes the equilibrium concentrations of the free and bound M^{2+} species in solution into account. The values for the 5'-end were taken from literature[355,382] as explained in the text.

M^{2+}	Binding site	log $K_{A,av1}$ [mM^{-1}]	log $K_{A,av2}$ [mM^{-1}]	log $K_{A,av3}$ [mM^{-1}]	log $K_{A,av4}$ [mM^{-1}]	log $K_{A,av5}$ [mM^{-1}]	log $K_{A,fin}$ [a] [mM^{-1}]	$\Delta_{fin-av1}$ [b] [mM^{-1}]
Mg^{2+}	Helix 1 (H1)	2.38 ± 0.04	2.59 ± 0.03	2.64 ± 0.03	2.65 ± 0.03	2.65 ± 0.03	2.65 ± 0.01	0.27 ± 0.04
Cd^{2+}	Helix 1 (H1)	2.10 ± 0.05	2.57 ± 0.02	2.71 ± 0.02	2.75 ± 0.02	2.77 ± 0.02	2.77 ± 0.01	0.67 ± 0.05
Mg^{2+}	Loop 1(L1)	2.13 ± 0.05	2.39 ± 0.03	2.43 ± 0.03	2.44 ± 0.03	2.45 ± 0.03	2.45 ± 0.01	0.32 ± 0.05
Cd^{2+}	Loop 1(L1)	2.23 ± 0.19	2.78 ± 0.26	2.89 ± 0.26	2.93 ± 0.26	2.95 ± 0.26	2.96 ± 0.01	0.73 ± 0.19
Mg^{2+}	Loop 2 (L2)	2.11 ± 0.06	2.40 ± 0.05	2.44 ± 0.05	2.45 ± 0.05	2.45 ± 0.05	2.45 ± 0.01	0.34 ± 0.06
Cd^{2+}	Loop 2 (L2)	2.47 ± 0.09	2.86 ± 0.27	2.99 ± 0.27	3.02 ± 0.27	3.04 ± 0.27	3.04 ± 0.01	0.57 ± 0.09

The chemical shift changes were obtained from 2D [^{1}H,^{1}H]-NOESY spectra of a 0.6 mM d3'-EBS1* RNA at pD 6.66 in 10 mM KCl at 25 °C. All error limits correspond to one standard deviation (1σ). [a]The maximal log $K_{A,fin}$ values correspond to the limiting value of an asymptotic fit, which was obtained by plotting log K_a values after each iteration round *versus* the number of the iteration round. The errors from the fits were multiplied by three to obtain reasonable error limits. [b]Difference in log K_A between log $K_{A,av1}$ and the maximal log $K_{A,fin}$ of the asymptotic fit.

(see Section 2.5.5). Out of 66 evaluated protons, 33 could be fitted by a Levenberg-Marquardt nonlinear least-squares regression for a single binding isotherm (Appendix 12A). Based on the first estimates for log K_A four binding sites were defined in d3'-EBS1*. In contrast to the binding sites determined for Mg^{2+} (Section 2.5.5), G13H8 and G14H1' were included in the binding site "loop 1" because their log K_A values are similar to the other ones in loop 1.

The first estimates for log $K_{A,est}$ for the single protons give already higher values than the ones for the Mg^{2+} titration (compare Appendix 10A with 12A). The estimates for averaged log $K_{A,av1}$ for the internal binding site helix 1 is 2.10 ± 0.05 mM^{-1}. The binding sites within the loop give slightly higher log $K_{A,av1}$ values with 2.23 ± 0.19 mM^{-1} for loop 1 and 2.47 ± 0.09 mM^{-1} for loop 2 (Table 21). Analogously to the calculation with Mg^{2+} (see Section 2.5.5), the available Cd^{2+} concentration was calculated based on the averaged affinities log $K_{A,av1}$ and subsequently the second iteration round was started. Seven iteration rounds were performed, but already after the fifth iteration round, the log K_A values did not change anymore within the error limits. The maximal log $K_{A,fin}$ values

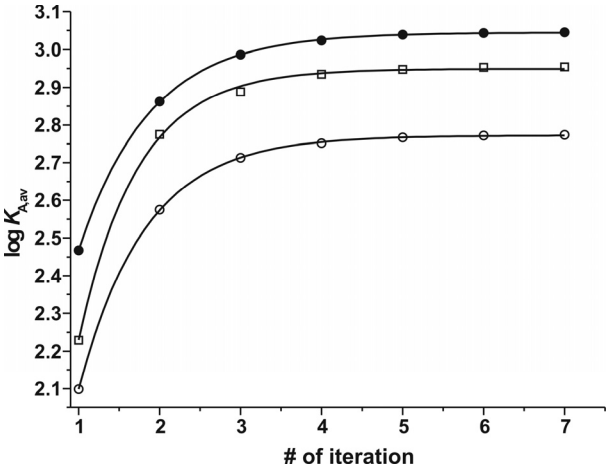

Figure 104 Plot of the average log K_A values of each binding site of d3'-EBS1* towards Cd^{2+} after every round *versus* the number of iteration and fitted to an asymptotic function. The plots for the binding sites at the helical region (H1, ○), loop 1 (L1, □) and loop 2 (L2, ●) are shown.

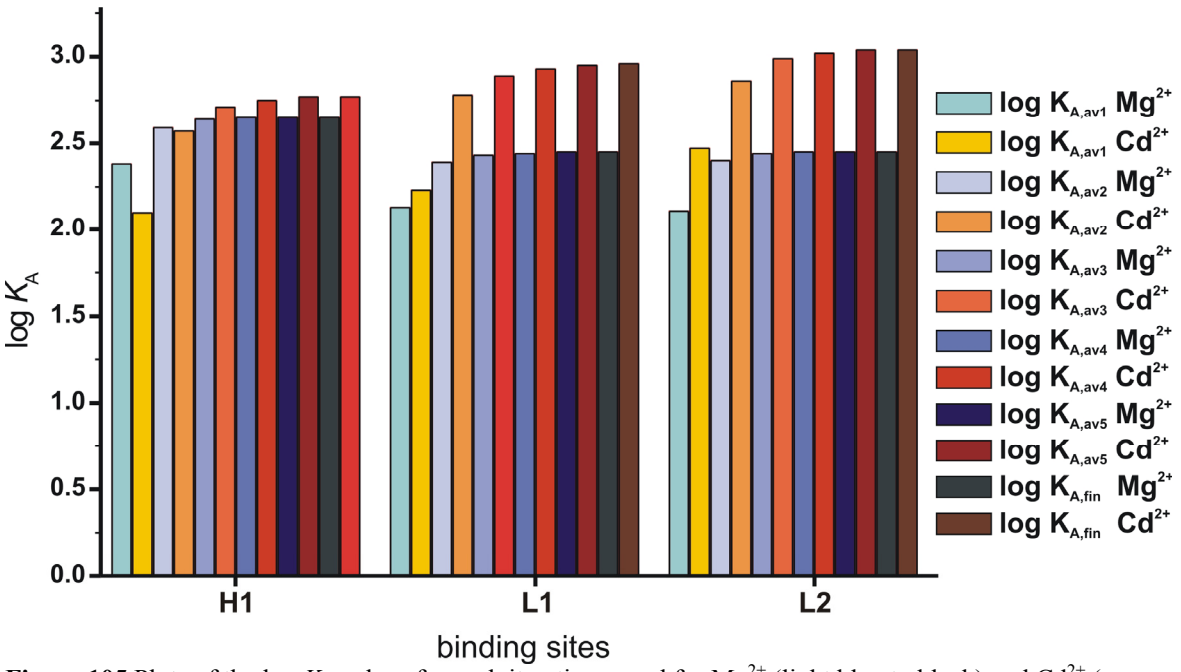

Figure 105 Plots of the log K_A values for each iteration round for Mg^{2+} (light blue to black) and Cd^{2+} (orange to red) coordinating to the binding sites H1, L1 and L2 in d3'-EBS1*.

(Table 21, column 8) were obtained by plotting log K_A values after each iteration round *versus* the number of the iteration round and fitting these data by an asymptotic function (Figure 104). The final log $K_{A,fin}$ for the binding site in the helix (H1) was calculated to 2.77 ± 0.01 mM^{-1}. The binding sites in the loop show higher affinities towards Cd^{2+} than helix 1. Thereby, loop 2 has a slightly higher affinity with a log $K_{A,fin}$ value of 3.04 ± 0.01 mM^{-1} than loop 1 with 2.96 ± 0.01 mM^{-1}. But loop 1 shows with 0.73 ± 0.19 log units the highest increase of log K_A over the course of the iteration procedure (Table 21). The results obtained for Cd^{2+} binding to the binding sites helix 1, loop 1 and loop 2, show a different binding behaviour of Cd^{2+} and Mg^{2+}. The latter one has the highest affinity, apart from the 5'-end, to the helix, whereas Cd^{2+} binds stronger to the loop region (Table 21, Figure 105). In addition, Cd^{2+} binds with slightly different affinities to the two binding sites in the loop, in contrast Mg^{2+} has the same affinity to these two sites. This view is supported by the chemical shift changes upon addition of Cd^{2+} or Mg^{2+}, respectively (Figure 103): Cd^{2+} influences the chemical shifts of EBS1* (G13 to G19) to a much higher degree than Mg^{2+}.

It is well known that Cd^{2+} has a much higher intrinsic affinity towards nucleic acids than Mg^{2+}, but can be very selective in replacing Mg^{2+}.[64] The results obtained from calculating affinity constants for the binding of Mg^{2+} and Cd^{2+} to d3'-EBS1*, respectively, support this view. The tighter Cd^{2+} binding to the loop is further supported by the larger chemical shift changes upon Cd^{2+} addition (Figure 103). It seems as if Cd^{2+} can better replace Mg^{2+} in helical than in single stranded loop regions. It is well possible that Cd^{2+} binds via its hexaqua-complex $Cd(H_2O)_6^{2+}$ in an outer-sphere fashion to the loop regions. Due to the flexibility of

the loop the accessibility is increased, so that the voluminous $Cd(H_2O)_6^{2+}$ could easiliy access the binding sites.

2.5.8 Calculation of affinity constants of Cd^{2+} to d3'-EBS1*·IBS1*

To assess the influence of IBS1* the intrinsic affinities of Cd^{2+} towards d3'-EBS1*·IBS1* were calculated. Like for the calculation of the affinity constants of Cd^{2+} towards d3'-EBS1*, ISTARv2.3 was applied. Assuming the same binding behaviour of Cd^{2+} to the 5'-end of d3'-EBS1* and d3'-EBS1*·IBS1*, respectively, the same literature values for the affinity constants of Cd^{2+} to the mononucleotides were used.[355,382] The integration of the two starting points G1H1'-H8 of the di- and triphosphate moieties in Sparky yielded for d3'-EBS1*·IBS1* the same ratio as for d3'-EBS1*, i.e. the presence of 70% triphosphate and 30% diphosphate.

Out of 98 evaluated protons, only 31 could be fitted to a 1:1 isotherm (Appendix 23). The remaining 67 protons experience hardly a chemical shift, or could not be evaluated in all spectra due to severe overlap or line broadening. Although it is expected that line broadening upon Cd^{2+} addition does not occur as quickly as with Mg^{2+} and thus the chemical shift changes of particular protons should be easier to follow, it was much more difficult to assign the spectra of d3'-EBS1*·IBS1* in the presence of Cd^{2+} than of Mg^{2+}. However, to draw conclusions about the binding behaviour of Cd^{2+} towards d3'-EBS1*·IBS1*, the 31 evaluated protons were used as a basis for the calculation of the affinity constants. It should be

Table 22 Affinity values log K_A for Mg^{2+} and Cd^{2+} (grey backgrounds) binding to d3'-EBS1*·IBS1* in D_2O. Listed are the averaged log K_A values (1σ) at the four high affinity binding sites, obtained from the change in chemical shifts of all aromatic and H1' protons after various rounds of iterative corrections for the metal ion concentration that is available at a certain site. The log K_A values are shown for the calculation with the modified version ISTARv2.3, which takes the equilibrium concentrations of the free and bound M^{2+} species in solution into account. The values for the 5'-end were taken from literature[355,382] as explained in the text.

M^{2+}	Binding site	log $K_{A,av1}$ [mM^{-1}]	log $K_{A,av2}$ [mM^{-1}]	log $K_{A,av3}$ [mM^{-1}]	log $K_{A,av4}$ [mM^{-1}]	log $K_{A,av5}$ [mM^{-1}]	log $K_{A,fin}$ [a] [mM^{-1}]	$\Delta_{fin-av1}$ [b] [mM^{-1}]
Mg^{2+}	Helix 1 (H1)	2.27 ± 0.05	2.68 ± 0.06	2.78 ± 0.06	2.80 ± 0.06	2.80 ± 0.06	2.80 ± 0.01	0.53 ± 0.05
Cd^{2+}	Helix 1 (H1)	2.40 ± 0.08	3.08 ± 0.07	3.19 ± 0.09	3.21 ± 0.08	3.21 ± 0.08	3.21 ± 0.01	0.81 ± 0.08
Mg^{2+}	Loop 1(L1)	2.60 ± 0.13	2.96 ± 0.12	3.04 ± 0.13	3.06 ± 0.13	3.06 ± 0.13	3.06 ± 0.01	0.46 ± 0.13
Cd^{2+}	Loop 1(L1)	3.70 ± 0.12	4.85 ± 0.33	4.94 ± 0.20	4.94 ± 0.18	4.94 ± 0.18	4.94 ± 0.01	1.24 ± 0.12
Mg^{2+}	Loop 2 (L2)	2.16 ± 0.04	2.64 ± 0.03	2.73 ± 0.03	2.75 ± 0.03	2.75 ± 0.03	2.75 ± 0.01	0.59 ± 0.04
Cd^{2+}	Loop 2 (L2)	2.36 ± 0.03	2.95 ± 0.04	3.09 ± 0.05	3.10 ± 0.05	3.10 ± 0.05	3.11 ± 0.01	0.75 ± 0.03

The chemical shift changes were obtained from 2D [^{1}H,^{1}H]-NOESY spectra of a 0.61 mM d3'-EBS1*·IBS1* RNA at pD 6.89 in 110 mM KCl at 25 °C. All error limits correspond to one standard deviation (1σ). [a]The maximal log $K_{A,fin}$ values correspond to the limiting value of an asymptotic fit, which was obtained by plotting log K_a values after each iteration round *versus* the number of the iteration round. The errors from the fits were multiplied by three to obtain reasonable error limits. [b]Difference in log K_A between log $K_{A,av1}$ and the maximal log $K_{A,fin}$ of the asymptotic fit

mentioned that such a small number of protons might lead to large errors of the averaged affinity constants, because the contribution of every single proton is much higher. Nevertheless, it was possible to calculate reliable affinity constants for d3'-EBS1*·IBS1*.

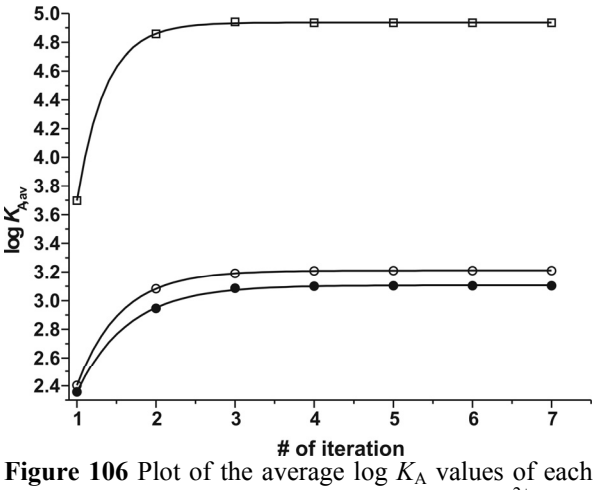

Figure 106 Plot of the average log K_A values of each binding site of d3'-EBS1*·IBS1* towards Cd^{2+} after every round *versus* the number of iteration and fitted to an asymptotic function. The plots for the binding sites at the helical region (H1, ○), loop 1 (L1, □) and loop 2 (L2, ●) are shown.

Based on the first estimates for log K_A four Cd^{2+} binding sites were determined for d3'-EBS1*·IBS1* (Appendix 23A). The first estimates for averaged weighted mean log $K_{A,av1}$ give for the internal binding site helix 1 in d3'-EBS1*·IBS1* a value of 2.40 ± 0.08 mM^{-1} (Table 22). The binding site loop 2, which has like helix 1 a helical pattern, has within the error limits the same log $K_{A,av1}$ value (2.36 ± 0.03 mM^{-1}). In contrast, the averaged weighted mean log $K_{A,av1}$ for the binding site loop 1 results with 3.70 ± 0.12 mM^{-1} in a much higher value than the helical binding sites (Table 22). After calculating the available Cd^{2+} concentration based on the averaged log $K_{A,av1}$, further iteration rounds were performed. Already after 5 iteration rounds, the log K_A values did not change anymore within the error limits. Figure 106 shows the plot of the average log K_A values of each binding site of d3'-EBS1*·IBS1* towards Cd^{2+} after every round *versus* the number of iteration, which were fitted to an asymptotic function and subsequently led to the final log $K_{A,fin}$ values.

The final log $K_{A,fin}$ for the binding site helix 1 and loop 2 in d3'-EBS1*·IBS1* give very similar values with 3.21 ± 0.01 mM^{-1} and 3.11 ± 0.01 mM^{-1}, respectively. The by far highest log $K_{A,fin}$ value was obtained for the binding site loop 1, which gives a value of 4.94 ± 0.01 mM^{-1}. In addition, the binding site loop 1 shows with 1.24 ± 0.12 log units the highest increase of log K_A over the course of the iteration procedure (Table 22). Cd^{2+} and Mg^{2+} show the same trend in log K_A values for the three binding sites, i.e. in both cases the binding site L1 has the highest affinity towards metal ions, whereas the helical binding sites H1 and L2 give similar values. Nevertheless, Cd^{2+} has a much higher affinity towards loop 1 than Mg^{2+} (Table 22, Figure 105). In addition, the difference between the log K_A values for H1, L2 and L1 are much higher for Cd^{2+} than for Mg^{2+}. These observations support the suggestion that Cd^{2+} is a better mimic for Mg^{2+} at helical sites due to the similar log K_A values of Cd^{2+} and Mg^{2+} at the binding sites H1 and L2. As it was already observed in d3'-EBS1*, Cd^{2+} has a

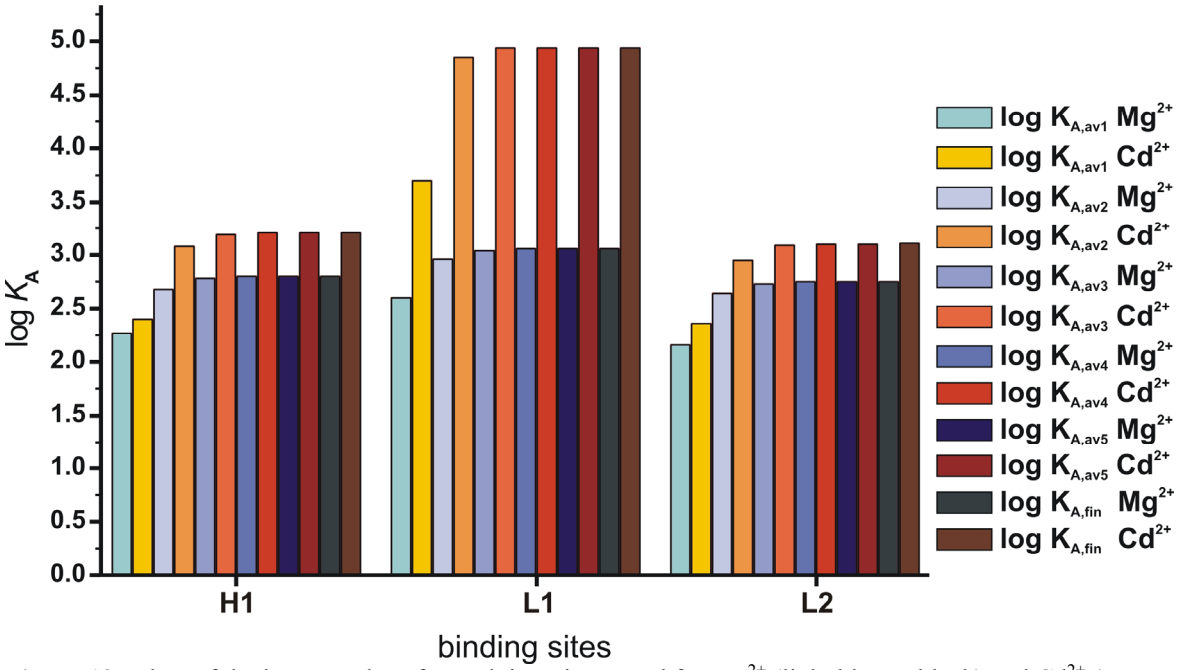

Figure 107 Plots of the log K_A values for each iteration round for Mg^{2+} (light blue to black) and Cd^{2+} (orange to red) coordinating to the binding sites H1, L1 and L2 in d3'-EBS1*·IBS1*.

much higher affinity towards single stranded regions than to helices due to the better accessibility to unpaired regions. The binding site loop 1 in d3'-EBS1*·IBS1* encompasses nucleotides in a helical region, but due to the unusual kink 5' of the binding site it does not represent a typical helix. As shown by the solution structure of d3'-EBS1*·IBS1* (Section 2.2.9), the phosphate oxygens of G13 and G14 protrude and are thus easiliy accessible for coordination of metal ions. It is well possible that a $Cd(H_2O)_6^{2+}$ binds in an outer-sphere mode via the water molecules to the phosphate groups.

Taken together, the obtained affinity constants for Cd^{2+} show for both cases, i.e. d3'-EBS1* and d3'-EBS1*·IBS1, a higher affinity towards RNA than Mg^{2+}, which is expected.[64] The stability constants of the $M(NXP)^{(y-2)}$- complexes increase in the order of $Ca^{2+} < Mg^{2+} < Mn^{2+} < Cd^{2+}$. Thus, Cd^{2+} forms the most stable complex in this series. The higher affinity of Mn^{2+} and Cd^{2+} agrees with the position of Mn^{2+} within the Irving William series[64,354,383,384] and the slightly higher stability of the Cd^{2+} complexes compared to the Mn^{2+} complexes is well in line with the *Stability Ruler* of Martin.[385-387]

2.6 CD spectroscopy reveals structural changes

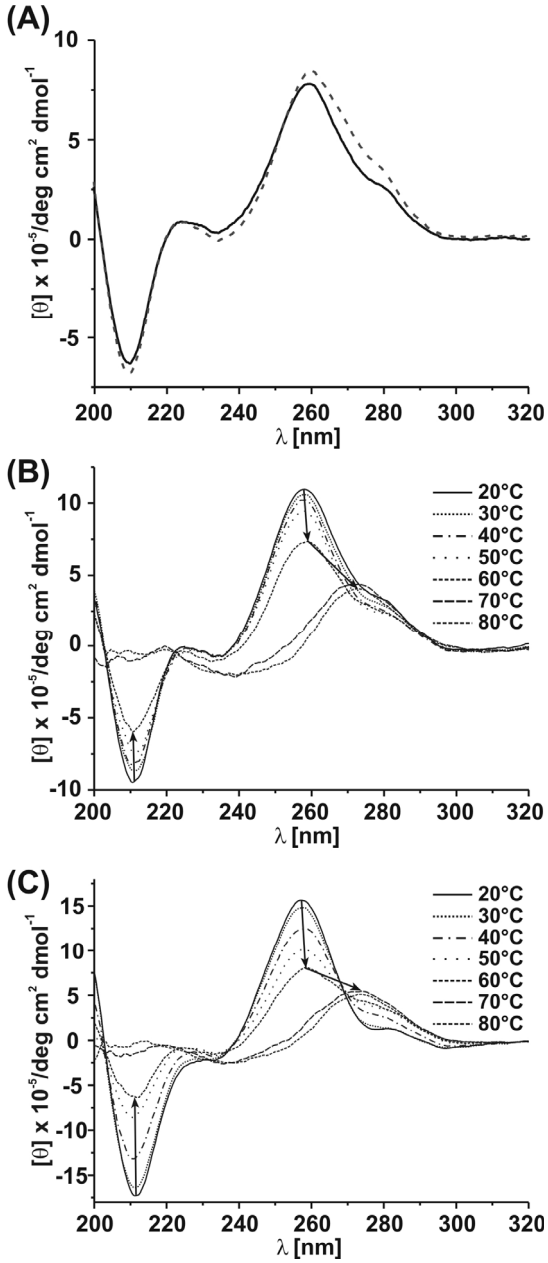

Figure 108 (A) Change in the CD signal of d3'-EBS1 (solid line) upon addition of 1 eq IBS1 (broken line) in the presence of 100 mM KCl. (B) Melting of d3'-EBS1* as observed with CD spectra in the presence of 10 mM KCl. (C) Change in CD spectra of d3'-EBS1*·IBS1* with increasing temperature in the presence of 100 mM KCl. The concentrations of the RNA are 10 μM (A) and 16 μM (B, C)

Circular dichroism is a powerful tool to monitor structural changes in proteins as well as in nucleic acids. Regular A-form RNA has a characteristic CD spectrum showing a large positive elipticity at 260 nm and a negative one at 210 nm.[388] Changes in the characteristic band at 260 nm correspond to hyperchromism of nucleobases as a result of helical stacking[389] and the band at 210 nm is associated with changes in loop structures.[296] Thus, changes in the shape of the CD spectrum can be directly related to structural changes in the RNA.

A comparison of the CD spectra of the wildtype d3'-EBS1 and d3'-EBS1·IBS1 (Figure 108A) show solely a general increase in intensity, i.e. the shape of the CD curve does not change, indicating that no structural change occurs. This is explained by the additional presence of nucleobases from IBS1, i.e. an increase of hyperchromism is seen. This finding indicates that IBS1 does not bind to EBS1 under these conditions being in agreement with UV melting studies described in Section 2.2.3.

d3'-EBS1* and d3'-EBS1*·IBS1* behave differently: Addition of the intronic sequence to d3'-EBS1* leads to a slight change in elipticity as can be seen best by the decreased intensity of the shoulder at 280 nm (compare solid lines in Figure 108B and C). This decrease is well in line with an expected different backbone structure in d3'-EBS1* compared to d3'-EBS1*·IBS1*, similar to previous observations with other RNAs.[296,389] Melting of the two RNAs has a twofold effect on both CD spectra: At room temperature, the CD signal of both d3'-EBS1* and d3'-EBS1*·IBS1* displays the characteristic shape of an A-form RNA together with a more distinct additional shoulder at

280 nm in the case of d3'-EBS1*·IBS1*. Upon heating to 60 °C, the elipticity at 210 nm and 260 nm decreases in both cases. However, whereas the CD signal at 280 nm of d3'-EBS1* looses intensity, in the case of the complex d3'-EBS1*-IBS1*, the opposite trend is observed giving an isosbestic point at 270 nm. A further increase in temperature to 80 °C then leads to a drastic change of the CD spectra as exhibited by a red-shift of the largest positive elipticity, giving rise to final spectra as expected for unstructured RNAs.

The above described observations are well in line with the formation of the d3'-EBS1*·IBS1* complex: The first melting transition (see also Table 4) corresponds to the dissociation of IBS1* yielding a spectral trace dominated by the still partly structured d3'-EBS1*. The hairpin stem of d3'-EBS1* then melts at higher temperature giving rise to the observed red shift and the new maximum elipticity at 280 nm.

In order to investigate the influence of Mg^{2+} on the formation of the recognition site complex, binding of IBS1* to d3'-EBS1* was monitored by CD spectroscopy under different conditions. The following three modes of actions can be envisaged: (i) Mg^{2+} is needed to pre-structure the EBS1* loop such that IBS1* can bind efficiently, (ii) Mg^{2+} is not needed for

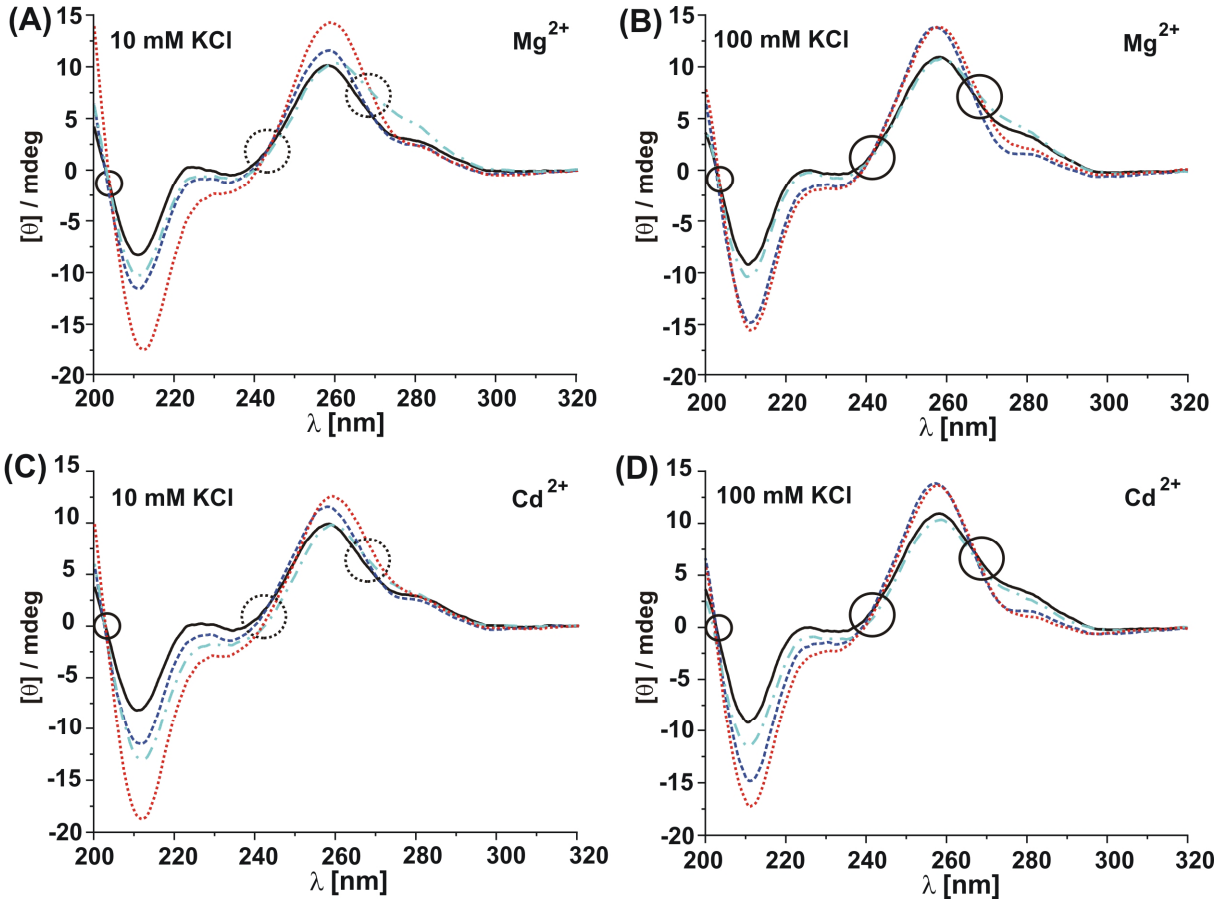

Figure 109 Changes in CD spectra of d3'-EBS1* (black solid line) upon addition of 1 eq IBS1* (dark blue dashed), 20 eq Mg^{2+} or Cd^{2+}, respectively (cyan dot-dashed) and 1 eq IBS1*/20 eq Mg^{2+} or Cd^{2+}, respectively (red dotted) in the presence of 10 mM KCl (A and C) and 100 mM KCl (B and D). Three isosbestic points at 205 nm, 245 nm and 270 nm (circles) are observed upon addition of IBS1* and IBS1*/20eq Mg^{2+} or Cd^{2+}, respectively, in the presence of 100 mM KCl. The concentration of d3'-EBS1* is 16 µM in all spectra shown.

binding of IBS1* to EBS1*, but for the final structure of the 5'-splice site, or (iii) Mg^{2+} is not needed at all. Hence, we recorded CD spectra between 200 nm and 320 nm of d3'-EBS1* alone, after the addition of one equivalent of IBS1*, or 20 equivalents of Mg^{2+}, respectively, and in the presence of both, i.e. one equivalent IBS1* and 20 equivalents Mg^{2+} (Figure 109A and B). Spectra were recorded at a background concentration of either 10 mM or 100 mM KCl.

In the presence of 10 mM KCl the addition of IBS1* to d3'-EBS1* leads to an increase in elipticity at 210 nm and 260 nm (Figure 109A). This increase is a consequence of binding of IBS1* to its cognate partner being consistent with the increasing number of stacked nucleobases upon addition of IBS1*. Subsequent addition of micromolar amounts of Mg^{2+} further increases significantly both bands suggesting that Mg^{2+} is needed to form the fully stable d3'-EBS1*·IBS1* complex (Figure 109A). The presence of higher concentrations of Mg^{2+} does not lead to any further changes in the CD spectrum. To investigate if the order of addition of Mg^{2+} or IBS1* to d3'-EBS1* has any influence on the final structure, a second experiment was performed, in which Mg^{2+} was added prior to IBS1*. These experiments show that the order of addition has no influence on the final structure. In the absence of IBS1*, the addition of Mg^{2+} leads to an intensification of the shoulder at around 280 nm and a slight shift to higher wavelength. Obviously Mg^{2+} binds to d3'-EBS1* inducing a structural change. The increasing elipticity at 280 nm suggests a longer single stranded, i.e. more unstructured region, similar to the melting of a double helix (see also Figure 108B and C). Indeed, the loop including EBS1* can form further basepairs, i.e. one Watson-Crick and two wobble base pairs, extending the duplex region and capped by a tetraloop (Figure 39B). Estimates of the folding energies of the open loop and the extended duplex region, respectively,[26,310] show that both forms have almost identical stabilities. The coordination of Mg^{2+} to d3'-EBS1* could thus lead to the melting of the EBS1* region thereby facilitating subsequent binding of IBS1*. Mg^{2+} binding to this region and EBS1* to be single stranded in the presence of Mg^{2+} is well in line with previously described Tb^{3+} cleavage experiments, where it has been shown that not only a metal ion binding site is located just 5' of EBS1 (also in the absence of IBS1), but in addition that EBS1 is not part of a duplex in the absence of 5'-exon.[91,97]

To investigate if Mg^{2+} is required to sculpt the 5'-splice site or if also monovalent ions can stabilize such a structure, the corresponding experiments were performed in the presence of 100 mM KCl (Figure 109B). As is the case in the presence of 10 mM KCl, also in 100 mM, the addition of IBS1* to d3'-EBS1* leads to an absolute increase in elipticity at 210 nm and

260 nm. However, at high K^+ concentration, the subsequent addition of Mg^{2+} does not result in a further increase in intensity. This suggests that at high concentration of K^+, binding of IBS1* is already fully achieved. Nevertheless, the small change in intensity at 280 nm indicates that Mg^{2+} still binds and has some influence on local structure, most probably in the unpaired region 5' of EBS1*. It is interesting to note that the shoulders at 280 nm of the d3'-EBS1* spectra in the absence and presence of Mg^{2+} show a similar elipticity. The addition of IBS1* reduces the same in both instances, which is different from the situation at 10 mM KCl. Taken together, the above results show that the presence of either Mg^{2+} or large excess of K^+ is sufficient to melt the EBS1* region prior to base pairing with IBS1* and to allow folding to the (almost) final d3'-EBS1*·IBS1* complex.

The group II intron *Sc*.ai5γ is known to be very sensitive to the presence of divalent metal ions other than Mg^{2+}.[70,390] Here, we investigated how Cd^{2+} binds to the 5'-splice site, as this metal ion is often used in so-called thiorescue experiments,[64,95,219,243] and has the least influence on splicing.[390] The changes of the CD spectra upon addition of Cd^{2+} to d3'-EBS1* or d3'-EBS1*·IBS1*, respectively, are shown in Figure 109C and D. At low K^+ concentration, Cd^{2+} again supports the formation of the d3'-EBS1*·IBS1* complex. Comparison of the overlay of CD spectra (Figure 109A and C) shows one major difference at 280 nm, i.e. Cd^{2+} has no influence on the intensity at this wavelength suggesting that it does bind differently to d3'-EBS1* compared to Mg^{2+} and does not promote melting of the EBS1* region. In the presence of 100 mM KCl the addition of Cd^{2+} to either d3'-EBS1* or d3'-EBS1*·IBS1* has no effect at 260 nm and 280 nm, but only at 210 nm, which is not observed in the case of Mg^{2+}. Again this suggests that Cd^{2+} binds slightly different than Mg^{2+} inducing a slightly different structure.

To summarize, the requirement of metal ions on the formation of the 5'-splice site have been investigated. Detailed circular dichroism studies showed that metal ions are required to form the stable EBS1*·IBS1* interaction. This can be achieved by either micromolar amounts of Mg^{2+} or high millimolar concentrations of K^+, although it seems as if Mg^{2+} is still needed for the final local structure. The role of these ions is most probably twofold: Firstly, Mg^{2+} (or 100 mM K^+) leads to an increased content of single strand in d3'-EBS1* suggesting the full melting of the EBS1* region. Obviously, this facilitates the base pairing with its cognate IBS1* sequence and hence also splicing in general. Secondly, small changes in the CD spectra upon addition of Mg^{2+} to d3'-EBS1*·IBS1* at both 10 and 100 mM KCl suggest minor structural changes in the RNA dimer. The most likely coordination site for metal ions in the complete 5'-splice site are the unpaired nucleotides just 5' of EBS1. Indeed, Tb^{3+}

cleavage experiments on the full length *Sc*.ai5γ are well in line with our results as they revealed EBS1 to be single stranded in the absence of IBS1 in addition to a strong metal ion binding site 5' of EBS1.[91,97]

All group II intron ribozymes investigated to date have a strict requirement for divalent metal ions for folding and catalysis.[129,203,207,243,287,391,392] In the case of *Sc*.ai5γ, a recent study showed that this group II intron is highly specific for Mg^{2+}, as the partial substitution of Mg^{2+} with other divalent ions like Ca^{2+}, Mn^{2+}, or Cd^{2+} leads in all cases to a significant loss in activity.[390] For example, in the presence of 90 mM Mg^{2+} and 10 mM Cd^{2+}, only about 75% of product was observed after 40 min compared to the reaction in 100 mM Mg^{2+}.[390] The here observed minor differences in Mg^{2+} and Cd^{2+} binding to d3'-EBS1*·IBS1* support this high selectivity for one kind of metal ion, as every small change in local structure will have an effect on the catalytic rate. However, the fact that Mg^{2+} can be (mostly) replaced by high concentrations of K^+ in the d3'-EBS1*·IBS1* complex is well in line with similar results from other small RNAs. For example, the hammerhead, hairpin, and VS ribozymes are still catalytically active at molar concentrations of M^+ ions (in the absence of Mg^{2+}), although at a significantly reduced rate.[74] The substitution of Mg^{2+} by large amounts of M^+ ions in small nucleotide systems is well known: The dephosphorylation of adenosine 5'-triphosphate works best in the presence of one equivalent each of Mg^{2+} and Zn^{2+}.[393] Mg^{2+} thereby only binds to phosphate oxygens whereas Zn^{2+} bridges phosphates and the purine N7 position. In the ATP system, the Mg^{2+} ion can be replaced by a 500-fold excess of Na^+, without resulting in a loss in dephosphorylation. It thus seems only reasonable that in the here investigated d3'-EBS1*·IBS1* system a 5000-fold excess of K^+ compared to Mg^{2+} is sufficient to induce a highly similar if not the same three dimensional local structure of the 5'-splice site.

3 Final Remarks and Outlook

Group II introns have the ability to splice themselves out of the precursor mRNA, but are also able to reinsert themselves into RNA and even DNA, therefore being infectious genetic elements. The base pairing interaction between IBS1 and EBS1 is thereby not only required for splice site recognition, but since the transesterification reactions are reversible, the same base-pairings are essential for reverse splicing into RNA or DNA target sites during intron mobility.[266,278] In this thesis, we report the solution structure of the splice site recognition complex in the absence and presence of the substrate, i.e. IBS1, thus providing a detailed view on this site at atomic resolution. Since reinsertion is also possible into DNA, it is of special interest to investigate the structural and also the metal ion requirements on a RNA-DNA hybrid, i.e. solving the solution structure, in which IBS1 is a DNA sequence. UV melting studies can reveal if this hybrid is more stable than the sole RNA construct. If this is the case, it could be even possible to solve the solution structure of the RNA-DNA hybrid with the wildtype sequence. These investigations would provide a detailed view on the binding of DNA to RNA, thus revealing knowledge about the ability of group II introns to migrate into DNA sequences.

The here described metal ion binding studies show that upon IBS1* binding, the metal ion binding site 5' of EBS1* shifts downstream. It is assumed that this shift occurs due to the induced structural change 5' of EBS1*. Through the kink in the backbone, the phosphate oxygens of G13 and G14 protrude to the outside and thus it is easier for metal ions to bind at this site. To further investigate the reasons for the shift of the metal ion binding site 5' of EBS1*, metal ion binding studies on the sole EBS1*·IBS1* can be performed. This will provide an understanding about the importance of the presence of the loop in the splice site recognition complex and will proof if indeed the metal ion binding site shifts due to the structural change. To get further insights into the metal ion requirements of the splice site, one can also envision a wide array of further experiments with other metal ions, monovalent as well as divalent.

The obtained detailed insights into metal ion binding and structural properties of the splice site recognition site in the absence and presence of IBS1* provide a view of the single parts of the ribozyme. With these informations, it will be now of special interest to investigate the behaviour of the splice site in the context of the active core of the ribozyme. The crystal structure of a group IIC intron in the absence of the exon shows that EBS1 is located in the catalytic center close to D5 and that two metal ions are located in close proximity to this

site.[249] One might ask if these two metal ions are still present if the exon is present. It is evident that with their length of up to several thousand nucleotides structures of full-length group II introns cannot be solved using NMR. Thus, to obtain a structure of the complete ribozyme, X-ray crystallography has to be used. This is indeed a time-consuming and challenging task. To further use NMR as a tool, one can only slightly increase the length of the RNA. Since the strcuture of the EBS1-site with the d3'-stem is solved and thus the spectral assignment of this construct is complete, one can think of solving the structure of a larger construct encompassing also α' and the bulge below, and even go as far as to include also the hairpin, which includes α to additionally gain information about the tertiary interaction between α and α'. It would also be of great interest to include EBS2 and IBS2 into the structure determination.

Circular dichroism studies reveal that the formation of the EBS1·IBS1 duplex does not necessarily require divalent metal ions, as large amounts of monovalent metal ions also promote the duplex. Nevertheless, micromolar amounts of divalent metal ions, e.g. Mg^{2+} or Cd^{2+}, strongly promote the formation of the 5'-splice site. It has been shown that Mg^{2+} and Cd^{2+} have different influences on the melting of the EBS1 site. It will be interesting to examine the role of Ca^{2+} and Mn^{2+} on the formation of the d3'-EBS1*·IBS1* complex, as it has been shown that these metal ions as well as Cd^{2+} leads to a significant loss in activity.[390]

There is indeed a wide array of different metal ions and techniques to further study the metal ion and structural requirements on the manifold interactions between metal ions and RNAs.

4 Materials and Methods

4.1 Materials

DNA oligonucleotides were purchased from Operon (Cologne, Germany) and Microsynth (Balgach, Switzerland). Oligonucleotide substrates 5'-CGUGGUGGGACAUUUUCGAG CGGU-3' (17/7), 5'-CGUGGUGGGACA***G***U***G***UCGAGCGGU-3' (17/7*) and 5'-CGUGGUGGGACA***G***U***GC***CGAGCGGU-3' (17/7-GC) for the activity assays were ordered from W. M. Keck (New Haven, USA), deprotected with DMF and triethylamintrihydrofluoride, precipitated with 1-butanole, and subsequently purified by HPLC according to the instructions by the manufacturer. IBS1 5'-CAUUUUC-3', EBS1 5'-GGAAAUG-3', IBS1* 5'-CAGUGUC-3', EBS1* 5'-GGCACUG-3', and IBS1GC 5'-CAGUGCC-3' were ordered HPLC-purified on a 1 µM scale from Curevac (Tübingen, Germany) and dialysed 3 times against 300 ml of a 100 mM KCl solution and 3 times against 300 ml double distilled water before use. Dialysis procedure was performed as previously described.[394] The Spectra/Por® Biotech Dialysis membrane tubings (Cellulose Ester, irradiated, 500 MWCO) were from Spectrum®labs (Breda, The Netherlands).

The *Taq* DNA polymerase (5 U/µl) was bought from New England BioLabs Inc. (Frankfurt, Germany). Ligation was performed using *T4* DNA Ligase (110u) from Promega (Madison, USA). Polynucleotide Kinase (PNK) was also from Promega. Restriction enzymes *Hind*III and *Eco*RI for plasmid linerization were purchased from Roche Diagnostics (Penzberg, Germany). The isolation and purification of the linearized plasmid was done by the Perfectprep® Gel cleanup kit from Eppendorf (Schönenbuch, Switzerland). For the purification of the plasmid after the mini preparation the High Pure Plasmid Isolation Kit from Roche (Penzberg, Germany) was utilized. For the maxi preparation the BioRad Aurum™ Plasmid Maxi Kit (Hercules, USA) was used. The digested plasmid was purified with QIAGEN-tip 100 from a QIAGEN Plasmid Midi Kit (Hilden, Germany). The adenosine 5'-[γ-^{32}P]triphosphate was purchased as triethylammonium salt from GE Healthcare (Otelfingen, Switzerland) as well as the MicroSpin G-25 size exclusion columns.

The nucleotide 5'-triphosphates of adenosine (ATP), cytidine (CTP) and guanosine (GTP) were from GE Healthcare (Chalfont St. Giles, UK), and uridine (UTP) was obtained from Acros (Geel, Belgium). Aqueous acrylamide solution (AccuGel 29:1) and TBE (Tris-borate-EDTA) buffer for the purification of RNA and DNA were purchased from National Diagnostics (Hussle Hull, UK), and urea (UltraPure) from Eurobio (Les Ulis, France). The T7

RNA polymerase used for *in vitro* transcription was home-made.[292,395] ^{15}N,^{13}C -labeled NTPs were from Silantes GmbH (München, Germany), now part of Cambridge Isotope Laboratories (CIL, Andover, USA). Selectively deuterated ribonucleotides were also purchased from CIL in a 100 mg mixture of ATP, CTP, GTP and UTP. For desalting Vivaspin 20 concentartors with a molecular weight cut-off of 3 kDa from VivaScience (Hannover, Germany) were used. Magnesium chloride for the metal ion titrations was utilized as a 1 M solution in H_2O in ultra-pure quality from Fluka-Sigma-Aldrich (Buchs, Switzerland). The exact concentrations of the $MgCl_2$, $CdCl_2$ and $MnCl_2$ stock solutions in 99.999% D_2O (Fluka-Sigma-Aldrich) was determined by potentiometric pH titrations via its $M(EDTA)^{2-}$ complex by measuring the equivalents of protons liberated from $H(EDTA)^{3-}$ upon complex formation. Deuterated reagents, that are D_2O (100%), D_2O (99.999% D), D_2O (99.98% D), H_2O/D_2O (90:10), NaOD (99.9% D) and DCl (99.5% D) were purchased from Armar Chemicals (Doettlingen, Switzerland). Pf1 phages in DEPC-treated water was purchased from Asla Biotech (Riga, Latvia) as a 50 mg/ml RNAase and Protease free solution in 10 mM K-phosphate buffer, pH 7.6. All used chemicals were at least puriss p.a. and used without further purification.

4.2 Instrumentation

The electroelution apparatus *Biotrap* and the BT1 and BT2 elutrap membranes are from Schleicher & Schuell, now Whatman (London, UK). The used centrifuges were a 5415R, 5415D, 5804R with rotor F-45-24-11 and 5804R with rotor A-4-44 from Eppendorf (Hamburg, Germany), as well as a RC-5C Plus from Sorvall (Langenselbold, Germany) with a SA-600, a SH-3000 and a SLA-3000 rotor. The purified RNA samples were dried in a Concentrator 5301 from Eppendorf (Hamburg, Germany). Gels were dried on a Biometra Maxidry geldryer (Goettingen, Germany).

The RNA was purified by a Merck Hitachi Elite La Chrom HPLC system. For reversed phase chromatography a C18 Beckmann Coulter Ultrasphere column was employed. Ion exchange chromatography was performed with either an analytical 4x250 mm or a semi-preparative 9x250 mm DNAPac® PA-100 from Dionex (Sunnyvale, USA).

NMR spectra were recorded on a Bruker AV2-400 MHz spectrometer with a 5mm QNP probehead, a Bruker DRX 500 MHz spectrometer using a 5 mm BBI probehead, a Bruker AV600 MHz spectrometer with a CP-TCI z-axis pulsed-field gradient cryoprobe or an AV700 MHz spectrometer equipped with a CP-TXI z-axis pulsed-field gradient cryoprobe at the NMR facility of the Chemical Institutes at the University of Zurich.

UV measurements were carried out on a Varian UV-vis-NIR spectrophometer (Cary 500 Scan, Varian Inc., Palo Alto, USA) equipped with a Cary Temperature Controller by Varian. The cuvettes were a 10 mm QS cuvette for the concentration determination and a 1 mm QS cuvette (both from Hellma, Müllheim, Germany) for UV melting studies as well as for CD measurements.

CD measurements were recorded on a J-810 spectrapolarimeter (Jasco Inc., Japan). Data evaluation was done by using the JASCO spectra manager-spectra analysis.

Dynamic Light Scattering was measured on a DynaPro Titan machine from Wyatt Technology Corporation (Santa Barbara, USA), employing the Dynamics V6 software.

The scintillation counter 22000CA Liquid Scintillation Analyzer was purchased from Canberra Packard. Phosphoimaging was performed with a Molecular Dynamics Storm 860 Phosphorimager (Amersham Biosciences, now GE Healthcare, Otelfingen, Switzerland). Quantitation of the gels was performed using the software ImageQuant (GE Healthcare, Otelfingen, Switzerland).

The H_2O used in all experiments was treated with a TKA genepure water purification system (TKA Wasseraufbereitungssysteme, Niederelbert, Germany).

4.3 General procedures

4.3.1 Sample preparation for NMR, CD and UV melting studies

The wildtype d3'-EBS1 (5'-GGAGUAUGUAUUGGAAAUGAGCAUACUCC-3'), d3'-EBS1* (5'-GGAGUAUGUAUUGGCACUGAGCAUACUCC-3') and d3'-TL (5'-GGAGUAUGUGAAAGCAUACUCC) were synthesized by *in vitro* transcription with T7 RNA polymerase from synthetic double stranded DNA oligonucleotide templates.[292] The reaction mixture contained 5 mM of each NTP, 0.9 μM of the double stranded DNA template, 0.1% Triton X-100, 40 mM Tris-HCl (pH 7.5), 40 mM DTT, 2 mM spermidine and 30 mM $MgCl_2$ for d3'-EBS1, 35 mM $MgCl_2$ for d3'-EBS1* and 50 mM $MgCl_2$ for d3'-TL, respectively. The amount of T7-polymerase was optimized individually for each polymerase batch. N (29 nucleotides) and n+1 (30 nucleotides) lengths RNAs were obtained in a ratio of approximately 60:40, and care was initially taken to separate them. It was found that the combined RNA species did not affect the chemical shifts in 2D [^{1}H,^{1}H]-NOESY spectra and thus also not the overall structure. Natural isotope abundance as well as fully ^{15}N,^{13}C -enriched samples of all three constructs were transcribed and used for NMR measurements. d3'-EBS1* was also transcribed with selectively deuterated NTPs. The RNA was purified by

denaturing 15% (w/v) polyacrylamide gel electrophoresis (PAGE), UV-shadowed and excised from the gel, followed by electroelution and ethanol-precipitation. In order to receive a hairpin conformation instead of a duplex, the RNA was dissolved in 100 ml 85°C ddH_2O, left for one minute and cooled down quickly on ice. The RNA was concentrated using Vivaspin 20 at 14 °C and 4'500 g and washed with ddH_2O. All samples were lyophilized, resolved in D_2O (200 µl) containing KCl (10 mM for d3'-EBS1* and d3'-TL, respectively, and 110 mM for d3'-EBS1*·IBS1*) and EDTA (10 µM). The RNA concentrations were determined with a Varian Cary 500 Scan UV-VIS-NIR spectrophometer, using an extinction coefficient at 260 nm (ε_{260}) 341.8 $mM^{-1}cm^{-1}$ for d3'-EBS1, 325.8 $mM^{-1}cm^{-1}$ for d3'-EBS1*, 257.7 $mM^{-1}cm^{-1}$ for d3'-TL, 66 $mM^{-1}cm^{-1}$ for IBS1, 91.5 $mM^{-1}cm^{-1}$ for EBS1, 73.6 $mM^{-1}cm^{-1}$ for IBS1*, 75.5 $mM^{-1}cm^{-1}$ for EBS1* and 71.1 $mM^{-1}cm^{-1}$ for IBS1GC. The concentrations of the RNA samples for NMR measurements varied between 0.4 and 1.2 mM. The pH was adjusted to 6.4 for samples in H_2O/D_2O and to pD 6.8 for samples in D_2O, using DCl or NaOD solutions. To measure the pD value, 0.4 log units were added to the pH meter reading.[73,396] All samples were lyophylized and resuspended in either H_2O/D_2O (90:10) or 100% D_2O prior to the acquisition of the NMR spectra. Samples for CD measurements and UV melting studies were resuspended in ddH_2O.

4.3.2 UV melting studies

Temperature dependent absorption measurements were performed at 260 nm in quartz cuvettes with 1 mm path length (volume 200 µl). Before measuring the samples were degassed for 30 sec and carefully covered with paraffin oil. The melting experiments were carried out by constantly raising the temperature from 5 °C to 80 °C (for EBS1·IBS1, EBS1·IBS1-GC and EBS1*·IBS1*), 5 °C to 90 °C (for d3'-EBS1*·IBS1*) and 15 °C to 75 °C (d3'-EBS1*), with a heating rate of 0.5 °C/min. Absorption spectra were recorded every 0.5 °C during three heating and three cooling cycles. Samples for concentration dependent UV measurements contained 1.0, 1.7, 3.5, 5.8, 13.3, 19.0, 36.5 and 70.1 µM d3'-EBS1* at pH 6.8. RNA concentrations for the other samples varied between 7.3 and 10.9 µM. Sodium ion concentrations ranged from 10 – 200 mM. All spectroscopic data were analysed using Origin® version 6.0 (OriginLab™ Corporation). The van't Hoff analysis was performed with the Hyperchromicity calculation – Thermal, which is part of the Cary WinUV package, with a non-self complementary, bimolecular function for EBS1*·IBS1* and with a self complementary monomolecular function for the d3'-stem.

4.3.3 Circular dichroism

CD spectra were recorded over the spectral range of 200-320 nm (3 spectra accumulations) and a scan speed of 50 nm min^{-1}. A quartz cuvette with 1 mm pathlength and 200 µl volume was used. For the metal ion titration studies a solution of 16 µM d3'-EBS1* with 10 mM KCl or 100 mM KCl, respectively, pH 6.8 (solution A), and a solution of 16 µM d3'-EBS1* with 10 mM KCl or 100 mM KCl, respectively, 1 mM $MgCl_2$, pH 6.8 (solution B), were prepared. The titration was done by removing small aliquots of solution A and adding the equivalent aliquot of solution B, so that the total sample volume remained constant. The same procedure was performed for the titration of d3'-EBS1*·IBS1* with Mg^{2+}, but in these experiments equivalent amounts of d3'-EBS1* and IBS1* (16 µM) were used. For the titrations with IBS1* small aliquots were added to solution A in the absence and presence of 320 µM Mg^{2+}, respectively, up to a final concentration of 32 µM IBS1*. All titrations were measured at 20 °C. The titrations with Cd^{2+} were performed analogously. For the titration of the d3'-EBS1 with IBS1 a 10 µM d3'-EBS1 solution (100 mM KCl, pH 6.8) was used and small aliquots of IBS1 were added up to a final concentration of 20 µM. Temperature dependent CD measurements were carried out between 20 °C and 84 °C with a heating rate of 1 °C/min and three accumulation cycles at each step.

4.3.4 Dynamic Light Scattering measurements

Dynamic light scattering (DLS) is a good tool to measure the hydrodynamic radius of molecules. DLS was measured at 293 K and 298 K in a 12 µl cuvette using the conditions from the NMR experiments (samples were in D_2O, pD 6.8, 10 mM KCl for d3'-TL and d3'-EBS1*, 100 mM KCl for EBS1*IBS1* and 110 mM KCl for d3'- EBS1*IBS1*). Samples were measured at concentrations of 0.25 mM or 0.5 mM, respectively. Before measuring, the samples were centrifuged for 45 min at 4 °C and 16'100 g prior to the experiment in order to avoid any dust that might hamper DLS measurements. At least ten measurements with ten acquisitions of each sample were recorded.

4.3.5 Preparation of the Pf1 aligned NMR samples to measure RDCs

For RDC measurements, d3'-EBS1* and d3'-EBS1*·IBS1* were aligned in 25.6 mg/ml Pf1 phage. First the magnetic alignment of the phage was checked by measuring the splitting of the HOD signal from the solvent. Therefore, a phage sample only of phages in 90%

H_2O/10% D_2O was prepared and a 1D ^2H NMR spectrum was recorded at 298 K. The splitted signal comes from the large deuterium quadrupole moment that is not isotropically averaged for water bound to the aligned phage particles and directly correlates with the ability of the phage to align RNA.[319] For a 25.6 mg/ml concentrated sample a splitting of 24.2 Hz was found for the phage alone. One sample with and one without phages were prepared for d3'-EBS1* or d3'-EBS1*·IBS1*, respectively. The d3'-EBS1* sample without phages was lyophylized and redissolved in 200 µl of 90% H_2O/10% D_2O to a final RNA concentration of 0.69 mM, including KCl for a final salt concentration of 10 mM KCl and EDTA for a final concentration of 10 µM. The pH was adjusted to 6.85. A droptest with 2 µl of the RNA sample and 1 µl of 50 mg/ml Pf1 phage showed no precipitation. Therefore the second lyophylized sample of d3'-EBS1* was prepared with phages by adding 156 µl of 90% H_2O/10% D_2O, adjusting the pH to 6.53 and 164 µl of 50 mg/ml Pf1 phages were added to a final volume of 320 µl. The final RNA concentration was 0.69 mM, salt concentrations were 10 mM KCl and 10 µM EDTA. The final RNA concentration of both samples of d3'-EBS1*·IBS1* was 0.48 mM, KCl concentrations were 50 mM and EDTA concentrations 10 µM. The phage concentration was 25.6 mg/ml in a volume of 320 µl. The pH for d3'-EBS1*·IBS1* without phages was set to 6.45 and with phages to 6.67. The droptest for d3'-EBS1*·IBS1* without phages also showed no precipitation.

4.3.6 NMR spectroscopy

Non-exchangeable proton resonances were assigned from 2D [^{1}H,^{1}H]-NOESY spectra in D_2O acquired at 60, 120 and 250 ms mixing times at 288 K, 293 K, 298 K and/or 303 K. 2D [^{13}C,^{1}H]-HSQCs were recorded separately for the aromatic (sw = 70 ppm, O1 = 135 ppm) and the aliphatic (sw = 120 ppm, O1 = 50 ppm) range of the ^{13}C resonances. 2D [^{1}H,^{1}H]-TOCSY spectra at 45 ms mixing time were used to clarify the sugar pucker conformation. In A-form RNA the sugar pucker conformation is usually 3'-endo and can be distinguished from the 2'-endo form, which gives a strong crosspeak between H1' and H2' and even between H1' and the H3' of the ribose sugar in a 2D [^{1}H,^{1}H]-TOCSY spectrum. Natural abundance 2D [^{13}C,^{1}H]-HSQCs were acquired for the EBS1*·IBS1* construct at 700 MHz over 24 hours.

Exchangeable proton resonances were assigned from 2D [^{1}H,^{1}H]-NOESY spectra in 90% H_2O/10% D_2O acquired at 278 K, 283 K and 293 K with mixing times of 150 ms and watergate H_2O suppression. Assignment was supported by [^{15}N,^{1}H]-HSQC experiments. The base pairing scheme was established by a 2D J_{NN} HNN-COSY spectrum,[118] which correlates

the imino nitrogen of uracil (N3) and guanine (N1) across the H-bond to the N1 of adenine or the N3 of cytosine on the other side of the double helix.

All ^{1}H spectra were recorded with RNA constructs of natural isotope abundance and experiments involving ^{13}C and ^{15}N isoptopes were recorded with fully $^{15}N,^{13}C$-enriched samples, except for EBS1*·IBS1*.

One-bond ^{1}H-^{13}C RDCs were measured from the splitting of the peak along the carbon dimension of 2D [$^{13}C,^{1}H$]-HSQCs (separately for the aromatic and the sugar region) at 298 K and one-bond ^{1}H-^{15}N RDCS in the nitrogen and proton dimensions of 2D [$^{15}N,^{1}H$]-HSQCs at 278 K for d3'-EBS1* and d3'-EBS1*·IBS1* in isotropic (unaligned) and Pf1-containing (aligned) solution (for sample conditions see section 4.3.5). The couplings for the aromatic (H2, H5, H6 and H8), for H1' sugar protons as well as the imino H1 and H3 protons were extracted with Sparky by determining the difference between ^{1}H-^{13}C and ^{1}H-^{15}N for isotropic and partially aligned samples.

For d3'-EBS1*·IBS1* with d3'-EBS1* hairpin $^{15}N,^{13}C$ labeled and IBS1* at natural abundance, as well as for a mixture of $^{15}N,^{13}C$ labeled and unlabeled d3'-EBS1* in a 1:1 ratio, double X half-filtered NOESY-HSQC spectra were recorded at 278 K with a ^{15}N filter in F1 (with watergate H_2O suppression) at 278 K with 16 scans and 2048 experiments in F3, 32 experiments in F2 and 132 experiments in F1. The used 3D pulse sequence from the Bruker pulse program library was noesyhsqcf3gpwx13d. The acquisition time was 73 ms, the coupling constants $^{1}J(N\text{-}H)$ (cnst4), $^{1}J(C\text{-}H)_{min}$ (cnst6) and $^{1}J(C\text{-}H)_{max}$ (cnst7) were set to 90 Hz, 160 Hz and 200 Hz, respectively. The relaxation delay (D1) was 1 s, the delay for homospoil/gradient recovery (D16) 200 μs and the mixing time 150 ms.

The 2D X-filter experiments of d3'-EBS1*·IBS1* (d3'-EBS1* labeled, EBS1* unlabeled) were recorded using a phase sensitive 2D w_1,w_2-$^{15}N,^{13}C$ -filtered NOESY experiment (Bruker pulse program: noesygpphwgxf.2) with watergate H_2O suppression as well as a TOCSY version of it (Bruker pulse program: dipsigpphwgxf.2).[325-328] These experiments were recorded at 298 K in 90% H_2O/10% D_2O. The NOESY experiment was recorded with 64 scans and 2048 experiments in F2 as well as 256 experiments in F1 and the TOCSY experiment with with 32 scans and 2048 experiments in F2 as well as 256 experiments in F1. For the NOESY as well as for the TOCSY experiment, the same parameters as for the double X half-filtered NOESY-HSQC experiment (see above) were used.

To calculate the hydrodynamic radius of EBS1*·IBS1*, d3'-TL, d3'-EBS1* and d3'-EBS1*·IBS1* DOSY experiments were acquired. The used 2D pulse sequence from the Bruker pulse program library was stebpgp1s, employing stimulated echo and bipolar gradient

pulses for diffusion. The diffusion time (Δ), the gradient length (δ) and the recovery delay after gradient pulses were set to 350 ms, 2 ms and 200 μs, respectively, and the gradient strength was incremented from 11.8 to 32 G/cm in 64-80 steps. For each FID 64 scans were collected with 21006 data points in F2. The diffusion coefficients were calculated using the DOSY routine of Topspin 1.3. For the calculation of the hydrodynamic radii of the molecules the Stokes-Einstein equation was used:

$$D = \frac{kT}{6\pi r\eta} \qquad \text{equation 19}$$

and rearrangement of equation 19 yields:

$$r = \frac{kT}{6\pi D\eta} \qquad \text{equation 20}$$

where k is the Boltzmann constant with $1.381 \cdot 10^{-23}$ NmK^{-1}, T the temperature in K at which the experiment was acquired (here 293 K or 298 K, respectively), η is the dynamic viscosity of the solvent ($1 \cdot 10^{-3}$ Nsm^{-2} for H_2O at 293 K and $0.89 \cdot 10^{-3}$ Nsm^{-2} for H_2O at 298 K), D is the diffusion coefficient, which was obtained from the DOSY experiment in m^2s^{-1}.

All spectra were processed with XWINNMR and Topspin 1.2, 1.3 or 2.0 (Bruker). 1D spectra were analyzed with MestreC (http://www.mestrec.com/) or with Topspin 1.2, 1.3 or 2.0. Sparky (http://www.cgl.ucsf.edu/home/sparky/) was used for multidimensional spectra assignment. NOE peak volumes were integrated with the Gaussian peak fitting function in Sparky.

4.4 Structure calculations

4.4.1 Structure calculation of d3'-EBS1*

NOE distances were estimated from the integrated peak volumes obtained from the 2D [^{1}H,^{1}H]-NOESY spectrum that was acquired at 293 K with a mixing time of 250 ms. Distances were calibrated using the CALIBA macro in DYANA.[397] The NOEs were grouped into four categories, corresponding to strong (1.8 – 3 Å), medium (1.8 – 4.5 Å), weak (3.0 – 6.0 Å), and very weak (4.0 – 7.0 Å) (Appendix 6). NOEs obtained from 2D [^{1}H,^{1}H]-NOESY crosspeaks in 90% H_2O/10% D_2O at 278 K were qualitatively assigned as strong, medium, weak, or very weak (Appendix 6).

Based on 1D ^{31}P NMR spectra, the torsion angles α and ζ were set to exclude the trans-range (except for G1, which was left unconstrained, as well as C29, where only α was

constrained) (Appendix 8).[121] Sugar pucker restraints were included based on 2D [^{1}H,^{1}H]-TOCSY experiments with a mixing time of 45 ms.[34] G1, A10 to A20, and C29 were left unconstrained. The other backbone torsional angles (β, γ, ε) were set to standard A-form values in the helical region of the structure (G2-U9, G21-C28). Based on the intranucleotide H1' to aromatic NOEs of a 60 ms NOESY spectrum the torsion angle χ was restrained to *anti* (–160 ± 20°) for all residues. Additional H-bond restraints were added for base pairs whose existence was proven by ^{1}H-^{1}H crosspeaks across the helix in the imino region and by HN-crosscorrelations from the 2D J_{NN} HNN-COSY spectrum.[118]

200 initial structures were calculated with CNS 1.2 from an extended structure with random initial velocities using NOE distance, dihedral and H-bond restraints.[119] The structures were subsequently refined with the introduction of RDCs in XPLOR-NIH (Appendix 7).[120] The RDCs were measured using Sparky by determining the difference between ^{1}H-^{13}C and ^{1}H-^{15}N for isotropic and partially aligned samples. The D_a and R values of the alignment tensor were estimated using PALES[323,324] and further refined by manual gridsearch.[398] The final D_a was set to –41 Hz and R to 0.3. Structures were refined by cooling from 2000 K to 100 K. 500 steps of energy minimization using the Powell algorithm followed simulated annealing. For comparison 200 structures each were calculated with and without the introduction of RDCs. After refinement, the structures were evaluated for convergence. Acceptance criteria were low overall energies and no significant NOE (>0.2 Å) or dihedral (>5°) violations. The twenty lowest-energy structures out of 200 calculated were visualized and analyzed using MOLMOL.[29] Six additional structures of low overall energy also satisfied all RDC and NOE restraints, but these were discarded owing to antiparallel alignment: that is, RDC restraints can be satisfied either by A-form geometry or by antiparallel helical orientations that are rotated 180° about the order tensor frame S_{xx} and S_{yy}.[399]

4.4.2 Structure calculation of d3'-EBS1*·IBS1*

NOE distances were estimated from the integrated peak volumes obtained from the 2D [^{1}H,^{1}H]-NOESY spectrum that was acquired at 298 K with a mixing time of 250 ms. Distances were calibrated using the CALIBA macro in DYANA.[397] The NOEs were grouped into four categories, corresponding to strong (1.8 – 3 Å), medium (1.8 – 4.5 Å), weak (3.0 – 6.0 Å), and very weak (4.0 – 7.0 Å) (Appendix 17). NOEs obtained from 2D [^{1}H,^{1}H]-NOESY

crosspeaks in 90% H_2O/10% D_2O at 278 K were qualitatively assigned as strong, medium, weak, or very weak (Appendix 17).

Based on 1D ^{31}P NMR spectra, the torsion angles α and ζ were set to exclude the trans-range (except for G1, which was left unconstrained, as well as C29 and C65, where only α was constrained) (Appendix 19).[121] Based on TOCSY experiments with a 45-ms mixing time, nucleotides with strong H1'-H2' and H1'-H3' crosspeaks were restrained to S-type range (δ = 145 ± 20°) (A10, U11, and U12), those with absent H1'-H2' crosspeaks to N-type range (δ = 85 ± 20°), and nucleotides with intermediate crosspeak intensities (G1, C29, and C65) were left unconstrained.[34] The other backbone torsional angles (β, γ, ε) were set to standard A-form values in the helical region of the structure (G2-U9, G21-C28, G13-G19, and C59-U64). Based on the intranucleotide H1' to aromatic NOEs of a 60 ms NOESY spectrum the torsion angle χ was restrained to *anti* (–160 ± 20°) for all residues. Additional H-bond restraints were added for base pairs whose existence was proven by ^{1}H-^{1}H crosspeaks across the helix in the imino region and by HN-crosscorrelations from the 2D J_{NN} HNN-COSY spectrum.[118]

200 initial structures were calculated with CNS 1.2 from an extended structure with random initial velocities using NOE distance, dihedral and H-bond restraints.[119] The structures were subsequently refined with the introduction of RDCs in XPLOR-NIH (Appendix 18).[120] The RDCs were measured using Sparky by determining the difference between ^{1}H-^{13}C and ^{1}H-^{15}N for isotropic and partially aligned samples. The D_a and R values of the alignment tensor were estimated using PALES[323,324] and further refined by manual gridsearch.[398] The final D_a was set to –40 Hz and R to 0.1. Structures were refined by cooling from 2000 K to 100 K. 500 steps of energy minimization using the Powell algorithm followed simulated annealing. For comparison 200 structures each were calculated with and without the introduction of RDCs. After refinement, the structures were evaluated for convergence. Acceptance criteria were low overall energies and no significant NOE (>0.2 Å) or dihedral (>5°) violations. The twenty lowest-energy structures out of 200 calculated were visualized and analyzed using MOLMOL.[29]

Conformational analysis, the wormsearch for comparison of structures, and motif search were performed with the AMIGOS algorithms (http://pylelab.org/software/index.html).[15,16]

4.4.3 Electrostatic surface potential calculation of d3'-EBS1* and d3'-EBS1*·IBS1*

The electrostatic surface potential of d3'-EBS1* and d3'-EBS1*·IBS1* was calculated with the program QNIFFT[80] and visualized with PYMOL (W. L. DeLano, 2002, http://www.pymol.org). The electrostatic potential of nucleic acids was calculated by means of the non-linear Poisson-Boltzmann (NLPB) equation. A surface potential representation elucidates areas of unusual negative or positive potential, which is an indication of potential molecular interactions, e.g. between RNA and metal ions.[80]

4.4.4 Structure calculation of d3'-TL

NOE distances were estimated from the integrated peak volumes obtained from the 2D [^{1}H,^{1}H]-NOESY spectrum that was acquired at 303 K with a mixing time of 250 ms. Distances were calibrated using the CALIBA macro in DYANA.[397] The NOEs were grouped into four categories, corresponding to strong (1.8 – 3 Å), medium (1.8 – 4.5 Å), weak (3.0 – 6.0 Å), and very weak (4.0 – 7.0 Å) (Appendix 28). NOEs obtained from [^{1}H,^{1}H]-NOESY crosspeaks in 90% H_2O/10% D_2O at 278 K were qualitatively assigned as strong, medium, weak, or very weak (Appendix 28).

Based on 1D ^{31}P NMR spectra, the torsion angles α and ζ were set to exclude the trans-range (except for G1, which was left unconstrained, as well as C22, where only α was constrained) (Appendix 29).[121] Based on TOCSY experiments with a 45 ms mixing time, nucleotides with strong H1'-H2' and H1'-H3' crosspeaks were restrained to S-type range (δ = 145 ± 20°) (A11), those with absent H1'-H2' crosspeaks to N-type range (δ = 85 ± 20°), and nucleotides with intermediate crosspeak intensities (G1, G10, A12, A13, and C22) were left unconstrained.[34] The other backbone torsional angles (β, γ, ε) were set to standard A-form values in the helical region of the structure (G2-U9, G14-C21). Based on the intranucleotide H1' to aromatic NOEs of a 60 ms NOESY spectrum the torsion angle χ was restrained to *anti* (–160 ± 20°) for all residues. Additional H-bond restraints were added for base pairs whose existence was proven by ^{1}H-^{1}H crosspeaks across the helix in the imino region and by HN-crosscorrelations from the 2D J_{NN} HNN-COSY spectrum.[118]

200 initial structures were calculated with CNS 1.2 from an extended structure with random initial velocities using NOE distance, dihedral and H-bond restraints.[119] The structures were subsequently refined in XPLOR-NIH.[120] After refinement, the structures were evaluated for convergence. Acceptance criteria were low overall energies and no

significant NOE (>0.2 Å) or dihedral (>5°) violations. The twenty lowest-energy structures out of 200 calculated were visualized and analyzed using MOLMOL.[29]

4.4.5 Structure calculation of EBS1*·IBS1*

NOE distances were estimated from the integrated peak volumes obtained from the 2D [^{1}H,^{1}H]-NOESY spectrum that was acquired at 288 K with a mixing time of 250 ms. Distances were calibrated using the CALIBA macro in DYANA.[397] The NOEs were grouped into four categories, corresponding to strong (1.8 – 3.0 Å), medium (1.8 – 4.5 Å), weak (3.0 – 6.0 Å), and very weak (4.0 – 7.0 Å) (Appendix 33). NOEs obtained from [^{1}H,^{1}H]-NOESY crosspeaks in 90% H_2O/10% D_2O at 278 K were qualitatively assigned as strong, medium, weak, or very weak (Appendix 33).

Based on 1D ^{31}P NMR spectra, the torsion angles α and ζ were set to exclude the trans-range (Appendix 34).[121] Sugar pucker restraints were included based on TOCSY experiments with 45 ms mixing time.[34] For EBS1*·IBS1* all nucleotides were constrained to N-type (δ = 85 ± 20°) due to missing H1'-H2' and H1'-H3' crosspeaks, except for G19 which was left unconstrained. The other backbone torsional angles (β, γ, ε) were set to standard A-form values. Based on the intranucleotide H1' to aromatic NOEs of a 60 ms NOESY spectrum the torsion angle χ was restrained to *anti* (–160 ± 20°) for all residues. Additional H-bond restraints were added for base pairs whose existence was proven by ^{1}H-^{1}H crosspeaks across the helix in the imino region.

200 initial structures were calculated with CNS 1.2 from an extended structure with random initial velocities using NOE distance, dihedral and H-bond restraints.[119] The structures were subsequently refined in XPLOR-NIH.[120]

After refinement, the structures were evaluated for convergence. Acceptance criteria were low overall energies and no significant NOE (>0.2 Å) or dihedral (>5°) violations. The twenty lowest-energy structures out of 200 calculated were visualized and analyzed using MOLMOL.[29]

4.5 Metal ion titration studies

4.5.1 Mg^{2+} line broadening and chemical shift analysis of d3'-EBS1* and d3'-EBS1*·IBS1*

Mg^{2+} line broadening and chemical shift changes of non-exchangeable protons were monitored by a series of 2D [^{1}H,^{1}H]-NOESY spectra at 298 K with 0.5 mM d3'-EBS1* (100% D_2O, *I* = 10 mM (KCl), 10 µM EDTA, pD = 6.96) and steps of 0, 0.5, 1, 1.5, 2, 2.5, 3, 4, 5, 6, 6.5, and 7 mM $MgCl_2$. The chemical shift map shown in Figure 77 was drawn by subtraction of the chemical shift of all observed H1', H2, H5, H6 and H8 protons at 0 mM Mg^{2+} from the corresponding chemical shifts at 2 mM Mg^{2+}. The 2D [^{1}H,^{1}H]-NOESY series for d3'-EBS1*·IBS1* was measured at 298 K with 0.9 mM d3'-EBS1*·IBS1* (100% D_2O, *I* = 110 mM (KCl), 10 µM EDTA, pD = 6.83) and steps at 0, 0.5, 1, 2 3, 4, 5, 6, 7, 8, 10 mM $MgCl_2$. The chemical shift map shown in Figure 77 was drawn by subtraction of the chemical shift of all observed H1', H2, H5, H6 and H8 protons at 0 mM Mg^{2+} from the corresponding chemical shifts at 3 mM Mg^{2+}.

Changes in chemical shifts of the imino protons of d3'-EBS1* and d3'-EBS1*·IBS1* were monitored by recording a series of 1D [^{1}H]-NMR experiments, using a spin echo water suppression scheme. In the titration series for d3'-EBS1*, spectra of 0.64 mM RNA (10 mM KCl, 10 µM EDTA, pH = 6.52) in 90% H_2O/10% D_2O were acquired with 0, 0.5, 1, 2, 3, 4, 5, 6, 7, and 8 mM Mg^{2+} at 278 K. The chemical shift values at 0 mM Mg^{2+} were subtracted from the values at 3 mM Mg^{2+} to yield the chemical shift map of the imino protons shown in Figure 76A. For d3'-EBS1*·IBS1* the titration series was recorded with 0.54 mM RNA (110 mM KCl, 10 µM EDTA, pH = 6.58) and steps at 0, 0.5, 1, 2, 3, 4, 5, 6, 7, 8, 9, 10, 12, 16, 20, 25, and 30 mM $MgCl_2$. The chemical shift values at 0 mM Mg^{2+} were subtracted from the values at 3 mM Mg^{2+} to yield the chemical shift map of the imino protons shown in Figure 76B. All spectra were recorded at 700 MHz proton frequency on a Bruker Avance spectrometer equipped with a CP-TXI z-axis pulsed-field gradient cryoprobe.

4.5.2 Mn^{2+} line broadening studies of d3'-EBS1* and d3'-EBS1*·IBS1*

Mn^{2+} binding to the non-exchangeable protons of d3'-EBS1* was monitored by titrating $MnCl_2$ in steps of 0, 5, 10, 15, 30, 45, 60, 90, 120, 150, 200, 300 µM to a sample of 0.54 mM d3'-EBS1* (100% D_2O, *I* = 10 mM (KCl), pD = 6.73) and acquisition of 2D [^{1}H,^{1}H]-NOESY spectra each with 48 scans and 2048 experiments in F2 as well as 256 experiments in F1 at

298 K. In addition a selectively deuterated d3'-EBS1* sample was measured containing 0.6 mM RNA (100% D_2O, I = 10 mM (KCl), pD = 6.72) in order to be able to follow also the line broadening of the signals, which are overlayed by the H5-H6 crosspeaks in non-deuterated samples. The titration steps were 0, 15, 30, 45, 60, 90, 120, 150, 180, 210, 240, 270, 300 µM Mn^{2+}. Each 2D [^{1}H,^{1}H]-NOESY spectrum was recorded with 48 scans and 2048 experiments in F2 as well as 256 experiments in F1 at 298 K. A 0.6 mM sample of d3'-EBS1*·IBS1* with the d3'-EBS1* hairpin selectively deuterated was used (100% D_2O, I = 110 mM (KCl), 20 µM EDTA, pD = 6.6) for the line broadening experiments with d3'-EBS1*·IBS1*. The 2D [^{1}H,^{1}H]-NOESY series was measured at 298 K with steps of 20, 30, 45, 60, 75, 90, 120, 150, 180, 210, 240, 270, 300, 330, 360, and 390 µM $MnCl_2$ (i.e. $[Mn^{2+}]_{tot}$ = 0, 10, 25, 40, 55, 70, 100, 130, 160, 190, 220, 250, 280, 310, 340, and 370 µM due to the binding of Mn^{2+} to EDTA). Each spectra were recorded with 48 scans and 2048 experiments in F2 as well as 256 experiments in F1.

Mn^{2+} binding to the imino protons of d3'-EBS1* and d3'-EBS1*·IBS1* was observed by recording 64 scans of a 1D [^{1}H]-NMR series, using a pulse sequence with spin echo water suppression. The sample of d3'-EBS1* contained 0.52 mM RNA (I = 10 mM (KCl), pH = 6.79) and d3'-EBS1*·IBS1* 0.54 mM RNA (I = 110 mM (KCl), pH = 6.89). 1D [^{1}H]-NMR experiments were measured in 90% H_2O/10% D_2O at 278 K for both samples in steps of 0, 10, 20, 30, 45, 60, 90, 120, 150, 180, 210, 240, 270, 300, 330, 360, 390, and 450 µM Mn^{2+}. All spectra were recorded at 700 MHz proton frequency on a Bruker Avance spectrometer equipped with a CP-TXI z-axis pulsed-field gradient cryoprobe. The line broadening effect of Mn^{2+} coordination to the non-exchangeable as well as to the exchangeable protons was evaluated qualitatively.

4.5.3 Cd^{2+} titrations - chemical shift analysis of d3'-EBS1* and d3'-EBS1*·IBS1*

Changes in chemical shifts of the non-exchangeable protons (H1', H2, H6 and H8) of d3'-EBS1* were monitored by 2D [^{1}H,^{1}H]-NOESY spectra upon addition of 0, 0.5, 1, 1.5, 2, 2.5, 3, 4, 5, 6, 7, and 8 mM $CdCl_2$. The d3'-EBS1* sample was selectively deuterated with a concentration of 0.6 mM (I = 10 mM (KCl), 10 µM EDTA, pD = 6.66). The chemical shift values at 3 mM Cd^{2+} were subtracted from the values at 0 mM Cd^{2+} to yield the chemical shift map of the imino protons shown in Figure 101. 2D [^{1}H,^{1}H]-NOESY spectra of d3'-EBS1*·IBS1* were recorded at steps of 0, 0.5, 1, 1.5, 2, 2.5, 3, 3.5, 4, 5, 6, and 8 mM $CdCl_2$.

The concentration of d3'-EBS1*·IBS1* was 0.61 mM (*I* = 10 mM (KCl), 10 µM EDTA, pD = 6.89). All spectra were measured at 298 K at 700 MHz proton frequency. The chemical shift values at 0 mM Cd^{2+} were subtracted from the values at 3 mM Cd^{2+} to yield the chemical shift map of the imino protons shown in Figure 101.

The change in chemical shifts of the exchangeable protons of d3'-EBS1* and d3'-EBS1*·IBS1* was monitored by the acquisition of a series of 1D [^{1}H]-NMR, using a spin echo water suppression scheme. In the titration series of d3'-EBS1*, spectra of a 0.55 mM RNA sample (*I* = 10 mM (KCl), 10 µM EDTA, pH = 6.72) in 90% H_2O/10% D_2O were acquired with 0, 0.5, 1, 2, 3, 4, 5, 6, 7, 8, 9, 10, 12, 16, 20, 25, and 30 mM Cd^{2+} at 278 K. The d3'-EBS1*·IBS1* sample contained 0.59 mM RNA (*I* = 110 mM (KCl), 10 µM EDTA, pH = 6.71). In this experiments 1D [^{1}H]-NMR with the same Cd^{2+} concentration steps like in d3'-EBS1* at 278 K were acquired. The chemical shift maps of the imino protons shown in Figure 99A and B were obtained by subtracting the chemical shift of a certain proton at 0 mM Cd^{2+} from the value at 2 mM Cd^{2+}. All spectra were acquired at 700 MHz proton frequency.

4.5.4 $[Co(NH_3)_6]^{3+}$ titrations of d3'-EBS1* and d3'-EBS1*·IBS1*

$[Co(NH_3)_6]^{3+}$ was titrated to 0.5 mM d3'-EBS1* (*I* = 10 mM (KCl), 10 µM EDTA, pH = 6.52 in 90% H_2O/10% D_2O) in steps of 0, 0.5, 1, 1.5, 2, and 2.5 mM. At each titration step 64 scans of a 1D [^{1}H]-NMR experiment with spin echo water suppression were recorded. All experiments were acquired at 278 K and 700 MHz. The chemical shift changes were evaluated by subtracting the chemical shift at 0 mM $[Co(NH_3)_6]^{3+}$ from the one at 2 mM $[Co(NH_3)_6]^{3+}$ for each imino proton. At 2.5 mM $[Co(NH_3)_6]^{3+}$ a 2D [^{1}H,^{1}H]-NOESY with watergate H_2O suppression was recorded with 64 scans and 256 experiments to observe NOE crosspeaks between the ammine protons of $[Co(NH_3)_6]^{3+}$ and the imino protons of d3'-EBS1*.

For the titration of 0.54 mM d3'-EBS1*·IBS1* (*I* = 110 mM (KCl), 10 µM EDTA, pH = 6.61 in 90% H_2O/10% D_2O) 1D [^{1}H]-NMR experiment with spin echo water suppression were acquired at titration points of 0, 0.5, 1, 1.5, and 2 mM $[Co(NH_3)_6]^{3+}$. The resonance line at 2 mM $[Co(NH_3)_6]^{3+}$ were already broadened, thus no titration step with 2.5 mM $[Co(NH_3)_6]^{3+}$ was performed. At 1.5 and 2 mM $[Co(NH_3)_6]^{3+}$ 2D [^{1}H,^{1}H]-NOESY experiments with watergate H_2O suppression were recorded with 140 scans and 320 experiments to observe NOE crosspeaks between the ammine protons of $[Co(NH_3)_6]^{3+}$ and the imino of d3'-EBS1*·IBS1*. Acquisition of the spectra was performed at 278 K and in addition for 2 mM $[Co(NH_3)_6]^{3+}$ a second 2D [^{1}H,^{1}H]-NOESY spectrum at 283 K was acquired. The

chemical shift changes were evaluated by subtracting the chemical shift at 0 mM $[Co(NH_3)_6]^{3+}$ from the one at 2 mM $[Co(NH_3)_6]^{3+}$ for each imino proton.

4.6 Stability constant calculations

4.6.1 Calculation of stability constants log K_A of Mg^{2+} binding to d3'-EBS1*

The concentration of d3'-EBS1* in the Mg^{2+} titration experiments was 0.5 mM. Mg^{2+} binding to d3'-EBS1* was monitored by observing the changes in chemical shifts of the non-exchangeable protons in 2D [^{1}H,^{1}H]-NOESY experiments acquired in the presence of 0, 0.5, 1, 1.5, 2, 2.5, 3, 4, 5, 6, 6.5, and 7 mM $MgCl_2$ (100% D_2O, I = 10 mM (KCl), 10 µM EDTA, pD = 6.96). The chemical shifts of the aromatic as well as sugar (H1') protons were plotted against the Mg^{2+} concentration and fitted to a single binding isotherm using a Levenberg-Marquardt nonlinear least-square regression.[34,85] From these fits, first estimates for millimolar affinity constants $K_{A,est}$ values were calculated by using the total amount of Mg^{2+} present in solution. The quality of the single plots was checked carefully and subsequently by including the line broadening data four individual binding sites were defined. In a second step, for each individual binding site an average log $K_{A,av}$ was calculated.

The averaged log $K_{A,av1}$ values of the first estimates were used to calculate the amount of Mg^{2+} bound to each binding site and thus to determine the actual free Mg^{2+} concentration as previously described.[351]

For each internal binding site "*i*" in d3'-EBS1* the equilibrium

$$RNA_i + Mg^{2+} \rightleftharpoons RNA_i \bullet Mg^{2+}$$

and the definition of its affinity constant

$$K_{A_i} = \frac{\left[RNA_i \bullet Mg^{2+}\right]}{\left[Mg^{2+}\right]_i \left[RNA_i\right]} \qquad \text{equation 21}$$

holds together with

$$\left[Mg^{2+}\right]_{tot} = \left[RNA_i \bullet Mg^{2+}\right]_i + \left[Mg^{2+}\right]_{tot-i} \text{ and} \qquad \text{equation 22}$$

$$\left[RNA_i\right]_{tot} = \left[RNA_i \bullet Mg^{2+}\right]_i + \left[RNA\right]_{tot-i} \qquad \text{equation 23}$$

$[Mg^{2+}]_{tot}$ and $[RNA]_{tot}$ correspond to the total concentration of Mg^{2+} or RNA of each individual binding site, respectively, $[RNA{\cdot}Mg^{2+}]_i$ to the concentration of the bound species, and $[Mg^{2+}]_{tot-i}$ and $[RNA]_{tot-i}$ to the concentration of the free species present in solution. The change in chemical shift in such a 1:1 binding equilibrium can be described by

$$\Delta\delta_{obs}=\Delta\delta_{RNA_i}+\left(\Delta\delta_{RNA\bullet Mg}-\Delta\delta_{RNA}\right)\frac{\left[Mg^{2+}\right]_{tot}+\left[RNA_i\right]_{tot}+\frac{1}{K_{Ai}}-\sqrt{\left(\left[Mg^{2+}\right]_{tot}+\left[RNA_i\right]_{tot}+\frac{1}{K_{Ai}}\right)^2-4\left[Mg^{2+}\right]_{tot}\left[RNA_i\right]_{tot}}}{2\left[RNA_i\right]_{tot}} \quad \text{equation 24}$$

where $\Delta\delta_{obs}$ is the observed chemical shift, $\Delta\delta_{RNA}$ the one of the unbound (free), and $\Delta\delta_{RNAi\cdot Mg}$ of the fully bound species.

From equations 21, 22, 23 and 24 follows:

$$K_{A_i}=\frac{\left[RNA_i\bullet Mg^{2+}\right]}{\left(\left[Mg^{2+}\right]_{tot}-\left[RNA_i\bullet Mg^{2+}\right]\right)\left(\left[RNA_i\right]_{tot}-\left[RNA_i\bullet Mg^{2+}\right]\right)} \quad \text{equation 25}$$

and

$$K_{A_i}\left(\left[Mg^{2+}\right]_{tot}\left[RNA_i\right]_{tot}-\left[Mg^{2+}\right]_{tot}\left[RNA_i\bullet Mg^{2+}\right]-\left[RNA_i\right]_{tot}\left[RNA_i\bullet Mg^{2+}\right]+\left[RNA_i\bullet Mg^{2+}\right]^2\right)=\left[RNA_i\bullet Mg^{2+}\right] \quad \text{equation 26}$$

This equation is of second order for $[RNA\bullet Mg^{2+}]_i$ and can be rewritten as

$$K_{A_i}\left[RNA\bullet Mg^{2+}\right]_i^2-\left[RNA_i\bullet Mg^{2+}\right]\left(K_{A_i}\left[Mg^{2+}\right]_{tot}+K_{A_i}\left[RNA_i\right]_{tot}+1\right)+K_{A_i}\left[Mg^{2+}\right]_{tot}\left[RNA_i\right]_{tot}=0 \quad \text{equation 27}$$

Thus, two solutions are possible for this equation, of which only one value is physically meaningful, i.e. a positive concentration for $[RNA_i\bullet Mg^{2+}]$, which corresponds to the amount of Mg^{2+} bound at each site "*i*" $\left[Mg^{2+}\right]_{bound,i}$:

$[RNA\cdot Mg^{2+}] =$

$$\left[Mg^{2+}\right]_{bound,i}=\frac{\left(K_{A_i}\left[Mg^{2+}\right]_{tot}+K_{A_i}\left[RNA_i\right]_{tot}+1\right)-\sqrt{\left(-\left(K_{A_i}\left[Mg^{2+}\right]_{tot}+K_{A_i}\left[RNA_i\right]_{tot}+1\right)\right)^2-4K_{A_i}{}^2\left[Mg^{2+}\right]_{tot}\left[RNA_i\right]_{tot}}}{2K_{A_i}} \quad \text{equation 28}$$

The actual Mg^{2+} concentration available for each of the four binding sites "*i*" $[Mg^{2+}]_{avail,i}$ is thus given by

$$\left[Mg^{2+}\right]_{avail,i}=\left[Mg^{2+}\right]_{tot}-\sum\left[Mg^{2+}\right]_{bound,tot}+\left[Mg^{2+}\right]_{bound,i} \quad \text{equation 29}$$

$\left[Mg^{2+}\right]_{avail.i}$ was then plotted *versus* the chemical shift values of the protons present at or close to this particular binding site, to yield a second set of log $K_{A,est2}$ values for each evaluated proton. Again, these second log $K_{A,est2}$ estimates were averaged for each of the four individual binding sites to give a higher and more accurate log $K_{A,av2}$ for each site. Based on these new log $K_{A,av2}$ values, again the amount of bound Mg^{2+} ions to each binding site was calculated, and the described procedure repeated. After five rounds of this iterative approximation procedure, the log $K_{A,av}$ values for each binding site did not change anymore within their error limits. At this point, the log $K_{A,av}$ values of each site were plotted *versus* the corresponding

iteration round and fit to an asymptotic curve fit according to $y=a-bc^x$ in Origin 7.0, where parameter *a* is the final affinity constant log $K_{A,fin}$ for each binding site.

All individual steps are fully automized in ISTAR using the Matlab toolbox (Matlab 2006a, The MathWorks Inc.).

To take the equilibrium concentrations of free and bound metal ions into account, the script "istar_run_sites.m" includes additionally the following lines:

```
bound = [];
for k = 1 : length(istar_cmetal_ion_initial)

   % Build a list of the weighted mean Ka averages after the i-th
   % iteration for all sites with a given metal ion concentration.
   avgs = [];
   for j = 1:nSites
      avgs = cat(2, avgs, Ka_avgs{i,j}.wm);
   end

   % Estimate the amount of metal bounds to each site for
   % a given concentration of metal ion.
   b = istar_estimate_bounds(avgs, site_cRNA, istar_cmetal_ion_initial(k));

   % concatenate the results onto the 'bound' matrix. Each row is
   % a different site, and each column is a different metal ion
   % concentration.
   bound = cat(1, bound, b);
end

bound
```

With this addition the script "istar_estimate_bounds.m" is called and $[M^{2+}]_{bound} = [M^{2+}{\cdot}xRNA]$ is calculated by using equation 14. The script includes the following lines:

```
function b = istar_estimate_bounds(Ka, site_cRNA, target)
   % Estimate the bound metal ion concentration for each site using the
```

```
    % average Ka for each site and the concentration of RNA at a site. The
    % assumed total metal ion concentration is in target.
    %
    % The estimates are found using the fsolve minimization function.


function f = bound(x)
    f = (Ka .* x .* site_cRNA) ./ ((Ka .* x) + 1);
end

function v = F(x)
    v = sum(bound(x)) + x - target;
end

options = optimset('TolFun',1e-13, 'Display', 'off');
[x,fval,exitflag,output] = fsolve(@F, 0, options);
if (exitflag ~= 1) disp(output); end
b = bound(x);

end
```

To check the definition of the binding sites in the loop region, the protons included in the loop were rearranged to define other binding sites. The 5'-end with G1H8, and the helix 1 comprising A3H1,G4H1, G4H8, U5H6, A25H8, C26H1, C26H6, U27H6 were left unaltered. The new defined binding site L1 in the loop contains A10H1, A10H2, A10H8, U11H1, U11H5, U11H6, U12H6, whereas the binding site L2 consists of A16H1, A16H8, U18H1, U18H6, G19H1, G19H8, A20H1, A20H2, A20H8, G21H1. The calculation was then performed as described above with ISTARv2.2 and ISTARv2.3.

4.6.2 Calculation of stability constants log K_A of Mg^{2+} binding to d3'-EBS1*·IBS1*

The concentration of d3'-EBS1*·IBS1* in the Mg^{2+} titration experiments was 0.9 mM. Mg^{2+} binding to d3'-EBS1*·IBS1* was monitored by observing the changes in chemical shifts

of the non-exchangeable protons in 2D [^{1}H,^{1}H]-NOESY experiments acquired in the presence of 0, 0.5, 1, 2 3, 4, 5, 6, 7, 8, and 10 mM $MgCl_2$ (100% D_2O, I = 110 mM (KCl), 10 µM EDTA, pD = 6.83). The chemical shifts of the aromatic as well as sugar (H1') protons were plotted against the Mg^{2+} concentration and fitted to a single binding isotherm using a Levenberg-Marquardt nonlinear least-square regression.[34,85] From these fits, first estimates for millimolar affinity constants log $K_{A,est}$ values were calculated by using the total amount of Mg^{2+} present in solution. The quality of the single plots was checked carefully and subsequently by including the line broadening data four individual binding sites were defined (Appendix 21).

As discussed in Section 2.5.5.6 a starting value for the 5'-end of d3'-EBS1*·IBS1* had to be defined because severe line broadening led to disappearance of the 5'-end NOEs upon Mg^{2+} addition in the 2D [^{1}H,^{1}H]-NOESY spectra. To allow a fixed value for log K_A as input, the script "istar_run_sites" of the program ISTAR has to include the following lines:

```
if (~exist('ensemble'))
   if (isfield(site, 'avgs'))
      ensemble = [];
   else
```

and the script "istar_calc":

```
if (isfield(site, 'avgs'))
   avgs = site.avgs;
   fits = {};
```

When these lines are included, it is possible to include the input file with the fixed value (here: 3.03 ± 0.05):

```
%%%%%%%%%%%%%%%%%%%%%%%%%%%%%%%%
site.name      = 'GTP';
site.cRNA      = 0.9;
site.initials  = [6 6 0.1];
site.initialsl = [4 4 0.01];
site.initialsh = [9 9 100];

site.avgs.am = 0;
site.avgs.erramabs = 0;
```

```
site.avgs.lam = 0;
site.avgs.lamabs = 0;
site.avgs.lwm = 0;
site.avgs.lerrwmabs = 0;
site.avgs.lwmrel = 0;
site.avgs.lwm = 3.03;
site.avgs.lerrwmabs = 0.05;
site.avgs.wm = (10 ^ site.avgs.lwm) / 1000;
site.avgs.errwmab = ((((10^site.avgs.lwm)*2.3026)^2*site.avgs.lerrwmabs^2)^0.5)/1000;
site.avgs.errwmrel = 0;
```

If one or more sites have a higher affinity towards M^{2+} than the other binding sites, the equilibrium concentrations of free and bound metal ions have to be considered. The averaged affinity constants were calculated by a modified ISTAR version, namely ISTARv2.3, as already described in section 4.6.1.

To check the definition of the binding sites in the loop region, the protons included in the loop and the EBS1*·IBS1* were rearranged to define five binding sites. The 5'-end with the fixed value, and the helix 1 comprising A3H1, G4H1, G4H8, U5H6, A25H2, C26H1, C26H6, U27H6 were left unaltered, as well as the first binding site in the loop L1 with G13H1, G13H8, G14H1, G14H8. The other two binding sites in the loop contain: C15H1, C15H6, A16H2, A16H8, U18H6, G61H1, G61H8, U62H6, G63H1, G63H8, U64H1 for L2 and U11H5, U11H6, U12H1, U12H6, G19H1, A20H1, A20H8, G21H1, C59H1, C59H5, C59H6, A60H2, A60H8 for L3. After rearranging the binding sites, the calculation was performed as described above with ISTARv2.3 including the equilibrium concentrations of bound and free M^{2+}.

4.6.3 Calculation of stability constants log K_A of Cd^{2+} binding to d3'-EBS1*

The concentration of d3'-EBS1* in the Cd^{2+} titration experiments was 0.6 mM. Cd^{2+} binding to d3'-EBS1* was monitored by observing the changes in chemical shifts of the non-exchangeable protons in 2D [^{1}H,^{1}H]-NOESY experiments acquired in the presence of 0, 0.5, 1, 1.5, 2, 2.5, 3, 4, 5, 6, 7, and 8 mM $CdCl_2$ (100% D_2O, I = 10 mM (KCl), 10 µM EDTA, pD = 6.66). The chemical shifts of the aromatic as well as sugar (H1') protons were plotted

against the Cd^{2+} concentration and fitted to a single binding isotherm using a Levenberg-Marquardt nonlinear least-square regression.[34,85] From these fits, first estimates for millimolar affinity constants log $K_{A,est}$ values were calculated by using the total amount of Cd^{2+} present in solution. The quality of the single plots was checked carefully. On the basis of the first estimates log $K_{A,est}$ together with the chemical shift change pattern, four metal ion binding sites were determined for Cd^{2+}. Considering the similar values of the first estimation G13 and G14 were included in the binding site L1 (Appendix 12). The modified ISTARv2.3 was used, which takes the equilibrium concentration of bound and unbound metal ions into account (see Section 4.6.1).

The 5'-end reflects a special case: upon addition of only 0.5 mM Cd^{2+} a second starting point appears, which was assigned to a diphosphate moiety. It is assumed that two Cd^{2+} bind to the triphospate at the 5'-end and one to the diphospahte. Since it was not possible to fit the data for G1 to a 1:1 binding isotherm, literature values were used in the calculation.[355,382] Through peak integration in Sparky a triphosphate:diphosphate ratio of 70:30 was found, which was taken into consideration in the calculation. The following scripts with fixed affinity constants for TP1 (5.82 ± 0.05), TP2 (2.52 ± 0.15) and DP (4.86 ± 0.03) were used:

```
%%%%%%%%%%%%%%%%%%%%%%%%%%%%%%%%
site.name              = 'TP1';
site.cRNA              = 0.42;
site.initials          = [6 6 0.1];
site.initialsl         = [4 4 0.01];
site.initialsh         = [9 9 100];

site.avgs.am       = 0;
site.avgs.erramabs  = 0;
site.avgs.lam      = 0;
site.avgs.lamabs    = 0;
site.avgs.lwm      = 0;
site.avgs.lerrwmabs = 0;
site.avgs.lwmrel    = 0;
site.avgs.lwm      = 5.82;
site.avgs.lerrwmabs = 0.05;
site.avgs.wm       = (10 ^ site.avgs.lwm) / 1000;
```

```
site.avgs.errwmab    =
((((10^site.avgs.lwm)*2.3026)^2*site.avgs.lerrwmabs^2)^0.5)/1000;
site.avgs.errwmrel   = 0;

%%%%%%%%%%%%%%%%%%%%%%%%%%%%%
site.name              = 'TP2';
site.cRNA               = 0.42;
site.initials          = [6 6 0.1];
site.initialsl         = [4 4 0.01];
site.initialsh         = [9 9 100];

site.avgs.am        = 0;
site.avgs.erramabs   = 0;
site.avgs.lam       = 0;
site.avgs.lamabs     = 0;
site.avgs.lwm       = 0;
site.avgs.lerrwmabs  = 0;
site.avgs.lwmrel     = 0;
site.avgs.lwm       = 2.52;
site.avgs.lerrwmabs  = 0.15;
site.avgs.wm        = (10 ^ site.avgs.lwm) / 1000;
site.avgs.errwmab    =
((((10^site.avgs.lwm)*2.3026)^2*site.avgs.lerrwmabs^2)^0.5)/1000;
site.avgs.errwmrel   = 0;

%%%%%%%%%%%%%%%%%%%%%%%%%%%%%
site.name              = 'DP';
site.cRNA               = 0.18;
site.initials          = [6 6 0.1];
site.initialsl         = [4 4 0.01];
site.initialsh         = [9 9 100];

site.avgs.am        = 0;
site.avgs.erramabs   = 0;
```

```
site.avgs.lam       = 0;
site.avgs.lamabs    = 0;
site.avgs.lwm       = 0;
site.avgs.lerrwmabs = 0;
site.avgs.lwmrel    = 0;
site.avgs.lwm       = 4.86;
site.avgs.lerrwmabs = 0.03;
site.avgs.wm        = (10 ^ site.avgs.lwm) / 1000;
site.avgs.errwmab   =
((((10^site.avgs.lwm)*2.3026)^2*site.avgs.lerrwmabs^2)^0.5)/1000;
site.avgs.errwmrel  = 0;
```

The weighted mean $K_{A,av}$ values of 7 iteration rounds were plotted *versus* the corresponding iteration number and fitted to an asymptotic function in Origin 7.0 to obtain a final log $K_{A,fin}$ value for each binding site as described in section 4.6.1.

4.6.4 Calculation of stability constants log K_A of Cd^{2+} binding to d3'-EBS1*·IBS1*

The concentration of d3'-EBS1*·IBS1* in the Cd^{2+} titration experiments was 0.61 mM. Cd^{2+} binding to d3'-EBS1*·IBS1* was monitored by observing the changes in chemical shifts of the non-exchangeable protons in 2D [^{1}H,^{1}H]-NOESY experiments acquired in the presence of 0, 0.5, 1, 1.5, 2, 2.5, 3, 3.5, 4, 5, 6, and 8 mM $CdCl_2$ (100% D_2O, I = 110 mM (KCl), 10 µM EDTA, pD = 6.89). From the first estimates log $K_{A,est}$ and the chemical shift change pattern four metal ion binding sites were determined (Appendix 23). The calculation of the affinity constants was performed analogous to the one for Cd^{2+} binding to d3'-EBS1* (see section 4.6.3). Like in the case of d3'-EBS1* a triphosphate:diphosphate ratio of 70:30 was found for d3'-EBS1*·IBS1*, thus the concentration for TP was 0.427 mM and for DP 0.183 mM. These values were inserted into the scripts for the fixed affinity constants for TP1, TP2 and DP (see Section 4.6.3).

4.7 Biochemical assays

4.7.1 RNA preparation for the activity assays

The D135 RNA construct is a reduced form of the mitochondrial intron ai5γ from *S. cerevisiae*. It contains elements spanning Domain 1 – 5 beginning at the first nucleotide of the intron and terminates with a 36-nucleotide 3'-tail that lies immediately downstream of D5. Domains 2 and 4 were shortened into hairpins that are capped by UUCG loops. Both constructs, the wtD135 and the mutated D135GC (mutations A331C and A333C) were transcribed by T7 RNA polymerase using *Hind*III-linearized plasmids (pT7D135[286] and pT7D135GC) as templates, yielding 618-nucleotide RNA transcripts. pT7D135GC was obtained by cloning the D135GC construct, including a T7 promotor at the 5'-end, by assembly-PCR (see Appendix 43) and subsequent cloned back into the pB5$^-$ vector at the *Eco*RI and *Hind*III restriction sites. pT7D135GC was sequenced by Microsynth (Balgach, Switzerland). The transcription was performed in 5 x 1 ml reaction volume containing a total amount of 6.75 µg predigested plasmid, 1000 µl 5x transcription buffer (200 mM Tris-HCl (pH 7.5), 200 mM DTT and 10 mM spermidine), 5 mM of each NTP, 0.1% Triton X-100, 20 mM $MgCl_2$ and an appropriate amount of homemade T7 RNA polymerase, which was tested before in transcription trials. The reaction mixture was incubated for 6 hours at 37 °C and 300 rpm. The reaction was stopped by ethanol precipitation with 3 volumes of 100% EtOH (abs.) and addition of 250 mM NaCl at –20 °C over night. The RNA was purified by denaturing 5% PAGE, UV-shadowed, excised from the gel and eluted by shaking the crushed gel pieces in 4 volumes of 10 mM MOPS, 1 mM EDTA, 250 mM NaCl, pH 6.0 for 2 hours at 4 °C. After crushing and soaking the RNA was recovered by EtOH precipitation at –20 °C over night. The precipitated pellet was spinned down at 4 °C, 13'000 g for 30 minutes, dried in a Concentrator 5301 from Eppendorf and resuspended in 100 µl of 10 mM MOPS, 10 µM EDTA, pH 6.0. The concentration of the RNA was determined by UV spectrophometry using an extinction coefficient $\varepsilon = 618\ mM^{-1}cm^{-1}$.

Substrate oligonucleotides 17/7, 17/7* and 17/7-GC were labeled with [γ-^{32}P]ATP at the 5'-end with polynucleotide kinase (PNK, 10 U/µl). To 50 µM of each substrate 2 µl of [γ-^{32}P]ATP (150 mCi/ml) and 1 µl of PNK (10 U/µl) was added and incubated for 30 minutes at 37 °C. The excessive [γ-^{32}P]ATP was removed by applying the labeled RNA onto a MicroSpin G-25 size exclusion column. The RNA was purified by denaturing 18% PAGE and visualized by autoradiography.[221] The labeled RNA was eluted by shaking the crushed gel

pieces in two volumes of 10 mM MOPS, 1 mM EDTA, 250 mM NaCl, pH 6.0 for 3 hours at 4 °C. The concentration was calculated via the specific activities from the scintillation counts.

4.7.2 Single turnover kinetics

Cleavage reactions were carried out in a reaction volume of 20 µl at 42 °C in 80 mM MOPS (pH 7.5), 100 mM $MgCl_2$, and 500 mM KCl. Ribozyme (100 nM final) and substrate oligonucleotides (1 nM final) were incubated separately at 95 °C for 1 minute in 80 mM MOPS (pH 7.5), and 500 mM KCl. Samples were cooled to 42 °C, $MgCl_2$ was added to a final concentration of 100 mM and the RNA was allowed to fold for 15 minutes. Cleavage reactions were initiated by adding the labeled substrate to the ribozyme. Aliquots (1 µl) were removed from the reaction volume at 0, 1, 2, 3, 4, 6, 8, 10, and 12 minutes, mixed with 3 µl of quenching buffer (formamide loading buffer: 82% formamide, 0.01 M EDTA, 0.01% bromphenole blue, 0.01% xyanole cyanide), and subjected to 18% polyacrylamide gels. Gels were analyzed and products were quantified using a Molecular Dynamics Storm 860 Phosphorimager. Quantification was performed using the software ImageQuant (Amersham Biosciences). The reaction rate constants were calculated based on a single exponential expression:

$$frac[precursor] = A_1 - A_2 e^{-kx} \qquad \text{equation 30}$$

where A_1 is the fraction of the unreacted precursor, A_2 the fraction of reacted substrate and k is the first-order rate constant in min^{-1}.[286]

5 Summary

Before carrying out their assigned function, most RNAs have to undergo several steps of post-transcriptional alteration. One of the most important of these processing steps is splicing, in which the non-coding introns are removed from the coding sequence of the mRNA and the remaining exons are joined. This can be performed either by the spliceosome, which consists of numerous small nuclear RNAs and proteins, or by group II introns, which are ribozymes, i.e. "enzymes" consisting exclusively of RNA. Group II introns are present in the genes of plants, fungi, yeast and many bacteria. They have the ability to undergo self-splicing and do not require proteins for successful splicing, since all the catalytic components required for splicing are located within the intron.[203,261,262,292] Nevertheless, their splicing very much resembles the spliceosomal pathway.[261,262] Results on structure and metal ion binding in the catalytic core of group II introns can therefore be directly transferred to the spliceosomal system.

Group II introns are large molecular machines consisting of a conserved set of six domains (D1 – D6) that are defined by characteristic secondary structure elements (Figure S1). D1, the largest of the six domains, is an independent folding unit that serves as the molecular scaffold for the docking of the other domains. The correct recognition of the splice site is ensured by base-pairing of two regions in D1, exon-binding site 1 and 2 (EBS1 and EBS2), with the two intron-binding sites (IBS1 and IBS2) located at the end of the adjoining 5'-exon.[203,292] EBS1 is located within the loop of a hairpin structure in domain 1 (Figure S1). Together with IBS1, it forms the 5'-splice-site recognition complex. D1 and D5 are together with the linker region the only intronic components essential for catalysis. In addition, metal ions are crucial for folding and are involved in catalysis.[69,292]

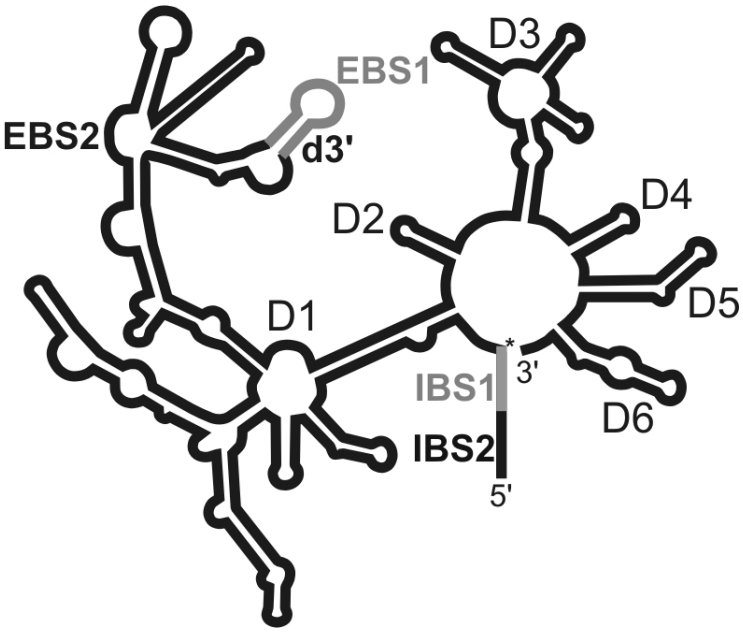

Figure S1 Schematic representation of a group II intron with its six domains arranged around a central wheel together with exonic IBS1 and IBS2.

The goal of this study was to solve the solution structure of a 5'-splice-site recognition complex in

the absence (d3'-EBS1*) and presence of the substrate (d3'-EBS1*·IBS1*) by nuclear magnetic resonance (NMR) spectroscopy and to investigate the effect of metal ions on these structures.

In the NMR studies, a RNA construct consisting of the d3'-stem loop closed by a 11-nucleotide loop that includes EBS1 of the group II intron ai5γ located in the *cox1* gene of *Saccharomyces cerevisiae* was used. A GGAG sequence was added to the 5'-end to stabilize the helical region and to improve the efficiency of the *in vitro* transcription (Figure S2).[(292)] The 7-nt IBS1 was obtained commercially since it is too short for successful *in vitro* transcription.

2D [^{1}H,^{1}H]-NOESY spectra of the wildtype d3'-EBS1·IBS1 show severe peak overlap in the region of the sequential walk indicating that no stable structure is formed. Along the same line, UV melting studies of the wildtype EBS1·IBS1 interaction reveal a very low melting temperature (T_m = 15.5 °C at 100 mM KCl). Higher concentrations of KCl do not lead to a considerable increase of T_m, thus indicating a poor stability of the EBS1·IBS1 complex in the absence of the covalent exon-intron linkage and/or EBS2·IBS2. Therefore, the EBS1–IBS1 interaction was modified by replacing two AU by GC base pairs (EBS1*·IBS1*) to stabilize the interaction. The modified construct does not alter the efficiency of the splicing activity as

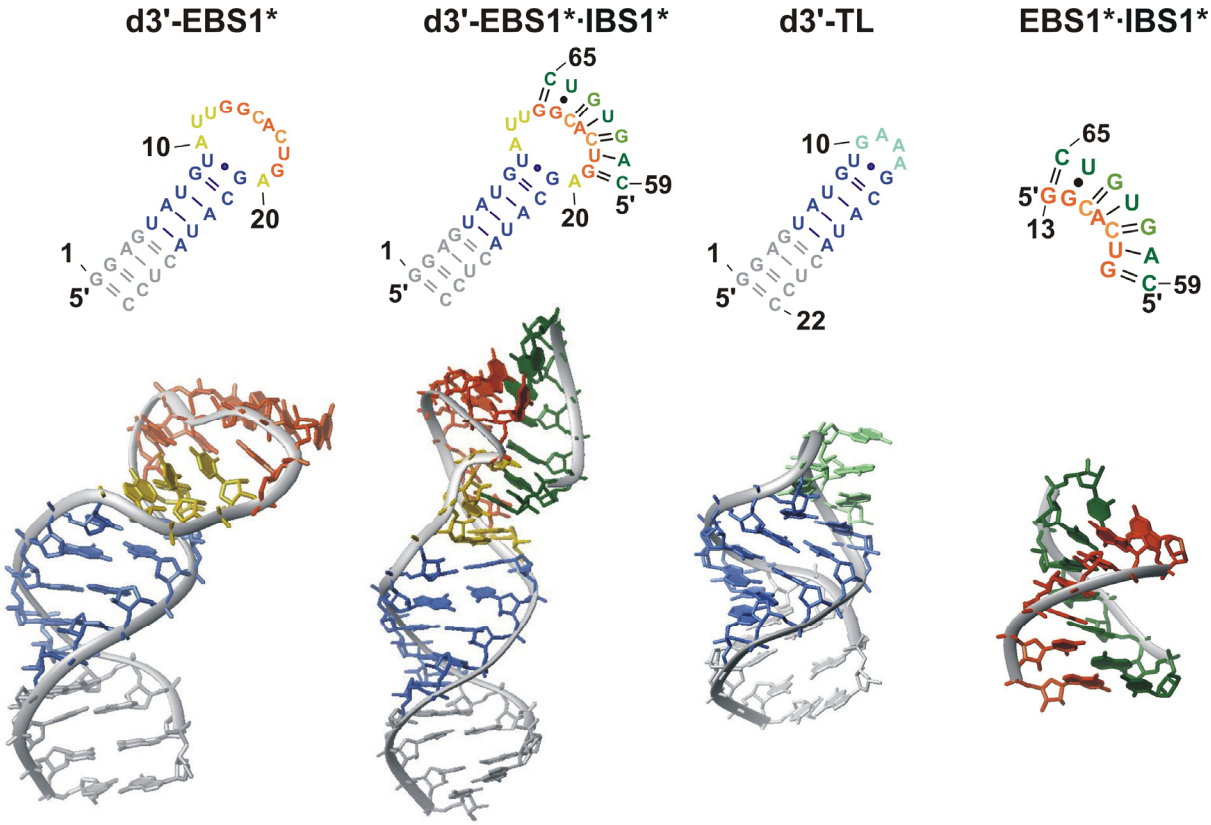

Figure S2 Secondary structures together with the lowest energy structures of d3'-EBS1*, d3'-EBS1*·IBS1*, d3'-TL and EBS1*·IBS1* (from left to right).

shown by single turnover cleavage assays.[289] In addition, the obtained results suggest that the G-U wobble pair in the EBS1-IBS1 interaction is crucial for successful splicing.

Concentration dependent UV melting studies, X-filter-NOESY-HSQC experiments, diffusion ordered spectroscopy (DOSY) as well as dynamic light scattering (DLS) studies have shown that d3'-EBS1* indeed forms a hairpin in solution. This verification is important for NMR measurements because the symmetry of a duplex leads to a spectrum, which can be similar to the one of a hairpin.

NMR spectra of d3'-EBS1* acquired in H_2O show eight Watson-Crick base pairs and only one strong cross-peak originating from a G–U wobble pair. This implies that the loop region does not form any further base pairs, but instead forms a 11-nt unpaired loop prior to IBS1* binding. Upon addition of IBS1*, six additional Watson-Crick base pairs and one additional G–U wobble pair are formed, showing that IBS1* is completely bound to EBS1*. The data are in agreement with the secondary structure of the d3'-EBS1* construct in the absence and presence of IBS1* as proposed by theoretical folding, which was performed with the mfold server.[26]

The comparatively low number of Nuclear Overhauser Effects (NOEs) per nucleotide (17.72) for d3'-EBS1* derives from the unstructured loop region, for which only 13.72 NOEs per residue were observed in comparison to the helix with its 20.16 NOEs per residue. As already shown by the base-pairing situation, the loop does not adopt a rigid structure, but is rather flexible and free to bind IBS1*. Upon addition of IBS1*, the loop is stabilized due to the formation of a second helix.

The solution structures in the absence and presence of IBS1* were solved to a final r.m.s.d. of 2.06 ± 0.86 Å for d3'-EBS1* and 0.69 ± 0.17 Å for d3'-EBS1*·IBS1* for all heavy atoms of the 20 lowest-energy structures (Figure S2). However, independent superposition of the helical region and of the loop in d3'-EBS1* results in much lower r.m.s. deviations of only 0.41 ± 0.10 Å for the helix, but in higher r.m.s. deviations of 2.59 ± 1.23 Å for the loop, thus further supporting the flexibility of the loop.

The full construct d3'-EBS1*·IBS1* shows an unusual kink between nucleotide U12 and G13 directly 5' of EBS1*. To determine whether such a motif is already known, a detailed wormsearch[16] of the protein data bank (RCSB PDB) was performed. This search revealed several structures with a similar motif. The found motif in the crystal structure of the 50S ribosomal subunit with release factor RF1, tRNAs and mRNA bound to the ribosome[346] shows the best fit. This structure shares with d3'-EBS1*·IBS1* an unpaired nucleotide in the

motif. This indicates that unpaired nucleotides are required to overcome sterical hindrances in order to form such motifs.

In addition, two individual parts of the splice site recognition complex have been solved, i.e. the d3'-stem, which is closed by a GAAA tetraloop (d3'-TL) and the EBS1*·IBS1* interaction alone (Figure S2).[289] The latter complex reveals no structural differences from the corresponding interaction in d3'-EBS1*·IBS1*.

Many tertiary structure elements are stabilized by interactions with divalent metal ions, e.g. Mg^{2+}.[64,69] In addition, monovalent ions appear to play a special role in binding to high-affinity sites.[66] One metal ion binding site is located at the 5'-splice-site recognition complex.[97,292] To study the effect of Mg^{2+} binding to the recognition site in the absence and presence of IBS1* at the atomic level, the chemical shift changes of non-exchangeable

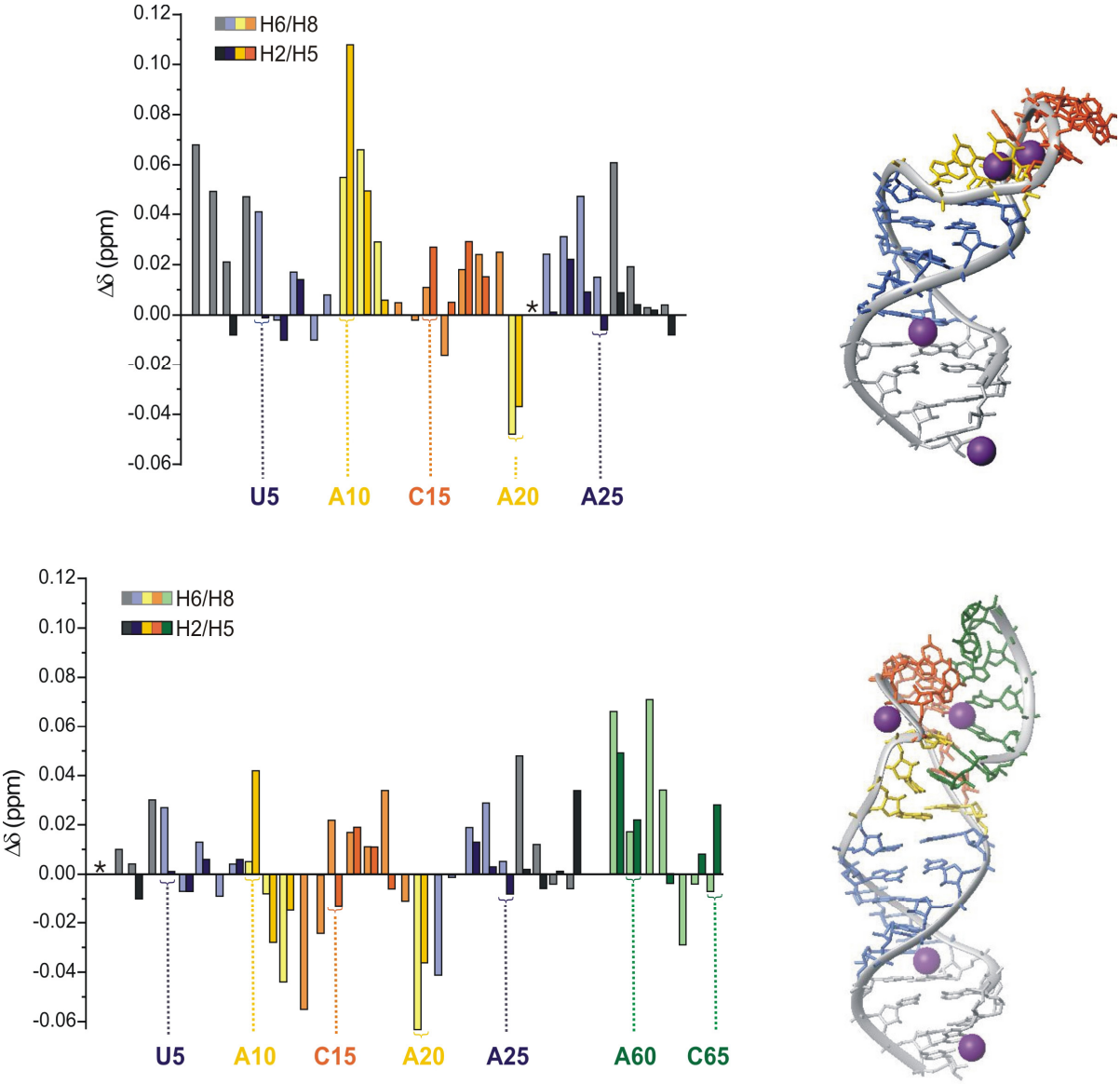

Figure S3 Changes in chemical shift upon Mg^{2+} binding to d3'-EBS1* (upper panel) and d3'-EBS1*·IBS1* (lower panel).

protons as a function of Mg^{2+} concentration were monitored by recording 2D [^{1}H,^{1}H]-NOESY spectra in D_2O of d3'-EBS1* and d3'-EBS1*·IBS1*. The effect of Mg^{2+} (as well as Cd^{2+}) binding to the RNA was monitored by changes in the chemical shift of the non-exchangeable sugar and nucleobase protons (Figure S3). The observed H8, H2, H6, H5 protons of the nucleobases and the H1' proton of the sugar moieties are positioned close to potential metal ion co-ordination sites, such as N7 of purines, the phosphate oxygens, or the 2'-OH at the sugars.

Analysis of chemical shift changes of the non-exchangeable protons indicates that, in both constructs, A10, U11 and A20 are more strongly affected by Mg^{2+} than other regions. Furthermore, in d3'-EBS1*·IBS1*, U12, G13 and G14 show a very strong chemical shift change and also IBS1* (C59 to C65) is strongly influenced. These findings are in agreement with Tb^{3+} cleavage experiments, which showed a high-affinity site for metal ion binding directly 5' of EBS1.[97] Due to the binding of IBS1* resulting in the formation of d3'-EBS1*·IBS1* containing a second helix, the phosphate oxygens of G13 and G14 protrude to the outside and are therefore preferred for binding to Mg^{2+} than in d3'-EBS1*, where G13 and G14 are involved in the flexibility of the loop. However, chemical shift changes can be induced by direct metal ion binding or by structural changes, i.e. reduced or increased stacking interactions, induced by metal ion binding.

Substantial line broadening of some peaks in these Mg^{2+} titration experiments was also observed. This effect is well known and can be traced back to binding kinetics of the metal ion at its binding site being in the intermediate exchange regime on the NMR timescale.[42,350] Line broadening experiments can therefore be used to detect specific Mg^{2+}-binding sites, since their effect should be visible only on protons in close proximity to the bound Mg^{2+}.[351] Line broadening experiments can also be performed with the paramagnetic Mn^{2+} ion. Line broadening upon addition of a paramagnetic ion is more straight forward to interpret than changes observed during titration with Mg^{2+} ions. The unpaired electron spin of the paramagnetic ion strongly interacts with the nearby nuclear spin in a distance-dependent manner.[81] Thorough evaluation of all these experiments led to the identification of numerous specific metal ion binding sites in both constructs. The 5'-splice site is thereby of particular interest. In the absence of IBS1*, a metal ion binding site is located at the 5'-end of the loop including A10, U11 and U12. Upon addition of IBS1*, this metal ion binding site is shifted downstream to G13 and G14 due to structural changes induced by the formation of the second helix. Together with the detailed view of the solution structures of d3'-EBS1* and d3'-EBS1*·IBS1*, the localization of the metal ion binding site just 5' of the splice site suggests

that this binding site plays a crucial role in the catalytic process. Divalent metal ions at this site help to stabilize the unusual conformation at U12 and G13, which is induced upon IBS1* binding, and to compensate the negative charge of the backbone at this site.

To assess the metal ion binding properties of divalent metal ions not only qualitatively, but also in a quantitative way, the intrinsic affinity constants of Mg^{2+} to d3'-EBS1* and d3'-EBS1*·IBS1* were determined. Thereby an iterative correction procedure was used, which takes the metal ions bound to other sites into account.[351] Excluding the 5'-end, the three metal ion binding sites in d3'-EBS1* show similar affinities towards Mg^{2+}. The two binding sites in the loop even show within the error limits the same intrinsic affinity. This picture changes when IBS1* is added: the binding site "loop 1" in d3'-EBS1*·IBS1*, which is located at G13 and G14, exhibits the strongest affinity towards Mg^{2+} with a final log $K_{A,fin}$ of 3.06 ± 0.01 mM^{-1}. This is in good agreement with the suggestion that a metal ion at this site is needed to stabilize the unusual conformation, which is induced by the formation of a second helix.

To evaluate the effect of other divalent metal ions besides Mg^{2+}, the metal ion titration experiments were additionally performed with Cd^{2+}. Cd^{2+} binding towards d3'-EBS1* and d3'-EBS1*·IBS1* was evaluated qualitatively as well as quantitatively. The obtained results show that Cd^{2+} binds to similar sites than Mg^{2+} in d3'-EBS1* and d3'-EBS1*·IBS1*, albeit in a different mode, and that Cd^{2+} has a much higher affinity[64] towards d3'-EBS1* and d3'-EBS1*·IBS1* than Mg^{2+}.

Moreover, the metal ion requirements for the formation of the 5'-splice site recognition complex were characterized using Circular Dichroism. These studies reveal that the formation of the EBS1*·IBS1* duplex does not necessarily require divalent metal ions, as large amounts of monovalent metal ions also promote duplex formation, albeit at a 5000 times higher concentration. Nevertheless, micromolar amounts of divalent metal ions, e.g. Mg^{2+} or Cd^{2+}, strongly promote the formation of the 5'-splice site. These observations illustrate that a high charge density independent of the nature of the ion is needed for binding of EBS1 to IBS1, but divalent metal ions are presumably the better players.[289]

In conclusion, this work is the first report of a NMR solution structure of a 5'-splice-site recognition complex of a group II intron ribozyme or a spliceosome in the absence and presence of substrate. Addition of substrate induces structural changes that shift the metal ion binding site located in close proximity of the catalytic site. These results thus provide us with a fundamental understanding of the relationship between three-dimensional structure and metal ion binding at the atomic level.

6 Zusammenfassung

Während der Proteinbiosynthese wird die genetische Information von der DNA über RNA zu den Proteinen übersetzt. Dabei durchläuft die RNA verschiedene Vorstufen, bevor sie ihre eigentliche Funktion ausführen kann. Eine essentielle Rolle spielt dabei das sogenannte Spleißen. Dabei werden die nicht-kodierenden Introns präzise aus den RNA-Vorläufern herausgeschnitten und die kodierenden Exons wieder miteinander verknüpft. Sogenannte Spleißosome, die aus vielen kleinen Kern-RNA und Proteinen bestehen, können das Spleißen katalysieren. Es gibt aber auch Introns, die die Fähigkeit haben, sich selbst aus der Vorläufer-RNA herauszuschneiden ohne die Hilfe von Proteinen. Zu diesen selbstspleißenden Introns gehören die Introns der Gruppe II, die im Mittelpunkt dieser Arbeit stehen. Diese Introns sind Ribozyme, d.h. "Enzyme", die ausschliesslich aus RNA bestehen. Sie kommen in den Genen von Pflanzen, Pilzen, Hefen und einigen Bakterien vor.[203,261,262,292] Obwohl sie in höheren Eukaryoten nicht vorkommen, ist der Mechanismus des Spleißens ähnlich dem des Spleißosoms.[261,262]

Introns der Gruppe II bestehen aus sechs Domänen (D1 – D6) (Figur S1). Jede Domäne hat typische sekundäre Strukturelemente mit eigenen Funktionen. Dabei ist D1 die grösste Domäne, an die die anderen Domänen durch tertiäre Wechselwirkungen andocken und somit die katalytisch aktive Tertiärstruktur bilden. Für ein erfolgreiches Spleißen muss das Exon durch das Intron erkannt werden. Die Erkennung erfolgt an zwei Stellen in D1, der Exonbindungsstellen 1 und 2 (EBS1 und EBS2). Wie der Name schon verrät, binden diese Stellen das Exon, d.h. durch Basenpaarung mit den Intronbindungsstellen 1 und 2 (IBS1 und IBS2) am angrenzenden 5'-Exon (Figur S1) wird sichergestellt, dass an der richtigen Stelle geschnitten wird.[203,292] EBS1 befindet sich im *loop* einer Haarnadelstruktur in D1 und bildet mit IBS1 die Erkennungsstelle für das Spleißen am 5'-Ende. Es wurde

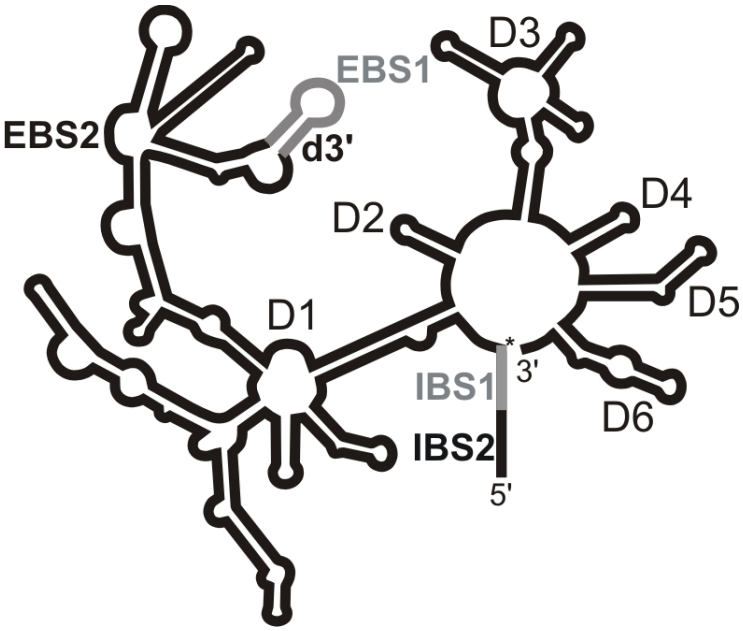

Figur S1 Schematische Darstellung eines Introns der Gruppe II mit seinen sechs Domänen. IBS1 und IBS2, die zum angrenzenden 5'-Exon gehören, sind dargestellt.

herausgefunden, dass D1 und D5 die einzigen Komponenten sind, die für die Katalyse unbedingt benötigt werden. Zusätzlich spielen Metallionen sowohl bei der Katalyse als auch bei der Faltung eine entscheidende Rolle.[69,292]

Ziel dieser Doktorarbeit war es, die NMR Strukturen der Spleißstelle am 5'-Ende in Abwesenheit (d3'-EBS1*) und Anwesenheit des Subrates (d3'-EBS1*·IBS1*) zu lösen und den Effekt von Metallionen auf diese Strukturen zu untersuchen.

Das verwendete RNA Konstrukt besteht aus einer Haarnadelstruktur, die sowohl den d3'-Stamm als auch EBS1 beinhaltet (Figur S2). Dieses Konstrukt ist Teil des Gruppe II Introns *Sc*.ai5γ, das sich im *cox1* Gen von *Saccharomyces cerevisiae* befindet. Um die Helix zu stabilisieren und die Effizienz der *in vitro* Transkription zu steigern, wurde eine GGAG Sequenz am 5'-Ende hinzugefügt.[292] Da kurze RNA Sequenzen nicht mittels *in vitro* Transkription hergestellt werden können, wurde IBS1, das aus nur 7 Nukleotiden besteht, gekauft.

Die 2D [^{1}H,^{1}H]-NOESY Spektren vom Wildtyp d3'-EBS1·IBS1 zeigten in der Region des *sequential walks* massive Überlappungen der Peaks. Dies war ein erster Hinweis dafür, dass keine stabile Struktur geformt wird, was mittels UV Schmelzkurven bestätigt werden konnte. Das Konstrukt, das nur EBS1·IBS1 beinhaltet, hat eine sehr geringe Schmelztemperatur (T_m =

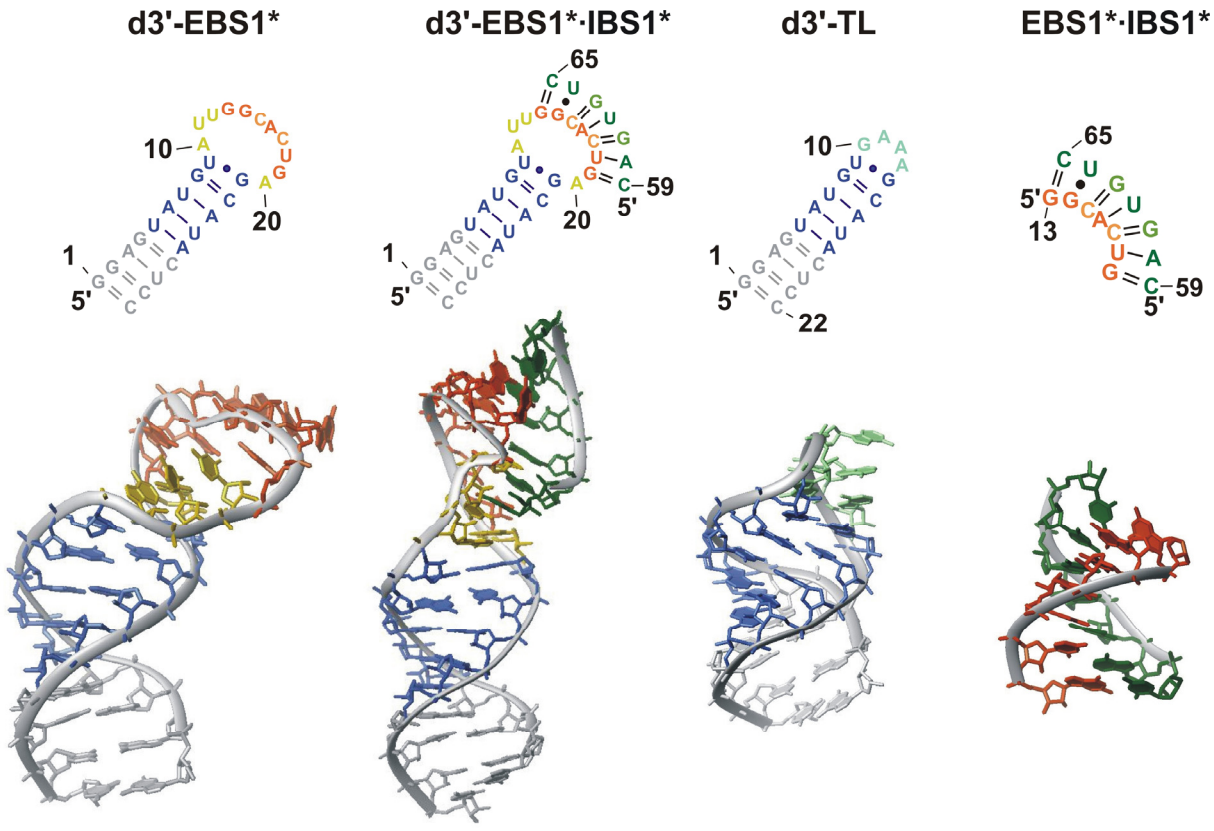

Figur S2 Sekundärstrukturen zusammen mit den NMR Strukturen von d3'-EBS1*, d3'-EBS1*·IBS1*, d3'-TL und EBS1*·IBS1* (von links nach rechts).

15.5 °C mit 100 mM KCl). Der Versuch, die Wechselwirkung durch höhere Salzkonzentrationen zu verstärken, scheiterte. Dies zeigt, dass der EBS1·IBS1 Komplex in der Abwesenheit der kovalenten Exon-Intron Bindung und/oder EBS2·IBS2 unstabil ist (siehe Figur S1). Um die Stabilität zu erhöhen, wurden zwei AU durch zwei GC Basenpaare ersetzt (EBS1*·IBS1*). Es konnte gezeigt werden, dass die katalytische Aktivität trotz der veränderten Basenpaarung nicht beeinflusst wird.[289] Dennoch scheint das G-U *wobble* Paar unabdingbar für erfolgreiches Spleissen zu sein.

Um Strukturen mittels NMR aufklären zu können, muss sichergestellt werden, dass die zu untersuchende RNA in Lösung nur eine Struktur bildet. Bei der hier untersuchten RNA ist es möglich, dass sich neben der Haarnadelstruktur, aus zwei dieser RNA Stränge auch eine Duplex formen kann. Leider ist es nicht möglich mittels 2D [^{1}H,^{1}H]-NOESY Spektren diese zwei Spezies zu unterscheiden, da die Spektren wegen der Symmetrie der Duplex sehr ähnlich aussehen können. Dass wirklich eine Haarnadelstruktur in Lösung vorliegt, wurde mittels konzentrationsäbhängiger UV Schmelzkurven, X-filter-NOESY-HSQC Experimenten, *diffusion ordered spectroscopy* (DOSY) und *dynamic light scattering* (DLS) bestimmt.

NMR Spektren von d3'-EBS1*, die in H_2O aufgenommen wurden, zeigen acht Watson-Crick Basenpaare und ein G-U *wobble* Paar. Das bedeutet, dass keine weiteren Basenpaare gebildet werden und somit in Abwesenheit von IBS1* wirklich ein *loop* gebildet wird, der 11 Nukleotide lang ist. Schon der mfold server hat diese Sekundärstruktur als stabilste vorgeschlagen.[26] Wird IBS1* hinzugefügt, bilden sich sechs weitere Watson-Crick Basenpaare und ein zusätzliches G-U *wobble* Paar. Das beweist, dass IBS1* komplett an EBS1* gebunden ist.

Die vergleichsweise geringe Anzahl an Kern-Overhauser-Effekten (NOEs) pro Nukleotid (17.72) im Falle von d3'-EBS1* ist auf den unstrukturierten *loop* zurückzuführen, für die nur 13.72 NOEs pro Nukleotid gefunden wurden. Für die Helix konnten 20.16 NOEs beobachtet werden. Dies zeigt zusätzlich, dass der *loop* keine starre Form einnimmt und daher flexibel und ungebunden ist. Diese Flexibilität führt dazu, dass das Substrat leicht gebunden werden kann. Durch die Zugabe von IBS1* wird eine zweite Helix gebildet, die den *loop* die Flexibilität nimmt.

Die NMR Strukturen von d3'-EBS1* und d3'-EBS1*·IBS1* konnten zu einer Abweichung vom quadratischen Mittelwert der 20 Strukturen mit der geringsten Energie von 2.06 ± 0.86 Å bzw. 0.69 ± 0.17 Å bestimmt werden (Figur S2). Die unabhängige Überlagerung der Helices in d3'-EBS1* zeigen kleine mittlere Abweichungen (0.41 ± 0.10 Å), während die mittlere

Abweichung für den *loop* wesentlich höher ist (2.59 ± 1.23 Å). Dieses Ergebnis zeigt zusätzlich, dass der *loop* in Abwesenheit von IBS1* flexibel ist.

Im Konstrukt d3'-EBS1*·IBS1* wurde ein ungewöhnlicher Knick zwischen den Nukleotiden U12 und G13 im Rückgrat beobachtet. Um herauszufinden, ob solch eine Struktur schon bekannt ist, wurde ein sogenannter *wormsearch* in der Proteindatenbank (RCSB PDB) durchgeführt. Diese Suche ergab mehrere Strukturen, die einen ähnlichen Knick aufweisen. Die beste Übereinstimmung mit dem Knick in d3'-EBS1*·IBS1* wurde in der Kristallstruktur der 50S ribosomalen Untereinheit[346] gefunden. Das Motiv in der Kristallstruktur hat ein ungepaartes Nukleotid, das benötigt wird, um sterische Hindernisse zu überwinden. d3'-EBS1*·IBS1* enthält sogar drei ungepaarte Nukleotide, die die Bildung dieses ungewöhnlichen Knicks ermöglichen.

Zusätzlich zu d3'-EBS1* und d3'-EBS1*·IBS1* wurden zwei weitere Strukturen gelöst. Diese repräsentieren die einzelnen Teile von d3'-EBS1*·IBS1*, d.h. auf der einen Seite der d3'-Stamm, der durch einen GAAA *tetraloop* geschlossen wird (d3'-TL), und auf der anderen Seite die individuelle EBS1*·IBS1* Verbindung (Figur S2).[289] Zwischen EBS1*·IBS1* und der entsprechenden Wechselwirkung in d3'-EBS1*·IBS1* konnten keine strukturellen Unterschiede gefunden werden.

Es ist bekannt, dass viele tertiäre Strukturelemente durch divalente Metallionen wie z.B. Mg^{2+} stabilisiert werden,[64,69] aber auch monovalente Metallionen können eine wichtige Rolle spielen.[66] Um den Einfluss von divalenten Metallionen auf d3'-EBS1* und d3'-EBS1*·IBS1* besser untersuchen zu können, wurden die Änderungen der chemischen Verschiebung der Protonresonanzen von d3'-EBS1* und d3'-EBS1*·IBS1* bei Zugabe von Mg^{2+} und Cd^{2+} untersucht (Figur S3). Da die Protonen H8, H2, H6, H5 der Basen und auch die H1'-Protonen des Zuckers nah an potentiellen Metallionen-Koordinationsstellen liegen (wie z.B. N7 der Purine, Phosphatsauerstoffe oder die 2'-OH Gruppe des Zuckers), kann die chemische Verschiebung bei Zugabe der Metallionen Informationen darüber geben, wo das Metall bindet.

Die Untersuchung der oben genannten Protonen zeigt, dass in beiden Konstrukten die Nukleotide A10, U11 and A20 am meisten durch Mg^{2+} beeinflusst werden. In d3'-EBS1*·IBS1* weisen zusätzlich die Nukleotide U12, G13 and G14 und auch IBS1* (C59 bis C65) eine starke Änderung der chemischen Verschiebung auf. Diese Beobachtungen stimmen gut mit den Tb^{3+}-Spaltungsexperimenten überein, die eine Metallionenbindungsstelle am 5'-Ende von EBS1 zeigen.[97] Aufgrund der zweiten Helix, die gebildet wird, wenn IBS1* an EBS1* bindet, ragen die Phosphatsauerstoffe in d3'-EBS1*·IBS1* von G13 und G14 heraus.

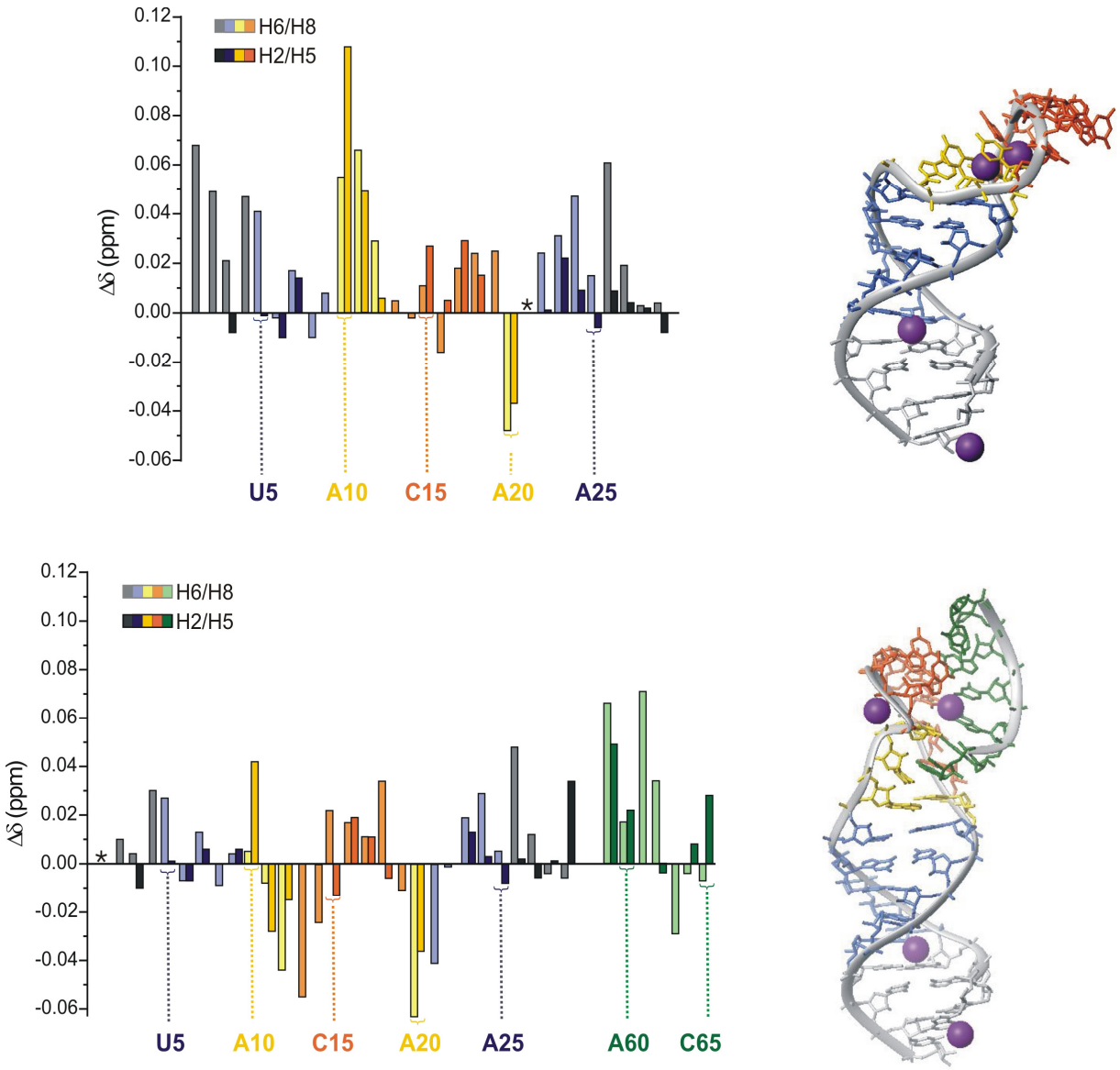

Figur S3 Änderungen der chemischen Verschiebung der Protonresonanzen von d3'-EBS1* (oben) und d3'-EBS1*·IBS1* (unten) bei Zugabe von Mg^{2+}.

Metallionen haben es somit einfacher, an diese Stellen zu binden. Jedoch können Änderungen der chemischen Verschiebung nicht nur durch direkte Koordination eines Metallions auftreten, sondern auch durch strukturelle Veränderungen, die das Metallion hervorruft, wenn es in der Nähe bindet. Solche strukturellen Veränderungen können z.B. erhöhte oder erniedrigte Stapelungen der Basen sein.

Mg^{2+} hat nicht nur einen Einfluss auf die chemische Verschiebung der Protonen, sondern auch auf die Linienbreite der Peaks. Wenn Mg^{2+} an eine Stelle bindet, werden die Peaks in ihrer unmittelbaren Nähe breiter.[351] Durch diesen Effekt kann man spezifische Mg^{2+}-Bindungsstellen detektieren. Im Gegensatz zu Mg^{2+} sind Mn^{2+}-Ionen paramagnetisch, dadurch verstärken sie den Effekt der Linienverbreiterung und sind daher sehr gut geeignet, um spezifische Metallionen-Bindungsstellen zu ermitteln. Mittels dieser Experimente wurden in beiden Konstrukten je vier Metallionenbindungsstellen identifiziert. Von speziellem

Interesse ist dabei die 5'-Spleißstelle. Ist das Substrat IBS1* nicht gebunden, befindet sich eine der vier Metallionenbindungsstellen in d3'-EBS1* vor dem 5'-Ende von EBS1* (bei A10, U11 und U12). Wenn IBS1* gebunden ist, verschiebt sich diese Bindungsstelle aufgrund struktureller Veränderungen stromabwärts zu G13 und G14. Die Metallionenbindungsstelle an der 5'-Spleißstelle spielt vermutlich eine wichtige Rolle im katalytischen Prozess. Divalente Metallionen helfen dabei, die ungewöhnliche Konformation zu stabilisieren, die aufgrund der Bindung von IBS1* an EBS1* entsteht und kompensieren zudem die negative Ladung am Rückgrat dieser Stelle.

Um ein genaueres Bild der Metallionenbindungsstellen zu erhalten, wurden die Affinitätskonstanten für Mg^{2+} an d3'-EBS1* und d3'-EBS1*·IBS1* berechnet. Dafür wurde ein iteratives Korrekturverfahren verwendet, das Metallionen, die schon an andere Stellen gebunden sind, in Betracht zieht.[351] Abgesehen vom 5'-Ende, das eine besondere Rolle bei *in vitro* transkribierter RNA spielt, haben die drei anderen Bindungsstellen in d3'-EBS1* ähnliche Affinitäten zu Mg^{2+}. Dabei zeigen die beiden Bindungsstellen im *loop* sogar dieselbe Affinität. Wenn IBS1* gebunden ist, ändern sich die Affinitätskonstanten erheblich. Die Bindungsstelle "*loop 1"*, die sich in d3'-EBS1*·IBS1* an den Nukleotiden G13 und G14 befindet, zeigt mit einem log $K_{A,fin}$ Wert von 3.06 ± 0.01 mM^{-1} die höchste Affinität gegenüber Mg^{2+}. Dieser Wert unterstützt die Vermutung, dass ein Metallion an dieser Stelle benötigt wird, um die ungewöhnliche Konformation zu stabilisieren, die durch die Bildung einer zweiten Helix zustande kommt.

Um den Effekt anderer Metallionen zu untersuchen, wurden die Titrationen zusätzlich mit Cd^{2+} durchgeführt. Sowohl die qualitative als auch die quantitative Analyse zeigen, dass Cd^{2+} zwar an ähnliche Stellen in d3'-EBS1* und d3'-EBS1*·IBS1* bindet wie Mg^{2+}, aber mit höherer Affinität. Aus der Literatur ist bekannt, dass Cd^{2+} im allgemeinen stärker an RNA bindet als Mg^{2+}.[64]

Circular Dichroismus wurde als zusätzliche Methode verwendet, um die Bedingungen an Metallionen für die Bildung der 5'-Spleißstelle zu untersuchen. Diese Untersuchungen zeigen, dass divalente Metallionen nicht unbedingt benötigt werden, um IBS1* an EBS1* zu binden. Eine Bedingung ist jedoch, dass genügend monovalente Ionen vorliegen, d.h. etwa in 5000 fach höherer Konzentration als divalente Ionen. Divalente Ionen wie Mg^{2+} oder Cd^{2+} können aber schon in mikromolaren Mengen dafür sorgen, dass die 5'-Spleißstelle gebildet wird. Das zeigt, dass eine hohe Ladungsdichte ausreichend ist, um EBS1 und IBS1 aneinander zu binden.[289]

Die in dieser Doktorarbeit gelösten NMR Strukturen der 5'-Spleißstelle mit und ohne Substrat und die detaillierten Untersuchungen der Bindung von Metallionen liefern ein umfassendes Bild über die Beziehung zwischen dreidimensionaler Struktur und Metallbindungen auf atomarer Basis. Die hier gewonnenen detaillierten Ergebnisse bilden eine solide Grundlage für Untersuchungen der Metallionenbindung an die 5'-Spleißstelle im Kontext des kompletten Ribozyms. Diese Ergebnisse sind essentiell, um die Rolle von Metallionen im katalytischen Prozess genau zu verstehen.

7 Appendices

Appendix 1 Comparison of the imino regions of 2D [^{1}H,^{1}H]-NOESY spectra of the upper and lower band of d3'-EBS1*

The left panel shows the imino region of the lower band of d3'-EBS1*, which is assigned to 29 nucleotides and the right panel the n+1 band of d3'-EBS1*. The corresponding imino resonances that are the same in both spectra are indicated by dotted lines. Black lines show the walk from G1 to G2 and U27 (left), and G1b, G2b and U27b (right), respectively.

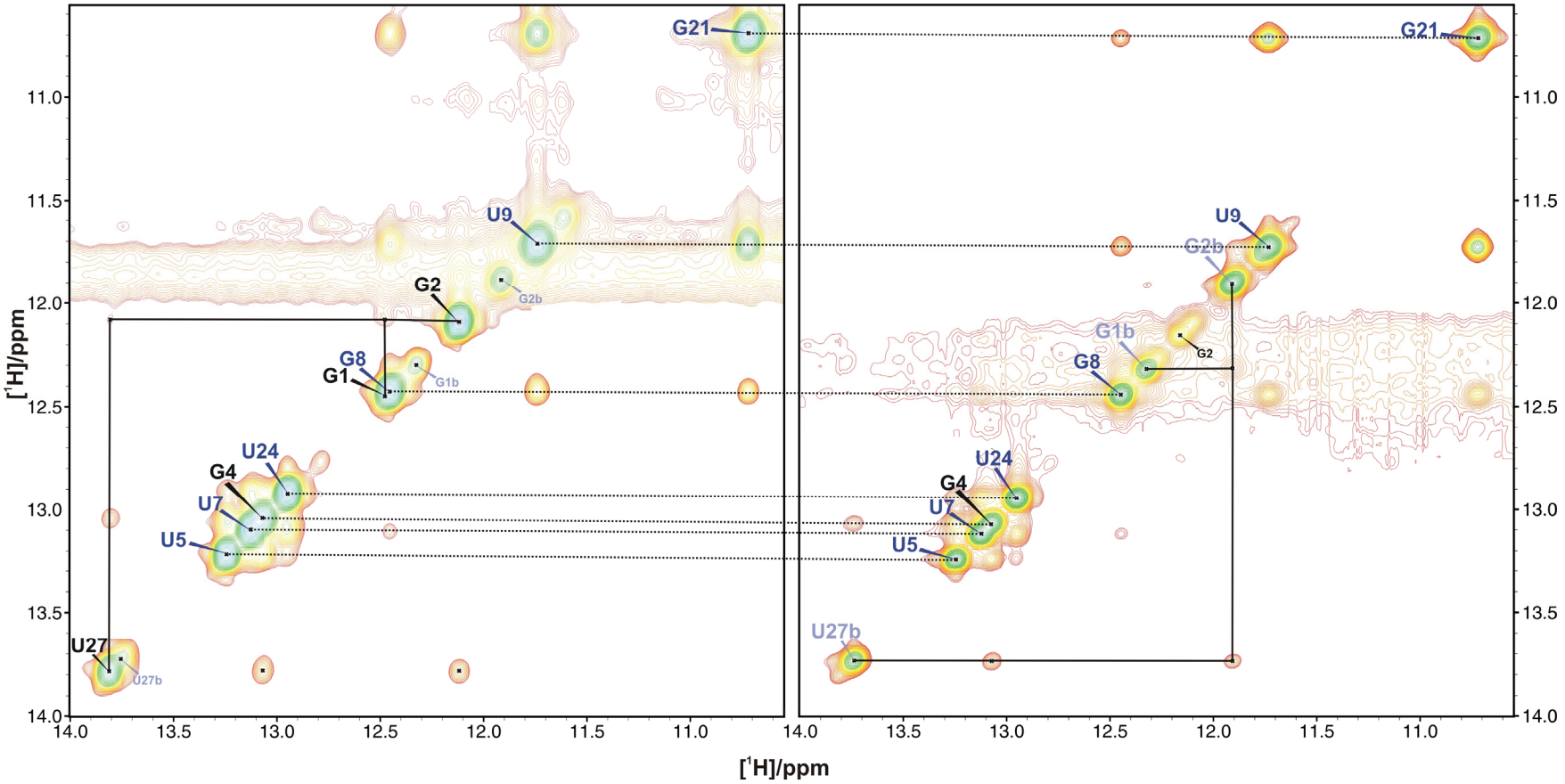

Appendix 2 ^{1}H chemical shift assignments for d3'-EBS1*

	H1	H1'	H2	H2'	H21	H22	H3	H3'	H4'	H41	H42	H5	H5'	H5''	H6	H61	H62	H8
G1	12.440	5.674	-	4.784	7.653	5.645	-	4.544	4.416	-	-	-	-	4.114	-	-	-	7.979
G2	12.093	5.760	-	4.545	7.847	5.670	-	4.418	4.450	-	-	-	-	4.114	-	-	-	7.379
A3	-	5.847	7.351	4.609	-	-	-	4.485	4.397	-	-	-	4.006	3.936	-	8.031	6.710	7.604
G4	13.049	5.406	-	4.279	8.070	5.944	-	4.182	4.324	-	-	-	-	3.886	-	-	-	6.921
U5	-	5.375	-	4.469	-	-	13.221	4.398	4.386	-	-	4.950	-	3.937	7.534	-	-	-
A6	-	5.847	6.888	4.357	-	-	-	4.500	4.421	-	-	-	-	4.016	-	7.576	6.179	7.999
U7	-	5.265	-	4.362	-	-	13.106	4.295	4.273	-	-	4.893	-	3.942	7.438	-	-	-
G8	12.426	5.596	-	4.387	7.571	5.668	-	4.293	-	-	-	-	-	-	-	-	-	7.434
U9	-	5.444	-	4.064	-	-	11.701	4.408	-	-	-	5.261	-	-	7.481	-	-	-
A10	-	5.858	7.691	4.530	-	-	-	4.471	4.371	-	-	-	4.175	4.002	-	-	-	8.108
U11	-	5.364	-	4.282	-	-	-	-	-	-	-	5.287	-	3.968	7.547	-	-	-
U12	-	5.479	-	4.122	-	-	-	4.367	4.180	-	-	5.513	-	3.890	7.599	-	-	-
G13	-	5.507	-	4.432	-	-	-	4.478	4.236	-	-	-	-	-	-	-	-	7.607
G14	-	5.523	-	4.597	-	-	-	4.524	4.312	-	-	-	-	3.972	-	-	-	7.668
C15	-	5.623	-	4.108	-	-	-	4.379	4.075	-	-	5.595	3.912	3.883	7.505	-	-	-
A16	-	5.786	7.818	4.556	-	-	-	4.365	4.386	-	-	-	4.081	3.947	-	-	-	8.070
C17	-	5.602	-	4.260	-	-	-	4.203	-	-	-	5.646	-	3.957	7.485	-	-	-
U18	-	5.670	-	4.188	-	-	-	4.446	4.238	-	-	5.617	-	3.979	7.590	-	-	-
G19	-	5.465	-	4.534	-	-	-	4.282	3.957	-	-	-	-	3.738	-	-	-	7.624
A20	-	5.842	7.785	4.595	-	-	-	4.414	4.341	-	-	-	-	3.972	-	-	-	7.867
G21	10.688	5.391	-	4.451	7.582	6.031	-	4.244	-	-	-	-	-	-	-	-	-	7.395
C22	-	5.207	-	4.253	-	-	-	4.400	4.345	7.993	6.625	5.255	-	-	7.509	-	-	-
A23	-	5.779	7.140	4.326	-	-	-	4.554	4.341	-	-	-	-	3.974	-	7.563	6.154	7.871
U24	-	5.302	-	4.239	-	-	12.924	4.342	4.399	-	-	4.950	-	-	7.512	-	-	-
A25	-	5.842	6.984	4.378	-	-	-	4.526	-	-	-	-	-	4.028	-	7.604	6.150	7.995
C26	-	5.210	-	4.032	-	-	-	4.202	4.126	8.048	6.717	5.051	-	3.910	7.385	-	-	-
U27	-	5.380	-	4.341	-	-	13.784	4.368	4.261	-	-	5.165	-	3.911	7.751	-	-	-
C28	-	5.439	-	4.060	-	-	-	4.309	4.249	8.027	6.704	5.478	-	3.915	7.762	-	-	-
C29	-	5.566	-	3.828	-	-	-	3.856	4.011	8.023	6.654	5.319	-	-	7.503	-	-	-

Chemical shifts were extracted from the 2D [^{1}H,^{1}H]-NOESY spectrum at 293 K (100% D_2O, 10 mM KCl, 10 µM EDTA, pD = 6.66) and the 2D [^{1}H,^{1}H]-NOESY spectrum at 278 K (90% H_2O/10% D_2O, 10 mM KCl, 10 µM EDTA, pH = 6.52), both acquired at 700 MHz proton frequency.

Appendix 3 ^{13}C and ^{15}N assignments for d3'-EBS1*

	C6	C5	C8	C2	C1'	N1	N3
G1	-	-	136.22	-	88.61	146.88	-
G2	-	-	137.89	-	90.10	146.57	-
A3	-	-	-	150.52	88.42	-	-
G4	-	-	133.14	-	89.92	147.76	-
U5	139.56	100.32	-	-	90.93	-	161.51
A6	-	-	135.99	150.32	-	-	-
U7	138.47	100.24		-	90.27	-	161.60
G8	-	-	137.98	-	88.38	147.32	-
U9	134.57	101.55	-	-	91.29	-	157.75
A10	-	-	138.64	152.13	90.11	-	-
U11	140.16	101.45	-	-	90.06	-	-
U12	140.28	102.16	-	-	89.33	-	-
G13	-	-	136.38	-	88.45	-	-
G14	-	-	136.70	-	87.40	-	-
C15	140.21	96.22	-	-	88.39	-	-
A16	-	-	138.60	152.30	87.99	-	-
C17	140.71	96.07	-	-	89.99	-	-
U18	140.95	102.47	-	-	88.45	-	-
G19	-	-	136.21	-	88.90	-	-
A20	-	-	137.97	151.79	90.04	-	-
G21	-	-	133.30	-	90.20	144.22	-
C22	138.79	94.98	-	-	90.91	-	-
A23	-	-	136.82	150.33	90.24	-	-
U24	140.28	100.01	-	-	90.32	-	161.08
A25	-	-	136.98	150.60	88.26	-	-
C26	134.23	94.42	-	-	91.04	-	-
U27	139.75	100.38	-	-	89.84	-	162.41
C28	138.91	94.63	-	-	90.04	-	-
C29	138.17	95.25	-	-	90.00	-	-

Appendix 4 2D J_{NN} HNN-COSY of d3'-EBS1* (90% H_2O/10% D_2O, pH = 6.87, 10 mM KCl, 10 µM EDTA) acquired on a 700 MHz Bruker Avance spectrometer equipped with a CP-TXI z-axis pulsed-field gradient cryoprobe at 278 K.

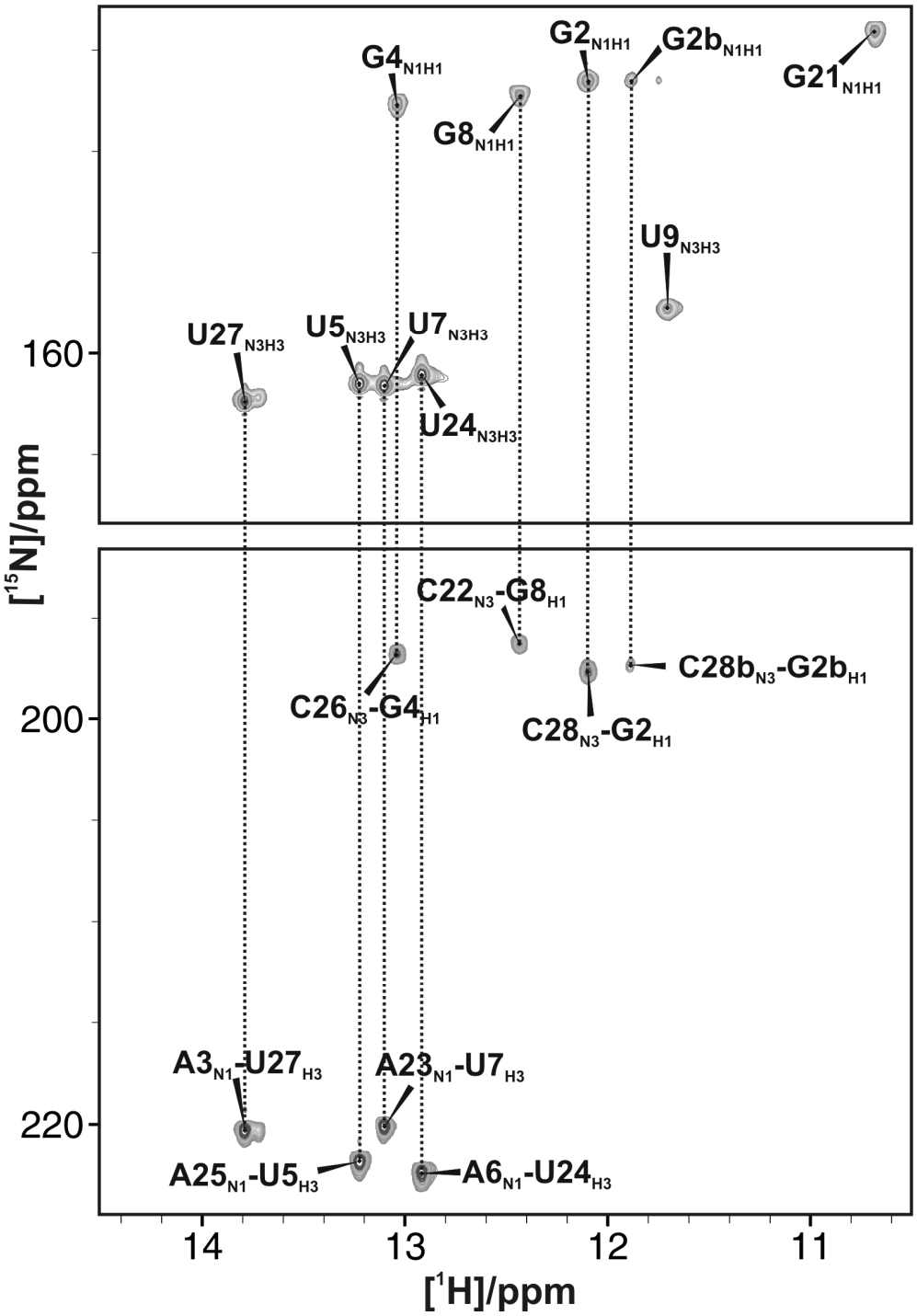

Appendix 5 Illustration of the surface area of d3'-EBS1*

The colours correspond to the one used in the seondary structure as shown in Figure 25.

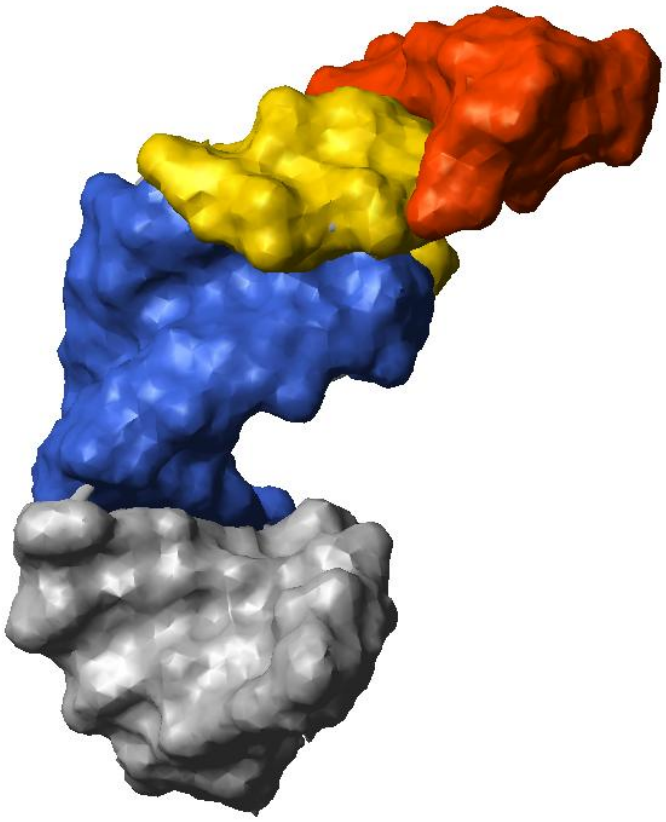

Appendix 6 All distance constraints in d3'-EBS1*

Distance constraints of non-exchangeable protons in d3'-EBS1* based on a 2D [^{1}H,^{1}H]-NOESY spectrum acquired at 700 MHz proton frequency at 293 K (100% D_2O, 10 mM KCl, 10 µM EDTA, pD = 6.66). Specified are the estimated distances in Å, the lower and the upper boundaries.

```
assign (residue  1 and name  H1') (residue  1 and name  H8)  3.80  2.00  0.70
assign (residue  1 and name  H2') (residue  1 and name  H8)  3.80  2.00  0.70
assign (residue  1 and name  H3') (residue  1 and name  H8)  3.80  2.00  0.70
assign (residue  1 and name  H4') (residue  1 and name  H8)  5.00  2.00  1.00
assign (residue  1 and name  H5") (residue  1 and name  H8)  2.50  0.70  0.50

assign (residue  1 and name  H1') (residue  2 and name  H1')  5.00  2.00  1.00
assign (residue  1 and name  H1') (residue  2 and name  H8)  3.80  2.00  0.70
assign (residue  1 and name  H2') (residue  2 and name  H1')  5.00  2.00  1.00
assign (residue  1 and name  H2') (residue  2 and name  H8)  2.50  0.70  0.50
assign (residue  1 and name  H3') (residue  2 and name  H8)  3.80  2.00  0.70
assign (residue  1 and name  H8)  (residue  2 and name  H8)  5.00  2.00  1.00

assign (residue  2 and name  H1') (residue  2 and name  H8)  3.80  2.00  0.70
assign (residue  2 and name  H2') (residue  2 and name  H8)  3.80  2.00  0.70
assign (residue  2 and name  H3') (residue  2 and name  H8)  2.50  0.70  0.50
assign (residue  2 and name  H4') (residue  2 and name  H8)  5.00  2.00  1.00
assign (residue  2 and name  H5") (residue  2 and name  H8)  3.80  2.00  0.70

assign (residue  2 and name  H1') (residue  3 and name  H1')  5.00  2.00  1.00
assign (residue  2 and name  H1') (residue  3 and name  H8)  5.00  2.00  1.00
assign (residue  2 and name  H2') (residue  3 and name  H1')  3.80  2.00  0.70
assign (residue  2 and name  H2') (residue  3 and name  H8)  2.50  0.70  0.50
assign (residue  2 and name  H3') (residue  3 and name  H8)  3.80  2.00  0.70
assign (residue  2 and name  H8)  (residue  3 and name  H8)  5.00  2.00  1.00

assign (residue  3 and name  H1') (residue  3 and name  H2)  5.00  2.00  1.00
assign (residue  3 and name  H1') (residue  3 and name  H8)  3.80  2.00  0.70
assign (residue  3 and name  H2') (residue  3 and name  H2)  5.00  2.00  1.00
assign (residue  3 and name  H2') (residue  3 and name  H8)  3.80  2.00  0.70
assign (residue  3 and name  H3') (residue  3 and name  H8)  2.50  0.70  0.50
assign (residue  3 and name  H4') (residue  3 and name  H8)  5.00  2.00  1.00
assign (residue  3 and name  H5') (residue  3 and name  H8)  3.80  2.00  0.70
assign (residue  3 and name  H5") (residue  3 and name  H8)  3.80  2.00  0.70

assign (residue  3 and name  H1') (residue  4 and name  H1')  5.00  2.00  1.00
assign (residue  3 and name  H1') (residue  4 and name  H8)  3.80  2.00  0.70
assign (residue  3 and name  H2') (residue  4 and name  H1')  3.80  2.00  0.70
assign (residue  3 and name  H2') (residue  4 and name  H8)  2.50  0.70  0.50
assign (residue  3 and name  H3') (residue  4 and name  H8)  3.80  2.00  0.70
assign (residue  3 and name  H2)  (residue  4 and name  H1')  2.50  0.70  0.50
assign (residue  3 and name  H2)  (residue  4 and name  H2')  3.80  2.00  0.70
assign (residue  3 and name  H2)  (residue  4 and name  H8)  5.00  2.00  1.00
assign (residue  3 and name  H2)  (residue 27 and name  H1')  5.00  2.00  1.00
```

```
assign (residue  3 and name  H2)   (residue 27 and name  H2')   5.00  2.00  1.00
assign (residue  3 and name  H2)   (residue 28 and name  H1')   3.80  2.00  0.70
assign (residue  3 and name  H2)   (residue 28 and name  H2')   5.00  2.00  1.00
assign (residue  3 and name  H2)   (residue 28 and name  H6)    5.00  2.00  1.00
assign (residue  3 and name  H8)   (residue  4 and name  H8)    5.00  2.00  1.00

assign (residue  4 and name  H1')  (residue  4 and name  H8)    3.80  2.00  0.70
assign (residue  4 and name  H2')  (residue  4 and name  H8)    3.80  2.00  0.70
assign (residue  4 and name  H3')  (residue  4 and name  H8)    2.50  0.70  0.50
assign (residue  4 and name  H4')  (residue  4 and name  H8)    3.80  2.00  0.70
assign (residue  4 and name  H5'') (residue  4 and name  H8)    3.80  2.00  0.70

assign (residue  4 and name  H1')  (residue  5 and name  H5)    5.00  2.00  1.00
assign (residue  4 and name  H1')  (residue  5 and name  H6)    3.80  2.00  0.70
assign (residue  4 and name  H2')  (residue  5 and name  H1')   3.80  2.00  0.70
assign (residue  4 and name  H2')  (residue  5 and name  H5)    3.80  2.00  0.70
assign (residue  4 and name  H2')  (residue  5 and name  H6)    2.50  0.70  0.50
assign (residue  4 and name  H3')  (residue  5 and name  H5)    2.50  0.70  0.50
assign (residue  4 and name  H3')  (residue  5 and name  H6)    2.50  0.70  0.50
assign (residue  4 and name  H8)   (residue  5 and name  H2')   6.00  2.00  1.00
assign (residue  4 and name  H8)   (residue  5 and name  H5)    3.80  2.00  0.70
assign (residue  4 and name  H8)   (residue  5 and name  H6)    5.00  2.00  1.00

assign (residue  5 and name  H1')  (residue  5 and name  H5)    5.00  2.00  1.00
assign (residue  5 and name  H1')  (residue  5 and name  H6)    3.80  2.00  0.70
assign (residue  5 and name  H2')  (residue  5 and name  H5)    5.00  2.00  1.00
assign (residue  5 and name  H2')  (residue  5 and name  H6)    3.80  2.00  0.70
assign (residue  5 and name  H3')  (residue  5 and name  H5)    3.80  2.00  0.70
assign (residue  5 and name  H3')  (residue  5 and name  H6)    2.50  0.70  0.50
assign (residue  5 and name  H4')  (residue  5 and name  H6)    5.00  2.00  1.00
assign (residue  5 and name  H5'') (residue  5 and name  H6)    3.80  2.00  0.70

assign (residue  5 and name  H1')  (residue  6 and name  H1')   5.00  2.00  1.00
assign (residue  5 and name  H1')  (residue  6 and name  H8)    5.00  2.00  1.00
assign (residue  5 and name  H1')  (residue 25 and name  H2)    5.00  2.00  1.00
assign (residue  5 and name  H2')  (residue  6 and name  H1')   3.80  2.00  0.70
assign (residue  5 and name  H2')  (residue  6 and name  H8)    2.50  0.70  0.50
assign (residue  5 and name  H2')  (residue 25 and name  H2)    5.00  2.00  1.00
assign (residue  5 and name  H3')  (residue  6 and name  H8)    3.80  2.00  0.70
assign (residue  5 and name  H3')  (residue 25 and name  H2)    5.00  2.00  1.00
assign (residue  5 and name  H6)   (residue  6 and name  H8)    5.00  2.00  1.00

assign (residue  6 and name  H1')  (residue  6 and name  H2)    3.80  2.00  0.70
assign (residue  6 and name  H1')  (residue  6 and name  H8)    3.80  2.00  0.70
assign (residue  6 and name  H2')  (residue  6 and name  H2)    5.00  2.00  1.00
assign (residue  6 and name  H2')  (residue  6 and name  H8)    3.80  2.00  0.70
assign (residue  6 and name  H3')  (residue  6 and name  H8)    2.50  0.70  0.50
assign (residue  6 and name  H4')  (residue  6 and name  H8)    5.00  2.00  1.00
assign (residue  6 and name  H5'') (residue  6 and name  H8)    3.80  2.00  0.70

assign (residue  6 and name  H1')  (residue  7 and name  H1')   5.00  2.00  1.00
```

```
assign (residue  6 and name  H1')  (residue  7 and name  H5)   5.00  2.00  1.00
assign (residue  6 and name  H1')  (residue  7 and name  H6)   5.00  2.00  1.00
assign (residue  6 and name  H1')  (residue 25 and name  H2)   3.80  2.00  0.70
assign (residue  6 and name  H2')  (residue  7 and name  H5)   3.80  2.00  0.70
assign (residue  6 and name  H2')  (residue  7 and name  H6)   3.80  2.00  0.70
assign (residue  6 and name  H2')  (residue 25 and name  H2)   5.00  2.00  1.00
assign (residue  6 and name  H3')  (residue  7 and name  H5)   2.50  0.70  0.50
assign (residue  6 and name  H3')  (residue  7 and name  H6)   3.80  2.00  0.70

assign (residue  6 and name  H2)   (residue  7 and name  H1')  3.80  2.00  0.70
assign (residue  6 and name  H2)   (residue  7 and name  H2')  6.00  2.00  1.00
assign (residue  6 and name  H2)   (residue  7 and name  H6)   5.00  2.00  1.00
assign (residue  6 and name  H2)   (residue 23 and name  H2)   5.00  2.00  1.00
assign (residue  6 and name  H2)   (residue 24 and name  H1')  5.00  2.00  1.00
assign (residue  6 and name  H2)   (residue 24 and name  H2')  5.00  2.00  1.00
assign (residue  6 and name  H2)   (residue 25 and name  H1')  3.80  2.00  0.70
assign (residue  6 and name  H2)   (residue 25 and name  H2')  5.00  2.00  1.00
assign (residue  6 and name  H2)   (residue 25 and name  H2)   3.80  2.00  0.70
assign (residue  6 and name  H2)   (residue 25 and name  H8)   5.00  2.00  1.00
assign (residue  6 and name  H8)   (residue  7 and name  H5)   3.80  2.00  0.70
assign (residue  6 and name  H8)   (residue  7 and name  H6)   5.00  2.00  1.00
assign (residue  6 and name  H8)   (residue 25 and name  H2)   5.00  2.00  1.00

assign (residue  7 and name  H1')  (residue  7 and name  H5)   5.00  2.00  1.00
assign (residue  7 and name  H1')  (residue  7 and name  H6)   3.80  2.00  0.70
assign (residue  7 and name  H2')  (residue  7 and name  H5)   5.00  2.00  1.00
assign (residue  7 and name  H2')  (residue  7 and name  H6)   3.80  2.00  0.70
assign (residue  7 and name  H3')  (residue  7 and name  H6)   2.50  0.70  0.50
assign (residue  7 and name  H4')  (residue  7 and name  H6)   5.00  2.00  1.00
assign (residue  7 and name  H5")  (residue  7 and name  H6)   3.80  2.00  0.70

assign (residue  7 and name  H1')  (residue  8 and name  H1')  5.00  2.00  1.00
assign (residue  7 and name  H1')  (residue  8 and name  H8)   3.80  2.00  0.70
assign (residue  7 and name  H1')  (residue 23 and name  H2)   6.00  2.00  1.00
assign (residue  7 and name  H2')  (residue  8 and name  H1')  3.80  2.00  0.70
assign (residue  7 and name  H2')  (residue  8 and name  H8)   2.50  0.70  0.50
assign (residue  7 and name  H2')  (residue 23 and name  H2)   6.00  2.00  1.00
assign (residue  7 and name  H3')  (residue  8 and name  H8)   3.80  2.00  0.70
assign (residue  7 and name  H3')  (residue 23 and name  H2)   5.00  2.00  1.00

assign (residue  8 and name  H1')  (residue  8 and name  H8)   3.80  2.00  0.70
assign (residue  8 and name  H2')  (residue  8 and name  H8)   3.80  2.00  0.70
assign (residue  8 and name  H3')  (residue  8 and name  H8)   2.50  0.70  0.50

assign (residue  8 and name  H1')  (residue  9 and name  H1')  6.00  2.00  1.00
assign (residue  8 and name  H1')  (residue  9 and name  H5)   5.00  2.00  1.00
assign (residue  8 and name  H1')  (residue  9 and name  H6)   3.80  2.00  0.70
assign (residue  8 and name  H1')  (residue 23 and name  H2)   3.80  2.00  0.70
assign (residue  8 and name  H2')  (residue  9 and name  H1')  3.80  2.00  0.70
assign (residue  8 and name  H2')  (residue  9 and name  H5)   2.50  0.70  0.50
assign (residue  8 and name  H2')  (residue  9 and name  H6)   2.50  0.70  0.50
```

```
assign (residue  8 and name  H2')  (residue 23 and name  H2)   5.00  2.00  1.00
assign (residue  8 and name  H3')  (residue  9 and name  H5)   2.50  0.70  0.50
assign (residue  8 and name  H3')  (residue  9 and name  H6)   3.80  2.00  0.70
assign (residue  8 and name  H3')  (residue 23 and name  H2)   5.00  2.00  1.00
assign (residue  8 and name  H8)   (residue  9 and name  H6)   5.00  2.00  0.70
assign (residue  8 and name  H8)   (residue 23 and name  H2)   5.00  2.00  1.00

assign (residue  9 and name  H1')  (residue  9 and name  H5)   5.00  2.00  1.00
assign (residue  9 and name  H1')  (residue  9 and name  H6)   3.80  2.00  0.70
assign (residue  9 and name  H2')  (residue  9 and name  H5)   5.00  2.00  1.00
assign (residue  9 and name  H2')  (residue  9 and name  H6)   3.80  2.00  0.70
assign (residue  9 and name  H3')  (residue  9 and name  H5)   5.00  2.00  1.00
assign (residue  9 and name  H3')  (residue  9 and name  H6)   2.50  0.70  0.50

assign (residue  9 and name  H1')  (residue 10 and name  H8)   3.80  2.00  0.70
assign (residue  9 and name  H2')  (residue 10 and name  H1')  3.80  2.00  0.70
assign (residue  9 and name  H2')  (residue 10 and name  H8)   2.50  0.70  0.50
assign (residue  9 and name  H3')  (residue 10 and name  H8)   3.80  2.00  0.70
assign (residue  9 and name  H6)   (residue 10 and name  H8)   5.00  2.00  1.00

assign (residue 10 and name H1')   (residue 10 and name  H2)   5.00  2.00  1.00
assign (residue 10 and name H1')   (residue 10 and name  H8)   3.80  2.00  0.70
assign (residue 10 and name H2')   (residue 10 and name  H8)   2.50  0.70  0.50
assign (residue 10 and name H3')   (residue 10 and name  H8)   3.80  2.00  0.70
assign (residue 10 and name H4')   (residue 10 and name  H8)   5.00  2.00  1.00
assign (residue 10 and name H5')   (residue 10 and name  H8)   3.80  2.00  0.70
assign (residue 10 and name H5")   (residue 10 and name  H8)   3.80  2.00  0.70

assign (residue 10 and name H1')   (residue 11 and name  H1')  5.00  2.00  1.00
assign (residue 10 and name H1')   (residue 11 and name  H6)   3.80  2.00  0.70
assign (residue 10 and name H1')   (residue 12 and name  H5)   6.00  2.00  1.00
assign (residue 10 and name H2')   (residue 11 and name  H1')  5.00  2.00  1.00
assign (residue 10 and name H2')   (residue 11 and name  H5)   2.50  0.70  0.50
assign (residue 10 and name H2')   (residue 11 and name  H6)   3.80  2.00  0.70
assign (residue 10 and name H3')   (residue 11 and name  H6)   3.80  2.00  0.70
assign (residue 10 and name H4')   (residue 11 and name  H5)   5.00  2.00  1.00
assign (residue 10 and name H2)    (residue 11 and name  H1')  3.80  2.00  0.70
assign (residue 10 and name H2)    (residue 20 and name  H2)   3.80  2.00  0.70
assign (residue 10 and name H2)    (residue 21 and name  H1')  5.00  2.00  1.00
assign (residue 10 and name H8)    (residue 11 and name  H5)   3.80  2.00  0.70
assign (residue 10 and name H8)    (residue 11 and name  H6)   5.00  2.00  1.00

assign (residue 11 and name H1')   (residue 11 and name  H6)   3.80  2.00  0.70
assign (residue 11 and name H2')   (residue 11 and name  H6)   5.00  2.00  1.00
assign (residue 11 and name H5")   (residue 11 and name  H6)   3.80  2.00  0.70

assign (residue 11 and name H1')   (residue 12 and name  H1')  5.00  2.00  1.00
assign (residue 11 and name H1')   (residue 12 and name  H5)   5.00  2.00  1.00
assign (residue 11 and name H1')   (residue 12 and name  H6)   5.00  2.00  1.00
assign (residue 11 and name H2')   (residue 12 and name  H1')  5.00  2.00  1.00
assign (residue 11 and name H2')   (residue 12 and name  H5)   3.80  2.00  0.70
```

```
assign (residue 11 and name H2')  (residue 12 and name  H6)   3.80  2.00  0.70
assign (residue 11 and name H5)   (residue 12 and name  H5)   3.80  2.00  0.70

assign (residue 12 and name H1')  (residue 12 and name  H5)   5.00  2.00  1.00
assign (residue 12 and name H1')  (residue 12 and name  H6)   3.80  2.00  0.70
assign (residue 12 and name H2')  (residue 12 and name  H5)   5.00  2.00  1.00
assign (residue 12 and name H2')  (residue 12 and name  H6)   3.80  2.00  0.70
assign (residue 12 and name H3')  (residue 12 and name  H5)   5.00  2.00  1.00
assign (residue 12 and name H3')  (residue 12 and name  H6)   2.50  0.70  0.50
assign (residue 12 and name H4')  (residue 12 and name  H6)   5.00  2.00  1.00
assign (residue 12 and name H5")  (residue 12 and name  H6)   3.80  2.00  0.70

assign (residue 12 and name H1')  (residue 13 and name  H8)   3.80  2.00  0.70
assign (residue 12 and name H1')  (residue 20 and name  H2)   2.50  0.70  0.50
assign (residue 12 and name H2')  (residue 13 and name  H1')  3.80  2.00  0.70
assign (residue 12 and name H2')  (residue 13 and name  H8)   3.80  2.00  0.70
assign (residue 12 and name H3')  (residue 13 and name  H8)   3.80  2.00  0.70
assign (residue 12 and name H6)   (residue 20 and name  H2)   3.80  2.00  0.70

assign (residue 13 and name H1')  (residue 13 and name  H8)   3.80  2.00  0.70
assign (residue 13 and name H2')  (residue 13 and name  H8)   2.50  0.70  0.50
assign (residue 13 and name H3')  (residue 13 and name  H8)   2.50  0.70  0.50
assign (residue 13 and name H4')  (residue 13 and name  H8)   5.00  2.00  1.00

assign (residue 13 and name H1')  (residue 14 and name  H8)   6.00  2.00  1.00
assign (residue 13 and name H2')  (residue 14 and name  H1')  5.00  2.00  1.00
assign (residue 13 and name H2')  (residue 14 and name  H8)   3.80  2.00  0.70
assign (residue 13 and name H3')  (residue 14 and name  H8)   3.80  2.00  0.70

assign (residue 14 and name H1')  (residue 14 and name  H8)   3.80  2.00  0.70
assign (residue 14 and name H2')  (residue 14 and name  H8)   2.50  0.70  0.50
assign (residue 14 and name H3')  (residue 14 and name  H8)   2.50  0.70  0.50
assign (residue 14 and name H4')  (residue 14 and name  H8)   5.00  2.00  1.00
assign (residue 14 and name H5")  (residue 14 and name  H8)   3.80  2.00  0.70

assign (residue 14 and name H1')  (residue 15 and name  H1')  5.00  2.00  1.00
assign (residue 14 and name H1')  (residue 15 and name  H5)   5.00  2.00  1.00
assign (residue 14 and name H1')  (residue 15 and name  H6)   5.00  2.00  1.00
assign (residue 14 and name H2')  (residue 15 and name  H1')  5.00  2.00  1.00
assign (residue 14 and name H2')  (residue 15 and name  H5)   3.80  2.00  0.70
assign (residue 14 and name H2')  (residue 15 and name  H6)   2.50  0.70  0.50
assign (residue 14 and name H3')  (residue 15 and name  H5)   3.80  2.00  0.70
assign (residue 14 and name H3')  (residue 15 and name  H6)   3.80  2.00  0.70
assign (residue 14 and name H8)   (residue 15 and name  H5)   6.00  2.00  1.00
assign (residue 14 and name H8)   (residue 15 and name  H6)   3.80  2.00  0.70

assign (residue 15 and name H1')  (residue 15 and name  H6)   3.80  2.00  0.70
assign (residue 15 and name H2')  (residue 15 and name  H5)   5.00  2.00  1.00
assign (residue 15 and name H2')  (residue 15 and name  H6)   2.50  0.70  0.50
assign (residue 15 and name H3')  (residue 15 and name  H5)   5.00  2.00  1.00
assign (residue 15 and name H3')  (residue 15 and name  H6)   2.50  0.70  0.50
```

```
assign (residue 15 and name H4')  (residue 15 and name  H6)   5.00  2.00  1.00
assign (residue 15 and name H5')  (residue 15 and name  H6)   3.80  2.00  0.70
assign (residue 15 and name H5")  (residue 15 and name  H6)   3.80  2.00  0.70

assign (residue 15 and name H1')  (residue 16 and name  H1')  5.00  2.00  1.00
assign (residue 15 and name H1')  (residue 16 and name  H2)   3.80  2.00  0.70
assign (residue 15 and name H1')  (residue 16 and name  H8)   5.00  2.00  1.00
assign (residue 15 and name H2')  (residue 16 and name  H1')  5.00  2.00  1.00
assign (residue 15 and name H2')  (residue 16 and name  H8)   3.80  2.00  0.70
assign (residue 15 and name H3')  (residue 16 and name  H8)   5.00  2.00  1.00
assign (residue 15 and name H6)   (residue 16 and name  H8)   5.00  2.00  1.00

assign (residue 16 and name H1')  (residue 16 and name  H2)   3.80  2.00  0.70
assign (residue 16 and name H1')  (residue 16 and name  H8)   3.80  2.00  0.70
assign (residue 16 and name H2')  (residue 16 and name  H2)   5.00  2.00  1.00
assign (residue 16 and name H2')  (residue 16 and name  H8)   2.50  0.70  0.50
assign (residue 16 and name H3')  (residue 16 and name  H8)   2.50  0.70  0.50
assign (residue 16 and name H4')  (residue 16 and name  H8)   5.00  2.00  1.00
assign (residue 16 and name H5')  (residue 16 and name  H8)   3.80  2.00  0.70
assign (residue 16 and name H5")  (residue 16 and name  H8)   3.80  2.00  0.70

assign (residue 16 and name H1')  (residue 17 and name  H1')  5.00  2.00  1.00
assign (residue 16 and name H1')  (residue 17 and name  H5)   5.00  2.00  1.00
assign (residue 16 and name H1')  (residue 17 and name  H6)   6.00  2.00  1.00
assign (residue 16 and name H2')  (residue 17 and name  H1')  3.80  2.00  0.70
assign (residue 16 and name H2')  (residue 17 and name  H5)   3.80  2.00  0.70
assign (residue 16 and name H2')  (residue 17 and name  H6)   3.80  2.00  0.70
assign (residue 16 and name H3')  (residue 17 and name  H5)   3.80  2.00  0.70
assign (residue 16 and name H3')  (residue 17 and name  H6)   3.80  2.00  0.70
assign (residue 16 and name H2)   (residue 17 and name  H1')  3.80  2.00  0.70
assign (residue 16 and name H2)   (residue 17 and name  H6)   5.00  2.00  1.00
assign (residue 16 and name H8)   (residue 17 and name  H5)   6.00  2.00  1.00
assign (residue 16 and name H8)   (residue 17 and name  H6)   3.80  2.00  0.70

assign (residue 17 and name H1')  (residue 17 and name  H6)   3.80  2.00  0.70
assign (residue 17 and name H2')  (residue 17 and name  H5)   5.00  2.00  1.00
assign (residue 17 and name H2')  (residue 17 and name  H6)   2.50  0.70  0.50
assign (residue 17 and name H3')  (residue 17 and name  H6)   2.50  0.70  0.50
assign (residue 17 and name H5")  (residue 17 and name  H6)   3.80  2.00  0.70

assign (residue 17 and name H1')  (residue 18 and name  H6)   5.00  2.00  1.00
assign (residue 17 and name H2')  (residue 18 and name  H1')  3.80  2.00  0.70
assign (residue 17 and name H2')  (residue 18 and name  H5)   3.80  2.00  0.70
assign (residue 17 and name H2')  (residue 18 and name  H6)   5.00  2.00  1.00
assign (residue 17 and name H3')  (residue 18 and name  H6)   3.80  2.00  0.70
assign (residue 17 and name H6)   (residue 18 and name  H6)   5.00  2.00  1.00

assign (residue 18 and name H1')  (residue 18 and name  H6)   3.80  2.00  0.70
assign (residue 18 and name H2')  (residue 18 and name  H5)   5.00  2.00  1.00
assign (residue 18 and name H2')  (residue 18 and name  H6)   2.50  0.70  0.50
assign (residue 18 and name H3')  (residue 18 and name  H6)   2.50  0.70  0.50
```

```
assign (residue 18 and name H4')   (residue 18 and name  H6)   5.00  2.00  1.00
assign (residue 18 and name H5")  (residue 18 and name  H6)   3.80  2.00  0.70

assign (residue 18 and name H1')   (residue 19 and name  H1')  5.00  2.00  1.00
assign (residue 18 and name H1')   (residue 19 and name  H8)   5.00  2.00  1.00
assign (residue 18 and name H2')   (residue 19 and name  H8)   3.80  2.00  0.70
assign (residue 18 and name H3')   (residue 19 and name  H8)   3.80  2.00  0.70

assign (residue 19 and name H1')   (residue 19 and name  H8)   3.80  2.00  0.70
assign (residue 19 and name H2')   (residue 19 and name  H8)   3.80  2.00  0.70
assign (residue 19 and name H3')   (residue 19 and name  H8)   2.50  0.70  0.50
assign (residue 19 and name H4')   (residue 19 and name  H8)   5.00  2.00  1.00

assign (residue 19 and name H1')   (residue 20 and name  H1')  5.00  2.00  1.00
assign (residue 19 and name H1')   (residue 20 and name  H8)   3.80  2.00  0.70
assign (residue 19 and name H2')   (residue 20 and name  H1')  5.00  2.00  1.00
assign (residue 19 and name H2')   (residue 20 and name  H8)   2.50  0.70  0.50
assign (residue 19 and name H3')   (residue 20 and name  H8)   3.80  2.00  0.70
assign (residue 19 and name H8)    (residue 20 and name  H8)   5.00  2.00  1.00

assign (residue 20 and name H1')   (residue 20 and name  H2)   3.80  2.00  0.70
assign (residue 20 and name H1')   (residue 20 and name  H8)   3.80  2.00  0.70
assign (residue 20 and name H2')   (residue 20 and name  H8)   3.80  2.00  0.70
assign (residue 20 and name H3')   (residue 20 and name  H8)   2.50  0.70  0.50
assign (residue 20 and name H4')   (residue 20 and name  H8)   5.00  2.00  1.00
assign (residue 20 and name H5")  (residue 20 and name  H8)   3.80  2.00  0.70

assign (residue 20 and name H2)    (residue 21 and name  H1')  3.80  2.00  0.70
assign (residue 20 and name H2)    (residue 21 and name  H2')  5.00  2.00  1.00
assign (residue 20 and name H1')   (residue 21 and name  H1')  5.00  2.00  1.00
assign (residue 20 and name H1')   (residue 21 and name  H8)   5.00  2.00  1.00
assign (residue 20 and name H2')   (residue 21 and name  H1')  5.00  2.00  1.00
assign (residue 20 and name H2')   (residue 21 and name  H8)   3.80  2.00  0.70
assign (residue 20 and name H3')   (residue 21 and name  H8)   3.80  2.00  0.70

assign (residue 21 and name H1')   (residue 21 and name  H8)   3.80  2.00  0.70
assign (residue 21 and name H2')   (residue 21 and name  H8)   3.80  2.00  0.70
assign (residue 21 and name H3')   (residue 21 and name  H8)   2.50  0.70  0.50

assign (residue 21 and name H1')   (residue 22 and name  H1')  5.00  2.00  1.00
assign (residue 21 and name H1')   (residue 22 and name  H6)   3.80  2.00  0.70
assign (residue 21 and name H2')   (residue 22 and name  H1')  3.80  2.00  0.70
assign (residue 21 and name H2')   (residue 22 and name  H5)   3.80  2.00  0.70
assign (residue 21 and name H2')   (residue 22 and name  H6)   2.50  0.70  0.50
assign (residue 21 and name H3')   (residue 22 and name  H5)   3.80  2.00  0.70
assign (residue 21 and name H3')   (residue 22 and name  H6)   3.80  2.00  0.70
assign (residue 21 and name H8)    (residue 22 and name  H5)   3.80  2.00  0.70
assign (residue 21 and name H8)    (residue 22 and name  H6)   3.80  2.00  0.70

assign (residue 22 and name H1')   (residue 22 and name  H6)   3.80  2.00  0.70
assign (residue 22 and name H2')   (residue 22 and name  H5)   5.00  2.00  1.00
```

```
assign (residue 22 and name H2')  (residue 22 and name  H6)   6.00  2.00  1.00
assign (residue 22 and name H3')  (residue 22 and name  H5)   5.00  2.00  1.00
assign (residue 22 and name H3')  (residue 22 and name  H6)   3.80  2.00  0.70
assign (residue 22 and name H4')  (residue 22 and name  H6)   5.00  2.00  1.00

assign (residue 22 and name H1')  (residue 23 and name  H1')  5.00  2.00  1.00
assign (residue 22 and name H1')  (residue 23 and name  H8)   3.80  2.00  0.70
assign (residue 22 and name H2')  (residue 23 and name  H1')  3.80  2.00  0.70
assign (residue 22 and name H2')  (residue 23 and name  H8)   2.50  0.70  0.50
assign (residue 22 and name H3')  (residue 23 and name  H8)   3.80  2.00  0.70
assign (residue 22 and name H6)   (residue 23 and name  H8)   5.00  2.00  1.00

assign (residue 23 and name H1')  (residue 23 and name  H2)   5.00  2.00  1.00
assign (residue 23 and name H1')  (residue 23 and name  H8)   3.80  2.00  0.70
assign (residue 23 and name H2')  (residue 23 and name  H2)   5.00  2.00  1.00
assign (residue 23 and name H2')  (residue 23 and name  H8)   3.80  2.00  0.70
assign (residue 23 and name H3')  (residue 23 and name  H8)   2.50  0.70  0.50
assign (residue 23 and name H4')  (residue 23 and name  H8)   5.00  2.00  1.00
assign (residue 23 and name H5")  (residue 23 and name  H8)   3.80  2.00  0.70

assign (residue 23 and name H1')  (residue 24 and name  H1')  6.00  2.00  1.00
assign (residue 23 and name H1')  (residue 24 and name  H5)   5.00  2.00  1.00
assign (residue 23 and name H1')  (residue 24 and name  H6)   5.00  2.00  1.00
assign (residue 23 and name H2')  (residue 24 and name  H1')  3.80  2.00  0.70
assign (residue 23 and name H2')  (residue 24 and name  H5)   3.80  2.00  0.70
assign (residue 23 and name H2')  (residue 24 and name  H6)   2.50  0.70  0.50
assign (residue 23 and name H3')  (residue 24 and name  H5)   2.50  0.70  0.50
assign (residue 23 and name H3')  (residue 24 and name  H6)   3.80  2.00  0.70
assign (residue 23 and name H2)   (residue 24 and name  H1')  3.80  2.00  0.70
assign (residue 23 and name H2)   (residue 24 and name  H2')  5.00  2.00  1.00
assign (residue 23 and name H2)   (residue 24 and name  H6)   5.00  2.00  1.00
assign (residue 23 and name H8)   (residue 24 and name  H5)   3.80  2.00  0.70
assign (residue 23 and name H8)   (residue 24 and name  H6)   5.00  2.00  1.00

assign (residue 24 and name H1')  (residue 24 and name  H5)   5.00  2.00  1.00
assign (residue 24 and name H1')  (residue 24 and name  H6)   3.80  2.00  0.70
assign (residue 24 and name H2')  (residue 24 and name  H6)   3.80  2.00  0.70
assign (residue 24 and name H3')  (residue 24 and name  H5)   5.00  2.00  1.00
assign (residue 24 and name H3')  (residue 24 and name  H6)   2.50  0.70  0.50
assign (residue 24 and name H4')  (residue 24 and name  H6)   5.00  2.00  1.00

assign (residue 24 and name H1')  (residue 25 and name  H1')  5.00  2.00  1.00
assign (residue 24 and name H1')  (residue 25 and name  H8)   3.80  2.00  0.70
assign (residue 24 and name H2')  (residue 25 and name  H1')  3.80  2.00  0.70
assign (residue 24 and name H2')  (residue 25 and name  H8)   2.50  0.70  0.50
assign (residue 24 and name H3')  (residue 25 and name  H8)   3.80  2.00  0.70
assign (residue 24 and name H5)   (residue 25 and name  H8)   5.00  2.00  1.00
assign (residue 24 and name H6)   (residue 25 and name  H8)   3.80  2.00  0.70

assign (residue 25 and name H1')  (residue 25 and name  H2)   3.80  2.00  0.70
assign (residue 25 and name H1')  (residue 25 and name  H8)   3.80  2.00  0.70
```

```
assign (residue 25 and name H2')  (residue 25 and name  H2)   5.00  2.00  1.00
assign (residue 25 and name H2')  (residue 25 and name  H8)   3.80  2.00  0.70
assign (residue 25 and name H3')  (residue 25 and name  H8)   2.50  0.70  0.50
assign (residue 25 and name H5")  (residue 25 and name  H8)   3.80  2.00  0.70

assign (residue 25 and name H1')  (residue 26 and name  H1')  5.00  2.00  1.00
assign (residue 25 and name H1')  (residue 26 and name  H5)   5.00  2.00  1.00
assign (residue 25 and name H1')  (residue 26 and name  H6)   3.80  2.00  0.70
assign (residue 25 and name H2')  (residue 26 and name  H1')  3.80  2.00  0.70
assign (residue 25 and name H2')  (residue 26 and name  H5)   3.80  2.00  0.70
assign (residue 25 and name H2')  (residue 26 and name  H6)   2.50  0.70  0.50
assign (residue 25 and name H3')  (residue 26 and name  H5)   3.80  2.00  0.70
assign (residue 25 and name H3')  (residue 26 and name  H6)   3.80  2.00  0.70
assign (residue 25 and name H2)   (residue 26 and name  H1')  3.80  2.00  0.70
assign (residue 25 and name H2)   (residue 26 and name  H2')  6.00  2.00  1.00
assign (residue 25 and name H2)   (residue 26 and name  H6)   5.00  2.00  1.00
assign (residue 25 and name H8)   (residue 26 and name  H5)   5.00  2.00  1.00
assign (residue 25 and name H8)   (residue 26 and name  H6)   3.80  2.00  0.70

assign (residue 26 and name H1')  (residue 26 and name  H5)   5.00  2.00  1.00
assign (residue 26 and name H1')  (residue 26 and name  H6)   3.80  2.00  0.70
assign (residue 26 and name H2')  (residue 26 and name  H5)   5.00  2.00  1.00
assign (residue 26 and name H2')  (residue 26 and name  H6)   3.80  2.00  0.70
assign (residue 26 and name H3')  (residue 26 and name  H5)   3.80  2.00  0.70
assign (residue 26 and name H3')  (residue 26 and name  H6)   2.50  0.70  0.50
assign (residue 26 and name H4')  (residue 26 and name  H5)   5.00  2.00  1.00
assign (residue 26 and name H4')  (residue 26 and name  H6)   5.00  2.00  1.00
assign (residue 26 and name H5")  (residue 26 and name  H6)   3.80  2.00  0.70

assign (residue 26 and name H1')  (residue 27 and name  H1')  5.00  2.00  1.00
assign (residue 26 and name H1')  (residue 27 and name  H6)   3.80  2.00  0.70
assign (residue 26 and name H2')  (residue 27 and name  H1')  3.80  2.00  0.70
assign (residue 26 and name H2')  (residue 27 and name  H5)   3.80  2.00  0.70
assign (residue 26 and name H2')  (residue 27 and name  H6)   2.50  0.70  0.50
assign (residue 26 and name H3')  (residue 27 and name  H5)   3.80  2.00  0.70
assign (residue 26 and name H3')  (residue 27 and name  H6)   3.80  2.00  0.70
assign (residue 26 and name H5)   (residue 27 and name  H5)   2.50  0.70  0.50
assign (residue 26 and name H6)   (residue 27 and name  H5)   2.50  0.70  0.50
assign (residue 26 and name H6)   (residue 27 and name  H6)   3.80  2.00  0.70

assign (residue 27 and name H1')  (residue 27 and name  H5)   5.00  2.00  1.00
assign (residue 27 and name H1')  (residue 27 and name  H6)   3.80  2.00  0.70
assign (residue 27 and name H2')  (residue 27 and name  H5)   5.00  2.00  1.00
assign (residue 27 and name H2')  (residue 27 and name  H6)   3.80  2.00  0.70
assign (residue 27 and name H3')  (residue 27 and name  H5)   5.00  2.00  1.00
assign (residue 27 and name H3')  (residue 27 and name  H6)   2.50  0.70  0.50
assign (residue 27 and name H4')  (residue 27 and name  H6)   5.00  2.00  1.00
assign (residue 27 and name H5")  (residue 27 and name  H6)   3.80  2.00  0.70

assign (residue 27 and name H1')  (residue 28 and nameH1')    6.00  2.00  1.00
assign (residue 27 and name H1')  (residue 28 and name  H5)   5.00  2.00  1.00
```

assign (residue 27 and name H1') (residue 28 and name H6) 3.80 2.00 0.70
assign (residue 27 and name H2') (residue 28 and name H1') 3.80 2.00 0.70
assign (residue 27 and name H2') (residue 28 and name H5) 3.80 2.00 0.70
assign (residue 27 and name H2') (residue 28 and name H6) 3.80 2.00 0.70
assign (residue 27 and name H3') (residue 28 and name H5) 3.80 2.00 0.70
assign (residue 27 and name H3') (residue 28 and name H6) 3.80 2.00 0.70
assign (residue 27 and name H5) (residue 28 and name H5) 5.00 2.00 1.00

assign (residue 28 and name H1') (residue 28 and name H6) 3.80 2.00 0.70
assign (residue 28 and name H2') (residue 28 and name H5) 5.00 2.00 1.00
assign (residue 28 and name H2') (residue 28 and name H6) 3.80 2.00 0.70
assign (residue 28 and name H3') (residue 28 and name H6) 2.50 0.70 0.50
assign (residue 28 and name H4') (residue 28 and name H6) 5.00 2.00 1.00
assign (residue 28 and name H5") (residue 28 and name H6) 3.80 2.00 0.70

assign (residue 28 and name H1') (residue 29 and name H1') 3.80 2.00 0.70
assign (residue 28 and name H1') (residue 29 and name H6) 3.80 2.00 0.70
assign (residue 28 and name H2') (residue 29 and name H1') 3.80 2.00 0.70
assign (residue 28 and name H2') (residue 29 and name H5) 3.80 2.00 0.70
assign (residue 28 and name H2') (residue 29 and name H6) 2.50 0.70 0.50
assign (residue 28 and name H3') (residue 29 and name H6) 3.80 2.00 0.70
assign (residue 28 and name H5) (residue 29 and name H5) 3.80 2.00 0.70
assign (residue 28 and name H6) (residue 29 and name H5) 3.80 2.00 0.70
assign (residue 28 and name H6) (residue 29 and name H6) 3.80 2.00 0.70

assign (residue 29 and name H1') (residue 29 and name H5) 5.00 2.00 1.00
assign (residue 29 and name H1') (residue 29 and name H6) 3.80 2.00 0.70
assign (residue 29 and name H2') (residue 29 and name H5) 5.00 2.00 1.00
assign (residue 29 and name H2') (residue 29 and name H6) 3.80 2.00 0.70
assign (residue 29 and name H3') (residue 29 and name H6) 2.50 0.70 0.50
assign (residue 29 and name H4') (residue 29 and name H5) 6.00 2.00 1.00
assign (residue 29 and name H4') (residue 29 and name H6) 3.80 2.00 0.70

Distance constraints of exchangeable protons in d3'-EBS1* based on a 2D [^{1}H,^{1}H]-NOESY spectrum acquired at 700 MHz proton frequency at 278 K (90% H_2O/10% D_2O, 10 mM KCl, 10 µM EDTA, pH = 6.52).

assign (residue 1 and name H1) (residue 2 and name H1') 6.00 2.00 1.00
assign (residue 1 and name H1) (residue 2 and name H1) 5.00 2.00 1.00
assign (residue 1 and name H1) (residue 2 and name H8) 6.00 2.00 1.00

assign (residue 1 and name H1) (residue 28 and name H1') 6.00 2.00 1.00
assign (residue 1 and name H1) (residue 29 and name H41) 2.50 0.70 0.50
assign (residue 1 and name H1) (residue 29 and name H42) 3.80 2.00 0.70
assign (residue 1 and name H1) (residue 29 and name H5) 6.00 2.00 1.00
assign (residue 1 and name H1) (residue 29 and name H6) 6.00 2.00 1.00

assign (residue 2 and name H1) (residue 3 and name H1') 6.00 2.00 1.00
assign (residue 2 and name H1) (residue 3 and name H2) 5.00 2.00 1.00
assign (residue 2 and name H1) (residue 3 and name H8) 6.00 2.00 1.00

```
assign (residue  2 and name  H1)   (residue 27 and name  H3)   5.00  2.00  1.00
assign (residue  2 and name  H1)   (residue 28 and name  H41)  2.50  0.70  0.50
assign (residue  2 and name  H1)   (residue 28 and name  H42)  3.80  2.00  0.70
assign (residue  2 and name  H1)   (residue 28 and name  H5)   6.00  2.00  1.00
assign (residue  2 and name  H1)   (residue 28 and name  H6)   6.00  2.00  1.00
assign (residue  2 and name  H1)   (residue 29 and name  H5)   6.00  2.00  1.00
assign (residue  2 and name  H1)   (residue 29 and name  H6)   5.00  2.00  1.00

assign (residue  4 and name  H1)   (residue  3 and name  H2)   5.00  2.00  1.00
assign (residue  4 and name  H1)   (residue  5 and name  H3)   3.80  2.00  1.00
assign (residue  4 and name  H1)   (residue  5 and name  H1')  6.00  2.00  1.00

assign (residue  4 and name  H1)   (residue 26 and name  H41)  2.50  0.70  0.50
assign (residue  4 and name  H1)   (residue 26 and name  H42)  3.80  2.00  0.70
assign (residue  4 and name  H1)   (residue 26 and name  H5)   5.00  2.00  1.00
assign (residue  4 and name  H1)   (residue 27 and name  H3)   3.80  2.00  0.70
assign (residue  4 and name  H1)   (residue 27 and name  H5)   5.00  2.00  1.00
assign (residue  4 and name  H1)   (residue 27 and name  H6)   5.00  2.00  1.00

assign (residue  5 and name  H3)   (residue  4 and name  H22)  6.00  2.00  1.00
assign (residue  5 and name  H3)   (residue  5 and name  H1')  5.00  2.00  1.00
assign (residue  5 and name  H3)   (residue  6 and name  H1')  5.00  2.00  1.00
assign (residue  5 and name  H3)   (residue  6 and name  H8)   5.00  2.00  1.00

assign (residue  5 and name  H3)   (residue 24 and name  H3)   3.80  2.00  0.70
assign (residue  5 and name  H3)   (residue 25 and name  H2)   3.80  2.00  0.70
assign (residue  5 and name  H3)   (residue 25 and name  H61)  2.50  0.70  0.50
assign (residue  5 and name  H3)   (residue 25 and name  H62)  3.80  0.30  0.40
assign (residue  5 and name  H3)   (residue 26 and name  H1')  6.00  2.00  1.00
assign (residue  5 and name  H3)   (residue 26 and name  H41)  3.80  0.30  0.40

assign (residue  7 and name  H3)   (residue  6 and name  H2)   5.00  2.00  1.00
assign (residue  7 and name  H3)   (residue  7 and name  H1')  5.00  2.00  1.00
assign (residue  7 and name  H3)   (residue  8 and name  H1')  5.00  2.00  1.00
assign (residue  7 and name  H3)   (residue  8 and name  H1)   3.80  2.00  0.70
assign (residue  7 and name  H3)   (residue  8 and name  H8)   5.00  2.00  1.00

assign (residue  7 and name  H3)   (residue 23 and name  H2)   3.80  2.00  0.70
assign (residue  7 and name  H3)   (residue 23 and name  H61)  2.50  0.70  0.50
assign (residue  7 and name  H3)   (residue 23 and name  H62)  3.80  0.30  0.40
assign (residue  7 and name  H3)   (residue 24 and name  H5)   5.00  2.00  1.00

assign (residue  8 and name  H1)   (residue  9 and name  H1')  6.00  2.00  1.00
assign (residue  8 and name  H1)   (residue  9 and name  H3)   3.80  2.00  0.70
assign (residue  8 and name  H1)   (residue  9 and name  H5)   6.00  2.00  1.00
assign (residue  8 and name  H1)   (residue  9 and name  H6)   6.00  2.00  1.00

assign (residue  8 and name  H1)   (residue 21 and name  H1)   5.00  2.00  1.00
assign (residue  8 and name  H1)   (residue 21 and name  H22)  6.00  2.00  1.00
assign (residue  8 and name  H1)   (residue 22 and name  H41)  2.50  0.70  0.50
```

```
assign (residue  8 and name  H1)   (residue 22 and name  H42) 3.80  2.00  0.70
assign (residue  8 and name  H1)   (residue 22 and name  H5)  6.00  2.00  1.00
assign (residue  8 and name  H1)   (residue 22 and name  H6)  6.00  2.00  1.00
assign (residue  8 and name  H1)   (residue 23 and name  H2)  5.00  2.00  1.00
assign (residue  8 and name  H1)   (residue 23 and name  H61) 6.00  2.00  1.00

assign (residue  9 and name  H3)   (residue 21 and name  H1)  2.50  0.70  0.50
assign (residue  9 and name  H3)   (residue 21 and name  H21) 5.00  2.00  1.00
assign (residue  9 and name  H3)   (residue 21 and name  H22) 3.80  0.30  0.40
assign (residue  9 and name  H3)   (residue 22 and name  H41) 3.80  0.30  0.40
assign (residue  9 and name  H3)   (residue 22 and name  H42) 3.80  0.30  0.40
assign (residue  9 and name  H3)   (residue 22 and name  H5)  6.00  2.00  1.00

assign (residue 21 and name H1)   (residue 22 and name  H1')  6.00  2.00  1.00
assign (residue 21 and name H1)   (residue 22 and name  H41) 6.00  2.00  1.00
assign (residue 21 and name H1)   (residue 22 and name  H42) 5.00  2.00  1.00
assign (residue 21 and name H1)   (residue 22 and name  H5)  6.00  2.00  1.00
assign (residue 21 and name H1)   (residue 22 and name  H6)  6.00  2.00  1.00

assign (residue 21 and name H1)   (residue  9 and name  H1')  5.00  2.00  1.00
assign (residue 21 and name H1)   (residue  9 and name  H5)  6.00  2.00  1.00
assign (residue 21 and name H1)   (residue  8 and name  H21) 5.00  2.00  1.00

assign (residue 24 and name H3)   (residue 23 and name  H2)  5.00  2.00  1.00
assign (residue 24 and name H3)   (residue 25 and name  H1')  5.00  2.00  1.00
assign (residue 24 and name H3)   (residue 25 and name  H8)  5.00  2.00  1.00

assign (residue 24 and name H3)   (residue  6 and name  H2)  3.80  2.00  0.70
assign (residue 24 and name H3)   (residue  6 and name  H61) 2.50  0.70  0.50
assign (residue 24 and name H3)   (residue  6 and name  H62) 3.80  0.30  0.40
assign (residue 24 and name H3)   (residue  7 and name  H3)  3.80  2.00  0.70
assign (residue 24 and name H3)   (residue  7 and name  H5)  5.00  2.00  1.00

assign (residue 27 and name H3)   (residue 28 and name  H5)  5.00  2.00  1.00
assign (residue 27 and name H3)   (residue 28 and name  H6)  6.00  2.00  1.00

assign (residue 27 and name H3)   (residue  3 and name  H2)  3.80  2.00  0.70
assign (residue 27 and name H3)   (residue  3 and name  H8)  6.00  2.00  1.00
assign (residue 27 and name H3)   (residue  3 and name  H61) 2.50  0.70  0.50
assign (residue 27 and name H3)   (residue  3 and name  H62) 3.80  0.30  0.40
assign (residue 27 and name H3)   (residue  4 and name  H1')  6.00  2.00  1.00
```

Hydrogen-bond restraints whose existence was proven by 2D [^{1}H,^{1}H]-NOESY spectrum acquired at 278 K at 700 MHz proton frequency (90% H_2O/10% D_2O, 10 mM KCl, 10 μM EDTA, pH = 6.52) and by a 2D J_{NN} HNN-COSY experiment acquired at 278 K (90% H_2O/10% D_2O, 10 mM KCl, 10 μM EDTA, pH = 6.87).

G1-C29
assign (residue 1 and name H1) (residue 29 and name N3) 2.00 0.20 0.20
assign (residue 1 and name N1) (residue 29 and name N3) 2.90 0.30 0.30
assign (residue 1 and name O6) (residue 29 and name H41) 2.00 0.20 0.20
assign (residue 1 and name O6) (residue 29 and name N4) 2.90 0.30 0.30
assign (residue 1 and name H21) (residue 29 and name O2) 2.00 0.20 0.20
assign (residue 1 and name N2) (residue 29 and name O2) 2.90 0.30 0.30

G2-C28
assign (residue 2 and name H1) (residue 28 and name N3) 2.00 0.20 0.20
assign (residue 2 and name N1) (residue 28 and name N3) 2.90 0.30 0.30
assign (residue 2 and name O6) (residue 28 and name H41) 2.00 0.20 0.20
assign (residue 2 and name O6) (residue 28 and name N4) 2.90 0.30 0.30
assign (residue 2 and name H21) (residue 28 and name O2) 2.00 0.20 0.20
assign (residue 2 and name N2) (residue 28 and name O2) 2.90 0.30 0.30

A3-U27
assign (residue 3 and name N1) (residue 27 and name H3) 2.00 0.20 0.20
assign (residue 3 and name N1) (residue 27 and name N3) 2.90 0.30 0.30
assign (residue 3 and name H61) (residue 27 and name O4) 2.00 0.20 0.20
assign (residue 3 and name N6) (residue 27 and name O4) 2.90 0.30 0.30

G4-C26
assign (residue 4 and name H1) (residue 26 and name N3) 2.00 0.20 0.20
assign (residue 4 and name N1) (residue 26 and name N3) 2.90 0.30 0.30
assign (residue 4 and name O6) (residue 26 and name H41) 2.00 0.20 0.20
assign (residue 4 and name O6) (residue 26 and name N4) 2.90 0.30 0.30
assign (residue 4 and name H21) (residue 26 and name O2) 2.00 0.20 0.20
assign (residue 4 and name N2) (residue 26 and name O2) 2.90 0.30 0.30

U5-A25
assign (residue 5 and name H3) (residue 25 and name N1) 2.00 0.20 0.20
assign (residue 5 and name N3) (residue 25 and name N1) 2.90 0.30 0.30
assign (residue 5 and name O4) (residue 25 and name H61) 2.00 0.20 0.20
assign (residue 5 and name O4) (residue 25 and name N6) 2.90 0.30 0.30

A6-U24
assign (residue 6 and name N1) (residue 24 and name H3) 2.00 0.20 0.20
assign (residue 6 and name N1) (residue 24 and name N3) 2.90 0.30 0.30
assign (residue 6 and name H61) (residue 24 and name O4) 2.00 0.20 0.20
assign (residue 6 and name N6) (residue 24 and name O4) 2.90 0.30 0.30

U7-A23
assign (residue 7 and name H3) (residue 23 and name N1) 2.00 0.20 0.20
assign (residue 7 and name N3) (residue 23 and name N1) 2.90 0.30 0.30
assign (residue 7 and name O4) (residue 23 and name H61) 2.00 0.20 0.20

```
assign (residue  7 and name  O4)   (residue 23 and name  N6)   2.90  0.30  0.30
```

G8-C22

```
assign (residue  8 and name  H1)   (residue 22 and name  N3)   2.00  0.20  0.20
assign (residue  8 and name  N1)   (residue 22 and name  N3)   2.90  0.30  0.30
assign (residue  8 and name  O6)   (residue 22 and name  H41)  2.00  0.20  0.20
assign (residue  8 and name  O6)   (residue 22 and name  N4)   2.90  0.30  0.30
assign (residue  8 and name  H21)  (residue 22 and name  O2)   2.00  0.20  0.20
assign (residue  8 and name  N2)   (residue 22 and name  O2)   2.90  0.30  0.30
```

U9-G21

```
assign (residue  9 and name  H3)   (residue 21 and name  H1)   1.90  0.10  0.20
assign (residue  9 and name  H3)   (residue 21 and name  O6)   1.90  0.10  0.20
assign (residue  9 and name  N3)   (residue 21 and name  O6)   2.90  0.10  0.20
assign (residue  9 and name  O2)   (residue 21 and name  H1)   1.90  0.10  0.20
assign (residue  9 and name  O2)   (residue 21 and name  N1)   2.90  0.10  0.20
```

Appendix 7 All RDCs used in the structure calculation of d3'-EBS1*

The first number represents the RDC value, the second and third the lower and upper error limits.

G13	C1'H1'	-7.6	2.0	2.0
U5	C6H6	14.7	2.0	2.0
U11	C6H6	9.11	2.0	2.0
U12	C6H6	9.81	2.0	2.0
C17	C6H6	4.91	2.0	2.0
U18	C6H6	9.11	2.0	2.0
C22	C6H6	25.91	2.0	2.0
G19	C8H8	23.8	2.0	2.0
A20	C8H8	29.41	2.0	2.0
A10	C2H2	22.42	2.0	2.0
A20	C2H2	25.9	2.0	2.0
A25	C2H2	49.01	2.0	2.0
U9	C5H5	52.98	2.0	2.0
U11	C5H5	31.59	2.0	2.0
U12	C5H5	25.8	2.0	2.0
C22	C5H5	34.03	2.0	2.0
U24	C5H5	30.64	2.0	2.0
U27	C5H5	28.41	2.0	2.0
G1	N1H1	18.94	2.0	2.0
G2	N1H1	15.25	2.0	2.0
G4	N1H1	22.41	2.0	2.0
G8	N1H1	25.68	2.0	2.0
G21	N1H1	26.6	2.0	2.0
U5	N3H3	24.5	2.0	2.0
U7	N3H3	24.9	2.0	2.0
U9	N3H3	25.2	2.0	2.0
U24	N3H3	25.2	2.0	2.0
U27	N3H3	7.45	2.0	2.0

Appendix 8 Dihedral angle restraints for the structure calculation of d3'-EBS1*

Phosphate-sugar-backbone dihedral angle restraints. β, γ and ε are only restrained for A-helical regions for residues with a 3'-endo sugar pucker. The number in the middle represents the angle in °, the two numbers to the right and the left are the error limits and the last number is a weighting factor. The exact values were taken from the dihedral angle restraint file of the structure calculation for D5-36, which represents a RNA hairpin structure.[34]

```
assign  (residue n-1    and name O3' )
        (residue n      and name P   )
        (residue n      and name O5' )
        (residue n      and name C5' )      20.0    -62.1   10.0    2       {*alpha*}

assign  (residue n      and name P   )
        (residue n      and name O5' )
        (residue n      and name C5' )
        (residue n      and name C4' )      20.0    -179.9  10.0    2       {*beta*}

assign  (residue n      and name O5' )
        (residue n      and name C5' )
        (residue n      and name C4' )
        (residue n      and name C3' )      20.0    47.44   10.0    2       {*gamma*}

assign  (residue n      and name C4' )
        (residue n      and name C3' )
        (residue n      and name O3' )
        (residue n+1    and name P   )      20.0    -151.7  10.0    2       {*epsilon*}

assign  (residue n      and name C3' )
        (residue n      and name O3' )
        (residue n+1    and name P   )
        (residue n+1    and name O5' )      20.0    -73.6   10.0    2       {*zeta*}
```

Sugar pucker restraints for 2'-endo and 3'-endo sugars. Helical A-type RNA is usually 3'-endo and does not give a strong H1'-H2' crosspeak in 2D [^{1}H,^{1}H]-TOCSY experiments. G1, A10 to A20 of the loop, and C29 were left unconstrained. The sugar pucker restraints are based on a 2D [^{1}H^{1}H]-TOCSY that was acquired at 293 K and 700 MHz proton frequency with 45 ms mixing time (100% D_2O containing 10 mM KCl and 10 μM EDTA, pD = 6.96).

```
2'-endo sugar pucker
assign  (residue n and name C5'  )
        (residue n and name C4'  )
        (residue n and name C3'  )
        (residue n and name O3'  )   20.0    145.0   30.0    2       {*delta*}

assign  (residue n and name O4'  )
        (residue n and name C1'  )
        (residue n and name C2'  )
        (residue n and name C3'  )   20.0    25.0    30.0    2       {*nu1*}

assign  (residue n and name C1'  )
        (residue n and name C2'  )
        (residue n and name C3'  )
        (residue n and name C4'  )   20.0    -35.0   30.0    2       {*nu2*}

3'-endo sugar pucker
assign  (residue n and name C5'  )
        (residue n and name C4'  )
        (residue n and name C3'  )
        (residue n and name O3'  )   20.0    85.0    30.0    2       {*delta*}

assign  (residue n and name O4'  )
        (residue n and name C1'  )
        (residue n and name C2'  )
        (residue n and name C3'  )   20.0    -25.0   30.0    2       {*nu1*}

assign  (residue n and name C1'  )
        (residue n and name C2'  )
        (residue n and name C3'  )
        (residue n and name C4'  )   20.0    37.3    30.0    2       {*nu2*}
```

Restraints for the torsion angle χ, which defines the orientation of the base to the sugar around the glycosidic bond. All χ angles were constrained to be in an *anti* orientation because of the absence of strong H1'-H8/H6 crosspeaks in the short mixing time 2D [^{1}H,^{1}H]-NOESYs recorded in D_2O.

```
torsion angle χ
assign  (residue n and name O4'  )
        (residue n and name C1'  )
        (residue n and name N9   )
        (residue n and name C4   )   20.0    -160    20.0    2
```

Appendix 9 Chemical shift values of the H1', H2, H5, H6 and H8 protons of d3'-EBS1* (0.5 mM in 100% D_2O, 10 mM KCl, 10 μM EDTA, pD = 6.96) upon addition of Mg^{2+}. All the protons that were used for the calculation of the affinity constants are listed according to their binding sites. The chemical shifts were extracted from 2D [$^1H^1H$]-NOESY spectra recorded on a 700 MHz Bruker Avance spectrometer at 298 K. The values that were omitted in the fitting procedure to calculate the log K_A values are marked in bold.

Mg^{2+}[mM]	0	0.5	1	1.5	2	2.5	3	4	5	6	6.5	7
5' end												
G1H8	8.027	8.062	8.076	8.087	8.095	8.104	8.102	8.100	-	-	-	-
H1												
A3H1'	5.901	5.898	5.895	5.892	5.889	5.888	5.885	5.882	5.875	-	-	-
G4H1'	5.459	5.464	5.469	5.475	5.481	5.486	5.489	5.496	5.498	5.496	5.497	5.494
G4H8	6.968	6.979	6.990	7.002	7.015	7.027	7.034	7.050	7.058	7.057	7.062	7.064
U5H6	7.577	7.580	7.596	7.608	7.618	7.627	7.636	7.649	7.656	7.658	7.657	7.659
A25H8	8.041	8.043	8.052	8.054	8.056	8.062	8.062	8.067	8.066	8.067	8.063	8.063
C26H1	5.265	5.270	5.273	5.277	5.279	5.282	5.283	5.284	5.284	5.283	5.284	5.283
C26H6	7.428	7.443	7.458	7.475	7.489	7.502	7.511	7.532	7.537	7.551	7.553	7.557
U27H6	7.801	7.804	7.807	7.814	7.820	7.825	7.824	7.832	7.838	7.842	7.838	7.840
L1												
A10H1'	5.896	5.901	5.910	5.920	5.930	5.937	5.944	5.954	5.956	5.960	5.960	5.957
A10H2	7.703	7.725	7.750	7.780	7.811	7.828	7.851	7.876	7.908	7.894	-	-
A10H8	8.142	8.153	8.167	8.184	8.197	8.209	8.219	8.233	8.241	8.240	8.235	8.241
U11H1'	5.433	5.438	5.442	5.445	5.449	5.452	5.455	5.459	5.461	5.457	-	-
U11H5	5.338	5.347	5.358	5.373	5.387	5.400	5.409	5.425	5.435	5.442	5.445	-
U11H6	7.571	7.579	7.598	7.617	7.637	7.657	7.671	7.698	7.719	7.729	7.725	-
U12H6	7.624	7.629	7.634	7.646	7.653	7.660	7.668	7.671	7.672	7.673	7.671	7.672
A20H1'	5.909	5.907	5.903	5.898	5.893	5.891	5.888	5.886	5.887	-	-	-
A20H2	7.859	7.856	7.845	7.833	7.822	7.814	7.803	7.786	7.774	7.764	7.758	
A20H8	7.968	7.964	7.950	7.933	7.92	7.905	7.890	7.872	7.858	-	-	-
G21H1'	5.467	5.461	5.451	5.444	5.435	5.430	5.420	5.415	5.412	5.409	-	-
L2												
A16H1'	5.842	5.838	5.835	5.831	5.827	5.825	5.823	5.818	5.817	5.818	5.818	**5.822**
A16H8	8.133	8.132	8.129	8.122	8.117	8.119	8.114	8.107	8.104	8.102	8.100	8.098
U18H1'	5.711	5.716	5.721	5.728	5.735	5.739	5.740	5.74	5.731	5.726	5.728	5.711
U18H6	7.628	7.632	7.637	7.643	7.652	7.658	7.659	7.665	7.666	7.663	7.662	7.662
G19H1'	5.517	5.524	5.530	5.536	5.540	5.546	5.550	5.556	**5.547**	-	-	-
G19H8	7.682	7.687	7.694	7.700	7.707	7.716	7.723	7.731	7.742	7.746	-	-
free												
U5H1'	5.432	5.428	5.425	5.422	5.420	5.418	5.417	5.414	5.411	5.406	5.404	5.402
A6H2	6.946	6.944	6.941	6.938	6.936	6.934	6.932	6.931	6.924	6.923	6.922	6.946
U7H6	7.481	7.485	7.485	7.492	7.498	7.505	7.508	7.513	7.518	7.521	7.521	7.520
G8H1'	5.651	5.649	5.644	5.641	5.638	5.635	5.633	5.631	5.628	5.625	5.627	5.629
G8H8	7.483	7.482	7.479	7.476	7.473	7.469	7.466	7.462	7.454	7.450	7.449	7.447
U9H1'	5.481	5.483	5.489	5.497	5.505	5.511	5.514	5.518	5.522	5.517	-	-
U12H1'	5.549	5.547	5.541	5.534	5.524	5.518	5.510	5.496	5.487	5.476	5.476	-
C22H1'	5.273	5.272	5.268	5.264	5.261	5.258	5.255	5.251	5.249	5.247	5.245	5.243
C22H6	7.562	7.566	7.572	7.578	7.586	7.591	7.590	7.597	7.596	7.592	7.594	7.599
A23H2	7.195	7.200	7.206	7.211	7.217	7.224	7.227	7.233	7.235	7.234	7.232	7.232
A23H8	7.919	7.925	7.931	7.942	7.950	7.958	7.961	7.97	7.973	7.972	7.976	7.972
U24H6	7.553	7.563	7.577	7.587	7.600	7.613	7.616	7.628	7.637	7.637	7.642	7.643
U27H1	5.435	5.433	5.431	5.428	5.425	5.423	5.420	5.416	5.412	5.408	5.405	5.406

Appendix 10 Affinity constants log $K_{A,est}$ values for Mg^{2+} binding to d3'-EBS1*

A Listed are the individual log $K_{A,est}$ values obtained from the change in chemical shifts of all aromatic and H1' protons in d3'-EBS1* after the first round of calculation in which the Mg^{2+} concentration corresponds to the total amount of Mg^{2+} added at each titration point.[a] The nucleotides belonging to the four individual binding sites are shaded by alternative grey scales.

	5'-end		H1							L1					
residue	G1	G2	A3	G4	U5	A6	U7	G8	U9	A10	U11	U12	G13	G14	C15
H1'	n.d.[c]	n.d.[b]	2.39 ± 0.22	2.65± 0.15	1.76 ± 0.21	n.d.[b]	n.d.[b]	2.55 ± 0.13	2.56 ± 0.23	2.51 ± 0.13	2.32± 0.08	1.63 ± 0.25	n.d.[b]	n.d.[b]	n.d.[d]
H2/H5	–	–	n.d.[b]	–	n.d.[b]	1.84 ± 0.19	n.d.[b]	–	n.d.[b]	2.36 ± 0.15	2.24 ± 0.10	n.d.[b]	–	–	n.d.[d]
H6/H8	3.3 ± 0.13	n.d.[c]	n.d.[b]	2.42 ± 0.1	2.45 ± 0.12	n.d.[c]	2.25 ± 0.17	1.39 ± 0.29	n.d.[b]	2.59 ± 0.12	2.14 ± 0.14	2.68 ± 0.16	n.d.[b]	n.d.[b]	n.d.[d]

			H1						L1			L2		
residue	C29	C28	U27	C26	A25	U24	A23	C22	G21	A20	G19	U18	C17	A16
H1'	n.d.[d]	n.d.[b]	1.62 ± 0.16	3.02 ± 0.12	n.d.[b]	n.d.[d]	n.d.[c]	2.18 ± 0.10	2.43 ± 0.13	2.55 ± 0.23	2.17 ± 0.08	2.59 ± 0.28	n.d.[d]	2.59 ± 0.13
H2/H5	n.d.[d]	n.d.[b]	n.d.[b]	n.d.[b]	n.d.[b]	n.d.[b]	2.66 ± 0.15	n.d.[d]	–	1.85 ± 0.14	–	n.d.[d]	n.d.[d]	n.d.[b]
H6/H8	n.d.[b]	n.d.[b]	2.29 ± 0.16	2.33 ± 0.06	2.89 ± 0.19	2.49 ± 0.08	2.58 ± 0.13	2.79 ± 0.18	n.d.[c]	1.78 ± 0.30	1.91 ± 0.16	2.77 ± 0.19	n.d.[d]	2.08± 0.17

B Affinity constants log $K_{A,est5}$ for Mg^{2+} binding to d3'-EBS1* after the fifth iteration round without equilibrium taken into account.

	5'-end		H1							L1					
residue	G1	G2	A3	G4	U5	A6	U7	G8	U9	A10	U11	U12	G13	G14	C15
H1'	n.d.[c]	n.d.[b]	2.86 ± 0.12	3.04 ± 0.11	2.20 ± 0.22	n.d.[b]	n.d.[b]	3.00 ± 0.10	3.13 ± 0.12	2.94 ± 0.06	2.84 ± 0.13	2.23 ± 0.05	n.d.[b]	n.d.[b]	n.d.[d]
H2/H5	–	–	n.d.[b]	–	n.d.[b]	2.31 ± 0.16	n.d.[b]	–	n.d.[b]	2.84 ± 0.10	2.69 ± 0.03	n.d.[b]	–	–	n.d.[d]
H6/H8	3.73 ± 0.17	n.d.[c]	n.d.[b]	2.79 ± 0.06	2.85 ± 0.05	n.d.[c]	2.71 ± 0.09	2.08 ± 0.08	n.d.[b]	3.02 ± 0.06	2.60 ± 0.06	3.15 ± 0.10	n.d.[b]	n.d.[b]	n.d.[d]

			H1						L1			L2		
residue	C29	C28	U27	C26	A25	U24	A23	C22	G21	A20	G19	U18	C17	A16
H1'	n.d.[d]	n.d.[b]	2.19 ± 0.09	3.51 ± 0.12	n.d.[b]	n.d.[d]	n.d.[c]	2.64 ± 0.05	2.92± 0.08	3.17 ± 0.11	2.84 ± 0.18	3.33 ± 0.17	n.d.[d]	3.03 ± 0.10
H2/H5	n.d.[d]	n.d.[b]	n.d.[b]	n.d.[b]	n.d.[b]	n.d.[b]	3.13 ± 0.11	n.d.[d]	–	2.37 ± 0.03	–	n.d.[d]	n.d.[d]	n.d.[b]
H6/H8	n.d.[b]	n.d.[b]	2.67 ± 0.10	2.70 ± 0.12	3.36 ± 0.18	2.93 ± 0.06	3.04 ± 0.07	3.33 ± 0.14	n.d.[c]	2.50 ± 0.11	2.44 ± 0.07	3.25 ± 0.14	n.d.[d]	2.52 ± 0.11

C Affinity constants log $K_{A,est5}$ for Mg^{2+} binding to d3'-EBS1* after the fifth iteration round with equilibrium taken into account.

	5'-end		H1							L1					
residue	G1	G2	A3	G4	U5	A6	U7	G8	U9	A10	U11	U12	G13	G14	C15
H1'	n.d.[c]	n.d.[b]	2.72 ± 0.17	2.94 ± 0.12	2.17 ± 0.18	n.d.[b]	n.d.[b]	2.89 ± 0.10	2.95 ± 0.17	2.83 ± 0.09	2.71 ± 0.06	2.15 ± 0.09	n.d.[b]	n.d.[b]	n.d.[d]
H2/H5	–	–	n.d.[b]	–	n.d.[b]	2.24 ± 0.14	n.d.[b]	–	n.d.[b]	2.71 ± 0.10	2.58 ± 0.05	n.d.[b]	–	–	n.d.[d]
H6/H8	3.48 ± 0.14	n.d.[c]	n.d.[b]	2.70 ± 0.07	2.74 ± 0.08	n.d.[c]	2.61 ± 0.12	1.98 ± 0.10	n.d.[b]	2.90 ± 0.09	2.49 ± 0.08	3.01 ± 0.13	n.d.[b]	n.d.[b]	n.d.[d]

			H1						L1		L2			
residue	C29	C28	U27	C26	A25	U24	A23	C22	G21	A20	G19	U18	C17	A16
H1'	n.d.[d]	n.d.[b]	2.10 ± 0.08	3.36 ± 0.10	n.d.[b]	n.d.[d]	n.d.[c]	2.54 ± 0.06	2.79 ± 0.08	2.96 ± 0.17	2.65 ± 0.07	3.05 ± 0.21	n.d.[d]	2.92 ± 0.10
H2/H5	n.d.[d]	n.d.[b]	n.d.[b]	n.d.[b]	n.d.[b]	n.d.[b]	3.01 ± 0.12	n.d.[d]	–	2.26 ± 0.06	–	n.d.[d]	n.d.[d]	n.d.[b]
H6/H8	n.d.[b]	n.d.[b]	2.72 ± 0.17	2.62 ± 0.03	3.21 ± 0.18	2.83 ± 0.05	2.92 ± 0.09	3.17 ± 0.15	n.d.[c]	2.31 ± 0.12	2.33 ± 0.08	3.10 ± 0.16	n.d.[d]	2.42 ± 0.12

[a]The chemical shift changes were obtained from [^{1}H,^{1}H]-NOESY spectra in D_2O (0.5 mM d3'-EBS1* RNA, pD 6.96, 10 mM KCl, 10 µM EDTA, 25 ºC). The log K_A values were calculated with a Levenberg-Marquardt nonlinear least-squares regression for a single binding isotherm. The four individual binding sites were identified by Mg^{2+} titrations as well as by Mg^{2+} and Mn^{2+} line broadening data. All error limits given correspond to one standard deviation (1σ). [b]n.d., not determined because chemical shift changes were too small. [c]n.d., not determined as peaks are getting too broad with higher Mg^{2+} concentrations, [d]n.d., not determined because a 1:1 binding fit was not possible.

Appendix 11 Chemical shift values of the H1', H2, H6 and H8 protons of d3'-EBS1* (0.6 mM in 100% D_2O, 10 mM KCl, 10 µM EDTA, pD = 6.66) upon addition of Cd^{2+}. The d3'-EBS1* sample was selectively deuterated, thus no resonances for H5 are observable. All the protons that were used for the calculation of the affinity constants are listed according to their binding sites. The chemical shifts were extracted from 2D [$^1H^1H$]-NOESY spectra recorded on a 700 MHz Bruker Avance spectrometer at 298 K. The values that were omitted in the fitting procedure to calculate the log K_A values are marked in bold.

Cd^{2+}[mM]	**0**	**0.5**	**1**	**1.5**	**2**	**2.5**	**3**	**4**	**5**	**6**	**7**	**8**
5'-end	Literature values for DP, TP1 and TP2 used because a fit to 1:1 binding behaviour was not possible											
H1												
A3H2	7.406	7.410	7.429	7.450	7.464	7.474	7.482	7.490	7.494	7.492	**7.485**	**7.484**
A3H8	7.655	7.660	7.674	7.683	7.690	7.700	7.707	7.715	7.717	7.714	-	-
G4H8	6.970	6.981	6.998	7.023	7.043	7.063	7.083	7.113	7.144	7.163	7.162	-
U5H1'	5.425	5.426	5.430	5.434	5.438	5.441	5.444	5.446	5.450	5.449	5.451	5.450
U5H6	7.576	7.583	7.604	7.634	7.659	7.685	7.703	7.732	7.758	7.779	-	-
A25H2	**7.040**	7.037	7.041	7.046	7.049	7.053	7.057	7.060	7.062	7.061	7.062	7.063
A25H8	8.045	8.044	8.048	8.051	8.055	8.058	8.062	8.066	8.066	8.068	8.068	8.072
C26H6	7.428	7.434	7.441	7.447	7.452	7.457	7.464	7.473	7.480	7.484	**7.476**	**7.476**
U27H6	7.801	7.804	7.813	7.822	7.829	7.838	7.843	7.853	7.858	7.859	7.870	7.879
L1												
A10H2	7.706	7.739	7.753	7.759	**7.781**	7.770	7.771	-	-	-	-	-
A10H8	8.146	8.165	8.175	8.186	8.189	8.208	8.215	8.229	-	-	-	-
U11H1'	5.444	5.464	5.477	5.482	**5.489**	5.483	5.483	**5.477**	-	-	-	-
G13H8	7.679	7.695	7.718	7.745	7.784	7.824	7.844	7.841	7.833	-	-	-
G14H1'	5.590	5.603	5.610	5.611	5.611	**5.606**	**5.607**	5.613	-	-	-	-
L2												
C17H1'	5.643	5.634	5.628	5.619	5.613	5.614	5.611	5.613	-	-	-	-
C17H6	7.563	7.598	7.617	7.629	7.633	7.639	7.646	7.648	-	-	-	-
G19H1'	5.527	5.549	5.563	5.577	5.591	5.607	5.618	5.629	-	-	-	-
free												
G2H1'	**5.804**	**5.801**	5.790	5.801	5.812	5.821	5.823	5.827	5.828	5.827	-	-
G2H8	7.435	7.455	7.491	7.539	7.572	7.600	7.621	7.645	7.667	7.667	-	-
A6H1'	5.896	5.899	5.900	5.902	5.903	**5.903**	5.906	5.908	**5.913**	5.914	5.915	-
U7H1'	5.316	5.316	5.314	5.310	5.308	5.304	5.301	5.294	5.289	5.282	5.278	5.273
U9H1'	5.470	5.463	5.454	5.446	5.441	5.439	5.435	**5.444**	-	-	-	-
U11H6	7.566	7.568	7.574	7.585	**7.624**	7.619	7.627	7.629	-	-	-	-
U12H6	7.619	7.619	7.624	7.633	7.646	7.661	**7.673**	7.667	-	-	-	-
G14H8	7.742	7.753	7.763	7.779	7.790	7.822	7.835	7.873	7.877	-	-	-
C15H1'	5.680	5.679	5.672	**5.612**	5.630	5.625	5.616	5.620	-	-	-	-
C15H6	7.582	7.615	7.624	7.629	7.636	7.638	**7.636**	7.647	-	-	-	-
A23H2	7.192	7.195	7.198	7.201	7.203	7.209	7.214	7.227	7.237	7.244	7.248	7.248
U24H1'	5.350	5.352	5.354	5.356	5.357	5.360	5.361	5.364	5.365	5.361	5.362	5.365
U24H6	7.555	7.560	7.566	7.573	7.580	7.591	7.598	7.612	7.631	7.634	-	-
A25H1'	5.890	5.892	5.894	5.897	5.900	5.903	5.906	5.909	5.913	5.915	5.918	-
C26H1'	5.262	**5.262**	**5.262**	5.257	5.252	5.249	5.245	5.240	5.234	5.228	5.223	5.221
C29H6	7.551	7.558	7.563	7.575	7.583	7.591	7.595	7.604	7.609	7.612	7.608	7.609

Appendix 12 Affinity constants log $K_{A,est}$ values for Cd^{2+} binding to d3'-EBS1*

A Listed are the individual log $K_{A,est}$ values obtained from the change in chemical shifts of all aromatic and H1' protons in d3'-EBS1* after the first round of calculation in which the Cd^{2+} concentration corresponds to the total amount of Cd^{2+} added at each titration point.[a] The nucleotides belonging to the four individual binding sites are shaded by alternative grey scales.

	5'-end		H1							L1					
residue	G1	G2	A3	G4	U5	A6	U7	G8	U9	A10	U11	U12	G13	G14	C15
H1'	n.d.[d]	3.49 ± 0.26	n.d.[b]	n.d.[b]	2.53 ± 0.13	1.73 ± 0.20	n.d.[d]	n.d.[b]	2.56 ± 0.19	n.d.[b]	3.74 ± 0.17	n.d.[c]	n.d.[d]	3.96 ± 0.95	2.37 ± 0.71
H2/H5	-	-	2.67 ± 0.18	-	-	n.d.[d]	n.d.[b]	-	-	3.45 ± 0.11	-	-	-	-	-
H6/H8	n.d.[d]	2.51 ± 0.14	2.59 ± 0.17	2.02 ± 0.15	1.98 ± 0.17	n.d.[d]	n.d.[b]	n.d.[d]	n.d.[d]	2.06 ± 0.29	1.69 ± 0.15	1.67 ± 0.15	2.56 ±0.34	1.40 ± 0.15	3.38 ± 0.19

			H1						L1		L2			
residue	C29	C28	U27	C26	A25	U24	A23	C22	G21	A20	G19	U18	C17	A16
H1'	n.d.[d]	n.d.[b]	n.d.[b]	1.24 ± 0.46	1.95 ± 0.12	2.53 ± 0.16	n.d.[b]	n.d.[b]	n.d.[d]	n.d.[c]	2.30 ± 0.25	n.d.[d]	3.04 ± 0.24	n.d.[c]
H2/H5	-	-	-	-	2.83 ± 0.13	-	1.50 ± 0.45	-	-	n.d.[d]	-	-	-	n.d.[d]
H6/H8	2.60 ± 0.13	n.d.[d]	2.16 ± 0.12	2.02 ± 0.09	2.31 ± 0.18	1.22 ± 0.68	n.d.[d]	n.d.[d]	n.d.[c]	n.d.[c]	n.d.[d]	n.d.[c]	3.25 ±0.06	n.d.[d]

B Affinity constants log $K_{A,est5}$ for Cd^{2+} binding to d3'-EBS1* after the fifth iteration round with equilibrium taken into account.

	5'-end		H1							L1					
residue	G1	G2	A3	G4	U5	A6	U7	G8	U9	A10	U11	U12	G13	G14	C15
H1'	n.d.[d]	3.75 ± 0.11	n.d.[b]	n.d.[b]	3.13 ± 0.06	2.46 ± 0.22	n.d.[d]	n.d.[b]	4.14 ± 0.71	n.d.[b]	5.72 ± 0.84	n.d.[c]	n.d.[d]	4.95 ± 0.65	3.95 ± 0.40
H2/H5	-	-	3.49 ± 0.04	-	-	n.d.[d]	n.d.[b]	-	-	4.44 ± 0.25	-	-	-	-	-
H6/H8	n.d.[d]	3.36 ± 0.06	3.31 ± 0.12	2.65 ± 0.06	2.73 ± 0.03	n.d.[d]	n.d.[b]	n.d.[d]	n.d.[d]	2.80 ± 0.40	± 0.15	3.14 ± 0.34	3.37 ± 0.25	2.65 ± 0.19	4.08 ± 1.51

			H1						L1		L2			
residue	C29	C28	U27	C26	A25	U24	A23	C22	G21	A20	G19	U18	C17	A16
H1'	n.d.[d]	n.d.[b]	n.d.[b]	2.27 ± 0.07	2.70 ± 0.06	3.17 ± 0.13	n.d.[b]	n.d.[b]	n.d.[d]	n.d.[c]	3.03 ± 0.27	n.d.[d]	4.31 ± 0.58	n.d.[c]
H2/H5	-	-	-	-	3.18 ± 0.08	-	2.32 ± 0.13	-	-	n.d.[d]	-	-	-	n.d.[d]
H6/H8	3.29 ± 0.08	n.d.[d]	2.72 ± 0.10	2.69 ± 0.11	2.92 ± 0.09	2.44 ± 0.12	n.d.[d]	n.d.[d]	n.d.[c]	n.d.[c]	n.d.[d]	n.d.[c]	4.10 ± 0.89	n.d.[d]

[a]The chemical shift changes were obtained from [^{1}H,^{1}H]-NOESY spectra in D_2O (0.6 mM d3'-EBS1* RNA (selectively deuterated), pD 6.66, 10 mM KCl, 10 µM EDTA, 25 ºC). The log K_A values were calculated with a Levenberg-Marquardt nonlinear least-squares regression for a single binding isotherm. All error limits given correspond to one standard deviation (1σ). [b]n.d., not determined because chemical shift changes were too small. [c]n.d., not determined as peaks are getting too broad with higher Cd^{2+} concentrations, [d]n.d., not determined because a 1:1 binding fit was not possible.

Appendix 13 ^{1}H chemical shift assignments for d3'-EBS1*·IBS1*

	H1	H1'	H2	H2'	H21	H22	H3	H3'	H4'	H41	H42	H5	H5'	H5''	H6	H61	H62	H8
G1	12.592	5.716	-	4.828	-	-	-	4.598	4.450	-	-	-	4.172	4.060	-	-	-	8.037
G2	12.227	5.804	-	4.581	7.972	5.830	-	4.390	4.441	-	-	-	4.131	4.013	-	-	-	7.415
A3	-	5.892	7.397	4.640	-	-	-	4.523	4.434	-	-	-	4.029	3.956	-	8.181	6.791	7.653
G4	13.160	5.459	-	4.305	7.644	6.241	-	4.234	4.366	-	-	-	4.247	3.936	-	-	-	6.968
U5	-	5.411	-	4.489	-	-	13.308	4.434	-	-	-	4.979			7.572	-	-	-
A6	-	5.888	6.927	4.387	-	-	-	4.529	4.344	-	-	-	4.143	4.063	-	7.681	6.276	8.022
U7	-	5.301	-	4.438	-	-	13.158	4.343	4.535	-	-	4.916		3.784	7.468	-	-	-
G8	12.581	5.598	-	4.430	7.634	5.754	-	4.274	4.348	-	-	-		3.990	-	-	-	7.431
U9	-	5.361	-	3.731	-	-	11.752	4.437	-	-	-	5.234			7.486	-	-	-
A10	-	5.900	7.696	4.586	-	-	-	4.648	4.655	-	-	-	4.233	4.047	-	7.889	5.242	8.247
U11	-	5.837	-	4.251	-	-	-	4.584	4.367	-	-	5.634	4.058	4.015	7.662	-	-	-
U12	-	5.877	-	4.403	-	-	-	4.369	4.115	-	-	5.823	-	3.784	7.702	-	-	-
G13	12.121	5.666	-	4.678	-	-	-	4.390	-	-	-	-	-	-	-	-	-	7.937
G14	11.460	5.781	-	4.532	8.135	6.087	-	4.413	-	-	-	-	-	-	-	-	-	7.446
C15	-	5.382	-	4.215	-	-	-	4.526	4.334	8.139	6.769	5.422	4.048	4.027	7.643	-	-	-
A16	-	5.832	7.314	4.385	-	-	-	4.244	4.431	-	-	-	4.042	3.928	-	-	-	7.882
C17	-	5.262	-	4.077	-	-	-	4.601	4.272	8.128	6.725	5.123	-	3.950	7.375	-	-	-
U18	-	5.430	-	4.546	-	-	13.381	4.419	4.271	-	-	5.222	-	-	7.658	-	-	-
G19	11.688	5.537	-	4.438	7.534	5.732	-	4.348	4.387	-	-	-	4.033	3.984	-	-	-	7.477
A20	-	5.799	7.567	4.513	-	-	-	4.401	4.391	-	-	-	-	4.011	-	7.472	5.375	7.590
G21	10.741	5.415	-	4.447	7.631	5.841	-	4.207	4.351	-	-	-	4.340	3.968	-	-	-	7.127
C22	-	5.253	-	4.254	-	-	-	4.440	4.424	8.079	6.677	5.251	-	-	7.566	-	-	-
A23	-	5.807	7.185	4.356	-	-	-	4.600	4.385	-	-	-	-	4.027	-	7.697	6.265	7.885
U24	-	5.350	-	4.271	-	-	13.018	4.352	4.587	-	-	4.972	-	-	7.564	-	-	-
A25	-	5.889	7.028	4.402	-	-	-	4.570	-	-	-	-	-	-	-	7.715	6.253	8.040
C26	-	5.266	-	4.069	-	-	-	4.268	4.291	8.165	6.783	5.095	-	3.964	7.454	-	-	-
U27	-	5.428	-	4.385	-	-	13.903	4.419	4.312	-	-	5.207	-	3.971	7.806	-	-	-
C28	-	5.485	-	4.108	-	-	-	4.355	4.315	8.192	6.792	5.529	-	3.962	7.810	-	-	-
C29	-	5.611	-	3.881	-	-	-	3.910	4.061	8.177	6.747	5.367	-	-	7.555	-	-	-
C59	-	5.299	-	4.431	-	-	-	4.517	4.249	7.885	6.583	5.052	4.006	3.784	7.414	-	-	-
A60	-	5.776	6.935	4.599	-	-	-	4.654	4.503	-	-	-	4.478	4.099	-	8.124	6.732	7.940
G61	13.148	5.548	-	4.430	8.141	6.020	-	4.409	4.191	-	-	-	-	4.015	-	-	-	7.272
U62	-	5.415	-	4.500	-	-	13.315	4.388	4.192	-	-	4.913	-	3.986	7.562	-	-	-
G63	12.666	5.665	-	4.471	7.651	5.762	-	4.303	4.374	-	-	-	4.010	3.963	-	-	-	7.428
U64	-	5.287	-	3.975	-	-	12.121	4.382	4.268	-	-	5.321	-	-	7.659	-	-	-
C65	-	5.764	-	3.868	-	-	-	4.008	4.115	8.302	6.759	5.537	4.399	3.922	7.640	-	-	-

Chemical shifts were extracted from the 2D [^{1}H,^{1}H]-NOESY spectrum at 293 K (100% D_2O, 10 mM KCl, 10 µM EDTA, pD = 6.66) and the 2D [^{1}H,^{1}H]-NOESY spectrum at 278 K (90% H_2O/10% D_2O, 10 mM KCl, 10 µM EDTA, pH = 6.52), both acquired at 700 MHz proton frequency.

Appendix 14 ^{13}C and ^{15}N assignments for d3'-EBS1*·IBS1*

	C6	C5	C8	C2	C1'	N1	N3
G1	-	-	136.25	-	89.96	146.91	-
G2	-	-	134.14	-	90.27	146.60	-
A3	-	-	136.51	150.52	89.45	-	-
G4	-	-	133.09	-	90.24	147.75	-
U5	139.32	100.27	-	-	-	-	161.49
A6	-	-	136.07	150.30	90.09	-	-
U7	138.23	100.25	-	-	90.31	-	161.49
G8	-	-	133.19	-	90.46	147.34	-
U9	134.55	-	-	-	90.44	-	157.76
A10	-	-	138.71	152.55	87.00	-	-
U11	140.55	102.39	-	-	88.07	-	-
U12	141.18	102.57	-	-	90.23	-	-
G13	-	-	137.78	-	90.02	-	-
G14	-	-	138.40	-	90.14	145.08	-
C15	138.76	95.22	-	-	90.96	-	-
A16	-	-	136.51	150.72	90.14	-	-
C17	137.99	94.64	-	-	90.76	-	-
U18	141.14	101.07	-	-	90.96	-	161.11
G19	-	-	133.45	-	90.00	146.29	-
A20	-	-	136.54	151.47	90.16	-	-
G21	-	-	133.70	-	90.85	144.60	-
C22	138.74	90.98	-	-	90.98	-	-
A23	-	-	136.68	150.39	90.08	-	-
U24	140.07	100.03	-	-	90.35	-	161.07
A25	-	-	136.96	150.62	87.20	-	-
C26	137.89	94.42	-	-	90.90	-	-
U27	139.67	100.48	-	-	90.49	-	162.40
C28	138.88	94.61	-	-	91.32	-	-
C29	138.22	95.30	-	-	90.09	-	-
C59	-	-	-	-	-	-	-
A60	-	-	-	-	-	-	-
G61	-	-	-	-	-	-	-
U62	-	-	-	-	-	-	-
G63	-	-	-	-	-	-	-
U64	-	-	-	-	-	-	-
C65	-	-	-	-	-	-	-

Chemical shifts for the EBS1*-part in d3'-EBS1*·IBS1* could not be obtained because EBS1* was at natural abundance.

Appendix 15 2D J_{NN} HNN-COSY of d3'-EBS1*·IBS1* (90% H_2O/10% D_2O, pH = 6.45, 50 mM KCl, 10 µM EDTA) acquired on a 700 MHz Bruker Avance spectrometer equipped with a CP-TXI z-axis pulsed-field gradient cryoprobe at 278 K.

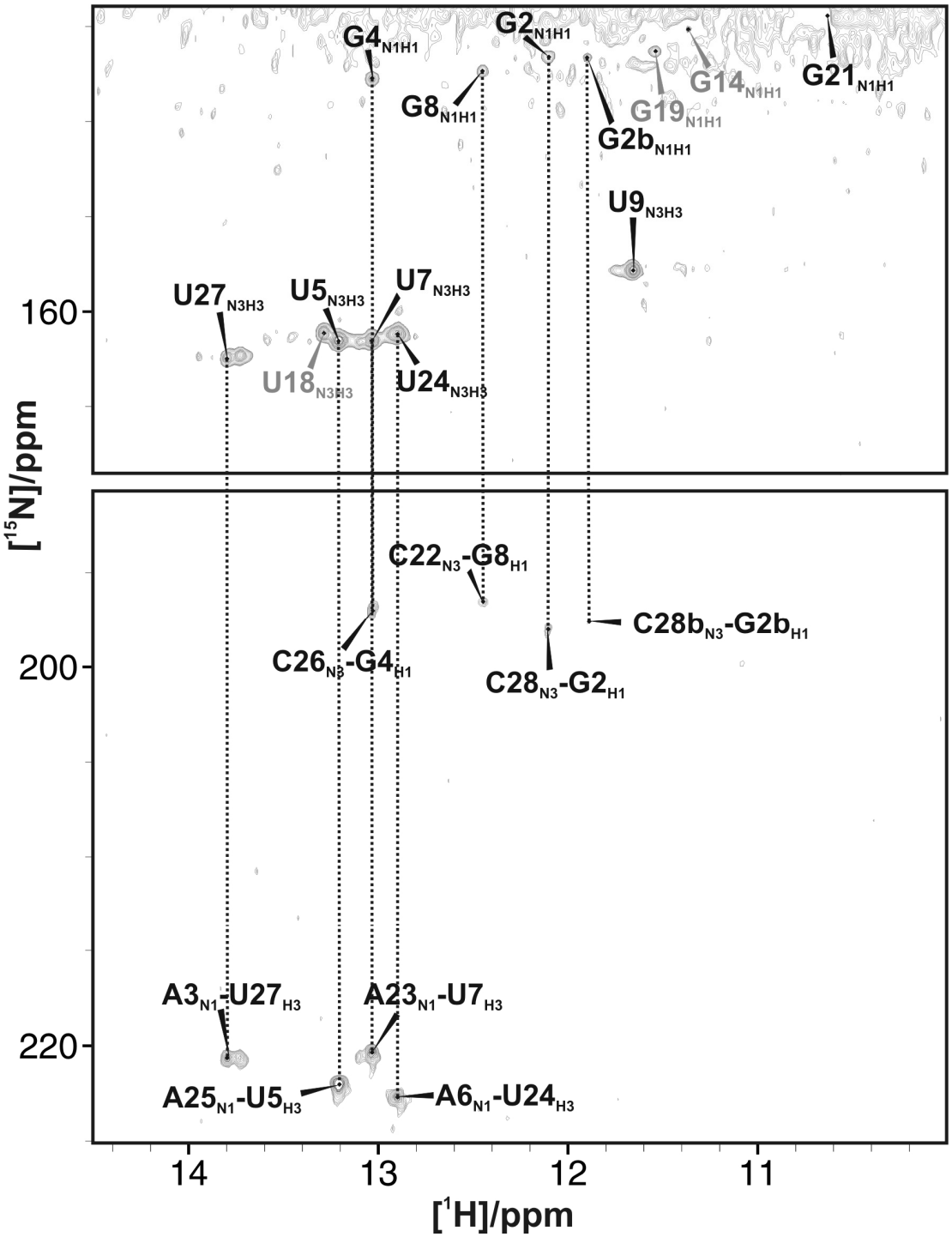

Appendix 16 Illustration of the surface area of d3'-EBS1*·IBS1*

The colours correspond to the one used in the seondary structure as shown in Figure 25. The hole, which is induced upon IBS1* binding, is clearly visible.

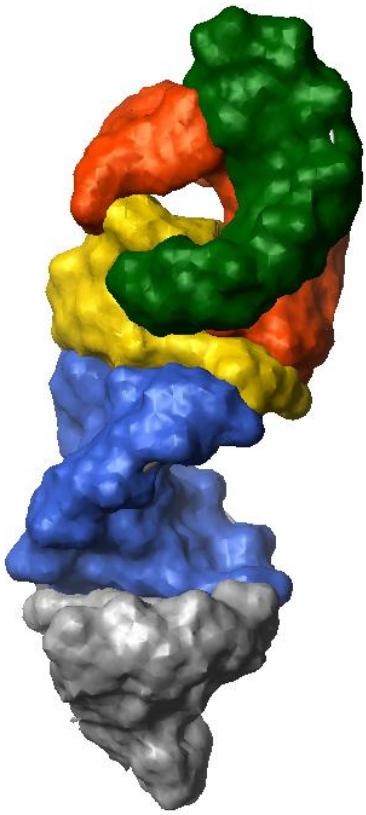

Appendix 17 All distance constraints in d3'-EBS1*·IBS1*

Distance constraints of non-exchangeable protons in d3'-EBS1* IBS1* based on a 2D [^{1}H,^{1}H]-NOESY spectrum acquired at 700 MHz proton frequency at 298 K (100% D_2O, 10 mM KCl, 110 µM EDTA, pD = 6.83). Specified are the estimated distances in Å, the lower and the upper boundaries.

```
assign (residue  1 and name  H1') (residue  1 and name  H8)  3.80  2.00  0.70
assign (residue  1 and name  H2') (residue  1 and name  H8)  3.80  2.00  0.70
assign (residue  1 and name  H3') (residue  1 and name  H8)  3.80  2.00  0.70
assign (residue  1 and name  H4') (residue  1 and name  H8)  5.00  2.00  1.00
assign (residue  1 and name  H5') (residue  1 and name  H8)  3.80  2.00  0.70
assign (residue  1 and name  H5") (residue  1 and name  H8)  3.80  2.00  0.70

assign (residue  1 and name  H1') (residue  2 and name  H1')  5.00  2.00  1.00
assign (residue  1 and name  H1') (residue  2 and name  H8)  3.80  2.00  0.70
assign (residue  1 and name  H2') (residue  2 and name  H1')  5.00  2.00  1.00
assign (residue  1 and name  H2') (residue  2 and name  H8)  2.50  0.70  0.50
assign (residue  1 and name  H3') (residue  2 and name  H8)  3.80  2.00  0.70
assign (residue  1 and name  H8)  (residue  2 and name  H8)  5.00  2.00  0.70

assign (residue  2 and name  H1') (residue  2 and name  H8)  3.80  2.00  0.70
assign (residue  2 and name  H2') (residue  2 and name  H8)  3.80  2.00  0.70
assign (residue  2 and name  H3') (residue  2 and name  H8)  2.50  0.70  0.50
assign (residue  2 and name  H4') (residue  2 and name  H8)  5.00  2.00  1.00
assign (residue  2 and name  H5') (residue  2 and name  H8)  3.80  2.00  0.70
assign (residue  2 and name  H5") (residue  2 and name  H8)  3.80  2.00  0.70

assign (residue  2 and name  H1') (residue  3 and name  H1')  5.00  2.00  1.00
assign (residue  2 and name  H1') (residue  3 and name  H8)  5.00  2.00  1.00
assign (residue  2 and name  H2') (residue  3 and name  H1')  3.80  2.00  0.70
assign (residue  2 and name  H2') (residue  3 and name  H8)  2.50  0.70  0.50
assign (residue  2 and name  H3') (residue  3 and name  H8)  3.80  2.00  0.70
assign (residue  2 and name  H8)  (residue  3 and name  H8)  5.00  2.00  1.00

assign (residue  3 and name  H1') (residue  3 and name  H2)  5.00  2.00  1.00
assign (residue  3 and name  H1') (residue  3 and name  H8)  3.80  2.00  0.70
assign (residue  3 and name  H2') (residue  3 and name  H2)  5.00  2.00  1.00
assign (residue  3 and name  H2') (residue  3 and name  H8)  3.80  2.00  0.70
assign (residue  3 and name  H3') (residue  3 and name  H8)  2.50  0.70  0.50
assign (residue  3 and name  H4') (residue  3 and name  H8)  5.00  2.00  1.00
assign (residue  3 and name  H5') (residue  3 and name  H8)  3.80  2.00  0.70
assign (residue  3 and name  H5") (residue  3 and name  H8)  3.80  2.00  0.70

assign (residue  3 and name  H1') (residue  4 and name  H1')  5.00  2.00  1.00
assign (residue  3 and name  H1') (residue  4 and name  H8)  3.80  2.00  0.70
assign (residue  3 and name  H2') (residue  4 and name  H1')  3.80  2.00  0.70
assign (residue  3 and name  H2') (residue  4 and name  H8)  2.50  0.70  0.50
assign (residue  3 and name  H3') (residue  4 and name  H8)  3.80  2.00  0.70
assign (residue  3 and name  H2)  (residue  4 and name  H1')  2.50  0.70  0.50
assign (residue  3 and name  H2)  (residue  4 and name  H2')  3.80  2.00  0.70
```

```
assign (residue  3 and name  H2)   (residue  4 and name   H8)   5.00  2.00  1.00
assign (residue  3 and name  H2)   (residue 27 and name  H1')  5.00  2.00  1.00
assign (residue  3 and name  H2)   (residue 27 and name  H2')  5.00  2.00  1.00
assign (residue  3 and name  H2)   (residue 28 and name  H1')  3.80  2.00  0.70
assign (residue  3 and name  H2)   (residue 28 and name  H2')  5.00  2.00  1.00
assign (residue  3 and name  H2)   (residue 28 and name  H6)   5.00  2.00  1.00
assign (residue  3 and name  H8)   (residue  4 and name  H8)   5.00  2.00  1.00

assign (residue  4 and name  H1')  (residue  4 and name  H8)   3.80  2.00  0.70
assign (residue  4 and name  H2')  (residue  4 and name  H8)   3.80  2.00  0.70
assign (residue  4 and name  H3')  (residue  4 and name  H8)   2.50  0.70  0.50
assign (residue  4 and name  H4')  (residue  4 and name  H8)   5.00  2.00  1.00
assign (residue  4 and name  H5')  (residue  4 and name  H8)   3.80  2.00  0.70
assign (residue  4 and name  H5'') (residue  4 and name  H8)   3.80  2.00  0.70

assign (residue  4 and name  H1')  (residue  5 and name  H1')  5.00  2.00  1.00
assign (residue  4 and name  H1')  (residue  5 and name  H5)   5.00  2.00  1.00
assign (residue  4 and name  H1')  (residue  5 and name  H6)   3.80  2.00  0.70
assign (residue  4 and name  H2')  (residue  5 and name  H1')  3.80  2.00  0.70
assign (residue  4 and name  H2')  (residue  5 and name  H5)   3.80  2.00  0.70
assign (residue  4 and name  H2')  (residue  5 and name  H6)   2.50  0.70  0.50
assign (residue  4 and name  H3')  (residue  5 and name  H5)   2.50  0.70  0.50
assign (residue  4 and name  H3')  (residue  5 and name  H6)   2.50  0.70  0.50
assign (residue  4 and name  H4')  (residue  5 and name  H5)   5.00  2.00  1.00
assign (residue  4 and name  H5')  (residue  5 and name  H5)   5.00  2.00  1.00
assign (residue  4 and name  H8)   (residue  5 and name  H5)   3.80  2.00  0.70
assign (residue  4 and name  H8)   (residue  5 and name  H6)   5.00  2.00  1.00

assign (residue  5 and name  H1')  (residue  5 and name  H5)   5.00  2.00  1.00
assign (residue  5 and name  H1')  (residue  5 and name  H6)   3.80  2.00  0.70
assign (residue  5 and name  H2')  (residue  5 and name  H5)   5.00  2.00  1.00
assign (residue  5 and name  H2')  (residue  5 and name  H6)   3.80  2.00  0.70
assign (residue  5 and name  H3')  (residue  5 and name  H5)   3.80  2.00  0.70
assign (residue  5 and name  H3')  (residue  5 and name  H6)   2.50  0.70  0.50

assign (residue  5 and name  H1')  (residue  6 and name  H1')  5.00  2.00  1.00
assign (residue  5 and name  H1')  (residue  6 and name  H8)   5.00  2.00  1.00
assign (residue  5 and name  H1')  (residue 25 and name  H2)   5.00  2.00  1.00
assign (residue  5 and name  H2')  (residue  6 and name  H1')  3.80  2.00  0.70
assign (residue  5 and name  H2')  (residue  6 and name  H8)   2.50  0.70  0.50
assign (residue  5 and name  H3')  (residue  6 and name  H8)   3.80  2.00  0.70
assign (residue  5 and name  H6)   (residue  6 and name  H8)   5.00  2.00  1.00

assign (residue  6 and name  H1')  (residue  6 and name  H2)   3.80  2.00  0.70
assign (residue  6 and name  H1')  (residue  6 and name  H8)   3.80  2.00  0.70
assign (residue  6 and name  H2')  (residue  6 and name  H2)   5.00  2.00  1.00
assign (residue  6 and name  H2')  (residue  6 and name  H8)   3.80  2.00  0.70
assign (residue  6 and name  H3')  (residue  6 and name  H8)   2.50  0.70  0.50
assign (residue  6 and name  H4')  (residue  6 and name  H8)   5.00  2.00  1.00
assign (residue  6 and name  H5')  (residue  6 and name  H8)   3.80  2.00  0.70
assign (residue  6 and name  H5'') (residue  6 and name  H8)   3.80  2.00  0.70
```

```
assign (residue  6 and name  H1')  (residue  7 and name  H1')  5.00  2.00  1.00
assign (residue  6 and name  H1')  (residue  7 and name  H5)   5.00  2.00  1.00
assign (residue  6 and name  H1')  (residue  7 and name  H6)   3.80  2.00  0.70
assign (residue  6 and name  H1')  (residue 25 and name  H2)   3.80  2.00  0.70
assign (residue  6 and name  H2')  (residue  7 and name  H1')  3.80  2.00  0.70
assign (residue  6 and name  H2')  (residue  7 and name  H5)   3.80  2.00  0.70
assign (residue  6 and name  H2')  (residue  7 and name  H6)   3.80  2.00  0.70
assign (residue  6 and name  H2')  (residue 25 and name  H2)   5.00  2.00  1.00
assign (residue  6 and name  H3')  (residue  7 and name  H5)   2.50  0.70  0.50
assign (residue  6 and name  H3')  (residue  7 and name  H6)   3.80  2.00  0.70

assign (residue  6 and name  H2)   (residue  7 and name  H1')  3.80  2.00  0.70
assign (residue  6 and name  H2)   (residue  7 and name  H2')  6.00  2.00  1.00
assign (residue  6 and name  H2)   (residue  7 and name  H6)   5.00  2.00  1.00
assign (residue  6 and name  H2)   (residue 23 and name  H2)   5.00  2.00  1.00
assign (residue  6 and name  H2)   (residue 24 and name  H1')  5.00  2.00  1.00
assign (residue  6 and name  H2)   (residue 24 and name  H2')  5.00  2.00  1.00
assign (residue  6 and name  H2)   (residue 25 and name  H1')  3.80  2.00  0.70
assign (residue  6 and name  H2)   (residue 25 and name  H2')  5.00  2.00  1.00
assign (residue  6 and name  H2)   (residue 25 and name  H2)   3.80  2.00  0.70
assign (residue  6 and name  H2)   (residue 25 and name  H8)   5.00  2.00  1.00
assign (residue  6 and name  H8)   (residue  7 and name  H5)   3.80  2.00  0.70
assign (residue  6 and name  H8)   (residue  7 and name  H6)   5.00  2.00  1.00
assign (residue  6 and name  H8)   (residue 25 and name  H2)   5.00  2.00  1.00

assign (residue  7 and name  H1')  (residue  7 and name  H5)   5.00  2.00  1.00
assign (residue  7 and name  H1')  (residue  7 and name  H6)   3.80  2.00  0.70
assign (residue  7 and name  H2')  (residue  7 and name  H5)   5.00  2.00  1.00
assign (residue  7 and name  H2')  (residue  7 and name  H6)   3.80  2.00  0.70
assign (residue  7 and name  H3')  (residue  7 and name  H5)   3.80  2.00  0.70
assign (residue  7 and name  H3')  (residue  7 and name  H6)   2.50  0.70  0.50
assign (residue  7 and name  H4')  (residue  7 and name  H6)   5.00  2.00  1.00
assign (residue  7 and name  H5")  (residue  7 and name  H6)   3.80  2.00  0.70

assign (residue  7 and name  H1')  (residue  8 and name  H1')  5.00  2.00  1.00
assign (residue  7 and name  H1')  (residue  8 and name  H8)   3.80  2.00  0.70
assign (residue  7 and name  H2')  (residue  8 and name  H1')  3.80  2.00  0.70
assign (residue  7 and name  H2')  (residue  8 and name  H8)   2.50  0.70  0.50
assign (residue  7 and name  H3')  (residue  8 and name  H8)   3.80  2.00  0.70
assign (residue  7 and name  H6)   (residue  8 and name  H8)   6.00  2.00  1.00
assign (residue  7 and name  H6)   (residue 23 and name  H2)   6.00  2.00  1.00

assign (residue  8 and name  H1')  (residue  8 and name  H8)   3.80  2.00  0.70
assign (residue  8 and name  H2')  (residue  8 and name  H8)   3.80  2.00  0.70
assign (residue  8 and name  H3')  (residue  8 and name  H8)   2.50  0.70  0.50
assign (residue  8 and name  H4')  (residue  8 and name  H8)   5.00  2.00  1.00
assign (residue  8 and name  H5")  (residue  8 and name  H8)   3.80  2.00  0.70

assign (residue  8 and name  H1')  (residue  9 and name  H1')  6.00  2.00  1.00
assign (residue  8 and name  H1')  (residue  9 and name  H5)   5.00  2.00  1.00
assign (residue  8 and name  H1')  (residue  9 and name  H6)   3.80  2.00  0.70
```

```
assign (residue  8 and name  H1')  (residue 23 and name  H2)   3.80  2.00  0.70
assign (residue  8 and name  H2')  (residue  9 and name  H1')  3.80  2.00  0.70
assign (residue  8 and name  H2')  (residue  9 and name  H5)   2.50  0.70  0.50
assign (residue  8 and name  H2')  (residue  9 and name  H6)   2.50  0.70  0.50
assign (residue  8 and name  H2')  (residue 23 and name  H2)   5.00  2.00  1.00
assign (residue  8 and name  H3')  (residue  9 and name  H6)   3.80  2.00  0.70
assign (residue  8 and name  H8)   (residue  9 and name  H5)   2.50  0.70  0.50
assign (residue  8 and name  H8)   (residue  9 and name  H6)   5.00  2.00  1.00
assign (residue  8 and name  H8)   (residue 23 and name  H2)   5.00  2.00  1.00

assign (residue  9 and name  H1')  (residue  9 and name  H5)   5.00  2.00  1.00
assign (residue  9 and name  H1')  (residue  9 and name  H6)   3.80  2.00  0.70
assign (residue  9 and name  H2')  (residue  9 and name  H5)   5.00  2.00  1.00
assign (residue  9 and name  H2')  (residue  9 and name  H6)   3.80  2.00  0.70
assign (residue  9 and name  H3')  (residue  9 and name  H5)   5.00  2.00  1.00
assign (residue  9 and name  H3')  (residue  9 and name  H6)   2.50  0.70  0.50

assign (residue  9 and name  H1')  (residue 10 and name  H8)   3.80  2.00  0.70
assign (residue  9 and name  H2')  (residue 10 and name  H1')  3.80  2.00  0.70
assign (residue  9 and name  H2')  (residue 10 and name  H8)   2.50  0.70  0.50
assign (residue  9 and name  H3')  (residue 10 and name  H8)   3.80  2.00  0.70
assign (residue  9 and name  H6)   (residue 10 and name  H8)   5.00  2.00  1.00

assign (residue 10 and name H1')  (residue 10 and name  H2)   5.00  2.00  1.00
assign (residue 10 and name H1')  (residue 10 and name  H8)   3.80  2.00  0.70
assign (residue 10 and name H2')  (residue 10 and name  H2)   5.00  2.00  1.00
assign (residue 10 and name H2')  (residue 10 and name  H8)   3.80  2.00  0.70
assign (residue 10 and name H3')  (residue 10 and name  H8)   3.80  2.00  0.70
assign (residue 10 and name H4')  (residue 10 and name  H8)   5.00  2.00  1.00
assign (residue 10 and name H5')  (residue 10 and name  H8)   3.80  2.00  0.70
assign (residue 10 and nameH5'')  (residue 10 and name  H8)   3.80  2.00  0.70

assign (residue 10 and name H1')  (residue 11 and name  H1')  5.00  2.00  1.00
assign (residue 10 and name H1')  (residue 11 and name  H5)   5.00  2.00  1.00
assign (residue 10 and name H1')  (residue 11 and name  H6)   5.00  2.00  1.00
assign (residue 10 and name H1')  (residue 59 and name  H5)   6.00  2.00  1.00
assign (residue 10 and name H1')  (residue 59 and name  H6)   5.00  2.00  1.00
assign (residue 10 and name H2')  (residue 11 and name  H1')  3.80  2.00  0.70
assign (residue 10 and name H2')  (residue 11 and name  H5)   3.80  2.00  0.70
assign (residue 10 and name H2')  (residue 11 and name  H6)   2.50  0.70  0.50
assign (residue 10 and name H2')  (residue 20 and name  H2)   6.00  2.00  1.00
assign (residue 10 and name H2')  (residue 59 and name  H5)   3.80  2.00  0.70
assign (residue 10 and name H3')  (residue 11 and name  H5)   3.80  2.00  0.70
assign (residue 10 and name H3')  (residue 11 and name  H6)   3.80  2.00  0.70
assign (residue 10 and name H2)   (residue 11 and name  H1')  5.00  2.00  1.00
assign (residue 10 and name H2)   (residue 11 and name  H2')  6.00  2.00  1.00
assign (residue 10 and name H2)   (residue 20 and name  H2)   3.80  2.00  0.70
assign (residue 10 and name H2)   (residue 21 and name  H1')  3.80  2.00  0.70
assign (residue 10 and name H2)   (residue 59 and name  H1')  3.80  2.00  0.70
assign (residue 10 and name H2)   (residue 59 and name  H2')  5.00  2.00  1.00
assign (residue 10 and name H2)   (residue 59 and name  H5)   5.00  2.00  1.00
```

```
assign (residue 10 and name H2)   (residue 59 and name  H6)   3.80  2.00  0.70
assign (residue 10 and name H8)   (residue 11 and name  H5)   5.00  2.00  1.00
assign (residue 10 and name H8)   (residue 11 and name  H6)   5.00  2.00  1.00

assign (residue 11 and name H1')  (residue 11 and name  H5)   5.00  2.00  1.00
assign (residue 11 and name H1')  (residue 11 and name  H6)   3.80  2.00  0.70
assign (residue 11 and name H2')  (residue 11 and name  H5)   5.00  2.00  1.00
assign (residue 11 and name H2')  (residue 11 and name  H6)   2.50  0.70  0.50
assign (residue 11 and name H3')  (residue 11 and name  H5)   3.80  2.00  0.70
assign (residue 11 and name H3')  (residue 11 and name  H6)   2.50  0.70  0.50
assign (residue 11 and name H4')  (residue 11 and name  H5)   6.00  2.00  1.00
assign (residue 11 and name H4')  (residue 11 and name  H6)   5.00  2.00  1.00
assign (residue 11 and name H5')  (residue 11 and name  H6)   3.80  2.00  0.70
assign (residue 11 and name H5'') (residue 11 and name  H6)   3.80  2.00  0.70

assign (residue 11 and name H1')  (residue 12 and name  H1')  3.80  2.00  0.70
assign (residue 11 and name H1')  (residue 12 and name  H6)   6.00  2.00  1.00
assign (residue 11 and name H1')  (residue 59 and name  H1')  6.00  2.00  1.00
assign (residue 11 and name H1')  (residue 59 and name  H5)   3.80  2.00  0.70
assign (residue 11 and name H1')  (residue 59 and name  H6)   3.80  2.00  0.70
assign (residue 11 and name H2')  (residue 12 and name  H1')  3.80  2.00  0.70
assign (residue 11 and name H2')  (residue 12 and name  H6)   3.80  2.00  0.70
assign (residue 11 and name H3')  (residue 12 and name  H6)   3.80  2.00  0.70
assign (residue 11 and name H5)   (residue 12 and name  H5)   5.00  2.00  1.00
assign (residue 11 and name H5)   (residue 12 and name  H6)   5.00  2.00  1.00
assign (residue 11 and name H5)   (residue 59 and name  H5)   3.80  2.00  0.70
assign (residue 11 and name H6)   (residue 12 and name  H6)   3.80  2.00  0.70
assign (residue 11 and name H6)   (residue 59 and name  H5)   3.80  2.00  0.70
assign (residue 11 and name H6)   (residue 59 and name  H6)   5.00  2.00  1.00

assign (residue 12 and name H1')  (residue 12 and name  H5)   5.00  2.00  1.00
assign (residue 12 and name H1')  (residue 12 and name  H6)   3.80  2.00  0.70
assign (residue 12 and name H2')  (residue 12 and name  H5)   5.00  2.00  1.00
assign (residue 12 and name H2')  (residue 12 and name  H6)   3.80  2.00  0.70
assign (residue 12 and name H3')  (residue 12 and name  H6)   3.80  2.00  0.70
assign (residue 12 and name H4')  (residue 12 and name  H6)   5.00  2.00  1.00

assign (residue 12 and name H1')  (residue 13 and name  H8)   5.00  2.00  1.00
assign (residue 12 and name H1')  (residue 59 and name  H1')  5.00  2.00  1.00
assign (residue 12 and name H1')  (residue 59 and name  H5')  3.80  2.00  0.70
assign (residue 12 and name H1')  (residue 59 and name  H5)   3.80  2.00  0.70
assign (residue 12 and name H1')  (residue 59 and name  H6)   3.80  2.00  0.70
assign (residue 12 and name H2')  (residue 13 and name  H8)   3.80  2.00  0.70
assign (residue 12 and name H3')  (residue 13 and name  H8)   3.80  2.00  0.70
assign (residue 12 and name H5)   (residue 59 and name  H5)   5.00  2.00  1.00
assign (residue 12 and name H6)   (residue 13 and name  H8)   5.00  2.00  1.00
assign (residue 12 and name H6)   (residue 59 and name  H5)   3.80  2.00  0.70

assign (residue 13 and name H1')  (residue 13 and name  H8)   3.80  2.00  0.70
assign (residue 13 and name H2')  (residue 13 and name  H8)   3.80  2.00  0.70
assign (residue 13 and name H3')  (residue 13 and name  H8)   2.50  0.70  0.50
```

```
assign (residue 13 and name H1')  (residue 14 and name  H1')  5.00  2.00  1.00
assign (residue 13 and name H1')  (residue 14 and name  H8)   3.80  2.00  0.70
assign (residue 13 and name H2')  (residue 14 and name  H1')  5.00  2.00  1.00
assign (residue 13 and name H2')  (residue 14 and name  H8)   2.50  0.70  0.50
assign (residue 13 and name H3')  (residue 14 and name  H8)   3.80  2.00  0.70
assign (residue 13 and name H8)   (residue 14 and name  H8)   3.80  2.00  0.70

assign (residue 14 and name H1')  (residue 14 and name  H8)   3.80  2.00  0.70
assign (residue 14 and name H2')  (residue 14 and name  H8)   3.80  2.00  0.70
assign (residue 14 and name H3')  (residue 14 and name  H8)   2.50  0.70  0.50

assign (residue 14 and name H1')  (residue 15 and name  H1')  5.00  2.00  1.00
assign (residue 14 and name H1')  (residue 15 and name  H5)   5.00  2.00  1.00
assign (residue 14 and name H1')  (residue 15 and name  H6)   3.80  2.00  0.70
assign (residue 14 and name H2')  (residue 15 and name  H1')  3.80  2.00  0.70
assign (residue 14 and name H2')  (residue 15 and name  H5)   3.80  2.00  0.70
assign (residue 14 and name H2')  (residue 15 and name  H6)   2.50  0.70  0.50
assign (residue 14 and name H3')  (residue 15 and name  H5)   3.80  2.00  0.70
assign (residue 14 and name H3')  (residue 15 and name  H6)   3.80  2.00  0.70
assign (residue 14 and name H8)   (residue 15 and name  H6)   3.80  2.00  0.70

assign (residue 15 and name H1')  (residue 15 and name  H6)   3.80  2.00  0.70
assign (residue 15 and name H2')  (residue 15 and name  H6)   3.80  2.00  0.70
assign (residue 15 and name H3')  (residue 15 and name  H5)   3.80  2.00  0.70
assign (residue 15 and name H3')  (residue 15 and name  H6)   2.50  0.70  0.50
assign (residue 15 and name H4')  (residue 15 and name  H6)   5.00  2.00  1.00
assign (residue 15 and name H5')  (residue 15 and name  H6)   3.80  2.00  0.70
assign (residue 15 and name H5")  (residue 15 and name  H6)   3.80  2.00  0.70

assign (residue 15 and name H1')  (residue 16 and name  H1')  5.00  2.00  1.00
assign (residue 15 and name H1')  (residue 16 and name  H8)   3.80  2.00  0.70
assign (residue 15 and name H2')  (residue 16 and name  H1')  3.80  2.00  0.70
assign (residue 15 and name H2')  (residue 16 and name  H2)   6.00  2.00  1.00
assign (residue 15 and name H2')  (residue 16 and name  H8)   2.50  0.70  0.50
assign (residue 15 and name H3')  (residue 16 and name  H8)   3.80  2.00  0.70
assign (residue 15 and name H6)   (residue 16 and name  H8)   3.80  2.00  0.70

assign (residue 16 and name H1')  (residue 16 and name  H2)   5.00  2.00  1.00
assign (residue 16 and name H1')  (residue 16 and name  H8)   3.80  2.00  0.70
assign (residue 16 and name H2')  (residue 16 and name  H2)   5.00  2.00  1.00
assign (residue 16 and name H2')  (residue 16 and name  H8)   3.80  2.00  0.70
assign (residue 16 and name H3')  (residue 16 and name  H8)   2.50  0.70  0.50
assign (residue 16 and name H4')  (residue 16 and name  H8)   5.00  2.00  1.00
assign (residue 16 and name H5')  (residue 16 and name  H8)   3.80  2.00  0.70
assign (residue 16 and name H5")  (residue 16 and name  H8)   3.80  2.00  0.70
assign (residue 16 and name H2)   (residue 16 and name  H8)   5.00  2.00  1.00

assign (residue 16 and name H1')  (residue 17 and name  H1')  5.00  2.00  1.00
assign (residue 16 and name H1')  (residue 17 and name  H5)   5.00  2.00  1.00
assign (residue 16 and name H1')  (residue 17 and name  H6)   3.80  2.00  0.70
assign (residue 16 and name H2')  (residue 17 and name  H1')  3.80  2.00  0.70
```

```
assign (residue 16 and name H2')  (residue 17 and name  H5)   3.80  2.00  0.70
assign (residue 16 and name H2')  (residue 17 and name  H6)   2.50  0.70  0.50
assign (residue 16 and name H3')  (residue 17 and name  H5)   3.80  2.00  0.70
assign (residue 16 and name H3')  (residue 17 and name  H6)   3.80  2.00  0.70
assign (residue 16 and name H2)   (residue 17 and name  H1')  3.80  2.00  0.70
assign (residue 16 and name H2)   (residue 17 and name  H2')  5.00  2.00  1.00
assign (residue 16 and name H2)   (residue 17 and name  H6)   3.80  2.00  0.70
assign (residue 16 and name H2)   (residue 62 and name  H1')  5.00  2.00  1.00
assign (residue 16 and name H2)   (residue 62 and name  H2')  5.00  2.00  1.00
assign (residue 16 and name H2)   (residue 63 and name  H1')  3.80  2.00  0.70
assign (residue 16 and name H2)   (residue 63 and name  H2')  5.00  2.00  1.00
assign (residue 16 and name H2)   (residue 63 and name  H8)   5.00  2.00  1.00
assign (residue 16 and name H8)   (residue 17 and name  H5)   3.80  2.00  0.70
assign (residue 16 and name H8)   (residue 17 and name  H6)   3.80  2.00  0.70

assign (residue 17 and name H1')  (residue 17 and name  H5)   5.00  2.00  1.00
assign (residue 17 and name H1')  (residue 17 and name  H6)   3.80  2.00  0.70
assign (residue 17 and name H2')  (residue 17 and name  H5)   5.00  2.00  1.00
assign (residue 17 and name H2')  (residue 17 and name  H6)   3.80  2.00  0.70
assign (residue 17 and name H3')  (residue 17 and name  H5)   3.80  2.00  0.70
assign (residue 17 and name H3')  (residue 17 and name  H6)   2.50  0.70  0.50
assign (residue 17 and name H4')  (residue 17 and name  H5)   6.00  2.00  1.00
assign (residue 17 and name H4')  (residue 17 and name  H6)   5.00  2.00  1.00

assign (residue 17 and name H1')  (residue 18 and name  H1')  5.00  2.00  1.00
assign (residue 17 and name H1')  (residue 18 and name  H6)   3.80  2.00  0.70
assign (residue 17 and name H2')  (residue 18 and name  H1')  3.80  2.00  0.70
assign (residue 17 and name H2')  (residue 18 and name  H5)   3.80  2.00  0.70
assign (residue 17 and name H2')  (residue 18 and name  H6)   2.50  0.70  0.50
assign (residue 17 and name H3')  (residue 18 and name  H6)   3.80  2.00  0.70
assign (residue 17 and name H4')  (residue 18 and name  H5)   6.00  2.00  1.00
assign (residue 17 and name H5)   (residue 18 and name  H5)   2.50  0.70  0.50
assign (residue 17 and name H6)   (residue 18 and name  H5)   2.50  0.70  0.50
assign (residue 17 and name H6)   (residue 18 and name  H6)   3.80  2.00  0.70

assign (residue 18 and name H1')  (residue 18 and name  H5)   5.00  2.00  1.00
assign (residue 18 and name H1')  (residue 18 and name  H6)   3.80  2.00  0.70
assign (residue 18 and name H2')  (residue 18 and name  H5)   5.00  2.00  1.00
assign (residue 18 and name H2')  (residue 18 and name  H6)   3.80  2.00  0.70
assign (residue 18 and name H3')  (residue 18 and name  H5)   5.00  2.00  1.00
assign (residue 18 and name H3')  (residue 18 and name  H6)   2.50  0.70  0.50

assign (residue 18 and name H1')  (residue 19 and name  H1')  3.80  2.00  0.70
assign (residue 18 and name H1')  (residue 19 and name  H8)   3.80  2.00  0.70
assign (residue 18 and name H1')  (residue 60 and name  H2)   5.00  2.00  1.00
assign (residue 18 and name H2')  (residue 19 and name  H1')  5.00  2.00  1.00
assign (residue 18 and name H2')  (residue 19 and name  H8)   2.50  0.70  0.50
assign (residue 18 and name H2')  (residue 60 and name  H2)   5.00  2.00  1.00
assign (residue 18 and name H3')  (residue 19 and name  H8)   3.80  2.00  0.70
assign (residue 18 and name H6)   (residue 19 and name  H8)   5.00  2.00  1.00
```

```
assign (residue 19 and name H1')  (residue 19 and name  H8)   3.80  2.00  0.70
assign (residue 19 and name H2')  (residue 19 and name  H8)   3.80  2.00  0.70
assign (residue 19 and name H3')  (residue 19 and name  H8)   2.50  0.70  0.50
assign (residue 19 and name H4')  (residue 19 and name  H8)   5.00  2.00  1.00
assign (residue 19 and name H5')  (residue 19 and name  H8)   3.80  2.00  0.70
assign (residue 19 and name H5'') (residue 19 and name  H8)   3.80  2.00  0.70

assign (residue 19 and name H1')  (residue 20 and name  H1')  3.80  2.00  0.70
assign (residue 19 and name H1')  (residue 20 and name  H8)   3.80  2.00  0.70
assign (residue 19 and name H1')  (residue 60 and name  H2)   3.80  2.00  0.70
assign (residue 19 and name H2')  (residue 20 and name  H1')  3.80  2.00  0.70
assign (residue 19 and name H2')  (residue 20 and name  H8)   2.50  0.70  0.50
assign (residue 19 and name H2')  (residue 60 and name  H2)   3.80  2.00  0.70
assign (residue 19 and name H3')  (residue 20 and name  H8)   3.80  2.00  0.70
assign (residue 19 and name H8)   (residue 20 and name  H8)   5.00  2.00  1.00
assign (residue 19 and name H8)   (residue 60 and name  H2)   3.80  2.00  0.70

assign (residue 20 and name H1')  (residue 20 and name  H2)   5.00  2.00  1.00
assign (residue 20 and name H1')  (residue 20 and name  H8)   3.80  2.00  0.70
assign (residue 20 and name H2')  (residue 20 and name  H2)   5.00  2.00  1.00
assign (residue 20 and name H2')  (residue 20 and name  H8)   3.80  2.00  0.70
assign (residue 20 and name H3')  (residue 20 and name  H8)   2.50  0.70  0.50
assign (residue 20 and name H4')  (residue 20 and name  H8)   5.00  2.00  1.00
assign (residue 20 and name H5'') (residue 20 and name  H8)   3.80  2.00  0.70

assign (residue 20 and name H1')  (residue 21 and name  H1')  6.00  2.00  1.00
assign (residue 20 and name H1')  (residue 21 and name  H8)   3.80  2.00  0.70
assign (residue 20 and name H2')  (residue 21 and name  H1')  3.80  2.00  0.70
assign (residue 20 and name H2')  (residue 21 and name  H8)   2.50  0.70  0.50
assign (residue 20 and name H3')  (residue 21 and name  H8)   3.80  2.00  0.70

assign (residue 20 and name H2)   (residue 21 and name  H2')  5.00  2.00  1.00
assign (residue 20 and name H2)   (residue 59 and name  H1')  2.50  0.70  0.50
assign (residue 20 and name H8)   (residue 21 and name  H8)   3.80  2.00  0.70

assign (residue 21 and name H1')  (residue 21 and name  H8)   3.80  2.00  0.70
assign (residue 21 and name H2')  (residue 21 and name  H8)   3.80  2.00  0.70
assign (residue 21 and name H3')  (residue 21 and name  H8)   2.50  0.70  0.50
assign (residue 21 and name H4')  (residue 21 and name  H8)   5.00  2.00  1.00
assign (residue 21 and name H5')  (residue 21 and name  H8)   3.80  2.00  0.70
assign (residue 21 and name H5'') (residue 21 and name  H8)   3.80  2.00  0.70

assign (residue 21 and name H1')  (residue 22 and name  H1')  5.00  2.00  1.00
assign (residue 21 and name H1')  (residue 22 and name  H5)   5.00  2.00  1.00
assign (residue 21 and name H1')  (residue 22 and name  H6)   3.80  2.00  0.70
assign (residue 21 and name H2')  (residue 22 and name  H1')  3.80  2.00  0.70
assign (residue 21 and name H2')  (residue 22 and name  H5)   3.80  2.00  0.70
assign (residue 21 and name H2')  (residue 22 and name  H6)   2.50  0.70  0.50
assign (residue 21 and name H3')  (residue 22 and name  H5)   3.80  2.00  0.70
assign (residue 21 and name H3')  (residue 22 and name  H6)   3.80  2.00  0.70
assign (residue 21 and name H8)   (residue 22 and name  H5)   3.80  2.00  0.70
```

```
assign (residue 21 and name H8)   (residue 22 and name  H6)   3.80  2.00  0.70

assign (residue 22 and name H1')  (residue 22 and name  H6)   3.80  2.00  0.70
assign (residue 22 and name H2')  (residue 22 and name  H5)   5.00  2.00  1.00
assign (residue 22 and name H2')  (residue 22 and name  H6)   6.00  2.00  1.00
assign (residue 22 and name H3')  (residue 22 and name  H5)   5.00  2.00  1.00
assign (residue 22 and name H3')  (residue 22 and name  H6)   3.80  2.00  0.70
assign (residue 22 and name H4')  (residue 22 and name  H6)   5.00  2.00  1.00

assign (residue 22 and name H1')  (residue 23 and name  H1')  5.00  2.00  1.00
assign (residue 22 and name H1')  (residue 23 and name  H8)   3.80  2.00  0.70
assign (residue 22 and name H2')  (residue 23 and name  H1')  3.80  2.00  0.70
assign (residue 22 and name H2')  (residue 23 and name  H8)   2.50  0.70  0.50
assign (residue 22 and name H3')  (residue 23 and name  H8)   3.80  2.00  0.70
assign (residue 22 and name H6)   (residue 23 and name  H8)   5.00  2.00  1.00

assign (residue 23 and name H1')  (residue 23 and name  H2)   5.00  2.00  1.00
assign (residue 23 and name H1')  (residue 23 and name  H8)   3.80  2.00  0.70
assign (residue 23 and name H2')  (residue 23 and name  H2)   5.00  2.00  1.00
assign (residue 23 and name H2')  (residue 23 and name  H8)   3.80  2.00  0.70
assign (residue 23 and name H3')  (residue 23 and name  H8)   2.50  0.70  0.50
assign (residue 23 and name H4')  (residue 23 and name  H8)   5.00  2.00  1.00
assign (residue 23 and name H5")  (residue 23 and name  H8)   3.80  2.00  0.70

assign (residue 23 and name H1')  (residue 24 and name  H1')  5.00  2.00  1.00
assign (residue 23 and name H1')  (residue 24 and name  H5)   5.00  2.00  1.00
assign (residue 23 and name H1')  (residue 24 and name  H6)   5.00  2.00  1.00
assign (residue 23 and name H2')  (residue 24 and name  H1')  3.80  2.00  0.70
assign (residue 23 and name H2')  (residue 24 and name  H5)   3.80  2.00  0.70
assign (residue 23 and name H2')  (residue 24 and name  H6)   2.50  0.70  0.50
assign (residue 23 and name H3')  (residue 24 and name  H5)   2.50  0.70  0.50
assign (residue 23 and name H3')  (residue 24 and name  H6)   3.80  2.00  0.70
assign (residue 23 and name H2)   (residue 24 and name  H1')  3.80  2.00  0.70
assign (residue 23 and name H2)   (residue 24 and name  H2')  5.00  2.00  1.00
assign (residue 23 and name H2)   (residue 24 and name  H6)   5.00  2.00  1.00
assign (residue 23 and name H8)   (residue 24 and name  H5)   3.80  2.00  0.70
assign (residue 23 and name H8)   (residue 24 and name  H6)   5.00  2.00  1.00

assign (residue 24 and name H1')  (residue 24 and name  H5)   5.00  2.00  1.00
assign (residue 24 and name H1')  (residue 24 and name  H6)   3.80  2.00  0.70
assign (residue 24 and name H2')  (residue 24 and name  H5)   5.00  2.00  1.00
assign (residue 24 and name H2')  (residue 24 and name  H6)   3.80  2.00  0.70
assign (residue 24 and name H3')  (residue 24 and name  H5)   5.00  2.00  1.00
assign (residue 24 and name H3')  (residue 24 and name  H6)   2.50  0.70  0.50
assign (residue 24 and name H4')  (residue 24 and name  H5)   5.00  2.00  1.00
assign (residue 24 and name H4')  (residue 24 and name  H6)   5.00  2.00  1.00

assign (residue 24 and name H1')  (residue 25 and name  H1')  5.00  2.00  1.00
assign (residue 24 and name H1')  (residue 25 and name  H8)   3.80  2.00  0.70
assign (residue 24 and name H2')  (residue 25 and name  H1')  3.80  2.00  0.70
assign (residue 24 and name H2')  (residue 25 and name  H8)   2.50  0.70  0.50
```

```
assign (residue 24 and name H3')  (residue 25 and name  H8)   3.80  2.00  0.70
assign (residue 24 and name H5)   (residue 25 and name  H8)   5.00  2.00  1.00
assign (residue 24 and name H6)   (residue 25 and name  H8)   3.80  2.00  0.70

assign (residue 25 and name H1')  (residue 25 and name  H2)   3.80  2.00  0.70
assign (residue 25 and name H1')  (residue 25 and name  H8)   3.80  2.00  0.70
assign (residue 25 and name H2')  (residue 25 and name  H2)   5.00  2.00  1.00
assign (residue 25 and name H2')  (residue 25 and name  H8)   3.80  2.00  0.70
assign (residue 25 and name H3')  (residue 25 and name  H8)   2.50  0.70  0.50

assign (residue 25 and name H1')  (residue 26 and name  H1')  5.00  2.00  1.00
assign (residue 25 and name H1')  (residue 26 and name  H5)   5.00  2.00  1.00
assign (residue 25 and name H1')  (residue 26 and name  H6)   3.80  2.00  0.70
assign (residue 25 and name H2')  (residue 26 and name  H1')  3.80  2.00  0.70
assign (residue 25 and name H2')  (residue 26 and name  H5)   3.80  2.00  0.70
assign (residue 25 and name H2')  (residue 26 and name  H6)   2.50  0.70  0.50
assign (residue 25 and name H3')  (residue 26 and name  H5)   3.80  2.00  0.70
assign (residue 25 and name H3')  (residue 26 and name  H6)   3.80  2.00  0.70
assign (residue 25 and name H2)   (residue 26 and name  H1')  3.80  2.00  0.70
assign (residue 25 and name H2)   (residue 26 and name  H2')  5.00  2.00  1.00
assign (residue 25 and name H2)   (residue 26 and name  H6)   5.00  2.00  1.00
assign (residue 25 and name H8)   (residue 26 and name  H5)   5.00  2.00  1.00
assign (residue 25 and name H8)   (residue 26 and name  H6)   3.80  2.00  0.70

assign (residue 26 and name H1')  (residue 26 and name  H5)   5.00  2.00  1.00
assign (residue 26 and name H1')  (residue 26 and name  H6)   3.80  2.00  0.70
assign (residue 26 and name H2')  (residue 26 and name  H5)   5.00  2.00  1.00
assign (residue 26 and name H2')  (residue 26 and name  H6)   3.80  2.00  0.70
assign (residue 26 and name H3')  (residue 26 and name  H5)   3.80  2.00  0.70
assign (residue 26 and name H3')  (residue 26 and name  H6)   2.50  0.70  0.50
assign (residue 26 and name H4')  (residue 26 and name  H5)   5.00  2.00  1.00
assign (residue 26 and name H4')  (residue 26 and name  H6)   5.00  2.00  1.00
assign (residue 26 and name H5")  (residue 26 and name  H6)   3.80  2.00  0.70

assign (residue 26 and name H1')  (residue 27 and name  H1')  5.00  2.00  1.00
assign (residue 26 and name H1')  (residue 27 and name  H6)   3.80  2.00  0.70
assign (residue 26 and name H2')  (residue 27 and name  H1')  3.80  2.00  0.70
assign (residue 26 and name H2')  (residue 27 and name  H5)   3.80  2.00  0.70
assign (residue 26 and name H2')  (residue 27 and name  H6)   2.50  0.70  0.50
assign (residue 26 and name H3')  (residue 27 and name  H5)   3.80  2.00  0.70
assign (residue 26 and name H3')  (residue 27 and name  H6)   3.80  2.00  0.70
assign (residue 26 and name H5)   (residue 27 and name  H5)   2.50  0.70  0.50
assign (residue 26 and name H6)   (residue 27 and name  H5)   2.50  0.70  0.50
assign (residue 26 and name H6)   (residue 27 and name  H6)   3.80  2.00  0.70

assign (residue 27 and name H1')  (residue 27 and name  H5)   5.00  2.00  1.00
assign (residue 27 and name H1')  (residue 27 and name  H6)   3.80  2.00  0.70
assign (residue 27 and name H2')  (residue 27 and name  H5)   5.00  2.00  1.00
assign (residue 27 and name H2')  (residue 27 and name  H6)   3.80  2.00  0.70
assign (residue 27 and name H3')  (residue 27 and name  H5)   5.00  2.00  1.00
assign (residue 27 and name H3')  (residue 27 and name  H6)   2.50  0.70  0.50
```

```
assign (residue 27 and name H4')   (residue 27 and name  H6)   5.00  2.00  1.00
assign (residue 27 and name H5")  (residue 27 and name  H6)   3.80  2.00  0.70

assign (residue 27 and name H1')   (residue 28 and name  H1')  6.00  2.00  1.00
assign (residue 27 and name H1')   (residue 28 and name  H5)   5.00  2.00  1.00
assign (residue 27 and name H1')   (residue 28 and name  H6)   3.80  2.00  0.70
assign (residue 27 and name H2')   (residue 28 and name  H1')  3.80  2.00  0.70
assign (residue 27 and name H2')   (residue 28 and name  H5)   3.80  2.00  0.70
assign (residue 27 and name H2')   (residue 28 and name  H6)   3.80  2.00  0.70
assign (residue 27 and name H3')   (residue 28 and name  H5)   3.80  2.00  0.70
assign (residue 27 and name H3')   (residue 28 and name  H6)   3.80  2.00  0.70
assign (residue 27 and name H5)    (residue 28 and name  H5)   5.00  2.00  1.00

assign (residue 28 and name H1')   (residue 28 and name  H6)   3.80  2.00  0.70
assign (residue 28 and name H2')   (residue 28 and name  H5)   5.00  2.00  1.00
assign (residue 28 and name H2')   (residue 28 and name  H6)   3.80  2.00  0.70
assign (residue 28 and name H3')   (residue 28 and name  H5)   5.00  2.00  1.00
assign (residue 28 and name H3')   (residue 28 and name  H6)   2.50  0.70  0.50
assign (residue 28 and name H4')   (residue 28 and name  H6)   5.00  2.00  1.00
assign (residue 28 and name H5")  (residue 28 and name  H6)   3.80  2.00  0.70

assign (residue 28 and name H1')   (residue 29 and name  H1')  3.80  2.00  0.70
assign (residue 28 and name H1')   (residue 29 and name  H5)   5.00  2.00  1.00
assign (residue 28 and name H1')   (residue 29 and name  H6)   3.80  2.00  0.70
assign (residue 28 and name H2')   (residue 29 and name  H1')  3.80  2.00  0.70
assign (residue 28 and name H2')   (residue 29 and name  H5)   3.80  2.00  0.70
assign (residue 28 and name H2')   (residue 29 and name  H6)   2.50  0.70  0.50
assign (residue 28 and name H3')   (residue 29 and name  H6)   3.80  2.00  0.70
assign (residue 28 and name H5)    (residue 29 and name  H1')  6.00  2.00  1.00
assign (residue 28 and name H5)    (residue 29 and name  H5)   3.80  2.00  0.70
assign (residue 28 and name H6)    (residue 29 and name  H5)   3.80  2.00  0.70
assign (residue 28 and name H6)    (residue 29 and name  H6)   3.80  2.00  0.70

assign (residue 29 and name H1')   (residue 29 and name  H5)   5.00  2.00  1.00
assign (residue 29 and name H1')   (residue 29 and name  H6)   3.80  2.00  0.70
assign (residue 29 and name H2')   (residue 29 and name  H5)   5.00  2.00  1.00
assign (residue 29 and name H2')   (residue 29 and name  H6)   3.80  2.00  0.70
assign (residue 29 and name H3')   (residue 29 and name  H5)   5.00  2.00  1.00
assign (residue 29 and name H3')   (residue 29 and name  H6)   2.50  0.70  0.50
assign (residue 29 and name H4')   (residue 29 and name  H5)   6.00  2.00  1.00
assign (residue 29 and name H4')   (residue 29 and name  H6)   3.80  2.00  0.70

assign (residue 59 and name H1')   (residue 59 and name  H5)   5.00  2.00  1.00
assign (residue 59 and name H1')   (residue 59 and name  H6)   3.80  2.00  0.70
assign (residue 59 and name H2')   (residue 59 and name  H5)   5.00  2.00  1.00
assign (residue 59 and name H2')   (residue 59 and name  H6)   3.80  2.00  0.70
assign (residue 59 and name H3')   (residue 59 and name  H5)   3.80  2.00  0.70
assign (residue 59 and name H3')   (residue 59 and name  H6)   2.50  0.70  0.50
assign (residue 59 and name H4')   (residue 59 and name  H5)   6.00  2.00  1.00
assign (residue 59 and name H4')   (residue 59 and name  H6)   3.80  2.00  0.70
assign (residue 59 and name H5')   (residue 59 and name  H5)   5.00  2.00  1.00
```

```
assign (residue 59 and name H5')   (residue 59 and name  H6)   3.80  2.00  0.70
assign (residue 59 and name H5")  (residue 59 and name  H5)   5.00  2.00  1.00
assign (residue 59 and name H5")  (residue 59 and name  H6)   3.80  2.00  0.70

assign (residue 59 and name H1')   (residue 60 and name  H1')  5.00  2.00  1.00
assign (residue 59 and name H1')   (residue 60 and name  H8)   3.80  2.00  0.70
assign (residue 59 and name H2')   (residue 60 and name  H1')  5.00  2.00  1.00
assign (residue 59 and name H2')   (residue 60 and name  H8)   2.50  0.70  0.50
assign (residue 59 and name H3')   (residue 60 and name  H8)   3.80  2.00  0.70
assign (residue 59 and name H6)    (residue 60 and name  H8)   5.00  2.00  1.00

assign (residue 60 and name H1')   (residue 60 and name  H2)   5.00  2.00  1.00
assign (residue 60 and name H1')   (residue 60 and name  H8)   3.80  2.00  0.70
assign (residue 60 and name H2')   (residue 60 and name  H2)   5.00  2.00  1.00
assign (residue 60 and name H2')   (residue 60 and name  H8)   3.80  2.00  0.70
assign (residue 60 and name H3')   (residue 60 and name  H8)   2.50  0.70  0.50
assign (residue 60 and name H4')   (residue 60 and name  H8)   5.00  2.00  1.00
assign (residue 60 and name H5')   (residue 60 and name  H8)   3.80  2.00  0.70
assign (residue 60 and name H5")  (residue 60 and name  H8)   3.80  2.00  0.70

assign (residue 60 and name H1')   (residue 61 and name  H1')  5.00  2.00  1.00
assign (residue 60 and name H1')   (residue 61 and name  H8)   3.80  2.00  0.70
assign (residue 60 and name H2')   (residue 61 and name  H1')  3.80  2.00  0.70
assign (residue 60 and name H2')   (residue 61 and name  H8)   2.50  0.70  0.50
assign (residue 60 and name H3')   (residue 61 and name  H8)   3.80  2.00  0.70

assign (residue 60 and name H2)    (residue 61 and name  H1')  3.80  2.00  0.70
assign (residue 60 and name H2)    (residue 61 and name  H4')  6.00  2.00  1.00
assign (residue 60 and name H2)    (residue 61 and name  H8)   5.00  2.00  1.00
assign (residue 60 and name H8)    (residue 61 and name  H8)   3.80  2.00  0.70

assign (residue 61 and name H1')   (residue 61 and name  H8)   3.80  2.00  0.70
assign (residue 61 and name H2')   (residue 61 and name  H8)   3.80  2.00  0.70
assign (residue 61 and name H3')   (residue 61 and name  H8)   2.50  0.70  0.50
assign (residue 61 and name H4')   (residue 61 and name  H8)   5.00  2.00  1.00
assign (residue 61 and name H5")  (residue 61 and name  H8)   3.80  2.00  0.70

assign (residue 61 and name H1')   (residue 62 and name  H1')  5.00  2.00  1.00
assign (residue 61 and name H1')   (residue 62 and name  H5)   5.00  2.00  1.00
assign (residue 61 and name H1')   (residue 62 and name  H6)   3.80  2.00  0.70
assign (residue 61 and name H2')   (residue 62 and name  H1')  3.80  2.00  0.70
assign (residue 61 and name H2')   (residue 62 and name  H5)   3.80  2.00  0.70
assign (residue 61 and name H2')   (residue 62 and name  H6)   2.50  0.70  0.50
assign (residue 61 and name H3')   (residue 62 and name  H6)   3.80  2.00  0.70
assign (residue 61 and name H8)    (residue 62 and name  H5)   5.00  2.00  1.00
assign (residue 61 and name H8)    (residue 62 and name  H6)   5.00  2.00  1.00

assign (residue 62 and name H1')   (residue 62 and name  H5)   5.00  2.00  1.00
assign (residue 62 and name H1')   (residue 62 and name  H6)   3.80  2.00  0.70
assign (residue 62 and name H2')   (residue 62 and name  H5)   5.00  2.00  1.00
assign (residue 62 and name H2')   (residue 62 and name  H6)   3.80  2.00  0.70
```

```
assign (residue 62 and name H3')  (residue 62 and name  H5)   5.00  2.00  1.00
assign (residue 62 and name H3')  (residue 62 and name  H6)   2.50  0.70  0.50
assign (residue 62 and name H4')  (residue 62 and name  H5)   6.00  2.00  1.00
assign (residue 62 and name H4')  (residue 62 and name  H6)   3.80  2.00  0.70
assign (residue 62 and name H5")  (residue 62 and name  H6)   3.80  2.00  0.70

assign (residue 62 and name H1')  (residue 63 and name  H1')  5.00  2.00  1.00
assign (residue 62 and name H1')  (residue 63 and name  H8)   3.80  2.00  0.70
assign (residue 62 and name H2')  (residue 63 and name  H1')  3.80  2.00  0.70
assign (residue 62 and name H2')  (residue 63 and name  H8)   2.50  0.70  0.50
assign (residue 62 and name H3')  (residue 63 and name  H8)   2.50  0.70  0.50
assign (residue 62 and name H5)   (residue 63 and name  H8)   5.00  2.00  1.00
assign (residue 62 and name H6)   (residue 63 and name  H8)   3.80  2.00  0.70

assign (residue 63 and name H1')  (residue 63 and name  H8)   3.80  2.00  0.70
assign (residue 63 and name H2')  (residue 63 and name  H8)   3.80  2.00  0.70
assign (residue 63 and name H3')  (residue 63 and name  H8)   2.50  0.70  0.50
assign (residue 63 and name H4')  (residue 63 and name  H8)   5.00  2.00  1.00
assign (residue 63 and name H5')  (residue 63 and name  H8)   3.80  2.00  0.70
assign (residue 63 and name H5")  (residue 63 and name  H8)   3.80  2.00  0.70

assign (residue 63 and name H1')  (residue 64 and name  H1')  5.00  2.00  1.00
assign (residue 63 and name H1')  (residue 64 and name  H5)   5.00  2.00  1.00
assign (residue 63 and name H1')  (residue 64 and name  H6)   3.80  2.00  0.70
assign (residue 63 and name H2')  (residue 64 and name  H1')  3.80  2.00  0.70
assign (residue 63 and name H2')  (residue 64 and name  H5)   3.80  2.00  0.70
assign (residue 63 and name H2')  (residue 64 and name  H6)   2.50  0.70  0.50
assign (residue 63 and name H3')  (residue 64 and name  H5)   2.50  0.70  0.50
assign (residue 63 and name H3')  (residue 64 and name  H6)   3.80  2.00  0.70
assign (residue 63 and name H8)   (residue 64 and name  H5)   3.80  2.00  0.70
assign (residue 63 and name H8)   (residue 64 and name  H6)   5.00  2.00  1.00

assign (residue 64 and name H1')  (residue 64 and name  H5)   5.00  2.00  1.00
assign (residue 64 and name H1')  (residue 64 and name  H6)   3.80  2.00  0.70
assign (residue 64 and name H2')  (residue 64 and name  H5)   5.00  2.00  1.00
assign (residue 64 and name H2')  (residue 64 and name  H6)   3.80  2.00  0.70
assign (residue 64 and name H3')  (residue 64 and name  H5)   5.00  2.00  1.00
assign (residue 64 and name H3')  (residue 64 and name  H6)   2.50  0.70  0.50
assign (residue 64 and name H4')  (residue 64 and name  H6)   3.80  2.00  0.70
assign (residue 64 and name H5')  (residue 64 and name  H6)   3.80  2.00  0.70
assign (residue 64 and name H5")  (residue 64 and name  H6)   3.80  2.00  0.70

assign (residue 64 and name H1')  (residue 65 and name  H1')  5.00  2.00  1.00
assign (residue 64 and name H1')  (residue 65 and name  H5)   5.00  2.00  1.00
assign (residue 64 and name H1')  (residue 65 and name  H6)   3.80  2.00  0.70
assign (residue 64 and name H2')  (residue 65 and name  H1')  3.80  2.00  0.70
assign (residue 64 and name H2')  (residue 65 and name  H5)   3.80  2.00  0.70
assign (residue 64 and name H2')  (residue 65 and name  H6)   2.50  0.70  0.50
assign (residue 64 and name H3')  (residue 65 and name  H5)   3.80  2.00  0.70
assign (residue 64 and name H3')  (residue 65 and name  H6)   3.80  2.00  0.70
assign (residue 64 and name H5)   (residue 65 and name  H5)   2.50  0.70  0.50
```

```
assign (residue 65 and name H1')  (residue 65 and name  H5)   5.00  2.00  1.00
assign (residue 65 and name H1')  (residue 65 and name  H6)   3.80  2.00  0.70
assign (residue 65 and name H2')  (residue 65 and name  H5)   3.80  2.00  0.70
assign (residue 65 and name H2')  (residue 65 and name  H6)   3.80  2.00  0.70
assign (residue 65 and name H3')  (residue 65 and name  H5)   3.80  2.00  0.70
assign (residue 65 and name H3')  (residue 65 and name  H6)   2.50  0.70  0.50
assign (residue 65 and name H4')  (residue 65 and name  H5)   6.00  2.00  1.00
assign (residue 65 and name H4')  (residue 65 and name  H6)   3.80  2.00  0.70
assign (residue 65 and name H5')  (residue 65 and name  H6)   3.80  2.00  0.70
assign (residue 65 and name H5'') (residue 65 and name  H5)   5.00  2.00  1.00
assign (residue 65 and name H5'') (residue 65 and name  H6)   3.80  2.00  0.70
```

Distance constraints of exchangeable protons in d3'-EBS1*·IBS1* based on a 2D [^{1}H,^{1}H]-NOESY spectrum acquired at 700 MHz proton frequency at 278 K (90% H_2O/10% D_2O, 110 mM KCl, 110 µM EDTA, pH = 6.83).

```
assign (residue  1 and name  H1)  (residue  2 and name  H1')  6.00  2.00  1.00
assign (residue  1 and name  H1)  (residue  2 and name  H1)   5.00  2.00  1.00

assign (residue  1 and name  H1)  (residue 28 and name  H1')  6.00  2.00  1.00
assign (residue  1 and name  H1)  (residue 29 and name  H41)  2.50  0.70  0.50
assign (residue  1 and name  H1)  (residue 29 and name  H42)  3.80  2.00  0.70
assign (residue  1 and name  H1)  (residue 29 and name  H5)   6.00  2.00  1.00

assign (residue  2 and name  H1)  (residue  3 and name  H1')  6.00  2.00  1.00
assign (residue  2 and name  H1)  (residue  3 and name  H2)   5.00  2.00  1.00
assign (residue  2 and name  H1)  (residue  3 and name  H8)   6.00  2.00  1.00

assign (residue  2 and name  H1)  (residue 27 and name  H3)   5.00  2.00  1.00
assign (residue  2 and name  H1)  (residue 28 and name  H5)   6.00  2.00  1.00
assign (residue  2 and name  H1)  (residue 28 and name  H41)  2.50  0.70  0.50
assign (residue  2 and name  H1)  (residue 28 and name  H42)  3.80  2.00  0.70
assign (residue  2 and name  H1)  (residue 28 and name  H6)   6.00  2.00  1.00
assign (residue  2 and name  H1)  (residue 29 and name  H4')  5.00  2.00  1.00
assign (residue  2 and name  H1)  (residue 29 and name  H5)   6.00  2.00  1.00
assign (residue  2 and name  H1)  (residue 29 and name  H6)   5.00  2.00  1.00

assign (residue  4 and name  H1)  (residue  3 and name  H2)   5.00  2.00  1.00
assign (residue  4 and name  H1)  (residue  4 and name  H2')  6.00  2.00  1.00
assign (residue  4 and name  H1)  (residue  5 and name  H3)   3.80  2.00  1.00

assign (residue  4 and name  H1)  (residue 26 and name  H41)  2.50  0.70  0.50
assign (residue  4 and name  H1)  (residue 26 and name  H42)  3.80  2.00  0.70
assign (residue  4 and name  H1)  (residue 26 and name  H5)   5.00  2.00  1.00
assign (residue  4 and name  H1)  (residue 27 and name  H2')  5.00  2.00  1.00
assign (residue  4 and name  H1)  (residue 27 and name  H3)   3.80  2.00  0.70
assign (residue  4 and name  H1)  (residue 27 and name  H5)   5.00  2.00  1.00
assign (residue  4 and name  H1)  (residue 27 and name  H6)   5.00  2.00  1.00

assign (residue  5 and name  H3)  (residue  4 and name  H22)  6.00  2.00  1.00
```

```
assign (residue  5 and name  H3)   (residue  6 and name   H1')   5.00  2.00  1.00
assign (residue  5 and name  H3)   (residue  6 and name   H2')   6.00  2.00  1.00
assign (residue  5 and name  H3)   (residue  6 and name   H8)    5.00  2.00  1.00

assign (residue  5 and name  H3)   (residue 24 and name  H3)    5.00  2.00  1.00
assign (residue  5 and name  H3)   (residue 25 and name  H2)    3.80  2.00  0.70
assign (residue  5 and name  H3)   (residue 25 and name  H2')   6.00  2.00  1.00
assign (residue  5 and name  H3)   (residue 25 and name  H61)  2.50  0.70  0.50
assign (residue  5 and name  H3)   (residue 25 and name  H62)  3.80  2.00  0.70
assign (residue  5 and name  H3)   (residue 26 and name  H1')   6.00  2.00  1.00
assign (residue  5 and name  H3)   (residue 26 and name  H41)  3.80  2.00  0.70
assign (residue  5 and name  H3)   (residue 26 and name  H42)  5.00  2.00  1.00

assign (residue  7 and name  H3)   (residue  6 and name   H2)    5.00  2.00  1.00
assign (residue  7 and name  H3)   (residue  8 and name   H1)    3.80  2.00  0.70
assign (residue  7 and name  H3)   (residue  8 and name   H1')   5.00  2.00  1.00
assign (residue  7 and name  H3)   (residue  8 and name   H2')   6.00  2.00  1.00
assign (residue  7 and name  H3)   (residue  8 and name   H8)    5.00  2.00  1.00

assign (residue  7 and name  H3)   (residue 23 and name  H2)    3.80  2.00  0.70
assign (residue  7 and name  H3)   (residue 23 and name  H2')   6.00  2.00  1.00
assign (residue  7 and name  H3)   (residue 23 and name  H61)  2.50  0.70  0.50
assign (residue  7 and name  H3)   (residue 23 and name  H62)  3.80  2.00  0.70
assign (residue  7 and name  H3)   (residue 24 and name  H2')   5.00  2.00  1.00

assign (residue  8 and name  H1)   (residue  9 and name   H1')   6.00  2.00  1.00
assign (residue  8 and name  H1)   (residue  9 and name   H3)    3.80  2.00  0.70
assign (residue  8 and name  H1)   (residue  9 and name   H5)    6.00  2.00  1.00
assign (residue  8 and name  H1)   (residue  9 and name   H6)    6.00  2.00  1.00

assign (residue  8 and name  H1)   (residue 21 and name  H1)    5.00  2.00  1.00
assign (residue  8 and name  H1)   (residue 21 and name  H22)   6.00  2.00  1.00
assign (residue  8 and name  H1)   (residue 22 and name  H41)  2.50  0.70  0.50
assign (residue  8 and name  H1)   (residue 22 and name  H42)  3.80  2.00  0.70
assign (residue  8 and name  H1)   (residue 22 and name  H5)    6.00  2.00  1.00
assign (residue  8 and name  H1)   (residue 22 and name  H6)    6.00  2.00  1.00
assign (residue  8 and name  H1)   (residue 23 and name  H2')   5.00  2.00  1.00
assign (residue  8 and name  H1)   (residue 23 and name  H2)    5.00  2.00  1.00
assign (residue  8 and name  H1)   (residue 23 and name  H61)  6.00  2.00  1.00

assign (residue  9 and name  H3)   (residue 10 and name  H61)  6.00  2.00  1.00
assign (residue  9 and name  H3)   (residue 10 and name  H62)  5.00  2.00  1.00

assign (residue  9 and name  H3)   (residue 21 and name  H1)    2.50  0.70  0.50
assign (residue  9 and name  H3)   (residue 21 and name  H21)   5.00  2.00  1.00
assign (residue  9 and name  H3)   (residue 21 and name  H22)   3.80  2.00  0.70
assign (residue  9 and name  H3)   (residue 22 and name  H41)  3.80  2.00  0.70
assign (residue  9 and name  H3)   (residue 22 and name  H42)  3.80  2.00  0.70
assign (residue  9 and name  H3)   (residue 22 and name  H5)    6.00  2.00  1.00

assign (residue 13 and name H1)   (residue 14 and name  H1)    5.00  2.00  1.00
```

```
assign (residue 13 and name H1)   (residue 64 and name  H3)   3.80  2.00  0.70
assign (residue 13 and name H1)   (residue 64 and name  H5)   5.00  2.00  1.00
assign (residue 13 and name H1)   (residue 64 and name  H6)   6.00  2.00  1.00
assign (residue 13 and name H1)   (residue 65 and name  H41)  2.50  0.70  0.50
assign (residue 13 and name H1)   (residue 65 and name  H42)  3.80  2.00  0.70

assign (residue 14 and name H1)   (residue 15 and name  H1')  6.00  2.00  1.00
assign (residue 14 and name H1)   (residue 15 and name  H41)  6.00  2.00  1.00
assign (residue 14 and name H1)   (residue 15 and name  H42)  5.00  2.00  1.00
assign (residue 14 and name H1)   (residue 15 and name  H5)   6.00  2.00  1.00
assign (residue 14 and name H1)   (residue 15 and name  H6)   6.00  2.00  1.00

assign (residue 14 and name H1)   (residue 63 and name  H1)   5.00  2.00  1.00
assign (residue 14 and name H1)   (residue 64 and name  H1')  5.00  2.00  1.00
assign (residue 14 and name H1)   (residue 64 and name  H2')  6.00  2.00  1.00
assign (residue 14 and name H1)   (residue 64 and name  H3)   2.50  0.70  0.50
assign (residue 14 and name H1)   (residue 64 and name  H5)   6.00  2.00  1.00
assign (residue 14 and name H1)   (residue 64 and name  H6)   6.00  2.00  1.00
assign (residue 14 and name H1)   (residue 65 and name  H2')  5.00  2.00  1.00
assign (residue 14 and name H1)   (residue 65 and name  H41)  5.00  2.00  1.00
assign (residue 14 and name H1)   (residue 65 and name  H5)   5.00  2.00  1.00

assign (residue 18 and name H3)   (residue 19 and nameH1)     3.80  2.00  0.70
assign (residue 18 and name H3)   (residue 19 and nameH8)     5.00  2.00  1.00

assign (residue 18 and name H3)   (residue 60 and name  H2)   3.80  2.00  0.70
assign (residue 18 and name H3)   (residue 60 and name  H61)  2.50  0.70  0.50
assign (residue 18 and name H3)   (residue 60 and name  H62)  3.80  2.00  0.70
assign (residue 18 and name H3)   (residue 61 and name  H1)   3.80  2.00  0.70

assign (residue 19 and name H1)   (residue 59 and name  H41)  2.50  0.70  0.50
assign (residue 19 and name H1)   (residue 59 and name  H42)  3.80  2.00  0.70
assign (residue 19 and name H1)   (residue 59 and name  H5)   6.00  2.00  1.00
assign (residue 19 and name H1)   (residue 59 and name  H6)   6.00  2.00  1.00

assign (residue 21 and name H1)   (residue 22 and name  H1')  6.00  2.00  1.00
assign (residue 21 and name H1)   (residue 22 and name  H41)  6.00  2.00  1.00
assign (residue 21 and name H1)   (residue 22 and name  H42)  5.00  2.00  1.00
assign (residue 21 and name H1)   (residue 22 and name  H5)   6.00  2.00  1.00
assign (residue 21 and name H1)   (residue 22 and name  H6)   6.00  2.00  1.00

assign (residue 21 and name H1)   (residue  9 and name  H1')  5.00  2.00  1.00
assign (residue 21 and name H1)   (residue  9 and name  H2')  6.00  2.00  1.00
assign (residue 21 and name H1)   (residue  9 and name  H5)   6.00  2.00  1.00
assign (residue 21 and name H1)   (residue  8 and name  H21)  5.00  2.00  1.00

assign (residue 24 and name H3)   (residue 23 and name  H2)   5.00  2.00  1.00
assign (residue 24 and name H3)   (residue 24 and name  H2')  5.00  2.00  1.00
assign (residue 24 and name H3)   (residue 25 and name  H1')  5.00  2.00  1.00
assign (residue 24 and name H3)   (residue 25 and name  H2')  6.00  2.00  1.00
assign (residue 24 and name H3)   (residue 25 and name  H8)   5.00  2.00  1.00
```

```
assign (residue 24 and name H3)   (residue  6 and name  H2')  6.00  2.00  1.00
assign (residue 24 and name H3)   (residue  6 and name  H2)   3.80  2.00  0.70
assign (residue 24 and name H3)   (residue  6 and name  H61)  2.50  0.70  0.50
assign (residue 24 and name H3)   (residue  6 and name  H62)  3.80  2.00  0.70
assign (residue 24 and name H3)   (residue  7 and name  H3)   3.80  2.00  0.70

assign (residue 27 and name H3)   (residue 27 and name  H2')  5.00  2.00  1.00
assign (residue 27 and name H3)   (residue 28 and name  H1')  5.00  2.00  1.00
assign (residue 27 and name H3)   (residue 28 and name  H5)   5.00  2.00  1.00
assign (residue 27 and name H3)   (residue 28 and name  H6)   6.00  2.00  1.00

assign (residue 27 and name H3)   (residue  3 and name  H2)   3.80  2.00  0.70
assign (residue 27 and name H3)   (residue  3 and name  H61)  2.50  0.70  0.50
assign (residue 27 and name H3)   (residue  3 and name  H62)  3.80  2.00  0.70

assign (residue 61 and name H1)   (residue 60 and name  H2)   5.00  2.00  1.00
assign (residue 61 and name H1)   (residue 62 and name  H1')  6.00  2.00  1.00
assign (residue 61 and name H1)   (residue 62 and name  H3)   3.80  2.00  0.70
assign (residue 61 and name H1)   (residue 62 and name  H5)   6.00  2.00  1.00
assign (residue 61 and name H1)   (residue 62 and name  H6)   6.00  2.00  1.00

assign (residue 61 and name H1)   (residue 17 and name  H41)  2.50  0.70  0.50
assign (residue 61 and name H1)   (residue 17 and name  H42)  3.80  2.00  0.70
assign (residue 61 and name H1)   (residue 17 and name  H5)   6.00  2.00  1.00
assign (residue 61 and name H1)   (residue 17 and name  H6)   6.00  2.00  1.00
assign (residue 61 and name H1)   (residue 18 and name  H5)   5.00  2.00  1.00
assign (residue 61 and name H1)   (residue 18 and name  H6)   5.00  2.00  1.00

assign (residue 62 and name H3)   (residue 63 and name  H1)   3.80  2.00  0.70
assign (residue 62 and name H3)   (residue 63 and name  H8)   5.00  2.00  1.00

assign (residue 62 and name H3)   (residue 16 and name  H2)   3.80  2.00  0.70

assign (residue 63 and name H1)   (residue 64 and name  H3)   3.80  2.00  0.70

assign (residue 63 and name H1)   (residue 15 and name  H41)  2.50  0.70  0.50
assign (residue 63 and name H1)   (residue 15 and name  H42)  3.80  2.00  0.70
assign (residue 63 and name H1)   (residue 15 and name  H5)   6.00  2.00  1.00
assign (residue 63 and name H1)   (residue 15 and name  H6)   6.00  2.00  1.00

assign (residue 64 and name H3)   (residue 65 and name  H2')  6.00  2.00  1.00
assign (residue 64 and name H3)   (residue 65 and nameH5)     5.00  2.00  1.00
assign (residue 64 and name H3)   (residue 65 and nameH6)     6.00  2.00  1.00

assign (residue 64 and name H3)   (residue 14 and name  H21)  5.00  2.00  1.00
assign (residue 64 and name H3)   (residue 14 and name  H22)  3.80  2.00  0.70
assign (residue 64 and name H3)   (residue 15 and name  H41)  3.80  2.00  0.70
assign (residue 64 and name H3)   (residue 15 and name  H42)  3.80  2.00  0.70
assign (residue 64 and name H3)   (residue 15 and name  H6)   5.00  2.00  1.00
```

Hydrogen-bond restraints whose existence was proven by 2D [^{1}H,^{1}H]-NOESY spectrum acquired at 278 K at 700 MHz proton frequency (90% H_2O/10% D_2O, 110 mM KCl, 110 μM EDTA, pH = 6.83) and by a 2D J_{NN} HNN-COSY experiment acquired at 278 K (90% H_2O/10% D_2O, 50 mM KCl, 10 μM EDTA, pH = 6.45).

G1-C29

```
assign (residue  1 and name  H1)  (residue 29 and name  N3)  2.00  0.20  0.20
assign (residue  1 and name  N1)  (residue 29 and name  N3)  2.90  0.30  0.30
assign (residue  1 and name  O6)  (residue 29 and name  H41) 2.00  0.20  0.20
assign (residue  1 and name  O6)  (residue 29 and name  N4)  2.90  0.30  0.30
assign (residue  1 and name  H21) (residue 29 and name  O2)  2.00  0.20  0.20
assign (residue  1 and name  N2)  (residue 29 and name  O2)  2.90  0.30  0.30
```

G2-C28

```
assign (residue  2 and name  H1)  (residue 28 and name  N3)  2.00  0.20  0.20
assign (residue  2 and name  N1)  (residue 28 and name  N3)  2.90  0.30  0.30
assign (residue  2 and name  O6)  (residue 28 and name  H41) 2.00  0.20  0.20
assign (residue  2 and name  O6)  (residue 28 and name  N4)  2.90  0.30  0.30
assign (residue  2 and name  H21) (residue 28 and name  O2)  2.00  0.20  0.20
assign (residue  2 and name  N2)  (residue 28 and name  O2)  2.90  0.30  0.30
```

A3-U27

```
assign (residue  3 and name  N1)  (residue 27 and name  H3)  2.00  0.20  0.20
assign (residue  3 and name  N1)  (residue 27 and name  N3)  2.90  0.30  0.30
assign (residue  3 and name  H61) (residue 27 and name  O4)  2.00  0.20  0.20
assign (residue  3 and name  N6)  (residue 27 and name  O4)  2.90  0.30  0.30
```

G4-C26

```
assign (residue  4 and name  H1)  (residue 26 and name  N3)  2.00  0.20  0.20
assign (residue  4 and name  N1)  (residue 26 and name  N3)  2.90  0.30  0.30
assign (residue  4 and name  O6)  (residue 26 and name  H41) 2.00  0.20  0.20
assign (residue  4 and name  O6)  (residue 26 and name  N4)  2.90  0.30  0.30
assign (residue  4 and name  H21) (residue 26 and name  O2)  2.00  0.20  0.20
assign (residue  4 and name  N2)  (residue 26 and name  O2)  2.90  0.30  0.30
```

U5-A25

```
assign (residue  5 and name  H3)  (residue 25 and name  N1)  2.00  0.20  0.20
assign (residue  5 and name  N3)  (residue 25 and name  N1)  2.90  0.30  0.30
assign (residue  5 and name  O4)  (residue 25 and name  H61) 2.00  0.20  0.20
assign (residue  5 and name  O4)  (residue 25 and name  N6)  2.90  0.30  0.30
```

A6-U24

```
assign (residue  6 and name  N1)  (residue 24 and name  H3)  2.00  0.20  0.20
assign (residue  6 and name  N1)  (residue 24 and name  N3)  2.90  0.30  0.30
assign (residue  6 and name  H61) (residue 24 and name  O4)  2.00  0.20  0.20
assign (residue  6 and name  N6)  (residue 24 and name  O4)  2.90  0.30  0.30
```

U7-A23

```
assign (residue  7 and name  H3)  (residue 23 and name  N1)  2.00  0.20  0.20
assign (residue  7 and name  N3)  (residue 23 and name  N1)  2.90  0.30  0.30
assign (residue  7 and name  O4)  (residue 23 and name  H61) 2.00  0.20  0.20
```

```
assign (residue  7 and name  O4)   (residue 23 and name  N6)   2.90  0.30  0.30
```

G8-C22

```
assign (residue  8 and name  H1)   (residue 22 and name  N3)   2.00  0.20  0.20
assign (residue  8 and name  N1)   (residue 22 and name  N3)   2.90  0.30  0.30
assign (residue  8 and name  O6)   (residue 22 and name  H41)  2.00  0.20  0.20
assign (residue  8 and name  O6)   (residue 22 and name  N4)   2.90  0.30  0.30
assign (residue  8 and name  H21)  (residue 22 and name  O2)   2.00  0.20  0.20
assign (residue  8 and name  N2)   (residue 22 and name  O2)   2.90  0.30  0.30
```

U9-G21

```
assign (residue  9 and name  H3)   (residue 21 and name  H1)   1.90  0.10  0.20
assign (residue  9 and name  H3)   (residue 21 and name  O6)   1.90  0.10  0.20
assign (residue  9 and name  N3)   (residue 21 and name  O6)   2.90  0.10  0.20
assign (residue  9 and name  O2)   (residue 21 and name  H1)   1.90  0.10  0.20
assign (residue  9 and name  O2)   (residue 21 and name  N1)   2.90  0.10  0.20
```

G13-C65

```
assign (residue 13 and name H1)   (residue 65 and name  N3)   2.00  0.20  0.20
assign (residue 13 and name N1)   (residue 65 and name  N3)   2.90  0.30  0.30
assign (residue 13 and name O6)   (residue 65 and name  H41)  2.00  0.20  0.20
assign (residue 13 and name O6)   (residue 65 and name  N4)   2.90  0.30  0.30
assign (residue 13 and name H21)  (residue 65 and name  O2)   2.00  0.20  0.20
assign (residue 13 and name N2)   (residue 65 and name  O2)   2.90  0.30  0.30
```

G14-U64

```
assign (residue 14 and name H1)   (residue 64 and name  H3)   1.90  0.10  0.20
assign (residue 14 and name H1)   (residue 64 and name  O2)   1.90  0.10  0.20
assign (residue 14 and name N1)   (residue 64 and name  O2)   2.90  0.10  0.20
assign (residue 14 and name O6)   (residue 64 and name  H3)   1.90  0.10  0.20
assign (residue 14 and name O6)   (residue 64 and name  N3)   2.90  0.10  0.20
```

C15-G63

```
assign (residue 15 and name N3)   (residue 63 and name  H1)   2.00  0.20  0.20
assign (residue 15 and name N3)   (residue 63 and name  N1)   2.90  0.30  0.30
assign (residue 15 and name H41)  (residue 63 and name  O6)   2.00  0.20  0.20
assign (residue 15 and name N4)   (residue 63 and name  O6)   2.90  0.30  0.30
assign (residue 15 and name O2)   (residue 63 and name  H21)  2.00  0.20  0.20
assign (residue 15 and name O2)   (residue 63 and name  N2)   2.90  0.30  0.30
```

A16-U62

```
assign (residue 16 and name N1)   (residue 62 and name  H3)   2.00  0.20  0.20
assign (residue 16 and name N1)   (residue 62 and name  N3)   2.90  0.30  0.30
assign (residue 16 and name H61)  (residue 62 and name  O4)   2.00  0.20  0.20
assign (residue 16 and name N6)   (residue 62 and name  O4)   2.90  0.30  0.30
```

C17-G61

```
assign (residue 17 and name N3)   (residue 61 and name  H1)   2.00  0.20  0.20
assign (residue 17 and name N3)   (residue 61 and name  N1)   2.90  0.30  0.30
assign (residue 17 and name H41)  (residue 61 and name  O6)   2.00  0.20  0.20
assign (residue 17 and name N4)   (residue 61 and name  O6)   2.90  0.30  0.30
```

```
assign (residue 17 and name O2)  (residue 61 and name  H21) 2.00  0.20  0.20
assign (residue 17 and name O2)  (residue 61 and name  N2)  2.90  0.30  0.30
```

U18-A60

```
assign (residue 18 and name H3)  (residue 60 and name  N1)  2.00  0.20  0.20
assign (residue 18 and name N3)  (residue 60 and name  N1)  2.90  0.30  0.30
assign (residue 18 and name O4)  (residue 60 and name  H61) 2.00  0.20  0.20
assign (residue 18 and name O4)  (residue 60 and name  N6)  2.90  0.30  0.30
```

G19-C59

```
assign (residue 19 and name H1)  (residue 59 and name  N3)  2.00  0.20  0.20
assign (residue 19 and name N1)  (residue 59 and name  N3)  2.90  0.30  0.30
assign (residue 19 and name O6)  (residue 59 and name  H41) 2.00  0.20  0.20
assign (residue 19 and name O6)  (residue 59 and name  N4)  2.90  0.30  0.30
assign (residue 19 and name H21) (residue 59 and name  O2)  2.00  0.20  0.20
assign (residue 19 and name N2)  (residue 59 and name  O2)  2.90  0.30  0.30
```

Appendix 18 All RDCs used in the structure calculation of d3'-EBS1*·IBS1*

The first number represents the RDC value, the second and third the lower and upper error limits.

U5	C6H6	16.12	2.0	2.0
U9	C6H6	19.28	2.0	2.0
U11	C6H6	24.6	2.0	2.0
U12	C6H6	15.87	2.0	2.0
U18	C6H6	20.58	2.0	2.0
C22	C6H6	24.6	2.0	2.0
C26	C6H6	16.02	2.0	2.0
U27	C6H6	13.72	2.0	2.0
C28	C6H6	26.07	2.0	2.0
G1	C8H8	36.9	2.0	2.0
G2	C8H8	21.68	2.0	2.0
A3	C8H8	17.11	2.0	2.0
G4	C8H8	24.75	2.0	2.0
A6	C8H8	15.55	2.0	2.0
G8	C8H8	39.52	2.0	2.0
A10	C8H8	31.86	2.0	2.0
A16	C8H8	43.95	2.0	2.0
G19	C8H8	34.9	2.0	2.0
A20	C8H8	24.93	2.0	2.0
A25	C8H8	29.71	2.0	2.0
A3	C2H2	24.12	2.0	2.0
A6	C2H2	38.59	2.0	2.0
A10	C2H2	36.64	2.0	2.0
A16	C2H2	13.28	2.0	2.0
A20	C2H2	40.98	2.0	2.0
A23	C2H2	40.26	2.0	2.0
G1	N1H1	17.3	2.0	2.0
G2	N1H1	18.21	2.0	2.0
G4	N1H1	22.19	2.0	2.0
G8	N1H1	14.99	2.0	2.0
G19	N1H1	37.11	2.0	2.0
G21	N1H1	23.8	2.0	2.0
U5	N3H3	20.27	2.0	2.0
U9	N3H3	22.4	2.0	2.0
U18	N3H3	14.7	2.0	2.0
U24	N3H3	18.42	2.0	2.0
U27	N3N3	10.44	2.0	2.0

Appendix 19 Dihedral angle restraints for the structure calculation of d3'-EBS1*·IBS1*

Phosphate-sugar-backbone dihedral angle restraints. β, γ and ε are only restrained for A-helical regions for residues with a 3'-endo sugar pucker. The number in the middle represents the angle in °, the two numbers to the right and the left are the error limits and the last number is a weighting factor. The exact values were taken from the dihedral angle restraint file of the structure calculation for D5-36, which represents a RNA hairpin structure.[34]

```
assign  (residue n-1    and name O3' )
        (residue n      and name P   )
        (residue n      and name O5' )
        (residue n      and name C5' )      20.0    -62.1   10.0    2       {*alpha*}

assign  (residue n      and name P   )
        (residue n      and name O5' )
        (residue n      and name C5' )
        (residue n      and name C4' )      20.0    -179.9  10.0    2       {*beta*}

assign  residue n       and name O5' )
        (residue n      and name C5' )
        (residue n      and name C4' )
        (residue n      and name C3' )      20.0    47.44   10.0    2       {*gamma*}

assign  (residue n      and name C4' )
        (residue n      and name C3' )
        (residue n      and name O3' )
        (residue n+1    and name P   )      20.0    -151.7  10.0    2       {*epsilon*}

assign  (residue n      and name C3' )
        (residue n      and name O3' )
        (residue n+1    and name P   )
        (residue n+1    and name O5' )      20.0    -73.6   10.0    2       {*zeta*}
```

Sugar pucker restraints for 2'-endo and 3'-endo sugars. Helical A-type RNA is usually 3'-endo and does not give a strong H1'-H2' crosspeak in 2D [^{1}H,^{1}H]-TOCSY experiments. The unpaired nucleotides A10, U11, and U12 were constrained to S-type (2'-endo). G1, C29, and C65 were left unconstrained. The sugar pucker restraints are based on a 2D [^{1}H^{1}H]-TOCSY that was acquired at 298 K and 700 MHz proton frequency with 45 ms mixing time (100% D_2O containing 110 mM KCl and 10 μM EDTA, pD = 6.83).

```
2'-endo sugar pucker
assign  (residue n and name C5'  )
        (residue n and name C4'  )
        (residue n and name C3'  )
        (residue n and name O3'  )    20.0    145.0   30.0    2       {*delta*}

assign  (residue n and name O4'  )
        (residue n and name C1'  )
        (residue n and name C2'  )
        (residue n and name C3'  )    20.0    25.0    30.0    2       {*nu1*}

assign  (residue n and name C1'  )
        (residue n and name C2'  )
        (residue n and name C3'  )
        (residue n and name C4'  )    20.0    -35.0   30.0    2       {*nu2*}

3'-endo sugar pucker
assign  (residue n and name C5'  )
        (residue n and name C4'  )
        (residue n and name C3'  )
        (residue n and name O3'  )    20.0    85.0    30.0    2       {*delta*}

assign  (residue n and name O4'  )
        (residue n and name C1'  )
        (residue n and name C2'  )
        (residue n and name C3'  )    20.0    -25.0   30.0    2       {*nu1*}

assign  (residue n and name C1'  )
        (residue n and name C2'  )
        (residue n and name C3'  )
        (residue n and name C4'  )    20.0    37.3    30.0    2       {*nu2*}
```

Restraints for the torsion angle χ, which defines the orientation of the base to the sugar around the glycosidic bond. All χ angles were constrained to be in an *anti* orientation because of the absence of strong H1'-H8/H6 crosspeaks in the short mixing time 2D [^{1}H,^{1}H]-NOESYs recorded in D_2O.

```
torsion angle χ
assign  (residue n and name O4'  )
        (residue n and name C1'  )
        (residue n and name N9   )
        (residue n and name C4   )    20.0    -160    20.0    2
```

Appendix 20 Chemical shift values of the H1', H2, H5, H6 and H8 protons of d3'-EBS1*·IBS1* (0.9 mM in 100% D_2O, 110 mM KCl, 10 µM EDTA, pD = 6.83) upon addition of Mg^{2+}. All the protons that were used for the calculation of the affinity constants are listed according to their binding sites. The chemical shifts were extracted from 2D [$^1H^1H$]-NOESY spectra recorded on a 700 MHz Bruker Avance spectrometer at 298 K. The values that were omitted in the fitting procedure to calculate the log K_A values are marked in bold.

Mg^{2+}[mM]	0	0.5	1	2	3	4	5	6	7	8	10
5'-end	Fixed value of 3.03 ± 0.05 due to broadening of resonances at the 5'-end in d3'-EBS1*·IBS1*										
H1											
A3H1'	5.892	5.889	5.886	5.879	5.869	5.867	5.859	5.858	-	-	-
G4H1'	5.459	5.461	5.464	5.468	5.470	5.471	**5.469**	5.471	5.471	5.471	-
G4H8	6.969	6.970	6.979	6.997	6.999	7.009	7.016	7.018	7.019	-	-
U5H6	7.569	7.576	7.577	7.583	7.596	7.603	**7.612**	7.603	7.603	-	-
A25H2	**7.029**	**7.029**	7.029	7.023	7.021	7.016	7.015	7.012	7.011	7.010	-
C26H1	5.267	5.269	5.271	5.273	5.275	**5.278**	**5.276**	5.279	5.280	5.281	-
C26H6	7.453	7.462	7.470	7.490	7.501	7.504	7.511	7.530	7.529	-	-
U27H6	7.804	7.807	7.810	7.815	7.816	7.817	**7.816**	7.822	7.825	-	-
L1											
G13H1'	5.675	5.666	5.655	5.611	5.607	5.610	5.606	5.608	5.607	-	-
G13H8	7.941	7.936	7.916	**7.887**	7.886	7.880	7.876	7.878	-	-	-
G14H1'	5.782	5.781	5.777	5.764	5.755	5.751	5.746	5.747	5.746	5.750	-
G14H8	7.448	7.442	7.441	7.432	7.424	7.422	7.416	7.417	7.417	-	-
L2											
A16H2	7.314	7.318	7.320	7.329	7.333	7.334	7.336	7.337	7.338	7.339	**7.334**
A16H8	7.882	7.884	7.888	7.893	7.899	7.902	7.905	7.908	-	-	-
U18H6	7.658	7.660	7.669	7.675	7.692	7.705	7.710	7.711	7.709	-	-
G19H1'	5.537	5.537	5.535	5.532	5.529	5.527	5.524	5.525	5.524	5.52	5.522
A20H1'	5.799	5.798	5.796	5.790	5.784	5.780	5.776	5.772	5.773	-	-
A20H8	7.593	7.586	7.574	7.549	7.530	7.518	7.498	7.485	7.484	-	-
G21H1'	5.415	5.408	5.402	5.378	5.364	5.352	5.336	5.329	5.330	5.329	-
C59H1'	5.299	5.301	5.303	5.309	5.313	5.316	5.321	5.319	5.318	5.321	-
C59H5	5.054	5.06	5.068	5.089	5.103	5.107	5.119	5.123	-	-	-
C59H6	7.416	7.424	7.437	7.462	7.482	7.490	7.508	7.507	-	-	-
A60H2	6.935	6.937	6.940	6.949	6.957	6.960	6.963	6.971	6.977	6.980	6.980
A60H8	7.940	7.942	7.948	7.955	7.957	7.962	7.961	7.967	-	-	-
G61H1'	5.548	5.551	5.556	5.566	5.574	5.576	5.581	5.585	5.593	-	-
G61H8	7.270	7.280	7.290	7.321	7.341	7.359	7.377	7.386	-	-	-
U62H6	7.561	7.564	7.573	7.583	7.595	7.601	7.601	7.606	-	-	-
G63H1'	5.665	5.663	5.662	5.658	5.655	5.654	5.653	**5.650**	**5.653**	5.651	5.651
G63H8	7.431	7.426	7.422	7.410	7.402	7.398	7.384	7.387	7.383	-	-
U64H1'	5.287	5.283	5.280	5.269	5.261	5.257	5.253	5.249	5.249	-	-
free											
A6H2	6.925	6.924	6.921	6.919	6.918	6.913	6.913	6.909	6.910	6.907	6.908
U7H1'	5.301	5.300	5.299	5.296	5.295	**5.292**	5.292	**5.293**	5.291	5.290	-
U7H5	4.915	4.916	4.918	4.921	4.921	4.922	4.922	**4.917**	-	-	-
G8H1'	5.598	5.597	5.596	5.594	5.591	5.590	5.588	5.587	5.588	-	-
G8H8	7.431	7.434	7.429	7.428	7.422	7.421	7.418	7.420	-	-	-
U11H1'	5.838	5.836	5.834	5.828	5.817	5.812	5.801	5.792	5.784	5.776	5.777
U11H5	5.632	5.631	5.627	5.614	5.604	5.599	5.587	5.585	5.581	5.572	5.573
U11H6	7.662	7.663	7.661	7.66	7.654	7.653	7.647	7.647	7.645	7.646	7.642
U12H1'	5.877	5.873	5.867	5.849	5.832	5.828	5.817	5.808	5.789	5.782	5.776
U12H6	7.707	7.702	7.696	7.681	7.663	7.653	7.641	7.631	7.610	7.605	7.597
C15H1'	5.382	5.380	5.379	5.372	5.366	5.360	5.357	5.356	-	-	-
C15H6	7.644	7.648	7.651	7.662	7.666	7.664	7.667	7.664	**7.658**	**7.657**	-
C17H6	7.374	7.377	7.379	7.382	7.385	7.389	7.394	7.394	-	-	-
A20H2	7.567	7.566	7.559	7.543	7.531	7.521	7.508	7.499	7.492	7.478	-
G21H8	7.129	7.124	7.121	7.103	7.088	7.069	7.045	7.031	7.033	-	-
C22H1'	5.254	5.251	5.248	5.239	5.232	5.226	5.218	5.214	-	-	-
A23H8	7.886	7.890	7.892	7.897	7.905	7.905	7.912	7.910	-	-	-
U24H6	7.563	7.564	7.570	7.586	7.592	7.596	7.596	7.595	-	-	-
C29H1'	5.611	5.607	5.603	5.591	5.582	5.573	5.568	5.558	-	-	-
C65H1'	5.764	5.762	5.762	5.758	5.753	5.749	5.746	5.745	5.743	-	-
C65H5	5.535	5.538	5.543	5.550	5.563	5.565	5.572	5.575	5.574	-	-

Appendix 21 Affinity constants log $K_{A,est}$ values for Mg^{2+} binding to d3'-EBS1*·IBS1*

A Listed are the individual log $K_{A,est}$ values obtained from the change in chemical shifts of all aromatic and H1' protons in d3'-EBS1*·IBS1* after the first round of calculation in which the Mg^{2+} concentration corresponds to the total amount of Mg^{2+} added at each titration point.[a] The nucleotides belonging to the four individual binding sites are shaded by alternative grey scales.

	5'-end		H1										L1		
residue	G1	G2	A3	G4	U5	A6	U7	G8	U9	A10	U11	U12	G13	G14	
H1'	n.d.[c]	n.d.[c]	1.94 ± 0.31	3.09 ± 0.15	n.d.[b]	n.d.[b]	2.29 ± 0.12	2.25 ± 0.24	n.d.[d]	n.d.[b]	1.54 ± 0.37	1.78± 0.18	3.13 ± 0.32	2.65 ± 0.24	
H2/H5	-	-	n.d.[d]	-	n.d.[b]	2.17 ± 0.21	2.97 ± 0.28	-	n.d.[b]	n.d.[d]	2.09 ± 0.15	n.d.[d]	-	-	
H6/H8	n.d.[c]	n.d.[c]	n.d.[b]	2.40 ± 0.20	2.51 ± 0.32	n.d.[b]	n.d.[b]	2.12 ± 0.72	n.d.[b]	n.d.[b]	1.89 ± 0.31	1.72 ± 0.17	2.79 ± 0.26	2.52 ± 0.19	

			H1						L2						
residue	C29	C28	U27	C26	A25	U24	A23	C22	G21	A20	G19	U18	C17	A16	C15
H1'	1.61 ± 0.25	n.d.[b]	n.d.[d]	2.30 ± 0.07	n.d.[b]	n.d.[b]	n.d.[b]	1.51 ± 0.27	2.31 ± 0.16	1.97 ± 0.26	2.25 ± 0.20	n.d.[d]	n.d.[b]	n.d.[b]	1.91 ± 0.36
H2/H5	n.d.[c]	n.d.[b]	n.d.[b]	n.d.[b]	2.42 ± 0.16	n.d.[b]	n.d.[b]	n.d.[b]	-	1.42 ± 0.24	-	n.d.[d]	n.d.[b]	2.71 ± 0.11	n.d.[c]
H6/H8	n.d.[b]	n.d.[b]	2.28 ± 0.24	2.19 ± 0.22	n.d.[b]	2.72 ± 0.32	2.27 ± 0.32	n.d.[b]	1.24 ± 0.10	2.04 ± 0.15	n.d.[d]	2.28 ± 0.31	1.67 ± 0.47	2.11 ± 0.13	3.05 ± 0.33

	L2						
residue	C59	A60	G61	U62	G63	U64	C65
H1'	2.41 ± 0.12	n.d.[b]	2.04 ± 0.20	n.d.[b]	2.62 ± 0.11	2.35 ± 0.14	1.81 ± 0.32
H2/H5	2.29 ± 0.18	2.00 ± 0.17	-	n.d.[b]	-	n.d.[d]	2.27 ± 0.21
H6/H8	2.31 ± 0.18	2.48 ± 0.25	1.99 ± 0.16	2.45 ± 0.20	2.19 ± 0.23	n.d.[b]	n.d.[b]

B Affinity constants log $K_{A,est5}$ for Mg^{2+} binding to d3'-EBS1*·IBS1* after the fifth iteration round with equilibrium taken into account.

	5'-end		H1										L1		
residue	G1	G2	A3	G4	U5	A6	U7	G8	U9	A10	U11	U12	G13	G14	
H1'	n.d.[c]	n.d.[c]	2.62 ± 0.20	3.90 ± 0.09	n.d.[b]	n.d.[b]	2.94 ± 0.10	2.94 ± 0.17	n.d.[d]	n.d.[b]	2.24 ± 0.15	2.38 ± 0.12	4.08 ± 0.45	3.15 ± 0.22	
H2/H5	-	-	n.d.[d]	-	n.d.[b]	2.70 ± 0.17	4.61 ± 0.54	-	n.d.[b]	n.d.[d]	2.65 ± 0.10	n.d.[d]	-	-	
H6/H8	n.d.[c]	n.d.[c]	n.d.[b]	2.99 ± 0.17	3.10 ± 0.29	n.d.[b]	n.d.[b]	2.97 ± 0.53	n.d.[b]	n.d.[b]	2.51 ± 0.19	2.34 ± 0.09	3.41 ± 0.27	2.99 ± 0.17	

			H1						L2						
residue	C29	C28	U27	C26	A25	U24	A23	C22	G21	A20	G19	U18	C17	A16	C15
H1'	2.54 ± 0.12	n.d.[b]	n.d.[d]	2.82 ± 0.10	n.d.[b]	n.d.[b]	n.d.[b]	2.49 ± 0.09	2.86 ± 0.11	2.61 ± 0.15	2.74 ± 0.17	n.d.[d]	n.d.[b]	n.d.[b]	2.75 ± 0.18
H2/H5	n.d.[c]	n.d.[b]	n.d.[b]	n.d.[b]	2.81 ± 0.14	n.d.[b]	n.d.[b]	n.d.[b]	-	2.31 ± 0.10	-	n.d.[d]	n.d.[b]	3.34 ± 0.10	n.d.[c]
H6/H8	n.d.[b]	n.d.[b]	2.80 ± 0.26	2.74 ± 0.20	n.d.[b]	3.81 ± 0.30	3.03 ± 0.27	n.d.[b]	2.32 ± 0.23	2.65 ± 0.10	n.d.[d]	2.88 ± 0.24	2.54 ± 0.24	2.77 ± 0.08	4.64 ± 0.57

									L2						
residue									C59	A60	G61	U62	G63	U64	C65
H1'									2.97 ± 0.07	n.d.[b]	2.65 ± 0.17	n.d.[b]	3.15 ± 0.07	2.95 ± 0.09	2.60 ± 0.15
H2/H5									2.95 ± 0.14	2.49 ± 0.12	-	n.d.[b]	-	n.d.[d]	2.98 ± 0.15
H6/H8									2.96 ± 0.14	3.13 ± 0.27	2.67 ± 0.08	3.12 ± 0.16	2.78 ± 0.18	n.d.[b]	n.d.[b]

[a]The chemical shift changes were obtained from [^{1}H,^{1}H]-NOESY spectra in D_2O (0.9 mM d3'-EBS1*·IBS1* RNA, pD 6.83, 110 mM KCl, 10 µM EDTA, 25 ºC). The log K_A values were calculated with a Levenberg-Marquardt nonlinear least-squares regression for a single binding isotherm. The four individual binding sites were identified by Mg^{2+} titrations as well as by Mg^{2+} and Mn^{2+} line broadening data. All error limits given correspond to one standard deviation (1σ). [b]n.d., not determined because chemical shift changes were too small. [c]n.d., not determined as peaks are getting too broad with higher Mg^{2+} concentrations, [d] n.d., not determined because a 1:1 binding fit was not possible.

.

Appendix 22 Chemical shift values of the H1', H2, H5, H6 and H8 protons of d3'-EBS1*·IBS1* (0.61 mM in 100% D_2O, 110 mM KCl, 10 µM EDTA, pD = 6.89) upon addition of Cd^{2+}. All the protons that were used for the calculation of the affinity constants are listed according to their binding sites. The chemical shifts were extracted from 2D [$^1H^1H$]-NOESY spectra recorded on a 700 MHz Bruker Avance spectrometer at 298 K. The values that were omitted in the fitting procedure to calculate the log K_A values are marked in bold.

Cd^{2+}[mM]	**0**	**0.5**	**1**	**1.5**	**2**	**2.5**	**3**	**3.5**	**4**	**5**	**7**
5'-end	Literature values for DP, TP1 and TP2 used because a fit to 1:1 binding behaviour was not possible										
H1											
A3H1'	5.898	5.893	**5.894**	5.888	**5.889**	5.886	5.884	**5.879**	5.880	5.881	-
A3H2	7.402	7.408	7.419	7.424	7.434	7.437	7.445	7.447	7.451	7.454	-
G4H1'	5.469	5.468	5.465	5.460	5.458	5.454	**5.446**	5.447	5.448	5.444	5.444
G4H8	6.976	6.982	**6.977**	7.011	7.021	7.039	**7.039**	7.040	7.042	7.037	-
U5H6	7.583	7.592	7.594	7.614	7.631	7.639	7.654	7.662	7.664	7.668	7.667
C26H1	5.275	5.274	5.270	5.268	**5.271**	5.263	5.260	5.256	5.255	5.252	5.252
L1											
G13H1'	5.712	5.696	5.685	5.683	**5.678**	**5.677**	5.680	5.679	**5.681**	**5.682**	**5.684**
L2											
U11H1'	5.837	5.835	5.836	5.833	5.829	5.823	5.822	5.821	5.818	5.818	5.813
U11H5	5.638	5.635	5.629	5.622	5.615	5.610	5.605	5.599	5.599	5.595	5.595
U12H1'	5.863	5.858	5.851	5.851	**5.839**	5.842	5.84	**5.842**	5.832	5.831	5.826
U12H5	5.821	5.818	5.815	5.812	5.810	5.807	5.806	5.806	5.807	5.806	5.803
U12H6	7.694	7.689	7.685	7.683	7.681	7.680	7.677	7.676	7.673	7.672	7.670
A16H2	**7.316**	7.316	**7.316**	**7.320**	7.325	7.329	7.333	7.333	7.336	7.339	7.340
C17H1'	5.268	5.262	5.253	5.241	5.233	5.225	5.221	5.215	5.214	5.204	5.198
C17H5	5.127	**5.123**	**5.125**	**5.128**	5.141	5.142	**5.156**	**5.156**	5.155	5.157	5.156
C17H6	7.383	7.376	7.368	7.363	7.336	7.335	7.336	7.334	7.337	7.335	7.343
A20H1'	5.803	5.794	5.787	5.781	5.776	5.772	5.774	5.767	5.768	5.768	-
A20H8	7.592	7.575	7.566	7.552	7.536	7.521	7.523	7.514	7.498	7.491	-
G21H1'	5.416	5.393	5.369	5.350	5.335	5.333	5.315	5.299	5.296	5.279	-
C59H1'	5.298	5.303	5.310	5.315	5.322	5.323	5.325	5.328	5.334	5.334	-
C59H5	5.044	5.070	5.098	5.122	5.132	5.148	5.159	5.168	5.177	5.195	5.225
C59H6	7.412	7.435	7.459	7.480	7.502	7.516	7.531	7.543	7.555	7.568	7.586
free											
A6H2	6.929	6.927	6.926	6.922	6.920	6.918	6.915	6.912	6.914	6.912	6.904
U7H1'	5.307	5.304	5.301	5.300	5.297	5.296	5.294	5.292	5.290	5.288	5.285
U9H6	7.490	7.487	**7.489**	7.482	7.479	**7.484**	**7.474**	**7.479**	7.478	7.475	7.472
U18H1'	5.435	5.437	5.438	5.440	5.444	**5.457**	5.448	5.452	5.453	5.455	-
G19H1'	5.544	5.543	5.545	5.554	5.561	5.566	5.572	**5.588**	5.581	5.582	-
U62H1'	5.418	**5.418**	**5.418**	5.424	5.429	**5.433**	5.433	**5.431**	5.434	5.438	-
U64H5	5.321	5.323	5.329	5.332	**5.332**	5.334	**5.338**	**5.335**	5.338	-	-
C65H1'	5.766	5.763	5.760	5.756	5.755	5.750	5.751	5.747	5.749	5.750	5.748
C65H5	5.561	5.566	5.569	5.572	5.574	5.576	5.576	**5.570**	**5.573**	-	-

Appendix 23 Affinity constants log $K_{A,est}$ values for Cd^{2+} binding to d3'-EBS1*·IBS1*

A Listed are the individual log $K_{A,est}$ values obtained from the change in chemical shifts of all aromatic and H1' protons in d3'-EBS1*·IBS1* after the first round of calculation in which the Cd^{2+} concentration corresponds to the total amount of Cd^{2+} added at each titration point.[a] The nucleotides belonging to the four individual binding sites are shaded by alternative grey scales.

	5'-end		H1								L2		L1		
residue	G1	G2	A3	G4	U5	A6	U7	G8	U9	A10	U11	U12	G13	G14	
H1'	n.d.[c]	n.d.[c]	2.66 ± 0.23	2.37 ± 0.21	n.d.[b]	n.d.[b]	2.18 ± 0.08	n.d.[b]	n.d.[b]	n.d.[b]	2.10 ± 0.29	2.33 ± 0.14	3.70 ± 0.12	n.d.[d]	
H2/H5	-	-	2.39 ± 0.13	-	n.d.[b]	1.95 ± 0.25	n.d.[b]	-	n.d.[b]	n.d.[d]	2.50 ± 0.17	2.80 ± 0.14	-	-	
H6/H8	n.d.[c]	n.d.[c]	n.d.[b]	2.79 ± 0.31	2.53 ± 0.21	n.d.[d]	n.d.[b]	n.d.[b]	2.58 ± 0.23	n.d.[b]	n.d.[d]	2.52 ± 0.08	n.d.[d]	n.d.[c]	

			H1						L2						
residue	C29	C28	U27	C26	A25	U24	A23	C22	G21	A20	G19	U18	C17	A16	C15
H1'	n.d.[d]	n.d.[b]	n.d.[b]	2.31 ± 0.21	n.d.[d]	n.d.[b]	n.d.[b]	n.d.[b]	2.37 ± 0.10	2.87 ± 0.13	1.71 ± 0.70	1.51 ± 0.72	2.41 ± 0.09	n.d.[b]	n.d.[d]
H2/H5	n.d.[c]	n.d.[b]	n.d.[c]	n.d.[d]	n.d.[b]	n.d.[c]	n.d.[b]	n.d.[b]	-	n.d.[b]	-	n.d.[d]	2.36 ± 0.41	2.53 ± 0.18	n.d.[b]
H6/H8	n.d.[d]	n.d.[b]	n.d.[d]	n.d.[b]	n.d.[b]	n.d.[b]	n.d.[b]	n.d.[b]	n.d.[d]	2.19 ± 0.18	n.d.[b]	n.d.[d]	2.24 ± 0.21	n.d.[b]	n.d.[b]

	L2						
residue	C59	A60	G61	U62	G63	U64	C65
H1'	2.45 ± 0.15	n.d.[d]	n.d.[d]	2.08 ± 0.43	n.d.[b]	n.d.[d]	2.84 ± 0.20
H2/H5	2.39 ± 0.05	n.d.[d]	-	n.d.[c]	-	2.70 ± 0.31	2.82 ± 0.12
H6/H8	2.44 ± 0.05	n.d.[d]	n.d.[c]	n.d.[d]	n.d.[b]	n.d.[b]	n.d.[b]

B Affinity constants log $K_{A,est5}$ for Cd^{2+} binding to d3'-EBS1*·IBS1* after the fifth iteration round with equilibrium taken into account.

	5'-end		H1								L2		L1		
residue	G1	G2	A3	G4	U5	A6	U7	G8	U9	A10	U11	U12	G13	G14	
H1'	n.d.[c]	n.d.[c]	3.45 ± 0.67	3.23 ± 0.15	n.d.[b]	n.d.[b]	2.88 ± 0.20	n.d.[b]	n.d.[b]	n.d.[b]	3.03 ± 0.12	± 0.14	4.94 ± 0.90	n.d.[d]	
H2/H5	-	-	3.23 ± 0.29	-	n.d.[b]	2.81 ± 0.22	n.d.[b]	-	n.d.[b]	n.d.[d]	3.97 ± 0.14	3.97 ± 0.43	-	-	
H6/H8	n.d.[c]	n.d.[c]	n.d.[b]	4.27 ± 0.42	3.48 ± 0.11	n.d.[d]	n.d.[b]	n.d.[b]	4.07 ± 0.09	n.d.[b]	n.d.[d]	3.14 ± 0.29	n.d.[d]	n.d.[c]	

			H1						L2						
residue	C29	C28	U27	C26	A25	U24	A23	C22	G21	A20	G19	U18	C17	A16	C15
H1'	n.d.[d]	n.d.[b]	n.d.[b]	3.03 ± 0.17	n.d.[d]	n.d.[b]	n.d.[b]	n.d.[b]	3.27 ± 0.39	4.15 ± 0.74	3.19 ± 0.11	3.00 ± 0.18	3.23 ± 0.18	n.d.[b]	n.d.[d]
H2/H5	n.d.[c]	n.d.[b]	n.d.[c]	n.d.[d]	n.d.[b]	n.d.[c]	n.d.[b]	n.d.[b]	-	n.d.[b]	-	n.d.[d]	3.20 ± 0.26	3.10 ± 0.09	n.d.[b]
H6/H8	n.d.[d]	n.d.[b]	n.d.[d]	n.d.[b]	n.d.[b]	n.d.[b]	n.d.[b]	n.d.[b]	n.d.[d]	3.26 ± 0.30	n.d.[b]	n.d.[d]	4.15 ± 0.90	n.d.[b]	n.d.[b]

	L2						
residue	C59	A60	G61	U62	G63	U64	C65
H1'	3.51 ± 0.39	n.d.[d]	n.d.[d]	3.59 ± 0.36	n.d.[b]	n.d.[d]	4.05 ± 0.47
H2/H5	3.04 ± 0.27	n.d.[d]	-	n.d.[c]	-	3.95 ± 0.90	4.73 ± 0.35
H6/H8	3.20 ± 0.20	n.d.[d]	n.d.[c]	n.d.[d]	n.d.[b]	n.d.[b]	n.d.[b]

[a]The chemical shift changes were obtained from [^{1}H,^{1}H]-NOESY spectra in D_2O (0.61 mM d3'-EBS1*·IBS1* RNA, pD 6.89, 110 mM KCl, 10 µM EDTA, 25 ºC). The log K_A values were calculated with a Levenberg-Marquardt nonlinear least-squares regression for a single binding isotherm. All error limits given correspond to one standard deviation (1σ). [b]n.d., not determined because chemical shift changes were too small. [c]n.d., not determined as peaks are getting too broad with higher Mg^{2+} concentrations, [d] n.d., not determined because a 1:1 binding fit was not possible.

.

Appendix 24 ^{1}H chemical shift assignments for d3'-TL

	H1	H1'	H2	H2'	H21	H22	H3	H3'	H4'	H41	H42	H5	H5'	H5''	H6	H61	H62	H8
G1	12.462	5.781	-	4.883	7.891	5.604	-	4.655	4.514	-	-	-	4.365	4.229	-	-	-	8.074
G2	12.085	5.854	-	4.652	7.822	5.665	-	4.528	4.547	-	-	-	4.437	4.233	-	-	-	7.489
A3	-	5.954	7.465	4.716	-	-	-	4.590	4.487	-	-	-	-	4.127	-	8.049	6.710	7.710
G4	13.040	5.511	-	4.390	8.082	5.943	-	4.289	4.434	-	-	-	4.370	3.997	-	-	-	7.012
U5	-	5.485	-	4.558	-	-	13.209	4.510	4.412	-	-	5.058	-	4.053	7.629	-	-	-
A6	-	5.959	7.007	4.443	-	-	-	4.619	4.525	-	-	-	-	4.137	-	7.573	6.181	8.111
U7	-	5.382	-	4.396	-	-	13.137	-	4.486	-	-	4.985	-	-	7.554	-	-	-
G8	12.298	5.719	-	4.403	7.628	5.726	-	4.431	-	-	-	-	-	4.058	-	-	-	7.507
U9	-	5.351	-	4.184	-	-	11.203	4.418	4.299	-	-	5.312	4.050	4.018	7.488	-	-	-
G10	10.387	5.555	-	4.510	-	5.931	-	4.666	4.402	-	-	-	4.331	4.053	-	-	-	7.656
A11	-	5.628	7.764	4.617	-	-	-	4.428	4.089	-	-	-	-	3.936	-	-	-	8.296
A12	-	5.465	7.700	4.365	-	-	-	4.583	4.266	-	-	-	3.962	3.855	-	-	-	7.914
A13	-	5.984	8.087	4.586	-	-	-	5.005	4.454	-	-	-	-	4.275	-	-	-	8.153
G14	10.983	4.053	-	4.331	8.070	5.937	-	4.266	-	-	-	-	-	3.914	-	-	-	7.701
C15	-	5.360	-	4.371	-	-	-	4.482	-	8.072	6.702	5.288	-	-	7.569	-	-	-
A16	-	5.880	7.208	4.412	-	-	-	4.643	4.443	-	-	-		4.091	-	7.559	6.180	7.983
U17	-	5.382	-	4.336	-	-	12.918	4.444	4.378	-	-	5.052	-	-	7.569	-	-	-
A18	-	5.933	7.083	4.484	-	-	-	4.601	4.456	-	-	-	-	4.116	-	7.658	6.165	8.067
C19	-	5.298	-	4.142	-	-	-	4.283	4.349	8.057	6.738	5.158	-	4.014	7.435	-	-	-
U20	-	5.488	-	4.439	-	-	13.774	4.469	-	-	-	5.267	-	4.019	7.837	-	-	-
C21	-	5.544	-	4.160	-	-	-	4.367	-	8.051	6.703	5.589	-	4.021	7.853	-	-	-
C22	-	5.681	-	3.936	-	-	-	4.117	4.441	7.950	6.710	5.436	-	3.974	7.608	-	-	-

Chemical shifts were extracted from the 2D [^{1}H,^{1}H]-NOESY spectrum at 303 K (100% D_2O, 10 mM KCl, 10 µM EDTA, pD = 6.61) and the 2D [^{1}H,^{1}H]-NOESY spectrum at 278 K (90% H_2O/10% D_2O, 10 mM KCl, 10 µM EDTA, pH = 6.61), both acquired at 700 MHz proton frequency.

Appendix 25 ^{13}C and ^{15}N assignments for d3'-TL

	C6	C5	C8	C2	C1'	N1	N3
G1	-	-	136.31	-	88.78	146.59	-
G2	-	-	136.72	-	90.06	146.26	-
A3	-	-	137.00	150.65	90.20	-	-
G4	-	-	133.23	-	90.23	147.44	-
U5	138.42	100.44	-	-	90.81	-	161.24
A6	-	-	137.07	150.50	88.76	-	-
U7	137.54	100.46	-	-	90.42	-	161.52
G8	-	-	133.19	-	90.05	146.55	-
U9	134.31	102.01	-	-	90.96	-	156.77
G10	-	-	134.20	-	88.87	145.59	-
A11	-	-	139.59	151.66	88.71	-	-
A12	-	-	-	151.75	89.44	-	-
A13	-	-	137.92	152.71	90.02	-	-
G14	-	-	134.68	-	-	144.07	-
C15	138.53	94.75	-	-	90.59	-	-
A16	-	-	136.90	150.45	90.35	-	-
U17	138.04	100.11	-	-	90.28	-	160.68
A18	-	-	136.92	150.68	90.04	-	-
C19	137.88	94.46	-	-	91.07	-	-
U20	139.81	100.50	-	-	91.07	162.10	-
C21	139.02	94.56	-	-	91.50	-	-
C22	139.45	95.33	-	-	90.04	-	-

Appendix 26 2D J_{NN} HNN-COSY of d3'-TL (90% H_2O/10% D_2O, pH = 6.82, 10 mM KCl, 10 µM EDTA) acquired on a 700 MHz Bruker Avance spectrometer equipped with a CP-TXI z-axis pulsed-field gradient cryoprobe at 278 K.

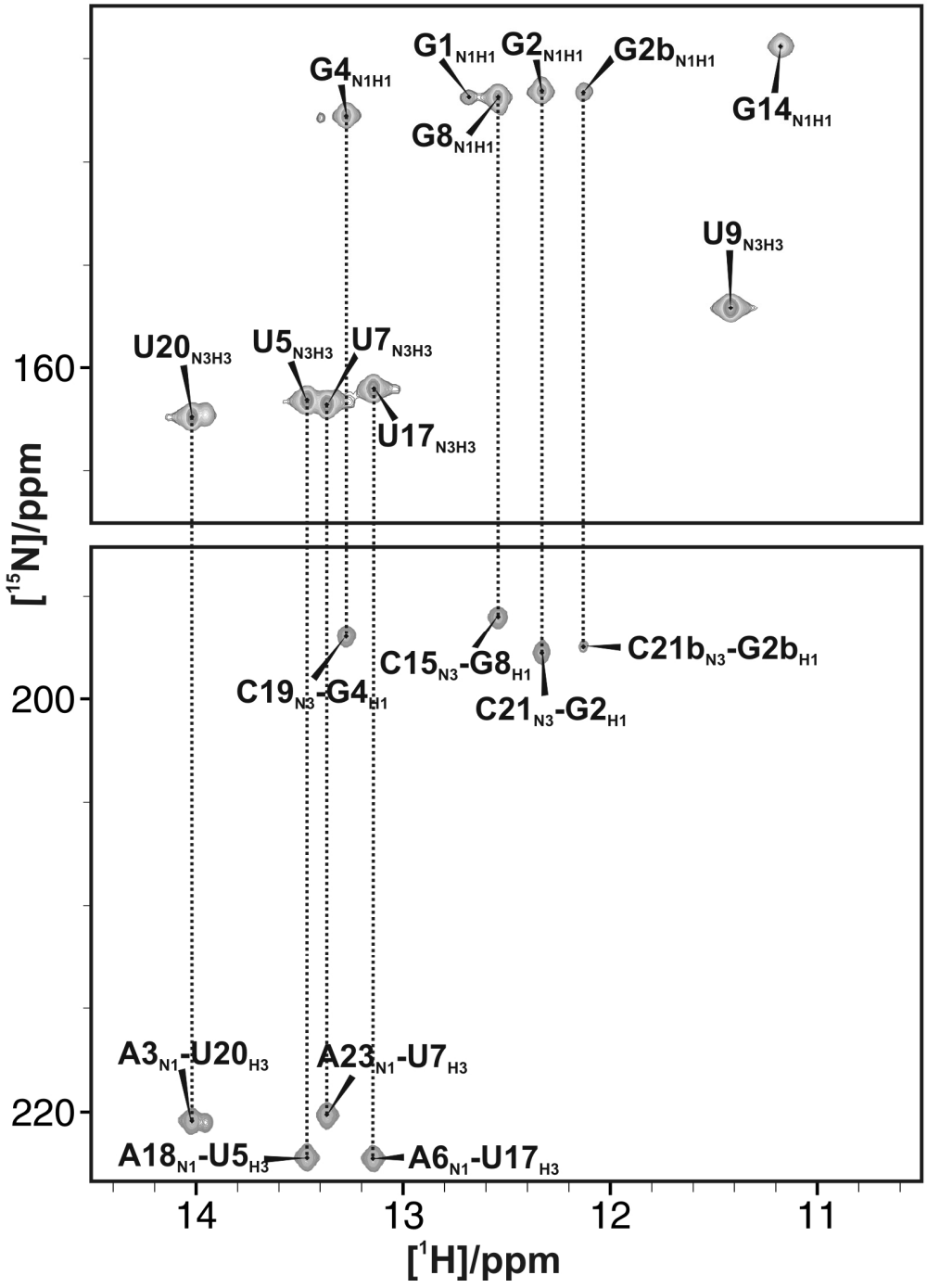

Appendix 27 Illustration of the surface area of d3'-TL

The colours correspond to the one used in the seondary structure as shown in Figure 25.

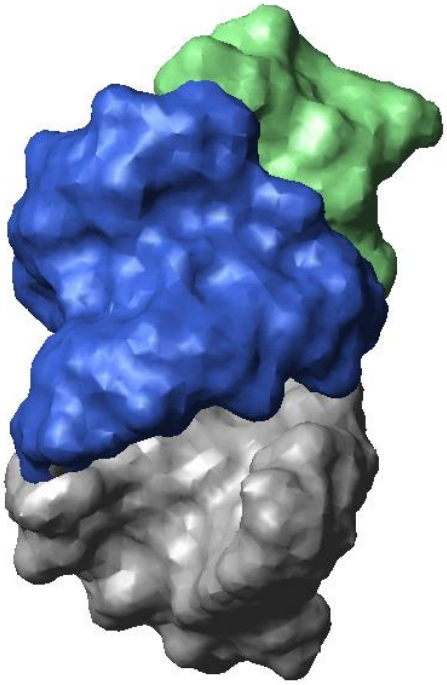

Appendix 28 All distance constraints in d3'-TL

Distance constraints of non-exchangeable protons in d3'-TL based on a 2D [^{1}H,^{1}H]-NOESY spectrum acquired at 700 MHz proton frequency at 303 K (100% D_2O, 10 mM KCl, 10 µM EDTA, pD = 6.61). Specified are the estimated distances in Å, the lower and the upper boundaries.

```
assign (residue  1 and name  H1')  (residue  1 and name  H8)   3.80  2.00  0.70
assign (residue  1 and name  H2')  (residue  1 and name  H8)   3.80  2.00  0.70
assign (residue  1 and name  H3')  (residue  1 and name  H8)   3.80  2.00  0.70
assign (residue  1 and name  H4')  (residue  1 and name  H8)   5.00  2.00  1.00
assign (residue  1 and name  H5')  (residue  1 and name  H8)   3.80  2.00  0.70
assign (residue  1 and name  H5'') (residue  1 and name  H8)   2.50  0.70  0.50

assign (residue  1 and name  H1')  (residue  2 and name  H1')  5.00  2.00  1.00
assign (residue  1 and name  H1')  (residue  2 and name  H8)   3.80  2.00  0.70
assign (residue  1 and name  H2')  (residue  2 and name  H1')  5.00  2.00  1.00
assign (residue  1 and name  H2')  (residue  2 and name  H5')  3.80  2.00  0.70
assign (residue  1 and name  H2')  (residue  2 and name  H5'') 5.00  2.00  1.00
assign (residue  1 and name  H2')  (residue  2 and name  H8)   2.50  0.70  0.50
assign (residue  1 and name  H3')  (residue  2 and name  H8)   3.80  2.00  0.70
assign (residue  1 and name  H8)   (residue  2 and name  H8)   5.00  2.00  1.00

assign (residue  2 and name  H1')  (residue  2 and name  H8)   3.80  2.00  0.70
assign (residue  2 and name  H2')  (residue  2 and name  H8)   3.80  2.00  0.70
assign (residue  2 and name  H3')  (residue  2 and name  H8)   2.50  0.70  0.50
assign (residue  2 and name  H4')  (residue  2 and name  H8)   5.00  2.00  1.00
assign (residue  2 and name  H5')  (residue  2 and name  H8)   3.80  2.00  0.70
assign (residue  2 and name  H5'') (residue  2 and name  H8)   3.80  2.00  0.70

assign (residue  2 and name  H1')  (residue  3 and name  H1')  5.00  2.00  1.00
assign (residue  2 and name  H1')  (residue  3 and name  H8)   5.00  2.00  1.00
assign (residue  2 and name  H2')  (residue  3 and name  H1')  3.80  2.00  0.70
assign (residue  2 and name  H2')  (residue  3 and name  H8)   2.50  0.70  0.50
assign (residue  2 and name  H3')  (residue  3 and name  H8)   3.80  2.00  0.70
assign (residue  2 and name  H4')  (residue  3 and name  H8)   6.00  2.00  1.00
assign (residue  2 and name  H8)   (residue  3 and name  H8)   5.00  2.00  1.00

assign (residue  3 and name  H1')  (residue  3 and name  H2)   5.00  2.00  1.00
assign (residue  3 and name  H1')  (residue  3 and name  H8)   3.80  2.00  0.70
assign (residue  3 and name  H2')  (residue  3 and name  H2)   5.00  2.00  1.00
assign (residue  3 and name  H2')  (residue  3 and name  H8)   3.80  2.00  0.70
assign (residue  3 and name  H3')  (residue  3 and name  H8)   2.50  0.70  0.50
assign (residue  3 and name  H4')  (residue  3 and name  H8)   5.00  2.00  1.00
assign (residue  3 and name  H5'') (residue  3 and name  H8)   3.80  2.00  0.70

assign (residue  3 and name  H1')  (residue  4 and name  H1')  5.00  2.00  1.00
assign (residue  3 and name  H1')  (residue  4 and name  H8)   3.80  2.00  0.70
assign (residue  3 and name  H2')  (residue  4 and name  H1')  3.80  2.00  0.70
assign (residue  3 and name  H2')  (residue  4 and name  H8)   2.50  0.70  0.50
assign (residue  3 and name  H3')  (residue  4 and name  H8)   3.80  2.00  0.70
```

```
assign (residue  3 and name  H4')  (residue  4 and name  H8)   6.00  2.00  1.00
assign (residue  3 and name  H2)   (residue  4 and name  H1')  2.50  0.70  0.50
assign (residue  3 and name  H2)   (residue  4 and name  H2')  3.80  2.00  0.70
assign (residue  3 and name  H2)   (residue  4 and name  H8)   5.00  2.00  1.00
assign (residue  3 and name  H8)   (residue  4 and name  H8)   5.00  2.00  1.00
assign (residue  3 and name  H2)   (residue 20 and name  H1')  5.00  2.00  1.00
assign (residue  3 and name  H2)   (residue 21 and name  H1')  3.80  2.00  0.70
assign (residue  3 and name  H2)   (residue 21 and name  H2')  6.00  2.00  1.00

assign (residue  4 and name  H1')  (residue  4 and name  H8)   3.80  2.00  0.70
assign (residue  4 and name  H2')  (residue  4 and name  H8)   3.80  2.00  0.70
assign (residue  4 and name  H3')  (residue  4 and name  H8)   2.50  0.70  0.50
assign (residue  4 and name  H4')  (residue  4 and name  H8)   3.80  2.00  0.70
assign (residue  4 and name  H5')  (residue  4 and name  H8)   3.80  2.00  0.70
assign (residue  4 and name  H5'') (residue  4 and name  H8)   3.80  2.00  0.70

assign (residue  4 and name  H1')  (residue  5 and name  H1')  6.00  2.00  1.00
assign (residue  4 and name  H1')  (residue  5 and name  H5)   5.00  2.00  1.00
assign (residue  4 and name  H1')  (residue  5 and name  H6)   3.80  2.00  0.70
assign (residue  4 and name  H2')  (residue  5 and name  H1')  3.80  2.00  0.70
assign (residue  4 and name  H2')  (residue  5 and name  H5)   3.80  2.00  0.70
assign (residue  4 and name  H2')  (residue  5 and name  H6)   2.50  0.70  0.50
assign (residue  4 and name  H3')  (residue  5 and name  H5)   2.50  0.70  0.50
assign (residue  4 and name  H3')  (residue  5 and name  H6)   2.50  0.70  0.50
assign (residue  4 and name  H8)   (residue  5 and name  H5)   3.80  2.00  0.70
assign (residue  4 and name  H8)   (residue  5 and name  H6)   5.00  2.00  1.00

assign (residue  5 and name  H1')  (residue  5 and name  H5)   5.00  2.00  1.00
assign (residue  5 and name  H1')  (residue  5 and name  H6)   3.80  2.00  0.70
assign (residue  5 and name  H2')  (residue  5 and name  H5)   5.00  2.00  1.00
assign (residue  5 and name  H2')  (residue  5 and name  H6)   3.80  2.00  0.70
assign (residue  5 and name  H3')  (residue  5 and name  H5)   3.80  2.00  0.70
assign (residue  5 and name  H3')  (residue  5 and name  H6)   2.50  0.70  0.50
assign (residue  5 and name  H4')  (residue  5 and name  H5)   6.00  2.00  1.00
assign (residue  5 and name  H4')  (residue  5 and name  H6)   5.00  2.00  1.00
assign (residue  5 and name  H5'') (residue  5 and name  H5)   6.00  2.00  1.00
assign (residue  5 and name  H5'') (residue  5 and name  H6)   3.80  2.00  0.70

assign (residue  5 and name  H1')  (residue  6 and name  H1')  5.00  2.00  1.00
assign (residue  5 and name  H1')  (residue  6 and name  H8)   5.00  2.00  1.00
assign (residue  5 and name  H1')  (residue 18 and name  H2)   5.00  2.00  1.00
assign (residue  5 and name  H2')  (residue  6 and name  H1')  3.80  2.00  0.70
assign (residue  5 and name  H2')  (residue  6 and name  H8)   2.50  0.70  0.50
assign (residue  5 and name  H2')  (residue 18 and name  H2)   5.00  2.00  1.00
assign (residue  5 and name  H3')  (residue  6 and name  H8)   3.80  2.00  0.70
assign (residue  5 and name  H5)   (residue  6 and name  H8)   6.00  2.00  1.00
assign (residue  5 and name  H6)   (residue  6 and name  H8)   5.00  2.00  1.00

assign (residue  6 and name  H1')  (residue  6 and name  H2)   3.80  2.00  0.70
assign (residue  6 and name  H1')  (residue  6 and name  H8)   3.80  2.00  0.70
assign (residue  6 and name  H2')  (residue  6 and name  H2)   5.00  2.00  1.00
```

```
assign (residue  6 and name  H2')  (residue  6 and name  H8)   3.80  2.00  0.70
assign (residue  6 and name  H3')  (residue  6 and name  H8)   2.50  0.70  0.50
assign (residue  6 and name  H4')  (residue  6 and name  H8)   5.00  2.00  1.00
assign (residue  6 and name  H5'')  (residue  6 and name  H8)   3.80  2.00  0.70

assign (residue  6 and name  H1')  (residue  7 and name  H1')   5.00  2.00  1.00
assign (residue  6 and name  H1')  (residue  7 and name  H5)   5.00  2.00  1.00
assign (residue  6 and name  H1')  (residue  7 and name  H6)   5.00  2.00  1.00

assign (residue  6 and name  H1')  (residue 18 and name  H2)   3.80  2.00  0.70
assign (residue  6 and name  H2')  (residue  7 and name  H1')   5.00  2.00  1.00
assign (residue  6 and name  H2')  (residue  7 and name  H5)   3.80  2.00  0.70
assign (residue  6 and name  H2')  (residue  7 and name  H6)   3.80  2.00  0.70
assign (residue  6 and name  H2')  (residue 18 and name  H2)   5.00  2.00  1.00
assign (residue  6 and name  H3')  (residue  7 and name  H6)   3.80  2.00  0.70
assign (residue  6 and name  H3')  (residue  7 and name  H5)   2.50  0.70  0.50
assign (residue  6 and name  H2)  (residue  7 and name  H1')   3.80  2.00  0.70
assign (residue  6 and name  H2)  (residue  7 and name  H2')   6.00  2.00  1.00
assign (residue  6 and name  H2)  (residue  7 and name  H6)   5.00  2.00  1.00
assign (residue  6 and name  H2)  (residue 18 and name  H1')   3.80  2.00  0.70
assign (residue  6 and name  H2)  (residue 18 and name  H2')   5.00  2.00  1.00
assign (residue  6 and name  H2)  (residue 18 and name  H2)   3.80  2.00  0.70
assign (residue  6 and name  H2)  (residue 18 and name  H8)   5.00  2.00  1.00
assign (residue  6 and name  H2)  (residue 16 and name  H2)   5.00  2.00  1.00
assign (residue  6 and name  H2)  (residue 17 and name  H1')   5.00  2.00  1.00
assign (residue  6 and name  H2)  (residue 17 and name  H2')   5.00  2.00  1.00
assign (residue  6 and name  H8)  (residue  7 and name  H5)   3.80  2.00  0.70
assign (residue  6 and name  H8)  (residue  7 and name  H6)   5.00  2.00  1.00
assign (residue  6 and name  H8)  (residue 18 and name  H2)   5.00  2.00  1.00

assign (residue  7 and name  H1')  (residue  7 and name  H5)   5.00  2.00  1.00
assign (residue  7 and name  H1')  (residue  7 and name  H6)   3.80  2.00  0.70
assign (residue  7 and name  H2')  (residue  7 and name  H5)   5.00  2.00  1.00
assign (residue  7 and name  H2')  (residue  7 and name  H6)   3.80  2.00  0.70
assign (residue  7 and name  H4')  (residue  7 and name  H6)   5.00  2.00  1.00

assign (residue  7 and name  H1')  (residue  8 and name  H1')   5.00  2.00  1.00
assign (residue  7 and name  H1')  (residue  8 and name  H5'')   6.00  2.00  1.00
assign (residue  7 and name  H1')  (residue  8 and name  H8)   3.80  2.00  0.70
assign (residue  7 and name  H1')  (residue 16 and name  H2)   6.00  2.00  1.00
assign (residue  7 and name  H2')  (residue  8 and name  H1')   3.80  2.00  0.70
assign (residue  7 and name  H2')  (residue  8 and name  H8)   2.50  0.70  0.50
assign (residue  7 and name  H2')  (residue 16 and name  H2)   6.00  2.00  1.00
assign (residue  7 and name  H5)  (residue  8 and name  H8)   3.80  2.00  0.70
assign (residue  7 and name  H6)  (residue  8 and name  H8)   3.80  2.00  0.70

assign (residue  8 and name  H1')  (residue  8 and name  H8)   3.80  2.00  0.70
assign (residue  8 and name  H2')  (residue  8 and name  H8)   3.80  2.00  0.70
assign (residue  8 and name  H3')  (residue  8 and name  H8)   2.50  0.70  0.50
assign (residue  8 and name  H5'')  (residue  8 and name  H8)   3.80  2.00  0.70
```

```
assign (residue  8 and name  H1')  (residue  9 and name  H1')  6.00  2.00  1.00
assign (residue  8 and name  H1')  (residue  9 and name  H5)   5.00  2.00  1.00
assign (residue  8 and name  H1')  (residue  9 and name  H6)   3.80  2.00  0.70
assign (residue  8 and name  H1')  (residue 16 and name  H2)   3.80  2.00  0.70
assign (residue  8 and name  H2')  (residue  9 and name  H1')  3.80  2.00  0.70
assign (residue  8 and name  H2')  (residue  9 and name  H5)   2.50  0.70  0.50
assign (residue  8 and name  H2')  (residue  9 and name  H6)   2.50  0.70  0.50
assign (residue  8 and name  H2')  (residue 16 and name  H2)   5.00  2.00  1.00
assign (residue  8 and name  H3')  (residue  9 and name  H5)   2.50  0.70  0.50
assign (residue  8 and name  H3')  (residue  9 and name  H6)   3.80  2.00  0.70
assign (residue  8 and name  H8)   (residue  9 and name  H5)   2.50  0.70  0.50
assign (residue  8 and name  H8)   (residue  9 and name  H6)   5.00  2.00  0.70
assign (residue  8 and name  H8)   (residue 16 and name  H2)   5.00  2.00  1.00

assign (residue  9 and name  H1')  (residue  9 and name  H5)   5.00  2.00  1.00
assign (residue  9 and name  H1')  (residue  9 and name  H6)   3.80  2.00  0.70
assign (residue  9 and name  H2')  (residue  9 and name  H5)   5.00  2.00  1.00
assign (residue  9 and name  H2')  (residue  9 and name  H6)   3.80  2.00  0.70
assign (residue  9 and name  H3')  (residue  9 and name  H5)   5.00  2.00  1.00
assign (residue  9 and name  H3')  (residue  9 and name  H6)   2.50  0.70  0.50
assign (residue  9 and name  H4')  (residue  9 and name  H6)   3.80  2.00  0.70
assign (residue  9 and name  H5')  (residue  9 and name  H6)   3.80  2.00  0.70
assign (residue  9 and name  H5'') (residue  9 and name  H6)   3.80  2.00  0.70

assign (residue  9 and name  H1')  (residue 10 and name  H1')  5.00  2.00  1.00
assign (residue  9 and name  H1')  (residue 10 and name  H8)   5.00  2.00  1.00
assign (residue  9 and name  H2')  (residue 10 and name  H1')  3.80  2.00  0.70
assign (residue  9 and name  H2')  (residue 10 and name  H8)   2.50  0.70  0.50
assign (residue  9 and name  H3')  (residue 10 and name  H8)   3.80  2.00  0.70
assign (residue  9 and name  H5)   (residue 10 and name  H8)   5.00  2.00  1.00
assign (residue  9 and name  H6)   (residue 10 and name  H8)   3.80  2.00  0.70

assign (residue 10 and name H1')   (residue 10 and name  H8)   3.80  2.00  0.70
assign (residue 10 and name H2')   (residue 10 and name  H8)   3.80  2.00  0.70
assign (residue 10 and name H3')   (residue 10 and name  H8)   3.80  2.00  0.70
assign (residue 10 and name H4')   (residue 10 and name  H8)   5.00  2.00  1.00
assign (residue 10 and name H5')   (residue 10 and name  H8)   3.80  2.00  0.70
assign (residue 10 and name H5'')  (residue 10 and name  H8)   3.80  2.00  0.70

assign (residue 10 and name H1')   (residue 11 and name  H1')  6.00  2.00  1.00
assign (residue 10 and name H1')   (residue 11 and name  H8)   3.80  2.00  0.70
assign (residue 10 and name H1')   (residue 12 and name  H8)   3.80  2.00  0.70
assign (residue 10 and name H2')   (residue 11 and name  H1')  6.00  2.00  1.00
assign (residue 10 and name H2')   (residue 11 and name  H8)   3.80  2.00  0.70
assign (residue 10 and name H2')   (residue 12 and name  H8)   3.80  2.00  0.70
assign (residue 10 and name H3')   (residue 11 and name  H8)   5.00  2.00  1.00
assign (residue 10 and name H3')   (residue 12 and name  H8)   5.00  2.00  1.00

assign (residue 11 and name H1')   (residue 11 and name  H2)   5.00  2.00  1.00
assign (residue 11 and name H1')   (residue 11 and name  H8)   3.80  2.00  0.70
assign (residue 11 and name H2')   (residue 11 and name  H2)   5.00  2.00  1.00
```

```
assign (residue 11 and name H2')  (residue 11 and name  H8)   3.80  2.00  0.70
assign (residue 11 and name H3')  (residue 11 and name  H8)   3.80  2.00  0.70
assign (residue 11 and name H4')  (residue 11 and name  H8)   5.00  2.00  1.00
assign (residue 11 and name H5")  (residue 11 and name  H8)   3.80  2.00  0.70

assign (residue 11 and name H1')  (residue 12 and name  H1')  5.00  2.00  1.00
assign (residue 11 and name H1')  (residue 12 and name  H8)   5.00  2.00  1.00
assign (residue 11 and name H2')  (residue 12 and name  H1')  3.80  2.00  0.70
assign (residue 11 and name H2')  (residue 12 and name  H8)   2.50  0.70  0.50
assign (residue 11 and name H3')  (residue 12 and name  H8)   3.80  2.00  0.70
assign (residue 11 and name H4')  (residue 12 and name  H8)   5.00  2.00  1.00
assign (residue 11 and name H2)   (residue 12 and name  H1')  3.80  2.00  0.70
assign (residue 11 and name H2)   (residue 12 and name  H2')  6.00  2.00  1.00
assign (residue 11 and name H8)   (residue 12 and name  H8)   6.00  2.00  1.00

assign (residue 12 and name H1')  (residue 12 and name  H2)   5.00  2.00  1.00
assign (residue 12 and name H1')  (residue 12 and name  H8)   3.80  2.00  0.70
assign (residue 12 and name H2')  (residue 12 and name  H2)   5.00  2.00  1.00
assign (residue 12 and name H2')  (residue 12 and name  H8)   3.80  2.00  0.70
assign (residue 12 and name H3')  (residue 12 and name  H8)   3.80  2.00  0.70
assign (residue 12 and name H4')  (residue 12 and name  H8)   5.00  2.00  1.00
assign (residue 12 and name H5')  (residue 12 and name  H8)   3.80  2.00  0.70
assign (residue 12 and name H5")  (residue 12 and name  H8)   5.00  2.00  1.00

assign (residue 12 and name H1')  (residue 13 and name  H1')  5.00  2.00  1.00
assign (residue 12 and name H1')  (residue 13 and name  H2)   6.00  2.00  1.00
assign (residue 12 and name H1')  (residue 13 and name  H8)   5.00  2.00  1.00
assign (residue 12 and name H2')  (residue 13 and name  H1')  3.80  2.00  0.70
assign (residue 12 and name H2')  (residue 13 and name  H8)   2.50  0.70  0.50
assign (residue 12 and name H3')  (residue 13 and name  H8)   3.80  2.00  0.70
assign (residue 12 and name H2)   (residue 13 and name  H1')  6.00  2.00  1.00
assign (residue 12 and name H2)   (residue 13 and name  H2)   3.80  2.00  0.70
assign (residue 12 and name H8)   (residue 13 and name  H8)   5.00  2.00  1.00

assign (residue 13 and name H1')  (residue 13 and name  H2)   5.00  2.00  1.00
assign (residue 13 and name H1')  (residue 13 and name  H8)   3.80  2.00  0.70
assign (residue 13 and name H2')  (residue 13 and name  H8)   3.80  2.00  0.70
assign (residue 13 and name H3')  (residue 13 and name  H8)   2.50  0.70  0.50
assign (residue 13 and name H4')  (residue 13 and name  H8)   5.00  2.00  1.00
assign (residue 13 and name H5")  (residue 13 and name  H8)   2.50  0.70  0.50

assign (residue 13 and name H1')  (residue 14 and name  H8)   3.80  2.00  0.70
assign (residue 13 and name H2')  (residue 14 and name  H8)   2.50  0.70  0.50
assign (residue 13 and name H3')  (residue 14 and name  H8)   2.50  0.70  0.50
assign (residue 13 and name H2)   (residue 14 and name  H8)   6.00  2.00  1.00
assign (residue 13 and name H8)   (residue 14 and name  H8)   3.80  2.00  0.70

assign (residue 14 and name H1')  (residue 14 and name  H8)   3.80  2.00  0.70
assign (residue 14 and name H2')  (residue 14 and name  H8)   3.80  2.00  0.70
assign (residue 14 and name H3')  (residue 14 and name  H8)   2.50  0.70  0.50
assign (residue 14 and name H5")  (residue 14 and name  H8)   3.80  2.00  0.70
```

```
assign (residue 14 and name H1')  (residue 15 and name  H5)   5.00  2.00  1.00
assign (residue 14 and name H1')  (residue 15 and name  H6)   3.80  2.00  0.70
assign (residue 14 and name H2')  (residue 15 and name  H1')  3.80  2.00  0.70
assign (residue 14 and name H2')  (residue 15 and name  H5)   3.80  2.00  0.70
assign (residue 14 and name H2')  (residue 15 and name  H6)   2.50  0.70  0.50
assign (residue 14 and name H3')  (residue 15 and name  H6)   3.80  2.00  0.70
assign (residue 14 and name H8)   (residue 15 and name  H5)   3.80  2.00  0.70
assign (residue 14 and name H8)   (residue 15 and name  H6)   3.80  2.00  0.70

assign (residue 15 and name H1')  (residue 15 and name  H5)   5.00  2.00  1.00
assign (residue 15 and name H1')  (residue 15 and name  H6)   3.80  2.00  0.70
assign (residue 15 and name H2')  (residue 15 and name  H5)   5.00  2.00  1.00
assign (residue 15 and name H2')  (residue 15 and name  H6)   6.00  2.00  1.00
assign (residue 15 and name H3')  (residue 15 and name  H5)   5.00  2.00  1.00
assign (residue 15 and name H3')  (residue 15 and name  H6)   3.80  2.00  0.70

assign (residue 15 and name H1')  (residue 16 and name  H1')  5.00  2.00  1.00
assign (residue 15 and name H1')  (residue 16 and name  H8)   3.80  2.00  0.70
assign (residue 15 and name H2')  (residue 16 and name  H1')  3.80  2.00  0.70
assign (residue 15 and name H2')  (residue 16 and name  H8)   2.50  0.70  0.50
assign (residue 15 and name H3')  (residue 16 and name  H8)   3.80  2.00  0.70
assign (residue 15 and name H5)   (residue 16 and name  H8)   6.00  2.00  1.00
assign (residue 15 and name H6)   (residue 16 and name  H8)   5.00  2.00  1.00

assign (residue 16 and name H1')  (residue 16 and name  H2)   5.00  2.00  1.00
assign (residue 16 and name H1')  (residue 16 and name  H8)   3.80  2.00  0.70
assign (residue 16 and name H2')  (residue 16 and name  H2)   5.00  2.00  1.00
assign (residue 16 and name H2')  (residue 16 and name  H8)   3.80  2.00  0.70
assign (residue 16 and name H3')  (residue 16 and name  H8)   2.50  0.70  0.50
assign (residue 16 and name H4')  (residue 16 and name  H8)   5.00  2.00  1.00
assign (residue 16 and name H5'') (residue 16 and name  H8)   3.80  2.00  0.70

assign (residue 16 and name H1')  (residue 17 and name  H1')  6.00  2.00  1.00
assign (residue 16 and name H1')  (residue 17 and name  H5)   5.00  2.00  1.00
assign (residue 16 and name H1')  (residue 17 and name  H6)   5.00  2.00  1.00
assign (residue 16 and name H2')  (residue 17 and name  H1')  3.80  2.00  0.70
assign (residue 16 and name H2')  (residue 17 and name  H5)   3.80  2.00  0.70
assign (residue 16 and name H2')  (residue 17 and name  H6)   2.50  0.70  0.50
assign (residue 16 and name H3')  (residue 17 and name  H5)   2.50  0.70  0.50
assign (residue 16 and name H3')  (residue 17 and name  H6)   3.80  2.00  0.70
assign (residue 16 and name H2)   (residue 17 and name  H1')  3.80  2.00  0.70
assign (residue 16 and name H2)   (residue 17 and name  H2')  5.00  2.00  1.00
assign (residue 16 and name H2)   (residue 17 and name  H6)   5.00  2.00  1.00
assign (residue 16 and name H8)   (residue 17 and name  H5)   3.80  2.00  0.70
assign (residue 16 and name H8)   (residue 17 and name  H6)   5.00  2.00  1.00

assign (residue 17 and name H1')  (residue 17 and name  H5)   5.00  2.00  1.00
assign (residue 17 and name H1')  (residue 17 and name  H6)   3.80  2.00  0.70
assign (residue 17 and name H2')  (residue 17 and name  H5)   5.00  2.00  1.00
assign (residue 17 and name H2')  (residue 17 and name  H6)   3.80  2.00  0.70
```

```
assign (residue 17 and name H3')  (residue 17 and name  H5)   5.00  2.00  1.00
assign (residue 17 and name H3')  (residue 17 and name  H6)   2.50  0.70  0.50
assign (residue 17 and name H4')  (residue 17 and name  H5)   6.00  2.00  1.00
assign (residue 17 and name H4')  (residue 17 and name  H6)   5.00  2.00  1.00

assign (residue 17 and name H1')  (residue 18 and name  H1')  5.00  2.00  1.00
assign (residue 17 and name H1')  (residue 18 and name  H8)   3.80  2.00  0.70
assign (residue 17 and name H2')  (residue 18 and name  H1')  3.80  2.00  0.70
assign (residue 17 and name H2')  (residue 18 and name  H8)   2.50  0.70  0.50
assign (residue 17 and name H3')  (residue 18 and name  H8)   3.80  2.00  0.70
assign (residue 17 and name H5)   (residue 18 and name  H8)   5.00  2.00  1.00
assign (residue 17 and name H5)   (residue 18 and name  H2')  6.00  2.00  1.00
assign (residue 17 and name H6)   (residue 18 and name  H8)   3.80  2.00  0.70

assign (residue 18 and name H1')  (residue 18 and name  H2)   3.80  2.00  0.70
assign (residue 18 and name H1')  (residue 18 and name  H8)   3.80  2.00  0.70
assign (residue 18 and name H2')  (residue 18 and name  H2)   5.00  2.00  1.00
assign (residue 18 and name H2')  (residue 18 and name  H8)   3.80  2.00  0.70
assign (residue 18 and name H3')  (residue 18 and name  H8)   2.50  0.70  0.50
assign (residue 18 and name H4')  (residue 18 and name  H8)   5.00  2.00  1.00
assign (residue 18 and name H5")  (residue 18 and name  H8)   3.80  2.00  0.70

assign (residue 18 and name H1')  (residue 19 and name  H1')  5.00  2.00  1.00
assign (residue 18 and name H1')  (residue 19 and name  H5)   5.00  2.00  1.00
assign (residue 18 and name H1')  (residue 19 and name  H6)   3.80  2.00  0.70
assign (residue 18 and name H2')  (residue 19 and name  H1')  3.80  2.00  0.70
assign (residue 18 and name H2')  (residue 19 and name  H5)   3.80  2.00  0.70
assign (residue 18 and name H2')  (residue 19 and name  H6)   2.50  0.70  0.50
assign (residue 18 and name H3')  (residue 19 and name  H5)   3.80  2.00  0.70
assign (residue 18 and name H3')  (residue 19 and name  H6)   3.80  2.00  0.70
assign (residue 18 and name H2)   (residue 19 and name  H1')  3.80  2.00  0.70
assign (residue 18 and name H2)   (residue 19 and name  H2')  6.00  2.00  1.00
assign (residue 18 and name H8)   (residue 19 and name  H5)   5.00  2.00  1.00
assign (residue 18 and name H8)   (residue 19 and name  H6)   3.80  2.00  0.70

assign (residue 19 and name H1')  (residue 19 and name  H5)   5.00  2.00  1.00
assign (residue 19 and name H1')  (residue 19 and name  H6)   3.80  2.00  0.70
assign (residue 19 and name H2')  (residue 19 and name  H5)   5.00  2.00  1.00
assign (residue 19 and name H2')  (residue 19 and name  H6)   3.80  2.00  0.70
assign (residue 19 and name H3')  (residue 19 and name  H5)   3.80  2.00  0.70
assign (residue 19 and name H3')  (residue 19 and name  H6)   2.50  0.70  0.50
assign (residue 19 and name H4')  (residue 19 and name  H5)   5.00  2.00  1.00
assign (residue 19 and name H4')  (residue 19 and name  H6)   5.00  2.00  1.00
assign (residue 19 and name H5")  (residue 19 and name  H5)   6.00  2.00  1.00
assign (residue 19 and name H5")  (residue 19 and name  H6)   3.80  2.00  0.70

assign (residue 19 and name H1')  (residue 20 and name  H1')  5.00  2.00  1.00
assign (residue 19 and name H1')  (residue 20 and name  H5)   5.00  2.00  1.00
assign (residue 19 and name H1')  (residue 20 and name  H6)   3.80  2.00  0.70
assign (residue 19 and name H2')  (residue 20 and name  H1')  3.80  2.00  0.70
assign (residue 19 and name H2')  (residue 20 and name  H5)   3.80  2.00  0.70
```

```
assign (residue 19 and name H2')  (residue 20 and name  H6)   2.50  0.70  0.50
assign (residue 19 and name H3')  (residue 20 and name  H5)   3.80  2.00  0.70
assign (residue 19 and name H3')  (residue 20 and name  H6)   3.80  2.00  0.70
assign (residue 19 and name H5)   (residue 20 and name  H5)   2.50  0.70  0.50
assign (residue 19 and name H5)   (residue 20 and name  H6)   5.00  2.00  1.00
assign (residue 19 and name H6)   (residue 20 and name  H5)   2.50  0.70  0.50
assign (residue 19 and name H6)   (residue 20 and name  H6)   3.80  2.00  0.70

assign (residue 20 and name H1')  (residue 20 and name  H5)   5.00  2.00  1.00
assign (residue 20 and name H1')  (residue 20 and name  H6)   3.80  2.00  0.70
assign (residue 20 and name H2')  (residue 20 and name  H5)   5.00  2.00  1.00
assign (residue 20 and name H2')  (residue 20 and name  H6)   3.80  2.00  0.70
assign (residue 20 and name H3')  (residue 20 and name  H5)   5.00  2.00  1.00
assign (residue 20 and name H3')  (residue 20 and name  H6)   2.50  0.70  0.50
assign (residue 20 and name H5")  (residue 20 and name  H5)   6.00  2.00  1.00
assign (residue 20 and name H5")  (residue 20 and name  H6)   3.80  2.00  0.70

assign (residue 20 and name H1')  (residue 21 and name  H1')  6.00  2.00  1.00
assign (residue 20 and name H1')  (residue 21 and name  H5)   5.00  2.00  1.00
assign (residue 20 and name H1')  (residue 21 and name  H6)   3.80  2.00  0.70
assign (residue 20 and name H2')  (residue 21 and name  H1')  3.80  2.00  0.70
assign (residue 20 and name H2')  (residue 21 and name  H5)   3.80  2.00  0.70
assign (residue 20 and name H2')  (residue 21 and name  H6)   3.80  2.00  0.70
assign (residue 20 and name H3')  (residue 21 and name  H5)   3.80  2.00  0.70
assign (residue 20 and name H3')  (residue 21 and name  H6)   3.80  2.00  0.70
assign (residue 20 and name H5)   (residue 21 and name  H5)   5.00  2.00  1.00
assign (residue 20 and name H5)   (residue 21 and name  H6)   6.00  2.00  1.00
assign (residue 20 and name H6)   (residue 21 and name  H5)   5.00  2.00  1.00
assign (residue 20 and name H6)   (residue 21 and name  H6)   5.00  2.00  1.00

assign (residue 21 and name H1')  (residue 21 and name  H5)   5.00  2.00  1.00
assign (residue 21 and name H1')  (residue 21 and name  H6)   3.80  2.00  0.70
assign (residue 21 and name H2')  (residue 21 and name  H5)   5.00  2.00  1.00
assign (residue 21 and name H2')  (residue 21 and name  H6)   3.80  2.00  0.70
assign (residue 21 and name H3')  (residue 21 and name  H5)   5.00  2.00  1.00
assign (residue 21 and name H3')  (residue 21 and name  H6)   2.50  0.70  0.50
assign (residue 21 and name H5")  (residue 21 and name  H5)   6.00  2.00  1.00
assign (residue 21 and name H5")  (residue 21 and name  H6)   3.80  2.00  0.70

assign (residue 21 and name H1')  (residue 22 and name  H1')  3.80  2.00  0.70
assign (residue 21 and name H1')  (residue 22 and name  H5)   5.00  2.00  1.00
assign (residue 21 and name H1')  (residue 22 and name  H6)   3.80  2.00  0.70
assign (residue 21 and name H2')  (residue 22 and name  H1')  3.80  2.00  0.70
assign (residue 21 and name H2')  (residue 22 and name  H5)   3.80  2.00  0.70
assign (residue 21 and name H2')  (residue 22 and name  H6)   2.50  0.70  0.50
assign (residue 21 and name H3')  (residue 22 and name  H5)   3.80  2.00  0.70
assign (residue 21 and name H3')  (residue 22 and name  H6)   3.80  2.00  0.70
assign (residue 21 and name H5)   (residue 22 and name  H5)   3.80  2.00  0.70
assign (residue 21 and name H5)   (residue 22 and name  H6)   6.00  2.00  1.00
assign (residue 21 and name H6)   (residue 22 and name  H5)   3.80  2.00  0.70
assign (residue 21 and name H6)   (residue 22 and name  H6)   3.80  2.00  0.70
```

```
assign (residue 22 and name H1')  (residue 22 and name  H5)   5.00  2.00  1.00
assign (residue 22 and name H1')  (residue 22 and name  H6)   3.80  2.00  0.70
assign (residue 22 and name H2')  (residue 22 and name  H5)   5.00  2.00  1.00
assign (residue 22 and name H2')  (residue 22 and name  H6)   3.80  2.00  0.70
assign (residue 22 and name H3')  (residue 22 and name  H5)   5.00  2.00  1.00
assign (residue 22 and name H3')  (residue 22 and name  H6)   2.50  0.70  0.50
assign (residue 22 and name H4')  (residue 22 and name  H5)   6.00  2.00  1.00
assign (residue 22 and name H4')  (residue 22 and name  H6)   3.80  2.00  0.70
assign (residue 22 and name H5")  (residue 22 and name  H5)   6.00  2.00  1.00
assign (residue 22 and name H5")  (residue 22 and name  H6)   3.80  2.00  0.70
```

Distance constraints of exchangeable protons in d3'-TL based on a 2D [^{1}H,^{1}H]-NOESY spectrum acquired at 700 MHz proton frequency at 278 K (90% H_2O/10% D_2O, 10 mM KCl, 10 µM EDTA, pH = 6.61).

```
assign (residue  1 and name  H1)  (residue  2 and name  H1')  6.00  2.00  1.00
assign (residue  1 and name  H1)  (residue  2 and name  H1)   5.00  2.00  1.00
assign (residue  1 and name  H1)  (residue  2 and name  H8)   6.00  2.00  1.00

assign (residue  1 and name  H1)  (residue 21 and name  H1')  6.00  2.00  1.00
assign (residue  1 and name  H1)  (residue 22 and name  H41)  2.50  0.70  0.50
assign (residue  1 and name  H1)  (residue 22 and name  H42)  3.80  2.00  0.70
assign (residue  1 and name  H1)  (residue 22 and name  H5)   6.00  2.00  1.00
assign (residue  1 and name  H1)  (residue 22 and name  H6)   6.00  2.00  1.00

assign (residue  2 and name  H1)  (residue  3 and name  H1')  6.00  2.00  1.00
assign (residue  2 and name  H1)  (residue  3 and name  H2)   5.00  2.00  1.00
assign (residue  2 and name  H1)  (residue  3 and name  H8)   6.00  2.00  1.00

assign (residue  2 and name  H1)  (residue 20 and name  H3)   5.00  2.00  1.00
assign (residue  2 and name  H1)  (residue 21 and name  H41)  2.50  0.70  0.50
assign (residue  2 and name  H1)  (residue 21 and name  H42)  3.80  2.00  0.70
assign (residue  2 and name  H1)  (residue 21 and name  H5)   6.00  2.00  1.00
assign (residue  2 and name  H1)  (residue 21 and name  H6)   6.00  2.00  1.00
assign (residue  2 and name  H1)  (residue 22 and name  H5)   6.00  2.00  1.00
assign (residue  2 and name  H1)  (residue 22 and name  H6)   5.00  2.00  1.00

assign (residue  4 and name  H1)  (residue  3 and name  H2)   5.00  2.00  1.00
assign (residue  4 and name  H1)  (residue  5 and name  H1')  6.00  2.00  1.00
assign (residue  4 and name  H1)  (residue  5 and name  H3)   3.80  2.00  1.00
assign (residue  4 and name  H1)  (residue  5 and name  H5)   6.00  2.00  1.00
assign (residue  4 and name  H1)  (residue  5 and name  H6)   6.00  2.00  1.00

assign (residue  4 and name  H1)  (residue 19 and name  H2')  6.00  2.00  1.00
assign (residue  4 and name  H1)  (residue 19 and name  H41)  2.50  0.70  0.50
assign (residue  4 and name  H1)  (residue 19 and name  H42)  3.80  2.00  0.70
assign (residue  4 and name  H1)  (residue 19 and name  H5)   5.00  2.00  1.00
assign (residue  4 and name  H1)  (residue 20 and name  H3)   3.80  2.00  0.70
assign (residue  4 and name  H1)  (residue 20 and name  H5)   5.00  2.00  1.00
assign (residue  4 and name  H1)  (residue 20 and name  H6)   5.00  2.00  1.00
```

```
assign (residue  5 and name  H3)   (residue  4 and name   H22) 6.00  2.00  1.00
assign (residue  5 and name  H3)   (residue  5 and name   H1') 5.00  2.00  1.00
assign (residue  5 and name  H3)   (residue  6 and name   H1') 5.00  2.00  1.00
assign (residue  5 and name  H3)   (residue  6 and name   H8)  5.00  2.00  1.00

assign (residue  5 and name  H3)   (residue 17 and name  H3)  3.80  2.00  0.70
assign (residue  5 and name  H3)   (residue 18 and name  H2)  3.80  2.00  0.70
assign (residue  5 and name  H3)   (residue 18 and name  H61) 2.50  0.70  0.50
assign (residue  5 and name  H3)   (residue 18 and name  H62) 3.80  0.30  0.40
assign (residue  5 and name  H3)   (residue 19 and name  H1') 6.00  2.00  1.00
assign (residue  5 and name  H3)   (residue 19 and name  H41) 3.80  0.30  0.40

assign (residue  7 and name  H3)   (residue  6 and name   H2)  5.00  2.00  1.00
assign (residue  7 and name  H3)   (residue  7 and name   H1') 5.00  2.00  1.00
assign (residue  7 and name  H3)   (residue  8 and name   H1') 5.00  2.00  1.00
assign (residue  7 and name  H3)   (residue  8 and name   H1)  3.80  2.00  0.70
assign (residue  7 and name  H3)   (residue  8 and name   H8)  5.00  2.00  1.00

assign (residue  7 and name  H3)   (residue 16 and name  H2)  3.80  2.00  0.70
assign (residue  7 and name  H3)   (residue 16 and name  H61) 2.50  0.70  0.50
assign (residue  7 and name  H3)   (residue 16 and name  H62) 3.80  0.30  0.40
assign (residue  7 and name  H3)   (residue 17 and name  H5)  5.00  2.00  1.00
assign (residue  7 and name  H3)   (residue 17 and name  H6)  5.00  2.00  1.00

assign (residue  8 and name  H1)   (residue  9 and name   H1') 6.00  2.00  1.00
assign (residue  8 and name  H1)   (residue  9 and name   H3)  3.80  2.00  0.70
assign (residue  8 and name  H1)   (residue  9 and name   H5)  6.00  2.00  1.00
assign (residue  8 and name  H1)   (residue  9 and name   H6)  6.00  2.00  1.00

assign (residue  8 and name  H1)   (residue 14 and name  H1)  5.00  2.00  1.00
assign (residue  8 and name  H1)   (residue 14 and name  H22) 6.00  2.00  1.00
assign (residue  8 and name  H1)   (residue 15 and name  H41) 2.50  0.70  0.50
assign (residue  8 and name  H1)   (residue 15 and name  H42) 3.80  2.00  0.70
assign (residue  8 and name  H1)   (residue 15 and name  H5)  6.00  2.00  1.00
assign (residue  8 and name  H1)   (residue 15 and name  H6)  6.00  2.00  1.00
assign (residue  8 and name  H1)   (residue 16 and name  H2)  5.00  2.00  1.00
assign (residue  8 and name  H1)   (residue 16 and name  H61) 6.00  2.00  1.00

assign (residue  9 and name  H3)   (residue  8 and name   H21) 5.00  2.00  1.00
assign (residue  9 and name  H3)   (residue 10 and name  H1)  5.00  2.00  1.00
assign (residue  9 and name  H3)   (residue 10 and name  H1') 5.00  2.00  1.00

assign (residue  9 and name  H3)   (residue 14 and name  H1)  2.50  0.70  0.50
assign (residue  9 and name  H3)   (residue 14 and name  H21) 5.00  2.00  1.00
assign (residue  9 and name  H3)   (residue 14 and name  H22) 3.80  0.30  0.40
assign (residue  9 and name  H3)   (residue 15 and name  H41) 3.80  0.30  0.40
assign (residue  9 and name  H3)   (residue 15 and name  H42) 3.80  0.30  0.40
assign (residue  9 and name  H3)   (residue 15 and name  H5)  6.00  2.00  1.00
assign (residue  9 and name  H3)   (residue 15 and name  H6)  5.00  2.00  1.00

assign (residue 10 and name H1)    (residue  9 and name   H6)  6.00  2.00  1.00
```

```
assign (residue 10 and name H1)   (residue 12 and name  H2')   6.00  2.00  1.00
assign (residue 10 and name H1)   (residue 12 and name  H8)    3.80  2.00  0.70
assign (residue 10 and name H1)   (residue 13 and name  H8)    5.00  2.00  1.00

assign (residue 14 and name H1)   (residue 15 and name  H41)  6.00  2.00  1.00
assign (residue 14 and name H1)   (residue 15 and name  H42)  5.00  2.00  1.00
assign (residue 14 and name H1)   (residue 15 and name  H5)   6.00  2.00  1.00

assign (residue 14 and name H1)   (residue  8 and name  H21)  5.00  2.00  1.00
assign (residue 14 and name H1)   (residue  9 and name  H1')  5.00  2.00  1.00
assign (residue 14 and name H1)   (residue  9 and name  H5)   6.00  2.00  1.00
assign (residue 14 and name H1)   (residue  9 and name  H6)   6.00  2.00  1.00
assign (residue 14 and name H1)   (residue 10 and name  H1')  3.80  2.00  0.70
assign (residue 14 and name H1)   (residue 15 and name  H1')  6.00  2.00  1.00
assign (residue 14 and name H1)   (residue 15 and name  H6)   6.00  2.00  1.00

assign (residue 17 and name H3)   (residue 16 and name  H2)   5.00  2.00  1.00
assign (residue 17 and name H3)   (residue 18 and name  H1')  5.00  2.00  1.00
assign (residue 17 and name H3)   (residue 18 and name  H8)   5.00  2.00  1.00

assign (residue 17 and name H3)   (residue  6 and name  H2)   3.80  2.00  0.70
assign (residue 17 and name H3)   (residue  6 and name  H61)  2.50  0.70  0.50
assign (residue 17 and name H3)   (residue  6 and name  H62)  3.80  0.30  0.40
assign (residue 17 and name H3)   (residue  7 and name  H3)   3.80  2.00  0.70
assign (residue 17 and name H3)   (residue  7 and name  H5)   5.00  2.00  1.00
assign (residue 17 and name H3)   (residue  7 and name  H6)   5.00  2.00  1.00

assign (residue 20 and name H3)   (residue 21 and name  H5)   5.00  2.00  1.00
assign (residue 20 and name H3)   (residue 21 and name  H6)   6.00  2.00  1.00

assign (residue 20 and name H3)   (residue  3 and name  H2)   3.80  2.00  0.70
assign (residue 20 and name H3)   (residue  3 and name  H8)   6.00  2.00  1.00
assign (residue 20 and name H3)   (residue  3 and name  H61)  2.50  0.70  0.50
assign (residue 20 and name H3)   (residue  3 and name  H62)  3.80  0.30  0.40
assign (residue 20 and name H3)   (residue  4 and name  H1')  6.00  2.00  1.00
```

Hydrogen-bond restraints whose existence was proven by 2D [^{1}H,^{1}H]-NOESY spectrum acquired at 278 K at 700 MHz proton frequency (90% H_2O/10% D_2O, 10 mM KCl, 10 μM EDTA, pH = 6.61) and by a 2D J_{NN} HNN-COSY experiment acquired at 278 K (90% H_2O/10% D_2O, 10 mM KCl, 10 μM EDTA, pH = 6.82).

G1-C22
assign (residue 1 and name H1) (residue 22 and name N3) 2.00 0.20 0.20
assign (residue 1 and name N1) (residue 22 and name N3) 2.90 0.30 0.30
assign (residue 1 and name O6) (residue 22 and name H41) 2.00 0.20 0.20
assign (residue 1 and name O6) (residue 22 and name N4) 2.90 0.30 0.30
assign (residue 1 and name H21) (residue 22 and name O2) 2.00 0.20 0.20
assign (residue 1 and name N2) (residue 22 and name O2) 2.90 0.30 0.30

G2-C21
assign (residue 2 and name H1) (residue 21 and name N3) 2.00 0.20 0.20
assign (residue 2 and name N1) (residue 21 and name N3) 2.90 0.30 0.30
assign (residue 2 and name O6) (residue 21 and name H41) 2.00 0.20 0.20
assign (residue 2 and name O6) (residue 21 and name N4) 2.90 0.30 0.30
assign (residue 2 and name H21) (residue 21 and name O2) 2.00 0.20 0.20
assign (residue 2 and name N2) (residue 21 and name O2) 2.90 0.30 0.30

A3-U20
assign (residue 3 and name N1) (residue 20 and name H3) 2.00 0.20 0.20
assign (residue 3 and name N1) (residue 20 and name N3) 2.90 0.30 0.30
assign (residue 3 and name H61) (residue 20 and name O4) 2.00 0.20 0.20
assign (residue 3 and name N6) (residue 20 and name O4) 2.90 0.30 0.30

G4-C19
assign (residue 4 and name H1) (residue 19 and name N3) 2.00 0.20 0.20
assign (residue 4 and name N1) (residue 19 and name N3) 2.90 0.30 0.30
assign (residue 4 and name O6) (residue 19 and name H41) 2.00 0.20 0.20
assign (residue 4 and name O6) (residue 19 and name N4) 2.90 0.30 0.30
assign (residue 4 and name H21) (residue 19 and name O2) 2.00 0.20 0.20
assign (residue 4 and name N2) (residue 19 and name O2) 2.90 0.30 0.30

U5-A18
assign (residue 5 and name H3) (residue 18 and name N1) 2.00 0.20 0.20
assign (residue 5 and name N3) (residue 18 and name N1) 2.90 0.30 0.30
assign (residue 5 and name O4) (residue 18 and name H61) 2.00 0.20 0.20
assign (residue 5 and name O4) (residue 18 and name N6) 2.90 0.30 0.30

A6-U17
assign (residue 6 and name N1) (residue 17 and name H3) 2.00 0.20 0.20
assign (residue 6 and name N1) (residue 17 and name N3) 2.90 0.30 0.30
assign (residue 6 and name H61) (residue 17 and name O4) 2.00 0.20 0.20
assign (residue 6 and name N6) (residue 17 and name O4) 2.90 0.30 0.30

U7-A16
assign (residue 7 and name H3) (residue 16 and name N1) 2.00 0.20 0.20
assign (residue 7 and name N3) (residue 16 and name N1) 2.90 0.30 0.30
assign (residue 7 and name O4) (residue 16 and name H61) 2.00 0.20 0.20

```
assign (residue  7 and name  O4)   (residue 16 and name  N6)   2.90  0.30  0.30
```

G8-C15

```
assign (residue  8 and name  H1)   (residue 15 and name  N3)   2.00  0.20  0.20
assign (residue  8 and name  N1)   (residue 15 and name  N3)   2.90  0.30  0.30
assign (residue  8 and name  O6)   (residue 15 and name  H41)  2.00  0.20  0.20
assign (residue  8 and name  O6)   (residue 15 and name  N4)   2.90  0.30  0.30
assign (residue  8 and name  H21)  (residue 15 and name  O2)   2.00  0.20  0.20
assign (residue  8 and name  N2)   (residue 15 and name  O2)   2.90  0.30  0.30
```

U9-G14

```
assign (residue  9 and name  H3)   (residue 14 and name  H1)   1.90  0.10  0.20
assign (residue  9 and name  H3)   (residue 14 and name  O6)   1.90  0.10  0.20
assign (residue  9 and name  N3)   (residue 14 and name  O6)   2.90  0.10  0.20
assign (residue  9 and name  O2)   (residue 14 and name  H1)   1.90  0.10  0.20
assign (residue  9 and name  O2)   (residue 14 and name  N1)   2.90  0.10  0.20
```

G10-A13

```
assign (residue 10 and name H21)  (residue 13 and name  N7)   1.90  0.10  0.20
assign (residue 10 and name N2)   (residue 13 and name  N7)   2.90  0.10  0.20
assign (residue 10 and name N3)   (residue 13 and name  H61)  2.00  0.10  0.20
assign (residue 10 and name N3)   (residue 13 and name  N6)   2.50  0.10  0.20
```

Appendix 29 Dihedral angle restraints fort he structure calculation of d3'-TL

Phosphate-sugar-backbone dihedral angle restraints. β,γ and ε are only restrained for A-helical regions for residues with a 3'-endo sugar pucker. The number in the middle represents the angle in °, the two numbers to the right and the left are the error limits and the last number is a weighting factor. The exact values were taken from the dihedral angle restraint file of the structure calculation for D5-36, which represents a RNA hairpin structure.[34]

```
assign  (residue n-1    and name O3' )
        (residue n      and name P   )
        (residue n      and name O5' )
        (residue n      and name C5' )      20.0    -62.1   10.0    2       {*alpha*}

assign  (residue n      and name P   )
        (residue n      and name O5' )
        (residue n      and name C5' )
        (residue n      and name C4' )      20.0    -179.9  10.0    2       {*beta*}

assign  residue n       and name O5' )
        (residue n      and name C5' )
        (residue n      and name C4' )
        (residue n      and name C3' )      20.0    47.44   10.0    2       {*gamma*}

assign  (residue n      and name C4' )
        (residue n      and name C3' )
        (residue n      and name O3' )
        (residue n+1    and name P   )      20.0    -151.7  10.0    2       {*epsilon*}

assign  (residue n      and name C3' )
        (residue n      and name O3' )
        (residue n+1    and name P   )
        (residue n+1    and name O5' )      20.0    -73.6   10.0    2       {*zeta*}
```

Sugar pucker restraints for 2'-endo and 3'-endo sugars. Helical A-type RNA is usually 3'-endo and does not give a strong H1'-H2' crosspeak in 2D [^{1}H,^{1}H]-TOCSY experiments. A11 was constrained to S-type range (2'-endo). G1, and C22, as well as G10, A12, A13 of the tetraloop were left unconstrained. The sugar pucker restraints are based on a 2D [^{1}H^{1}H]-TOCSY that was acquired at 303 K and 700 MHz proton frequency with 45 ms mixing time (100% D_2O containing 10 mM KCl and 10 μM EDTA, pD = 6.4).

```
2'-endo sugar pucker
assign  (residue n and name C5'  )
        (residue n and name C4'  )
        (residue n and name C3'  )
        (residue n and name O3'  )    20.0    145.0  30.0   2       {*delta*}

assign  (residue n and name O4'  )
        (residue n and name C1'  )
        (residue n and name C2'  )
        (residue n and name C3'  )    20.0    25.0   30.0   2       {*nu1*}

assign  (residue n and name C1'  )
        (residue n and name C2'  )
        (residue n and name C3'  )
        (residue n and name C4'  )    20.0    -35.0  30.0   2       {*nu2*}

3'-endo sugar pucker
assign  (residue n and name C5'  )
        (residue n and name C4'  )
        (residue n and name C3'  )
        (residue n and name O3'  )    20.0    85.0   30.0   2       {*delta*}

assign  (residue n and name O4'  )
        (residue n and name C1'  )
        (residue n and name C2'  )
        (residue n and name C3'  )    20.0    -25.0  30.0   2       {*nu1*}

assign  (residue n and name C1'  )
        (residue n and name C2'  )
        (residue n and name C3'  )
        (residue n and name C4'  )    20.0    37.3   30.0   2       {*nu2*}
```

Restraints for the torsion angle χ, which defines the orientation of the base to the sugar around the glycosidic bond. All χ angles were constrained to be in an *anti* orientation because of the absence of strong H1'-H8/H6 crosspeaks in the short mixing time 2D [^{1}H,^{1}H]-NOESYs recorded in D_2O.

```
torsion angle χ
assign  (residue n and name O4'  )
        (residue n and name C1'  )
        (residue n and name N9   )
        (residue n and name C4   )    20.0    -160   20.0   2
```

Appendix 30 ^{1}H chemical shift assignments for EBS1*·IBS1*

	H1	H1'	H2	H2'	H21	H22	H3	H3'	H4'	H41	H42	H5	H5'	H5''	H6	H61	H62	H8
G13	12.301	5.284	-	4.240	-	-	-	4.417	4.005	-	-	-	3.628	3.710	-	-	-	7.667
G14	11.393	5.645	-	4.457	7.521	6.053	-	4.389	4.283	-	-	-	-	-	-	-	-	7.232
C15	-	5.278	-	4.206	-	-	-	4.403	4.373	8.069	6.679	5.308	-	3.918	7.533	-	-	-
A16	-	5.732	7.209	4.375	-	-	-	4.494	4.300	-	-	-	-	3.942	-	7.705	6.056	7.840
C17	-	5.205	-	4.022	-	-	-	4.194	4.178	8.037	6.767	5.035	-	3.862	7.374	-	-	-
U18	-	5.322	-	4.191	-	-	13.569	4.347	4.336	-	-	5.153	-	3.860	7.606	-	-	-
G19	12.222	5.677	-	3.865	-	-	-	4.122	4.049	-	-	-	-	-	-	-	-	7.509
C59	-	5.231	-	4.349	-	-	-	4.094	4.368	8.038	6.896	5.762	3.813	3.712	7.869	-	-	-
A60	-	5.793	7.041	4.582	-	-	-	4.290	4.341	-	-	-	-	4.018	-	-	6.183	8.013
G61	13.141	5.399	-	4.167	8.069	5.934	-	4.265	4.252	-	-	-	-	3.908	-	-	-	7.075
U62	-	5.315	-	4.469	-	-	13.366	4.329	4.229	-	-	4.858	-	3.880	7.474	-	-	-
G63	12.472	5.590	-	4.449	7.587	5.792	-	4.249	4.300	-	-	-	3.928	3.871	-	-	-	7.419
U64	-	5.640	-	3.900	-	-	11.992	4.009	3.809	-	-	5.227	-	-	7.626	-	-	-
C65	-	5.512	-	4.338	-	-	-	4.323	3.865	8.038	6.741	5.477	-	-	7.627	-	-	-

Appendix 31 ^{13}C and ^{15}N assignments for EBS1*·IBS1*

	C6	C5	C8	C2	C1'
G13	-	-	137.41	-	-
G14	-	-	134.17	-	90.05
C15	137.35	95.44	-	-	90.54
A16	-	-	136.41	150.58	90.08
C17	137.91	94.32	-	-	90.72
U18	138.54	101.02	-	-	90.69
G19	-	-	134.81	-	88.30
C59	141.71	95.09	-	-	90.74
A60	-	-	138.03	150.03	90.02
G61	-	-	133.64	-	90.07
U62	138.14	100.51	-	-	90.46
G63	-	-	133.14	-	87.97
U64	137.88	101.47	-	-	91.02
C65	140.08	94.74	-	-	90.23

Appendix 32 Illustration of the surface area of EBS1*·IBS1*

The colours correspond to the one used in the secondary structure as shown in Figure 25.

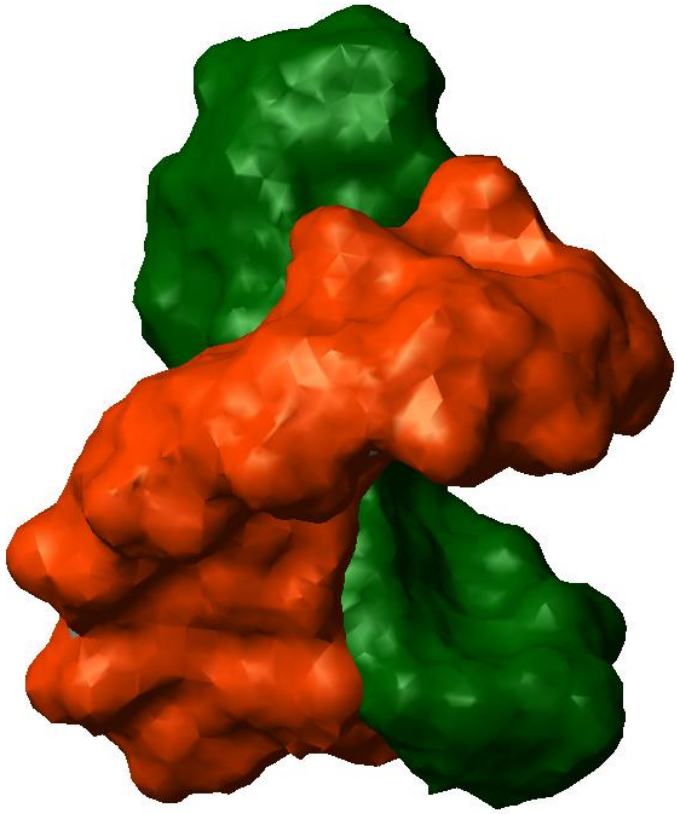

Appendix 33 All distance constraints in EBS1*·IBS1*

Distance constraints of non-exchangeable protons in EBS1*·IBS1* based on a 2D [^{1}H,^{1}H]-NOESY spectrum acquired at 700 MHz proton frequency at 288 K (100% D_2O, 100 mM KCl, 10 µM EDTA, pD = 6.7). Specified are the estimated distances in Å, the lower and the upper boundaries.

```
assign (residue 13 and name H1')   (residue 13 and name  H8)   3.80  2.00  0.70
assign (residue 13 and name H2')   (residue 13 and name  H8)   3.80  2.00  0.70
assign (residue 13 and name H3')   (residue 13 and name  H8)   2.50  0.70  0.50
assign (residue 13 and name H4')   (residue 13 and name  H8)   5.00  2.00  1.00
assign (residue 13 and name H5')   (residue 13 and name  H8)   3.80  2.00  0.70
assign (residue 13 and name H5'')  (residue 13 and name  H8)   3.80  2.00  0.70

assign (residue 13 and name H1')   (residue 14 and name  H1')  5.00  2.00  1.00
assign (residue 13 and name H1')   (residue 14 and name  H8)   5.00  2.00  0.70
assign (residue 13 and name H2')   (residue 14 and name  H1')  5.00  2.00  1.00
assign (residue 13 and name H2')   (residue 14 and name  H8)   3.80  2.00  0.70
assign (residue 13 and name H3')   (residue 14 and name  H8)   3.80  2.00  0.70
assign (residue 13 and name H8)    (residue 14 and name  H8)   3.80  2.00  0.70

assign (residue 14 and name H1')   (residue 14 and name  H8)   3.80  2.00  0.70
assign (residue 14 and name H2')   (residue 14 and name  H8)   3.80  2.00  0.70
assign (residue 14 and name H3')   (residue 14 and name  H8)   2.50  0.70  0.50
assign (residue 14 and name H4')   (residue 14 and name  H8)   5.00  2.00  1.00

assign (residue 14 and name H1')   (residue 15 and name  H1')  3.80  2.00  0.70
assign (residue 14 and name H1')   (residue 15 and name  H5)   5.00  2.00  1.00
assign (residue 14 and name H1')   (residue 15 and name  H6)   3.80  2.00  0.70
assign (residue 14 and name H2')   (residue 15 and name  H1')  3.80  2.00  0.70
assign (residue 14 and name H2')   (residue 15 and name  H5)   3.80  2.00  0.70
assign (residue 14 and name H2')   (residue 15 and name  H6)   3.80  2.00  0.70
assign (residue 14 and name H3')   (residue 15 and name  H5)   3.80  2.00  0.70
assign (residue 14 and name H3')   (residue 15 and name  H6)   3.80  2.00  0.70
assign (residue 14 and name H8)    (residue 15 and name  H5)   2.50  0.70  0.50
assign (residue 14 and name H8)    (residue 15 and name  H6)   3.80  2.00  0.70

assign (residue 15 and name H1')   (residue 15 and name  H5)   5.00  2.00  1.00
assign (residue 15 and name H1')   (residue 15 and name  H6)   3.80  2.00  0.70
assign (residue 15 and name H2')   (residue 15 and name  H5)   5.00  2.00  1.00
assign (residue 15 and name H2')   (residue 15 and name  H6)   3.80  2.00  0.70
assign (residue 15 and name H3')   (residue 15 and name  H5)   3.80  2.00  0.70
assign (residue 15 and name H3')   (residue 15 and name  H6)   2.50  0.70  0.50
assign (residue 15 and name H4')   (residue 15 and name  H5)   6.00  2.00  1.00
assign (residue 15 and name H4')   (residue 15 and name  H6)   3.80  2.00  0.70
assign (residue 15 and name H5'')  (residue 15 and name  H6)   3.80  2.00  0.70

assign (residue 15 and name H1')   (residue 16 and name  H1')  5.00  2.00  1.00
assign (residue 15 and name H1')   (residue 16 and name  H8)   3.80  2.00  0.70
assign (residue 15 and name H2')   (residue 16 and name  H8)   2.50  0.70  0.50
assign (residue 15 and name H3')   (residue 16 and name  H8)   3.80  2.00  0.70
```

```
assign (residue 15 and name H5)  (residue 16 and name  H8)   5.00  2.00  1.00
assign (residue 15 and name H6)  (residue 16 and name  H8)   3.80  2.00  0.70

assign (residue 16 and name H1')  (residue 16 and name  H2)   3.80  2.00  0.70
assign (residue 16 and name H1')  (residue 16 and name  H8)   3.80  2.00  0.70
assign (residue 16 and name H2')  (residue 16 and name  H2)   3.80  2.00  0.70
assign (residue 16 and name H2')  (residue 16 and name  H8)   3.80  2.00  0.70
assign (residue 16 and name H3')  (residue 16 and name  H8)   2.50  0.70  0.50
assign (residue 16 and name H4')  (residue 16 and name  H8)   5.00  2.00  1.00
assign (residue 16 and name H5")  (residue 16 and name  H8)   3.80  2.00  0.70
assign (residue 16 and name H2)  (residue 16 and name  H8)   5.00  2.00  1.00

assign (residue 16 and name H1')  (residue 17 and name  H1')   5.00  2.00  1.00
assign (residue 16 and name H1')  (residue 17 and name  H5)   5.00  2.00  1.00
assign (residue 16 and name H1')  (residue 17 and name  H6)   3.80  2.00  0.70
assign (residue 16 and name H2')  (residue 17 and name  H1')   3.80  2.00  0.70
assign (residue 16 and name H2')  (residue 17 and name  H5)   3.80  2.00  0.70
assign (residue 16 and name H2')  (residue 17 and name  H6)   2.50  0.70  0.50
assign (residue 16 and name H3')  (residue 17 and name  H5)   3.80  2.00  0.70
assign (residue 16 and name H3')  (residue 17 and name  H6)   3.80  2.00  0.70
assign (residue 16 and name H2)  (residue 17 and name  H1')   2.50  0.70  0.50
assign (residue 16 and name H2)  (residue 17 and name  H2')   5.00  2.00  1.00
assign (residue 16 and name H2)  (residue 17 and name  H3')   5.00  2.00  1.00
assign (residue 16 and name H2)  (residue 17 and name  H6)   3.80  2.00  0.70
assign (residue 16 and name H2)  (residue 62 and name  H1')   5.00  2.00  1.00
assign (residue 16 and name H2)  (residue 62 and name  H2')   5.00  2.00  1.00
assign (residue 16 and name H2)  (residue 63 and name  H1')   2.50  0.70  0.50
assign (residue 16 and name H2)  (residue 63 and name  H2')   3.80  2.00  0.70
assign (residue 16 and name H2)  (residue 63 and name  H8)   3.80  2.00  0.70
assign (residue 16 and name H8)  (residue 17 and name  H5)   3.80  2.00  0.70
assign (residue 16 and name H8)  (residue 17 and name  H6)   3.80  2.00  0.70

assign (residue 17 and name H1')  (residue 17 and name  H5)   5.00  2.00  1.00
assign (residue 17 and name H1')  (residue 17 and name  H6)   3.80  2.00  0.70
assign (residue 17 and name H2')  (residue 17 and name  H5)   5.00  2.00  1.00
assign (residue 17 and name H2')  (residue 17 and name  H6)   3.80  2.00  0.70
assign (residue 17 and name H3')  (residue 17 and name  H5)   3.80  2.00  0.70
assign (residue 17 and name H3')  (residue 17 and name  H6)   2.50  0.70  0.50
assign (residue 17 and name H4')  (residue 17 and name  H5)   5.00  2.00  1.00
assign (residue 17 and name H4')  (residue 17 and name  H6)   5.00  2.00  1.00
assign (residue 17 and name H5")  (residue 17 and name  H5)   6.00  2.00  1.00
assign (residue 17 and name H5")  (residue 17 and name  H6)   3.80  2.00  0.70

assign (residue 17 and name H1')  (residue 18 and name  H1')   5.00  2.00  1.00
assign (residue 17 and name H1')  (residue 18 and name  H5)   5.00  2.00  1.00
assign (residue 17 and name H1')  (residue 18 and name  H6)   3.80  2.00  0.70
assign (residue 17 and name H2')  (residue 18 and name  H1')   3.80  2.00  0.70
assign (residue 17 and name H2')  (residue 18 and name  H5)   3.80  2.00  0.70
assign (residue 17 and name H2')  (residue 18 and name  H6)   2.50  0.70  0.50
assign (residue 17 and name H3')  (residue 18 and name  H5)   3.80  2.00  0.70
assign (residue 17 and name H3')  (residue 18 and name  H6)   3.80  2.00  0.70
```

```
assign (residue 17 and name H5)  (residue 18 and name  H5)  2.50  0.70  0.50
assign (residue 17 and name H5)  (residue 18 and name  H6)  3.80  2.00  0.70
assign (residue 17 and name H6)  (residue 18 and name  H5)  2.50  0.70  0.50
assign (residue 17 and name H6)  (residue 18 and name  H6)  3.80  2.00  0.70

assign (residue 18 and name H1') (residue 18 and name  H5)  5.00  2.00  1.00
assign (residue 18 and name H1') (residue 18 and name  H6)  3.80  2.00  0.70
assign (residue 18 and name H2') (residue 18 and name  H5)  5.00  2.00  1.00
assign (residue 18 and name H2') (residue 18 and name  H6)  2.50  0.70  0.50
assign (residue 18 and name H3') (residue 18 and name  H5)  5.00  2.00  1.00
assign (residue 18 and name H3') (residue 18 and name  H6)  2.50  0.70  0.50
assign (residue 18 and name H4') (residue 18 and name  H5)  6.00  2.00  1.00
assign (residue 18 and name H4') (residue 18 and name  H6)  5.00  2.00  1.00
assign (residue 18 and name H5") (residue 18 and name  H5)  6.00  2.00  1.00
assign (residue 18 and name H5") (residue 18 and name  H6)  3.80  2.00  0.70

assign (residue 18 and name H1') (residue 19 and name  H1') 3.80  2.00  0.70
assign (residue 18 and name H1') (residue 19 and name  H8)  3.80  2.00  0.70
assign (residue 18 and name H1') (residue 60 and name  H2)  3.80  2.00  0.70
assign (residue 18 and name H2') (residue 19 and name  H1') 5.00  2.00  1.00
assign (residue 18 and name H2') (residue 19 and name  H8)  2.50  0.70  0.50
assign (residue 18 and name H2') (residue 60 and name  H2)  5.00  2.00  1.00
assign (residue 18 and name H3') (residue 19 and name  H8)  3.80  2.00  0.70
assign (residue 18 and name H6)  (residue 19 and name  H8)  3.80  2.00  0.70

assign (residue 19 and name H1') (residue 19 and name  H8)  3.80  2.00  0.70
assign (residue 19 and name H1') (residue 60 and name  H2)  3.80  2.00  0.70
assign (residue 19 and name H2') (residue 19 and name  H8)  3.80  2.00  0.70
assign (residue 19 and name H2') (residue 60 and name  H2)  3.80  2.00  0.70
assign (residue 19 and name H3') (residue 19 and name  H8)  2.50  0.70  0.50
assign (residue 19 and name H4') (residue 19 and name  H8)  5.00  2.00  1.00
assign (residue 19 and name H8)  (residue 60 and name  H2)  3.80  2.00  0.70

assign (residue 59 and name H1') (residue 59 and name  H5)  5.00  2.00  1.00
assign (residue 59 and name H1') (residue 59 and name  H6)  3.80  2.00  0.70
assign (residue 59 and name H2') (residue 59 and name  H5)  5.00  2.00  1.00
assign (residue 59 and name H2') (residue 59 and name  H6)  6.00  2.00  1.00
assign (residue 59 and name H3') (residue 59 and name  H5)  3.80  2.00  0.70
assign (residue 59 and name H3') (residue 59 and name  H6)  2.50  0.70  0.50
assign (residue 59 and name H4') (residue 59 and name  H5)  5.00  2.00  1.00
assign (residue 59 and name H4') (residue 59 and name  H6)  3.80  2.00  0.70
assign (residue 59 and name H5') (residue 59 and name  H5)  5.00  2.00  1.00
assign (residue 59 and name H5') (residue 59 and name  H6)  3.80  2.00  0.70
assign (residue 59 and name H5") (residue 59 and name  H5)  3.80  2.00  0.70
assign (residue 59 and name H5") (residue 59 and name  H6)  2.50  0.70  0.50

assign (residue 59 and name H1') (residue 60 and name  H1') 5.00  2.00  1.00
assign (residue 59 and name H1') (residue 60 and name  H8)  3.80  2.00  0.70
assign (residue 59 and name H2') (residue 60 and name  H1') 5.00  2.00  1.00
assign (residue 59 and name H2') (residue 60 and name  H8)  2.50  0.70  0.50
assign (residue 59 and name H3') (residue 60 and name  H8)  3.80  2.00  0.70
```

```
assign (residue 59 and name H6)  (residue 60 and name  H8)   3.80  2.00  0.70

assign (residue 60 and name H1')  (residue 60 and name  H2)   3.80  2.00  0.70
assign (residue 60 and name H1')  (residue 60 and name  H8)   3.80  2.00  0.70
assign (residue 60 and name H2')  (residue 60 and name  H2)   5.00  2.00  1.00
assign (residue 60 and name H2')  (residue 60 and name  H8)   3.80  2.00  0.70
assign (residue 60 and name H3')  (residue 60 and name  H8)   2.50  0.70  0.50
assign (residue 60 and name H4')  (residue 60 and name  H8)   6.00  2.00  1.00
assign (residue 60 and name H5")  (residue 60 and name  H8)   3.80  2.00  0.70

assign (residue 60 and name H1')  (residue 61 and name  H1')  5.00  2.00  1.00
assign (residue 60 and name H1')  (residue 61 and name  H8)   3.80  2.00  0.70
assign (residue 60 and name H2')  (residue 61 and name  H1')  3.80  2.00  0.70
assign (residue 60 and name H2')  (residue 61 and name  H8)   3.80  2.00  0.70
assign (residue 60 and name H3')  (residue 61 and name  H8)   3.80  2.00  0.70
assign (residue 60 and name H2)  (residue 61 and name  H1')  3.80  2.00  0.70
assign (residue 60 and name H2)  (residue 61 and name  H2')  6.00  2.00  1.00
assign (residue 60 and name H2)  (residue 61 and name  H8)   5.00  2.00  1.00
assign (residue 60 and name H8)  (residue 61 and name  H8)   3.80  2.00  0.70

assign (residue 61 and name H1')  (residue 61 and name  H8)   3.80  2.00  0.70
assign (residue 61 and name H2')  (residue 61 and name  H8)   3.80  2.00  0.70
assign (residue 61 and name H3')  (residue 61 and name  H8)   3.80  2.00  0.70
assign (residue 61 and name H4')  (residue 61 and name  H8)   5.00  2.00  1.00
assign (residue 61 and name H5")  (residue 61 and name  H8)   3.80  2.00  0.70

assign (residue 61 and name H1')  (residue 62 and name  H1')  3.80  2.00  0.70
assign (residue 61 and name H1')  (residue 62 and name  H5)   5.00  2.00  1.00
assign (residue 61 and name H1')  (residue 62 and name  H6)   3.80  2.00  0.70
assign (residue 61 and name H2')  (residue 62 and name  H1')  3.80  2.00  0.70
assign (residue 61 and name H2')  (residue 62 and name  H5)   3.80  2.00  0.70
assign (residue 61 and name H2')  (residue 62 and name  H6)   3.80  2.00  0.70
assign (residue 61 and name H3')  (residue 62 and name  H5)   3.80  2.00  0.70
assign (residue 61 and name H3')  (residue 62 and name  H6)   5.00  2.00  0.70
assign (residue 61 and name H8)  (residue 62 and name  H5)   5.00  2.00  0.70
assign (residue 61 and name H8)  (residue 62 and name  H6)   5.00  2.00  0.70

assign (residue 62 and name H1')  (residue 62 and name  H5)   5.00  2.00  1.00
assign (residue 62 and name H1')  (residue 62 and name  H6)   3.80  2.00  0.70
assign (residue 62 and name H2')  (residue 62 and name  H6)   3.80  2.00  0.70
assign (residue 62 and name H3')  (residue 62 and name  H5)   5.00  2.00  1.00
assign (residue 62 and name H3')  (residue 62 and name  H6)   3.80  2.00  0.70
assign (residue 62 and name H4')  (residue 62 and name  H5)   5.00  2.00  1.00
assign (residue 62 and name H4')  (residue 62 and name  H6)   3.80  2.00  0.70
assign (residue 62 and name H5")  (residue 62 and name  H6)   5.00  2.00  1.00

assign (residue 62 and name H1')  (residue 63 and name  H1')  5.00  2.00  1.00
assign (residue 62 and name H1')  (residue 63 and name  H8)   3.80  2.00  0.70
assign (residue 62 and name H2')  (residue 63 and name  H1')  3.80  2.00  0.70
assign (residue 62 and name H2')  (residue 63 and name  H8)   3.80  2.00  0.70
assign (residue 62 and name H3')  (residue 63 and name  H8)   2.50  0.70  0.50
```

```
assign (residue 62 and name H5)   (residue 63 and name  H8)   5.00  2.00  1.00
assign (residue 62 and name H6)   (residue 63 and name  H8)   3.80  2.00  0.70

assign (residue 63 and name H1')  (residue 63 and name  H8)   3.80  2.00  0.70
assign (residue 63 and name H2')  (residue 63 and name  H8)   5.00  2.00  1.00
assign (residue 63 and name H3')  (residue 63 and name  H8)   3.80  2.00  0.70
assign (residue 63 and name H4')  (residue 63 and name  H8)   5.00  2.00  1.00
assign (residue 63 and name H5')  (residue 63 and name  H8)   3.80  2.00  0.70
assign (residue 63 and name H5'') (residue 63 and name  H8)   3.80  2.00  0.70

assign (residue 63 and name H1')  (residue 64 and name  H1')  5.00  2.00  1.00
assign (residue 63 and name H1')  (residue 64 and name  H5)   5.00  2.00  0.70
assign (residue 63 and name H1')  (residue 64 and name  H6)   3.80  2.00  0.70
assign (residue 63 and name H2')  (residue 64 and name  H5)   3.80  2.00  0.70
assign (residue 63 and name H2')  (residue 64 and name  H6)   3.80  2.00  0.70
assign (residue 63 and name H3')  (residue 64 and name  H5)   2.50  0.70  0.50
assign (residue 63 and name H3')  (residue 64 and name  H6)   3.80  2.00  0.70
assign (residue 63 and name H8)   (residue 64 and name  H5)   3.80  2.00  0.70
assign (residue 63 and name H8)   (residue 64 and name  H6)   3.80  2.00  0.70

assign (residue 64 and name H1')  (residue 64 and name  H5)   5.00  2.00  1.00
assign (residue 64 and name H1')  (residue 64 and name  H6)   3.80  2.00  0.70
assign (residue 64 and name H2')  (residue 64 and name  H5)   5.00  2.00  1.00
assign (residue 64 and name H2')  (residue 64 and name  H6)   3.80  2.00  0.70
assign (residue 64 and name H3')  (residue 64 and name  H5)   5.00  2.00  1.00
assign (residue 64 and name H3')  (residue 64 and name  H6)   3.80  2.00  0.70
assign (residue 64 and name H4')  (residue 64 and name  H5)   6.00  2.00  1.00
assign (residue 64 and name H4')  (residue 64 and name  H6)   3.80  2.00  0.70

assign (residue 64 and name H1')  (residue 65 and name  H1')  5.00  2.00  1.00
assign (residue 64 and name H1')  (residue 65 and name  H5)   3.80  2.00  0.70
assign (residue 64 and name H1')  (residue 65 and name  H6)   3.80  2.00  0.70
assign (residue 64 and name H2')  (residue 65 and name  H1')  3.80  2.00  0.70
assign (residue 64 and name H2')  (residue 65 and name  H5)   3.80  2.00  0.70
assign (residue 64 and name H2')  (residue 65 and name  H6)   3.80  2.00  0.70
assign (residue 64 and name H3')  (residue 65 and name  H5)   3.80  2.00  0.70
assign (residue 64 and name H3')  (residue 65 and name  H6)   3.80  2.00  0.70
assign (residue 64 and name H5)   (residue 65 and name  H5)   2.50  0.70  0.50
assign (residue 64 and name H6)   (residue 65 and name  H5)   5.00  2.00  0.70
assign (residue 64 and name H6)   (residue 65 and name  H6)   5.00  2.00  0.70

assign (residue 65 and name H1')  (residue 65 and name  H5)   5.00  2.00  1.00
assign (residue 65 and name H1')  (residue 65 and name  H6)   3.80  2.00  0.70
assign (residue 65 and name H2')  (residue 65 and name  H5)   5.00  2.00  1.00
assign (residue 65 and name H2')  (residue 65 and name  H6)   3.80  2.00  0.70
assign (residue 65 and name H3')  (residue 65 and name  H5)   3.80  2.00  0.70
assign (residue 65 and name H3')  (residue 65 and name  H6)   3.80  2.00  0.70
assign (residue 65 and name H4')  (residue 65 and name  H5)   5.00  2.00  1.00
assign (residue 65 and name H4')  (residue 65 and name  H6)   3.80  2.00  0.70
```

Distance constraints of exchangeable protons in EBS1*·IBS1* based on a 2D [^{1}H,^{1}H]-NOESY spectrum acquired at 700 MHz proton frequency at 278 K (90% H_2O/10% D_2O, 100 mM KCl, 10 μM EDTA, pH = 6.7).

```
assign (residue 13 and name H1)  (residue 14 and name  H1)   5.00  2.00  1.00

assign (residue 13 and name H1)  (residue 64 and name  H3)   3.80  2.00  0.70

assign (residue 14 and name H1)  (residue 15 and name  H1')  6.00  2.00  1.00
assign (residue 14 and name H1)  (residue 15 and name  H41)  6.00  2.00  1.00
assign (residue 14 and name H1)  (residue 15 and name  H42)  5.00  2.00  1.00
assign (residue 14 and name H1)  (residue 15 and name  H5)   6.00  2.00  1.00
assign (residue 14 and name H1)  (residue 15 and name  H6)   6.00  2.00  1.00

assign (residue 14 and name H1)  (residue 63 and name  H1)   5.00  2.00  1.00
assign (residue 14 and name H1)  (residue 64 and name  H3)   2.50  0.70  0.50
assign (residue 14 and name H1)  (residue 64 and name  H5)   6.00  2.00  1.00
assign (residue 14 and name H1)  (residue 64 and name  H6)   6.00  2.00  1.00
assign (residue 14 and name H1)  (residue 65 and name  H41)  5.00  2.00  1.00
assign (residue 14 and name H1)  (residue 65 and name  H42)  5.00  2.00  1.00
assign (residue 14 and name H1)  (residue 65 and name  H5)   5.00  2.00  1.00

assign (residue 18 and name H3)  (residue 19 and name  H1)   3.80  2.00  0.70
assign (residue 18 and name H3)  (residue 19 and name  H8)   5.00  2.00  1.00

assign (residue 18 and name H3)  (residue 60 and name  H2)   3.80  2.00  0.70
assign (residue 18 and name H3)  (residue 60 and name  H62)  3.80  0.30  0.40
assign (residue 18 and name H3)  (residue 61 and name  H1)   3.80  2.00  0.70

assign (residue 19 and name H1)  (residue 59 and name  H41)  2.50  0.70  0.50
assign (residue 19 and name H1)  (residue 59 and name  H42)  3.80  2.00  0.70
assign (residue 19 and name H1)  (residue 59 and name  H5)   6.00  2.00  1.00

assign (residue 61 and name H1)  (residue 60 and name  H2)   5.00  2.00  1.00
assign (residue 61 and name H1)  (residue 62 and name  H3)   3.80  2.00  0.70
assign (residue 61 and name H1)  (residue 62 and name  H5)   6.00  2.00  1.00

assign (residue 61 and name H1)  (residue 16 and name  H2)   6.00  2.00  1.00
assign (residue 61 and name H1)  (residue 16 and name  H61)  5.00  2.00  1.00
assign (residue 61 and name H1)  (residue 17 and name  H41)  2.50  0.70  0.50
assign (residue 61 and name H1)  (residue 17 and name  H42)  3.80  2.00  0.70
assign (residue 61 and name H1)  (residue 17 and name  H5)   6.00  2.00  1.00
assign (residue 61 and name H1)  (residue 18 and name  H5)   5.00  2.00  1.00
assign (residue 61 and name H1)  (residue 18 and name  H6)   5.00  2.00  1.00

assign (residue 62 and name H3)  (residue 63 and name  H1)   3.80  2.00  0.70
assign (residue 62 and name H3)  (residue 63 and name  H1')  5.00  2.00  1.00
assign (residue 62 and name H3)  (residue 63 and name  H8)   5.00  2.00  1.00

assign (residue 62 and name H3)  (residue 15 and name  H42)  5.00  2.00  1.00
assign (residue 62 and name H3)  (residue 16 and name  H2)   3.80  2.00  0.70
```

```
assign (residue 62 and name H3)  (residue 16 and name  H61) 5.00  2.00  1.00
assign (residue 62 and name H3)  (residue 16 and name  H62) 5.00  2.00  1.00
assign (residue 62 and name H3)  (residue 17 and name  H1') 5.00  2.00  1.00
assign (residue 62 and name H3)  (residue 17 and name  H41) 3.80  2.00  0.70
assign (residue 62 and name H3)  (residue 17 and name  H42) 5.00  2.00  1.00

assign (residue 63 and name H1)  (residue 64 and name  H3)  3.80  2.00  0.70
assign (residue 63 and name H1)  (residue 64 and name  H5)  6.00  2.00  1.00

assign (residue 63 and name H1)  (residue 14 and name  H22) 5.00  2.00  1.00
assign (residue 63 and name H1)  (residue 15 and name  H41) 2.50  0.70  0.50
assign (residue 63 and name H1)  (residue 15 and name  H42) 3.80  2.00  0.70
assign (residue 63 and name H1)  (residue 15 and name  H5)  6.00  2.00  1.00
assign (residue 63 and name H1)  (residue 15 and name  H6)  6.00  2.00  1.00
assign (residue 63 and name H1)  (residue 16 and name  H1') 6.00  2.00  1.00
assign (residue 63 and name H1)  (residue 16 and name  H2)  6.00  2.00  1.00

assign (residue 64 and name H3)  (residue 65 and name  H41) 6.00  2.00  1.00
assign (residue 64 and name H3)  (residue 65 and name  H42) 5.00  2.00  1.00
assign (residue 64 and name H3)  (residue 65 and name  H5)  5.00  2.00  1.00
assign (residue 64 and name H3)  (residue 65 and name  H6)  6.00  2.00  1.00

assign (residue 64 and name H3)  (residue 14 and name  H1') 6.00  2.00  1.00
assign (residue 64 and name H3)  (residue 14 and name  H21) 5.00  2.00  1.00
assign (residue 64 and name H3)  (residue 14 and name  H22) 3.80  0.30  0.40
assign (residue 64 and name H3)  (residue 15 and name  H41) 3.80  0.30  0.40
assign (residue 64 and name H3)  (residue 15 and name  H42) 3.80  0.30  0.40
```

Hydrogen-bond restraints whose existence was proven by 2D [^{1}H,^{1}H]-NOESY spectrum acquired at 278 K at 700 MHz proton frequency (90% H_2O/10% D_2O, 100 mM KCl, 10 μM EDTA, pH = 6.7).

G13-C65

```
assign (residue 13 and name  H1)   (residue 65 and name N3)    2.00  0.20  0.20
assign (residue 13 and name  N1)   (residue 65 and name N3)    2.90  0.30  0.30
assign (residue 13 and name  O6)   (residue 65 and name H41)   2.00  0.20  0.20
assign (residue 13 and name  O6)   (residue 65 and name N4)    2.90  0.30  0.30
assign (residue 13 and name  H21)  (residue 65 and name O2)    2.00  0.20  0.20
assign (residue 13 and name  N2)   (residue 65 and name O2)    2.90  0.30  0.30
```

G14-U64

```
assign (residue 14 and name  H1)   (residue 64 and name H3)    1.90  0.10  0.20
assign (residue 14 and name  H1)   (residue 64 and name O2)    1.90  0.10  0.20
assign (residue 14 and name  N1)   (residue 64 and name O2)    2.90  0.10  0.20
assign (residue 14 and name  O6)   (residue 64 and name H3)    1.90  0.10  0.20
assign (residue 14 and name  O6)   (residue 64 and name N3)    2.90  0.10  0.20
```

C15-G63

```
assign (residue 15 and name  N3)   (residue 63 and name H1)    2.00  0.20  0.20
assign (residue 15 and name  N3)   (residue 63 and name N1)    2.90  0.30  0.30
assign (residue 15 and name  H41)  (residue 63 and name O6)    2.00  0.20  0.20
assign (residue 15 and name  N4)   (residue 63 and name O6)    2.90  0.30  0.30
assign (residue 15 and name  O2)   (residue 63 and name H21)   2.00  0.20  0.20
assign (residue 15 and name  O2)   (residue 63 and name N2)    2.90  0.30  0.30
```

A16-U62

```
assign (residue 16 and name  N1)   (residue 62 and name H3)    2.00  0.20  0.20
assign (residue 16 and name  N1)   (residue 62 and name N3)    2.90  0.30  0.30
assign (residue 16 and name  H61)  (residue 62 and name O4)    2.00  0.20  0.20
assign (residue 16 and name  N6)   (residue 62 and name O4)    2.90  0.30  0.30
```

C17-G61

```
assign (residue 17 and name  N3)   (residue 61 and name H1)    2.00  0.20  0.20
assign (residue 17 and name  N3)   (residue 61 and name N1)    2.90  0.30  0.30
assign (residue 17 and name  H41)  (residue 61 and name O6)    2.00  0.20  0.20
assign (residue 17 and name  N4)   (residue 61 and name O6)    2.90  0.30  0.30
assign (residue 17 and name  O2)   (residue 61 and name H21)   2.00  0.20  0.20
assign (residue 17 and name  O2)   (residue 61 and name N2)    2.90  0.30  0.30
```

U18-A60

```
assign (residue 18 and name  H3)   (residue 60 and name N1)    2.00  0.20  0.20
assign (residue 18 and name  N3)   (residue 60 and name N1)    2.90  0.30  0.30
assign (residue 18 and name  O4)   (residue 60 and name H61)   2.00  0.20  0.20
assign (residue 18 and name  O4)   (residue 60 and name N6)    2.90  0.30  0.30
```

G19-C59

```
assign (residue 19 and name  H1)   (residue 59 and name N3)    2.00  0.20  0.20
assign (residue 19 and name  N1)   (residue 59 and name N3)    2.90  0.30  0.30
assign (residue 19 and name  O6)   (residue 59 and name H41)   2.00  0.20  0.20
```

```
assign (residue 19 and name  O6)    (residue 59 and name N4)    2.90  0.30  0.30
assign (residue 19 and name  H21)   (residue 59 and name O2)    2.00  0.20  0.20
assign (residue 19 and name  N2)    (residue 59 and name O2)    2.90  0.30  0.30
```

Appendix 34 Dihedral angle restraints fort he structure calculation of EBS1*·IBS1*

Phosphate-sugar-backbone dihedral angle restraints. β,γ and ε are only restrained for A-helical regions for residues with a 3'-endo sugar pucker. The number in the middle represents the angle in °, the two numbers to the right and the left are the error limits and the last number is a weighing factor. The exact values were taken from the dihedral angle restraint file of the structure calculation for D5-36, which represents a RNA hairpin structure.[34]

```
assign  (residue n-1    and name O3' )
        (residue n      and name P   )
        (residue n      and name O5' )
        (residue n      and name C5' )      20.0    -62.1   10.0    2       {*alpha*}

assign  (residue n      and name P   )
        (residue n      and name O5' )
        (residue n      and name C5' )
        (residue n      and name C4' )      20.0    -179.9  10.0    2       {*beta*}

assign  residue n       and name O5' )
        (residue n      and name C5' )
        (residue n      and name C4' )
        (residue n      and name C3' )      20.0    47.44   10.0    2       {*gamma*}

assign  (residue n      and name C4' )
        (residue n      and name C3' )
        (residue n      and name O3' )
        (residue n+1    and name P   )      20.0    -151.7  10.0    2       {*epsilon*}

assign  (residue n      and name C3' )
        (residue n      and name O3' )
        (residue n+1    and name P   )
        (residue n+1    and name O5' )      20.0    -73.6   10.0    2       {*zeta*}
```

Sugar pucker restraints for 2'-endo and 3'-endo sugars. Helical A-type RNA is usually 3'-endo and does not give a strong H1'-H2' crosspeak in 2D [^{1}H,^{1}H]-TOCSY experiments. G19 was left unconstrained. The sugar pucker restraints are based on a 2D [^{1}H^{1}H]-TOCSY that was acquired at 288 K and 700 MHz proton frequency with 45 ms mixing time (100% D_2O containing 100 mM KCl and 10 μM EDTA, pD = 6.7).

```
2'-endo sugar pucker
assign  (residue n and name C5'  )
        (residue n and name C4'  )
        (residue n and name C3'  )
        (residue n and name O3'  )   20.0    145.0   30.0    2       {*delta*}

assign  (residue n and name O4'  )
        (residue n and name C1'  )
        (residue n and name C2'  )
        (residue n and name C3'  )   20.0    25.0    30.0    2       {*nu1*}

assign  (residue n and name C1'  )
        (residue n and name C2'  )
        (residue n and name C3'  )
        (residue n and name C4'  )   20.0    -35.0   30.0    2       {*nu2*}

3'-endo sugar pucker
assign  (residue n and name C5'  )
        (residue n and name C4'  )
        (residue n and name C3'  )
        (residue n and name O3'  )   20.0    85.0    30.0    2       {*delta*}

assign  (residue n and name O4'  )
        (residue n and name C1'  )
        (residue n and name C2'  )
        (residue n and name C3'  )   20.0    -25.0   30.0    2       {*nu1*}

assign  (residue n and name C1'  )
        (residue n and name C2'  )
        (residue n and name C3'  )
        (residue n and name C4'  )   20.0    37.3    30.0    2       {*nu2*}
```

Restraints for the torsion angle χ, which defines the orientation of the base to the sugar around the glycosidic bond. All χ angles were constrained to be in an *anti* orientation because of the absence of strong H1'-H8/H6 crosspeaks in the short mixing time 2D [^{1}H,^{1}H]-NOESYs recorded in D_2O.

```
torsion angle χ
assign  (residue n and name O4'  )
        (residue n and name C1'  )
        (residue n and name N9   )
        (residue n and name C4   )   20.0    -160    20.0    2
```

Appendix 35 Chemical shift comparison of H2 resonances in d3'-EBS1*, d3'-EBS1*·IBS1*, d3'-TL and EBS1*·IBS1*.

	d3'-EBS1*	d3'-EBS1*·IBS1*	d3'-TL	EBS1*·IBS1*
A3H2	7.351[a]	7.397[a]	7.465[a]	-
A6H2	6.888[a]	6.927[a]	7.007[a]	-
A10H2	7.691[b]	7.696[b]	-	-
A11H2	-	-	7.764[c]	-
A12H2	-	-	7.700[c]	-
A13H2	-	-	8.087[c]	-
A16H2	7.818[b]	7.314[a]		7.209[a]
A20H2	7.785[b]	7.567[b]		-
A23H2 (A16H2)	7.140[a]	7.185[a]	7.208[a]	-
A25H2 (A18H2)	6.984[a]	7.028[a]	7.083[a]	-
A60H2	-	6.935[a]	-	7.041[a]

[a]H2 resonances are in the range of a typical A-U base pair, [b]Chemical shift is more downfield than H2 located in an AU, but more upfield than H2 of GAAA tetraloops, [c]H2 resonances in a GAAA tetraloop

Appendix 36 NMR restraints and structural statistics for the EBS1*·IBS1*, d3'-TL, d3'-EBS1* and d3'-EBS1*·IBS1* structures.[a]

	EBS1*·IBS1*	d3'-TL	d3'-EBS1*	d3'-EBS1*·IBS1*
NOE-derived distance restraints	281	462	514	751
Intranucleotide	105	157	178	259
Internucleotide ($\|i - j\| = 1$)	126	223	252	347
Long-range ($\|i - n\| \geq 2$)	50	82	84	145
Repulsive	0	0	0	0
NOE restraints per residue	20.07	21	17.72	20.86
Dihedral restraints	118	162	180	288
Hydrogen bond restraints	37	49	45	82
Dipolar coupling restraints	0	0	28	37
r.m.s.d. (for all heavy atoms to the best structure (Å))				
Overall	0.20 ± 0.09	0.73 ± 0.23	2.06 ± 0.86	0.69 ± 0.17
Loop (residue number)	-	0.46 ± 0.16 (10-13)	2.59 ± 1.23 (10-20)	0.27 ± 0.10 (13-19,59-65)
Helix (1-9, 21-29 (14-22 in d3'-TL))	-	0.11 ± 0.05	0.41 ± 0.10	0.45 ± 0.11
NOE violations > 0.2 Å	0	0	0	0
Dihedral violations > 5°	0	0	0	0

[a]All statistics are given for the 20 lowest energy structures out of 200 calculated structures. For d3'-EBS1' and d3'- EBS1*·IBS1* values are given for the structures with RDCs.

Appendix 37 The software AMIGOS

The η-θ-plot for d3'-EBS1* as received by AMIGOS. The loop nucleotides A10 to A20 are indicated in blue. The left panel shows the η-θ-plot for the lowest energy structure in d3'-EBS1* and the right panel the one for the second lowest. It is obvious that the spots are distributed all over the η-θ-plot adopting no specific values for the loop nucleotides.

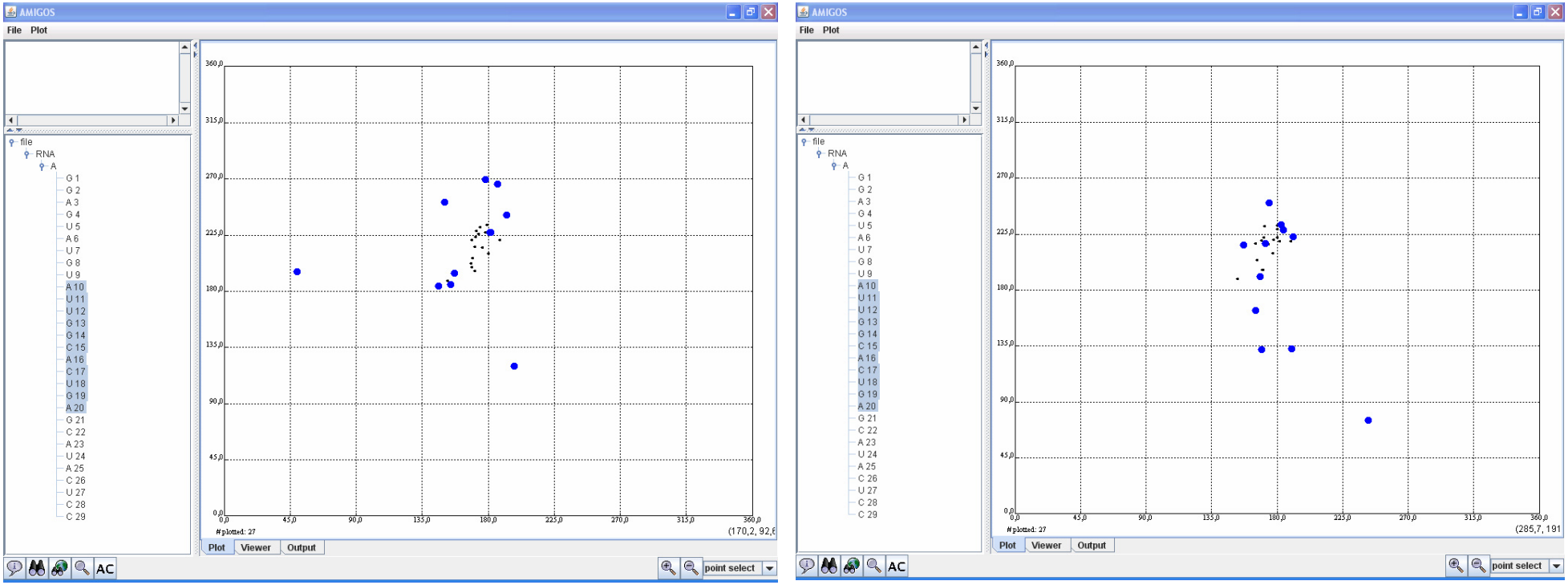

The η-θ-plot for d3'-EBS1*·IBS1* as obtained by AMIGOS. For A10, U11, U12 and G13 (blue) in d3'-EBS1*·IBS1* deviations from a normal helical structure are found. All other nucleotides are centered at around η=170° and θ=225°, which represents the helical region.

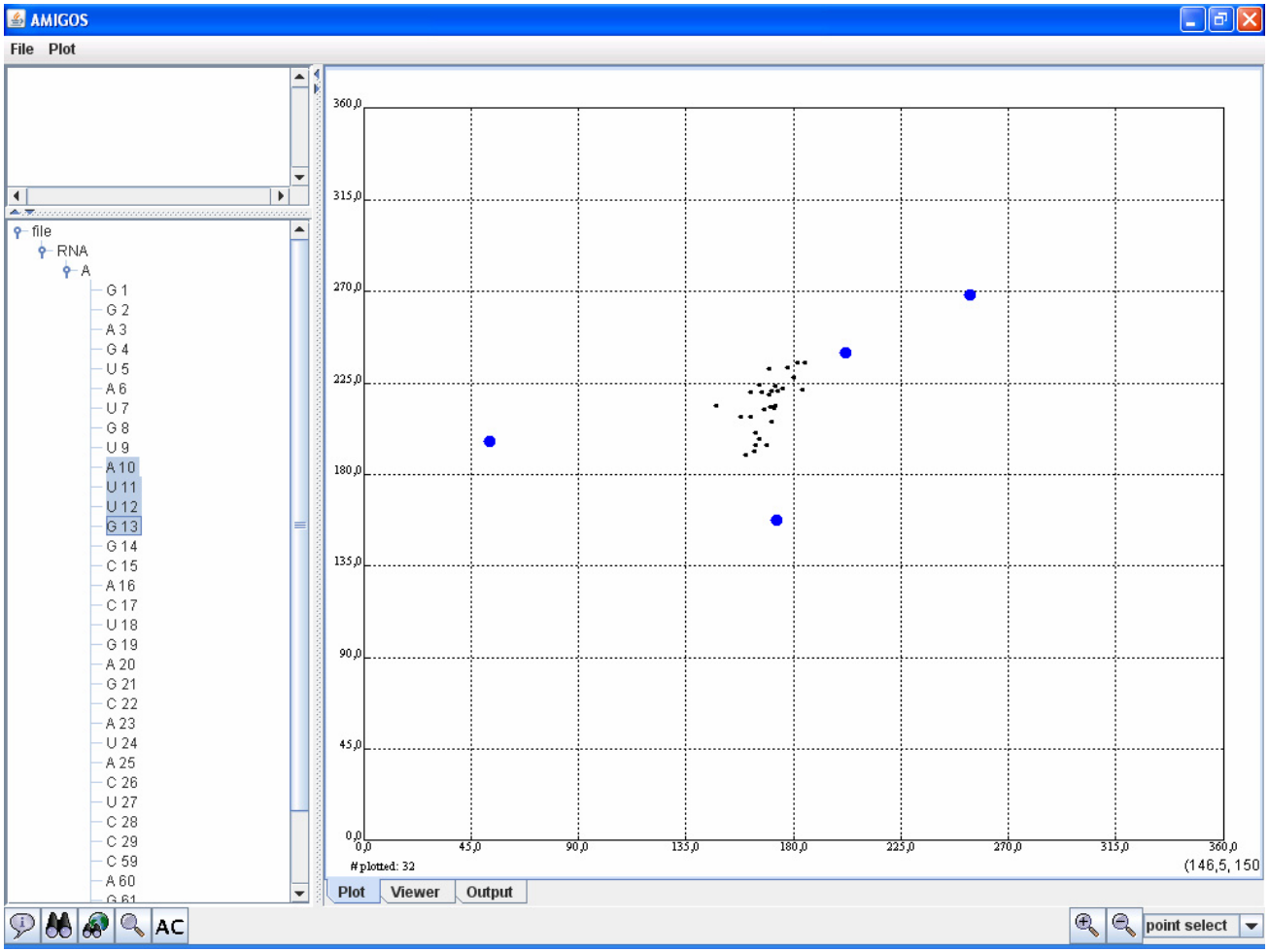

Results of the AMIGOS wormsearch of known RNA structures for the nucleotides 10-14 and 11-14 of d3'-EBS1*·IBS1*. Start and End indicate the number of the nucleotides, which gave a reasonable well match in the wormsearch. The corresponding sequences are shown.The values represent the absolute value of the single residues towards the corresponding residue in d3'-EBS1*·IBS1* as it was calculated from the η-θ-plot. The best match of 2B66 is indicated in bold.

PDB	chain	Start	End	Seq	Total	res0	res1	re2	res3	res4
wormsearch: 10-14										
d3'-EBS1*IBS1*		10	14	AUUGG	0	0	0	0	0	0
1EUQ	B	944	950	CAGCG	97.87759	43.028873	93.848625	145.42145	124.263855	25.537352
1VS5	A	1047	1051	GGUGC	98.85327	50.18504	6.5090976	211.97299	28.811956	23.157354
2B66	A	1362	1366	CCGAA	40.014633	10.127505	58.142056	38.098747	49.90842	24.092009
2TPK	A	6	10	CCAGC	38.235546	29.71432	46.065662	38.5315	40.88823	33.88619
30S Ribosomal subunit:										
1IBM	A	264	268	UGGCC	84.83577	26.654346	66.78514	172.8922	26.28625	15.2363825
1N32	A	264	268	UGGCC	84.95777	27.14307	64.31683	173.30914	32.097878	12.222274
1N33	A	264	268	UGGCC	86.318016	26.053318	60.542934	178.70619	29.78649	9.308026
1N34	A	264	268	UGGCC	93.33392	24.023993	61.47204	194.63397	34.704517	10.647086
1XMQ	A	264	268	UGGCC	86.48814	27.268625	67.364456	176.70332	27.568398	11.634621
1XNQ	A	264	268	UGGCC	84.90872	25.3514	64.9892	174.04578	24.096548	17.566698
1XNR	A	264	268	UGGCC	91.988075	28.935312	61.428818	191.71227	28.346191	11.882005
2UU9	A	264	268	UGGCC	84.22915	24.435871	66.081856	172.39337	23.771248	14.975975
2UUA	A	264	268	UGGCC	83.96363	26.266161	67.75392	170.04016	30.443453	11.335393
2UUB	A	264	268	UGGCC	84.343636	25.288273	67.571106	171.74203	26.079762	13.72636
2UUC	A	264	268	UGGCC	84.784454	24.917912	64.37058	174.02565	28.298439	9.582287
2UXC	A	264	268	UGGCC	84.25533	26.67774	68.17536	170.97908	26.126919	14.790474
2VQE	A	264	268	UGGCC	84.37889	26.532204	67.484665	171.59831	26.331663	14.195504
2VQF	A	264	268	UGGCC	84.29548	26.52095	67.9881	171.38016	24.80653	14.709609
wormsearch: 11-14										
d3'-EBS1*IBS1*		11	14	AUUGG	0	0	0	0	0	
2TPK	A	7	10	CAGC	40.083797	46.065662	38.5315	40.88823	33.88619	
2B66	**A**	**59**	**62**	**UGGC**	**61.78671**	**76.818504**	**57.03111**	**76.77048**	**14.934918**	
2B66	A	1363	1366	CGAA	44.45022	58.142056	38.098747	49.90842	24.092009	
1JP0	A	5	8	GUGC	90.06331	26.991262	119.98966	125.223816	40.47895	

1JU7	A	10	13	CAGG	75.127365	108.38342	83.82536	51.53081	33.87329
1LUX	A	33	36	UOMGAA	84.58973	43.121315	100.357056	66.27605	110.89719
30S Ribosomal subunit									
2F4V	A	265	268	GGCC	97.149315	58.371212	182.0735	26.315306	22.394268
1IBK	A	265	268	GGCC	92.06117	67.454315	168.6466	26.184032	14.955569
1XMO	A	265	268	GGCC	92.11321	68.068275	168.59888	26.42232	13.504138
1XMQ	A	265	268	GGCC	95.73063	67.364456	176.70332	27.568398	11.634621
1XNQ	A	265	268	GGCC	94.08077	64.9892	174.04578	24.096548	17.566698
1N33	A	265	268	GGCC	95.623245	60.542934	178.70619	29.78649	9.308026
1IBM	A	265	268	GGCC	93.90831	66.78514	172.8922	26.28625	15.2363825
2UXC	A	265	268	GGCC	93.251144	68.17536	170.97908	26.126919	14.790474
1N32	A	265	268	GGCC	94.01113	64.31683	173.30914	32.097878	12.222274
2UUB	A	265	268	GGCC	93.44751	67.571106	171.74203	26.079762	13.72636
2UUC	A	265	268	GGCC	93.96957	64.37058	174.02565	28.298439	9.582287
2UU9	A	265	268	GGCC	93.3751	66.081856	172.39337	23.771248	14.975975
2VQF	A	265	268	GGCC	93.30766	67.9881	171.38016	24.80653	14.709609
2VQE	A	265	268	GGCC	93.401054	67.484665	171.59831	26.331663	14.195504
2UUA	A	265	268	GGCC	92.95099	67.75392	170.04016	30.443453	11.335393

Appendix 38 Additional hydrogen bond restraints, which were added in the calculation of d3'-EBS1*·IBS1* to force a triple base pair between U12, A60 and U18 in order to check if it has any influence on the structure.

U12-A60

```
assign (residue 12 and name H3)  (residue 60 and name  N7)  2.00  0.20  0.20
assign (residue 12 and name N3)  (residue 60 and name  N7)  2.90  0.30  0.30
assign (residue 12 and name O4)  (residue 60 and name  H61) 2.00  0.20  0.20
assign (residue 12 and name O4)  (residue 60 and name  N6)  2.90  0.30  0.30
```

Appendix 39 Structural statistic for the d3'-EBS1*·IBS1* with (1) and without (2) a forced triple base pair

	1	**2**
NOE-derived distance restraints	751	751
Intranucleotide	259	259
Internucleotide ($\|i - j\| = 1$)	347	347
Long-range ($\|i - n\| \geq 2$)	145	145
Repulsive	0	0
NOE restraints per residue	20.86	20.86
Dihedral restraints	288	288
Hydrogen bond restraints	86	82
Dipolar coupling restraints	37	37
r.m.s.d. (for all heavy atoms to the best structure (Å))		
Overall	0.91 ± 0.36	0.69 ± 0.17
Helix (1-9,21-29)	0.60 ± 0.20	0.45 ± 0.11
EBS1*·IBS1* (13-19,59-65)	0.31 ± 0.10	0.27 ± 0.10
NOE violations > 0.2 Å	0	0
Dihedral violations > 5°	0	0

Appendix 40 The 20 lowest energy structures of d3'-EBS1*·IBS1* with a forced triple base pair including U12, A60, and U18. (A) Overall superposition of all heavy atoms in d3'-EBS1*. (B) Superposition of all heavy atoms in the stem (nucleotides 1-9, and 21-29) of d3'-EBS1* of the 20 lowest energy structures. (C) Superposition of all heavy atoms in the EBS1*·IBS1* (nucleotides 13-19, and 59-65) of d3'-EBS1* of the 20 lowest energy structures.

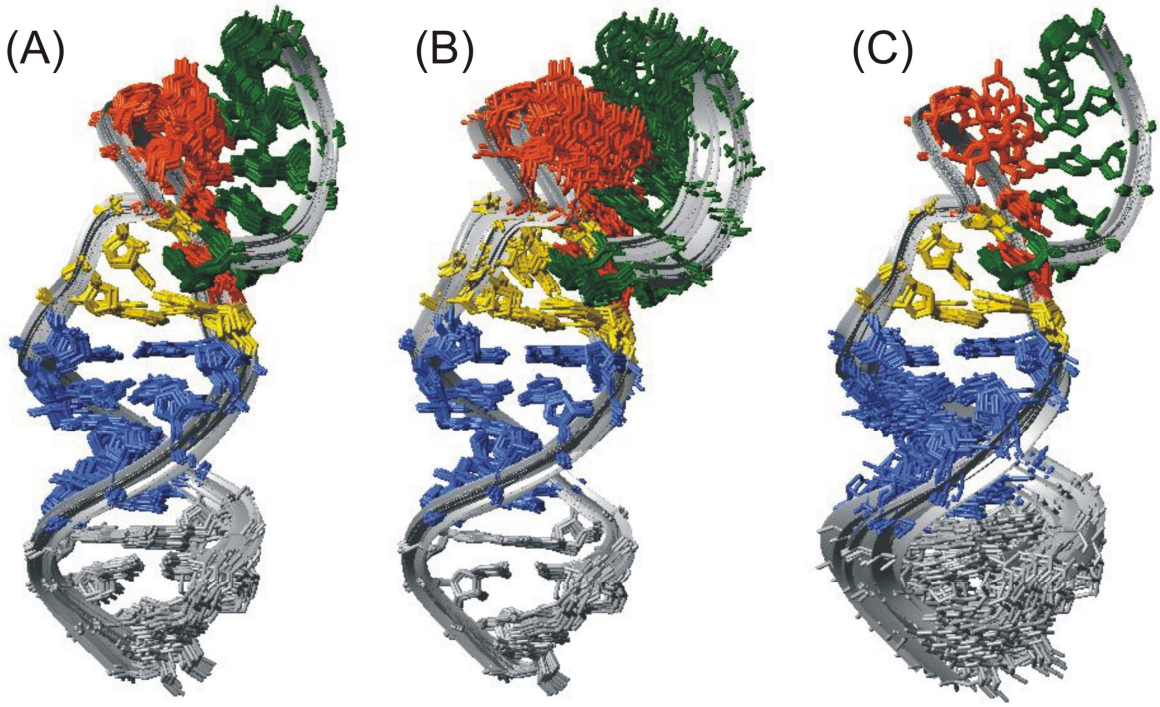

Appendix 41 Comparison of chemical shifts (in ppm) in the helical stem of d3'-EBS1, d3'-TL, d3'-EBS1*, and d3'-EBS1*·IBS1*. All spectra were measured at 293 K at 700 MHz. Ionic strengthes are 10 mM KCl for d3'-EBS1, d3'-TL, d3'-EBS1* and 110 mM KCl for d3'-EBS1*·IBS1*. The numbering scheme was taken from d3'-EBS1, d3'-EBS1*, and d3'-EBS1*·IBS1*. The error for the chemical shifts is ± 0.002 ppm. All chemical shifts, which differ more than 0.02 ppm from the chemical shift of d3'-EBS1, are marked in bold.

	d3'-EBS1	d3'-TL	d3'-EBS1*	d3'-EBS1*·IBS1*
G1H1'	5.672	5.673	5.674	5.655
G1H8	7.981	7.979	7.979	7.981
G2H1'	5.760	5.755	5.760	5.752
G2H8	7.376	7.379	7.378	7.361
A3H1'	5.842	5.846	5.847	5.837
A3H2	7.345	7.350	7.352	7.341
A3H8	7.599	7.607	7.604	7.606
G4H1'	5.408	5.404	5.406	5.409
G4H8	6.927	6.918	6.923	6.927
U5H1'	5.369	5.377	5.374	5.359
U5H5	4.947	4.953	4.952	**4.921**
U5H6	7.541	7.543	7.535	7.534
A6H1'	5.847	5.857	5.848	5.837
A6H2	6.883	6.890	6.887	6.869
A6H8	7.993	**8.017**	7.999	7.975
U7H1'	5.263	5.273	5.266	5.248
U7H5	4.892	4.890	4.893	**4.866**
U7H6	7.447	**7.470**	7.437	7.429
G8H1'	5.597	**5.620**	5.595	**5.544**
G8H8	7.432	**7.404**	7.437	**7.380**
U9H1'	5.426	**5.260**	**5.444**	**5.300**
U9H5	5.260	5.240	5.261	**5.182**
U9H6	7.464	**7.403**	7.480	**7.436**
A10H1'	5.815	-	**5.859**	**5.835**
A10H8	8.096	-	**8.109**	**8.191**
G21H1'	-		5.393	5.358
G21H8	-	7.562	7.397	7.084
C22H1'	5.200	**5.256**	5.207	5.192
C22H5	5.257	5.169	5.255	**5.196**
C22H6	7.495	**7.473**	7.511	7.511
A23H1'	5.777	5.773	5.779	**5.752**
A23H2	7.146	**7.093**	7.140	7.132
A23H8	7.887	7.892	7.870	**7.838**
U24H1'	5.300	**5.274**	5.302	5.297
U24H5	4.955	4.956	4.947	**4.921**
U24H6	7.524	**7.484**	7.512	7.520
A25H1'	5.838	5.829	5.841	5.837
A25H2	6.972	6.962	6.983	6.970
A25H8	7.989	7.973	7.996	7.995
C26H1'	5.207	5.187	5.211	5.213

C26H5	5.049	5.054	5.048	5.044
C26H6	7.392	**7.346**	7.386	**7.417**
U27H1'	5.375	5.379	5.380	5.373
U27H5	5.164	5.170	5.165	5.158
U27H6	7.751	7.737	7.749	7.761
C28H1'	5.434	5.438	5.438	5.431
C28H5	5.475	5.476	5.477	5.474
C28H6	7.759	7.757	7.762	7.761
C29H1'	5.557	5.564	5.564	5.551
C29H5	5.311	5.322	5.319	5.318
C29H6	7.497	7.500	7.503	7.502

Appendix 42 Double X half-filtered NOESY-HSQC with a ^{15}N filter in F1 of d3'-EBS1*·IBS1*.
Shown are projections onto the HSQC-planes. Only resonances between $^{15}N/^{13}C$-labeled d3'-EBS1* and unlabeled IBS1* are observed.

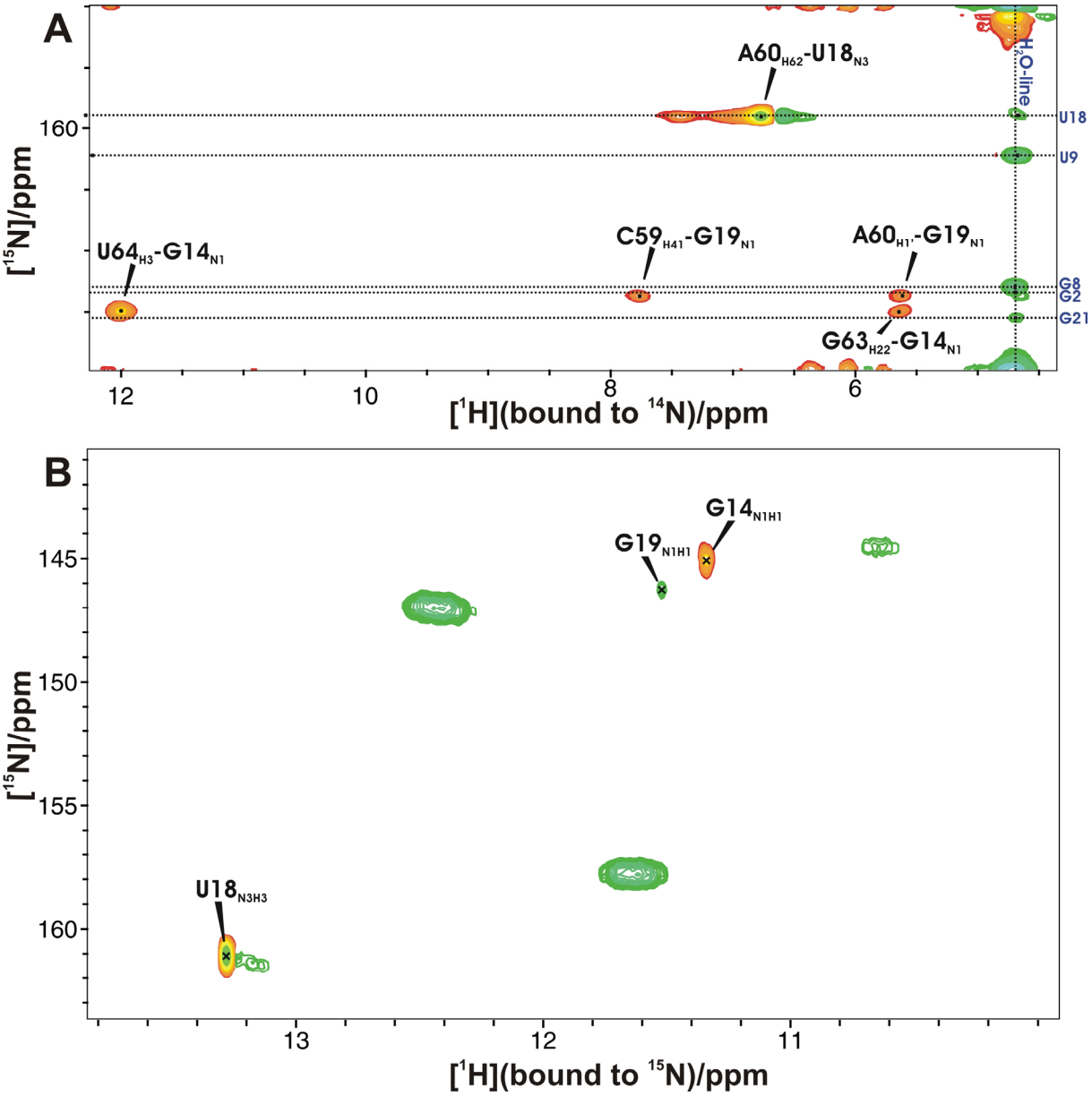

Appendix 43 Primer sequences used for the assembly-PCR to insert the two mutations A331C and A333C into the D135 construct of *Sc*.ai5γ. The position of the primers relative to the T7 promoter (T7P) and D135 sequence on the pT7D135 plasmid is given below. The two restriction sites used, EcoR1 and HindIII, are also indicated.

Primer	Sequence
P1	5'- GGGCGAATTCGTGAATTGTAATACGAC
P2	5'- CTACCCAAGCTTGCATGCCTGCAGG
P3	5'- GGTTGATGTTATGTATTGGCACTGAGCATACGATAAATCATATAACC
P4	5'- GGTTATATGATTTATCGTATGCTCAGTGCCAATACATAACATCAACC

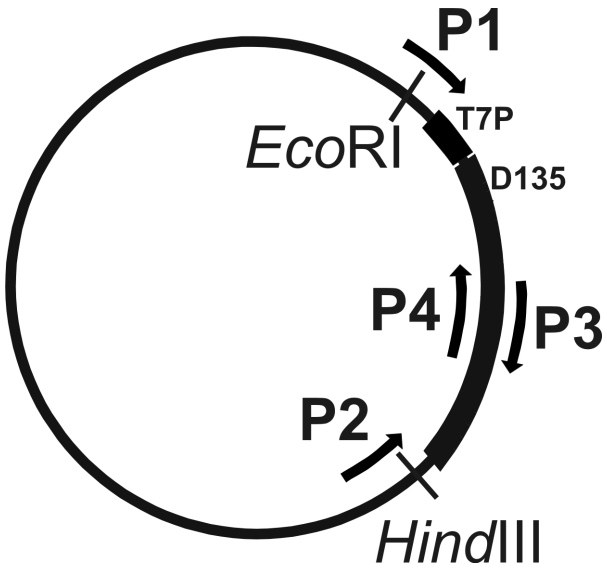

8 Literature

(1) Crick, F. (1970) *Nature* **227**, 561-563.
(2) Mathews, C. K., van Holde, K. E. (1990) *Biochemistry* (The Benjamin/Cummings Publishing Company, Inc., Redwood City).
(3) Vitreschak, A. G., Rodionov, D. A., Mironov, A. A., Gelfand, M. S. (2004) *Trends Genetics* **20**, 44-50.
(4) Gesteland, R. F., Cech, T. R., Atkins, J. F. (1999) *The RNA World: The Nature of Modern RNA Suggests a Prebiotic RNA* (Cold Spring Harbor Laboratory Press.
(5) Keenan, R. J., Freymann, D. M., Stroud, R. M., Walter, P. (2001) *Annu. Rev. Biochem.* **70**, 755-775.
(6) Woese, C. R. (1967) *The genetic code* (Harper & Row, New York).
(7) Crick, F. (1968) *J. Mol. Biol.* **38**, 367-379.
(8) Orgel, L. E. (1968) *J. Mol. Biol.* **38**, 381-393.
(9) Kruger, K., Grabowski, P. J., Zaug, A. J., Sands, J., Gottschling, D. E., Cech, T. R. (1982) *Cell* **31**, 147-157.
(10) Guerrier-Takada, C., Gardiner, K., Marsh, T., Pace, N., Altman, S. (1983) *Cell* **35**, 849-857.
(11) Gilbert, W. (1986) *Nature* **319**, 618.
(12) Saenger, W. (1984) *Principles of Nucleic Acid Structure* (Springer Verlag, New York).
(13) Zhao, X., Yu, Y.-T. (2004) *RNA* **10**, 996-1002.
(14) Rozenski, J., Crain, P., McCloskey, J. (1999) *Nucleic Acids Res.* **27**, 196-197.
(15) Duarte, C. M., Pyle, A. M. (1998) *J. Mol. Biol.* **284**, 1465-1478.
(16) Wadley, L. M., Keating, K. S., Duarte, C. M., Pyle, A. M. (2007) *J. Mol. Biol.* **372**, 942-957.
(17) Wang, A. H. J., Quigley, G. J., Kolpak, F. J., Crawford, J. L., van Boom, J. H., van der Marel, G., Rich, A. (1979) *Nature* **282**, 680-686.
(18) Patel, D. J., Kozlowski, S. A., Nordheim, A., Rich, A. (1982) *Proc. Nat. Acad. Sci. USA* **79**, 1413-1417.
(19) Wüthrich, K. (1986) *NMR of Proteins and Nucleic Acids* (John Wiley & Sons, New York).
(20) Golden, B. L., Gooding, A. R., Podell, E. R., Cech, T. R. (1998) *Science* **282**, 259-264.
(21) Cate, J. H., Gooding, A. R., Podell, E., Zhou, K., Golden, B. L., Kundrot, C. E., Cech, T. R., Doudna, J. A. (1996) *Science* **273**, 1678-1685.
(22) Latham, J. A., Cech, T. R. (1989) *Science* **245**, 276-282.
(23) Nagaswamy, U., Larios-Sanz, M., Hury, J., Collins, S., Zhang, Z., Zhao, Q., Fox, G. E. (2002) *Nucleic Acids Res.* **30**, 395-397.
(24) Chastain, M., Tinoco, I., Jr. (1991) *Prog. Nucleic Acid Res. Mol. Biol.* **41**, 131-177.
(25) Tian, B., Bevilacqua, P. C., Diegelman-Parente, A., Mathews, M. B. (2004) *Nature Rev. Mol. Cell Biol.* **5**, 1013-1023.
(26) Zuker, M. (2003) *Nucleic Acids Res.* **31**, 3406-3415.
(27) McCall, M., Brown, T., Kennard, O. (1985) *J. Mol. Biol.* **183**, 385-396.
(28) Moore, P. B. (1999) in *The RNA World*, eds. Gesteland, R. F., Cech, T. R. & Atkins, J. F. (Cold Spring Harbor Press, Cold Spring Harbor), 381-401.
(29) Koradi, R., Billeter, M., Wüthrich, K. (1996) *J. Mol. Graphics* **14**, 51-55, 29-32.
(30) Dock-Bregeon, A. C., Chevrier, B., Podjarny, A., Johnson, J., de Bear, J. S., Gough, G. R., Gilham, P. T., Moras, D. (1989) *J. Mol. Biol.* **209**, 459-474.

(31) Drew, H. R., Wing, R. M., Takano, T., Broka, C., Tanaka, S., Itakura, K., Dickerson, R. E. (1981) *Proc. Nat. Acad. Sci. USA* **78**, 2179-2183.
(32) Groebe, D. R., Uhlenbeck, O. C. (1988) *Nucleic Acids Res.* **16**, 11725-11735.
(33) Antao, V. P., Lai, S. Y., Tinoco, I., Jr. (1991) *Nucleic Acids Res.* **19**, 5901-5905.
(34) Sigel, R. K. O., Sashital, D. G., Abramovitz, D. L., Palmer III, A. G., Butcher, S. E., Pyle, A. M. (2004) *Nat. Struct. Mol. Biol.* **11**, 187-192.
(35) Jaeger, J. A., Turner, D. H., Zuker, M. (1989) *Proc. Natl. Acad. Sci. USA* **86**, 7706-7710.
(36) Hirao, I., Nishimura, Y., Naraoka, T., Watanabe, K., Arata, Y., Miura, K.-i. (1989) *Nucleic Acids Res.* **17**, 2223-2231.
(37) Cheong, C., Varani, G., Tinoco, I. (1990) *Nature* **346**, 680-682.
(38) Robertus, J. D., Ladner, J. E., Finch, J. T., Rhodes, D., Brown, R. S., Clark, B. F. C., Klug, A. (1974) *Nature* **250**, 546-551.
(39) Hermann, T., Patel, D. J. (1999) *J. Mol. Biol.* **294**, 829-849.
(40) Noller, H. F. (2005) *Science* **309**, 1508-1514.
(41) Nissen, P., Ippolito, J. A., Ban, N., Moore, P. B., Steitz, T. A. (2001) *Proc. Natl. Acad. Sci. USA* **98**, 4899-4903.
(42) Davis, J. H., Tonelli, M., Scott, L. G., Jaeger, L., Williamson, J. R., Butcher, S. E. (2005) *J. Mol. Biol.* **351**, 371-382.
(43) Cate, J. H., Yusupov, M. M., Yusupova, G. Z., Earnest, T. N., Noller, H. F. (1999) *Science* **285**, 2095-2104.
(44) Wimberly, B. T., Brodersen, D. E., Clemons, W. M., Morgan-Warren, R. J., Carter, A. P., Vonrhein, C., Hartsch, T., Ramakrishnan, V. (2000) *Nature* **407**, 327-339.
(45) Schluenzen, F., Tocilj, A., Zarivach, R., Harms, J., Gluehmann, M., Janell, D., Bashan, A., Bartels, H., Agmon, I., Franceschi, F., Yonath, A. (2000) *Cell* **102**, 615-623.
(46) Ban, N., Nissen, P., Hansen, J., Moore, P. B., Steitz, T. A. (2000) *Science* **289**, 905-920.
(47) Yusupov, M. M., Yusupova, G. Z., Baucom, A., Lieberman, K., Earnest, T. N., Cate, J. H. D., Noller, H. F. (2001) *Science* **292**, 883-896.
(48) Klein, D. J., Schmeing, T. M., Moore, P. B., Steitz, T. A. (2001) *EMBO J.* **20**, 4214-4221.
(49) Steitz, T. A., Moore, P. B. (2003) *Trends Biochem. Sci.* **28**, 411-418.
(50) Nissen, P., Hansen, J., Ban, N., Moore, P. B., Steitz, T. A. (2000) *Science* **289**, 920-930.
(51) Quigley, G. J., Rich, A. (1976) *Science* **194**, 796-806.
(52) Su, L., Chen, L., Egli, M., Berger, J. M., Rich, A. (1999) *Nat. Struct. Biol.* **6**, 285-292.
(53) Chang, K.-Y., Tinoco, I. (1997) *J. Mol. Biol.* **269**, 52-66.
(54) Rietveld, K., Van Poelgeest, R., Pleij, C. W. A., Van Boom, J. H., Bosch, L. (1982) *Nucleic Acids Res.* **10**, 1929-1946.
(55) Brierley, I., Digard, P., Inglis, S. C. (1989) *Cell* **57**, 537-547.
(56) Rastogi, T., Beattie, T. L., Olive, J. E., Collins, R. A. (1996) *EMBO J.* **15**, 2820–2825.
(57) Ke, A., Zhou, K., Ding, F., Cate, J. H. D., Doudna, J. A. (2004) *Nature* **429**, 201-205.
(58) Adams, P. L., Stahley, M. R., Kosek, A. B., Wang, J., Strobel, S. A. (2004) *Nature* **430**, 45-50.
(59) Theimer, C. A., Blois, C. A., Feigon, J. (2005) *Mol. Cell* **17**, 671-682.
(60) Wagner, E. G. H., Simons, R. W. (1994) *Annu. Rev. Microbiol.* **48**, 713-742.
(61) Battiste, J. L., Mao, H., Rao, N. S., Tan, R., Muhandiram, D. R., Kay, L. E., Frankel, A. D., Williamson, J. R. (1996) *Science* **273**, 1547-1551.
(62) Pley, H. W., Flaherty, K. M., McKay, D. B. (1994) *Nature* **372**, 68-74.
(63) Pyle, A. M. (1993) *Science* **261**, 709-714.

(64) Freisinger, E., Sigel, R. K. O. (2007) *Coord. Chem. Rev.* **251**, 1834-1851.
(65) Pyle, A. M. (1996) *Met. Ions Biol. Syst.* **32**, 479-519.
(66) Shiman, R., Draper, D. E. (2000) *J. Mol. Biol.* **302**, 79-91.
(67) Basu, S., Rambo, R. P., Strauss-Soukup, J., Cate, J. H., Ferre-D'Amare, A. R., Strobel, S. A., Doudna, J. A. (1998) *Nat. Struct. Biol.* **5**, 986-992.
(68) Cate, J. H., Hanna, R. L., Doudna, J. A. (1997) *Nat. Struct. Biol.* **4**, 553-558.
(69) Sigel, R. K. O., Pyle, A. M. (2007) *Chem. Rev.* **107**, 97-113.
(70) Sigel, R. K. O. (2005) *Eur. J. Inorg. Chem.*, 2281-2292.
(71) Fedor, M. J. (2002) *Curr. Opin. Struct. Biol.* **12**, 289-295.
(72) Grosshans, C. A., Cech, T. R. (1989) *Biochemistry* **28**, 6888-6894.
(73) Lumry, R., Smith, E., Glantz, R. (1951) *J. Am. Chem. Soc.* **73**, 4330-4340.
(74) Murray, J. B., Seyhan, A. A., Walter, N. G., Burke, J. M., Scott, W. G. (1998) *Chem. Biol.* **5**, 587-595.
(75) O'Rear, J. L., Wang, S., Feig, A. L., Beigelman, L., Uhlenbeck, O. C., Herschlag, D. (2001) *RNA* **7**, 537-545.
(76) Curtis, E. A., Bartel, D. P. (2001) *RNA* **7**, 546-552.
(77) Geyer, C. R., Sen, D. (1997) *Chem. Biol.* **4**, 579-593.
(78) Manning, G. S. (1978) *Quart. Rev. Biophys.* **11**, 179-246.
(79) Misra, V. K., Draper, D. E. (1998) *Biopolymers* **48**, 113-135.
(80) Chin, K., Sharp, K. A., Honig, B., Pyle, A. M. (1999) *Nat. Struct. Biol.* **6**, 1055-1061.
(81) Gonzalez, R. L., Jr., Tinoco Jr., I. (1999) *J. Mol. Biol.* **289**, 1267-1282.
(82) Rüdisser, S., Tinoco, I., Jr. (2000) *J. Mol. Biol.* **295**, 1211-1223.
(83) Kieft, J. S., Tinoco, I., Jr. (1997) *Structure* **5**, 713-721.
(84) Huppler, A., Nikstad, L. J., Allmann, A. M., Brow, D. A., Butcher, S. E. (2002) *Nat. Struct. Biol.* **9**, 431-435.
(85) Sigel, R. K. O., Freisinger, E., Lippert, B. (2000) *J. Biol. Inorg. Chem.* **5**, 287-299.
(86) Piccirilli, J. A., Vyle, J. S., Caruthers, M. H., Cech, T. R. (1993) *Nature* **361**, 85-88.
(87) Christian, E. L., Yarus, M. (1992) *J. Mol. Biol.* **228**, 743-758.
(88) Correll, C. C., Freeborn, B., Moore, P. B., Steitz, J. A. (1997) *Cell* **91**, 705-712.
(89) Pichler, A., Berens, C., Schroeder, R. (2000) *Ribozyme*, 7-25,A1-A3.
(90) Swisher, J. F., Su, L. J., Brenowitz, M., Anderson, V. E., Pyle, A. M. (2002) *J. Mol. Biol.* **315**, 297-310.
(91) Sigel, R. K. O., Pyle, A. M. (2003) *Met. Ions Biol. Syst.* **40**, 477-512.
(92) Christian, E. L., Yarus, M. (1993) *Biochemistry* **32**, 4475-4480.
(93) Yoshida, A., Sun, S., Piccirilli, J. A. (1999) *Nat. Struct. Biol.* **6**, 318-321.
(94) Kuo, L. Y., Piccirilli, J. A. (2001) *Biochim. Biophys. Acta* **1522**, 158-166.
(95) Shan, S.-O., Yoshida, A., Sun, S., Piccirilli, J. A., Herschlag, D. (1999) *Proc. Natl. Acad. Sci. USA* **96**, 12299-12304.
(96) Shan, S.-O., Kravchuk, A. V., Piccirilli, J. A., Herschlag, D. (2001) *Biochemistry* **40**, 5161-5171.
(97) Sigel, R. K. O., Vaidya, A., Pyle, A. M. (2000) *Nat. Struct. Biol.* **7**, 1111-1116.
(98) Dorner, S., Barta, A. (1999) *Biol. Chem.* **380**, 243-251.
(99) Morrissey, S. R., Horton, T. E., DeRose, V. J. (2000) *J. Am. Chem. Soc.* **122**, 3473-3481.
(100) Maderia, M., Horton, T. E., DeRose, V. J. (2000) *Biochemistry* **39**, 8193-8200.
(101) Brown, R. S., Hingerty, B. A., Dewan, J. C., Klug, A. (1983) *Nature* **303**, 543-546.
(102) Rubin, J. R., Sundaralingam, M. (1983) *J. Biomol. Struct. Dyn.* **1**, 639-646.
(103) Behlen, L. S., Samspon, J. R., DiRenzo, A. B., Uhlenbeck, O. C. (1990) *Biochemistry* **29**, 2515-2523.
(104) Ciesiolka, J., Hardt, W. D., Schlegl, J., Erdmann, V. A., Hartmann, R. K. (1994) *Eur. J. Biochem.* **219**, 49-56.

(105) Streicher, B., Westhof, E., Schroeder, R. (1996) *EMBO J.* **15**, 2556–2564.
(106) Hertweck, M., Mueller, M. W. (2001) *Eur. J. Biochem.* **268**, 4610-4620.
(107) Berens, C., Streicher, B., Schroeder, R., Hillen, W. (1998) *Chem. Biol.* **5**, 163-175.
(108) Hoch, I., Berens, C., Westhof, E., Schroeder, R. (1998) *J. Mol. Biol.* **282**, 557-569.
(109) James, T. L., Noggle, J. H. (1969) *Proc. Natl. Acad. Sci. U. S. A.* **62**, 644-9.
(110) Kirchner, R., Vogtherr, M., Limmer, S., Sprinzl, M. (1998) *Antisense Nucleic Acid Drug Dev.* **8**, 507-516.
(111) Hud, N. V., Schultze, P., Feigon, J. (1998) *J. Am. Chem. Soc.* **120**, 6403-6404.
(112) Allain, F. H. T., Varani, G. (1995) *Nucleic Acids Res.* **23**, 341-350.
(113) Butcher, S. E., Allain, F. H.-T., Feigon, J. (2000) *Biochemistry* **39**, 2174-2182.
(114) Feigon, J., Butcher, S. E., Finger, L. D., Hud, N. V. (2001) *Methods Enzymol.* **338**, 400-420.
(115) Erat, M. C., Zerbe, O., Fox, T., Sigel, R. K. O. (2007) *ChemBioChem* **8**, 306-314.
(116) Puglisi, E. V., Puglisi, J. D. (1998) in *RNA structure and function*, eds. Simons, R. W. & Grunberg-Manago, M. (Cold Spring Harbor Laboratory Press, Cold Spring Harbor), 117-146.
(117) Fürtig, B., Richter, C., Wöhnert, J., Schwalbe, H. (2003) *ChemBioChem* **4**, 936-962.
(118) Luy, B., Marino, J. P. (2000) *J. Am. Chem. Soc.* **122**, 8095-8096.
(119) Brünger, A. T., Adams, P. D., Clore, G. M., DeLano, W. L., Gros, P., Grosse-Kunstleve, R. W., Jiang, J.-S., Kuszewski, J., Nilges, M., Pannu, N. S., Read, R. J., Rice, L. M., Simonson, T., Warren, G. L. (1998) *Acta Crystallogr.* **D54**, 905-921.
(120) Schwieters, C. D., Kuszewski, J. J., Tjandra, N., Clore, G. M. (2003) *J. Magn. Res.* **160**, 65-73.
(121) Varani, G., Aboul-ela, F., Allain, F. H.-T. (1996) *Prog. Nucl. Mag. Res. Sp.* **29**, 51-127.
(122) Latham, M. P., Brown, D. J., McCallum, S. A., Pardi, A. (2005) *ChemBioChem* **6**, 1492-1505.
(123) Wijmenga, S. S., van Buuren, B. N. M. (1998) *Prog. Nucl. Mag. Res. Sp.* **32**, 287-387.
(124) Winkler, W. C., Nahvi, A., Roth, A., Collins, J. A., Breaker, R. R. (2004) *Nature* **428**, 281-286.
(125) Joyce, G. F. (1993) *Pure Appl. Chem.* **65**, 1205-1212.
(126) Beaudry, A. A., Joyce, G. F. (1992) *Science* **257**, 635-641.
(127) Lehmann, K., Schmidt, U. (2003) *Critical Rev. Biochem. Mol. Biol.* **38**, 249-303.
(128) Serganov, A., Patel, D. J. (2007) *Nat. Rev. Genet.* **8**, 776-790.
(129) Steitz, T. A., Steitz, J. A. (1993) *Proc. Nat. Acad. Sci. USA* **90**, 6498-6502.
(130) Forster, A. C., Symons, R. H. (1987) *Cell* **49**, 211-220.
(131) Buzayan, J. M., Hampel, A., Bruening, G. (1986) *Nucleic Acids Res.* **14**, 9729-9743.
(132) Kuo, M. Y., Sharmeen, L., Dinter-Gottlieb, G., Taylor, J. (1988) *J. Virol.* **62**, 4439-4444.
(133) Saville, B. J., Collins, R. A. (1990) *Cell* **61**, 685-696.
(134) Walter, F., Westhof, E. (2002) in *Encyclopedia of Life Sciences*.
(135) Butcher, S. E. (2001) *Curr. Opin. Struct. Biol.* **11**, 315-320.
(136) Klein, D. J., Ferre-D'Amare, A. R. (2006) *Science* **313**, 1752-1756.
(137) Roth, A., Nahvi, A. L. I., Lee, M., Jona, I., Breaker, R. R. (2006) *RNA* **12**, 607-619.
(138) Salehi-Ashtiani, K., Luptak, A., Litovchick, A., Szostak, J. W. (2006) *Science* **313**, 1788-1792.
(139) Teixeira, A., Tahiri-Alaoui, A., West, S., Thomas, B., Ramadass, A., Martianov, I., Dye, M., James, W., Proudfoot, N. J., Akoulitchev, A. (2004) *Nature* **432**, 526-530.
(140) Prody, G. A., Bakos, J. T., Buzayan, J. M., Schneider, I. R., Bruening, G. (1986) *Science* **231**, 1577-1580.

(141) Ruffner, D. E., Stormo, G. D., Uhlenbeck, O. C. (1990) *Biochemistry* **29**, 10695-10702.
(142) Symons, R. H. (1997) *Nucleic Acids Res.* **25**, 2683-2689.
(143) Uhlenbeck, O. C. (1987) *Nature* **328**, 596-600.
(144) Blount, K. F., Uhlenbeck, O. C. (2005) *Annu. Rev. Biophys. Biomol. Struct.* **34**, 415-440.
(145) McKay, D. B. (1996) *RNA* **2**, 395-403.
(146) Scott, W. G. (1999) *Q. Rev. Biophys.* **32**, 241-284.
(147) Wedekind, J. E., McKay, D. B. (1998) *Annu. Rev. Bioph. Biomol. Struct.* **27**, 475-502.
(148) Scott, W. G., Finch, J. T., Klug, A. (1995) *Cell* **81**, 991-1002.
(149) Martick, M., Scott, W. G. (2006) *Cell* **126**, 309-320.
(150) Koizumi, M., Ohtsuka, E. (1991) *Biochemistry* **30**, 5145-5150.
(151) Slim, G., Gait, M. J. (1991) *Nucleic Acids Res.* **19**, 1183-1188.
(152) Wang, S., Karbstein, K., Peracchi, A., Beigelman, L., Herschlag, D. (1999) *Biochemistry* **38**, 14363-14378.
(153) Nelson, J. A., Uhlenbeck, O. C. (2006) *Mol. Cell* **23**, 447-450.
(154) Cai, Z., Tinoco Jr., I. (1996) *Biochemistry* **35**, 6026-6036.
(155) Butcher, S. E., Allain, F. H.-T., Feigon, J. (1999) *Nat. Struct. Biol.* **6**, 212-216.
(156) Rupert, P. B., Ferre-D'Amare, A. R. (2001) *Nature* **410**, 780-786.
(157) Hampel, A., Tritz, R. (1989) *Biochemistry* **28**, 4929-4933.
(158) Fedor, M. J. (2000) *J. Mol. Biol.* **297**, 269-291.
(159) Berzal-Herranz, A., Joseph, S., Chowrira, B. M., Butcher, S. E., Burke, J. M. (1993) *EMBO J.* **12**, 2567–2573.
(160) Anderson, P., Monforte, J., Tritz, R., Nesbitt, S., Hearst, J., Hamper, A. (1994) *Nucleic Acids Res.* **22**, 1096-1100.
(161) Butcher, S. E., Heckmann, J. E., Burke, J. M. (1995) *J. Biol. Chem.* **270**, 29648-29652.
(162) Butcher, S. E., Allain, F. H. T., Feigon, J. (2000) *Biochemistry* **39**, 2174-2182.
(163) Walter, N. G., Yang, N., Burke, J. M. (2000) *J. Mol. Biol.* **298**, 539-555.
(164) Perrotta, A. T., Been, M. D. (1991) *Nature* **350**, 434-436.
(165) Ferre-D'Amare, A. R., Zhou, K., Doudna, J. A. (1998) *Nature* **395**, 567-574.
(166) Perrotta, A. T., Been, M. D. (1990) *Nucleic Acids Res.* **18**, 6821-6827.
(167) Shih, I. h., Been, M. D. (2002) *Annu. Rev. Biochem.* **71**, 887-917.
(168) Perrotta, A. T., Been, M. D. (1996) *Nucleic Acids Res.* **24**, 1314-1321.
(169) Suh, Y.-A., Kumar, P. K. R., Taira, K., Nishikawa, S. (1993) *Nucleic Acids Res.* **21**, 3277-3280.
(170) Ananvoranich, S., Perreault, J.-P. (2000) *Biochem. Biophys. Res. Co.* **270**, 600-607.
(171) Wadkins, T. S., Perrotta, A. T., Ferre-D'Amare, A. R., Doudna, J. A., Been, M. D. (1999) *RNA* **5**, 720-727.
(172) Beattie, T. L., Olive, J. E., Collins, R. A. (1995) *Proc. Natl. Acad. Sci. USA* **92**, 4686-4690.
(173) Lilley, D. M. (2004) *RNA* **10**, 151-158.
(174) Michiels, P. J., Schouten, C. H., Hilbers, C. W., Heus, H. A. (2000) *RNA* **6**, 1821-1832.
(175) Anderson, A. A., Collins, R. A. (2000) *Mol. Cell* **5**, 469-478.
(176) Azubel, M., Wolf, S. G., Sperling, J., Sperling, R. (2004) *Mol. Cell* **15**, 833-839.
(177) Stoltzfus, A. (2004) *Current Biology* **14**, R351-R352.
(178) Kazantsev, A. V., Krivenko, A. A., Harrington, D. J., Holbrook, S. R., Adams, P. D., Pace, N. R. (2005) *Proc. Natl. Acad. Sci. USA* **102**, 13392-13397.
(179) Stahley, M. R., Strobel, S. A. (2005) *Science* **309**, 1587-1590.
(180) Frank, D. N., Pace, N. R. (1998) *Annu. Rev. Biochem.* **67**, 153-180.

(181) Mörl, M., Marchfelder, A. (2001) *EMBO Rep.* **2**, 17-20.
(182) James, B. D., Olsen, G. J., Liu, J., Pace, N. R. (1988) *Cell* **52**, 19-26.
(183) Chen, J. L., Pace, N. R. (1997) *RNA* **3**, 557-560.
(184) Fang, X.-w., Pan, T., Sosnick, T. R. (1999) *Nat. Struct. Mol. Biol.* **6**, 1091-1095.
(185) Beebe, J. A., Kurz, J. C., Fierke, C. A. (1996) *Biochemistry* **35**, 10493-10505.
(186) Warnecke, J. M., Sontheimer, E. J., Piccirilli, J. A., Hartmann, R. K. (2000) *Nucleic Acids Res.* **28**, 720-727.
(187) Warnecke, J. M., Held, R., Busch, S., Hartmann, R. K. (1999) *J. Mol. Biol.* **290**, 433-445.
(188) Haugen, P., Simon, D. M., Bhattacharya, D. (2005) *Trends in Genetics* **21**, 111-119.
(189) Cech, T. R. (1990) *Annu. Rev. Biochem.* **59**, 543-568.
(190) Cech, T. R. (1993) in *The RNA World*, eds. Gesteland, R. & Atkins, J. (Cold Spring Harbor Press, Cold Spring Harbor), 239-270.
(191) Vicens, Q., Cech, T. R. (2006) *Trends Biochem. Sci.* **31**, 41-51.
(192) Adams, P. L., Stahley, M. R., Gill, M. L., Kosek, A. B., Wang, J., Strobel, S. A. (2004) *RNA* **10**, 1867-1887.
(193) Guo, F., Gooding, A. R., Cech, T. R. (2004) *Mol. Cell* **16**, 351-362.
(194) Golden, B. L., Kim, H., Chase, E. (2005) *Nat. Struct. Mol. Biol.* **12**, 82-89.
(195) Uchimaru, T., Uebayasi, M., Tanabe, K., Taira, K. (1993) *FASEB J.* **7**, 137-142.
(196) Beese, L. S., Steitz, T. A. (1991) *EMBO J.* **10**, 25–33.
(197) Sjogren, A. S., Pettersson, E., Sjoberg, B. M., Stromberg, R. (1997) *Nucleic Acids Res.* **25**, 648-653.
(198) Shan, S., Kravchuk, A. V., Piccirilli, J. A., Herschlag, D. (2001) *Biochemistry* **40**, 5161-5171.
(199) Lipchock, S. V., Strobel, S. A. (2008) *Proc. Natl. Acad. Sci. USA* **105**, 5699-5704.
(200) Michel, F., Umesono, K., Ozeki, H. (1989) *Gene* **82**, 5-30.
(201) Lambowitz, A. M., Belfort, M. (1993) *Annu. Rev. Biochem.* **62**, 587-622.
(202) Michel, F., Ferat, J. L. (1995) *Annu. Rev. Biochem.* **64**, 435-461.
(203) Pyle, A. M., Lambowitz, A. M. (2006) in *The RNA World*, eds. Gesteland, R. F., Cech, T. R. & Atkins, J. F. (Cold Spring Harbor Laboratory Press, Cold Spring Harbor), 469-505.
(204) Vallès, Y., Halanych, K. M., Boore, J. L. (2008) *PLoS ONE* **3**, e1488.
(205) Michel, F., Jacquier, A., Dujon, B. (1982) *Biochimie* **64**, 867-881.
(206) Toor, N., Hausner, G., Zimmerly, S. (2001) *RNA* **7**, 1142-1152.
(207) Toor, N., Robart, A. R., Christianson, J., Zimmerly, S. (2006) *Nucleic Acids Res.* **34**, 6461–6471.
(208) Podar, M., Chu, V. T., Pyle, A. M., Perlman, P. S. (1998) *Nature* **391**, 915-918.
(209) Granlund, M., Michel, F., Norgren, M. (2001) *J. Bacteriol.* **183**, 2560-2569.
(210) Mörl, M., Schmelzer, C. (1990) *Cell* **60**, 629-636.
(211) Aizawa, Y., Xiang, Q., Lambowitz, A. M., Pyle, A. M. (2003) *Mol. Cell* **11**, 795-805.
(212) Dai, L., Toor, N., Olson, R., Keeping, A., Zimmerly, S. (2003) *Nucleic Acids Res.* **31**, 424-426.
(213) Qin, P. Z., Pyle, A. M. (1998) *Curr. Opin. Struct. Biol.* **8**, 301-308.
(214) Costa, M., Michel, F., Westhof, E. (2000) *EMBO J.* **19**, 5007-5018.
(215) De Lencastre, A., Pyle, A. M. (2008) *RNA* **14**, 11-24.
(216) Swisher, J., Duarte, C. M., Su, L. J., Pyle, A. M. (2001) *EMBO J.* **20**, 2051-2061.
(217) De Lencastre, A., Hamill, S., Pyle, A. M. (2005) *Nat. Struct. Mol. Biol.* **12**, 626-627.
(218) Qin, P. Z., Pyle, A. M. (1997) *Biochemistry* **36**, 4718-4730.
(219) Boudvillain, M., deLencastre, A., Pyle, A. M. (2000) *Nature* **406**, 315-318.
(220) Fedorova, O., Mitros, T., Pyle, A. M. (2003) *J. Mol. Biol.* **330**, 197-209.
(221) Pyle, A. M., Green, J. B. (1994) *Biochemistry* **33**, 2716-2725.

(222) Pyle, A. M., Fedorova, O., Waldsich, C. (2007) *Trends Biochem. Sci.* **32**, 138-145.
(223) Su, L. J., Waldsich, C., Pyle, A. M. (2005) *Nucleic Acids Res.* **33**, 6674-6687.
(224) Jacquier, A., Michel, F. (1987) *Cell* **50**, 17-29.
(225) Qin, P. Z., Pyle, A. M. (1999) *J. Mol. Biol.* **291**, 15-27.
(226) Su, L. J., Qin, P. Z., Michels, W. A., Pyle, A. M. (2001) *J. Mol. Biol.* **306**, 655-668.
(227) Jacquier, A., Michel, F. (1990) *J. Mol. Biol.* **213**, 437-447.
(228) Michels, W. J., Pyle, A. M. (1995) *Biochemistry* **34**, 2965-2977.
(229) Koch, J. L., Boulanger, S. C., Dib-Hajj, S. D., Hebbar, S. K., Perlman, P. S. (1992) *Mol. Cell. Biol.* **12**, 1950-1958.
(230) Pyle, A. M. (1996) in *Nucleic Acids and Molecular Biology*, eds. Eckstein, F. & Lilley, D. M. J. (Springer Verlag, New York), Vol. 10, 75-107.
(231) Costa, M., Deme, E., Jacquier, A., Michel, F. (1997) *J. Mol. Biol.* **267**, 520-536.
(232) Podar, M., Dib-Hajj, S., Perlman, P. S. (1995) *RNA* **1**, 828-840.
(233) Griffin, E. A., Qin, Z.-F., Michels, W. A., Pyle, A. M. (1995) *Chem. Biol.* **2**, 761-770.
(234) Mikheeva, S., Murray, H. L., Zhou, H., Turczyk, B. M., Jarrell, K. A. (2000) *RNA* **6**, 1509-1515.
(235) Belfort, M., Derbyshire, V., Parker, M. M., Cousineau, B., Lambowitz, A. M. (2002) *Mobile DNA II*, 761-783.
(236) Costa, M., Michel, F. (1995) *EMBO J.* **14**, 1276-1285.
(237) Abramovitz, D. L., Friedman, R. A., Pyle, A. M. (1996) *Science* **271**, 1410-1413.
(238) Konforti, B. B., Abramovitz, D. L., Duarte, C. M., Karpeisky, A., Beigelman, L., Pyle, A. M. (1998) *Mol. Cell* **1**, 433-441.
(239) Boulanger, S. C., Belcher, S. M., Schmidt, U., Dib-Hajj, S. D., Schmidt, T., Perlman, P. S. (1995) *Mol. Cell. Biol.* **15**, 4479-4488.
(240) Schmidt, U., Podar, M., Stahl, U., Perlman, P. S. (1996) *RNA* **2**, 1161-1172.
(241) Costa, M., Christian, E. L., Michel, F. (1998) *RNA* **4**, 1055-1068.
(242) Zhang, L., Doudna, J. A. (2002) *Science* **295**, 2084-2088.
(243) Gordon, P. M., Piccirilli, J. A. (2001) *Nat. Struct. Biol.* **8**, 893-898.
(244) Chu, V. T., Liu, Q., Podar, M., Perlman, P. S., Pyle, A. M. (1998) *RNA* **4**, 1186-1202.
(245) Chu, V. T., Adamidi, C., Liu, Q., Perlman, P. S., Pyle, A. M. (2001) *EMBO J.* **20**, 6866-6876.
(246) Liu, Q., Green, J. B., Khodadadi, A., Haeberli, P., Beigelman, L., Pyle, A. M. (1997) *J. Mol. Biol.* **267**, 163-171.
(247) Gaur, R. K., McLaughlin, L. W., Green, M. R. (1997) *RNA* **3**, 861-869.
(248) Menger, M., Eckstein, F., Porschke, D. (2000) *Biochemistry* **39**, 4500-4507.
(249) Toor, N., Keating, K. S., Taylor, S. D., Pyle, A. M. (2008) *Science* **320**, 77-82.
(250) Fedorova, O., Pyle, A. M. (2005) *EMBO J.* **24**, 3906–3916.
(251) Podar, M., Zhou, J., Zhang, M., Franzen, J. S., Perlman, P. S., Peebles, C. L. (1998) *RNA* **4**, 151-166.
(252) Podar, M., Perlman, P. S. (1999) *RNA* **5**, 318-329.
(253) Daniels, D. L., Michels, W. J., Jr., Pyle, A. M. (1996) *J. Mol. Biol.* **256**, 31-49.
(254) Padgett, R. A., Podar, M., Boulanger, S. C., Perlman, P. S. (1994) *Science* **266**, 1685-1688.
(255) Jacquier, A., Jacquesson-Breuleux, N. (1991) *J. Mol. Biol.* **219**, 415-428.
(256) Chin, K., Pyle, A. M. (1995) *RNA* **1**, 391-406.
(257) Van der Veen, R., Kwakman, J. H. J. M., Grivell, L. A. (1997) *EMBO J.* **6**, 3827-3831.
(258) Jarrell, K. A., Peebles, C. L., Dietrich, R. C., Romiti, S. L., Perlman, P. S. (1988) *J. Biol. Chem.* **263**, 3432-3439.
(259) Vogel, J., Borner, T. (2002) *EMBO J.* **21**, 3794-3803.
(260) Fedorova, O., Zingler, N. (2007) *Biol. Chem.* **388**, 665.

(261) Peebles, C. L., Perlman, P. S., Mecklenburg, K. L., Petrillo, M. L., Tabor, J. H., Jarrell, K. A., Cheng, H. L. (1986) *Cell* **44**, 213-223.
(262) Schmelzer, C., Schweyen, R. J. (1986) *Cell* **46**, 557-565.
(263) Nilsen, T. W. (1998) in *RNA Structure and Function*, eds. Simons, R. W. & Grunberg-Manago, M. (Cold Spring Harbor Laboratory Press, Cold Spring Harbor), 279-307.
(264) Moore, M. J., Query, C. C., Sharp, P. A. (1993) in *The RNA World*, eds. Gesteland, R. F. & Atkins, J. F. (Cold Spring Harbor Laboratory Press, Cold Spring Harbor), 303-357.
(265) Guthrie, C. (1991) *Science* **253**, 157-163.
(266) Lambowitz, A. M. (1989) *Cell* **56**, 323-326.
(267) Eskes, R., Liu, L., Ma, H., Chao, M. Y., Dickson, L., Lambowitz, A. M., Perlman, P. S. (2000) *Mol. Cell. Biol.* **20**, 8432-8446.
(268) Zimmerly, S., Guo, H., Eskes, R., Yang, J., Perlman, P. S., Lambowitz, A. M. (1995) *Cell* **83**, 529-538.
(269) Yang, J., Zimmerly, S., Perlman, P. S., Lambowitz, A. M. (1996) *Nature* **381**, 332-335.
(270) Guo, H., Karberg, M., Long, M., Jones, J. P., III, Sullenger, B., Lambowitz, A. M. (2000) *Science* **289**, 452-457.
(271) Toro, N. (2003) *Environ. Microbiol.* **5**, 143-151.
(272) Lambowitz, A. M., Zimmerly, S. (2004) *Annu. Rev. Gen.* **38**, 1-35.
(273) Matsuura, M., Saldanha, R., Ma, H., Wank, H., Yang, J., Mohr, G., Cavanagh, S., Dunny, G. M., Belfort, M., Lambowitz, A. M. (1997) *Genes Dev.* **11**, 2910-2924.
(274) Herschlag, D., Cech, T. R. (1990) *Biochemistry* **29**, 10172-10180.
(275) Hertel, K. J., Herschlag, D., Uhlenbeck, O. C. (1996) *EMBO J.* **15**, 3751-3757.
(276) Werner, M., Uhlenbeck, O. C. (1995) *Nucleic Acids Res.* **23**, 2092-2096.
(277) Xiang, Q., Qin, P. Z., Michels, W. J., Freeland, K., Pyle, A. M. (1998) *Biochemistry* **37**, 3839-3849.
(278) Lambowitz, A. M., Mohr, G., Zimmerly, S. (2005) in *Homing endonucleases and inteins*, eds. Belfort, M., Derbyshire, V., Stoddard, B. L. & Wood, D. W. (Springer-Verlag, Heidelberg), 121-145.
(279) Hebbar, S. K., Belcher, S. M., Perlman, P. S. (1992) *Nucleic Acids Res.* **20**, 1747-1754.
(280) Huang, H.-R., Chao, M. Y., Armstrong, B., Wang, Y., Lambowitz, A. M., Perlman, P. S. (2003) *Mol. Cell. Biol.* **23**, 8809-8819.
(281) Costa, M., Fontaine, J. M., Goër, S. L., Michel, F. (1997) *J. Mol. Biol.* **274**, 353-364.
(282) Adamidi, C., Fedorova, O., Pyle, A. M. (2003) *Biochemistry* **42**, 3409-3418.
(283) Huang, H.-R., Rowe, C. E., Mohr, S., Jiang, Y., Lambowitz, A. M., Perlman, P. S. (2005) *Proc. Natl. Acad. Sci. USA* **102**, 163-168.
(284) Fedorova, O., Waldsich, C., Pyle, A. M. (2007) *J. Mol. Biol.* **366**, 1099-1114.
(285) Schroeder, R., Barta, A., Semrad, K. (2004) *Nat. Rev. Mol. Cell Biol.* **5**, 908-919.
(286) Su, L. J., Brenowitz, M., Pyle, A. M. (2003) *J. Mol. Biol.* **334**, 639.
(287) Sontheimer, E. J., Gordon, P. M., Piccirilli, J. A. (1999) *Genes Dev.* **13**, 1729-1741.
(288) Gordon, P. M., Sontheimer, E. J., Piccirilli, J. A. (2000) *RNA* **6**, 199-205.
(289) Kruschel, D., Sigel, R. K. O. (2008) *J. Inorg. Biochem.*, doi:10.1016/j.jinorgbio.2008.08.006
(290) Milligan, J. F., Groebe, D. R., Witherell, G. W., Uhlenbeck, O. C. (1987) *Nucleic Acids Res.* **15**, 8783-8798.
(291) Milligan, J. F., Uhlenbeck, O. C. (1989) *Methods Enzymol.* **180**, 51-62.
(292) Gallo, S., Furler, M., Sigel, R. K. O. (2005) *CHIMIA* **59**, 812-816.
(293) Eskes, R., Yang, J., Lambowitz, A. M., Perlman, P. S. (1997) *Cell* **88**, 865-874.
(294) Marky, L. A., Breslauer, K. J. (1987) *Biopolymers* **26**, 1601-1620.

(295) Breslauer, K. J. (1994) *Methods Mol. Biol.* **26**, 347-372.
(296) Stampfl, S., Lempradl, A., Koehler, G., Schroeder, R. (2007) *ChemBioChem* **8**, 1137 - 1145.
(297) SantaLucia, J., Jr., Turner, D. H. (1997) *Biopolymers* **44**, 309-319.
(298) Puglisi, J. D., Tinoco, I. (1989) *Methods Enzymol.* **180**, 304-325.
(299) Hilbers, C. W., Heus, H. A., Van Dongen, M. J. P., Wijmenga, S. S. (1994) in *Nucleic Acids and Molecular Biology*, eds. Eckstein, F. & Lilley, D. M. J. (Springer Verlag, Berlin), Vol. 8, 56-104.
(300) Napierala, M., Krzyzosiak, W. J. (1997) *J. Biol. Chem.* **272**, 31079-31085.
(301) Lapham, J., Rife, J. P., Moore, P. B., Crothers, D. M. (1997) *J. Biomol. NMR* **10**, 255-262.
(302) Marky, L. A., Blumenfeld, K. S., Kozlowski, S., Breslauer, K. J. (1983) *Biopolymers* **22**, 1247-1257.
(303) Borer, P. N., Lin, Y., Wang, S., Roggenbuck, M. W., Gott, J. M., Uhlenbeck, O. C., Pelczer, I. (1995) *Biochemistry* **34**, 6488-6503.
(304) Marky, L. A., Kallenbach, N. R., McDonough, K. A., Seeman, N. C., Breslauer, K. J. (1987) *Biopolymers* **26**, 1621-1634.
(305) Aboul-ela, F., Nikonowicz, E. P., Pardi, A. (1994) *FEBS Lett.* **347**, 261-264.
(306) Cabello-Villegas, J., Nikonowicz, E. P. (2000) *Nucleic Acids Res.* **28**, e74.
(307) Johannsen, S., Paulus, S., Düpre, N., Müller, J., Sigel, R. K. O. (2008) *J. Inorg. Biochem.* **102**, 1141-1151.
(308) Micura, R., Pils, W., Höbartner, C., Grubmayr, K., Ebert, M.-O., Jaun, B. (2001) *Nucleic Acids Res.* **29**, 3997-4005.
(309) Eimer, W., Williamson, J. R., Boxer, S. G., Pecora, R. (1990) *Biochemistry* **29**, 799-811.
(310) Mathews, D. H., Sabina, J., Zuker, M., Turner, D. H. (1999) *J. Mol. Biol.* **288**, 911-940.
(311) MacDonald, D., Lu, P. (2002) *Curr. Opin. Struct. Biol.* **12**, 337-343.
(312) Metzler, W. J., Wang, C., Kitchen, D. B., Levy, R. M., Pardi, A. (1990) *J. Mol. Biol.* **214**, 711-736.
(313) Venters, R. A., Thompson, R., Cavanagh, J. (2002) *J. Mol. Struct.* **602**, 275-292.
(314) Blackledge, M. (2005) *Prog. Nucl. Mag. Res. Sp.* **46**, 23-61.
(315) Zhou, H., Vermeulen, A., Jucker, F. M., Pardi, A. (1999) *Biopolymers* **52**, 168-180.
(316) Vermeulen, A., Zhou, H., Pardi, A. (2000) *J. Am. Chem. Soc.* **122**, 9638 - 9647.
(317) Marvin, D. A., Wachtel, E. J. (1975) *Nature* **253**, 19-23.
(318) Torbet, J., Maret, G. (1979) *J. Mol. Biol.* **134**, 843-845.
(319) Hansen, M. R., Mueller, L., Pardi, A. (1998) *Nat. Struct. Biol.* **5**, 1065 - 1074.
(320) Hansen, M. R., Hanson, P., Pardi, A. (2000) *Methods Enzymol.* **317**, 220-240.
(321) Tjandra, N., Bax, A. (1997) *Science* **278**, 1111-1114.
(322) Erat, M. C. (2007) in *Two domains of branching and catalysis act as specific metal ion binding platforms within the group II intron ribozyme core* (Dissertation, University of Zürich, Institute of Inorganic Chemistry, Zürich), 1-348.
(323) Zweckstetter, M., Bax, A. (2000) *J. Am. Chem. Soc.* **122**, 3791-3792.
(324) Zweckstetter, M. (2008) *Nat. Protoc.* **3**, 679-690
(325) Breeze, A. L. (2000) *Prog. Nucl. Mag. Res. Sp.* **36**, 323-372.
(326) Zwahlen, C., Legault, P., Vincent, S. J. F., Greenblatt, J., Konrat, R., Kay, L. E. (1997) *J. Am. Chem. Soc.* **119**, 6711-6721.
(327) Ogura, K., Terasawa, H., Inagaki, F. (1996) *J. Biomol. NMR* **8**, 492-498.
(328) Iwahara, J., Wojciak, J. M., Clubb, R. T. (2001) *J. Biomol. NMR* **19**, 231-241.
(329) Nonin, S., Leroy, J. L., Guéron, M. (1995) *Biochemistry* **34**, 10652-10659.
(330) Wu, M., Tinoco Jr., I. (1998) *Proc. Natl. Acad. Sci. USA* **95**, 11555–11560.

(331) Greenbaum, N. L., Radhakrishnan, I., Hirsh, D., Patel, D. J. (1995) *J. Mol. Biol.* **252**, 314-327.
(332) Pasternack, L. B., Lin, S.-B., Chin, T.-M., Lin, W.-C., Huang, D.-H., Kan, L.-S. (2002) *Biophys. J.* **82**, 3170-3180.
(333) J. Richards, R., Theimer, C. A., Finger, L. D. F., Juli (2006) *Nucl. Acid. Res.* **34**, 816–825.
(334) Plant, E. P., Pérez-Alvarado, G. C., Jacobs, J. L., Mukhopadhyay, B., Hennig, M., Dinman, J. D. (2005) *PLoS Biol.* **3**, e172.
(335) Joli, F., Bouchemal, N., Laigle, A., Hartmann, B., Hantz, E. (2006) *Nucleic Acids Res.* **34**, 5740–5751.
(336) Cerdan, R., Payet, D., Yang, J.-C., Travers, A. A., Neuhaus, D. (2001) *Protein Sci.* **10**, 504–518.
(337) Brodsky, A. S., Williamson, J. R. (1997) *J. Mol. Biol.* **267**, 624-639.
(338) Puglisi, J. D., Tan, R., Calnan, B. J., Frankel, A. D., Williamson, J. R. (1992) *Science* **257**, 76-80.
(339) Harms, J., Schluenzen, F., Zarivach, R., Bashan, A., Gat, S., Agmon, I., Bartels, H., Franceschi, F., Yonath, A. (2001) *Cell* **107**, 679-688.
(340) Holland, J. A., Hoffman, D. W. (1996) *Nucleic Acids Res.* **24**, 2841-2848.
(341) Long, K. S., Crothers, D. M. (1999) *Biochemistry* **38**, 10059 - 10069.
(342) Ye, X., Gorin, A., Ellington, A. D., Patel, D. J. (1996) *Nat. Struct. Biol.* **3**, 1026-1033.
(343) Ye, X., Kumar, R. A., Patel, D. J. (1995) *Chem. Biol.* **2**, 827-840.
(344) Leontis, N. B., Westhof, E. (2001) *RNA* **7**, 499-512.
(345) Ramachandran, G. N., Ramakrishnan, C., Sasisekharan, V. (1963) *J. Mol. Biol.* **7**, 95-99.
(346) Petry, S., Brodersen, D. E., Murphy Iv, F. V., Dunham, C. M., Selmer, M., Tarry, M. J., Kelley, A. C., Ramakrishnan, V. (2005) *Cell* **123**, 1255-1266.
(347) Holland, J. A., Hansen, M. R., Du, Z., Hoffman, D. W. (1999) *RNA* **5**, 257 - 271.
(348) Heus, H. A., Pardi, A. (1991) *Science* **253**, 191-194.
(349) Bruker (2008) *Almanac*.
(350) Pecoraro, V. L., Hermes, J. D., Cleland, W. W. (1984) *Biochemistry* **23**, 5262-5271.
(351) Erat, M. C., Sigel, R. K. O. (2007) *Inorg. Chem.* **46**, 11224-11234.
(352) Bianchi, E. M., Sajadi, S. A. A., Song, B., Sigel, H. (2003) *Chem. Eur. J.* **9**, 881-892.
(353) Sigel, H., Griesser, R. (2005) *Chem. Soc. Rev.* **34**, 875-900.
(354) Sigel, R. K. O., Sigel, H. (2007) *Met. Ions Life Sci.* **2**, 109-180.
(355) Sigel, H., Bianchi, E. M., Corfù, N. A., Kinjo, Y., Tribolet, R., Martin, R. B. (2001) *Chem. Eur. J.* **7**, 3729-3737.
(356) Davis, J. H., Foster, T. R., Tonelli, M., Butcher, S. E. (2007) *RNA* **13**, 76-86.
(357) Knobloch, B., Sigel, R. K. O., Lippert, B., Sigel, H. (2004) *Angew. Chem., Int. Ed.*, 3793-3795.
(358) Klein, D. J., Moore, P. B., Steitz, T. A. (2004) *RNA* **10**, 1366-1379.
(359) Ennifar, E., Walter, P., Dumas, P. (2003) *Nucleic Acids Res.* **31**, 2671-2682.
(360) Sigel, H., Bianchi, E. M., Corfu, N. A., Kinjo, Y., Tribolet, R., Martin, R. B. (2001) *J. Chem. Soc., Perkin Trans.* **2**, 507-511.
(361) Sigel, H. (2004) *Pure Appl. Chem.* **76**, 375-388.
(362) Sajadi, S. A. A., Song, B., Gregan, F., Sigel, H. (1999) *Inorg. Chem.* **38**, 439-448.
(363) Sigel, R. K. O., Sigel, H. (2007) *Met. Ions Life Sci.* **2**, 109-180.
(364) Martin, R. B. (1963) *Science* **139**, 1198-1203.
(365) Markley, J. C., Godde, F., Sigurdsson, S. T. (2001) *Biochemistry* **40**, 13849-13856.
(366) Maderia, M., Hunsicker, L. M., DeRose, V. J. (2000) *Biochemistry* **39**, 12113-12120.
(367) Nikonowicz, E. P., Smith, J. S. (1999) *Phosphorus, Sulfur, and Silicon and the Related Elements* **144**, 305 - 308.

(368) Yoshida, A., Sun, S., Piccirilli, J. A. (1999) *Nat. Struct. Mol. Biol.* **6**, 318-321.
(369) Kuimelis, R. G., McLaughlin, L. W. (1996) *Biochemistry* **35**, 5308-5317.
(370) Eigen, M. (1963) *Pure Appl. Chem.* **6**, 97-115.
(371) Bennetto, H. P., Caldin, E. F. (1971) *J. Chem. Soc., A*, 2198-2207.
(372) Frey, C. M., Stuehr, J. E. (1974) *Met. Ions Biol. Syst.* **1**, 51-116.
(373) Sigel, H., Amsler, P. E. (1976) *J. Am. Chem. Soc.* **98**, 7390-7400.
(374) Glassman, T. A., Suchy, J., Cooper, C. (1973) *Biochemistry* **12**, 2430-2437.
(375) Glassman, T. A., Cooper, C., Kuntz, G. P. P., Swift, T. J. (1974) *FEBS Lett.* **39**, 73-74.
(376) Frey, C. M., Stuehr, J. E. (1978) *J. Am. Chem. Soc.* **100**, 139-145.
(377) Butenhof, K. J., Cochenour, D., Banyasz, J. L., Stuehr, J. E. (1986) *Inorg. Chem.* **25**, 691-696.
(378) Bishop, E. O., Kimber, S. J., Orchard, D., Smith, B. E. (1981) *Biochim. Biophys. Acta* **635**, 63-72.
(379) Sigel, H. (1990) *Coord. Chem. Rev.* **100**, 453-539.
(380) Arena, G., Cali, R., Cucinotta, V., Musumeci, S. R., Sammartano, S. (1983) *J. Chem. Soc., Dalton Trans.*, 1271-1278.
(381) Mucha, A., Knobloch, B., Jezowska-Bojczuk, M., Kozlowski, H., Sigel, R. K. O. (2008) *Chem. Eur. J.* **14**, 6663-6671.
(382) Bianchi, E. M. (2003) in *Comparison of the Stabilities and Solution Structures of Metal Ion Complexes Formed with 5-Di- and 5-Triphosphates of Purine Nucleotides* (Dissertation, University of Basel, Department of Chemistry, Basel), 1-216.
(383) Irving, H., Williams, R. J. P. (1948) *Nature*, 746 - 747
(384) Irving, H., Williams, R. J. P. (1953) *J. Chem. Soc.*, 3192 - 3210.
(385) Martin, R. B. (1986) *Met. Ions Biol. Syst.* **20**, 21-65.
(386) Martin, R. B. (1994) in *Encyclopedia of Inorganic Chemistry*, ed. King, R. B. (Wiley, Chichester), Vol. 4, 2185-2196.
(387) Martin, R. B. (1996) in *Encyclopedia of Molecular Biology and Molecular Medicine*, ed. Meyers, R. A. (VCH, Weinheim), Vol. 1, 125-134.
(388) Sarkar, M., Sigurdsson, S., Tomac, S., Sen, S., Rozners, E., Sjöberg, B., Strömberg, R., Gräslund, A. (1996) *Biochemistry* **35**, 4678-4688.
(389) Pan, T., Sosnick, T. R. (1997) *Nat. Struct. Biol.* **4**, 931-938.
(390) Erat, M. C., Sigel, R. K. O. (2008) *J. Biol. Inorg. Chem.* **13**, 1025-1036.
(391) Gordon, P. M., Sontheimer, E. J., Piccirilli, J. A. (2000) *Biochemistry* **39**, 12939-12952.
(392) Pyle, A. M. (2002) *J. Biol. Inorg. Chem.* **7**, 679-690.
(393) Sigel, H. (1992) *Inorg. Chim. Acta* **198-200**, 1-11.
(394) Sodhi, R., Rajput, Y. S. (2003) *Anal. Biochem.* **315**, 141-142.
(395) Davanloo, P., Rosenberg, A. H., Dunn, J. J., Studier, F. W. (1984) *Proc. Natl. Acad. Sci. USA* **A81**, 2035-2039.
(396) Glasoe, P. K., Long, F. A. (1960) *J. Phys. Chem.* **64**, 188-190.
(397) Güntert, P., Mumenthaler, C., Wüthrich, K. (1997) *J. Mol. Biol.* **273**, 283-298.
(398) Clore, G. M., Gronenborn, A. M., Tjandra, N. (1998) *Journal of Magnetic Resonance* **131**, 159-162.
(399) Al-Hashimi, H. M., Gorin, A., Majumdar, A., Gosser, Y., Patel, D. J. (2002) *J. Mol. Biol.* **318**, 637-649.

Acknowledgements

Last but not least I would like to thank all the people who supported me during my time in Zürich:

All members of the Sigel and Freisinger groups at the University of Zürich. Thank you very much for all your support, help and friendship. Special thanks go to MAYA FURLER who helped me a lot in getting acquainted with all the new methods and techniques in the beginning of my time in Zürich. BERND KNOBLOCH (our brain!) and MICHÈLE ERAT for introducing me to NMR and a lot of useful discussions and hints. My labmates SOFIA GALLO and MIRIAM STEINER for a wonderful atmosphere in the lab with great scientific as well as personal discussions, as well as VERONIKA ZELENAY and ARIEL MUCHA, who joined us in the lab for some time. SILKE JOHANNSEN and SUSANN PAULUS for all their help and support in all areas of my life and thanks for joining me for coffee breaks! DANIELA DONGHI, who joined our group for a short time during my last months in Zürich, thanks for sharing my ups and downs during this period. I would like to thank my student DANIEL MARTI for his efforts and patience in recording CD spectra. Special thanks go to SILKE JOHANNSEN, BERND KNOBLOCH, SUSANN PAULUS and MIRIAM STEINER for carefully reading my thesis. Thank you very much for the time you spend on correcting it and leading me back on the right way when I have lost the thread. EMINA BESIC, JOACHIM SCHNABL, MAXIMILANE KORTH, and all other past and present members of the SF-lab! Thank you very much for everything, I really had a great time here in Zürich and I will miss you all!

All members of the Institute of Inorganic Chemistry at the University of Zürich, especially NATHALIE FICHTER, PATRIZIA ALLEGRO, BEATRICE SPICHTIG and TANJA SPÖRRI for administrative services, MANFRED JÖHRI for technical support, HANSPETER STALDER for constructing and reparing our equipment and BERNHARD SPINGLER for a lot of help.

OLIVER ZERBE and the NMR team NADJA BROSS and SIMON JURT, as well as THOMAS FOX for setting up and running the NMR facilities, for all your help, tips and tricks. Special thanks go to HELENA KOVACS from Bruker Biospin for showing us the NMR world from the technical side and for a lot of help and discussions.

SAM BUTCHER and JARED DAVIS from the University of Wisconsin in Madison (USA) as well as RONALD MICURA, CHRISTOPH KREUTZ and RENATE MARTINA RIEDER from the Leopold-Franzens University Innsbruck (Austria) for giving me a lot of suggestions concerning my "RNA-problems". ANNA MARIE PYLE and her group at Yale University in New Haven (USA) for supporting our work and for the generous gift of pT7D135 plasmid.

Big thanks go to the *Boehringer Ingelheim Fond*, not only for their financial support, but also for a great time during the summer seminars and for always having an open ear for our worries and concerns. Financial support by the Swiss National Science Foundation and the University of Zürich is also gratefully acknowledged.

Finally, I would like to thank my family and friends:
Meinen Eltern möchte ich von tiefstem Herzen für ihre Liebe und ihr Verständnis danken. Danke, dass ihr mich meinen Weg gehen lasst und mich immer dabei unterstützt.
My friends EVA, SILKE, DEBO, CADDY, RAMON, MARTIN, and ESTHER: thank you for your friendships, for supporting and motivating me, for sharing with me good and bad times during my time in Zürich. My "old" friends BRITTA, SABRINA and SILKE for their continous friendship, for answering the phone when I call and listening to me for hours. CAMILO, NATALIA and CARINA, for sharing with me the ups and downs of being a PhD student. GABRIELLE, my flatmate, for a great time sharing our lifes and for all the conversations and advices. And especially NIKOS for being my friend and for all the discussions during our coffee and sport breaks. I will miss you all and I hope to see you all again wherever we will end up in the end.